PHARMACOLOGICAL EFFECTS OF TRADITIONAL CHINESE MEDICINE ON CARDIOVASCULAR DISEASE

EDITED BY: Jianxun Liu, Guanhua Du and Xiu-Wei Yang
PUBLISHED IN: Frontiers in Pharmacology

frontiers Research Topics

frontiers

ISSN 1664-8714
ISBN 978-2-88971-798-9
DOI 10.3389/978-2-88971-798-9

About Frontiers

Frontiers is more than just an open-access publisher of scholarly articles: it is a pioneering approach to the world of academia, radically improving the way scholarly research is managed. The grand vision of Frontiers is a world where all people have an equal opportunity to seek, share and generate knowledge. Frontiers provides immediate and permanent online open access to all its publications, but this alone is not enough to realize our grand goals.

Frontiers Journal Series

The Frontiers Journal Series is a multi-tier and interdisciplinary set of open-access, online journals, promising a paradigm shift from the current review, selection and dissemination processes in academic publishing. All Frontiers journals are driven by researchers for researchers; therefore, they constitute a service to the scholarly community. At the same time, the Frontiers Journal Series operates on a revolutionary invention, the tiered publishing system, initially addressing specific communities of scholars, and gradually climbing up to broader public understanding, thus serving the interests of the lay society, too.

Dedication to Quality

Each Frontiers article is a landmark of the highest quality, thanks to genuinely collaborative interactions between authors and review editors, who include some of the world's best academicians. Research must be certified by peers before entering a stream of knowledge that may eventually reach the public - and shape society; therefore, Frontiers only applies the most rigorous and unbiased reviews.
Frontiers revolutionizes research publishing by freely delivering the most outstanding research, evaluated with no bias from both the academic and social point of view. By applying the most advanced information technologies, Frontiers is catapulting scholarly publishing into a new generation.

What are Frontiers Research Topics?

Frontiers Research Topics are very popular trademarks of the Frontiers Journals Series: they are collections of at least ten articles, all centered on a particular subject. With their unique mix of varied contributions from Original Research to Review Articles, Frontiers Research Topics unify the most influential researchers, the latest key findings and historical advances in a hot research area! Find out more on how to host your own Frontiers Research Topic or contribute to one as an author by contacting the Frontiers Editorial Office: frontiersin.org/about/contact

PHARMACOLOGICAL EFFECTS OF TRADITIONAL CHINESE MEDICINE ON CARDIOVASCULAR DISEASE

Topic Editors:
Jianxun Liu, China Academy of Chinese Medical Sciences, China
Guanhua Du, Chinese Academy of Medical Sciences and Peking Union Medical College, China
Xiu-Wei Yang, Peking University, China

Cardiovascular diseases include ischemic and hemorrhagic diseases involving the heart, brain, whole body tissue, and includes coronary heart disease, heart failure, arrhythmia, atherosclerosis and stroke. This particular group of diseases continue to be a leading cause of death throughout the world with mortality rate remaining high. Currently, drugs administered orally and intravenously and surgical treatments are used to treat such diseases.

Traditional Chinese medicine (TCM) refers to natural herbal medicines and their processed products used for preventing and treating disease under the guidance of traditional Chinese medicine's theory. The implementation of prevention and treatment programs of ischemic cardiovascular diseases with the use of TCM have been associated with positive outcomes; in terms of a reduction in the disability and mortality rate of some patients. Other studies have also shown that specific multi-component TCM preparations have therapeutic benefits based on multi-target and multi-pathway mechanisms, which may have advantages over the current single-component and single-target therapy. Based these characteristics, approved pharmaceutical drugs based in TCM, such as Compound Danshen Dripping Pills, Naoxintong Capsules, Tonxinluo Capsules, and Danhong Injection, are currently used to treat cardiovascular diseases.

However, there are a number of areas that still need further investigation. For example, the identification of effective components in herbal medicine is essential in furthering our understanding of what occurs at a pharmacological level; the metabolizing pharmacological pathways of such components; the cellular target of the components; and the lack of standardized guidelines to enhance clinical research.

Citation: Liu, J., Du, G., Yang, X.-W., eds. (2021). Pharmacological Effects of Traditional Chinese Medicine on Cardiovascular Disease.
Lausanne: Frontiers Media SA. doi: 10.3389/978-2-88971-798-9

Table of Contents

frontiers in Pharmacology

ORIGINAL RESEARCH
published: 21 June 2019
doi: 10.3389/fphar.2019.00614

Danggui Buxue Tang, a Chinese Herbal Decoction Containing Astragali Radix and Angelicae Sinensis Radix, Modulates Mitochondrial Bioenergetics in Cultured Cardiomyoblasts

*Kenneth K.L. Kwan[1,2], Yun Huang[1,2], Ka W. Leung[1,2], Tina T.X. Dong[1,2] and Karl W.K. Tsim[1,2]**

[1] Shenzhen Key Laboratory of Edible and Medicinal Bioresources, Shenzhen Research Institute, Shenzhen, China, [2] Division of Life Science and Center for Chinese Medicine, The Hong Kong University of Science and Technology, Hong Kong, Hong Kong

OPEN ACCESS

Edited by:
Michael Heinrich,
UCL School of Pharmacy,
United Kingdom

Reviewed by:
Betty Yuen Kwan Law,
Macau University of Science and Technology, Macau
Pui Kei Wu,
Medical College of Wisconsin, United States

***Correspondence:**
Karl W.K. Tsim
botsim@ust.hk

Specialty section:
This article was submitted to Ethnopharmacology, a section of the journal Frontiers in Pharmacology

Received: 09 January 2019
Accepted: 15 May 2019
Published: 21 June 2019

Citation:
Kwan KKL, Huang Y, Leung KW, Dong TTX and Tsim KWK (2019) Danggui Buxue Tang, a Chinese Herbal Decoction Containing Astragali Radix and Angelicae Sinensis Radix, Modulates Mitochondrial Bioenergetics in Cultured Cardiomyoblasts. Front. Pharmacol. 10:614. doi: 10.3389/fphar.2019.00614

Danggui Buxue Tang (DBT) is an ancient herbal mixture containing Astragali Radix and Angelicae Sinensis Radix, and which are commonly consumed for "qi-invigorating" (i.e., stimulating vital energy/energy metabolism) as traditional Chinese medicine (TCM). The pharmacological activities of DBT in anti-oxidation, estrogenic, hematopoietic, and immunogenic have been reported; however, the role of DBT in cellular energy metabolism has not been determined. Here, we employed an extracellular flux analyzer to evaluate the mitochondrial respiration of cultured H9C2 cardiomyoblasts in present of DBT. The herbal extract of DBT was qualified chemically for the major ingredients, i.e. astragaloside, calycosin, formononetin, Z-ligustilide, and ferulic acid. The anti-oxidant activities of DBT, as well as its major ingredients, were determined by Folin-Ciocalteu assay, 2,2-diphenyl-1-picrylhydrazyl (DPPH) radical scavenging assay, and protective effect in tert-butyl hydroperoxide (tBHP)-treated cultured cardiomyoblasts. In addition, a real-time oxygen consumption rate (OCR) in herbal extract-treated cultured cardiomyoblasts was revealed by using a Seahorse extracellular flux analyzer. In addition, the transcript expressions of peroxisome proliferator-activated receptor gamma coactivator 1-alpha (PCG-1α) and other genes relating to mitochondria biogenesis were determined in cardiomyoblasts under different herbal treatments. DBT possessed the strongest anti-oxidant activity and protective effects on the oxidatively stressed cardiomyoblasts. By revealing the OCR in mitochondria, the health state of cultured cardiomyoblasts under DBT was improved *via* increase of basal respiration, proton leak, non-mitochondria, and adenosine triphosphate (ATP) production. Furthermore, the transcriptional activities of genes responsible for mitochondrial biogenesis and DNA replication were stimulated by application of DBT in cultures.

Keywords: Astragalus, Angelica, anti-oxidative activity, Chinese medicine, extracellular flux analyzer, mitochondrial bioenergetics, oxygen consumption rate

INTRODUCTION

Traditional Chinese medicine (TCM) has been used as medicine, or health supplement, in China over thousands of years (Lu and Lu, 2014). Historically, TCM herbal decoction is prepared by a unique methodology with specific combination of different herbs as a formula. Among thousands of herbal formulae, Danggui Buxue Tang (DBT) is an ancient Chinese herbal decoction having a simple combination of two herbs. DBT was first described in *Neiwaishang Bianhuo Lun* by Li Dongyuan in China in AD 1247. DBT contains two common herbs, Astragali Radix [AR; roots of *Astragalus membranaceus* (Fisch). Bunge or *A. membranaceus* (Fisch). Bunge var. *mongholicus* (Bunge) Hsiao] and Angelicae Sinensis Radix (ASR; roots of *Angelica sinensis* Oliv). at the weight ratio of 5 to 1 (Lin et al., 2017). DBT is a well-known herbal decoction in clinical treatment for women suffering from menopausal symptoms (Gong et al., 2016a). Until now, numerous components have been identified in DBT decoction, and astragaloside IV, calycosin, formononetin, Z-ligustilide, and ferulic acid are considered to be major and active ingredients (Zheng et al., 2011). According to TCM theory, DBT promotes "qi" (vital energy) enhancement and "blood" (body circulation) nourishment. DBT has been proposed to possess pharmacological properties both *in vivo* and *in vitro*, which includes: i) stimulating hematopoietic function (Yim et al., 2000), ii) exhibiting estrogenic property (Choi et al., 2011), iii) accelerating bone regeneration (Wang et al., 2015), iv) promoting immune system (Yang et al., 2014), v) protecting cardiovascular and pulmonary system (Mak et al., 2006), and vi) engaging formation of capillary and blood vessel (Gong et al., 2016a).

DBT and its chemical ingredients showed protective effects to different organs in various models of oxidative stress-related defects. For example, the antioxidant properties of ASR-derived ferulic acid (Kikuzaki et al., 2002) and AR-derived astragalosides and isoflavonoids were clearly shown in both *in vitro* and *in vivo* (Chen et al., 2011). In ferulic acid knock-out DBT, a significant decrease of anti-oxidative property was revealed, and which strongly suggested the role of ferulic acid in DBT (Gong et al., 2016b). To achieve maximal anti-oxidative functions, astragalosides from AR inhibited ROS generation, as induced by high glucose, in rat retinal capillary endothelial cells (Qiao et al., 2017). In addition, the flavonoids from AR, e.g. calycosin and formononetin, inhibited ROS-related lipid peroxidation (Toda and Shirataki, 1998).

Mitochondrial bioenergetics is a measurement of cellular energy status. In live cells, a Seahorse extracellular flux analyzer could be used to reveal the profiling of mitochondrial bioenergetics. These bioenergetics parameters are oxygen consumption rate (OCR), spare respiratory capacity (SRC), referring to ability of mitochondria to increase ATP to theoretical maximum (Dranka et al., 2010), and proton leakage, representing part of OCR pushing the substrate cycle of proton pumping and proton leak across inner mitochondrial membrane and not coupling to ATP production (Brand, 2005).

An important function of mitochondria is to enhance ATP production and oxidative phosphorylation for balance of bioenergy (Owen and Sunram-Lea, 2011). In addition, mitochondrial has a crucial role in cell death, signaling transmission, and energy homeostasis (Friedman and Nunnari, 2014). Thus, the malfunction of mitochondria is proposed to be the primary cause of energy decline, as well as onset of aging process, including neurodegenerative disease and diabetes (Sivitz and Yorek, 2010). Improving the profile of mitochondrial bioenergetics could be an approach to prevent cell damage (Wallacea et al., 1997). Thus, the application of TCM in maintaining health status of mitochondria should be considered. DBT is commonly consumed in daily life, and which has been claimed to be "qi-invigorating" (i.e., stimulating vital energy/energy metabolism), but the effect of DBT in mitochondrial bioenergetics is still a mystery. Here, a detail oxidative phosphorylation parameter in mitochondria, after application of DBT, or other herbal extracts, in cultured cardiomyoblasts were determined in live cell dynamically by fluorescence-based respirometer. In addition, the expression of mitochondrial genes, as well as the morphology of mitochondria, was determined here in cultured cardiomyoblasts.

MATERIALS AND METHODS

Standardization of DBT Extracts

The preparation of herbal extracts, e.g., DBT and water extracts of ASR and AR, was described previously (Song et al., 2004). Roots of 3-year-old *A. membranaceus* var. *mongholicus* (AR) from Shanxi Province and 2-year-old *A. sinensis* roots (ASR) from Minxian of Gansu Province were used. The authentication of plant materials was identified by Dr. Tina Dong at Hong Kong University of Science and Technology (HKUST). The authentication of these herbs was according to Hong Kong Materia Medica Standards. The voucher specimens (voucher # 02-9-1 for ASR and voucher # 02-10-4 for AR) were stored in Centre for Chinese Medicine of HKUST. To prepare the herbal extract, DBT (exact amounts of AR and ASR in a weight ratio of 5:1), AR, and ASR were boiled in 8 vol of water (v/w) for 2 h, and the extraction was repeated twice. The extracts were dried by lyophilization and stored at −80°C. Qualification of chemical markers of DBT and water extracts of ASR and AR was performed on an Agilent HPLC 1200 series system (Agilent, Waldbronn, Germany), equipped with a degasser, a binary pump, an autosampler, a thermos-stated column compartment, and a diode array detector. The mixtures were filtered by a 0.22-μm filter before separated by an Agilent ZORBAX Eclipse XDB-C18 column (1.8 μm, 50 mm × 4.6 mm). The mobile phase composed of 0.1% formic acid in acetonitrile (A) and 0.1% formic acid in water (B) according to the following gradient program: 0–2 min, isocratic gradient 20–20% (A); 2–7 min, linear gradient 20–34% (A); 7–12 min, isocratic gradient 34–34% (A); 12–16 min, linear gradient 34–65% (A); and 16–18 min, linear grad 65–80% (A). A pre-balance period of 5 min was used between each run. The flow rate was set at 0.4 ml/min; the column temperature was 25°C; and the injection volume was 5 μl. To determine amount of chemical markers of DBT, ASR, and AR extracts, the effluent was introduced into MS for further analysis. Mass spectrometry was performed on an Agilent QQQ-MS/MS (6410A) equipped with an ESI ion source was operated in positive and negative ion. The dry gas temperature was 325°C; drying gas

flow rate: 10 L/min; capillary voltage: 4,000 V; nebulizer pressure: 35 psi; and delta electro multiplier voltage: 400 V. For the multiple reaction monitoring (MS/MS) analysis, two transition pairs were chosen for acquisition in MRM mode for calycosin, formononetin, Z-ligustilide, ferulic acid, and astragalosides. The collision energy value and fragmentor voltage were optimized in advance to obtain the highest abundance.

Cell Cultures

The rat embryonic cardiomyoblast, H9C2 cell line, was obtained from American Type Culture Collection (ATCC, Manassas, VA). H9C2 cell line was maintained in high-glucose content Dulbecco's modified Eagle's medium (DMEM) supplemented with 100 IU/ml penicillin, 100 μg/ml streptomycin, and 10% fetal bovine serum (FBS) at 37°C in a 5% CO_2 water-saturated incubator. All culture reagents were purchased from Invitrogen Technologies (Carlsbad, CA).

Cell Viability Assay

Cell viability was performed by 3-(4,5-dimethylthiazol-2-yl)-2,5-diphenyltetra-zolium bromide (MTT) assay. Cells were seeded in 96-well plates at a density of 5,000 cells/ml. After 24-h drug treatment, cells in each well were incubated with 50 μl MTT (2 mg/ml, Invitrogen) at a final concentration of 0.5 mg/ml for 3 h at 37°C. After removal of the solution, DMSO was used to re-suspend the purple precipitate inside the cells at room temperature, and the absorbance was detected at 570 nm. The cell viability was calculated as a percentage of absorbance; while the value of vehicle control was set as 100%.

Folin-Ciocalteu Assay

To reveal the amount of total phenolic compound, 20 μl of each herb sample together with 40 μl 10% (v/v) Folin-Ciocalteu solution (Sigma-Aldrich, St Louis, MO) was added into 96-well microplate and shaken for 10 min at room temperature in dark. Then, 160 μl Na_2CO_3 (700 mM) was introduced into the well. The assay plates were shaken and incubated at room temperature without light exposure for 2 h before optical displacement (OD) value at 765 nm was measured. At the same time, gallic acid (Sigma-Aldrich) was used as the reference chemical marker, and total phenolic amount of each extract was referring amount of gallic acid.

2,2-Diphenyl-1-picrylhydrazyl Radical Scavenging Assay

The free radical scavenging activity of herbs extracts was measured by 2,2-diphenyl-1-picrylhydrazyl (DPPH) colorimetric assay. In brief, 150 μl of 0.1 mM DPPH solution with 50 μl of each extract (0–9 mg/ml) was added into 96-well microplate for 10 min at room temperature. The color of DPPH solution was changed from purple to yellow, indicating free radical scavenging or redox reaction. The OD value at 517 nm was measured. DPPH radical scavenging capacity was calculated as inhabitation percentage based on the following equation: inhibition $[(\%) = (A_0\text{-}A_1)/A_0] \times 100$, where A_0 is the OD value of the vehicle control, and A_1 is the OD value of each herbs sample aliquot. In this assay, gallic acid (0–100 μM) was served as a positive control.

Oxidative Stress Assay

To investigate the ability of DBT against tert-butyl hydroperoxide (tBHP)-induced cytotoxicity of oxidative stress, the cells were cultured in 96-well plate. After drug treatment for 24 h, tBHP (400 μM) were added into the wells for 3 h before MTT at 37°C, MTT was dissolved in 1 × PBS at a final concentration of 0.5 mg/ml. After the solution was removed, the purple organic crystal inside the cells was re-suspended in dimethyl sulfoxide (DMSO) and then measured at 570 nm absorbance. Before performed this experiment. The amount of tBHP (Sigma-Aldrich) and positive control (vitamin C, 1 mM) were optimized in cultured H9C2 cells.

Mitochondrial Bioenergetics Analysis

To determine mitochondrial bioenergetics of H9C2 cell, real-time oxygen consumption by mitochondria in live cells was monitored by a Seahorse Bioscience XFp extracellular flux analyzer (Agilent). When the cell was exposed to various stimuli through multiple mitochondrial specific inhibitors from injection ports, the rate of oxygen consumption (OCR) by mitochondria in live cells could be measured by the change of fluorescence intensity at Seahorse XFp sensor cartridge. The seeding density of H9C2 cell was optimized at 5,000 cells per well, and thus this density was utilized for the experiments. In addition, mitochondrial-specific inhibitors and uncouplers (Sigma-Aldrich) were used at 1 μM oligomycin (complex V inhibitor), 3 μM FCCP (mitochondrial oxidative phosphorylation uncoupler), and 1 μM rotenone/antimycin A (inhibitors of complex I and complex III, respectively) to elicit maximal effects on mitochondrial respiration. The fluorescence background noise and interference were normalized by background correction wells (the wells without cells). Cells were seeded on XFp cell mini-plates (Agilent) and treated with herbal extracts for 24 h. The sensor cartridge of XFp analyzer was hydrated in a 37°C non-CO_2 water-saturated incubator a day before the experiment. During the sensor calibration, cells were incubated in 37°C non-CO_2 incubator in 180 μl assay medium (XF base medium, 10 mM glucose, 1 mM pyruvate, and 2 mM L-glutamine, pH 7.4 at 37°C) for 1 h prior to assay. The plate was placed into calibrated XFp extracellular flux analyzer. The OCR had three cycles of reading: 2 min of mixing solution, 2 min of reagent incubation, and 2 min of fluorescing intensity measurements consisted in each measurement cycle. The OCR was normalized to amount of cellular protein/well and corrected for extra-mitochondrial O_2 consumption. After Seahorse XFp assay, the cells were lysed with high salt lysis buffer (50 mM Tris-HCl, pH 8.0, 500 mM NaCl, 5 mM EDTA, and 1% Triton X-100), and the amount of total protein of intact cells was determined using Bradford reagent (Bio-Rad; Hercules, CA). The bovine serum albumin (BSA) was used for the standard curve for the determination of protein content. The OCR data were expressed as pmol/min/μg protein. Each complex of the mitochondrial respiratory chain was provided in bioenergetics profile. In brief, six parameters of mitochondrial function were calculated from

bioenergetics profile: basal respiration, ATP production, proton leak, maximal respiration, spare respiration capacity, and non-mitochondrial respiration.

Mitochondrial Membrane Potential Assay

H9C2 cell was seeded on 96-well black multiwall plate at 4,000 cell/ml with clear bottom and grown for 24 h. The cultures were washed with 1× PBS twice and loaded with 100 µl JC-1 dye (20 µM; Sigma-Aldrich) at 37°C for 10 min under 5% CO_2 r (v/v) at 37°C. The cells were washed with PBS twice for staining and incubated with DBT, as well as extracts of ASR, AR, and their mixture. Carbonyl cyanide-p-trifluoromethoxy-phenylhydrazone (FCCP; 100 µM), a mitochondrial uncoupler, was used as a negative control in the measurement. The accumulation of JC-1 dye in mitochondria was quantified by red fluorescence intensity (excitation 527 nm and emission 590 nm), which was monitored every 1 min for up to 60 min at 37°C. The changes in mitochondrial membrane potential were expressed as the percentage of initial level of corresponding control.

Real-Time Polymerase Chain Reaction

Cultured H9C2 cells were seeded in a 6-well plate at 4,000 cells/ml and treated with herbal extracts, or other reagents, for 24 h. Total RNA was isolated by RNAzol reagent from Molecular Research Center Inc. (Cincinnati, OH), followed by reverse transcription into cDNA according to the manufacturer's instructions (Invitrogen). RT-PCR was performed by using Fast Start Universal SYBR Green Master (ROX) according to manufacturer's instructions (Roche Diagnostics; Mannheim, Germany). The primers for rat PCG-1α gene were 5'-GGA GCA ATA AAG CAA AGA GCA-3' and 5'-GTG TGA GGA GGG TCA TCG TT-3'; the primers for rat TFAM were 5'-CAG AGT TGT CAT TGG GAT TGG-3' and 5'-TTC AGT GGG CAG AAG TCC AT-3'; the primers for rat NRF1 were 5'-TTG ATG GAC ACT TGG GTA GC-3' and 5'-GCC AGA AGG ACT GAA AGC AG-3'; the primers for rat PLOG were 5'-CTC CTA CCT GCC TGT CAA CC-3' and 5'-GCT CCA TCA GCG ACT TCT TC-3'; the primers for rat TOP1MT were 5'-CCA AGG TGT TTC GGA CCT AC-3' and 5'-GTT TGC CCG GTT GTA AGC TA-3'; the primers for rat TWINKLE were 5'-GAG GAC AGG GAG GAG GTC TT-3'and 5'-TGG TAA GGC CAA ACA TCA CA-3'. The rat GAPDH RNA was used as internal control in all case, and its primer sequences were: 5-AAC GGA TTT GGC CGT ATT GG-3' and 5-CTT CCC GTT CAG CTC TGG G-3'. The SYSB green signal was detected by LightCycler 480 Ⅱ real-time PCR system (Roche; Basel, Switzerland). The transcript levels were quantified by using ΔΔCt value method under LightCycler 480 software release 1.5.1.62 SP3 in which the values of EPO genes were normalized first by GAPDH mRNA in the same sample before comparison. The products of PCR were analyzed by gel electrophoresis, and the analysis of melting curve was for confirmation of amplification.

MitoTracker Staining and Confocal Microscopy

Cardiomyoblasts were seeded in 6-well plates at a density of 4,000 cells/ml on a glass slide. The cell was treated with herbal extract for 24 h. Following the treatment, the treated cell was strained by MitoTracker FM red (Invitrogen) at concentration of 150 nM for 30 min. The MitoTracker FM red was removed and washed by PBS, three times. The 63× objective was used in a laser scanning confocal microscope (LSM7 DUO, Zeiss). Fluorescence intensity was measured by Zeiss software, and mitochondria parameters were measured by ImageJ (Dagda et al., 2009).

Transmission Electron Microscopy

H9C2 cells were seeded in 6-well plates at a density of 4,000 cells/ml on 100-mm culture dish. After the drug treatment, H9C2 cells were trypsinized and were fixed in 2.5% glutaraldehyde for 24 h. Then, the fixed cells were firmed by 1% osmium tetroxide. After, the cells were dehydrated and embedded in durcupan. The embedded samples were cut into 60 nm by using a diamond knife and mounted on Cu-grids. The images were viewed by transmission electron microscope (Philips CM100). The mitochondria parameters were measured by ImageJ.

Statistical Analysis

Tandem mass spectrometry data were processed using Agilent Mass Hunter workstation software version B.01.00. Principal component analysis (PCA) of the sample was conducted using SIMCA-P version 13.0 (Umetrics, Sweden). The mitochondrial bioenergetics profile was visualized on Wave Desktop 2.3.0. All data were expressed as mean ± standard error of the mean (SEM). Statistical tests were performed with Student's t-test and Dunnett's test (one-way analysis of variance with multiple comparisons, SPSS, version 13). Statistically, difference was classified as significant (*) where $p < 0.05$, more significant (**) where $p < 0.01$, and highly significant (***) where $p < 0.001$.

RESULTS

Phenolic Compounds in DBT

In chemical standardization of herbal extracts, an optimized LC-MS method was used to determine the amounts of major ingredients within DBT, e.g. astragaloside IV, calycosin, formononetin, ferulic acid, and Z-ligustilide, as reported (Zheng et al., 2012; **Supplementary Figure 1A**). The LC profiles of those chosen markers in herbal extracts were revealed (**Supplementary Figure 1B**); while the amounts of those chemical markers were calibrated (**Table 1** and **Supplementary Table 1**). A well-standardized herbal decoction is a must as to ensure the repeatability of all experiments. A PCA analysis of marker contents in DBT was conducted. Two ranking PCs, PC1 and PC2, described ~53.9% and ~43.1% of the total variability, respectively, and which accounted for ~96% of total variance. The score plot showed that DBT, ASR, AR, and ASR+AR (simply adding AR extract and ASR extract in 5:1 ratio) could be clarified into four distinct groups (**Supplementary Figure 1C**). The loading plots for PC1 versus PC2 indicated different role of each variable in the extracts (**Supplementary Figure 1D**).

TABLE 1 | Quantitative assessment of five chemicals in DBT, AR, and ASR extracts.

Marker chemical	DBT (ng/mL)[a]	AR (ng/mL)[b]	ASR (ng/mL)[c]
Calycosin	3,051.91 ± 16.36[d]	1,140.59 ± 0.12	–
Formononetin	764.54 ± 0.423	224.45 ± 10.84	–
Ferulic acid	267.46 ± 24.9	–	1,086.42 ± 40.86
Z-ligustilide	4.98 ± 0.43	–	34.19 ± 1.26
Astragal side IV	737.79 ± 5.73	475.24 ± 1.31	–

[a]*Amount of chemicals in 1 mg/ml of DBT, determined by LC-MS/MS.*
[b]*Amount of chemicals in 1 mg/ml AR extract, determined by LC-MS/MS.*
[c]*Amount of chemicals in 1 mg/ml ASR extract, determined by LC-MS/MS.*
[d]*Values are in mean ± SD, n = 3.*

Anti-Oxidative Effect of DBT

To conduct a comprehensive analysis of anti-oxidative effects of herbal extracts of DBT, AR, ASR, and ASR+AR, free radical scavenging activity and total phenolic compounds were examined. Gallic acid was used as a reference marker, and total phenolic content of each herbal extract was represented by an equivalent amount of gallic acid. As shown in **Figure 1A,** DBT contained significant higher content of phenolic compounds, i.e., equivalent to ~13 mg gallic acid/g of sample. The extracts of ASR, AR, and ASR+AR contained equivalent ~8.5, ~5, and ~7 mg gallic acid/g, respectively. Moreover, the free radical scavenging activity was determined here, and gallic acid served as a control showing a dose-dependent manner (**Figure 1B**). At the same time, DBT showed significant higher, at least ~2.5 folds, in DPPH scavenging activity, as compared to that of other herbal extracts (**Figure 1C**). Here, we proposed a correlation between free radical scavenging ability and amount of phenolic compounds in DBT might be closely related (**Figure 1A** and **C**). Thus, the anti-oxidative element within the herbal extract could be represented by total phenolic compounds.

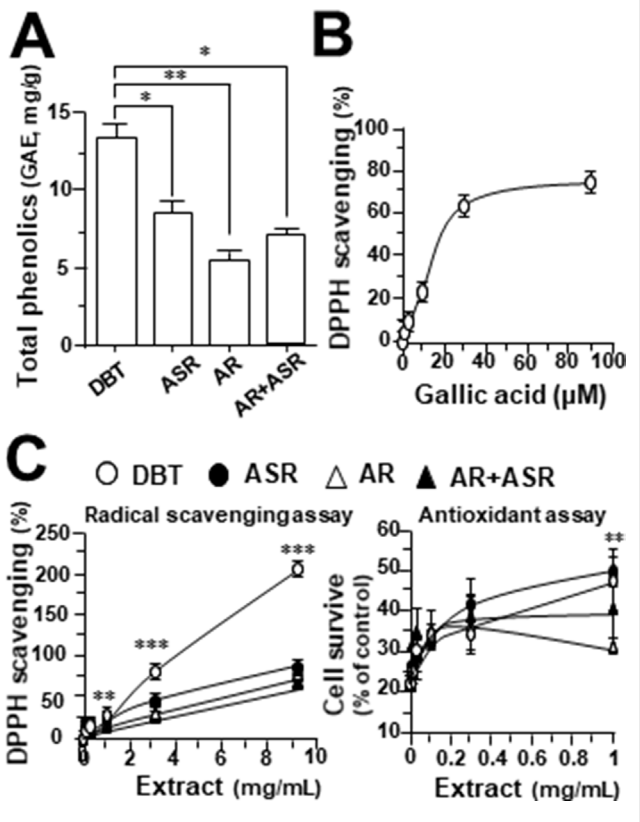

FIGURE 1 | (A) Total amount of phenolic compounds in herbal extracts was measured using Folin-Ciocalteu assay, corresponding to equivalent amount of gallic acid (i.e., GAE in mg/g). **(B)** Radical scavenging ability was detected by colorimetric reaction in gallic acid. **(C)** Protection effect of herbal extract to H9C2 cells against oxidative stress, i.e. DPPH scavenging (left) and cell protection against 400 μM tBHP (right). The values are in percentage of control (no treatment) in mean ± SD, $n = 4$. Statistical difference was made of the sample with the lowest value of corresponding content or indicated, $^{*}p < 0.05$, $^{**}p < 0.01$, and $^{***}p < 0.001$.

H9C2 cell, a commonly used cardiomyoblast, was employed here in testing the role of DBT. A stress inducer, tBHP, was chosen to damage cultured cardiomyocytes in a dose-dependent manner (**Supplementary Figure 2A**). A sub-maximal induction of cell death at ~400 μM was used for subsequent assay. The applied herbal extract by itself in cultures did not affect the cell viability (**Supplementary Figure 2B**). Application of herbal extracts of DBT, AR, ASR, and ASR+AR protected cardiomyocytes against oxidative insult in a dose-dependent manner (**Figure 1C**, right). Among the herbal extracts, DBT and ASR showed significant higher, at least ~1.5 folds, in protecting cell from damage, as compared to that of AR and ASR+AR extracts at 1 mg/mL (**Figure 1C**, right).

DBT Regulates Mitochondrial Bioenergetics

By using Seahorse XFp extracellular flux analyzer, various parameters of mitochondrial bioenergetics during myocardium energy metabolism could be measured **(Supplementary Figure 3A**). Firstly, seeding cell density and FCCP concentration were optimized for the measurement of cellular metabolic functions. As shown in **Supplementary Figure 3B**, the optimal cell density of H9C2 cells was set at 5,000 cells/well, as to adjust an initial OCR to appropriate range (100–160 pmol/min) for further analysis. Meanwhile, the concentration of FCCP was optimized to 3 μM yielding maximal OCR (**Supplementary Figure 3B**). The concentration of oligomycin (1 μM) and rotenone/antimycin A (1 μM) were optimized according to the manufacturer's instruction. The effects of increasing concentration of herbal

extracts on OCR of cultured H9C2 cells were plotted against time. All extracts could dose-dependently increase basal respiration, proton leak, ATP production, and non-mitochondrial respiration to different degree (**Figure 2**). In mitochondrial bioenergetics, the effects of DBT, as well as other herbal extracts, to the parameters of maximum respiration and SRC were rather different. By analyzing the results of mitochondrial bioenergetics, all herbal extracts could regulate OCR reading in dose-dependent manners (**Figure 3**). DBT in many cases showed the best induction in basal respiration, proton leak, ATP production, and non-mitochondria respiration (**Figure 3**). The non-mitochondria respiration was the most sensitive parameter in responding to DBT challenge, i.e., ~10-fold induction at high dose of DBT. In addition, the responsive dose of cultured cardiomyoblasts to herbal extracts was rather sensitive. In many cases, a low dose of herbal extract could achieve a maximal response (**Figure 3**).

The mitochondrial bioenergetics was carried out in tBHP-treated cardiomyoblasts under the treatments of herbal extracts (**Figure 4**). Similar to the control cell, the herbal extracts increased, dose-dependently, basal respiration, proton leak, ATP production, and non-mitochondrial respiration to different degree. The robust inductive effects in OCR reading after the treatment of DBT could be revealed in basal respiration, ATP production and non-mitochondrial respiration: these outcomes were very similar to that in normal cultured cardiomyoblasts (**Figure 5**). These results showed that the effects of DBT could be revealed in normal or stressed cell cultures. Again, all extracts showed a robust response in a low dose treatment (**Figure 5**).

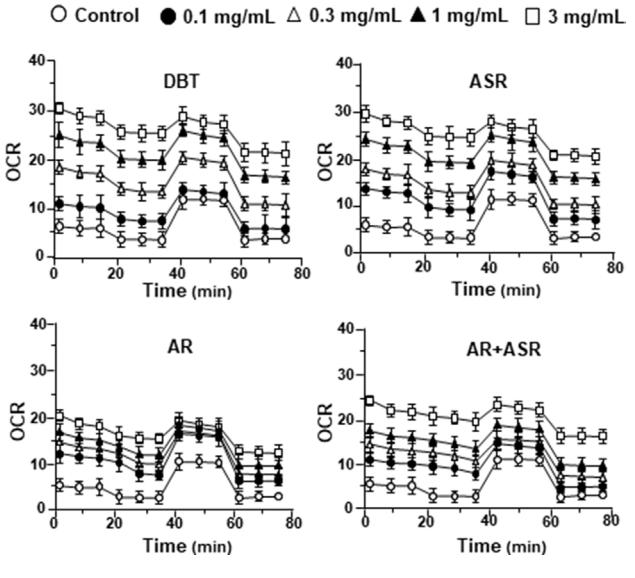

FIGURE 2 | The extracts of DBT, ASR, AR, and ASR+AR modulate mitochondrial bioenergetics of H9C2 cells. Cultured H9C2 cells were treated with herbal extracts, as indicated, for 24 h before measuring oxygen consumption rate (OCR in pmol/min/mg of protein) with XFp Cell Mito Stress Test. The response of H9C2 cells after oligomycin (1 μM), FCCP (3 μM), and rotenone/antimycin A (1 μM) applied to the wells were recorded. Blank is the naive cell. Data are expressed in mean ± SD, *n* = 3, each with triplicate samples.

To further investigate the bioenergetic roles of major ingredients in DBT, the mitochondrial bioenergetics was carried out in tBHP-treated cardiomyoblasts under the treatments of calycosin, formononetin, ferulic acid, Z-ligustilide, and astragaloside IV (**Figure S1A**). The robust inductive effects in OCR reading, after the treatment of astragaloside IV, could be revealed in basal respiration, ATP production, and SRC, but not for other DBT ingredients **(Figure 6).** Moreover, Z-ligustilide was able to induce proton leakage significantly (**Figure 6**).

DBT Stabilizes Mitochondrial Membrane Potential

To investigate mitochondrial membrane potential being regulated by DBT, the changes in the membrane potential were monitored by real-time photo-luminescent. The incubation of H9C2 cells with DBT induced an increase of mitochondrial membrane potential in a time-dependent manner. During initial time period (5–20 min), the membrane potential was induced by DBT application, and thereafter which was stabilized (**Figure 7A**). In contrast, a gradual decrease in mitochondrial membrane potential was observed after incubation with the extracts of AR, ASR, and AR + ASR. Furthermore, the effects of different herbal extracts on membrane potential in tBHP-treated H9C2 cells were tested. Interestingly, DBT applied in H9C2 cells caused a time-dependent manner increase of mitochondrial membrane potential during initial period (5–20 min): the maximum of stimulation being increased at 20 min after the herbal treatment (**Figure 7B**). However, the treatment of H9C2 with the extracts of ASR and AR caused a time-dependent stability in mitochondrial membrane potential. FCCP, a chemical uncoupler of mitochondria, served as a control to induce a gradual decrease in mitochondrial membrane potential in both types of cultures.

DBT Upregulates Mitochondrial Gene Expressions

To determine the molecular mechanism responsible for enhanced mitochondrial content by DBT treatment, the expression levels of mitochondrial biogenesis related gene (PGC-1α, NRF1, TFAM) and mitochondrial DNA replication related gene (PLOG, TOP1MT, TWINKLE) were determined by quantitative real-time PCR. The treatments with DBT and AR extracts for 24 h caused a significant increase of PGC-1α mRNA to ~3 folds (**Figure 8**). The PGC-1α mRNA induction was much less in cases of ASR and AR + ASR. In parallel, NRF1, a downstream target of PGC-1α, was also increased by ~3 folds in DBT- and AR-treated cardiomyocytes. TFAM, a downstream effector of NRF1 and a regulator of mitochondrial DNA expression, showed a significant change of expression under DBT and ASR treatments (**Figure 8**). The mitochondrial DNA replication related genes, i.e. PLOG, TOP1MT, and TWINKLE, were measured here. DBT, as well as other herbal extracts, induced the expressions of these transcripts by two to eight folds (**Figure 8**).

DBT Alters Mitochondrial Morphology

MitoTracker staining and confocal microscopy were used to examine the oxidative status of mitochondria (**Figure 9A**). In

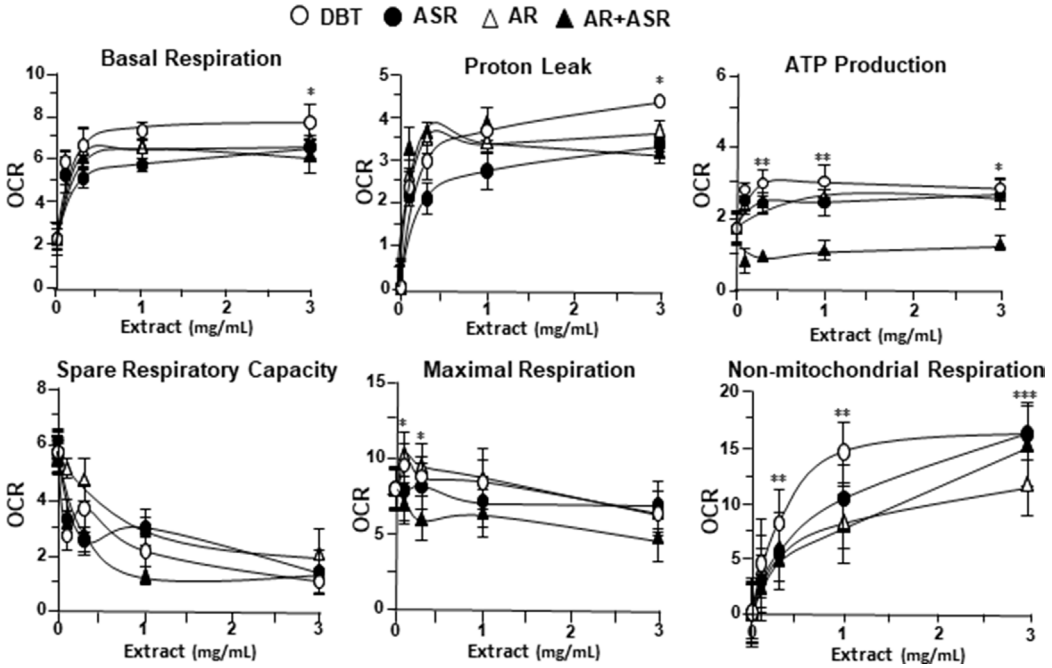

FIGURE 3 | The parameters of mitochondrial respiration in DBT, ASR, AR, and ASR+AR applied H9C2 cells. Cultured H9C2 cells were treated with herbal extracts as that in **Figure 2**. The effects of different extracts to basal respiration, proton leak, ATP production, spare respiratory capacity, maximal respiration, and non-mitochondrial respiration were measured and compared. The OCR value in pmol/min/mg of protein was shown. Data are expressed as mean ± SD, $n = 3$, each with triplicate samples. Statistical comparison was made of the sample with the lowest value of corresponding concentration, $^{*}p < 0.05$, $^{**}p < 0.01$, and $^{***}p < 0.001$.

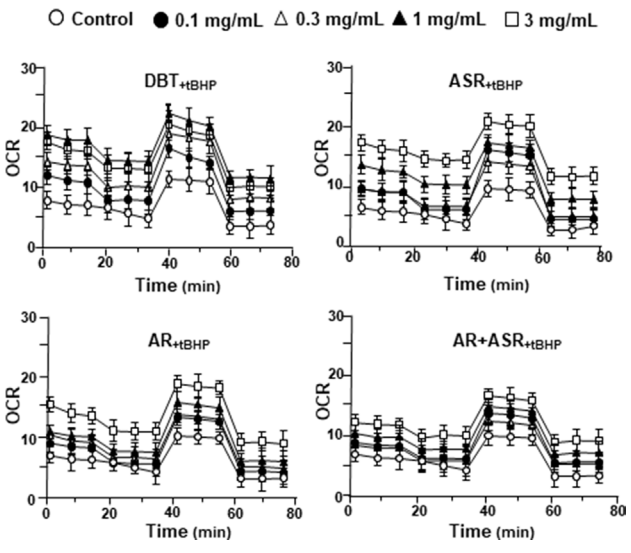

FIGURE 4 | The extracts of DBT, ASR, AR, and ASR+AR modulate mitochondrial bioenergetics of H9C2 cells under oxidative stress. Cultured H9C2 cells were treated with herbal extracts for 24 h. Then, the treated cells were exposed to 30 μM tBHP for 3 h before measuring oxygen consumption rate with XFp Cell Mito Stress Test, as in **Figure 2**. The OCR value in pmol/min/mg of protein was shown. Blank is the naive cell. Data are expressed as mean ± SD, $n = 3$, each with triplicate samples.

DBT-treated cardiomyocytes, the MitoTracker staining was markedly increased by ~160%, as compared to the control (**Figure 9B**). In addition, the mitochondria morphology of DBT-treated cells was changed, which included the average values of perimeter, circularity, and minor axis (**Figure 9B**). In addition, the mitochondria ultrastructure was revealed under a transmitted electron microscopy (**Figure 10A**). The mitochondria ultrastructure DBT-treated cardiomyocytes were found to have a decrease of circularity (**Figure 10B**). In contrast, the average length and area of mitochondria did not alter.

DISCUSSION

Mitochondria have crucial roles in cardiomyocytes' dynamic, survival, and maintenance of cardiac functions in daily life (Gottlieb and Gustafsson, 2011). Mature cardiomyocytes possess a large number of mitochondria occupying at least 30% of total cell volume (Piquereau et al., 2013). The close relationship between mitochondrial biogenesis and cardiac function was supported by the observation of heart failure under mitochondrial dysfunction (Pisano et al., 2015). We have previously reported the protective effects of DBT in cardiomyocyte's energy metabolism in mice having acute myocardial infarction or cardiac ischemia-reperfusion injury: this protective effect was triggered by mitochondrial enhancement

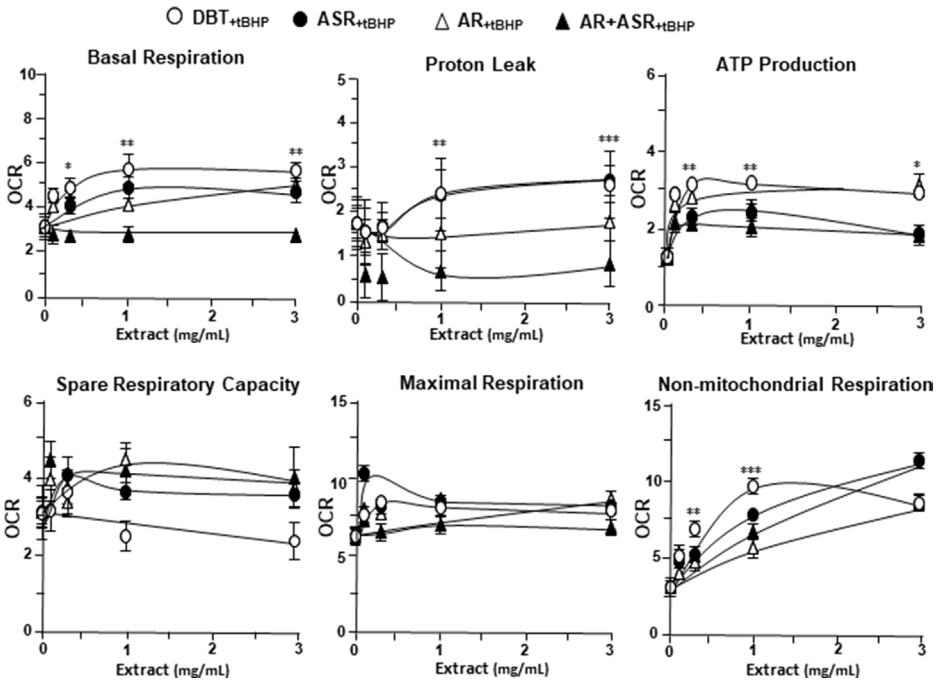

FIGURE 5 | The parameters of mitochondrial respiration in DBT, ASR, AR, and ASR+AR applied tBHP-treated H9C2 cells. Cultured H9C2 cells were treated as that in **Figure 4**. The effects of increasing concentration of herbal extracts to basal respiration, proton leak, ATP production, spare respiratory capacity, maximal respiration, and non-mitochondrial respiration was measured and compared. The OCR value in pmol/min/mg of protein was shown. Data are expressed as mean ± SD, $n = 3$, each with triplicate samples. Statistical comparison was made of the sample with the lowest value of corresponding concentration, $^{*}p < 0.05$, $^{**}p < 0.01$, and $^{***}p < 0.001$.

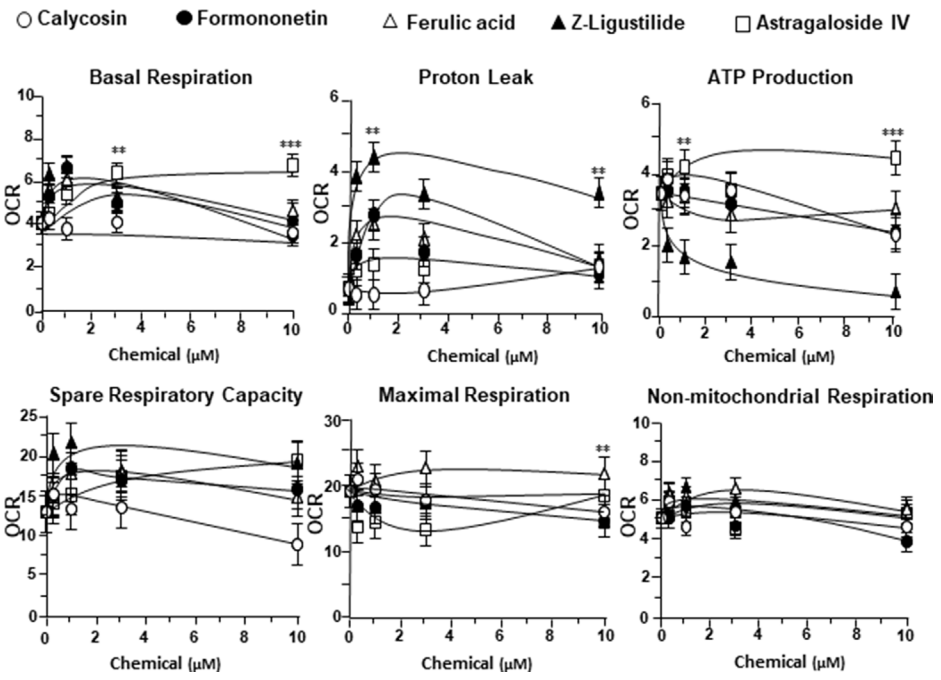

FIGURE 6 | The parameters of mitochondrial respiration in tBHP-treated H9C2 cells in the present of major chemicals from DBT. The effects of increasing concentration of different extracts to basal respiration, proton leak, ATP production, spare respiratory capacity, maximal respiration, and non-mitochondrial respiration were measured and compared. The OCR value in pmol/min/mg of protein was shown. Data are expressed as mean ± SD, $n = 3$, each with triplicate samples. Statistical comparison was made with the sample with the lowest value of corresponding concentration, $^{*}p < 0.05$, $^{**}p < 0.01$, and $^{***}p < 0.001$.

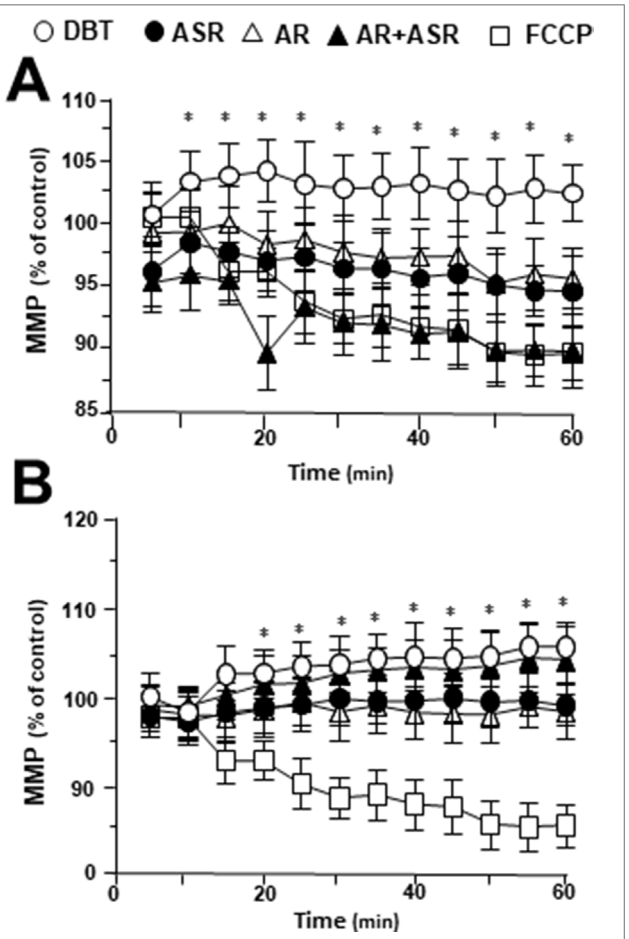

FIGURE 7 | Regulation of mitochondrial membrane potential in H9C2 cells treated with herbal extracts. In a 96-well black multi-well plates with a clear bottom, H9C2 cells were stained with JC-1 and then washed with 2× PBS. The fluorescence of JC-1 aggregates in different treatments was measured. FCCP (100 μM) was used as a negative control. **(A)** Time course of herbal extract-induced changes in mitochondrial membrane potential in H9C2 cells. **(B)** Time course of herbal extract-induced changes in mitochondrial membrane potential in H9C2 cells after treated with 400 μM tBHP. All herbal extract was at 0.1 mg/ml. Data are expressed as the percentage of fluorescence intensity of JC-1 aggregate to value of control (no treatment). Values are in mean ± SD, with $n = 3$. Statistical comparison was made with the sample with control, $^{*}p < 0.1$, $^{**}p < 0.01$, and $^{***}p < 0.001$.

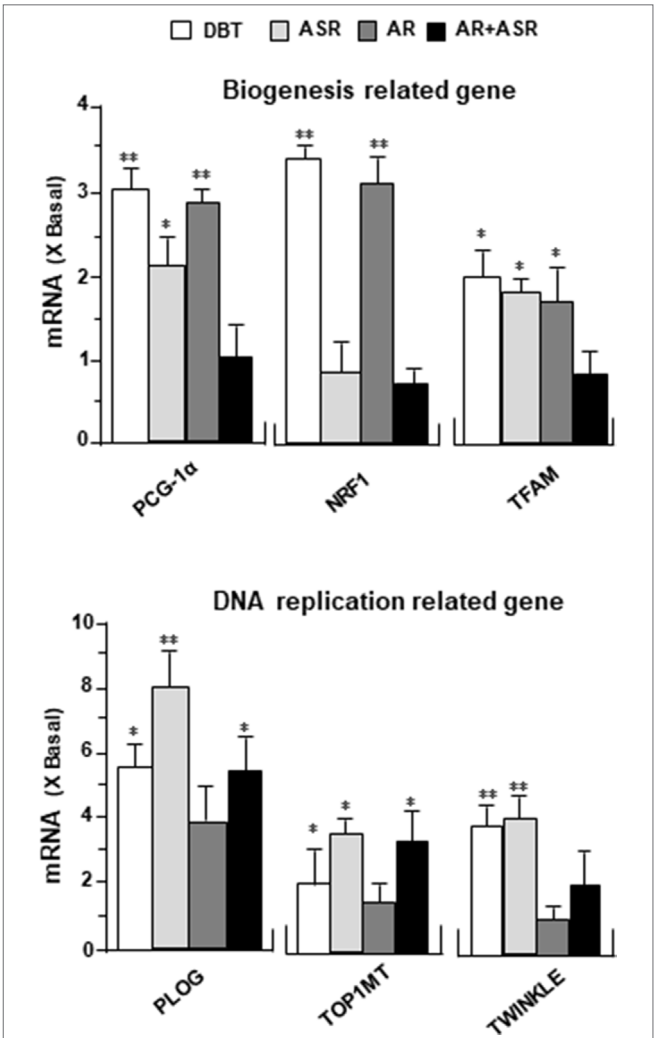

FIGURE 8 | DBT regulates mitochondrial biogenesis-related genes. The expression levels of (upper panel) mitochondrial biogenesis related gene (PGC-1α, NRF1, TFAM) and (lower panel) mitochondrial DNA replication related gene (PLOG, TOP1MT, TWINKLE) were quantified by RT-PCR, following treatment of H9C2 cells with DBT, ASR, AR, and ASR+AR at 0.1 mg/ml for 24 h. Data are expressed as the ratio to the background (no treatment). Values are in mean ± SD, with $n = 3$. Statistical comparison was made of the sample with the background, $^{*}p < 0.1$, $^{**}p < 0.01$, and $^{***}p < 0.001$.

as well as glutathione status in red blood cell (Mak et al., 2006). DBT is a Chinese herbal mixture being prescript for "qi-invigorating" action, and which is aiming to improve the "Yin-Yang balance" of an individual. The quantification of five major chemical ingredients, i.e., calycosin, astragaloside IV, formononetin, Z-ligustilide, and ferulic acid, in extracts of ASR, AR, and DBT were measured by using LC-MS. The result showed that DBT contained higher amount of these ingredients in decoction as compared to that of AR alone, ASR alone, or just AR+ASR (just mixing the extracts of AR and ASR together with boiling separately), and this result was in line to previous report (Zheng et al., 2014). The stability and solubility of bioactive ingredients in DBT could be increased after boiling of AR and ASR together in 5 to 1 ratio, in contrast to different herb ratios (Gao et al., 2016). On the other hand, the amount of bio-suppressive chemical (Z-ligustilide) was markedly reduced after boiling of two herbs together (Zheng et al., 2014). Based on the difference in contents of these compounds, the herbal extracts could be distinguished by an analysis of PCA, and the clustering of herbal extracts in PCA scoring plot was highly consistent with the chemical markers in loading plot. These results revealed that the chemical composition might be differed significantly in DBT, ASR, AR, and ASR+AR.

Due to flexibility and efficiency, Folin-Ciocalteu and DPPH radical scavenging assays were chosen here for chemical

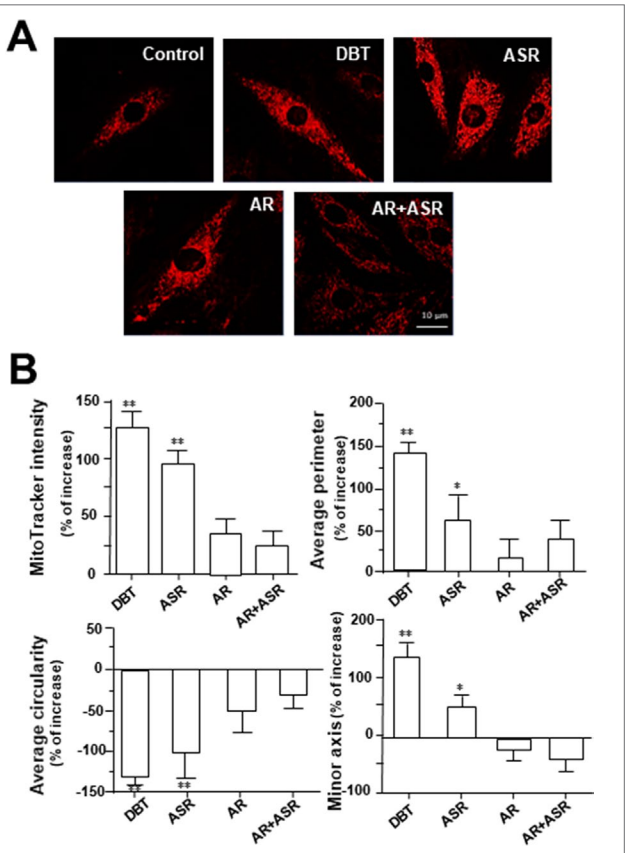

FIGURE 9 | DBT increases mitochondrial morphology in cultured cardiomyocyte. **(A)** H9C2 cells were stained with MitoTracker Red FM and then analyzed for fluorescence intensity using confocal microscope. The cultures were treated with herbal extracts at 0.1 mg/ml for 24 h. Representing photo was shown. **(B)** Quantitative analysis from **(A)** out of 10 randomly selected images taken under 63× objective after treatment with DBT, ASR, AR, and AR+ASR. Data are expressed as the percentage of change to background (no treatment), in mean ± SD, with $n = 4$. Statistical comparison was made of the sample with control, $^{*}p < 0.1$, $^{**}p < 0.01$, and $^{***}p < 0.001$.

assessment of total antioxidant activities of herbal extracts (Kedare and Singh, 2011; Margraf et al., 2015). Here, the radical scavenging ability was represented relatively by total phenolic compounds. DBT had higher radical scavenging ability than that from the extracts deriving from single herb or ASR+AR mixture. In line with previous studies, DBT showed higher protection effects to oxidatively stressed cells, which therefore might be due to an inhibition of tBHP-induced ROS in the present of herbal extract (Gong et al., 2016b). In accordance to this notion, ferulic acid, derived from ASR, was demonstrated to be a key ingredient in orchestrating the anti-oxidative properties of DBT by reducing the formation of free radicals (Gong et al., 2016b).

Mitochondrial function plays roles in a variety of cellular process and metabolism. The assessment of bioenergetic properties in isolated mitochondria was done in past few years (Chowański et al., 2017). However, the damage of mitochondria during such isolation process happens very often, and additionally this isolation requires large amounts of starting materials (Lanza and Nair, 2009). To better understand the effect of DBT in mitochondrial metabolic flux change. The oxidative status of herbal extract-treated H9C2 cells was measured by an analyzer in monitoring real-time extracellular flux and mitochondria respiration in a live cell, which therefore could offer a more dynamic window for drug examination.

After DBT treatment in cultured H9C2 cells, an increase of basal respiration and ATP production was revealed. Astragaloside IV was identified to be a major active compound in inducing basal respiration and ATP production. Basal respiration is oxidative phosphorylation in responding to ATP demand; while ATP production is reflecting to cellular energy status, which can improve the energy metabolism in cultured cardiomyoblasts (Brand and Nicholls, 2011). On the other hand, the proton leak, a sign of mitochondrial uncoupling, was induced by DBT in our assay. Among different DBT ingredients, Z-ligustilide is a major inducer in proton leak. An increase of the proton leak is reported to reduce the generation of ROS (Dott et al., 2014) and to show the cytoprotective effect in ischemic injury models (Brookes, 2005). Indeed, the mitochondrial uncoupling has been proposed to have favorable effects in diseases having association with oxidative stress, e.g., ischemic-reperfusion injury, Parkinson's disease, insulin resistance, aging, heart failure, ischemic-reperfusion injury, and obesity (Busiello et al., 2015). The non-mitochondria respiration, induced by DBT in the cultures, was having a dose-dependent increase; however, the induction was insignificant for DBT major chemicals. Thus, possible unidentified ingredients, e.g., polysaccharide, should be considered in triggering this non-mitochondria respiration. Besides the aforementioned bioenergetics parameters, we have shown the DBT-induced transcriptional expression of heme oxygenases *via* triggering hypoxia inducible factors (HIFs) (Dunn et al., 2014). Indeed, the effect of DBT on HIF pathway has been shown in previous report (Zheng et al., 2011). The protective effect of DBT under oxidative stress is in line to induction of heme oxygenases, because these enzymes are well known in affecting oxidation, differentiation, and apoptosis (Ayer et al., 2016). The detail mechanism therefore needs to further investigation.

In accounting the ATP production from oxidative phosphorylation, we have shown an increase of mitochondria membrane potential during DBT treatment. In our previous studies, astragaloside IV and calycosin are proposed to be active compounds in enhancing the stability of mitochondria membrane potential (Huang et al., 2018). Stability of mitochondria membrane potential is an important parameter in maintaining the mitochondrial function (Brand and Nicholls, 2011).

The energy lost in dissipating proton gradient *via* uncoupling protein (UCP) is the cause of heat generation, and therefore UCP is linking to thermogenesis (Dulloo and Samec, 2001). PGC-1α, a co-activator of PPARγ, serves as an inducible booster in mitochondrial biogenesis (Wenz, 2013). Here, PGC-1α, as well as its down stream effectors including NRF1, TFAM, and other related genes involved in NRF family, was found to be upregulated in DBT-treated cardiomyocytes. PGC-1α is strongly related with fatty acid oxidation, glucose utilization, antioxidant detoxication, angiogenesis, mtDNA

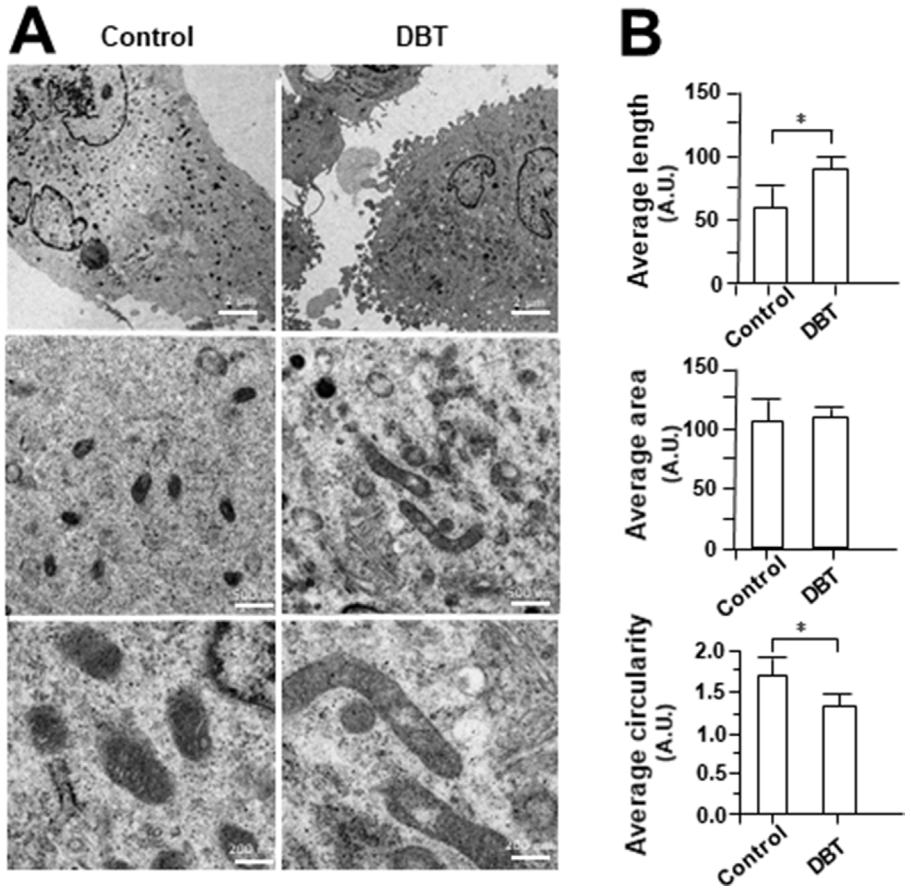

FIGURE 10 | Electron microscope of DBT-treated H9C2 cells. **(A)** Mitochondrial ultrastructure was visualized by transmission electron microscope after H9C2 were treated with DBT (0.1 mg/ml) for 24 h. **(B)** Quantitative analysis from **(A)**, and data are expressed as arbitrary unit (AU), in mean ± SD, with $n = 3$. Statistical comparison was made of the sample with control, $^*p < 0.1$.

transcription, and replication (Liang and Ward, 2006). Furthermore, the transcriptional level of mtDNA polymerase genes (PLOG,TOP1MT, and TWINKLE) were also upregulated after DBT treatment. Report has been shown the important of mtDNA in aging process (Copeland, 2010).

The decrease of circularity and increasing of perimeter and minor axis of mitochondria could be reflected to cell having less oxidative stress (Sripathi et al., 2018). These mitochondria morphological parameters in cardiomyocytes could be altered by DBT treatment. In line to this result, astragaloside IV has been shown to improve mitochondrial ultrastructure of angiotensin II-induced dysfunction in vascular smooth muscle cells (Lu et al., 2015). In addition, ferulic acid applying together with ascorbic acid could restore the catecholamine-induced cardiotoxicity in rats (Yogeeta et al., 2006). Ligustilide, another key chemical in DBT, restored the memory deficiency in APP/PS1 transgenic mice by increasing the mitochondrial length (Xu et al., 2018). Therefore, we speculated that DBT treatment in cultured cardiomyoblast might promote mitochondrial biogenesis.

In summary, this study provided a comprehensive analysis of DBT effects on mitochondrial bioenergetics, as well as to explain the difference of tonic effect between single herbs and formulation of DBT. In our future work, the molecular docking has to be done in revealing the possible interaction of various molecular protein targets with DBT major ingredients: because the direct targets in mitochondria being activated by DBT are not known.

AUTHOR CONTRIBUTIONS

KT and KK conceived and designed the experiments. KK, YH, and LW performed experiments, analyzed the results, and made the figures and tables. YH and TD contributed to the scientific discussions. KT and KK wrote the paper.

FUNDING

This study was supported by Hong Kong RGC Theme-based Research Scheme (T13-607/12R), Innovation and Technology Commission Innovation Technology Fund (UIM/288, UIM/302,

UIM/340, UIT/137, ITS/022/16FP; ITCPD/17-9), TUYF15SC01, Shenzhen Science and Technology Committee Research Grant (CKFW2016082916015476; ZDSYS201707281432317; JCYJ20170413173747440; JCYJ20160229205812004; JCYJ20160229210027564), and Guangzhou Science and Technology Committee Research Grant (GZSTI16SC02; GZSTI17SC02).

SUPPLEMENTARY MATERIAL

The Supplementary Material for this article can be found online at: https://www.frontiersin.org/articles/10.3389/fphar.2019.00614/full#supplementary-material

FIGURE S1 | PCA of chemical markers in different AR extracts. **(A)** Chemical Structure of calycosin, formononetin, ferulic acid, Z-ligustilide and astragaloside IV. **(B)** Identification of ferulic acid (1), calycosin (2), astragaloside IV (3), Z-ligustilide (4) and formononetin (5) was made by an MS detector. Representative chromatograms of standard markers (Standards), DBT, ASR and AR under MRM mode were shown. **(C)** The scoring plot of different extracts was presented by comparing the contents of chosen standards. PC1 and PC2 described ~80.2% and ~17.5% of the total variability, respectively. **(D)** The loading plot of PC1 versus PC2 for four markers was shown, *n* = 3.

FIGURE S2 | (A) Optimization of tBHP dose in MTT assay. Cultured H9C2 cells (1 x 104 cells/well) were exposed to tBHP at various concentrations. The cell viability was determined by MTT assay after treated for 3 hours, and the level of intracellular ROS was measured by fluorescent staining after 1 hour. Cell viability was expressed as % of control (cells without tBHP). tBHP at 400 μM was used for routine analysis. **(B)** The effects of DBT, ASR, AR and ASR+AR extracts and main ingredients for cell viability in H9C2 cells. Cultured H9C2 cells were treated with different extracts (0-3 mg/mL) for 24 hours. Cell viability was determined by MTT assay. Data are expressed as Mean ± SD, *n* = 3, each with triplicate samples.

FIGURE S3 | (A) Schematic diagram of metabolic parameters of mitochondrial respiration measured by Seahorse Bioscience XFp extracellular flux analyzer. Basal respiration represents energetic demand of the cell under baseline conditions. Proton leak shows the remaining basal respiration and is the difference in OCR after oligomycin and rotenone/antimycin A (R&A) injection. ATP production is the difference between basal respiration and proton leak and represents the portion of basal respiration that is being used to drive ATP production. Maximal respiration shows the maximum rate of respiration that the cell can achieve, which is calculated as the OCR after FCCP injection. Spare respiratory capacity is the difference between maximal and basal OCR and can be an indicator of cell fitness or flexibility. The non-mitochondrial rate was subtracted from all other rates, which is a result of a subset of cellular enzymes that continue to consume oxygen after rotenone/antimycin A addition. **(B)** Optimization of cell density, FCCP and tBHP dosage in XFp Mito Stress Test. **(Left)** Cultured H9C2 cells with increasing cell density were seeded in XFp Cell Culture Miniplate and cultured for 48 hours before basal OCR was measured. **(Center)** H9C2 cells (5,000 cells/well) were cultured for 48 hours, then treated with 1 μM oligomycin and three serial injections of FCCP at different concentrations (a high concentration range of 3, 6, 12 μM and a low concentration range of 0.75, 1.5, 3 μM). The resulting data set characterizes the cells' response to 6 doses of FCCP. **(Right)** Cultured H9C2 cells (5,000 cells/well) were exposed to tBHP at various concentrations for 24 hours, and OCR was determined. The above-mentioned OCR values were normalized with the cellular protein. Data are expressed as mean ± SD, *n* = 3, each with triplicate samples.

TABLE S1 | Mass spectra properties of marker chemicals in DBT, ASR and AR extracts.

REFERENCES

Ayer, A., Zarjou, A., Agarwal, A., and Stocker, R. (2016). Heme oxygenases in cardiovascular health and disease. *Physiol. Rev.* 96 (4), 1449–1508. doi: 10.1152/physrev.00003.2016

Brand, M. D. (2005). The efficiency and plasticity of mitochondrial energy transduction. *Biochem. Soc. Trans.* 33 (Pt 5), 897–904. doi: 10.1042/BST20050897

Brand, M. D., and Nicholls, D. G. (2011). Assessing mitochondrial dysfunction in cells. *Biochem. J.* 435 (Pt 2), 297–312. doi: 10.1042/BJ20110162

Brookes, P. S. (2005). Mitochondrial H(+) leak and ROS generation: an odd couple. *Free Radic. Biol. Med.* 38 (1), 12–23. doi: 10.1016/j.freeradbiomed.2004.10.016

Busiello, R. A., Savarese, S., and Lombardi, A. (2015). Mitochondrial uncoupling proteins and energy metabolism. *Front. Physiol.* 6, 36. doi: 10.3389/fphys.2015.00036

Chen, C., Zu, Y., Fu, Y., Luo, M., Zhao, B., Zhao, C., et al. (2011). Preparation and antioxidant activity of Radix Astragali residues extracts rich in calycosin and formononetin. *Biochem. Eng. J.* 56, 84–93. doi: 10.1016/j.bej.2011.04.015

Choi, R., Gao, Q., Cheung, A., Zhu, J., Lau, F., Li, J., (2011). A Chinese herbal decoction, Danggui Buxue Tang, stimulates proliferation, differentiation and gene expression of cultured osteosarcoma cells: genomic approach to reveal specific gene activation. *Evid. Based Complement Alternat. Med.* 2011, 307548–307513. doi: 10.1093/ecam/nen085

Chowański, S., Lubawy, J., Paluch-Lubawa, E., Spochacz, M., Rosiński, G., and Słocińska, M. (2017). The physiological role of fat body and muscle tissues in response to cold stress in the tropical cockroach *Gromphadorhina coquereliana*. *PLoS One* 12, e0173100. doi: 10.1371/journal.pone.0173100

Copeland, W. C. (2010). The mitochondrial DNA polymerase in health and disease. *Subcell. Biochem.* 50, 211–222. doi: 10.1007/978-90-481-3471-7_11

Dagda, R. K., Cherra, S. J., Kulich, S. M., Tandon, A., Park, D., and Chu, C. T. (2009). Loss of PINK1 function promotes mitophagy through effects on oxidative stress and mitochondrial fission. *J. Biol. Chem.* 284 (20), 13843–13855. doi: 10.1074/jbc.M808515200

Dott, W., Mistry, P., Wright, J., Cain, K., and Herbert, K. E. (2014). Modulation of mitochondrial bioenergetics in a skeletal muscle cell line model of mitochondrial toxicity. *Redox Biol.* 2, 224–233. doi: 10.1016/j.redox.2013.12.028

Dranka, B. P., Hill, B. G., and Darley-Usmar, V. M. (2010). Mitochondrial reserve capacity in endothelial cells: the impact of nitric oxide and reactive oxygen species. *Free Radic. Biol. Med.* 48 (7), 905–14. doi: 10.1016/j.freeradbiomed.2010.01.015

Dulloo, A. G., and Samec, S. (2001). Uncoupling proteins: their roles in adaptive thermogenesis and substrate metabolism reconsidered. *Br. J. Nutr.* 86, 123–139. doi: 10.1079/BJN2001412

Dunn, L. L., Midwinter, R. G., Ni, J., Hamid, H. A., Parish, C. R., and Stocker, R. (2014). New insights into intracellular locations and functions of heme oxygenase-1. *Antioxid. Redox. Signal.* 20, 1723–1742. doi: 10.1089/ars.2013.5675

Friedman, J. R., and Nunnari, J. (2014). Mitochondrial form and function. *Nature* 505, 335–343. doi: 10.1038/nature12985

Gao, Q. T., Cheung, J. K., Li, J., Chu, G. K., Duan, R., Cheung, A. W., et al. (2016). A Chinese herbal decoction, Danggui Buxue Tang, prepared from Radix Astragali and Radix Angelicae Sinensis stimulates the immune responses. *Planta Med.* 13, 1227–1231. doi: 10.1055/s-2006-947186

Gong, A., Lau, K., Zhang, L., Lin, H., Dong, T., and Tsim, K. (2016a). *Danggui Buxue Tang*, Chinese herbal decoction containing Astragali Radix and Angelicae Sinensis Radix, induces production of nitric oxide in endothelial cells: signaling mediated by phosphorylation of endothelial nitric oxide synthase. *Planta Med.* 82, 418–423. doi: 10.1055/s-0035-1558332

Gong, G. W., Huang, V. Y., Wang, H. Y., Lin, Q. Y., Dong, T. T. X., and Tsim, K. W. K. (2016b). Ferulic acid orchestrates anti-oxidative properties of Danggui Buxue Tang, an ancient herbal decoction: elucidation by chemical knock-out approach. *PLoS One* 11, 11. doi: 10.1371/journal.pone.0165486

Gottlieb, R. A., and Gustafsson, Å. B. (2011). Mitochondrial turnover in the heart. *Biochim. Biophys. Acta.* 18, 1295–1301. doi: 10.1016/j.bbamcr.2010.11.017

Huang, Y., Kwan, K, Leng, K., Wang, H., Kong, X., Dong, T., and Tsim, K. (2018). The extracts and major compounds derived from Astragali Radix after mitochondrial biogenetics in cultured cardiomyocytes: Companion of various

polar solvents and compounds. *Int. J. Mol. Sci.* 19 (6), 1574. doi: 10.3390/ijms19061574

Kedare, S., and Singh, R. (2011). Genesis and development of DPPH method of antioxidant assay. *J. Food Sci. Technol.* 48, 412–422. doi: 10.1007/s13197-011-0251-1

Kikuzaki, H., Hisamoto, M., Hirose, K., Akiyama, K., and Taniguchi, H. (2002). Antioxidant properties of ferulic acid and its related compounds. *J. Agric. Food Chem.* 50, 2161–2168. doi: 10.1021/jf011348w

Liang, H., and Ward, W. F. (2006). PGC-1α: a key regulator of energy metabolism. *Adv. Physiol. Educ.* 30, 145–151. doi: 10.1152/advan.00052.2006

Lanza, I. R., and Nair, K. S. (2009). Functional assessment of isolated mitochondria *in vitro*. *Methods Enzymol.* 457, 349–372. doi: 10.1016/S0076-6879(09)05020-4

Lin, H. Q., Gong, A. G. W., Wang, H. Y., Duan, R., Dong, T. T. X., Zhao, K. J., et al. (2017). *Danggui Buxue Tang* (Astragali Radix and Angelicae Sinensis Radix) for menopausal symptoms: a review. *J. Ethnopharmacol.* 199, 205–210. doi: 10.1016/j.jep.2017.01.044

Lu, I. W., and Lu, D. P. (2014). Impact of Chinese herbal medicine on American society and health care system: perspective and concern. *Evid. Based Complement Alternat. Med.* 2014, 251891–251896. doi: 10.1155/2014/251891

Lu, Y., Li, S., Wu, H., Bian, Z., Xu, J., and Gu, C. (2015). Beneficial effects of astragaloside IV against angiotensin II-induced mitochondrial dysfunction in rat vascular smooth muscle cells. *Int. J. Mol. Med.* 36 (5), 1223–1232. doi: 10.3892/ijmm.2015.2345

Mak, D. H. F., Chiu, P. Y., Dong, T. T. X., Tsim, K. W. K., and Ko, K. M. (2006). Dang-Gui Buxue Tang produces a more potent cardioprotective effect than its component herb extracts and enhances glutathione status in rat heart mitochondria and erythrocytes. *Phytother. Res.* 20, 561–567. doi: 10.1002/ptr.1904

Margraf, T., Karnopp, A. R., Rosso, N. D., and Granato, D. (2015). Comparison between Folin-Ciocalteu and Prussian blue assays to estimate the total phenolic content of juices and teas using 96-Well microplates. *J. Food. Sci.* 80, C2397–C2403. doi: 10.1111/1750-3841.13077

Owen, L., and Sunram-Lea, S. I. (2011). Metabolic agents that enhance ATP can improve cognitive functioning: a review of the evidence for glucose, oxygen, pyruvate, creatine, and i-carnitine. *Nutrients* 3, 735–755. doi: 10.3390/nu3080735

Piquereau, J., Caffin, F., Novotova, M., Lemaire, C., Veksler, V., Garnier, A., et al. (2013). Mitochondrial dynamics in the adult cardiomyocytes: which roles for a highly specialized cell? *Front. Physiol.* 4, 102. doi: 10.3389/fphys.2013.00102

Pisano, A., Cerbelli, B., Perli, E., Pelullo, M., Bargelli, V., and Preziuso, C. (2015). Impaired mitochondrial biogenesis is a common feature to myocardial hypertrophy and end-stage ischemic heart failure. *Cardiovasc. Pathol.* 25, 103–112. doi: 10.1016/j.carpath.2015.09.009

Qiao, Y., Fan, C., and Tang, M. (2017). Astragaloside IV protects rat retinal capillary endothelial cells against high glucose-induced oxidative injury. *Drug Des. Devel. Ther.* 11, 3567–3577. doi: 10.2147/DDDT.S152489

Sivitz, W. I., and Yorek, M. A. (2010). Mitochondrial dysfunction in diabetes: from molecular mechanisms to functional significance and therapeutic opportunities. *Antioxid. Redox. Signal* 12, 537–577. doi: 10.1089/ars.2009.2531

Sripathi, S. R., He, W., Offor, J., Gutsaeva, D. R., and Jahng, W. J. (2018). Mitochondrial trafficking by prohibitin-kinesin-myosin-cadherin complex in the eye, in *Mitochondrial Diseases.* IntechOpen. doi: 10.5772/intechopen.75994

Song, Z. H., Ji, Z. N., Lo, C. K., Dong, T. T., Zhao, K. J., and Li, O. T. (2004). Chemical and biological assessment of a traditional Chinese herbal decoction prepared from Radix Astragali and Radix Angelicae Sinensis: orthogonal array design to optimize the extraction of chemical constituents. *Planta Med.* 12, 1222–1227. doi: 10.1055/s-2004-835855

Toda, S., and Shirataki, Y. (1998). Inhibitory effects of isoflavones in roots of *Astragalus membranaceus* BUNGE (Astragali Radix) on lipid peroxidation by reactive oxygen species. *Phytother. Res.* 12, 59–61. doi: 10.1002/(SICI)1099-1573(19980201)12:1<59::AID-PTR182>3.0.CO;2-R

Wang, W. L., Sheu, S. Y., Chen, Y. S., Kao, S. T., Fu, Y. T., Kuo, T. F., et al. (2015). Enhanced bone tissue regeneration by porous gelatin composites loaded with the Chinese herbal decoction Danggui Buxue Tang. *PLoS One* 10 (6), e0131999. doi: 10.1371/journal.pone.0131999

Wallacea, K. B., Eells, J. T., Madeira, V. M. C., Cortopassi, G., and Jones, D. P. (1997). Mitochondria-mediated cell injury. *Fundam. Appl. Toxicol.* 1, 37–38. doi: 10.1006/faat.1997.2320

Wenz, T. (2013). Regulation of mitochondrial biogenesis and PGC-1α under cellular stress. *Mitochondrion* 13, 134–142. doi: 10.1016/j.mito.2013.01.006

Xu, Y. J., Mei, Y., Qu, Z. L., Zhang, S. J., Zhao, W., Fang, J. S., et al. (2018). Ligustilide ameliorates memory deficiency in APP/PS1 transgenic mice *via* restoring mitochondrial dysfunction. *Biomed. Res. Int.* 2018, 4606752. doi: 10.1155/2018/4606752

Yang, X., Yang, S., Huang, C., Du, S., Zhang, X., Liu, J., et al. (2014). Effect of Danggui Buxue Tang on immune-mediated aplastic anemia bone marrow proliferation mice. *Phytomedicine* 21, 640–646. doi: 10.1016/j.phymed.2013.10.018

Yim, T. K., Wu, W. K., Pak, W. F., Mak, D. H. F., Liang, S. M., and Ko, K. M. (2000). Myocardial protection against ischaemia-reperfusion injury by a *Polygonum multiflorum* extract supplemented 'Dang-Gui decoction for enriching blood', a compound formulation, ex vivo. *Phytother. Res.* 14, 195–199. doi: 10.1002/(SICI)1099-1573(200005)14:3<195::AID-PTR629>3.0.CO;2-4

Yogeeta, S. K., Raghavendran, H. R., Gnanapragasam, A., Subhashini, R., and Devaki, T. (2006). Ferulic acid with ascorbic acid synergistically extenuates the mitochondrial dysfunction during beta-adrenergic catecholamine induced cardiotoxicity in rats. *Chem. Biol. Interact.* 163 (1–2), 160–169. doi: 10.1016/j.cbi.2006.04.018

Zheng, K. Y. Z., Choi, R. C. Y., Cheung, A. W. H., Guo, A. J. Y., Bi, C. W. C., Zhu, K. Y., et al. (2011). Flavonoids from Radix Astragali induce the expression of erythropoietin in cultured cells: a signaling mediated *via the* accumulation of hypoxia-inducible factor-1α. *J. Agric. Food. Chem.* 59, 1697–1704. doi: 10.1021/jf104018u

Zheng, K. Y., Choi, R. C., Guo, A. J., Bi, C. W., Zhu, K. Y., Du, C. Y., et al. (2012). The membrane permeability of Astragali Radix-derived formononetin and calycosin is increased by Angelicae Sinensis Radix in Caco-2 cells: a synergistic action of an ancient herbal decoction Danggui Buxue Tang. *J. Pharm. Biomed. Anal.* 70, 671–679. doi: 10.1016/j.jpba.2012.05.018

Zheng, K., Zhang, Z., Du, C., Zhang, W., Bi, C., Choi, R., et al. (2014). Ferulic acid enhances the chemical and biological properties of Astragali Radix: a stimulator for Danggui Buxue Tang, an ancient Chinese herbal decoction. *Planta Med.* 80, 2/03. doi: 10.1055/s-0033-1360314

Conflict of Interest Statement: The authors declare that the research was conducted in the absence of any commercial or financial relationships that could be construed as a potential conflict of interest.

frontiers in Pharmacology

ORIGINAL RESEARCH
published: 10 September 2019
doi: 10.3389/fphar.2019.00985

Metabolic Profiling Analysis of Patients With Coronary Heart Disease Undergoing Xuefu Zhuyu Decoction Treatment

*Tianqi Tao, Tao He, Xiaoreng Wang and Xiuhua Liu**

Department of Pathophysiology, Chinese PLA General Hospital, Beijing, China

Coronary heart disease (CHD) remains the leading cause of morbidity and mortality worldwide. Traditional Chinese medicine (TCM) is one of the effective complementary and alternative therapies used to improve the prognosis of CHD patients. Xuefu Zhuyu (XFZY) decoction, a classical traditional Chinese medication for regulating Qi and promoting blood circulation, has a clinical benefit in CHD; however, the underlying mechanism is not clear. Recently, it was found that the metabolites involved in amino acid metabolism and the tricarboxylic acid cycle were altered in CHD patients with Qi and Yin deficiency syndrome. To understand the material foundation of Qi, it is of great significance to study the differential metabolites involved in Qi during treatment of CHD with Qi-regulating and blood-promoting herbs. In this study, we investigated the metabolic profiles of serum in CHD patients by nontargeted metabolomics analysis to detect differential metabolites between the XFZY decoction group and placebo group. Ten CHD patients were enrolled and treated with placebo granules or XFZY decoction granules in a random and double-blind manner. Serum samples of all patients were evaluated by untargeted high-performance liquid chromatography with tandem mass spectrometry-based metabolomics. In total, 513 metabolites were detected in the serum of CHD patients, and six of these metabolites participating in seven metabolic pathways were significantly different between CHD patients treated with XFZY decoction and the placebo group. Among the six differential metabolites, FA (20:2)-H and tetracarboxylic acid (24:0), involved in fatty acid metabolism; cis-aconitic acid, which participates in the tricarboxylic acid cycle; 2-deoxy-D-glucose, involved in glucose metabolism; and N-acetylglycine, involved in amino acid metabolism, were decreased, whereas spermine, which participates in amino acid metabolism, was increased as compared with the placebo group. Our findings, combined with the perspective of biological functions, indicate that 2-deoxy-D-glucose and spermine might constitute the partial material foundation of Qi in CHD patients treated with XFZY decoction.

Keywords: metabolomics, coronary heart disease, Xuefu Zhuyu decoction, LC-MS/MS, ethnopharmacology

OPEN ACCESS

Edited by:
Jianxun Liu,
China Academy of Chinese Medical Sciences, China

Reviewed by:
Dazhuo Shi,
China Academy of Chinese Medical Sciences, China
Jinggang Xia,
Capital Medical University, China

****Correspondence:***
Xiuhua Liu
xiuhualiu98@163.com

Specialty section:
This article was submitted to Ethnopharmacology, a section of the journal Frontiers in Pharmacology

Received: *30 June 2019*
Accepted: *31 July 2019*
Published: *10 September 2019*

Citation:
Tao T, He T, Wang X and Liu X (2019) Metabolic Profiling Analysis of Patients With Coronary Heart Disease Undergoing Xuefu Zhuyu Decoction Treatment. Front. Pharmacol. 10:985. doi: 10.3389/fphar.2019.00985

INTRODUCTION

Coronary heart disease (CHD) remains the major cause of morbidity and mortality worldwide, responsible for about one in every seven deaths (Lozano et al., 2012). It is predicted to continue until 2030, accounting for 14% of all deaths (Mirzaei et al., 2009). Currently, the incidence of CHD is still on the rise and is associated with a high mortality rate, despite the use of effective Western medicine treatments. Therefore, effective complementary and alternative therapy is necessary to improve functional status and quality of life in CHD patients. Traditional Chinese medicine (TCM) integrated with Western medicine in the treatment of CHD has made great progress. As an effective complementary and alternative therapy, TCM has improved the prognosis of CHD patients. According to the TCM theory, Qi is the commander of blood. Qi stagnation causes blood stasis, which leads to heart vessel blockage stasis. CHD with Qi stagnation and blood stasis is a common syndrome of CHD. Therefore, one of the critical treatments of CHD in TCM is to regulate Qi and promote blood circulation (Xu and Chen, 2007). Xuefu Zhuyu (XFZY) decoction, which originated from the ancient Chinese document "Yilin Gaicuo" in the late Qing Dynasty, has effects on regulating Qi and promoting blood circulation, which is the basic prescription for the treatment of CHD (Meng et al., 2018). Previous studies confirmed that XFZY decoction reduced the incidence of cardiovascular events and improved the prognosis of patients with CHD; however, the underlying mechanism is still unclear.

CHD is characterized by an atherosclerotic plaque-induced narrowing of the coronary arteries, which results in myocardial ischemia, infarction, and postinfarction heart failure. The abnormal substrate and energy metabolism induced by myocardial ischemia is fundamental in the development of CHD (Doenst et al., 2013). Because complete metabolism of glucose is more oxygen efficient than that of fatty acids (FA; Mjos, 1971), myocardial ischemia causes the limitation of FA oxidation and the effective utilization of glucose catabolism, which may lead to the decrease of adenosine triphosphate (ATP) production. In addition, several additional pathways that do not lead to ATP generation, such as the pentose phosphate pathway and the hexosamine biosynthetic pathway, are activated. Therefore, metabolic abnormality plays a key role in affecting the development and prognosis of CHD (Nicholson et al., 1999; Kordalewska and Markuszewski, 2015). Recently, it was found that metabolites involved in amino acid metabolism and tricarboxylic acid (TCA) cycle might partially constitute the material foundation of Qi, according to the Qi and blood theory of TCM (Zhou et al., 2019). Therefore, we studied differential metabolites in the serum of CHD patients to explore the effects of TCM on regulating Qi and promoting blood circulation. It is of great significance to elucidate the mechanism of improving the prognosis of CHD patients through Qi-regulating and blood-promoting herbs and to study Qi and blood in TCM theory.

Metabolomics is one of the youngest branches of "-omics" (such as genomics, transcriptomics, proteomics) techniques to offer the most up-to-date insight into the state of the system in the field of systems biology. It contains approaches to detect low-molecular-weight metabolites (molecular mass <1,500 Da), which reflects changes in the final representations of an organism's phenotype. In our study, we used nontargeted metabolomics analysis to focus on the differential metabolites in the serum from CHD patients treated with placebo and XFZY decoction. We aimed to provide references for the pathogenesis of CHD and the treatment of Qi-regulating and blood-promoting drugs, which refined the understanding of Qi and blood in TCM theory.

MATERIALS AND METHODS

Participants

In this study, a total of 10 CHD patients were recruited from the Chinese PLA General Hospital from April to July 2017. On the basis of routine Western medicine treatment according to the guidelines, participants were treated with placebo granules and XFZY decoction granules randomly and double blindly (twice a day for 12 weeks). The study was approved by the Ethics Review Committee of Chinese PLA General Hospital (No. S2015-048-01) and registered at www.chictr.org.cn (registration number ChiCTR-IOR-15006989).

Inclusion criteria included age <75 years and compliance with the diagnostic criteria for stable CHD according to the American College of Cardiology (ACC)/American Heart Association (AHA) guidelines in 2014 (Fihn et al., 2014). All participation was voluntary, and patients signed an informed agreement. We excluded patients with severe renal dysfunction (serum creatinine >220 μmol/l in males or >175 μmol/l in females), liver dysfunction (aspartate aminotransferase or alanine aminotransferase level three times higher than normal), uncontrolled blood pressure, diabetes mellitus, hemorrhagic diseases, malignant tumors, autoimmune diseases, or hematological or psychiatric diseases; pregnant women; and those who were allergic to components of the research drugs. We also excluded patients with a history of myocardial infarction, severe chronic heart failure, severe arrhythmia, or a cardiac pacemaker. Patients were treated with routine Western medicine according to the guidelines, including anti-ischemia drugs (β receptor blocker or calcium antagonist), antiplatelet drugs (aspirin or clopidogrel), anticoagulant drugs (heparin or low-weight-molecular heparin), and lipid-lowering drugs (statins). Complications, such as hypertension and dyslipidemia, were treated according to relevant guidelines. During the study, nitroglycerin was used to relieve acute angina pectoris. The specifications of nitroglycerin are 0.5 mg/tablet. The original treatment was maintained during the trial.

TCM Treatment

Both XFZY decoction granules and placebo granules were prepared and standardized from China Resources Sanjiu Medical & Pharmaceutical Company (Shenzhen, China). XFZY decoction granules refer to the proportion of components of XFZY decoction, and the botanical compositions are shown in **Table 1**. The voucher specimens of total compositions were

TABLE 1 | Botanical compositions of Xuefu Zhuyu decoction.

Herb (local name)	Medicinal parts	Amount in application (g)
Prunus persica (L.) Batsch (Tao Ren)	Seed	12
Angelica sinensis (Oliv.) Diels (Dang Gui)	Root	15
Conioselinum anthriscoides "Chuanxiong" (Chuan Xiong)	Root	10
Carthamus tinctorius L. (Hong Hua)	Flower	10
Paeonia lactiflora Pall. (Chi Shao)	Root	10
Rehmannia glutinosa (Gaertn.) DC. (Di Huang)	Root	15
Citrus × *aurantium* L. (Zhi Qiao)	Fruit	6
Bupleurum chinense DC. (Chai Hu)	Root	3
Platycodon grandiflorus (Jacq.) A.DC. (Jie Geng)	Root	4.5
Achyranthes bidentata Blume (Niu Xi)	Root	9
Glycyrrhiza uralensis Fisch. ex DC. (Gan Cao)	Root	6

All components in Xuefu Zhuyu decoction granules were fully validated using http://mpns.kew.org/mpns-portal/?_ga=1.111763972.1427522246.1459077346.

stored by China Resources Sanjiu Medical & Pharmaceutical Company (Shenzhen, China). The chemical compositions of XFZY decoction mainly consisted of ferulic acid, paeoniflorin, amygdalin, hydroxysafflor yellow A, catalpol, platycodin D, liquiritin, and ammonium glycyrrhizinate, as indicated by the high-performance liquid chromatography (HPLC) profile of the extract performed by the manufacturer (**Supplementary Figure 1**). The chemical structures of those major compounds are depicted in **Supplementary Figure 2**. The main components of placebo granules were caramel pigments (4 g), and maltodextrin (1,000 g). Using the technical requirements of the quality standards of TCM formula granules, a mixing solution was dried, and granules were then formed. Quality control (QC) of the pharmaceutical process was carried out in accordance with Pharmaceutical Production Quality Management Standards (2015).

Randomization, Control, and Double Blinding

Subjects were randomly grouped by researchers using a random-number table by SAS statistical software. The allocation ratio between the XFZY decoction group and placebo group was 1:1. Drugs were coded and packaged according to random numbers. The blind bottom could not be disassembled during the trial. A placebo group was established as the control of XFZY decoction to exclude the effect of the placebo on CHD treatment. The participants, staff, and researchers were blinded to the treatment group allocation.

Sample Collection and Preparation

All subjects fasted overnight, and 4 ml of peripheral venous blood was drawn in the morning of the day of the consultation. The blood was then coagulated for 30 min at 4°C and centrifuged at 3,000 × *g* for 15 min. The serum supernatant was collected. We then added 400 µl of prechilled methanol to 100 µl serum samples to precipitate the proteins. The mixture was shaken for 15 s, incubated at −80°C for 1 h, and then centrifuged at 13,400 × *g* for 20 min at 4°C. The supernatant was transferred to a new Eppendorf tube and dried before storage in the −80°C freezer. A pooled QC sample solution was prepared by combining equal volumes of serum from each sample and treated using the same procedure. This sample was used to monitor the reliability of the entire experiment. One QC sample was inserted in front of the batch of experimental samples, and each QC sample was inserted in an interval of 10 to 15 samples. Once a QC sample ended, the instrumental stability was monitored throughout the batch process (Li et al., 2018).

Untargeted LC-MS/MS Analysis and Metabolite Identification

Samples were analyzed by untargeted liquid chromatography with tandem mass spectrometry (LC-MS/MS) using an Ultimate 3000

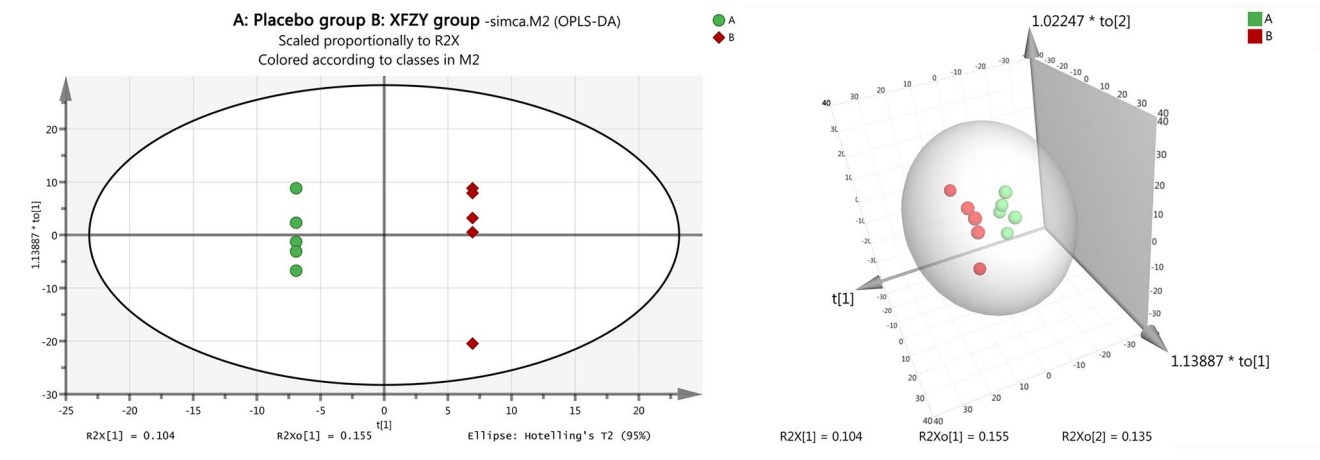

FIGURE 1 | The orthogonal projection to latent structure-discriminant analysis (OPLS-DA) score plots compared the Xuefu Zhuyu decoction group to the placebo group. The left image is the two-dimensional graph of the OPLS-DA score plots, and the right image is the three-dimensional graph of the OPLS-DA score plots. The placebo group is shown in green, and the Xuefu Zhuyu decoction group is shown in red.

UHPLC (Dionex) system combined with a Thermo Q-Exactive (Orbitrap) mass spectrometer (Thermo Fisher Scientific, San Jose, CA, USA). Data identifications were performed by Trace Finder (Thermo Fisher Scientific, San Jose, CA, USA). First, metabolites were potentially identified by accurate masses according to the endogenous MS database. Meanwhile, metabolites that matched with the spectra in the fragment database were confirmed at the MS/MS level. The mass tolerances of primary and secondary identifications were 10 and 15 ppm, respectively. Moreover, a 0.25-min retention time shift was applied (Ning et al., 2018).

Data Processing and Statistical Analysis

SIMCA 14.0 software (Umetrics AB, Umea, Sweden) was used for multivariate statistical analysis. Unsupervised principal component analysis (PCA) was employed to assess the quality, homogeneity, outlier identification, and dominating trends of the group separation inherent in the data set. A supervised orthogonal partial least squares discriminant analysis (OPLS-DA) was applied to distinguish between the classes and to identify the differential metabolites. Variable importance in the projection (VIP) value was generated in PLS-DA model. The quality of the multivariate statistical analysis model was evaluated by R^2X and Q^2. Student's *t* test was used to determine the difference in metabolites between the two groups. Metabolites with VIP > 1 and $P < 0.05$ were considered to be the most probable metabolites, which could be used to analyze the difference between the two groups and to assess the severity of CHD. Subsequently, the internal metabolite MS/MS database was used to identify metabolites by matching accurate quality and MS/MS spectra. MetaboAnalyst 4.0 (http://www.metaboanalyst.ca/; Wishart Research Group, McGill University, Canada) was used to show differential metabolites with a heat map and to predict the metabolic pathways (Chong et al., 2018). SPSS v13.0 (Chicago, IL, USA) was used for statistical analysis. Student's *t* test was performed for two-group comparisons on baseline characteristics. One-way analysis of variance was used to detect the homogeneity of variance. Values are presented as mean ± SD. $P < 0.05$ was considered statistically significant.

RESULTS

Baseline Characteristics

Ten CHD patients were randomly and double blindly divided into two groups: five patients were treated with placebo granules for 12 weeks, and five patients were treated with XFZY decoction granules for 12 weeks. Serum samples from 10 CHD patients were detected by nontargeted metabolomics analysis. The baseline characteristics of the subjects are shown in **Table 2** and include age, body mass index (BMI), blood pressure (systolic pressure, diastolic pressure), heart rate, five kinds of blood routine indices [including red blood cell (RBC), hemoglobin (HGB), white blood cell (WBC), neutrophil (NE), and platelet (PLT)], 10 kinds of biochemical indices [including alanine aminotransferase (ALT), aspartate aminotransferase (AST), serum creatinine (SCr), blood urea nitrogen (BUN), uric acid (UA), triglyceride (TG), total cholesterol (TC), low-density lipoprotein (LDL), high-density lipoprotein (HDL), and fasting glucose (Glu)], and four kinds of coagulation parameters [including prothrombin time (PT), activated partial thrombin time (APTT), fibrinogen (FIB), and thrombin time (TT)]. The average ages of the CHD patients in the two groups were 54.4 ± 5.73 years and 57.0 ± 15.84 years, respectively. The mean BMIs of the two groups were 28.26 ± 6.62 kg/m^2 and 28.49 ± 3.71 kg/m^2, respectively. With the statistical analysis by Student's *t* test, the levels of HGB and Glu were increased, whereas APTT was decreased in the XFZY decoction group as compared with those in the placebo group ($P < 0.05$). However, all values were within the normal range. There was no significant difference in other characteristics between the two groups ($P > 0.05$).

TABLE 2 | Baseline characteristics of patients.

	Placebo (n = 5)	XFZY (n = 5)	*P* Value
Gender (F/M)	2/3	1/4	0.690
Age, years	54.4 ± 5.73	57 ± 15.84	0.739
BMI, kg/m^2	28.26 ± 6.62	28.49 ± 3.71	0.946
Blood pressure, mmHg			
SBP	126.80 ± 15.40	133.60 ± 11.61	0.453
DBP	86.80 ± 6.42	82 ± 8.37	0.339
Heart rate, beats/min	67.20 ± 5.22	71.40 ± 15.19	0.575
Library data			
RBC, ×10^{12}/L	4.78 ± 0.08	5.12 ± 0.42	0.153
HGB, g/L	140.4 ± 7.57	159 ± 16.02	0.047*
WBC, ×10^9/L	6.03 ± 1.98	7.08 ± 2.34	0.465
NE, %	64.94 ± 9.80	63.99 ± 4.54	0.849
PLT, ×10^9/L	231 ± 47.43	231.6 ± 92.69	0.990
AST, U/L	20.18 ± 4.98	20.86 ± 7.06	0.865
ALT, U/L	22.80 ± 10.51	27.40 ± 8.86	0.476
SCr, μmol/L	68.34 ± 23.38	82.08 ± 15.89	0.309
UA, μmol/L	319.74 ± 90.24	319.84 ± 24.85	0.998
BUN, mmol/L	4.63 ± 1.20	5.31 ± 1.23	0.399
TG, mmol/L	2.22 ± 1.15	1.32 ± 0.38	0.135
CHOL, mmol/L	3.07 ± 1.59	4.48 ± 0.68	0.106
HDL, mmol/L	1.29 ± 0.48	1.18 ± 0.12	0.630
LDL, mmol/L	1.94 ± 0.47	2.70 ± 0.74	0.088
Glu, mmol/L	4.83 ± 0.37	5.64 ± 0.59	0.031*
PT, s	13.18 ± 0.63	12.52 ± 0.98	0.242
APTT, s	37.84 ± 1.63	32.94 ± 3.14	0.015*
FIB, g/L	2.84 ± 0.35	3.19 ± 0.44	0.201
TT, s	16.68 ± 0.66	16.72 ± 1.58	0.960

*Values are mean ± SD. *P < 0.05 versus placebo group.*

Analysis of QC Samples

We randomly selected 10 serum samples from CHD patients for metabolomics testing (five in the placebo group and five in the XFZY decoction group). In our research, we used a customized database and nontargeted metabolomics methods to analyze the data. From data collection to data analysis of clear compounds, we quantitatively identified hundreds of compounds according to the established Orbitrap workflow. A total of 513 metabolites were detected in the samples after treatment, which were identified with known MS/MS information. Samples were then subjected to PCA and OPLS-DA analysis.

Serum Metabolomics and Pathway Analysis

To evaluate the identification ability of 513 metabolites, we analyzed the metabolic differences between the two groups, merged all identified compounds (513 in total), and imported them into SIMCA-P software for PCA. The results showed that there was no significant difference between the two groups ($P > 0.05$). Further analysis with two- or three-dimensional orthogonal partial least -squares discriminant method obtained an OPLS-DA score chart (**Figure 1**), which confirmed that there was significant difference between the XFZY decoction group and the placebo group. The OPLS-DA model established a good model and made an accurate prediction ($R^2X = 76.2\%$ and $Q^2 = 39.1\%$).

After filtering 513 different metabolites in each group with the requirements of VIP > 1 and $P < 0.05$, six differential metabolites in the XFZY decoction group were changed as compared with the placebo group, namely, tetracosanoic acid (24:0), N-acetylglycine, FA (20:2)-H, 2-deoxy-D-glucose (2-DG), cis-aconitic acid, and spermine. Compared with the placebo group, tetracosanoic acid (24:0), N-acetylglycine, FA (20:2)-H, 2-DG, and cis-aconitic acid were downregulated, whereas spermine was upregulated in the XFZY decoction group.

As shown in **Table 3**, the differential metabolites related to FA metabolism were tetracosanoic acid (24:0) and FA (20:2)-H, which were obtained by election spray ionization negative (ESI–) mode with a mass of 367.358 and 307.264, respectively. Compared with the placebo group, tetracosanoic acid (24:0) and FA (20:2)-H in the XFZY decoction group were decreased, exhibiting that the ratio (XFZY/placebo) of tetracosanoic acid (24:0) or FA (20:2) was 0.46 (VIP = 2.40596, $P = 0.008$) or 0.78 (VIP = 2.21854, $P = 0.020$). 2-DG and cis-aconitic acid, which are related to glucose metabolism and obtained by ESI– mode, were downregulated with XFZY decoction treatment. The mass, VIP value, P value, and FC (XFZY/placebo) of 2-DG were 163.061, 2.03138, 0.039, and 0.50, respectively. The mass, VIP value, P value, and FC (XFZY/placebo) of cis-aconitic acid were 173.009, 1.9734, 0.048, and 0.81, respectively. The differential metabolites associated with amino acid metabolism were N-acetylglycine and spermine obtained by ESI+ mode. The concentration of N-acetylglycine in the XFZY decoction group was decreased as compared with the placebo group, which showed that the ratio (XFZY/placebo) of N-acetylglycine was 44% (VIP = 2.28626, $P = 0.015$). However, the concentration of spermine was increased by 208% compared with that in the placebo group (VIP = 1.99192, $P = 0.045$). As shown in **Figure 2**, the heat map illustrated total differential metabolites between the XFZY decoction group and placebo group: tetracosanoic acid, N-acetylglycine, FA, 2-DG, and cis-aconitic acid were downregulated, whereas spermine was upregulated.

MetaboAnalyst 4.0 software was used to analyze and predict the potential metabolic pathways involved in differential metabolites with XFZY decoction treatment. As shown in **Figure 3**, six differential metabolites were involved in seven metabolic pathways: citrate cycle (TCA cycle), β-alanine metabolism, glycerolipid metabolism, glutathione metabolism, glyoxylate and dicarboxylate metabolism, FA metabolism, and arginine and proline metabolism.

Further studies showed that cis-aconitic acid was involved in the TCA cycle as well as in glyoxylate and dicarboxylate metabolism. Spermine was predicted to participate in glutathione metabolism, arginine and proline metabolism, and β-alanine metabolism, respectively. FA (20:2) were predicted to be involved in FA metabolism and glycerolipid metabolism (**Table 4**).

DISCUSSION

CHD is the leading cause of morbidity and mortality throughout the world (Lozano et al., 2012). The high mortality rate of CHD asks for effective complementary and alternative therapy to improve the prognosis of CHD patients. TCM based on syndrome differentiation is one of the effective complementary and alternative therapies. XFZY decoction, a classical traditional Chinese medication that regulates Qi and promotes blood circulation, is confirmed to be of clinical benefit for CHD treatment; however, the underlying mechanism is still unknown. The key pathogenesis of CHD is based on the abnormal metabolism of myocardial substrates and the disturbance of energy metabolism induced by myocardial ischemia or hypoxia (Doenst et al., 2013). A recent study found that metabolites involved in the TCA cycle and amino acid metabolism (tryptophan, arginine, and proline metabolism) were significantly decreased in fasting morning urine of CHD patients with Qi and Yin deficiency syndrome, suggesting that the metabolites in amino acid metabolism and TCA cycle were partially the material foundation of Qi (Zhou et al., 2019).

TABLE 3 | Differential metabolites between the XFZY group and placebo group patients from LC-MS/MS analysis.

Differential metabolite	Related metabolism	ESI mode	Mass (m/z)	RT (min)	FC (XFZY/placebo)	VIP	*P* value
Tetracosanoic acid (24:0)	Fatty acid metabolism	Neg	367.358	14.85	0.46	2.40596	0.008
N-acetylglycine	Amino acid metabolism	Pos	118.050	8.29	0.44	2.28626	0.015
FA(20:2)-H	Fatty acid metabolism	Neg	307.264	13.25	0.78	2.21854	0.020
2-deoxy-D-glucose	Glucose metabolism	Neg	163.061	1.04	0.50	2.03138	0.039
Spermine	Amino acid metabolism	Pos	203.223	8.76	3.08	1.99192	0.045
cis-aconitic acid	Glucose metabolism	Neg	173.009	0.87	0.81	1.9734	0.048

XFZY, Xuefu Zhuyu decoction; ESI, election spray ionization; RT, retention time; VIP, variable importance in the projection; P, probability; FC, fold change; Pos, positive; Neg, negative; FA, fatty acid.

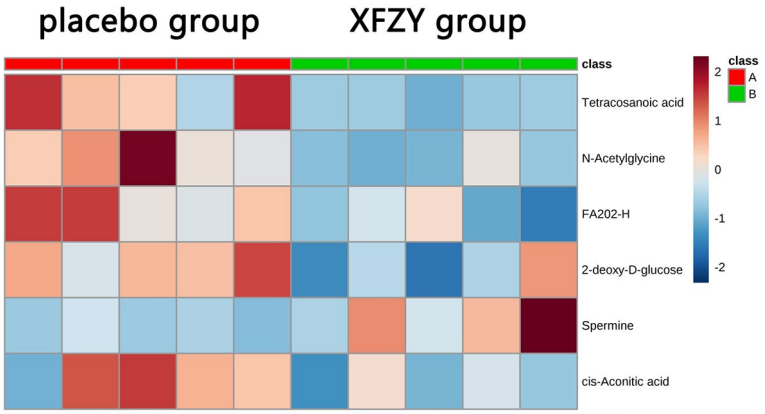

FIGURE 2 | The six differential metabolites in the two groups are shown in the heat map using MetaboAnalyst 4.0 (A: placebo group; B: Xuefu Zhuyu decoction group). The row represents the metabolites, and the column represents the individual samples. Red bands indicate upregulated metabolites, and blue bands indicate downregulated metabolites in the two groups. The deeper the color, the greater the difference in metabolites.

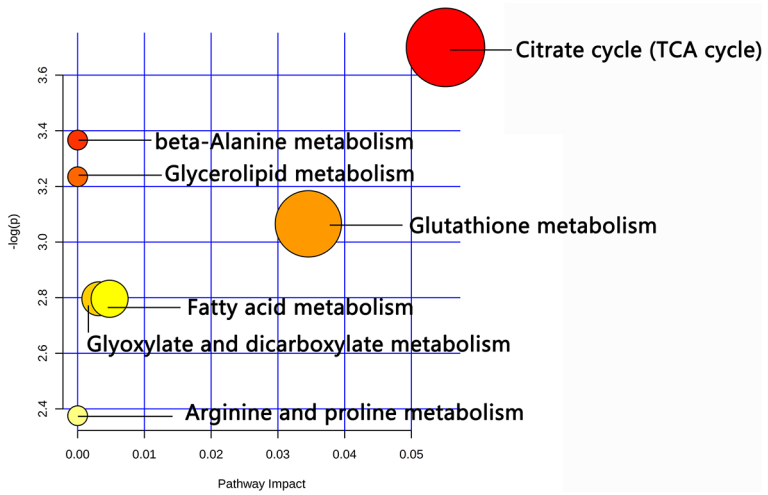

FIGURE 3 | The disturbed metabolic pathways showed differential metabolites changed in the Xuefu Zhuyu decoction group as compared with the placebo group by MetaboAnalyst 4.0 software. Node radius was based on pathway impact values. Node color was based on *P* value.

In TCM theory, Qi is the commander of blood. Qi replenishment causes the promotion of blood circulation, whereas Qi stagnation leads to blood stasis, which suggests that Qi plays a leading role in CHD with Qi stagnation and blood stasis. In our study, the effect of XFZY decoction on low-molecular-weight metabolites was investigated by nontargeted metabolomics analysis. Compared with the placebo group, 513 kinds of metabolites were detected, and six metabolites were significantly differential in the serum from CHD patients after treatment with XFZY decoction. Among the six differential metabolites, FA (20:2)-H and tetracarboxylic acid (24:0), which are involved in FA metabolism; cis-aconitic acid, which participates in the TCA cycle; 2-DG, which is involved in glucose metabolism; and N-acetylglycine, which is involved in amino acid metabolism, were decreased, whereas spermine, which is involved in amino acid metabolism (such as arginine and proline, glutathione, and β-alanine metabolism), was increased as compared with the placebo group. This suggests that those low-molecular-weight metabolites might be the material foundation of XFZY decoction for regulating Qi and promoting blood circulation in CHD treatment.

FA Metabolism

Because of continuous mechanical work, the heart has a high rate of ATP utilization. Because the high-energy phosphate pool in the heart is significantly small and could be exhausted within a few seconds, cardiomyocytes are very sensitive to changes in energy metabolism, and cardiac work strongly depends on ATP generation. Nearly 70% to 90% of ATP is produced by the oxidation of FA in cardiomyocytes (Doenst et al., 2013). Free FA are esterified to fatty acylCoA in the cytosol and are transported into the mitochondria matrix by carnitine. There, they form Acyl-CoA to enter β-oxidation (Berndt et al., 2019).

TABLE 4 | Differential metabolic pathway between the XFZY group and placebo group.

Pathway name	Match status	Match metabolites
Citrate cycle (TCA cycle)	1/20	cis-aconitic acid
β-alanine metabolism	1/28	Spermine
Glycerolipid metabolism	1/32	Fatty acid
Glutathione metabolism	1/38	Spermine
Glyoxylate and dicarboxylate metabolism	1/50	cis-aconitic acid
Fatty acid metabolism	1/50	Fatty acid
Arginine and proline metabolism	1/77	Spermine

XFZY, Xuefu Zhuyu decoction; TCA cycle, tricarboxylic acid cycle; match status, the number of accumulated metabolites/the number of all metabolites in metabolic pathways.

Xu et al. found that FA and carnitine in the plasma of CHD patients were decreased compared with controls (Xu et al., 2016). However, others detected the lipid profile of H9c2 cells and then found that different types of FA were increased or decreased in hypoxic cardiomyocytes, which demonstrates that FA (18:1) was decreased, whereas FA (16:0) and FA (18:0) were increased as compared with controls. This indicates that different FA might change differently in special periods of hypoxia or ischemia in cardiomyocytes (Sousa et al., 2016). FA (20:2)-H and tetracarboxylic acid (24:0) are very-long-chain FA and should be oxidized by peroxisome to form medium- or short-chain FA. They are then transported to the mitochondria matrix by carnitine for β-oxidation. This means that FA (20:2)-H and tetradecanoic acid (24:0) provide substrates for β-oxidation, and the decrease in carnitine indicates the limitation of FA β-oxidation. In this study, we found that FA (20:2)-H and tetradecanoic acid (24:0) were downregulated, whereas carnitine did not decrease after XFZY decoction treatment as compared with the placebo group, suggesting that XFZY decoction might promote FA β-oxidation, which led to the decrease of FA in the serum.

Glucose Metabolism

In myocardial metabolism, FA and glucose utilization is tightly linked and co-regulated. Utilization of one substrate may directly inhibit the utilization of the other, which is referred to as the "Randle cycle" (Randle, 1998). In ischemic myocardium, FA oxidation is limited, and the utilization of glucose is increased. As a glucose analogue, 2-DG inhibited the critical enzymes of glycolysis (hexokinase and phosphoglucose isomerase), which inhibited glycolysis with the downregulation of glucose-6-phosphate and fructose-6-phosphate. In addition, 2-DG possessed a mannose-like property, which competed with mannose during the initial steps of N-linked glycosylation, resulting in protein misfolding and endoplasmic reticulum stress (Xi et al., 2014). In rat models, 2-DG was encountered as cardiac toxicity, with microscopic findings of vacuolar degeneration and hypertrophy of the endothelial cells of the endocardium (Terse et al., 2016). Studies in tumors have found that at low doses, 2-DG mainly interfered with N-linked glycosylation, resulting in endoplasmic reticulum stress, apoptosis, and autophagy. At medium doses, 2-DG also blocked glycolysis, leading to ATP reduction, and the subsequent growth inhibition. At high doses, 2-DG started to disrupt the pentose phosphate pathway, which caused growth arrest and oxidative stress (Xi et al., 2014). It was found for the first time that 2-DG in the serum of CHD patients was decreased after treatment with XFZY decoction, which suggested that XFZY decoction could attenuate the inhibition of N-glycosylation and glycolysis; alleviate endoplasmic reticulum stress, apoptosis, and autophagy; promote ATP production; and protect cardiomyocytes by downregulating 2-DG.

Acetyl-CoA, a common end product of glucose and FA oxidation, enters the TCA cycle and provides energy for cardiomyocytes (Opie, 2004). Cis-aconitic acid is an important intermediate that participates in the TCA cycle. It combines with aconitase, which converts citric acid to isocitric acid, and maintains the progress of the TCA cycle. The decrease in cis-aconitic acid suggests the limitation of TCA cycle metabolism. Our study first found that cis-aconitic acid, one intermediate of the TCA cycle, had the same change as 2-DG. Compared with the placebo group, cis-aconitic acid was decreased after XFZY decoction treatment. Combined with the previous changes in FA metabolism, it suggested that the upregulation of FA metabolism might inhibit glucose metabolism, as shown in the decrease of the intermediate in the TCA cycle.

Amino Acid Metabolism

Amino acids can also be used as energy metabolites. They form precursors of glucose and FA metabolism through deamination or transamination and participate in metabolic pathways, such as the TCA cycle. In addition, amino acid-derived bioactive substances play an important role in the cardiovascular system. Spermine is a kind of polyamine that is further produced by putrescine converted from arginine and has many physiological functions. It was reported that spermine was significantly decreased after myocardial ischemia/reperfusion injury in rats, suggesting that spermine may play a key role in myocardial ischemia/reperfusion injury (Han et al., 2009). Animal experiments showed that spermine enhanced the antioxidant status: spermine supplementation and extended spermine administration could promote the expression of antioxidant enzymes, such as glutathione reductase by upregulating nuclear factor erythroid 2-related factor 2 (Nrf2) expression (Cao et al., 2018). Arginine plays a critical antiatherogenic role in the development of cardiovascular disease by regulating endothelial cell homeostasis. Nitric oxide (NO), produced by the oxidation of arginine in endothelial cells, promotes beneficial effects in the vasculature, including vasodilation, enhanced fibrinolysis, and inhibition of multiple atherothrombotic biological processes, such as platelet aggregation, leukocyte adhesion, endothelin generation, and smooth muscle cell proliferation (Nausch et al., 2008; Tang et al., 2009). β-alanine can be transaminated to pyruvate, providing a substrate for cardiac glucose oxidation. In our study, we found for the first time that the serum spermine concentration in CHD patients was increased after treatment with XFZY decoction. Bioinformatics analysis further indicated that spermine was involved in glutathione metabolism, arginine and proline metabolism, and β-alanine metabolism. It was suggested that XFZY decoction

could alleviate oxidative stress in cardiomyocytes by promoting glutathione metabolism, maintain endothelial function by upregulating arginine metabolism, and increase the production of aerobic oxidative substrates in cardiomyocytes by promoting β-alanine metabolism.

In our study, we further investigated the mechanism of XFZY decoction for regulating Qi and promoting blood circulation from the perspective of biological functions of low-molecular-weight metabolites. Some studies have shown that XFZY decoction alleviated cardiomyocyte apoptosis and oxidative stress (Meng et al., 2018) as well as the inhibition of platelet aggregation (Li et al., 1999). For the first time, we found that 2-DG was decreased whereas spermine was increased in the serum of CHD patients after treatment with XFZY decoction. Through exploration of the effects of those two differential metabolites on ischemic myocardium, we confirmed the potential mechanism of XFZY decoction in CHD treatment: the decrease of 2-DG alleviated apoptosis and autophagy and promoted glycolysis to generate ATP after treatment with XFZY decoction, and the increase in spermine alleviated apoptosis and oxidative stress and inhibited platelet aggregation in the XFZY decoction group, which explained the similar functions of XFZY decoction in previous animal experiments. The elevation of spermine also illustrated the increase of arginine metabolism, which might generate more NO to alleviate coronary atherosclerosis. In addition, the decrease in 2-DG promoted ATP synthesis. Because NO and ATP are regarded as a part of the involvement of Qi in TCM theory (Deng et al., 2012; Chen et al., 2018), it is suggested that the metabolites of Qi might be associated with 2-DG and spermine.

Limitation

Although we believe that our study investigated the effects of XFZY decoction on metabolic profiles in CHD patients and the results could partly explain the mechanism of XFZY decoction for regulating Qi and promoting blood circulation, some limitations should still be considered. One limitation is that the sample size in this study is small. Another limitation is that the follow-up time is not long enough, so we did not focus on the study of the primary or second end points. Because there was statistical difference between the placebo group and the XFZY decoction group before treatment, we excluded the metabolites that have similar trends in our analysis. In addition, metabolomics itself has some limitations. Because of the wide concentration range and chemical diversity of metabolites, there is no instrument to detect all metabolites in a single analysis. In this study on metabolomics of CHD, we detected the metabolites in the serum. However, the metabolites in the circulatory system may originate from nonmyocardial tissues. The use of metabolic drugs and the excretion function of the liver and kidney may also affect the level of metabolites. Those two reasons increased the uncertainty of applying metabolomics to clinical detection of CHD (Dias and Koal, 2016). Moreover, some energy metabolites, such as ATP, adenosine diphosphate (ADP), and phosphocreatine were not detected in this study. Considering the limitation of nontargeted metabolomics, we should optimize the methods, such as choosing targeted metabolomics in the future.

CONCLUSION

In conclusion, we found that XFZY decoction caused the changes in six metabolites in FA, glucose, and amino acid metabolism with the detection of the serum in CHD patients by nontargeted LC-MS/MS analysis. We further predicted seven metabolic pathways according to those differential metabolites. Among them, 2-DG and spermine might partially be the material foundation of Qi in TCM theory, which suggests potential targets of XFZY decoction for regulating Qi and promoting blood circulation in CHD treatment.

DATA AVAILABILITY

The datasets generated for this study are available on request to the corresponding author.

ETHICS STATEMENT

The studies involving human participants were reviewed and approved by the Ethics Review Committee of Chinese PLA General Hospital (No. S2015-048-01). The patients/participants provided their written informed consent to participate in this study.

AUTHOR CONTRIBUTIONS

XL conceived, designed, and supervised the clinical trial and experiments and contributed to manuscript revision. TT performed the trials and statistical analysis and drafted the manuscript. TH coperformed the trials. XW coperformed the statistical analysis. All authors read and approved the submitted version.

FUNDING

This work was supported by the National Basic Research Program of China (XL: No. 2015CB554402 and 2015CB554405) and the National Natural Science Foundation of China (XL: No. 31771287).

SUPPLEMENTARY MATERIAL

The Supplementary Material for this article can be found online at: https://www.frontiersin.org/articles/10.3389/fphar.2019.00985/full#supplementary-material

REFERENCES

Berndt, N., Eckstein, J., Heucke, N., Gajowski, R., Stockmann, M., Meierhofer, D., et al. (2019). Characterization of lipid and lipid droplet metabolism in human HCC. *Cells* 8, E512. doi: 10.3390/cells8050512

Cao, W., Xu, X., Jia, G., Zhao, H., Chen, X., Wu, C., et al. (2018). Roles of spermine in modulating the antioxidant status and Nrf2 signaling molecules expression in the thymus and spleen of suckling piglets—new insight. *J. Anim. Physiol. Anim. Nutr. (Berl.)* 102, e183–e192. doi: 10.1111/jpn.12726

Chen, J. C., Liu, J. X., Lin, C. R., Ren, J. G., Li, L., and Guo, H. (2018). Study on establishment of an animal model of Qi deficiency syndrome base on theory of over exertion leading to Qi consumption in traditional Chinese medicine. *Zhongguo Zhong Yao Za Zhi* 43, 2177–2183. doi: 10.19540/j.cnki.cjcmm.20180418.003

Chong, J., Soufan, O., Li, C., Caraus, I., Li, S., Bourque, G., et al. (2018). MetaboAnalyst 4.0: towards more transparent and integrative metabolomics analysis. *Nucleic Acids Res.* 46, W486–W494. doi: 10.1093/nar/gky310

Deng, L., Wang, Q., Yuan, H., Liu, J., Tang, Q., and Xu, X. (2012). Effect of catalpol and puerarin freeze-dried powder on coagulability, hemorheology and no in rats with Qi-deficiency and blood-stasis syndrome. *Zhongguo Zhong Yao Za Zhi* 37, 1472–1476.

Dias, D. A., and Koal, T. (2016). Progress in metabolomics standardisation and its significance in future clinical laboratory medicine. *EJIFCC* 27, 331–343. 28149265.

Doenst, T., Nguyen, T. D., and Abel, E. D. (2013). Cardiac metabolism in heart failure: implications beyond ATP production. *Circ. Res.* 113, 709–724. doi: 10.1161/CIRCRESAHA.113.300376

Fihn, S. D., Blankenship, J. C., Alexander, K. P., Bittl, J. A., Byrne, J. G., Fletcher, B. J., et al. (2014). 2014 ACC/AHA/AATS/PCNA/SCAI/STS focused update of the guideline for the diagnosis and management of patients with stable ischemic heart disease: a report of the American College of Cardiology/American Heart Association Task Force on Practice Guidelines, and the American Association for Thoracic Surgery, Preventive Cardiovascular Nurses Association, Society for Cardiovascular Angiography and Interventions, and Society of Thoracic Surgeons. *Circulation* 130, 1749–1767. doi: 10.1161/CIR.0000000000000095

Han, L., Xu, C., Guo, Y., Li, H., Jiang, C., and Zhao, Y. (2009). Polyamine metabolism in rat myocardial ischemia-reperfusion injury. *Int. J. Cardiol.* 132, 142–144. doi: 10.1016/j.ijcard.2007.07.163

Kordalewska, M., and Markuszewski, M. J. (2015). Metabolomics in cardiovascular diseases. *J. Pharm. Biomed. Anal.* 113, 121–136. doi: 10.1016/j.jpba.2015.04.021

Li, Y., Wang, Z., and Weng, J. (1999). Effect of xuefu zhuyu decoction on function of platelet and endothelial cell. *Zhongguo Zhong Xi Yi Jie He Za Zhi* 19, 289–291.

Li, Z. J., Chen, W., Jiang, H., Li, X. Y., Zhu, S. N., and Liu, X. H. (2018). Effects of postoperative parenteral nutrition enhanced by multivitamin on metabolic phenotype in postoperative gastric cancer patients. *Mol. Nutr. Food Res.* 62, e1700757. doi: 10.1002/mnfr.201700757

Lozano, R., Naghavi, M., Foreman, K., Lim, S., Shibuya, K., Aboyans, V., et al. (2012). Global and regional mortality from 235 causes of death for 20 age groups in 1990 and 2010: a systematic analysis for the global burden of disease study 2010. *Lancet* 380, 2095–2128. doi: 10.1016/S0140-6736(12)61728-0

Meng, F., Lai, H., Luo, Z., Liu, Y., Huang, X., Chen, J., et al. (2018). Effect of Xuefu Zhuyu decoction pretreatment on myocardium in sepsis rats. *Evid. Based Complement. Alternat. Med.* 2018, 2939307. doi: 10.1155/2018/2939307

Mirzaei, M., Truswell, A. S., Taylor, R., and Leeder, S. R. (2009). Coronary heart disease epidemics: not all the same. *Heart* 95, 740–746. doi: 10.1136/hrt.2008.154856

Mjos, O. D. (1971). Effect of free fatty acids on myocardial function and oxygen consumption in intact dogs. *J. Clin. Invest.* 50, 1386–1389. doi: 10.1172/JCI106621

Nausch, L. W., Ledoux, J., Bonev, A. D., Nelson, M. T., and Dostmann, W. R. (2008). Differential patterning of cGMP in vascular smooth muscle cells was revealed by single GFP-linked biosensors. *Proc. Natl. Acad. Sci. U. S. A.* 105, 365–370. doi: 10.1073/pnas.0710387105

Nicholson, J. K., Lindon, J. C., and Holmes, E. (1999). Metabonomics: understanding the metabolic responses of living systems to pathophysiological stimuli *via* multivariate statistical analysis of biological NMR spectroscopic data. *Xenobiotica* 29, 1181–1189. doi: 10.1080/004982599238047

Ning, P., Zheng, Y., Luo, Q., Liu, X., Kang, Y., Zhang, Y., et al. (2018). Metabolic profiles in community-acquired pneumonia: developing assessment tools for disease severity. *Crit. Care* 22, 130. doi: 10.1186/s13054-018-2049-2

Opie, L. H. (2004). The metabolic vicious cycle in heart failure. *Lancet* 364, 1733–1734. doi: 10.1016/S0140-6736(04)17412-6

Randle, P. J. (1998). Regulatory interactions between lipids and carbohydrates: the glucose fatty acid cycle after 35 years. *Diabetes Metab. Rev.* 14, 263–283. doi: 10.1002/(SICI)1099-0895(199812)14:4<263::AID-DMR233>3.0.CO;2-C

Sousa, B., Melo, T., Campos, A., Moreira, A. S., Maciel, E., Domingues, P., et al. (2016). Alteration in phospholipidome profile of myoblast H9c2 cell line in a model of myocardium starvation and ischemia. *J. Cell. Physiol.* 231, 2266–2274. doi: 10.1002/jcp.25344

Tang, W. H., Wang, Z., Cho, L., Brennan, D. M., and Hazen, S. L. (2009). Diminished global arginine bioavailability and increased arginine catabolism as metabolic profile of increased cardiovascular risk. *J. Am. Coll. Cardiol.* 53, 2061–2067. doi: 10.1016/j.jacc.2009.02.036

Terse, P. S., Joshi, P. S., Bordelon, N. R., Brys, A. M., Patton, K. M., Arndt, T. P., et al. (2016). 2-Deoxy–D-Glucose (2-DG) induced cardiac toxicity in Rat: NT proBNP and BNP as potential early cardiac safety biomarkers. *Int. J. Toxicol.* 35, 284–293. doi: 10.1177/1091581815624397

Xi, H., Kurtoglu, M., and Lampidis, T. J. (2014). The Wonders of 2-Deoxy-D-Glucose. *IUBMB. Life* 66, 110–121. doi: 10.1002/iub.1251

Xu, H., and Chen, K. J. (2007). Difficulties and countermeasures in research for prevention and treatment of coronary heart disease by integrative Chinese and Western medicine. *Zhongguo Zhong Xi Yi Jie He Za Zhi* 27, 647–649.

Xu, X., Gao, B., Guan, Q., Zhang, D., Ye, X., Zhou, L., et al. (2016). Metabolomic profile for the early detection of coronary artery disease by using UPLC-QTOF/MS. *J. Pharm. Biomed. Anal.* 129, 34–42. doi: 10.1016/j.jpba.2016.06.040

Zhou, H., Li, L., Zhao, H., Wang, Y., Du, J., Zhang, P., et al. (2019). A large-scale, multi-center urine biomarkers identification of coronary heart disease in TCM syndrome differentiation. *J. Proteome. Res.* 18, 1994–2003. doi: 10.1021/acs.jproteome.8b00799

Conflict of Interest Statement: The authors declare that the research was conducted in the absence of any commercial or financial relationships that could be construed as a potential conflict of interest.

frontiers in Pharmacology

ORIGINAL RESEARCH
published: 11 September 2019
doi: 10.3389/fphar.2019.00979

ITRAQ-Based Proteomics Analysis Reveals the Effect of Neoliensinine on KCl-Induced Vascular Smooth Muscle Contraction by Inhibiting Regulatory Light Chain Phosphorylation

*Guang-Ming Yang†, Ke Yan†, Peng Wang, Jun-Li Zhang, Zi-Hao Pan and Yang Pan**

School of Pharmacy, Nanjing University of Chinese Medicine, Nanjing, China

OPEN ACCESS

Edited by:
Xiu-Wei Yang,
Peking University, China

Reviewed by:
Ru Yan,
University of Macau, China
Minsheng Zhu,
Nanjing University, China
Xiaobin Jia,
China Pharmaceutical University, China

***Correspondence:**
Yang Pan
y.pan2006@163.com

†These authors have contributed equally to this work

Specialty section:
This article was submitted to Ethnopharmacology, a section of the journal Frontiers in Pharmacology

Received: *19 February 2019*
Accepted: *31 July 2019*
Published: *11 September 2019*

Citation:
Yang G-M, Yan K, Wang P, Zhang J-L, Pan Z-H and Pan Y (2019) ITRAQ-Based Proteomics Analysis Reveals the Effect of Neoliensinine on KCl-Induced Vascular Smooth Muscle Contraction by Inhibiting Regulatory Light Chain Phosphorylation. Front. Pharmacol. 10:979. doi: 10.3389/fphar.2019.00979

Smooth muscle (SM) contraction is one of the important physiological functions of the human body, and SM abnormal contraction will induce many diseases. The phosphorylated regulatory light chains (p-RLC) play a decisive role in SM contraction, and dephosphorylation of p-RLC is an effective way to relax SM. Our previous study showed that the novel benzylisoquinoline alkaloid, neoliensinine (Neo), could relax microvascular SM contracted by KCl hyperpolarization. In this study, mesenteric capillaries isolated from 45 mice were divided into normal tension group (Control), 124 mM KCl induced contraction model group (Model), and KCl and Neo-treatment group (Drug). The dephosphorylation levels of RLC in the three groups were measured. Compared with the model group, the phosphorylation of RLC in the drug group was decreased dramatically as expected, suggesting that the relaxation effect of Neo was caused by downregulating p-RLC of microvessel SM. In order to fully understand its fundamental mechanism, our research focused on the identification of target proteins in mice with KCl-induced contractile mesenteric capillary. Isobaric tags for relative and absolute quantification (ITRAQ) tagging was carried out by nanospray liquid chromatography–tandem mass spectrometry. The results allowed the upregulation of 164 differential abundance proteins (DAPs) among the 3,474 protein abundance disturbances identified from the model/control samples. Further comparison showed that there were 16 DAP convergences associated with vascular SM contraction between the drug/model and the drug/control samples. Among them, two proteins with known function, PLCβ and RhoGEF12, were selected as target proteins of the relaxation effect of Neo. The two selective target DAPs were verified by Western blot at protein level. The results suggested that changes of the two proteins were consistent with that of the iTRAQ results. Our present work reveals that Neo relaxes vascular smooth muscle *via* inhibition of RLC phosphorylation, and PLCβ and RhoGEF12 may be potential biomarkers for evaluating the effects mediated by Neo.

Keywords: vascular smooth muscle relaxation, neoliensinine, *Nelumbo nucifera* Gaertn, regulatory light chain phosphorylation, iTRAQ

INTRODUCTION

Smooth muscle (SM) exists in the circulatory system, respiratory system, reproductive systems, and other parts of the human body (Webb, 2003). Its failure to relax normally due to improper regulation can lead to hypertension (Heinze et al., 2014), gastrointestinal diseases (He et al., 2008), asthma (Christopher, 2009), and other problems. Therefore, many treatment strategies rely on medication for SM relaxation (Mak and Hanania, 2012). *Nelumbo nucifera* Gaertn, also known as Indian lotus, Chinese water lily, sacred lotus, India bean, Egyptian bean, or simply lotus, is currently classified as a single genus of Nelumbonaceae (Shen-Miller et al., 2002). Embryo of lotus seed, as an ancient folk herb, is widely used to overcome nervous disorders, insomnia, high fever (with restlessness), and cardiovascular diseases (SATCM, 1999; Khare, 2004; China Pharmacopoeia Committee, 2015). Previous studies have shown that isoquinoline alkaloids were the active components in the bitter embryos (Zhang and P, 2002; Itoh et al., 2011; Li et al., 2016; Sharma et al., 2017). These compounds were attracting ever-increasing attention for their biological activities in hypertension, arrhythmia, and ischemic stroke related to abnormal contraction of SM (Qian, 2002). In our previous study, neoliensinine (Neo) was reported to be a newly isolated tribenzylisoquinoline of *N. nucifera*. The stereochemical structure of Neo is shown in **Figure 1**. Neo has been shown to possess a unique skeleton different from that of existing isoquinolines and has a potent relaxation effect on constricted SM induced by KCl hyperpolarization, and the relaxation effect is weak reversible (or nearly irreversible) (Yang et al., 2018). However, until now, the mechanism of its action as a new relaxant is very little understood.

The structure of neoliensinine was elucidated to be2-[[(1*R*)-1-(4-methoxyphenyl) methyl-6-methoxy-2-methyl-3,4-dihydro-1H-isoquinolin-7-yl] oxy]-4-[[4-[[(1*R*)-6,7-dimethoxy-2-methyl-3,4-dihydro-1H-isoquinolin-1-yl] methyl]-2-[[(1*R*)-6-methoxy-1-[(4-methoxyphenyl)methyl]-2-methyl-3,4-dihydro-1H-isoquinolin-7-yl] oxy] phenyl-1-yl] oxy] phenol. As far as we know, naturally occurring tribenzylisoquinoline alkaloids that possess three benzylisoquinoline moieties have not been reported yet.

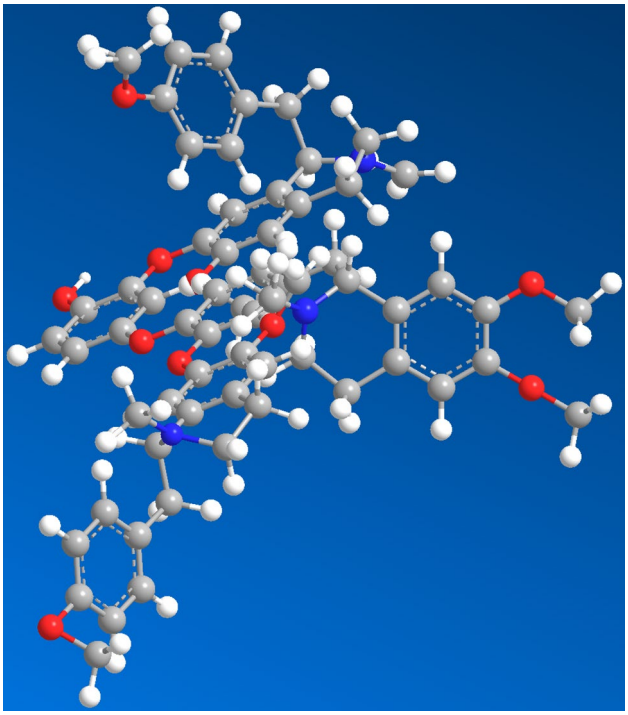

FIGURE 1 | The 3D structure of neoliensinine isolated from embryos of lotus seed, a unique tribenzylisoquinoline.

Generally, myosin light-chain kinase (MLCK) may phosphorylate the regulatory light chains (RLCs, also called MLC20) to form p-RLC within minutes of the smooth muscle being stimulated to contract by physiochemical agents. The smooth muscle then has the ability to maintain contractile force, keeping the phosphorylation of RLC at a certain level in the subsequent sustained phase (Hartshorne and Ito, 1998; He et al., 2008; Aguilar and Mitchell, 2010; He et al., 2011; Qiao et al., 2014). Therefore, dephosphorylation of p-RLC is an effective means to inhibit smooth muscle contraction.

As we have known, drugs exert their therapeutic effect by binding to and regulating specific protein or nucleic acid targets and identifying potential intervention targets, which is the first step to use reverse pharmacology approach to discover a drug (Overington et al., 2006; Landry and Gies, 2008; Rang et al., 2012). Among a variety of global quantification strategies used in MS-based proteomics, isobaric tags for relative and absolute quantification (iTRAQ) is an attractive option for detecting large amounts of proteins in specific biological environments using labeled peptides to identify different samples (Evans et al., 2012). Using iTRAQ approach, many researchers have made great progress in identifying drug targets (Wang et al., 2017). ITRAQ analysis is further strengthened using robust bioinformatic tools, such as Gene ontology (GO) annotation and the Kyoto Encyclopedia of Genes and Genomes (KEGG) enrichment, as well as statistical analyses that supports observations (Herbrich et al., 2013). In the present research, a mass-spectrometry-based iTRAQ was carried out to identify cell targets involved in Neo-mediated relaxation of microvascular arteries *in vitro* and to obtain comprehensive differential protein profiles in

Abbreviations: SM, smooth muscles; RLC (MLC20), regulatory light chains; p-RLC, phosphorylated regulatory light chains; MLCK, myosin light-chain kinase; mM, mmol/l; iTRAQ, isobaric tags for relative and absolute quantification; DAPs, differential abundance proteins; LC, liquid chromatography; MS, mass spectrometry; GO, Gene Ontology; KEGG, Kyoto Encyclopedia of Genes and Genomes; PH, pleckstrin homology; PIP2, phosphatidylinositol 4,5-bisphosphate; DAG, diacylglycerol; IP3, inositol 1,4,5-trisphosphate; GDI, guanine dissociation inhibitor; RhoGEFs, Rho-specific guanine nucleotide exchange factors; GDP, guanosine diphosphate; GTP, guanosine triphosphate; RGS, regulator of protein G signaling; DH, Dbl homology; HPLC, high-performance liquid chromatography; DMSO, dimethyl sulfoxide; TCA, trichloroacetic acid; TEMED, tetramethyl ethylenediamine; HEPES, 2-hydroxyethyl; DTT, dithiotheritol; EDTA, ethylene diamine tetra acetic acid; APS, ammonium persulphate; NJUMARC, Model Animal Research Center of Nanjing University; H-T, HEPES-Tyrode; PAGE, polyacrylamide gel electrophoresis; PMSF, phenylmethanesulfonylfluoride; FASP, filter-aided sample preparation; TEAB, triethylammonium bicarbonate; CID, collision-induced dissociation; FDR, false discovery rate; TOF, time of flight; PPI, protein–protein interactions.

control, model, and drug samples. Differentially expressed proteins were selected for further bioinformatics analysis to determine the optimal target proteins. This work will help to understand the molecular mechanism of Neo-triggered relaxation of microvascular vessels and further reveal the biological activity of Neo.

MATERIALS AND METHODS

Main Instruments

The main instruments used in this study were described as below: Sartorius PB-10 pH meter (Sartorius, Germany); Evolution 200 Ultraviolet–Visible Spectrophotometer (Thermo Fisher Scientific, USA); BT25S Electronic Balance (Sartorius, Germany, d = 0.01 mg); Ultrapure Water Machine (Millipore, USA); Bio-Rad ChemiDoc XRS$^+$ System with Image Lab software and Bio-Rad Mini-Protean® Tetra system; DMI3000B Inverted Research Grade Microscope with Leica Application Suite V4.4.0 (Leica, Germany); 5427R Microcentrifuge (Eppendorf, Germany); Triple TOF 5600 Mass Spectrometer fitted with Eksigent NanoLC-Ultra 2D system, Nanospray III source, and Protein Pilot 5.0 software (AB SCIEX, MA, USA); and high-performance liquid chromatography (HPLC) system (Agilent 1200, USA).

Solutions and Drugs

Embryos of lotus seed were purchased from Bozhou Medical Material Market (Anhui China) and collected from Jiangxi province, and authenticated by Professor Yang Pan (Nanjing University of Chinese Medicine) according to the Chinese Pharmacopoeia. A voucher specimen (NENU-2010-AH-BZ) was deposited in the School of Pharmacy, Nanjing University of Chinese Medicine, Nanjing, Jiangsu, China. Neo was isolated from embryos of lotus seed (*Nelumbo nucifera* Gaertn) by our laboratory, whose structure was elucidated by spectral analyses, with the purity above 95% confirmed by HPLC peak area normalization method (Yang et al., 2018). Neo was dissolved in dimethyl sulfoxide (DMSO) solution at the concentration of 10 mM as mother solution before pharmacological use. Trichloroacetic acid (TCA), Trizma base (T1503), glycine (G8898), Tris base, sucrose, TEMED [$(CH_3)_2NCH_2CH_2N(CH_3)_2$], sodium dodecyl sulfate (SDS), and urea (U6504) were all products of Sigma Chemical Company. HEPES, glycerol, EDTA, ammonium persulfate [APS, $(NH_4)_2S_2O_8$], and bromophenol blue were purchased from Sangon Biotech Co., Ltd. (Shanghai, China).

The protease inhibitor phenylmethanesulfonylfluoride (PMSF) and dithiotheritol (DTT) used in protein extraction were from Sigma Chemical Company. The bicinchoninic acid (BCA) protein assay kit, rabbit antiphospho-mouse myosin regulatory light chain (primary antibody), and horseradish peroxidase conjugated goat antirabbit IgG (secondary antibody) were provided by Thermo Scientific (USA). The SuperBright™ Prolong ECL substrate was an approval Western blot detection kit by Sudgen Biotechnology Inc. for local package in China (Nanjing, China). The 30% acrylamide/Bis (29:1) and polyvinylidene difluoride (PVDF) membrane were from Bio-Rad Laboratories, Inc. (USA). ITRAQ® Reagents, 8-plex amine-modifying labeling reagents for multiplexed relative and absolute protein quantitation was a registered product of AB Sciex Pte. Ltd., MA (USA). Acetonitrile of HPLC grade was from Tedia Company Inc. (USA). Deionized water was purified by a Milli-Q Water Purification system (Millipore, MA, USA). Antibodies (primary antibody) to Plcβ and Arhgrf12 were purchased from Affinity Biosciences, Inc. (USA). β-Actin antibody (primary antibody) was obtained from Proteintech Group, Inc. (USA). Antirabbit IgG horseradish-peroxidase-linked antibody (secondary antibody) for all above samples was also from Proteintech Group, Inc. (USA). PVDF membranes were purchased from Millipore, Inc. (USA).

Animals, Animal Welfare, and Ethical Statement

About 8-week-old male or female C57BL/6J mice were kindly provided by the Model Animal Research Center of Nanjing University (NJUMARC, Nanjing, China). Animals were cage acclimated for 7 days before surgery in temperature-controlled environment (24 ± 3°C) on a 12-h light/12-h dark cycle, with food and water. All animal experiments were strictly performed in accordance with the Guidelines of Care and Use of Laboratory Animals of NJUMARC. Animal protocols were approved by the Nanjing University Institutional Animal Care and Use Committee of NJUMARC.

During the experimental procedures, all animals were clinically normal, free of any infection or inflammation, and did not show any neurological deficits. To minimize animal suffering, the test mice were killed by cervical dislocation before preparation of mesenteric arteries.

Preparation of Mesenteric Arteries

The second-order branches of mesenteric arteries were prepared from C57BL/6J mice of either gender (18–22 g body weight) by the successful operation as previously reported (He et al., 2011). In short, mice were killed by cervical dislocation, and the entire mesentery was rapidly removed and immersed in HEPES-Tyrode (H-T) buffer solution (pH 7.4) with the following composition (in mM): NaCl, 136.9; KCl, 2.7; $MgCl_2$, 1.0; $CaCl_2$, 1.8; HEPES, 10.0; and glucose, 5.09 (adjust pH to 7.4 with 2 M NaOH). The pH value was measured using a Sartorius PB-10 pH meter (Sartorius, Germany). About six second-order branches of mesenteric artery were separated from each mouse and cleaned of adventitial adipose and connective tissue under a stereoscopic microscope, cut into 6.0–8.0-mm-long segments. The integrity of contractile reactivity of the arteries was assessed by being exposed to 124 mM KCl for contraction, and the segments exhibiting no contraction were discarded. Then, the well-chosen segments were washed with H-T buffer to remove KCl for further use.

Measurement of Myosin Regulatory Light Chain Phosphorylation

Multiple signal networks have been implicated in regulation of smooth muscle contraction, in which Ca^{2+}/calmodulin-dependent myosin light chain kinase (MLCK) is central to smooth muscle contraction, and MLCK dedicatedly phosphorylates the

regulatory light chain (RLC) at Ser19 site (Kamm and Stull, 1985; Somlyo and Somlyo, 2000; Ogut and Brozovich, 2003; Herring et al., 2006; He et al., 2008; Hong et al., 2013).

Pretreatment of isolated tissues. In order to reduce the error caused by individual differences, six mesenteric segments of each mouse with contractility were assigned equally to control, model, and drug samples, i.e., two segments for each one. The three samples were prepared from 30 mice to obtain sufficient protein amounts. The normotonic segments cultivated in H-T buffer (pH 7.4) were the control sample; the segments stimulated by 124 mM KCl for 5 min to constrict the blood vessels were used as the model sample; while the contractile segments induced by KCl for 5 min and then treated by 10 μM of Neo for 10 min were the drug sample. All artery tissue samples were quickly frozen by liquid nitrogen and immersed in ice-chilled 10% trichloroacetic acid/acetone to immobilize. Samples must be used immediately or stored at −80°C until further experiments.

Protein preparation. The immobilized tissues prepared above were homogenized with a glass tissue grinder homogenizer on ice after transferring into 10% trichloroacetic acid/H_2O. The precipitated proteins were yielded by centrifugation and dissolved in urea sample buffer for protein determination by the BCA assay (Smith et al., 1985; Wiechelman et al., 1988).

RLC phosphorylation assay. The equal concentrations of proteins of the samples were loaded and separated by urea/glycerol polyacrylamide gel electrophoresis (PAGE) where the nonphosphorylated RLC would be detached from the monophosphorylated RLC (Isotani et al., 2004). At last, using a monoclonal antibody against myosin light chain, and then secondary antibody sequentially, both nonphosphorylated and monophosphorylated RLC protein were visualized after blotting. All the electrophoresis, membrane electro-transfer, and image formation were carried out in sequence on Bio-Rad Laboratory Instruments (USA) equipped with a Min-ROTEAN Tetra system, a trans-blot cell with wire electrodes and PowerPac HC Power Supply System, and a ChemiDoc XRS$^+$ System with Image Lab software. Western blot analyses were run with biological triplicates (n = 3). ImageJ software was applied to calculate the grayscale image, which was a public domain, Java-based image processing program developed at the National Institutes of Health (Collins, 2007; Schneider et al., 2012).

ITRAQ Analysis

ITRAQ has unique advantages over other conventional proteomics techniques because it identifies and quantifies many proteins from mammalian proteomes by sensitive mass spectrometers (Evans et al., 2012). However, the reliability and efficiency of protein identification and quantitation from an iTRAQ workflow strongly depend on sample preparation before MS (Luczak et al., 2014; Spanos and Moore, 2016). Here, we described our methods of sample treatment for iTRAQ analysis.

Sample design. The second-order branches of mesenteric artery were isolated from 45 mice to make the total protein contents of each sample as high as 100 μg. The samples were divided into control, model, and drug groups as described before. Two sets of parallel experiments were conducted for replication.

Protein extraction and total content determination. The immobilized artery segments were grinded into a fine powder in liquid nitrogen, and the tissue powder were suspended in 10% trichloroacetic acid/acetone solution containing 0.1% dithiotheritol (DTT) and 1 mM PMSF. The mix was placed at −20°C overnight and centrifuged at 15,000 rpm for 20 min at 4°C. The precipitate resuspended was in the same solvent. The mix was placed again at −20°C for 2 h and centrifuged in the same conditions. The sediment was freeze dried into powder in a refrigerated vacuum dryer. About 100 μg of protein was dissolved in 800 μl of lysis buffer (7 M urea, 2 M thiourea, 4% CHAPS, 65 mM DTT, 0.5% ampholyte, 1 mM PMSF). The supernatant was centrifuged at 15,000 rpm for 10 min at 4°C. Then, the supernatant was collected, and protein concentration was quantified by the Bradford method (Bio-Rad) (Bradford, 1976).

Protein alkylation, digestion, and labeling. For each sample, 100 μg of protein was dissolved in precooled acetone. The mix was set at −20°C for 1 h and centrifuged at 15,000 rpm for 20 min at 4°C. Peptides were generated by a modified filter-aided sample preparation (FASP) protocol (Wiśniewski et al., 2009). In short, the sediment of 100 μg of protein was dissolved in dissolution buffer and reduced with 5 mM of DTT at 60°C for 1 h, and then alkylated with 10 mM of iodoacetamide at 25°C in darkness for 40 min. After that, the protein sample was buffer exchanged with 200 μl of cysteine-blocking reagent, i.e., 0.5 M of triethylammonium bicarbonate (TEAB, pH 8.5), using a spin ultra-filtration unit of nominal molecular weight cutoff 10 kDa (Millipore, MA), and placed under room temperature for 10 min. Sequencing-grade modified trypsin (Promega) was added to each sample at an enzyme to protein ratio of 1:50, and the samples were incubated at 37°C for 16 h. Digested peptides were collected by centrifugation and quantified using a NanoDrop spectrophotometer.

ITRAQ labeling. ITRAQ method is based on the covalent labeling of the *N*-terminus and side chain amines of peptides from protein digestions with tags of varying masses (Ross et al., 2004; Zieske, 2006). We performed iTRAQ labeling using an iTRAQ 8-plex reagent kit. One hundred micrograms of digested samples was labeled and conducted in duplicates as follows: control 1→model 1→drug 1: tag 113, 115, and 118; control 2→model 2→drug 2: tag 119, 117, and 121.

Peptide fractionation, desaltation, and nano-LC-MS/MS determination. After being labeled, all samples were fractionated using Agilent 1200 HPLC with a strong cation-exchange column and further separated with an Eksigent NanoLC-Ultra 2D system (Zieske, 2006).

High strong cation-exchange reverse phase fractionation chromatography was carried out using an Agilent 1200 HPLC system with a quaternary pump, online degasser, autosampler, column temperature controller, ultraviolet detector (UV), and a fraction collection device. The mobile phase included parts A and B. Part A was 0.1% trifluoro acetic acid (TAA) water solution, and part B was 0.1% TAA CH_3CN solution. The iTRAQ-tagged tryptic peptides were load onto Poly-SEA C18 column (150 mm × 2.0 mm, 5 μm, 300 Å, Michrom, USA) and eluted with gradient 0–5% B in 5 min, 5–50% B in 35 min, 50–80% B in 5 min, and 80% B hold for 10 min at a flowrate of 0.3 ml/min. Absorbances

at 215 and 282 nm were monitored, and a total of 10 fractions were collected and vacuum dried.

Online separation was performed with an Eksigent NanoLC-Ultra system. Each of the fractions was dissolved in 0.1% TAA and then centrifuged at 15,000 rpm for 20 min. A volume of 5 μl of the supernatant was first loaded onto C18 precolumn (3 cm × 100 μm, 3 μm, 150 Å) to be desalted, then eluted on the analytical column (Chrom XP Eksigent C18, 15 cm × 75 μm, 3 μm, 120 Å, AB, USA) by a gradient with a linear increase of 5–35% B at a flowrate of 2 μl/min over 70 min. The mobile phase system was the same as mentioned above.

Protein identification and quantification. At the peptide level, the signals of the reporter ions of each MS/MS spectrum allow for calculating the relative abundance (ratio) of the peptide(s) identified by this spectrum. The abundance of the reporter ions may consist of more than one single signal in the MS/MS data, and the signals must be integrated in some way from the histogram spectrum. At the protein level, the combined ratios of a protein's peptides represent the relative quantification of that protein (Zieske, 2006).

Data-dependent MS/MS was performed with a Triple TOF 5600 System fitted with Nanospray III source and pulled quartz tip as the emitter (New Objectives, USA). The electrospray voltage applied was 2.5 kV, curtain gas of 30 psi, nebulizer gas of 5 psi, and an interface heater temperature of 150°C. For information-dependent acquisition (IDA), survey scans were acquired in 250 ms, and as many as 35 product ion scans were collected if they exceeded a threshold of 150 counts per second (counts/s) with a two to five charge state. The total cycle time was fixed to 2.5 s. A rolling collision energy setting was applied to all precursor ions for collision-induced dissociation (CID). Dynamic exclusion was set for 1/2 of peak width (18 s), and the precursor was then refreshed off the exclusion list.

ITRAQ Data Analysis

Raw data were analyzed by Protein Pilot software v.5.0 against the database using the Paragon algorithm (Shilov et al., 2007). The iTRAQ data processed with protein identification was performed using the Uniport Database (update to June 12th, 2017, including 267,091 protein sequences). Searching parameters were as follows: trypsin was chosen as the enzyme with allowance at most two-missed cleavage; Gln→pyro-Glu (*N*-terminus Q), oxidation (M), deamidated as the potential variable modifications, and carbamidomethyl (C), iTRAQ 8-plex (*N*-terminus), iTRAQ 8-plex (K) as fixed modifications; a mass tolerance of 10 ppm was permitted for intact peptide mass and 0.02 Da for fragmented ions. The instrument was Triple TOF 5600, and iTRAQ quantification and biological modifications were selected as ID focus.

A Percolator algorithm was applied to estimate the false discovery rate (FDR) based on q-value, and only peptides with FDR values <1% were counted as the identified protein. For protein quantitation, one protein had to contain at least one unique peptide during the search, and peptides at the 95% confidence interval were considered for further analysis. The protein abundance perturbations were further confidently assessed by setting unused value ≥1.3.

A three-step process was performed in two biological replicates to screen differential abundance proteins (DAPs) (EF < 3). When the fold change was more than 1.5 in the model sample compared to the control one, the DAPs were predicated to be upregulated significantly. Then, by setting threshold of 0.7-fold decrease in drug/model samples, these upregulated DAPs were confirmed to be downregulated through Neo treatment. Finally, these downregulated proteins were expected to reach almost normal or lower levels in drug/control samples.

Bioinformatic Analysis of DAPs

KEGG is a knowledge base for systematic analysis of gene functions, linking genomic information with higher order functional information (Kanehisa and Goto, 2000; Kanehisa et al., 2016). KEGG databases are daily updated and freely available (http://www.genome.ad.jp/kegg/) (Kanehisa et al., 2017). In the present study, KEGG pathway analysis was employed to analyze the selected DAPs.

Western Blot Analysis

Protein samples of the three groups, i.e., the control, model, and drug groups, were subjected to SDS-PAGE. After being separated, proteins in samples were transferred to PVDF transfer membranes (Millipore, Inc. USA) by standard procedures. After being blocked with 3% bovine serum albumin in PBS for 1.5 h at 37°C, the membranes were incubated with primary antibody overnight at 4°C and secondary antibody (Proteintech Group, Inc. USA) sequentially at room temperature for 2 h. After washing, the blots were detected with ECL substrate (Millipore, Bedford, MA). Immunoreactive protein bands were detected with Tanon 5200 Chemiluminescence imaging system (Shanghai, China). β-Actin was chosen as the internal marker. The band intensities were quantified with ImageJ software. All experiments reported here were performed with at least triplicate independent replicates.

Datum Calculation and Statistical Analysis

Data are expressed as mean ± SEM of different experiments with more than three replicated measurements. The statistical analyses of differences among group means were obtained by analysis of one-way analysis of variance (ANOVA) (Fisher, 1918), taking $P < 0.05$ as significant according to Tukey's multiple comparison test.

RESULTS

The Decrease in RLC Phosphorylation by Neo

The morphological characters of the three mesenteric capillary samples, i.e., normotonic capillaries (control group), contractive capillaries evoked by 124 mM KCl (model group) for 5 min, and Neo-treated contractive capillaries (drug group), were observed using stereoscopy (**Figure 2A**). And urea/glycerol PAGE electrophoresis showed that RLC phosphorylation (p-RLC) changes shifted quite visibly among the control, model, and

drug groups (**Figure 2B**). The grayscale values calculated by image analysis system were well consistent with the results of Western blot as seen from the figure above. The p-RLC value of normal tension mesenteric arteries was almost zero without the presence of p-RLC protein bands. Thus, compared with the control sample, the RLC phosphorylation band of the model sample was observed clearly, and p-RLC protein level was extremely increased to 47.39% ($n = 3$, $P < 0.001$). On the other hand, the p-RLC of the drug sample was dramatically decreased to very a low level at 13.48% as compared to the model one ($n = 3$, $P < 0.001$) (**Figure 2C**), suggesting that neoliensinine relaxed smooth muscle by inhibiting the signaling converging on Ca^{2+}/calmodulin-dependent MLCK, or activating the countered enzyme MLCP, a serine/threonine-specific protein phosphatase that dephosphorylated p-RLC.

The second-order branches of mesenteric arteries were prepared from C57BL/6J mice of either gender. The mesenteric capillaries of each mouse were equally divided into three groups, i.e., normotonic capillaries (Control), contractive capillaries evoked by 124 mM KCl for 5 min (Model), and Neo-treated contractive capillaries (Drug) (**A**). All samples were quickly frozen and immobilized for protein sample preparation. RLC phosphorylation was measured by Western blot of urea/glycerol PAGE gels, and the ImageJ method was used to analyze the grayscale image (**B**). The gray values were the means ± SEM of three independent experiments ($n = 3$). Bars with different symbols indicated significant differences according to one-way analysis of variance, Tukey's multiple comparison test. The RLC phosphorylation of the control group was almost zero. Thus, compared with the control sample, the RLC phosphorylation of the model group was extremely increased (***, $P < 0.001$), while the RLC phosphorylation of the drug group was dramatically decreased to very low level as compared with the model one (###, $P < 0.001$) (**C**), suggesting that neoliensinine relaxed smooth muscle by inhibiting the signaling converging on Ca^{2+}/calmodulin-dependent MLCK. Blue squares represented the grayscale values of the unphosphorylated RLC, and red squares represented those of the phosphorylated RLC.

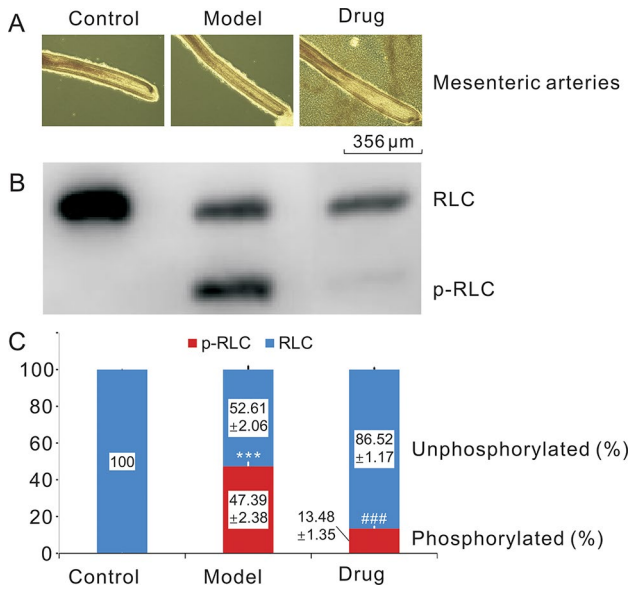

FIGURE 2 | Relaxing smooth muscle and reducing RLC phosphorylation effects of neoliensinine on microvascular constriction. **(A)** Mesenteric arteries of three groups, **(B)** RLC phosphorylation by Western blot, **(C)** histogram of RLC phosphorylation. ***$P < 0.001$ and ###$P < 0.001$.

Screening the Differential Abundance Proteins

An iTRAQ-based shotgun quantitation analysis was used to obtain the overall view of proteomic expression patterns of three experimental groups, including control, model, and drug groups. As a result, a total of 3,934 proteins in the control group were identified with <1% FDR, and 3,474 protein abundance perturbations were confidently assessed by setting unique peptide ≥1 and unused value ≥1.3 (**Supplementary Tables S1 and S2**). With a cutoff threshold of >1.5-fold change for increase and <0.7-fold change for decrease, 302 proteins showed differential accumulation in model/control samples, including 164 proteins upregulated and 138 proteins downregulated after KCl stimulation (**Supplementary Tables S3 and S4**). The 138 downregulated proteins were not further analyzed here and will be covered separately in the next article. In the case of the 164 upregulated proteins, 33 were decreased differentially by adoption of <0.7-fold in drug/model samples (**Supplementary Table S5**). Among the 33 downregulated proteins in drug/control samples, although expressions of 17 proteins remained to be higher than 1.5-fold of that of control group, expressions of 16 proteins were at normal or lower levels (**Table 1**), suggesting that Neo could interfere with these protein expressions significantly so as to relax vascular smooth muscle contracted by KCl.

Top 10 Key Pathways Based on the 16 DAPs

To narrow the molecular targets and make them more specific, the top 10 key pathways were extracted by KEGG pathway enrichment based on the 16 significant differential proteins selected before. They were classified into 10 functional categories as follows: platelet activation, vascular smooth muscle contraction, protein processing in endoplasmic reticulum (all $P < 0.01$), pathways in cancer, African trypanosomiasis, endocrine and other factor-regulated calcium reabsorption, long-term depression, long-term potentiation, renin secretion, and inositol phosphate metabolism (all $P < 0.05$) (**Figure 3**). There were only four proteins involved in the top 10 key pathways, and PLCβ and RhoGEF12 played a collective role in mediating processes of vascular smooth muscle contraction.

The top 10 key pathways (or biological processes) were extracted by KEGG pathway enrichment. The bars were colored with gradient color from deep blue (smaller P value) to sea blue (bigger P value), which represented the following: function 1, platelet activation; function 2, vascular smooth muscle contraction; function 3, protein processing in endoplasmic reticulum ($P < 0.01$); function 4, pathways in cancer; function 5,

African trypanosomiasis; function 6, endocrine and other factor-regulated calcium reabsorption; function 7, long-term depression; function 8, long-term potentiation; function 9, renin secretion; and function 10: inositol phosphate metabolism ($P < 0.05$). Our analysis revealed that two proteins PLCβ and RhoGEF12 were mainly involved in vascular smooth muscle contraction.

Protein Expressions of PLCβ and RhoGEF12 by Western Blot

The relative expressions of two target proteins, PLCβ and RhoGEF12, in control, model, and drug samples were analyzed by Western blot. **Figure 4** showed that the relative PLCβ and RhoGEF12 expressions were significantly increased in model group compared to those in control group, while they were notably decreased after exposure to Neo in drug samples compared to those in the model group. Thus, we concluded that treatment of Neo could decrease abnormally increased protein expressions of PLCβ and RhoGEF12 in smooth muscles simulated by KCl, which was consistent with the above iTRAQ results.

All samples were quickly frozen and immobilized for protein sample preparation. Protein expressions of PLCβ and RhoGEF12 were measured by Western blot of SDS-PAGE gels, and the ImageJ method was used to analyze the gray scale image (**A**). The gray values were the means ± SEM of three independent experiments ($n = 3$). Bars with different symbols indicated significant differences according to one-way analysis of variance (ANOVA), Tukey's multiple comparison test. Compared with the control sample, the expressions of PLCβ and RhoGEF12 in the model group was extremely increased (**, $P < 0.01$). On the other hand, the two protein expressions in the drug group were dramatically decreased as compared with the model one (#, $P < 0.05$), suggesting that neoliensinine relaxed smooth muscle by inhibiting the expressions of PLCβ and RhoGEF12.

TABLE 1 | Significant differential abundance proteins in microvascular smooth muscles contracted by high potassium with or without Neo treatment.

No.	Accession	Description	Gene name	Coverage%	Unique peptides	Model/Control[a]		Drug/Model[a]		Drug/Control[a]	
						Ratio	Trend[b]	Ratio	Trend[b]	Ratio	Trend[b]
1	B2RTM0|B2RTM0	Histone H4	Hist2h4	75.73	26	4.0878	+	0.6009	–	1.1934	=
2	Q8C7E4|Q8C7E4	Ribonuclease 4	Rnase4	47.97	5	1.8118	+	0.4053	–	0.8918	=
3	Q3TML0|Q3TML0	Protein disulfide-isomerase A6	Pdia6	39.33	21	1.7278	+	0.5197	–	0.8679	=
4	Q542P5|Q542P5	Carbonyl reductase 2, isoform CRA_b	Cbr2	56.15	16	1.8813	+	0.4372	–	0.8644	=
5	Q545V2|Q545V2	Protein S100	S100a4	41.58	4	3.2510	+	0.1462	–	0.8438	=
6	F8VQN6|F8VQN6	Rho guanine nucleotide exchange factor 12	Arhgef12	19.56	6	1.7119	+	0.4244	–	0.8390	=
7	Q571M2|Q571M2	MKIAA4025 protein (Fragment)	Hspa4	63.23	45	2.2777	+	0.5193	–	0.8136	=
8	F6XC54|F6XC54	Protein diaphanous homolog 1	Diaph1	24.10	14	1.8690	+	0.4649	–	0.7608	=
9	Q542X9|Q542X9	Superoxide dismutase [Cu–Zn]	Sod3	70.52	27	1.9040	+	0.3802	–	0.7293	=
10	Q3UKV0|Q3UKV0	Protein Eif2b3	Eif2b3	23.60	3	1.5633	+	0.4900	–	0.7169	=
11	Q3T9Z2|Q3T9Z2	Glyoxylate reductase/ hydroxy pyruvate reductase	Grhpr	49.09	12	2.3454	+	0.5056	–	0.6958	–
12	Q921W7|Q921W7	Putative uncharacterized protein Tes	Tes	36.75	8	3.5798	+	0.4937	–	0.6931	–
13	E3VRY6|E3VRY6	Large conductance Ca^{2+}-activated potassium channel ERL variant 4	Kcnma1	12.04	1	44.913	+	0.3659	–	0.6795	–
14	Q91UZ1|Q91UZ1	Phosphoinositide phospholipase C	Plcb4	40.34	21	2.0192	+	0.3706	–	0.4815	–
15	Q6NXL1|Q6NXL1	Protein Sec24d	Sec24d	26.45	11	3.5485	+	0.5153	–	0.4740	–
16	Q58EU7|Q58EU7	Rbp1 protein	Rbp1	78.52	18	3.5583	+	0.5040	–	0.3738	–

[a]*Model/control: the average ratios for model→control; drug/model: the average ratios for drug→model; drug/control: the average ratios for drug→control.*

[b]*+: by adoption of ratio >1.5-fold for upregulated cutoff values; –: by adoption of ratio <0.7-fold for downregulated cutoff values; =: by adoption of ratio <1.5-fold and >0.7-fold, not significantly changed.*

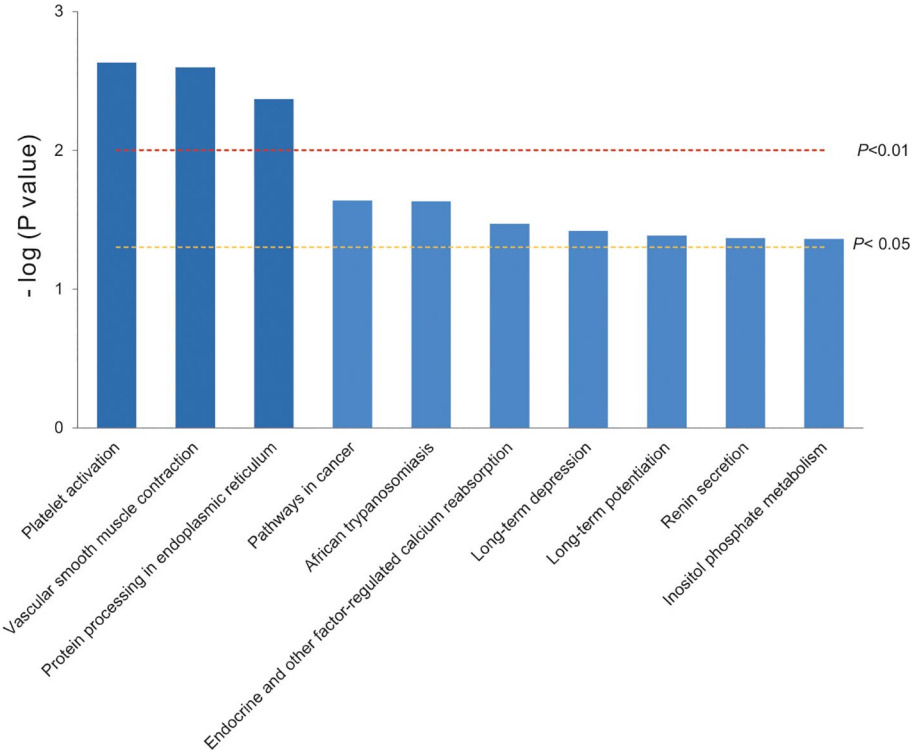

FIGURE 3 | The 10 key pathways extracted by KEGG pathway enrichment based on the 16 DAPs.

DISCUSSION

As we reported earlier, once KCl is added to mesenteric smooth muscle (SM), its initial contraction was characterized by rapid contraction and periodic relaxation. After only few seconds, SM entered a phase of sustained contraction tonically until neoliensinine was given at sufficient concentration. KCl stimulation for 5 min could achieve the optimal stable tension of SM and significantly increase the phosphorylation level of MLC20 in sustained phase (Yang et al., 2018). Based on these results, KCl was used to stimulate vessels for 5 min in subsequent experiments, and samples were collected for proteomics analyses to analyze changes in protein expression.

The phosphorylated regulatory light chains (p-RLC) regulated by myosin light-chain kinase (MLCK) was a crucial link in SM contraction, and decreasing or eliminating p-RLC may cause them to relax. We also demonstrated that RLC phosphorylation of contractive capillary SM increased significantly under KCl inducement and then decreased sharply to normal level after neoliensinine (Neo) treatment. The result indicated that Neo relaxed SM by inhibiting the convergence of Ca^{2+}/calmodulin-dependent MLCK signals. However, little is known about the details and molecular mechanisms. Our study used LC-MS/MS for iTRAQ proteomic analysis to explore and quantify dysregulated proteins in contractive mesenteric capillaries. Compared with other proteomics methods, it is a mature and high-throughput proteomics technique (Xu et al., 2014), and relative quantification of eight samples can be achieved

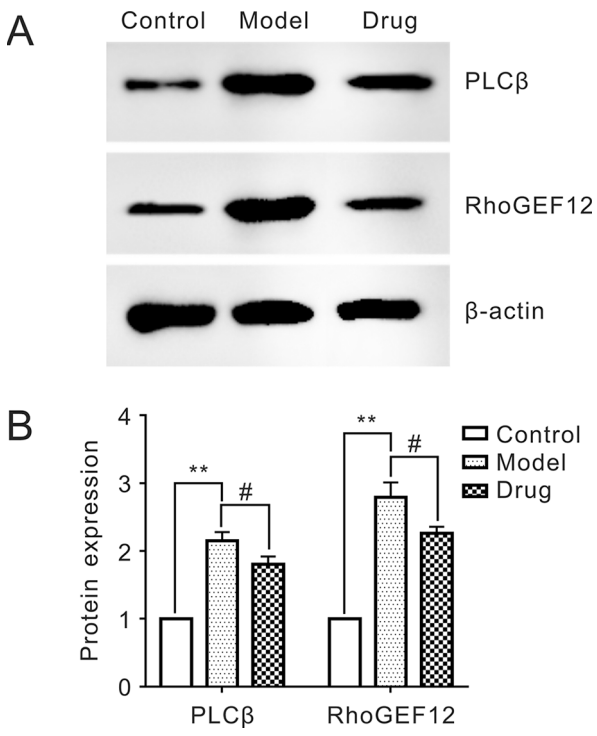

FIGURE 4 | Reducing expressions of PLCβ and RhoGEF12 of neoliensinine in mesenteric arteries contracted by KCl. **(A)** Protein expressions of PLCβ and RhoGEF12 by Western blot, **(B)** histogram of protein expressions of PLCβ and RhoGEF12. $^{**}P < 0.01$ and $^{\#}P < 0.05$.

simultaneously (Xu et al., 2017). Therefore, we designed three experimental groups to screen differential abundance proteins (DAPs) in mouse mesenteric capillaries: blank control group (control), high K-stimulation group (model), and KCl-inducement and Neo-treatment group (drug).

The important criterion for screening DAPs can be set by *P* value or error factor (EF). We selected EF to screen out DAPs. The closer EF gets to 1, the more reliable the result is. Generally, EF< 3 is a good result. In this MS, we chose EF< 3 as the criterion. As a result, based on the criterion of |fold change (FC)|≥1.5, 164 upregulated DAPs were found in the 3,474 protein abundance perturbations identified in model/control samples, among which 33 downregulated DAPs were filtered out in drug/model samples with a cutoff value of 0.7-fold. Of the 33 converging DAPs, only 16 DAPs (including 10 normal DAPs and 6 downregulated DAPs) were recommended for use as specific targets for Neo treatment in drug/model samples, which may be involved in Neo-mediated microvascular relaxation for further bioinformatics analysis. The results of both intragroup replicate and repetitive assessment showed that our results were fairly reproducible between comparisons.

Analysis of KEGG pathway clearly shows that the two candidate proteins, PLCβ and RhoGEF12, are involved in vascular smooth muscle contraction, which is consistent with the results of molecular mechanism research on Neo-mediated relaxation effect on KCl-induced small vessel contraction.

Smooth muscle can phasically contract with rapid contraction and relaxation or tonically with slow and sustained contraction (Aguilar and Mitchell, 2010). Normally, phosphorylation of RLC is initiated by MLCK at the initial phase of microvessel contraction and maintained by protein G activation of RhoA *via* RhoGEFs during sustained contraction. PLCβ acting as an upstream MLCK regulator, while RhoGEF12 acting as a member of RhoGEFs, play vital roles in initial and sustained phases of SM contraction, respectively. KCl-induced SM contraction is mainly performed through L-type calcium channel. Meanwhile, the activation of PLCβ and RhoGEF12 by KCl may be due to partial activation of GPCR *via* stimulation of Rho and ROCK (Janssen et al., 2004). The two proteins associated with RLC phosphorylation signaling pathway are further discussed below.

PLCβ isozymes are expressed in SM cells, which are activated by binding of its *C*-terminal or *N*-terminal pleckstrin homology (PH) domain to protein G (Rhee, 2001). Phosphatidylinositol 4,5-bisphosphate (PIP2) is the predominant phosphoinositide substrate hydrolyzed by PLCβ, resulting in the formation of diacylglycerol (DAG) and a diffusible Ca^{2+}-mobilizing messenger, inositol 1,4,5-trisphosphate (IP3) (Murthy and Makhlouf, 1991). Activation of PLCβ is transient (<2 min), mainly occurring in the initial phase of contraction (Murthy and Makhlouf, 1995; Murthy, 2006). Inhibition of IP_3 formation and IP_3-dependent Ca^{2+} results in the relaxation of initial Ca^{2+}-dependent contraction (Gohla et al., 2000).

Protein G-coupled receptors (GPCRs) can activate Rho/Rho-kinase, which inhibits the activity of myosin phosphatase (MLCP) through signal cascade reaction, while the increase in phosphorylated myosin (p-MLC) leads to sustained contraction of smooth muscle (Somlyo and Somlyo, 1994; Gohla et al., 2000; Tang et al., 2003). RhoA exists in two forms, the inactive and active ones. The inactive form of RhoA (RhoA. GDP) in the cytosol bound to a guanine dissociation inhibitor (GDI), and the activation of RhoA by protein G is mediated by various Rho-specific guanine nucleotide exchange factors (RhoGEFs). RhoGEFs promote the transformation of GDP to GTP, thereby activating RhoA, triggering the downstream signaling pathway, and causing continuous contraction of smooth muscle (García-Mata et al., 2006). Therefore, if the activity of RhoGEFs is blocked, the dephosphorylation of MLCP will be enhanced to cause smooth muscle relaxation.

Neoliensinine may relax vascular smooth muscle relaxation through blocking PLCβ expression in initial phase and RhoGEF12 expression in sustained phase, which also well explains the weak reversible (or nearly irreversible) relaxation effect of Neo. One possible explanation for the changes in protein expression is that KCl induces PLCβ (or RhoGEF12) activation in GPCR pathway, and the activated PLCβ (or RhoGEF12) are transferred to the membrane. The activated PLCβ (or RhoGEF12) is more easily dissolved and detected by iTRAQ analysis, while the treatment of neoliensinine makes both proteins inactive, and the inactivated PLCβ and RhoGEF12 are not easy to be dissolved and detected.

The iTRAQ proteomics analysis is intended to explore and semiquantify proteins of interest. Compared with other proteomics methods, it is a mature and high-throughput proteomics technique. In our study, the relative quantification of eight samples can be achieved simultaneously. Western blot is a technique that quantifies specific proteins in samples based on image analysis, and ImageJ software was used to analyze the grayscale image. It is inevitable that data from different methods may not be completely consistent. The samples for iTRAQ analysis and Western blot were from different mice, which may also lead to differences in the data from the two methods. However, the data trends of the two methods were the same, which could reasonably explain the protein changes of model/control group, drug/model group, and drug/control group.

CONCLUSION

In conclusion, neoliensinine can effectively relax constricted vascular smooth muscle (SM) by KCl hyperpolarization *via* downregulating p-RLC of microvessels. Through iTRAQ screening, we focused specifically on two target proteins, PLCβ or/and RhoGEF12; the two upstream factors may cause nonphosphorylation of RLC in initial phase and dephosphorylation of RLC in sustained phase, respectively. Western blot also confirmed the two selective target DAPs at the protein level, indicating that the change trend of the two proteins was consistent with that of iTRAQ results.

Our present work reveals that Neo inhibits RLC phosphorylation and relaxes vascular SM, and PLCβ and RhoGEF12 may be potential biomarkers for evaluating the effects mediated by Neo. The two underlying targets may provide new drug strategies for the treatment of SM-related diseases. However, it is still necessary to study the exact molecular mechanism of

neoliensinine-mediated microvascular SM relaxation using genetic materials.

DATA AVAILABILITY

All datasets generated for this study are included in the manuscript and the **Supplementary Files**.

ETHICS STATEMENT

This study was carried out in accordance with the recommendations of Guidelines of Care and Use of Laboratory Animals of NJUMARC, Nanjing University Institutional Animal Care and Use Committee of NJUMARC. The protocol was approved by the Nanjing University Institutional Animal Care and Use Committee of NJUMARC.

AUTHOR CONTRIBUTIONS

G-MY, J-LZ, and Z-HP performed experiments; G-MY, KY, PW, J-LZ, and YP analyzed data and conceptualized the work; and G-MY, KY, PW, and YP wrote the manuscript.

FUNDING

This research was supported by the National Natural Science Foundation of China (Grant Nos. 81373295 and 81473420), the Project Funded by the Priority Academic Program Development of Jiangsu Higher Education Institutions (PAPD), and the Top-notch Academic Programs Project of Jiangsu Higher Education Institutions (TAPP).

ACKNOWLEDGMENTS

The authors wish to thank Dr. Jie Sun of the Model Animal Research Center and MOE Key Laboratory of Animal Models of Disease for guidance of the smooth muscle relaxation related experiment, and Mr. Yun-Hui Zhang of Nanjing Heyelan Biotechnology Company for iTRAQ technical supports.

SUPPLEMENTARY MATERIAL

The Supplementary Material for this article can be found online at: https://www.frontiersin.org/articles/10.3389/fphar.2019.00979/full#supplementary-material

REFERENCES

Aguilar, H. N., and Mitchell, B. F. (2010). Physiological pathways and molecular mechanisms regulating uterine contractility. *Hum. Reprod. Update* 16, 725–744. doi: 10.1093/humupd/dmq016

Bradford, M. M. (1976). A rapid and sensitive method for the quantitation of microgram quantities of protein utilizing the principle of protein-dye binding. *Anal. Biochem.* 72, 248–254. doi: 10.1016/0003-2697(76)90527-3

China Pharmacopoeia Committee. (2015). *Chinese Pharmacopoeia*, vol. 1. (Beijing, China: Chinese Medical Science and Technology Press), 273–276.

Christopher, H. (2009). Asthma. *N. Engl. J. Med.* 360, 1002–1014. doi: 10.1056/NEJMra0804579

Collins, T. J. (2007). ImageJ for microscopy. *Biotechniques* 43, 25–30. doi: 10.2144/000112517

Fisher, R. A. (1918). "The correlation between relatives on the supposition of Mendelian inheritance," in *In Philosophical Transactions of the Royal Society of Edinburgh*. (Cambridge: Cambridge University Press), 399–433. doi: 10.1017/S0080456800012163

García-Mata, R., Wennerberg, K., Arthur, W. T., Noren, N. K., Ellerbroek, S. M., and Burridge, K. (2006). Analysis of activated GAPs and GEFs in cell lysates. *Method Enzymol.* 406, 425–437. doi: 10.1016/S0076-6879(06)06031-9

Gohla, A., Schultz, G., and Offermanns, S. (2000). Role for G12/G13 in agonist-Induced vascular smooth muscle cell contraction. *Circ. Res.* 87, 221–227. doi: 10.1161/01.RES.87.3.221

Hartshorne, D. J., and Ito, M. (1998). Myosin light chain phosphatase: subunit composition, interactions and regulation. *J. Muscle Res. Cell Motil.* 19, 325–341. doi: 10.1023/A:1005385302064

He, W. Q., Peng, Y. J., Zhang, W. C., Ning, L. V., Tang, J., Chen, C., et al. (2008). Myosin light chain kinase is central to smooth muscle contraction and required for gastrointestinal motility in mice. *Gastroenterology* 135, 610–620. doi: 10.1053/j.gastro.2008.05.032

He, W. Q., Qiao, Y. N., Zhang, C. H., Peng, Y. J., Chen, C., Wang, P., et al. (2011). Role of myosin light chain kinase in regulation of basal blood pressure and maintenance of salt-induced hypertension. *Am. J. Physiol.-Heart Circ. Physiol.* 301, H584–H591. doi: 10.1152/ajpheart.01212.2010

Heinze, C., Seniuk, A., Sokolov, M. V., Huebner, A. K., Klementowicz, A. E., Szijártó, I. A., et al. (2014). Disruption of vascular Ca2+-activated chloride currents lowers blood pressure. *J. Clin. Invest.* 124, 675–686. doi: 10.1172/JCI70025

Herbrich, S. M., Cole, R. N., West, K. J., Schulze, K., and Yager, J. D. (2013). Statistical inference from multiple iTRAQ experiments without using commonreference standards. *J. Proteome Res.* 12, 594–604. doi: 10.1021/pr300624g

Herring, B. P., El-Mounayri, O., Gallagher, P. J., Yin, F., and Zhou, J. L. (2006). Regulation of myosin light chain kinase and telokin expression in smooth muscle tissues. *Am. J. Physiol. Cell Physiol.* 291, C817–C827. doi: 10.1152/ajpcell.00198.2006

Hong, F., Facemyer, K. C., Carter, M. S., Jackson, D. R., Haldeman, B. D., Ruana, N., et al. (2013). The kinetics of myosin light chain kinase activation of smooth muscle myosin in an *in vitro* model system. *Biochemistry* 52, 1–23. doi: 10.1021/bi401001x

Isotani, E., Zhi, G., Lau, K. S., Huang, J., Mizuno, Y., Persechini, A., et al. (2004). Real-time evaluation of myosin light chain kinase activation in smooth muscle tissues from a transgenic calmodulin-biosensor mouse. *Proc. Natl. Acad. Sci. U. S. A.* 101, 6279–6284. doi: 10.1073/pnas.0308742101

Itoh, A., Saitoh, T., Tani, K., Uchigaki, M., Sugimoto, Y., Yamada, J., et al. (2011). Bisbenzylisoquinoline alkaloids from *Nelumbo nucifera*. *Chem. Pharm. Bull.* 59, 947–951. doi: 10.1248/cpb.59.947

Janssen, L. J., Tazzeo, T., Zuo, J., Pertens, E., and Keshavjee, S. (2004). KCl evokes contraction of airway smooth muscle *via* activation of RhoA and Rho-kinase. *Am. J. Physiol. Lung Cell Mol. Physiol.* 287, L852–L858. doi: 10.1152/ajplung.00130.2004

Kamm, K. E., and Stull, J. T. (1985). The funtion of myosin and myosin light chain kinase phosphorylation in smooth muscle. *Ann. Rev. Phamacol. Toxicol.* 25, 593–620. doi: 10.1146/annurev.pa.25.040185.003113

Kanehisa, M., Furumichi, M., Tanabe, M., Sato, Y., and Morishima, K. (2017). KEGG: new perspectives on genomes, pathways, diseases and drugs. *Nucleic Acids Res.* 45, D353–D361. doi: 10.1093/nar/gkw1092

Kanehisa, M., and Goto, S. (2000). KEGG: Kyoto encyclopedia of genes and genomes. *Nucleic Acids Res.* 28, 27–30. doi: 10.1093/nar/28.1.27

Kanehisa, M., Sato, Y., Kawashima, M., Furumichi, M., and Tanabe, M. (2016). KEGG as a reference resource for gene and protein annotation. *Nucleic Acids Res.* 44, D457–D462. doi: 10.1093/nar/gkv1070

Khare, C. P. (2004). *Indian herbal remedies: rational western therapy ayurvedic and other traditional usage*. NY, USA: Springer Science and Business Media. doi: 10.1007/978-3-642-18659-2

Landry, Y., and Gies, J. P. (2008). Drugs and their molecular targets: an updated overview. *Fund. Clin. Pharmacol.* 22, 1–18. doi: 10.1111/j.1472-8206.2007.00548.x

Li, P., Yang, G. M., Zhang, Y. L., Gu, Z. Y., Li, M., and Pan, Y. (2016). Isolation and identification of the lipopholic alkaloids of embryo loti. *J. Food Sci. Biotech*. 35, 19–27. doi: 10.3969/j.issn.1673-1689.2016.01.003

Luczak, M., Marczak, L., and Stobiecki, M. (2014). Optimization of plasma sample pretreatment for quantitative analysis using iTRAQ labeling and LC-MALDI-TOF/TOF. *Plos One* 9, e101694. doi: 10.1371/journal.pone.0101694

Mak, G., and Hanania, N. A. (2012). New bronchodilators. *Curr. Opin. Pharmacol.* 12, 238–245. doi: 10.1016/j.coph.2012.02.019

Murthy, K. S. (2006). Signaling for contraction and relaxation in smooth muscle of the gut. *Annu. Rev. Physiol.* 68, 345–374. doi: 10.1146/annurev.physiol.68.040504.094707

Murthy, K. S., and Makhlouf, G. M. (1991). Phosphoinositide metabolism in intestinal smooth muscle: preferential production of Ins (1, 4, 5)P3 in circular muscle cells. *Am. J. Physiol.* 261, G945–G951. doi: 10.1152/ajpgi.1991.261.6.G945

Murthy, K. S., and Makhlouf, G. M. (1995). Functional characterization of phosphoinositide-specific phospholipase C-β1and -β3 in intestinal smooth muscle. *Am. J. Physiol. Lung Cell* 269, C969–C978. doi: 10.1152/ajpcell.1995.269.4.C969

Ogut, O., and Brozovich, F. V. (2003). Regulation of force in vascular smooth muscle. *J. Mol. Cell. Cardiol.* 35, 347–355. doi: 10.1016/S0022-2828(03)00045-2

Overington, J. P., Al-Lazikani, B., and Hopkins, A. L. (2006). How many drug targets are there? *Nat. Rev. Drug Disco.* 5, 993–996. doi: 10.1038/nrd2199

Qian, J. Q. (2002). Cardiovascular pharmacological effects of bisbenzylisoquinoline alkaloid derivatives. *Acta Pharmacol. Sin.* 23, 1086–1092.

Qiao, Y. N., He, W. Q., Chen, C. P., Zhang, C. H., Zhao, W., Wang, P., et al. (2014). Myosin phosphatase target subunit 1 (MYPT1) regulates the contraction and relaxation of vascular smooth muscle and maintains blood pressure. *J. Biol. Chem.* 289, 22512–22523. doi: 10.1074/jbc.M113.525444

Rang, H. P., Dale, M. M., Ritter, J. M., Flower, R. J., and Henderson, G. (2012). *Rang and Dale's Pharmacology*. Edinburgh, New York: Elsevier/Churchill Livingstone. doi: 10.1016/B978-0-7020-3471-8.00001-9

Rhee, S. G. (2001). Regulation of phosphoinositide-specific phospholipase C. *Annu. Rev. Biochem.* 70, 281–312. doi: 10.1146/annurev.biochem.70.1.281

Ross, P. L., Huang, Y. N., Marchese, J. N., Williamson, B., Parker, K., Hattan, S., et al. (2004). Multiplexed protein quantitation in *Saccharomyces cerevisiae* using amine-reactive isobaric tagging reagents. *Mol. Cell. Proteomics* 3, 1154–1169. doi: 10.1074/mcp.M400129-MCP200

SATCM, B., E., and Z, H. B. C. (1999). Zhong Hua Ben Cao, Vol 3 (Shanghai, China: Shanghai Science and Technology Press).

Schneider, C. A., Rasband, W. S., and Eliceiri, K. W. (2012). NIH Image to ImageJ: 25 years of image analysis. *Nat. Methods* 9, 671–675. doi: 10.1038/nmeth.2089

Sharma, B. R., Gautam, L. N., Adhikari, D., and Karki, R. (2017). A comprehensive review on chemical profiling of *Nelumbo nucifera*: potential for drug development. *Phytother. Res.* 31, 3–26. doi: 10.1002/ptr.5732

Shen-Miller, J., Schopf, J. W., Harbottle, G., Cao, R. J., Ouyang, S., Zhou, K. S., et al. (2002). Long-living lotus: germination and soil-irradiation of centuries-old fruits, and cultivation, growth, and phenotypic abnormalities of offspring. *Am. J. Bot.* 89, 236–247. doi: 10.3732/ajb.89.2.236

Shilov, I. V., Seymour, S. L., Patel, A. A., Loboda, A., Tan, W. H., Keating, S. P., et al. (2007). The paragon algorithm, a next generation search engine that uses sequence temperature values and feature probabilities to identify peptides from tandem mass spectra. *Mol. Cell. Proteomics* 6, 1638–1655. doi: 10.1074/mcp.T600050-MCP200

Smith, P. K., Krohn, R. I., Hermanson, G. T., Mallia, A. K., Gartner, F. H., Provenzano, M. D., et al. (1985). Measurement of protein using bicinchoninic acid. *Anal. Biochem.* 150, 76–85. doi: 10.1016/0003-2697(85)90442-7

Somlyo, A. P., and Somlyo, A. (2000). Signal transduction by G-proteins, Rho-kinase and protein phosphatase to smooth muscle and non-muscle myosin II. *J. Physiol.* 522, 177–185. doi: 10.1111/j.1469-7793.2000.t01-2-00177.x

Somlyo, A. P., and Somlyo, A. V. (1994). Signal transduction and regulation in smooth muscle. *Nature* 372, 812–813. doi: 10.1038/372812a0

Spanos, C., and Moore, J. B. (2016). Sample preparation approaches for iTRAQ labeling and quantitative proteomic analyses in systems biology. *Methods Mol. Biol.* 1394, 15–24. doi: 10.1007/978-1-4939-3341-9_2

Tang, M., Wang, G., Lu, P., Karas, R. H., Aronovitz, M., Heximer, S. P., et al. (2003). Regulator of G-protein signaling-2 mediates vascular smooth muscle relaxation and blood pressure. *Nat. Med.* 9, 1506–1512. doi: 10.1038/nm958

Wang, J., Wong, Y. K., Zhang, J., Lee, Y. M., Hua, Z. C., Shen, H. M., et al. (2017). Drug target identification using an iTRAQ-based quantitative chemical proteomics approach-based on a target profiling study of andrographolide. *Method Enzymol.* 586, 291–309. doi: 10.1016/bs.mie.2016.09.049

Webb, R. C. (2003). Smooth muscle contraction and relaxation. *Adv. Physiol. Educ.* 27, 201–206. doi: 10.1152/advan.00025.2003

Wiechelman, K. J., Braun, R. D., and Fitzpatrick, J. D. (1988). Investigation of the bicinchoninic acid protein assay: identification of the groups responsible for color formation. *Anal. Biochem.* 175, 231–237. doi: 10.1016/0003-2697(88)90383-1

Wiśniewski, J. R., Zougman, A., Nagaraj, N., and Mann, M. (2009). Universal sample preparation method for proteome analysis. *Nat. Methods* 6, 359–362. doi: 10.1038/nmeth.1322

Xu, D. D., Deng, D. F., Li, X., Wei, L. L., Li, Y. Y., Yang, X. Y., et al. (2014). Discovery and identification of serum potential biomarkers for pulmonary tuberculosis using iTRAQ-coupled two-dimensional LC-MS/MS. *Proteomics* 14, 322–331. doi: 10.1002/pmic.201300383

Xu, J. W., Li, Y. L., Zhang, S. J., Jiang, H. Q., Wang, N., and Lin, H. Q. (2017). Identification of Tengfu Jiangya tablet target biomarkers with quantitative proteomic technique. *Evid. Compl. Alter. Med.* 2017, 1–12. doi: 10.1155/2017/7594805

Yang, G. M., Sun, J., Pan, Y., Zhang, J. L., Xiao, M., and Zhu, M. S. (2018). Isolation and identification of a tribenzylisoquinoline alkaloid from *Nelumbo nucifera* Gaertn, a novel potential smooth muscle relaxant. *Fitoterapia* 124, 58–65. doi: 10.1016/j.fitote.2017.10.020

Zhang, X., and P., Y. (2002). Research advances of alkaloids of medical plantNelumbo nucifera. *J. Nanjing TCM Univ. (Nat Sci)* 18, 382–384.

Zieske, L. R. (2006). A perspective on the use of iTRAQ reagent technology for protein complex and profiling studies. *J. Exp. Bot.* 57, 1501–1508. doi: 10.1093/jxb/erj168

Conflict of Interest Statement: The authors declare that the research was conducted in the absence of any commercial or financial relationships that could be construed as a potential conflict of interest.

The reviewer MZ declared a shared affiliation, with no collaboration, with the authors, JZ, ZP, YP, PW, GY, to the handling editor at the time of the review.

frontiers in Pharmacology

ORIGINAL RESEARCH
published: 13 September 2019
doi: 10.3389/fphar.2019.01040

Butyrate Improves the Metabolic Disorder and Gut Microbiome Dysbiosis in Mice Induced by a High-Fat Diet

*Feng Gao[1], Yi-Wei Lv[1], Jie Long[1], Jie-Mei Chen[1], Jiu-ming He[1], Xiong-Zhong Ruan[2] and Hai-bo Zhu[1]**

[1] State Key Laboratory for Bioactive Substances and Functions of Natural Medicines, Beijing Key Laboratory of New Drug Mechanisms and Pharmacological Evaluation Study, Institute of MateriaMedica, Chinese Academy of Medical Sciences & Peking Union Medical College, Beijing, China, [2] John Moorhead Research Laboratory, Department of Renal Medicine, University College London Medical School, University College London, London, United Kingdom

OPEN ACCESS

Edited by:
Jianxun Liu, China Academy of Chinese Medical Sciences, China

Reviewed by:
Yanyong Liu, Chinese Academy of Medical Sciences and Peking Union Medical College, China
Mingqian Sun, China Academy of Chinese Medical Sciences, China

***Correspondence:**
Hai-bo Zhu
zhuhaibo@imm.ac.cn

Specialty section:
This article was submitted to Ethnopharmacology, a section of the journal Frontiers in Pharmacology

Received: *07 June 2019*
Accepted: *16 August 2019*
Published: *13 September 2019*

Citation:
Gao F, Lv Y-W, Long J, Chen J-M, He J-m, Ruan X-Z and Zhu H-b (2019) Butyrate Improves the Metabolic Disorder and Gut Microbiome Dysbiosis in Mice Induced by a High-Fat Diet. Front. Pharmacol. 10:1040. doi: 10.3389/fphar.2019.01040

Background: Metabolic syndrome (MS) is one of the major causes of coronary artery diseases (CAD). Gut microbiome diversity and its natural fermentation products are not only correlated with MS and CAD, but their correlations also appear to be stronger than the associations with traditional risk factors. Therefore, the aim of this study was to provide a new potential pathway for the natural fermentation product butyrate to improve MS and to examine whether it is associated with serum metabolic profiles and gut flora composition.

Methods: C57BL/6J mice fed a high-fat diet (HFD) were treated with 400 mg/kg of sodium butyrate for 16 weeks. Blood and fecal samples were collected, and the metabolite concentrations and 16s rRNA were measured with liquid chromatography–MS and Illumina platform, respectively. The plasma differential metabolites and gut microbiome composition were analyzed with XCMS online and QIIME 2, respectively.

Results: Gut microbiome-derived butyrate reduced glucose intolerance and insulin resistance, resisting HFD-induced increase in the relative abundance of f_*Lachnospiraceae*, f_*Rikenellaceae*, and f_*Paraprevotellaceae*. Meanwhile, sodium butyrate increased the levels of α-linolenate, all-trans-retinal, resolvin E1, and leukotriene in the plasma, and the differential pathways showed enrichment in mainly resolvin E biosynthesis, histidine degradation, lipoxin biosynthesis, and leukotriene biosynthesis. Moreover, sodium butyrate increased the levels of phosphorylated-adenosine 5′-monophosphate-activated protein kinase (p-AMPK) and facilitated glucose transporter member 4 (GLUT4) in the adipose tissue.

Conclusion: Butyrate can induce AMPK activation and GLUT4 expression in the adipose tissue, improving cardiovascular disease (CVD)-related metabolic disorder, resisting HFD-induced gut microbiome dysbiosis, and promoting resolvin E1 and lipoxin biosynthesis. Oral supplement of the natural fermentation product butyrate can be a potential strategy for preventing CVD.

Keywords: AMPK, GLUT4, metabolomics, sodium butyrate, 16s rRNA

INTRODUCTION

Previous studies have indicated that the risk of developing cardiovascular disease (CVD) in patients with metabolic syndrome (MS) is approximately 2-fold higher than that in healthy people. Gut microbiome diversity is not only correlated with MS and CVD, but the correlations also appear to be stronger than the associations with traditional risk factors (Flego et al., 2016; Bogiatzi et al., 2018; Menni et al., 2018). Diet is an important factor affecting the diversity and composition of the gut microbiome, especially high-fat diet (HFD), which is not only associated with gut microbiome composition but is also a risk factor for MS and CVD (Daliri et al., 2018). However, how HFD affects MS and CVD via the gut microbiome still remains largely unknown.

Butyrate is a natural fermentation product of the gut, and it plays a crucial role in maintaining the homeostasis of host metabolism and gut microbiome diversity (Kasubuchi et al., 2015). A reduction in butyrate concentration in the gut is related to the development of the MS and CVD (Murugesan et al., 2018). Although oral butyrate supplement can improve HFD-induced MS and coronary artery disease in mice *via* histone deacetylases (Gao et al., 2009), a recent research indicated that oral butyrate treatment exerts a beneficial effect on glucose metabolism in healthy males instead of MS patients (Bouter et al., 2018), thus suggesting that the effects and molecular mechanism of butyrate in glucose metabolism and insulin resistance need to be confirmed further.

Butyrate is mostly produced in the intestinal epithelium, and its concentration is very low in the blood (Leonel and Alvarez-Leite, 2012). Therefore, butyrate-derived blood metabolites could be a potential pathway through which butyrate can regulate the physiological processes in the host. However, it has been rarely reported how butyrate impacts the metabolites in the blood. Comparative metabolomics based on the pathological process and circumstantial stimuli is an effective approach to discover the relationship between metabolites and pathways (Shan et al., 2018). 16s RNA sequencing is extensively applied to describe the gut microbiome profile.

Here, we used metabolomics and 16s RNA sequencing to identify the differential metabolites and gut microbiome related to MS, thus evaluating the effects of butyrate on glucose homeostasis and metabolic profiles. Discovery of a relationship between the natural fermentation product butyrate and MS provides opportunities to identify new strategies and targets for CVD.

MATERIALS AND METHODS

Treatment of Animals

Male C57BL/6J mice (4 weeks old) were purchased from Beijing Vital River Laboratory Animal Technology Co., Ltd. All animals were housed in a temperature-controlled environment with a 12 h light/12 h dark cycle and allowed free access to food and water. The animal study was reviewed and approved by the Ethics Committee of Institute of Materia Medica, Chinese Academy of Medical Sciences & Peking Union Medical College. After 1 week of adaptation, 36 mice were randomly assigned to control, HFD, and HFD plus sodium butyrate group. Animals in the control group were fed with a normal diet and given daily gavage with water. Animals in the HFD group were fed with an HFD and given daily gavage with water (10% lard, 1.00% cholesterol, 0.4% sodium cholate, and 10% custard powder) (Wang et al., 2017).

Sodium butyrate (molecular formula: $C_4H_7NaO_2$, molecular weight: 110.09, purity: 99%) was purchased from Shanghai Aladdin Biochemical Technology Co., Ltd. Animals in the sodium butyrate group were fed with HFD and given daily gavage with sodium butyrate (400 mg/kg, dissolved in water) for 16 weeks.

Glucose Tolerance Tests and Glucose-Induced Insulin

Blood samples of C57BL/6J mice were collected from the caudal vein after fasting for 16 h. The concentration of blood glucose was measured with a blood glucose meter (Accu-ChekActive [Model GB], Roche Diabetes Care Gmbh, Mannheim, Germany). Glucose-induced insulin secretion was measured with an Insulin Kit [Insulin (Mouse) Ultrasensitive EIA, 96w, "RUO" Alpco].

Measurement of Total Cholesterol, Triglyceride, and Glycosylated Protein

Blood samples of C57BL/6J mice were collected from the caudal vein after fasting for 12 h. Analyses of cholesterol (CHOD-PAP kit, BioSino Bio-Technology & Science Inc, Beijing, China), triglyceride (GPO-PAP kit, BioSino Bio-Technology & Science Inc, Beijing, China), and glycosylated protein (GSP-NBT, BioSino Bio-Technology & Science Inc, Beijing, China) were performed by using the standardized kits.

Serum Metabolomics

The metabolites in serum were determined by a Dionex UHPLC Ultimate 3000 system (Thermo Scientific, Dionex, Sunnyvale, CA, USA) coupled to a Q-Exactive mass spectrometer. Blood samples were collected at week 4. A quantity of 50 μL serum was precipitated with 150 μL acetonitrile. The mixture was vortexed for 300 s at 2500 rpm and then centrifuged at 10,000 rpm under 4°C for 5 min. The supernatant was collected and dried under nitrogen gas flow. The residues were dissolved in 100 μL acetonitrile:H_2O (2:98, V/V) for liquid chromatography–MS analysis. Chromatographic separation was performed on a Waters HSS T3 (C18) column (2.1 × 100 mm, 1.8 mm), and the column temperature was maintained around 35°C. The mobile phase consisted of 0.1% formic acid (A) and acetonitrile (B), and the flow rate was 250 μL/min. The injection volume was 10 μL. The gradient conditions were as follows: 0 min, 2% B; 9 min, 60% B; 18 min, 60% B; 20 min, 100% B; and 30 min, 100% B. The mass spectrometric settings for positive/negative ion modes were as follows: scan mode, full MS; scan range, m/z

100–1000; resolution, 70,000; automatic gain control target, 3 × 106; maximum IT, 100 ms; spray voltage (+/−), 3.5/3.2 kV; capillary temperature, 320°C; sheath gas flow rate (+/−), 40/7; and aux gas flow rate (+/−), 11/0. The non-linear alignment of data in the time domain and the spontaneous integration and isolation of peak intensities were performed by using XCMS online. Partial least squares discriminant analysis (PLS-DA), principal components analysis (PCA), principal coordinates analysis (PCoA), and volcano plot were performed using the Omicshare platform.

16s RNA Sequencing of Fecal Samples

Fecal samples from C57BL/6J mice were collected and stored at −80°C at week 4. The V3–V4 hypervariable domain of the 16S rRNA gene was amplified with the specific primers 341F: (5′-CCTAYGGGRBGCASCAG-3′ and 806R (5′-GGA CTACNNGGGTATCTAAT-3′) (**Supplementary Material**). Sequencing was performed using a single-end configuration by an Illumina sequencing platform. Phenotypic analysis was carried out by QIIME2 (version: 2018.11). The sequence quality control and feature table construction were performed with the DADA2 plugin. Phylogenetic diversity analyses were performed with q2-phylogeny and q2-diversity. The feature classifiers were trained by q2-feature-classifier within QIIME2. The box plot was generated using the Omicshare platform.

Western Blot Assay

Proteins were prepared from tissues and cells in radio immunoprecipitation assay (RIPA) lysis buffer with protease inhibitors and phosphatase inhibitor cocktail (Roche, Switzerland). Then, SDS-polyacrylamide gel electrophoresis (SDS-PAGE) was conducted, and bands were transferred to polyvinylidene fluoride (PVDF) membrane, followed by incubation with primary antibodies against phospho-AMPK (phosphorylated-adenosine 5′-monophosphate-activated protein kinase), phospho-ACC, phospho-LKB1 (Ser428), Glut4, GAPDH, and di-methyl-histone H3(Lys27) (diluted at 1:1000, catalog number: 3033, 3661, 3482, 2213, 5174, and 9728, respectively, Cell Signaling Technology, Boston, MA, USA). Corresponding secondary antibodies (diluted at 1:5000) were added, and bands were visualized with enhanced chemiluminescence reagents (Thermo Fisher Scientific, Waltham, MA, USA). Signals were normalized to those of β-actin (diluted at 1:5000, catalog number: 4967, Cell Signaling Technology, Boston, MA, USA).

Hematoxylin–Eosin Staining

Sections (3 μm) were obtained from each paraffin block using a microtome and stained with hematoxylin–eosin. Samples were immersed in xylene and alcohol, stained with hematoxylin for 5 min, stained with eosin for 3 min, and re-immersed in alcohol and xylene.

RESULTS

HFD Induces MS in Mice

To evaluate the impact of HFD on the homeostasis of glucose and lipids, we treated C57BL/6J male mice with HFD for 16 weeks. At the beginning of the experiment, mice were randomly divided into control and HFD groups. The levels of plasma glucose, total cholesterol, and triglycerides, which can characterize MS, were detected at week 4. As expected, compared to the control group, the weight was much higher in the HFD group (**Figure 1A**). In addition, we observed an apparent increase of triglyceride and total cholesterol in the HFD group at week 4 (**Figures 1B**, **C**), glucose intolerance and insulin resistance appeared at week 16 (**Figures 1D**–**G**). In the control group, hepatocytes were arranged radially around a vein in the center and hepatic structure was clearly visible. Few small-sized cavities were found, whereas in the HFD group many small-sized cavities were found (**Figure 1H**). These results indicated that HFD impaired the homeostasis of glucose and lipids, which is in agreement with previous studies (Araujo et al., 2011).

HFD Changes the Metabolic Profiles in Mice

To further investigate the change in metabolic profiles induced by HFD, we performed serum untargeted metabolomics using a liquid chromatograph–mass spectrometer. As shown by the metabolomics cloud plot (**Figure 2A**), a total of 4840 features were observed (p-value ≤ 0.05 and fold ≥ 1.5). The PCoA analysis displayed that there was a separate tendency of serum metabolites between the control and HFD groups (**Figure 2B**). The parameter values of R2 and Q2 from PLS-DA analysis were 0.988 and 0.95, respectively, indicating that this model showed excellent performance on predictive ability (**Figure 2C**). The values of variable importance in projection (VIP) above 1.0 and p-values below 0.05 were employed to identify significant metabolites related to group separation. Compared to the control group, a total of 682 metabolites were increased and 229 metabolites were decreased in the HFD group (**Figure 2D**). Differential pathways showed enrichment in nicotine degradation IV, noradrenaline and adrenaline degradation, sphingomyelin metabolism or ceramide salvage, phospholipases, and pentose phosphate pathway (**Figure 3**).

Gut Flora Composition Is Associated With Plasma Biomarker and Metabolic Profiles

To investigate how HFD changes the gut microbiome composition, we analyzed fecal samples of mice in the HFD and control groups using 16S rRNA gene sequencing (Kovatcheva-Datchary et al., 2015). PCoA based on the individual Bray–Curtis distance indicated that there was a significant separation tendency between these two groups (**Figure 4A**). Although p_Bacteroidetes and p_Firmicutes were the dominant bacteria at the phylum level, our results indicated

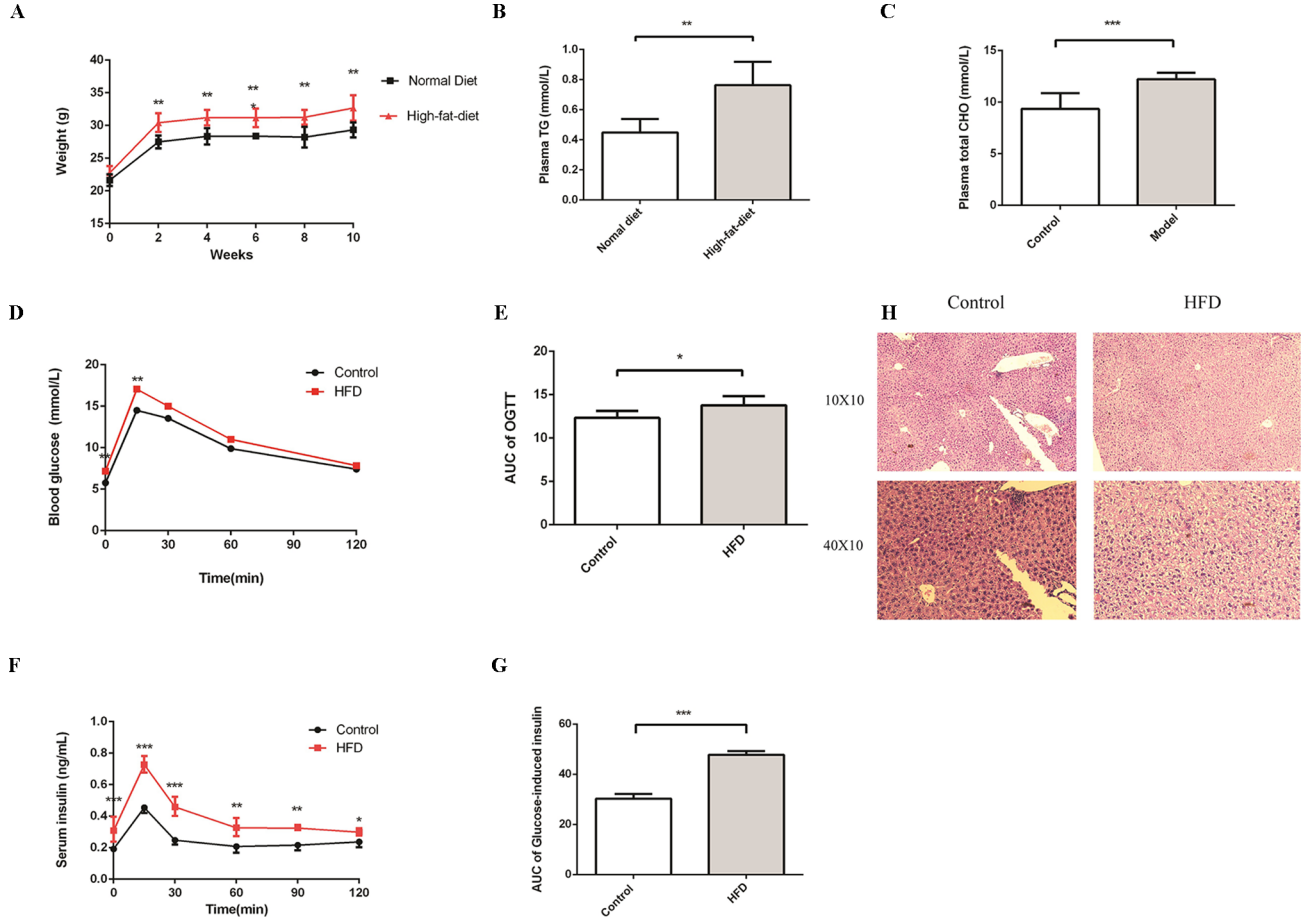

FIGURE 1 | HFD induces metabolic syndrome in C57BL/6J mice. Male C57BL/6J mice were allowed free access to the high-fat and normal diet. **(A)** The body weight of the HFD group was significantly higher compared to the control group. **(B** and **C)** Compared to the control group, the levels of plasma TG and Total CHO were significantly increased in the HFD group at week4 (n = 6, *p < 0.05). **(D** and **E)** After fasting for16 hours, mice received i.p. injections of 1 g/kg glucose. Blood glucose level was measured at 15, 30, 60, and 120 min. Compared to the control group, the level of blood glucose was significantly increased in the HFD group at 0 and 15 min (n = 5, *p < 0.05). Data are representative of five mice in each case. Data represent mean ± sem. *p < 0.05; **p < 0.01; ***p < 0.001 via unpaired t-test at each time point. **(F** and **G)** After fasting for16 hours, mice received i.p. injections of 1 g/kg glucose. Serum insulin levels were measured at 15, 30, 60, 90, and 120 min. Compared to the control group, the level of serum insulin was significantly increased in the HFD group (n = 5, *p < 0.05). Data are representative of five mice in each case. Data represent mean ± sem. *p < 0.05; **p < 0.01; ***p < 0.001 via unpaired t-test at each time point. **(H)** Compared to the control group, the number of cavities was increased in the HFD group.

that there was no significant difference between these two groups (**Figure 4B**). At the family level, we observed an increased relative abundance of f_Lachnospiraceae, f_Rikenellaceae, and f_*Paraprevotellaceae* and a decreased relative abundance of f_*Alcaligenaceae* in the HFD group (**Figure 4C**). Meanwhile, the ratios of f_*Lachnospiraceae*/p_*Firmicutes*, f_*Rikenellaceae*/p_*Bacteroides*, and f_*Paraprevotellaceae*/p_*Bacteroides* were also increased, suggesting that p_*Lachnospiraceae*, p_*Rikenellaceae*, and p_*Paraprevotellaceae* were the dominant bacteria in the HFD group and were associated with HFD-induced MS (**Figure 4D**).

To explore whether the alteration of gut composition is associated with plasma biomarkers and metabolic profiles, we performed a Pearson correlation analysis. The results are displayed in **Figure 5**, and they showed that relative abundance of f_*Lachnospiraceae*, f_*Rikenellaceae*, and f_*Paraprevotellaceae* had a positive correlation with the levels of total cholesterol, triglyceride, and glucose resistance, and a negative correlation with glucose tolerance. Moreover, f_*Lachnospiraceae*, f_*Rikenellaceae*, and f_*Paraprevotellaceae* relative abundances were associated with MS-related metabolites, including choline and L-argininosuccinate. Therefore, we deduced that gut composition is associated with metabolic profiles and plasma biomarkers, suggesting that gut composition could affect MS via metabolites.

Butyrate Improves HFD-Induced MS in Mice

To further determine the effects of butyrate on HFD-induced MS, we performed daily gavage of 6-week-old C57BL/6J mice fed an HFD with sodium butyrate (400 mg/kg) for 16 weeks. The levels of total cholesterol and triglyceride showed

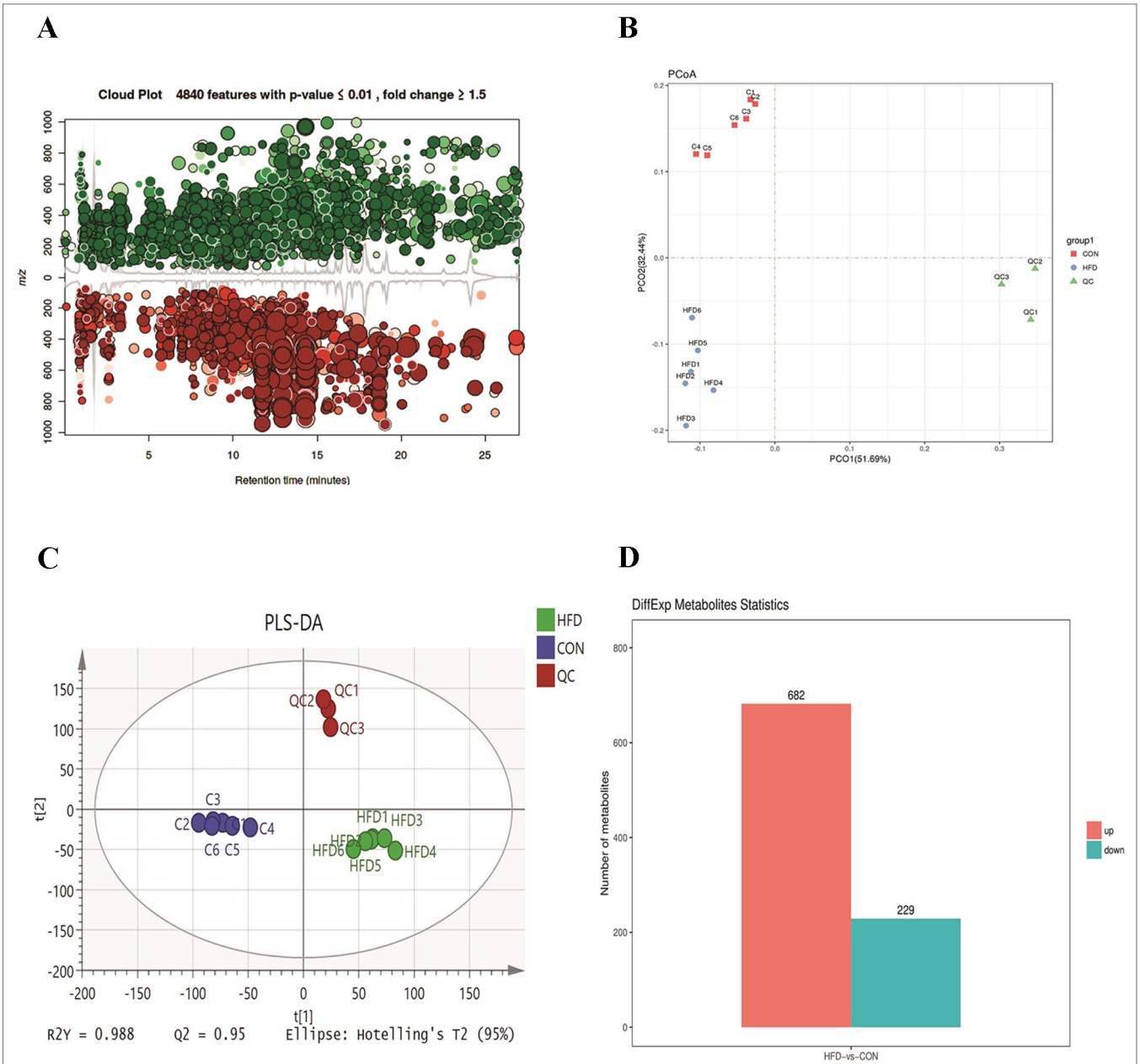

FIGURE 2 | HFD changes metabolic profiles in C57BL/6J mice. Blood samples were collected at week 4. Serum metabolomics analysis was performed with the pairwise method on the XCMS online platform. **(A)** Differential featured plots were shown. Only dysregulated features (p-value ≤ 0.05 and fold change ≥ 1.5) are displayed. Up-regulated features are shown in green, and down-regulated features are shown in red. **(B)** PCoA of the features intensities from all simples. The control group is shown in red; the HFD group is shown in blue; the quality control is shown in green **(C)** PLS-DA scores plot of the control and HFD group. Blue spots represent the control group, and the red spots represent the HFD group. **(D)** The red column represents up-regulated metabolites, and green column represents down-regulated metabolites in the HFD group.

no significant difference between the sodium butyrate and HFD group, whereas HFD-induced glucose intolerance and insulin resistance were significantly reduced (**Figures 6A–D**). Compared to the HFD group, weight gain was alleviated by sodium butyrate (**Figure 6E**). In the control group, few small-sized cavities were found in hepatocytes, whereas in the HFD group large-sized cavities were observed. Compared to the HFD group, the number of cavities was reduced in the butyrate group (**Figure 6F**). These data demonstrated that butyrate could improve HFD-induced glucose metabolism disorder instead of lipid metabolism disorder.

Given the effect of butyrate on glucose tolerance and insulin resistance, we examined the levels of p-AMPK and glucose transporter member 4 (GLUT4) in the liver and adipose tissue. As shown in **Figure 7**, sodium butyrate at 400 mg/kg increased the

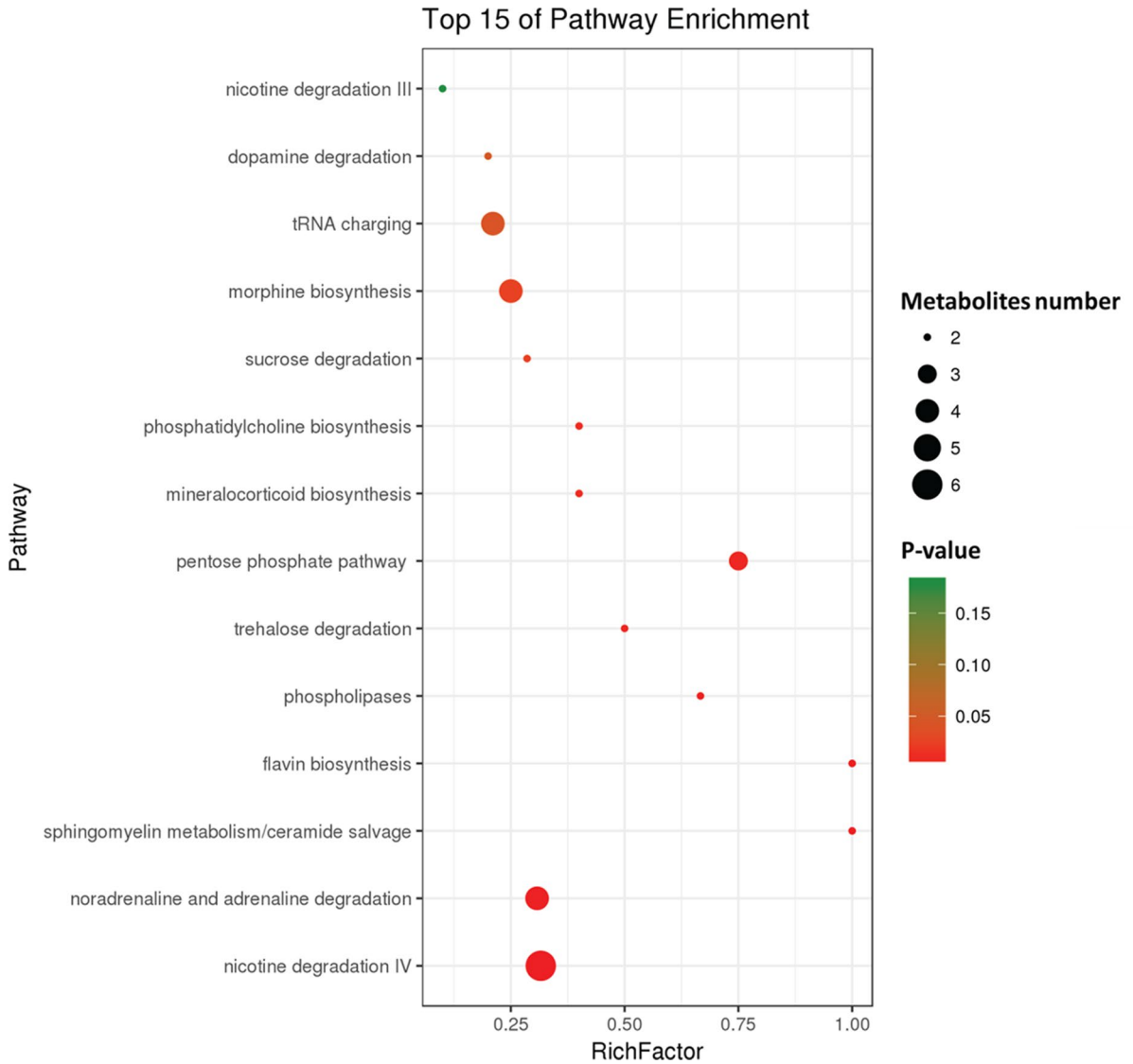

FIGURE 3 | Differential pathway analysis of the HFD and control group. The radius of each circle represents the number of metabolites relative to the number of metabolites represented by other circles. The colors from green to red indicate the elevated p-value.

levels of p-AMPK, GLUT4, and histone acetylation in the white adipose tissue and brown adipose tissue from C57 BL/6J mice.

Butyrate Alters the Metabolic Profiles in Mice

To further explore the effect of butyrate on HFD-induced MS, we used serum untargeted metabolomics to monitor the change in the metabolic profile induced by sodium butyrate. As shown in the metabolomics cloud plot (**Figure 8A**), we observed a total of 4369 features (p-value ≤ 0.05 and fold ≥ 1.5). The PCoA analysis displayed that there was a separate tendency of serum metabolites between the sodium butyrate and HFD groups (**Figure 8B**). The parameter values of the R2 and Q2 from PLS-DA analysis were 0.985 and 0.949, respectively (**Figure 8C**). Compared to the control group, a total of 229 metabolites were increased and 444 metabolites were decreased in the sodium butyrate group (**Figure 8D**). Differential pathways showed enrichment in resolvin E biosynthesis, histidine degradation, lipoxin biosynthesis, and leukotriene biosynthesis (**Figure 9**).

Butyrate-Mediated Metabolic Profile Alteration Is Associated With the Gut Microbiome

To further determine the effect of butyrate on gut microbiome composition, we performed daily gavage of 6-week-old C57BL/6J mice with sodium butyrate (400 mg/kg) and collected

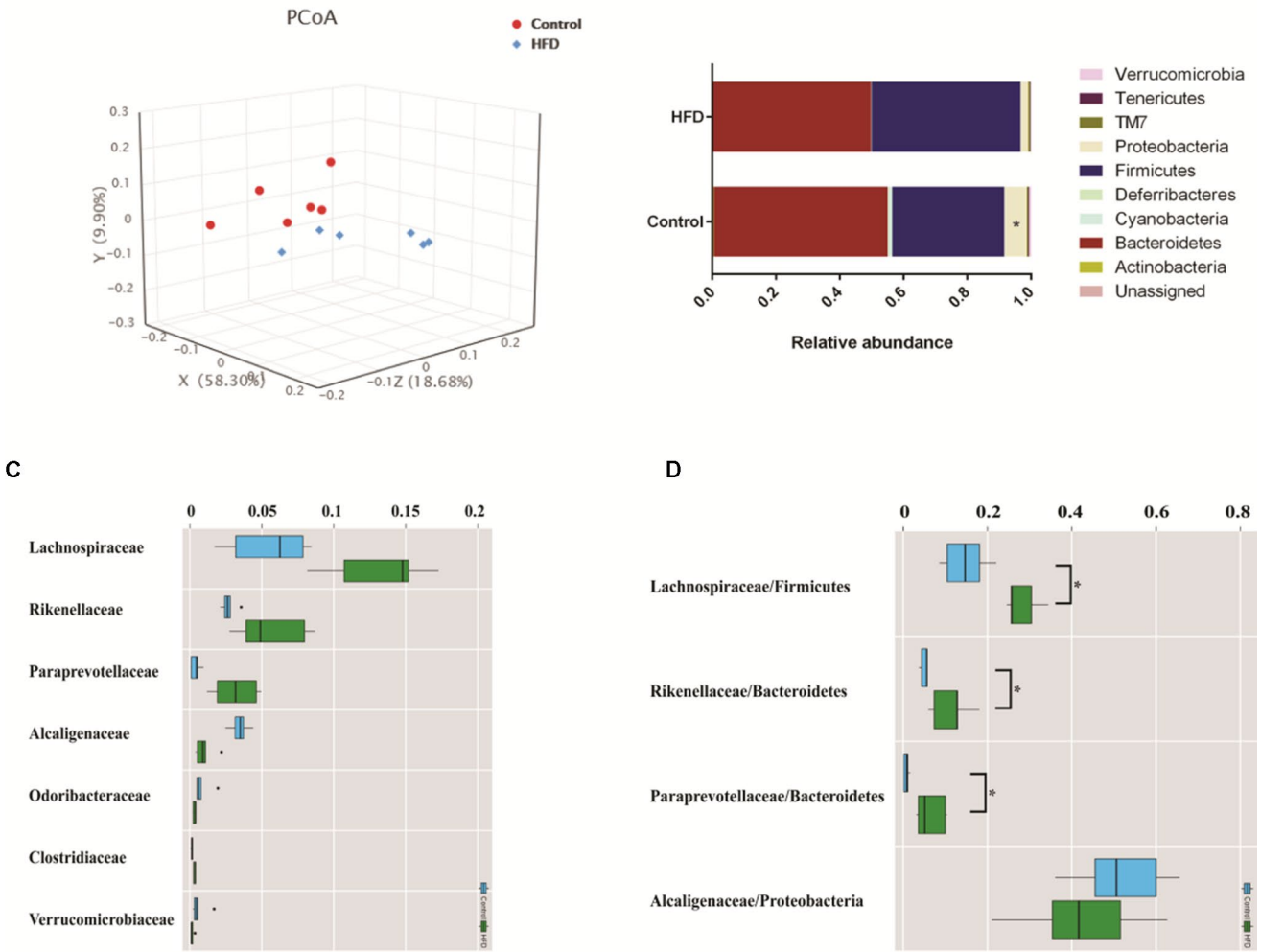

FIGURE 4 | HFD alters the composition of gut microbiome in C57BL/6J mice. Fecal samples were collected at week 4. Fecal DNA was subjected to 16S rRNA sequencing and analyzed with QIIME2. (version 2018.11). **(A)** Principal coordinates analysis (PCoA) plot of Bray–Curtis distance. Red spots represent samples from the control group, and blue spots represents samples from the HFD group. **(B)** The relative abundance of a major microbial phylum in the control and HFD group. Compared to the HFD group, proteobacteria was a higher abundance in the control group. Data are mean ± SD (*p < 0.05; Wilcoxon matched-pairs signed rank test and Mann–Whitney U test). **(C)** Relative abundance of a major microbial family in the control and HFD group. The seven abundant families are shown. Data are mean ± SD (*p < 0.05; Wilcoxon matched-pairs signed rank test and Mann–Whitney U test). **(D)** The ratio of the major microbial family/phylum in the control and HFD group. Data are mean ± SD (*p < 0.05; Wilcoxon matched-pairs signed rank test and Mann–Whitney U test).

fecal samples at week 4. Results are displayed in **Figure 10**, and they showed that sodium butyrate increased the relative abundance of p_*Verrucomicrobia* and decreased the relative abundance of p_*Firmicutes*. At the family level, the relative abundances of f_*Verrucomicrobiaceae*, f_*Bacteroidaceae*, and f_*Alcaligenaceae* were increased and the relative abundances of f_*Lachnospiraceae* and f_*Paraprevotellaceae* were decreased in the butyrate group. The ratios of f_*Lachnospiraceae*/f_*Firmicutes* and f_*Paraprevotellaceae*/f_*Bacteroidetes* were decreased, suggesting that butyrate can resist HFD-induced increase in f_*Lachnospiraceae* and f_*Paraprevotellaceae*. Subsequently, we performed a Pearson correlation analysis to confirm whether there is a correlation between the gut microbiome and butyrate-mediated metabolic profile alteration. The results are shown in **Figure 11**, and they showed that f_*Verrucomicrobia* was negatively associated with L-glutamine, 13-hydroxy-α-tocopherol, and hydroxy-bupropion, and it was positively correlated with resolvin E 1, (5)-HPETE, and linoleate. The pattern in f_*Lachnospiraceae* and f_*Paraprevotellaceae* was opposite to that in f_*Verrucomicrobia*.

DISCUSSION

MS is a cluster of metabolic disorders, including central adiposity with visceral fat accumulation, dysglycemia, insulin

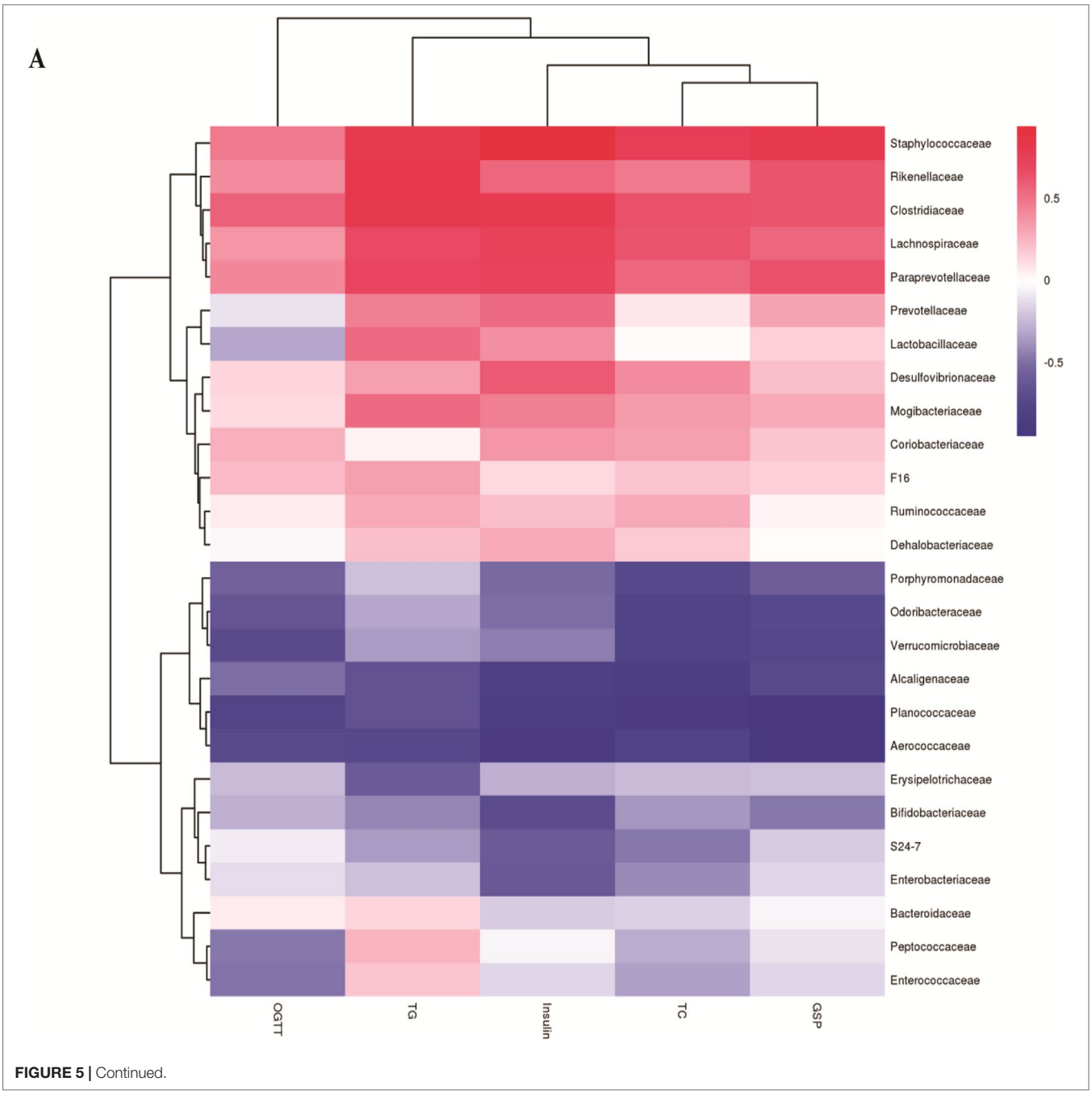

FIGURE 5 | Continued.

resistance, and dyslipidemia (Sherling et al., 2017). The risk of developing CVD in patients with MS is approximately 2-fold higher than that in healthy people (Samson and Garber, 2014). Gut flora composition and microbiome-derived metabolites are correlated with CVD and appear to have a strong correlation than traditional risk factors (Mazidi et al., 2016). Accumulating studies have suggested that HFD-induced gut flora dysbiosis is related to MS and CVD (Murphy et al., 2015).

Here, we found that C57BL/6J mice fed an HFD not only showed altered gut flora diversity but also increased relative abundances of f_*Lachnospiraceae*, f_*Rikenellaceae*, and f_*Paraprevotellaceae* and decreased relative abundance of f_ *Alcaligenaceae*. The increase in the above-mentioned bacteria had a positive correlation with total cholesterol, triglyceride, and insulin resistance, and a negative correlation with glucose tolerance. Meanwhile, the increase in f_*Lachnospiraceae*, f_*Rikenellaceae*, and f_*Paraprevotellaceae* was associated with plasma metabolite change. These data demonstrated that HFD-induced gut flora dysbiosis was associated with plasma biomarker and plasma profile.

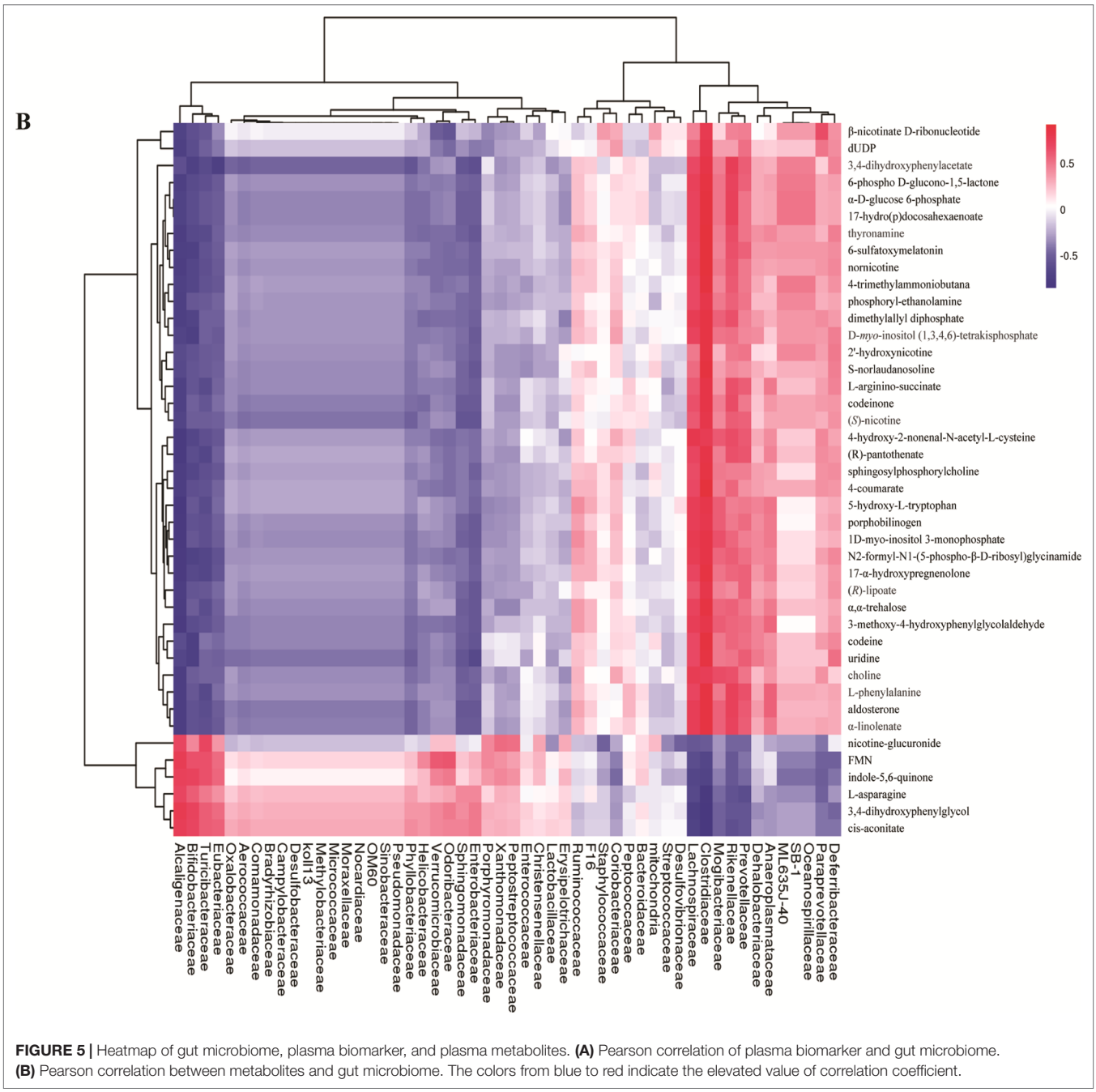

FIGURE 5 | Heatmap of gut microbiome, plasma biomarker, and plasma metabolites. **(A)** Pearson correlation of plasma biomarker and gut microbiome. **(B)** Pearson correlation between metabolites and gut microbiome. The colors from blue to red indicate the elevated value of correlation coefficient.

Previous studies have also supported the claim that f_*Lachnospiraceae* and f_*Rikenellaceae* are related to glucose metabolism disorder and insulin resistance (Brown and Hazen, 2015; Brown and Hazen, 2018). Our results also showed that f_*Lachnospiraceae* and f_*Rikenellaceae* are associated with plasma metabolites including choline and branched chain amino acids (BCAAs). Previous studies have displayed that choline-derived trimethylamine oxide (TMAO) can stimulate the macrophages to engulf ox-LDL and enhance platelet hyperreactivity, ultimately promoting atherosclerosis progression. Elevated levels of BCAAs selectively disrupt mitochondrial pyruvate utilization and promote MS, whereas promoting BCAA catabolism or normalizing glucose utilization by overexpressing GLUT1 in the heart can rescue the metabolism disorder (Li et al., 2017).

HFD-induced microbiome dysbiosis is a major cause of butyrate reduction in the gut and is related to MS. Butyrate is a major metabolite from microbial fermentation in the gut (Duncan et al., 2002; Khan and Jena, 2015). As an important energy source for the intestinal epithelium and intestinal

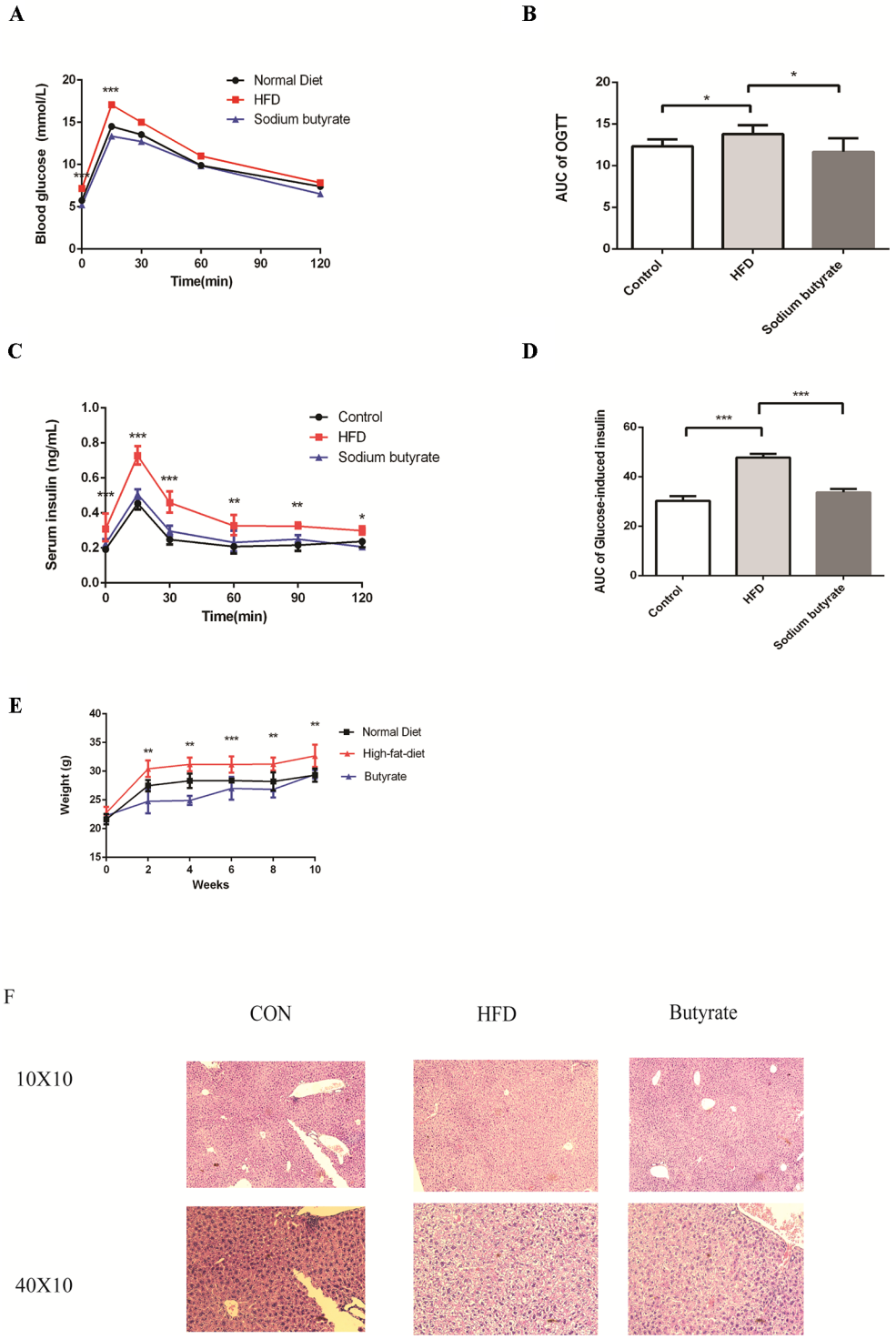

FIGURE 6 | Butyrate improves HFD-induced metabolic syndrome in C57BL/6J mice. Male C57BL/6J mice were divided into the HFD group and Butyrate group. Butyrate group was oral gavaged sodium butyrate (400 mg/kg) for 16 weeks. **(A** and **B)** After 16 hours of fasting, mice received i.p. injections of 1 g/kg glucose. Blood glucose levels were measured at 15, 30, 60, and 120 min. Compared to the HFD group, blood glucose level was significantly reduced at 0 and 15 min in the butyrate group (n = 5, *p < 0.05). Data are representative of five mice in each case. Data represent mean ± sem. *p < 0.05; **p < 0.01; ***p < 0.001 *via* unpaired t-test at each time point. **(C** and **D)** After 16 hours of fasting, mice received i.p. injections of 1 g/kg glucose. Serum insulin level was measured at 15, 30, 60, 90, and 120 min. Compared to the HFD group, serum insulin level was significantly reduced in the butyrate group (n = 5, *p < 0.05). Data are representative of five mice in each case. Data represent mean ± sem. *p < 0.05; **p < 0.01; ***p < 0.001 *via* unpaired t-test at each time point. **(E)** Body weight of mice on the high-fat diet was significantly higher than the butyrate group for 16 weeks. **(F)** Compared to the HFD group, few cavities were observed in the butyrate group.

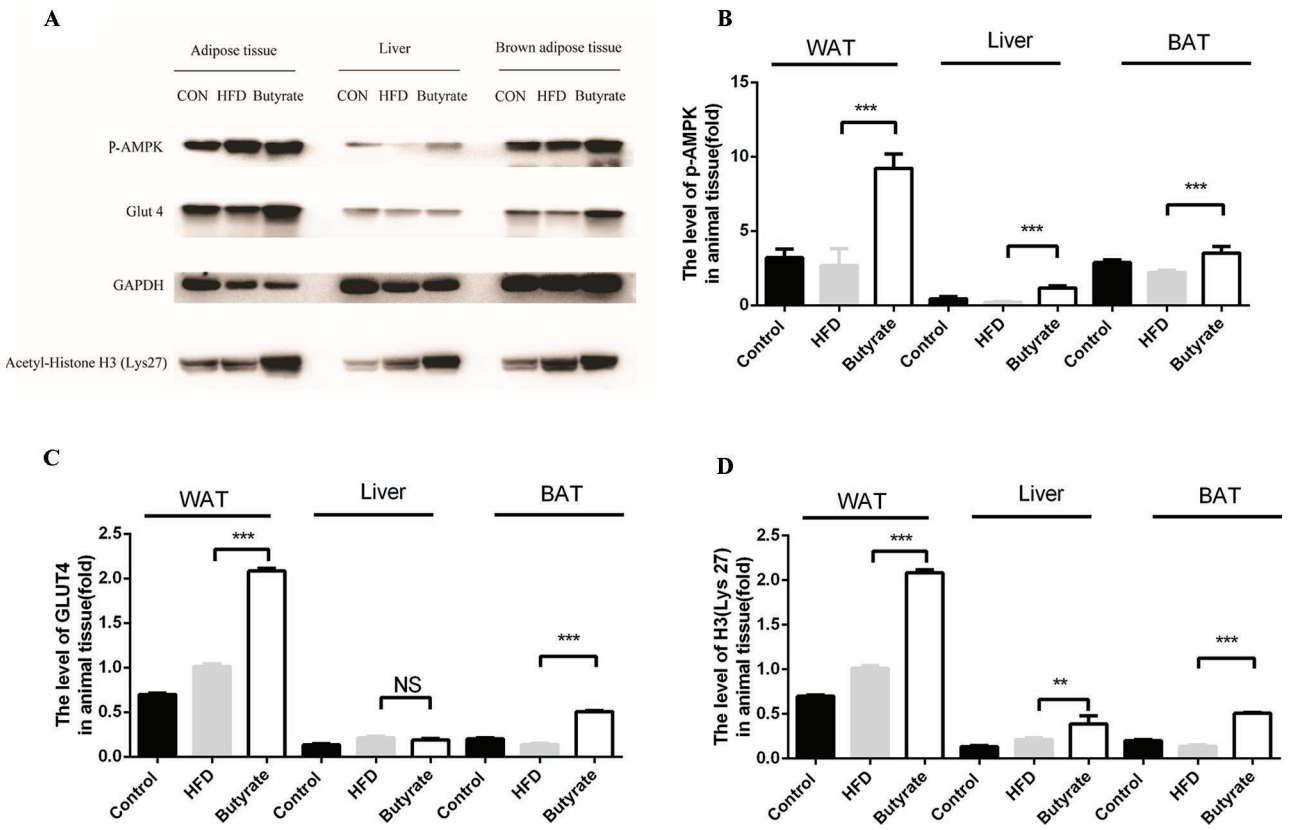

FIGURE 7 | Sodium butyrate supplement increases the expression of p-AMPK, Glut4, and H3 (Lys 27) in adipose tissue from C57BL/6J mice. Murine tissues were collected after sodium butyrate treatment for 16 weeks **(A)** The western blotting of p-AMPK, Glut4, and H3(Lys 27). **(B, C,** and **D)** Compared to the HFD group, the levels of p-AMPK, Glut4, and H3 (Lys 27) were increased in the sodium butyrate group ($p < 0.05$). Data represent mean ± sem. *$p < 0.05$; **$p < 0.01$; ***$p < 0.001$ *via* unpaired t-test.

epithelial cells, butyrate not only can maintain physiological function but also can directly regulate gene expression and physiological process via inhibiting histone deacetylation (Perry et al., 2016; Menni et al., 2018). Although a probiotic supplement can increase the butyrate level, probiotics can occasionally cause detrimental metabolic activities or produce host deleterious metabolites and cause inappropriate immune responses and systemic infections (Daliri et al., 2018). Therefore, oral butyrate supplement is a better way to increase the butyrate level in the gut. In our study, we observed that oral sodium butyrate supplement could reduce HFD-induced glucose metabolites and insulin resistance, in agreement with previous studies (Si et al., 2018). However, we did not observe a significant effect of sodium butyrate on lipid metabolism in C57BL/6J mice.

AMPK is an important energy sensor in mammalian cells, and it can sense glucose via fructose-1,6-bisphosphate and aldolase. AMPK activation can increase glucose uptake, glycolysis, and mitochondrial biogenesis to improve glucose metabolism disorder and atherosclerosis (Kim et al., 2016). GLUT4 is a member of glucose transporter protein family and is expressed primarily in skeletal muscle and adipose tissue. The primary function of GLUT4 is insulin-induced glucose uptake (Lizunov et al., 2013; Salt and Hardie, 2017). AMPK activation increases GLUT4 transfer to the plasma membrane and facilitates glucose uptake. Meanwhile, AMPK activation can increase PGC-1 expression to elevate GLUT4 expression (Fulco and Sartorelli, 2008). Given the effect of sodium butyrate on glucose metabolism and insulin resistance, we measured the levels of p-AMPK and GLUT4 in the liver and adipose tissue from sodium butyrate-treated C57BL/6J mice. As expected, we observed an increase in p-AMPK and GLUT4 levels in adipose tissue.

Butyrate is mostly produced by intestinal endothelium, and the concentration of butyrate is about 1–3 μM in the blood (Kasubuchi et al., 2015); thus, a metabolite derived from the interaction between butyrate and host could be responsible for improving MS. Previous studies have indicated that butyrate can stimulate intestinal epithelial cells to secrete glucagon-like peptide 1, thus increasing insulin sensitivity (Yadav et al., 2013). In our study, we observed that butyrate could increase the levels of α-linolenate, all-trans-retinal, resolvin E1, and leukotriene. The differential metabolic pathways are abundant in resolvin E1 biosynthesis, histidine degradation, lipoxin biosynthesis, and leukotriene biosynthesis. Resolvin E1 is a specialized pro-resolving lipid mediator, and it is

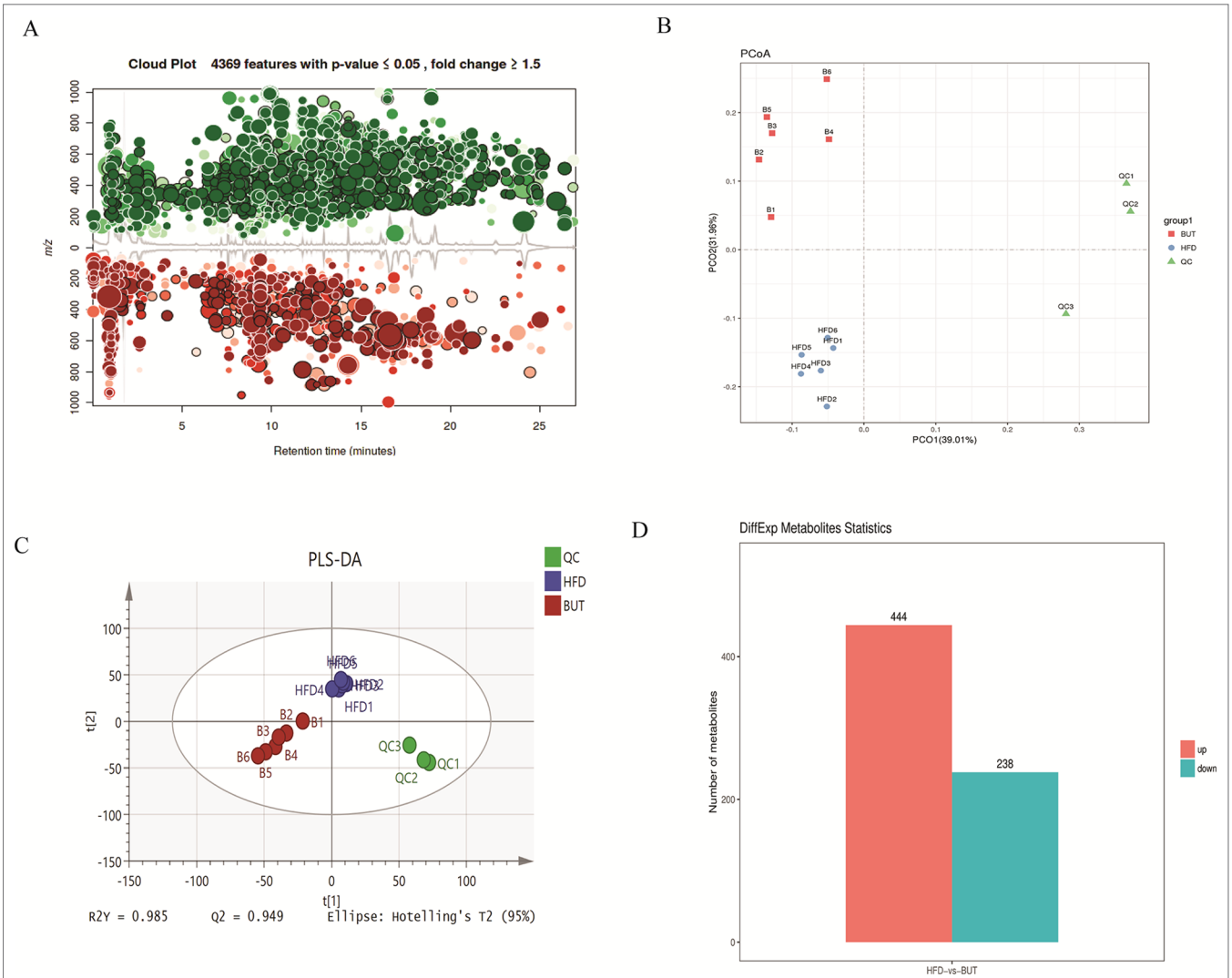

FIGURE 8 | Sodium butyrate alters metabolic profiles in C57BL/6J mice. Blood samples were collected at week 4. Serum metabolomics analysis was performed with the pairwise method on the XCMS online platform. **(A)** Differential featured plots were shown. Only dysregulated features (p-value ≤ 0.05 and fold change ≥ 1.5) are displayed. Up-regulated features are shown in green, and down-regulated features are shown in red. **(B)** PCoA of the features intensities from all simples. HFD group is shown in blue; butyrate group is shown in red; quality control group is shown in green. **(C)** PLS-DA scores plot of the butyrate and HFD group. Red spots represent the butyrate group; blue spots represent the HFD group; green spots represent the quality control group. **(D)** The red column represents up-regulated metabolites, and the green column represents down-regulated metabolites in the HFD group.

linked to metabolic dysregulation and the immune system in type 2 diabetes. Resolvin E1 can resist LPS and TNFα induction of ERV1 overexpression and diabetic overexpression activating phagocytosis and resolution signals in human neutrophils (Freire et al., 2017). Thus, butyrate-induced resolvin E1 biosynthesis could be a potential mechanism through which butyrate can reduce unexplained inflammation. Lipoxin can attenuate obesity-induced adipose inflammation and alter the adipose M1/M2 ratio, promoting HFD-induced MS (Borgeson et al., 2015). However, we did not find any studies on the effect of butyrate on resolvin E1 and lipoxin metabolism for improving MS. We speculated that butyrate-induced biosynthesis of resolvin E1 and lipoxin could be a new pathway through which butyrate can reduce unexplained inflammation.

In conclusion, our study demonstrated that HFD increases the relative abundances of f_*Lachnospiraceae*, f_*Rikenellaceae*, and f_*Paraprevotellaceae* related to the levels of choline and BCAAs, which play a crucial role in the pathological process of atherosclerosis. Oral butyrate supplement could resist HFD-induced increase in f_*Lachnospiraceae*, f_*Rikenellaceae*, and f_*Paraprevotellaceae*. Meanwhile, oral butyrate supplement can regulate resolvin E1 biosynthesis, histidine degradation, lipoxin biosynthesis, and leukotriene biosynthesis, thus providing a

FIGURE 9 | Differential pathway analysis of the HFD and butyrate group. The radius of each circle represents the number of metabolites relative to the number of metabolites represented by other circles. The colors from green to red indicate the elevated p-value.

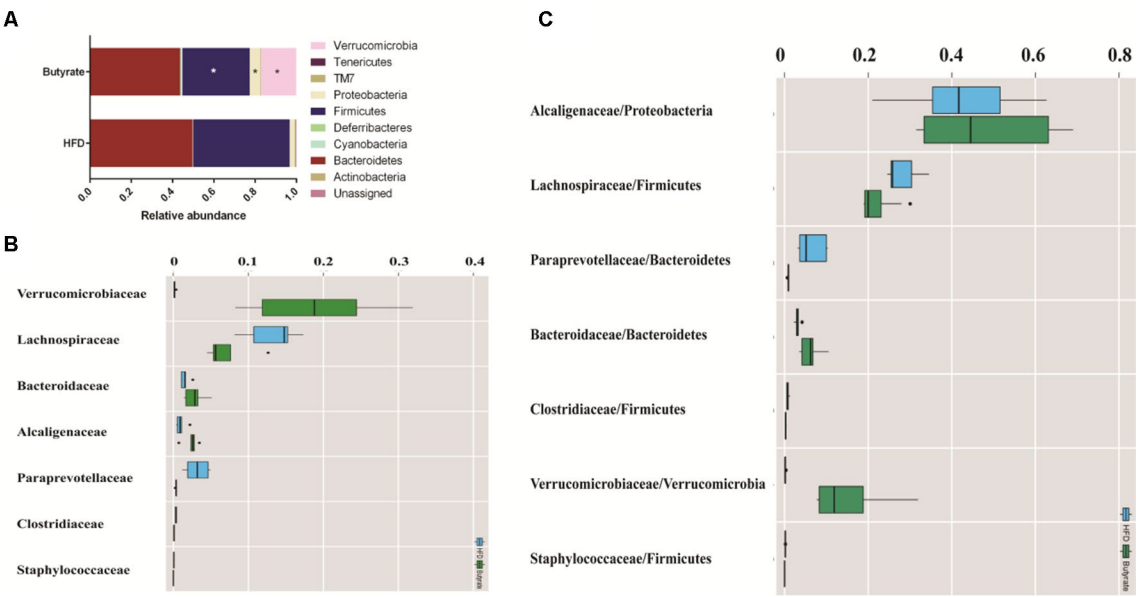

FIGURE 10 | Butyrate resists the gut flora perturbation of C57BL/6J mice induced by HFD. Fecal samples from both HFD and butyrate group were collected at 4 weeks. Fecal DNA was subjected to 16S rRNA sequencing, and sequences were analyzed using QIIME2 (version 2018.11). **(A)** Relative abundance of a major microbial phylum in the butyrate and HFD group. Data are mean ± SD (*$p < 0.05$; Wilcoxon matched-pairs signed rank test and Mann–Whitney U test). **(B)** Relative abundance of a major microbial family in the butyrate and HFD group. The seven abundant families are shown. Data are mean ± SD (*$p < 0.05$; Wilcoxon matched-pairs signed rank test and Mann–Whitney U test). **(C)** The ratio of the major microbial family/phylum in the butyrate and HFD group. Data are mean ± SD (*$p < 0.05$; Wilcoxon matched-pairs signed rank test and Mann–Whitney U test).

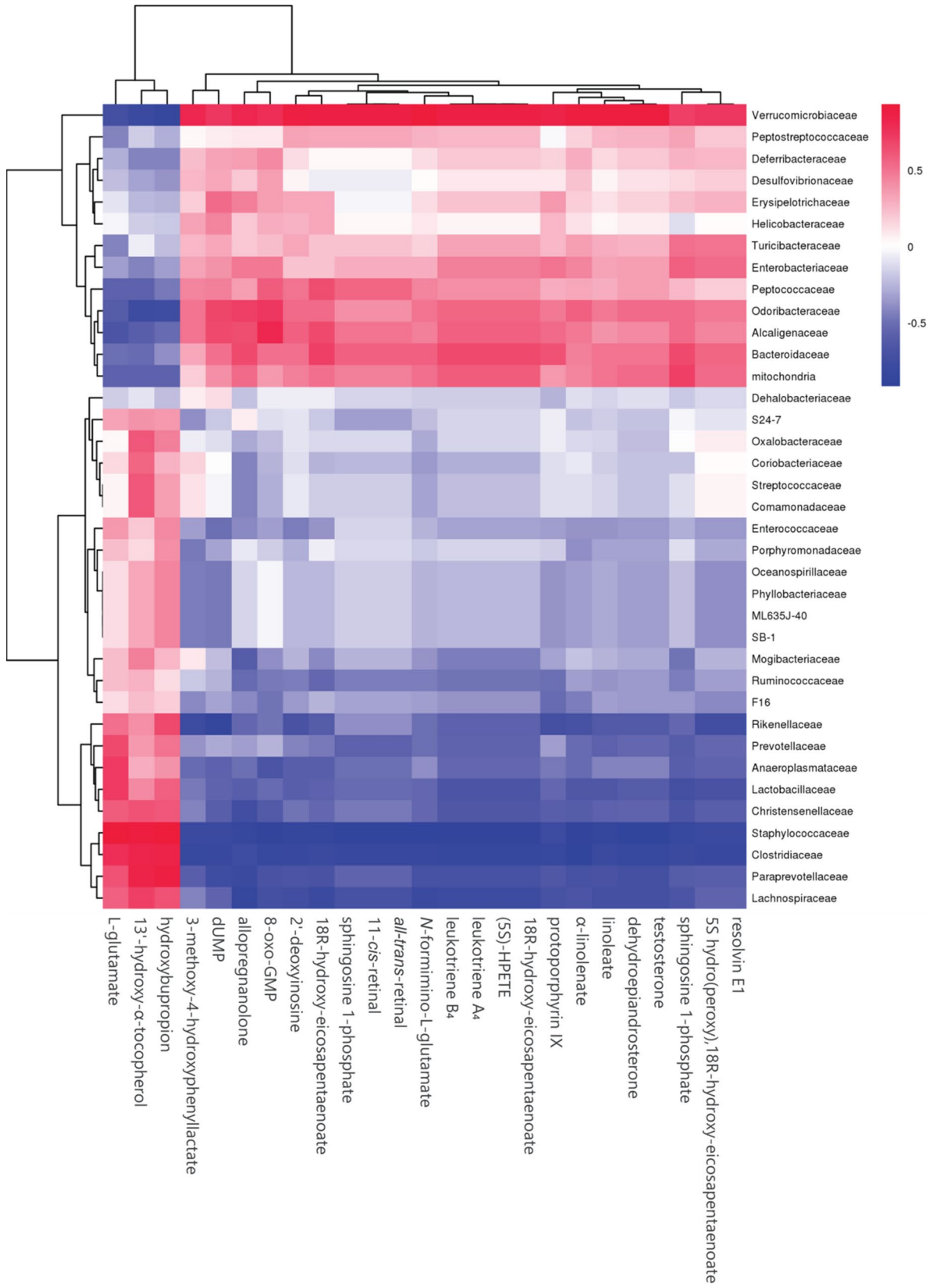

FIGURE 11 | Heatmap of plasma metabolites and gut microbiome. The colors from blue to red indicate the elevated value of the correlation coefficient.

new pathway through which butyrate can reduce unexplained inflammation related to CVD. Therefore, an oral supplement of the natural fermentation product butyrate can be a potential strategy for preventing CVD.

DATA AVAILABILITY

The data that support the findings of this study are openly available in [gene bank] at https://www.ncbi.nlm.nih.gov/genbank, reference number [MN059945 - MN060968]. Accession numbers can be found in the **Supplementary Material**.

ETHICS STATEMENT

The animal study was reviewed and approved by Ethics Committee of Institute of Materia Medica, Chinese Academy of Medical Sciences & Peking Union Medical College.

AUTHOR CONTRIBUTIONS

Conception and design of the study: FG and H-bZ; acquisition of data: FG, Y-WL, JL, and J-MC; analysis and interpretation of data: J-mH, X-ZR, and H-bZ.

FUNDING

This work was supported by funding support from The Drug Innovation Major Project 2018ZX09711001-003-011, CAMS Innovation Fund for Medical Sciences 2016-I2M-1-009, and the National Natural Sciences Foundation of China (NSFC) (grant number 91539126).

SUPPLEMENTARY MATERIAL

The Supplementary Material for this article can be found online at: https://www.frontiersin.org/articles/10.3389/fphar.2019.01040/full#supplementary-material

REFERENCES

Araujo, T. G., Leite, A. C., Martins da Fonseca, C. S., Carvalho, B. M., Schuler, A. R., and Lima, V. L. (2011). High-fat diet based on dried bovine brain: an effective animal model of dyslipidemia and insulin resistance. *J. Physiol. Biochem.* 67, 371–379. doi: 10.1007/s13105-011-0085-3

Bogiatzi, C., Gloor, G., Allen-Vercoe, E., Reid, G., Wong, R. G., Urquhart, B. L., et al. (2018). Metabolic products of the intestinal microbiome and extremes of atherosclerosis. *Atherosclerosis.* 273, 91–97. doi: 10.1016/j.atherosclerosis.2018.04.015

Borgeson, E., Johnson, A. M., Lee, Y. S., Till, A., Syed, G. H., Ali-Shah, S. T., et al. (2015). Lipoxin A4 attenuates obesity-induced adipose inflammation and associated liver and kidney disease. *Cell Metab.* 22, 125–137. doi: 10.1016/j.cmet.2015.05.003

Bouter, K., Bakker, G. J., Levin, E., Hartstra, A. V., Kootte, R. S., Udayappan, S. D., et al. (2018). Differential metabolic effects of oral butyrate treatment in lean versus metabolic syndrome subjects. *Clin. Transl. Gastroenterol.* 9, 155. doi: 10.1038/s41424-018-0025-4

Brown, J. M., and Hazen, S. L. (2015). The gut microbial endocrine organ: bacterially derived signals driving cardiometabolic diseases. *Annu. Rev. Med.* 66, 343–359. doi: 10.1146/annurev-med-060513-093205

Brown, J. M., and Hazen, S. L. (2018). Microbial modulation of cardiovascular disease. *Nat. Rev. Microbiol.* 16, 171–181. doi: 10.1038/nrmicro.2017.149

Daliri, E. B., Tango, C. N., Lee, B. H., and Oh, D. H. (2018). Human microbiome restoration and safety. *Int. J. Med. Microbiol.* 308, 487–497. doi: 10.1016/j.ijmm.2018.05.002

Duncan, S. H., Barcenilla, A., Stewart, C. S., Pryde, S. E., and Flint, H. J. (2002). Acetate utilization and butyryl coenzyme A (CoA):acetate-CoA transferase in butyrate-producing bacteria from the human large intestine. *Appl. Env. Microbiol.* 68, 5186–5190. doi: 10.1128/AEM.68.10.5186-5190.2002

Flego, D., Liuzzo, G., Weyand, C. M., and Crea, F. (2016). Adaptive immunity dysregulation in acute coronary syndromes: from cellular and molecular basis to clinical implications. *J. Am. Coll. Cardiol.* 68, 2107–2117. doi: 10.1016/j.jacc.2016.08.036

Freire, M. O., Dalli, J., Serhan, C. N., and Van Dyke, T. E. (2017). Neutrophil resolvin E1 receptor expression and function in type 2 diabetes. *J. Immunol. (Baltimore, Md: 1950).* 198, 718–728. doi: 10.4049/jimmunol.1601543

Fulco, M., and Sartorelli, V. (2008). Comparing and contrasting the roles of AMPK and SIRT1 in metabolic tissues. *Cell Cycle (Georgetown, Tex).* 7, 3669–3679. doi: 10.4161/cc.7.23.7164

Gao, Z., Yin, J., Zhang, J., Ward, R. E., Martin, R. J., Lefevre, M., et al. (2009). Butyrate improves insulin sensitivity and increases energy expenditure in mice. *Diabetes.* 58, 1509–1517. doi: 10.2337/db08-1637

Kasubuchi, M., Hasegawa, S., Hiramatsu, T., Ichimura, A., and Kimura, I. (2015). Dietary gut microbial metabolites, short-chain fatty acids, and host metabolic regulation. *Nutrients* 7, 2839–2849. doi: 10.3390/nu7042839

Khan, S., and Jena, G. (2015). The role of butyrate, a histone deacetylase inhibitor in diabetes mellitus: experimental evidence for therapeutic intervention. *Epigenomics* 7, 669–680. doi: 10.2217/epi.15.20

Kim, J., Yang, G., Kim, Y., Kim, J., and Ha, J. (2016). AMPK activators: mechanisms of action and physiological activities. *Exp. Mol. Med.* 48, e224. doi: 10.1038/emm.2016.16

Kovatcheva-Datchary, P., Nilsson, A., Akrami, R., Lee, Y. S., De Vadder, F., Arora, T., et al. (2015). Dietary fiber-induced improvement in glucose metabolism is associated with increased abundance of Prevotella. *Cell Metab.* 22, 971–982. doi: 10.1016/j.cmet.2015.10.001

Leonel, A. J., and Alvarez-Leite, J. I. (2012). Butyrate: implications for intestinal function. *Curr. Opin. Clin. Nutr. Metab. Care.* 15, 474–479. doi: 10.1097/MCO.0b013e32835665fa

Li, T., Zhang, Z., Kolwicz, S. C., Jr., Abell, L., Roe, N. D., Kim, M., et al. (2017). Defective branched-chain amino acid catabolism disrupts glucose metabolism and sensitizes the heart to ischemia-reperfusion injury. *Cell Metab.* 25, 374–385. doi: 10.1016/j.cmet.2016.11.005

Lizunov, V. A., Lee, J.-P., Skarulis, M. C., Zimmerberg, J., Cushman, S. W., and Stenkula, K. G. (2013). Impaired tethering and fusion of GLUT4 vesicles in insulin-resistant human adipose cells. *Diabetes.* 62, 3114–3119. doi: 10.2337/db12-1741

Mazidi, M., Rezaie, P., Kengne, A. P., Mobarhan, M. G., and Ferns, G. A. (2016). Gut microbiome and metabolic syndrome. *Diabetes Metab. Syndr.* 10, S150–S157. doi: 10.1016/j.dsx.2016.01.024

Menni, C., Lin, C., Cecelja, M., Mangino, M., Matey-Hernandez, M. L., Keehn, L., et al. (2018). Gut microbial diversity is associated with lower arterial stiffness in women. *Eur. Heart J.* 39 (25), 2390–2397. doi: 10.1093/eurheartj/ehy226

Murphy, E. A., Velazquez, K. T., and Herbert, K. M. (2015). Influence of high-fat diet on gut microbiota: a driving force for chronic disease risk. *Curr. Opin. Clin. Nutr. Metab. Care* 18, 515–520. doi: 10.1097/MCO.0000000000000209

Murugesan, S., Nirmalkar, K., Hoyo-Vadillo, C., Garcia-Espitia, M., Ramirez- Sanchez, D., and Garcia-Mena, J. (2018). Gut microbiome production of short-chain fatty acids and obesity in children. *Eur. J. Clin. Microbiol. Infect Dis.* 37, 621–625. doi: 10.1007/s10096-017-3143-0

Perry, R. J., Peng, L., Barry, N. A., Cline, G. W., Zhang, D., Cardone, R. L., et al. (2016). Acetate mediates a microbiome-brain-beta-cell axis to promote metabolic syndrome. *Nature* 534, 213–217. doi: 10.1038/nature18309

Salt, I. P., and Hardie, D. G. (2017). AMP-activated protein kinase: an ubiquitous signaling pathway with key roles in the cardiovascular system. *Circ. Res.* 120, 1825–1841. doi: 10.1161/CIRCRESAHA.117.309633

Samson, S. L., and Garber, A. J. (2014). Metabolic syndrome. *Endocrinol. Metab. Clin. North Am.* 43, 1–23. doi: 10.1016/j.ecl.2013.09.009

Shan, J., Peng, L., Qian, W., Xie, T., Kang, A., Gao, B., et al. (2018). Integrated serum and fecal metabolomics study of collagen-induced arthritis rats and the therapeutic effects of the zushima tablet. *Front. Pharmacol.* 9, 891. doi: 10.3389/fphar.2018.00891

Sherling, D. H., Perumareddi, P., and Hennekens, C. H. (2017). Metabolic syndrome. *J. Cardiovasc. Pharmacol. Ther.* 22, 365–367. doi: 10.1177/1074248416686187

Si, X., Shang, W., Zhou, Z., Strappe, P., Wang, B., Bird, A., et al. (2018). Gut Microbiome-induced shift of acetate to butyrate positively manages dysbiosis in high fat diet. *Mol. Nutr. Food Res.* 62 (3), 1700670. doi: 10.1002/mnfr.201700670

Wang, J., Ma, A., Zhao, M., and Zhu, H. (2017). AMPK activation reduces the number of atheromata macrophages in ApoE deficient mice. *Atherosclerosis* 258, 97–107. doi: 10.1016/j.atherosclerosis.2017.01.036

Yadav, H., Lee, J. H., Lloyd, J., Walter, P., and Rane, S. G. (2013). Beneficial metabolic effects of a probiotic *via* butyrate-induced GLP-1 hormone secretion. *J. Biol. Chem.* 288, 25088–25097. doi: 10.1074/jbc.M113.452516

Conflict of Interest Statement: The authors declare that the research was conducted in the absence of any commercial or financial relationships that could be construed as a potential conflict of interest.

The reviewer YL declared a shared affiliation, with no collaboration, with several of the authors, FG, Y-WL, JL, J-MC, J-MH, and H-BZ, to the handling editor at the time of the review.

frontiers in Pharmacology

ORIGINAL RESEARCH
published: 17 September 2019
doi: 10.3389/fphar.2019.01033

Piper sarmentosum Promotes Endothelial Nitric Oxide Production by Reducing Asymmetric Dimethylarginine in Tumor Necrosis Factor-α-Induced Human Umbilical Vein Endothelial Cells

Uma Mahgesswary Sundar[1], Azizah Ugusman[1], Hui Kien Chua[1], Jalifah Latip[2] and Amilia Aminuddin[1]*

[1] *Department of Physiology, Faculty of Medicine, Universiti Kebangsaan Malaysia Medical Centre, Kuala Lumpur, Malaysia,* [2] *Department of Pharmaceutical Chemistry, School of Chemical Sciences & Food Technology, Faculty of Science and Technology, Universiti Kebangsaan Malaysia, Bangi, Malaysia*

OPEN ACCESS

Edited by:
Steyner F. Cortes, Federal University of Minas Gerais, Brazil

Reviewed by:
Juliana Montani Raimundo, Federal University of Rio de Janeiro, Brazil
Roger Lyrio Santos, Federal University of Espirito Santo, Brazil

***Correspondence:**
Azizah Ugusman
dr.azizah@ppukm.ukm.edu.my

Specialty section:
This article was submitted to Ethnopharmacology, a section of the journal Frontiers in Pharmacology

Received: *28 May 2019*
Accepted: *14 August 2019*
Published: *17 September 2019*

Citation:
Sundar UM, Ugusman A, Chua HK, Latip J and Aminuddin A (2019) Piper sarmentosum Promotes Endothelial Nitric Oxide Production by Reducing Asymmetric Dimethylarginine in Tumor Necrosis Factor-α-Induced Human Umbilical Vein Endothelial Cells. Front. Pharmacol. 10:1033. doi: 10.3389/fphar.2019.01033

Asymmetric dimethylarginine (ADMA) is an endogenous inhibitor of endothelial nitric oxide synthase (eNOS). ADMA is degraded by dimethylarginine dimethylaminohydrolase (DDAH). Elevated levels of ADMA lead to reduction in nitric oxide (NO) production, which is linked to endothelial dysfunction and atherosclerosis. *Piper sarmentosum* is an herb that has shown stimulation on endothelial NO production by increasing both expression and activity of eNOS. Thus, this study determined whether the positive effect of *P. sarmentosum* on NO production is related to its modulation on the DDAH–ADMA pathway in cultured human umbilical vein endothelial cells (HUVEC) exposed to tumor necrosis factor-α (TNF-α). HUVEC were divided into four groups: control, treatment with 250 μg/ml of aqueous extract of *P. sarmentosum* leaves (AEPS), treatment with 30 ng/ml of TNF-α, and concomitant treatment with AEPS and TNF-α for 24 h. After treatments, HUVEC were collected to measure *DDAH1* messenger RNA (mRNA) expression using quantitative real-time polymerase chain reaction. DDAH1 protein level was measured using enzyme-linked immunosorbent assay (ELISA), and DDAH enzyme activity was measured using colorimetric assay. ADMA concentration was measured using ELISA, and NO level was measured using Griess assay. Compared to control, TNF-α-treated HUVEC showed reduction in *DDAH1* mRNA expression ($P < 0.05$), DDAH1 protein level ($P < 0.01$), and DDAH activity ($P < 0.05$). Treatment with AEPS successfully increased *DDAH1* mRNA expression ($P < 0.05$), DDAH1 protein level ($P < 0.01$), and DDAH activity ($P < 0.05$) in TNF-α-treated HUVEC. Treatment with TNF-α caused an increase in ADMA level ($P < 0.01$) and a decrease in endothelial NO production ($P < 0.001$). Whereas treatment with AEPS was able to reduce ADMA level ($P < 0.01$) and restore NO ($P < 0.001$) in TNF-α-treated HUVEC. The results suggested that AEPS promotes endothelial NO production by stimulating DDAH activity and thus reducing ADMA level in TNF-α-treated HUVEC.

Keywords: *Piper sarmentosum*, asymmetric dimethylarginine, dimethylarginine dimethylaminohydrolase, human umbilical vein endothelial cells, tumor necrosis factor-α, endothelial dysfunction

INTRODUCTION

Atherosclerotic cardiovascular disease is the leading cause of mortality worldwide (Benjamin et al., 2017). The earliest stage of atherosclerosis development is endothelial dysfunction that is associated with other cardiovascular risk factors such as hypertension, hypercholesterolemia, hyperhomocysteinemia, diabetes mellitus, obesity, and systemic inflammation, contributing to the pathogenesis of cardiovascular diseases (Su, 2015). Endothelial dysfunction is defined as the loss of the homeostatic mechanisms that operate in healthy endothelial cells. It is characterized by decreased bioavailability of nitric oxide (NO), which promotes vascular dysfunction and atherosclerosis progression (Su, 2015).

Endothelium-derived NO is synthesized by endothelial nitric oxide synthase (eNOS). NO acts as an endogenous anti-atherosclerotic molecule by inducing vasodilation (Sukhovershin et al., 2015) and inhibiting monocyte adhesion, smooth muscle cell proliferation, and platelet aggregation (Ishizaka et al., 2007). Decrease of NO leads to endothelial dysfunction and subsequently promotes atherosclerosis. Asymmetric dimethylarginine (ADMA) is a competitive inhibitor of eNOS, which reduces NO production. ADMA level was increased in individuals with hypercholesterolemia, hypertension, diabetes mellitus, and hyperhomocysteinemia, leading to increased risk of atherosclerosis (Jawalekar et al., 2013).

A small part of ADMA is excreted *via* the kidneys, while most ADMA is degraded by dimethylarginine dimethylaminohydrolase (DDAH) enzyme to dimethylamine and L-citrulline (Liu et al., 2016). Reduction in DDAH activity leads to an increase in ADMA, which in turn reduces eNOS activity and NO production (Czarnecka et al., 2017). Tumor necrosis factor-α (TNF-α) is a pro-inflammatory cytokine that reduces the expression and activity of eNOS. TNF-α also reduces DDAH activity and consequently increases ADMA level (Vairappan, 2015). There are two isoforms of DDAH, with DDAH1 predominantly found in the kidneys and brain while DDAH2 is present mainly in the kidneys and heart (Bulau et al., 2007). Several studies have identified the role of DDAH1 in ADMA degradation and NO synthesis while the physiological function of DDAH2 is still undetermined (Liu et al., 2016). Enzyme kinetics of these isoforms demonstrated a V_{max} value of 356 and 4.8 nmol/mg/min for ADMA of DDAH1 and DDAH2, respectively. Thus, the apparent rate of ADMA degradation for DDAH1 is 70 times higher than that of DDAH2 (Pope et al., 2009). Based on these enzyme kinetics studies, DDAH1 is recognized as the principal ADMA metabolizing pathway in the endothelium. In addition, overexpression of *DDAH1* was reported to reduce ADMA level in mice (Zhang et al., 2011). Hence, this study was focused mainly on *DDAH1* expression.

Piper sarmentosum is an herbaceous plant that is widely used in Chinese traditional medicine to treat fever, cough, pleurisy, toothache, and dyspepsia. The vernacular names of *P. sarmentosum* vary among different countries such as *daun kaduk* in Malaysia, *cha plu* in Thailand, and *qing ju* in China. The plant easily grows in tropical and subtropical regions, especially in shady and moist areas (Chaveerach et al., 2008). Aqueous extract of *P. sarmentosum* (AEPS) leaves is rich in flavonoids and possesses numerous pharmacological properties such as anti-inflammatory, antioxidant, antibacterial, and anti-osteoporosis activities (Chan and Wong, 2014). AEPS leaves also reduced the formation of atherosclerosis in hypercholesterolemic rabbits (Adel et al., 2010). The extract was able to reduce blood pressure and increase serum nitric oxide in spontaneously hypertensive rats (Zainudin et al., 2015). Subacute toxicity study in rats showed that AEPS leaves was safe for consumption (Zainudin et al., 2013). In addition, AEPS leaves promoted the production of NO in human umbilical vein endothelial cells (HUVEC) by increasing both expression and activity of eNOS (Ugusman et al., 2010). Therefore, this study was conducted to determine whether the positive effect of *P. sarmentosum* on NO production is related to its modulation on the DDAH–ADMA pathway in HUVEC treated with TNF-α. We hypothesized that AEPS stimulated endothelial NO generation by increasing DDAH and decreasing ADMA, hence protecting against endothelial dysfunction and atherosclerosis.

MATERIALS AND METHOD

Preparation and Chemical Analysis of Aqueous Extract of P. *sarmentosum*

Fresh leaves of *P. sarmentosum* were purchased in one batch from Herbagus Sdn. Bhd., Penang, Malaysia, and only this batch was used throughout the study. The leaves were identified by plant taxonomists in Herbarium, Universiti Kebangsaan Malaysia (UKM) (specimen voucher number: UKMB40240). AEPS was prepared according to the previous method (Ugusman et al., 2010). Fresh *P. sarmentosum* leaves were rinsed with water, dried under sunlight, and blended into powder. Then, 100 g of the powder were immersed in 900 ml of Milli-Q water (1:10, w/v) in a reflux extractor machine. The extract was boiled at 80°C for 3 h, and the resulting solution was filtered and frozen at −80°C. Finally, the extract was freeze-dried and stored at 4°C. Liquid chromatography (LC)–mass spectrometry (MS) Orbitrap full-scan analysis was conducted to identify the compounds present in AEPS. LC–ultraviolet (UV) analysis was performed using the Accela™ ultrahigh-performance LC (UHPLC) system (Thermo Scientific, San Jose, USA) equipped a with quarternary pump, a build degasser, a photodiode array (PDA) detector, and an autosampler. The column used for the chromatographic separation was a Luna Kinetex Reversed Phase C18 column [2.6-µm particle size, 2.1- mm inner diameter (ID) × 150 mm]. The conditions consisted of a gradient elution using acetonitrile as mobile phase A and 0.1% formic acid as phase B at a flow rate of 200 µl/min over 40 min. The following gradient was applied: 0–20 min, 5% A; 20–30 min, 35% A; 30–35 min, 100% A; 35–35.01 min, 5% A, returning to 5% A in 5 min, with 10 µl of sample injected. The compounds eluted and separated were further analyzed with a linear trap quadrupole) LTQ Orbitrap mass spectrometer (Thermo Scientific, San Jose, USA) operating in a negative ion mode. The operating parameters were as follows: source accelerating voltage, 4.0 kV; capillary temperature, 350°C; sheath gas flow, 40 arb; auxiliary gas, 20 arb. Mass spectra were acquired with a scan range of 300–1,000 *m*/*z*. All data were processed with the Xcalibur™ 2.1 software (Thermo Scientific, San Jose, USA). LC–MS Orbitrap full-scan analysis identified a total of 19 compounds in AEPS (**Figure 1**). The compounds were characterized using retention times (R_t) and mass spectra, as provided by electrospray ionization (ESI)–MS (summarized in **Table 1**).

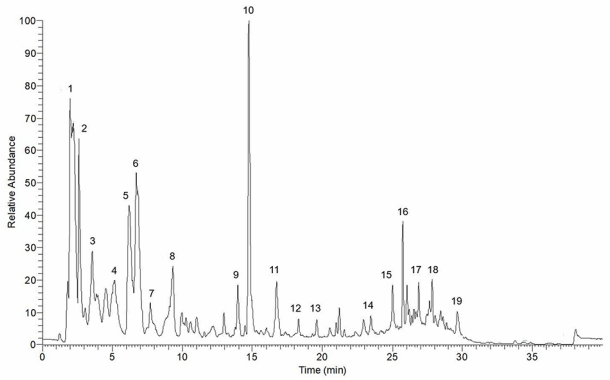

FIGURE 1 | Total ion chromatogram of aqueous extract of *P. sarmentosum* leaves (AEPS). Peaks are identified with numbers according to the elution order (refer to **Table 1**).

Isolation and Culture of HUVEC

HUVEC were isolated from human umbilical cords collected from the labor room of the Department of Obstetrics and Gynaecology, Hospital Kuala Lumpur. This study was approved by the Ethical Research Committee of Universiti Kebangsaan Malaysia Medical Centre and National Medical Research Registration (approval numbers: FF-2014-412 and NMRR-14-583-20729). Informed consent was obtained from all volunteers prior to delivery. HUVEC were isolated using collagenase infusion as described previously (Ugusman et al., 2010). The cells were cultured in endothelial cell medium (ECM) (ScienCell Research Laboratories, Inc., San Diego, CA) at 37°C in a humidified 5% CO_2 incubator. The cells were not exposed to shear stress as the cell culture media did not fluctuate during the experiments and the cells were maintained in static conditions (Albuquerque et al., 2000). HUVEC were subcultured until they reached passage 3 at 80% confluency.

3-(4,5-Dimethylthiazol-2-Yl)-2,5-Diphenyltetrazolium Bromide (MTT) Assay for Determination of Cell Viability and Griess Assay for Determination of NO Level

Optimal dose of TNF-α was determined based on its effect on HUVEC viability and NO production. Briefly, 5×10^4 HUVEC per well were seeded in a 96-well plate and allowed to attach for 24 h. The cells were then exposed to 10 to 40 ng/ml of TNF-α for 24 h. MTT assay was used to measure the viability of HUVEC while Griess assay was used to measure NO level in the culture medium. MTT assay was done according to a previous method (Ugusman et al., 2012). Briefly, 200 µl of MTT solution was added to each well, and the mixture was incubated for 4 h. Subsequently, the supernatants

TABLE 1 | Retention time (R_t) and mass spectra details for compounds identified in the negative mode of liquid chromatography (LC)–mass spectrometry (MS) Orbitrap full-scan analysis.

Peak	R_t (min)	m/z	Molecular weight	Molecular formula	Proposed compound
1	1.98	195.0503 (M-Na)	218.252	$C_{13}H_{14}O_3$	2,2-Dimethyl-2*H*-1-benzopyran-6-carboxylic acid; methyl ester
2	2.61	191.01933 (M-H)	192.214	$C_{11}H_{12}O_3$	1-Allyl-2-methoxy-4,5-methylenedioxybenzene/sarisan/asaricin
3	3.56	203.0820 (M-H)	204.35	$C_{15}H_{24}$	Sesquisabinene
4	5.16	315.0530 (M-H)	316.5	$C_{21}H_{32}O_2$	1-(3,4-Methylenedioxyphenyl)-1*E*-tetradecene
5	6.18	341.0863 (M-H)	342.3	$C_{15}H_{18}O_9$	1-*O*-Caffeoylgalactose
6	6.7	195.0504 (M-H)	196.202	$C_{10}H_{12}O_4$	2′-Hydroxy-4′,6′-dimethoxyacetophenone
7	7.72	431.0965 (M-H)	432.38	$C_{21}H_{20}O_{10}$	Vitexin
8	9.31	206.0816 (M-Na)	229.279	$C_{14}H_{15}NO_2$	*N*-[3-(4-Methoxyphenyl)propanoyl] pyrrole
9	13.9	209.0812 (M-H)	210.229	$C_{11}H_{14}O_4$	Kadsuketanone A
10	14.75	239.0918 (M-H)	240.255	$C_{12}H_{16}O_5$	3,4,5-Trimethoxydihydrocinnamic acid
11	16.71	237.0761 (M-H)	238.239	$C_{12}H_{14}O_5$	2,4,5-Trimethoxycinnamic acid
12	18.3	225.1125 (M-H)	226.275	$C_{15}H_{14}O_2$	1-Phenylethanol; benzoyl
13	19.6	361.1851 (M-H)	362.381	$C_{22}H_{18}O_5$	Isochamanetin
14	23.46	229.1441 (M-H)	230.348	$C_{13}H_{26}O_3$	Sarmentol A
15	25	243.1595 (M-H)	244.331	$C_{13}H_{24}O_4$	Sarmentoic acid
16	25.74	279.1568 (M-Na)	302.238	$C_{15}H_{10}O_7$	Quercetin
17	26.86	271.1906 (M-H)	272.256	$C_{15}H_{12}O_5$	Naringenin
18	27.83	293.2112 (M-Na)	316.5	$C_{21}H_{32}O_2$	1-(3,4-Methylenedioxyphenyl)-1*E*-tetradecene; (E)-form
19	29.63	265.1471 (M-H)	266.293	$C_{14}H_{18}O_5$	3,4-Dihydroxy-5-(3-methyl-2-butenyl)benzoic acid; 3′-isomer, 2′-hydroxy, ethyl ester

were aspirated, and the purple formazan crystal formed in each well was dissolved in 200 µl of DMSO. The absorbance of each well was read at 570 nm. A nitrate/nitrite colorimetric assay kit (Sigma-Aldrich, USA) was used to measure NO level indirectly in the cell culture medium as described previously (Ugusman et al., 2010). The principle of this assay is based on the measurement of total nitrite in the sample whereby nitrate reductase was utilized for enzymatic reduction of nitrate to nitrite. Total nitrite was measured at 540- nm absorbance after adding Griess reagents. Even though Griess reaction is less sensitive to quantitate NO generation compared to the direct method, it is the most extensively used method to measure NO indirectly; this method is fast and cheap and has a strong literature background (Csonka et al., 2015).

HUVEC were exposed to 50–300 µg/ml of AEPS for 24 h, and cell viability was measured using MTT assay to assess the extract's cytotoxicity effect. In order to determine the optimal dose of AEPS for subsequent experiments, HUVEC were treated concomitantly with 30 ng/ml of TNF-α and three different concentrations of AEPS (150, 250, and 300 µg/ml) for 24 h. AEPS at these concentrations was used as it had shown potent antioxidant effects in a previous study (Hafizah et al., 2010). Subsequently, HUVEC viability and NO production were measured using MTT assay and Griess assay, respectively.

Experimental Protocol

HUVEC at 1×10^5 cell density were seeded onto six-well tissue culture plates and allowed to grow until it reached 80% confluency. The cells were then divided into four groups: control, treatment with 250 µg/ml of AEPS, treatment with 30 ng/ml of TNF-α, and concomitant treatment with 250 µg/ml of AEPS and 30 ng/ml of TNF-α for 24 h. The dose of TNF-α (30 ng/ml) was chosen as it was the first dose that significantly reduced HUVEC viability and NO production. As for AEPS, 250 µg/ml of AEPS was used as it significantly increased HUVEC viability and NO production when exposed to 30 ng/ml of TNF-α.

Quantitative Real-Time Polymerase Chain Reaction (qRT-PCR) for Measurement of DDAH1 mRNA Expression

Extraction of RNA was done using TRI reagent (Molecular Research Center, Cincinnati, Ohio) as described previously (Ugusman et al., 2011). Following RNA extraction, cDNA synthesis was carried out using SuperScript® III First-Strand Synthesis SuperMix for qRT-PCR kit (Invitrogen, Carlsbad, USA). Master mixes containing SYBR® Select Master Mix (BIO-RAD Laboratories, Hercules, USA), cDNA samples, RNase- and DNase-free distilled water, and forward and reverse primers were prepared and pipetted into the PCR plate. Specific forward and reverse primers were used as follows: *DDAH1* (GenBank accession no. BC_033680), forward: 5′-ggacaaatcaacgaggtgct-3′, reverse: 5′-tagcggtggtcactcatctg-3′; and *GAPDH* (GenBank accession no. NM_002046), forward: 5′-tccctgagctgaacgggaag-3′, reverse: 5′-ggaggagtgggtgtcgctgt-3′. The reaction was conducted at initial denaturing at 95°C for 3 min; then involved 40 cycles of 61°C for 30 s, 95°C for 1 min, 55°C for 1 min, 70 cycles of 60°C for 10 s; and terminated by a cooling step at 4°C. Each experiment was performed in duplicate. The specificity of the PCRs was verified by analysis of melting curves and 1.5% agarose gel electrophoresis. The threshold cycle (C_T) value was determined, and the relative mRNA expression of *DDAH* was analyzed as follows:

$$\text{Relative mRNA expression} = 2^{-\Delta\Delta CT}$$

$$\Delta\Delta C_T = C_T GAPDH - C_T DDAH1$$

ELISA for Measurement of DDAH1 Protein Level

DDAH1 protein level in HUVEC was measured using a human DDAH1 ELISA kit (Cloud-Clone Corp., USA) according to the manufacturer's instructions. Briefly, 100 µl of HUVEC lysates was added into the plate and incubated for 2 h at 37°C. After incubation, liquid from each well was aspirated, and biotin-conjugated antibody specific to DDAH 1 was added. After washing, avidin conjugated to horseradish peroxidase (HRP) was added followed by 3,3′,5,5′-tetramethylbenzidine (TMB) substrate solution. Optical density (OD) of the wells was measured at 450 nm using a spectrophotometer.

Colorimetric Assay for Measurement of DDAH Enzyme Activity

The activity of DDAH was determined based on a previous method (Prescott and Jones, 1969). The principle of this assay was based on the measurement of L-citrulline produced by DDAH from ADMA degradation in the sample in a timed reaction. Serially diluted L-citrulline standard of different concentrations from 0 to 100 mM was prepared. HUVEC lysates were centrifuged at 3,000 g for 10 min, and the supernatant was collected. Then, 250 µl of 20% sulfuric acid solution containing 0.5% w/v antipyrine and 250 µl of 5% acetic acid solution containing 0.8% w/v diacetyl monoxime were mixed. Subsequently, 100 µl of the mixture was added to each sample. The mixtures were incubated in a shaker incubator at 60°C for 110 min in a dark state before the absorbance was measured at 466 nm. Concentration of L-citrulline in the sample was calculated based on the standard curve. Total protein concentration in the samples was determined using Bradford assay (Bradford, 1976). DDAH enzyme activity is calculated based on the following formula:

$$\text{DDAH activity} = \left(\left[\text{L-citrulline}\right]/110\right)/\left[\text{total protein}\right]$$

$$\text{Total protein}\ \left(\text{mg}\right)$$

ELISA for Measurement of ADMA Concentration

ADMA concentration in HUVEC was determined using a human ADMA ELISA kit (Cloud-Clone Corp., USA) according to the manufacturer's instructions. HUVEC lysate and biotin-labeled

ADMA were added into their respective wells. The mixture was mixed and incubated for an hour at 37°C. After incubation, liquid was aspirated and washed. Then, avidin conjugated to HRP was added to each well and incubated for 30 min at 37°C. The processes of aspiration and washing were repeated. After the last wash, TMB substrate solution and sulfuric acid were added. OD of each well was measured at 450 nm using a spectrophotometer.

Statistical Analysis

Data were analyzed using SPSS version 21.0 software. The Kolmogorov–Smirnov test was used to measure the normality of the data. Then, the data were analyzed using one-way ANOVA and *post hoc* Tukey test. The data were presented as mean ± standard error for the mean (SEM). Differences were considered significant at $P < 0.05$.

RESULTS

AEPS Protected Against TNF-α-Induced Cytotoxicity

Exposure to varied concentrations of AEPS up to 300 μg/ml did not cause noticeable toxicity to HUVEC whose viability was 80% and above (**Figure 2A**). Treatment with different TNF-α concentrations ranging from 10 to 40 ng/ml induced cell death and reduced NO level in a dose-dependent manner with 30 and 40 ng/ml of TNF-α causing significant reduction in HUVEC viability ($P < 0.05$) and NO level ($P < 0.05$) (**Figures 2B, C**). Thus, 30 ng/ml of TNF-α as the first dose causing significant reduction in HUVEC viability and NO level was selected for subsequent experiments. In the presence of AEPS, TNF-α-induced cytotoxicity was significantly reduced, as determined by MTT (**Figure 2D**) and Griess (**Figure 2E**) assays, as well as cell density and morphological examination (**Figure 2F**). Treatment of TNF-α-induced HUVEC with 150, 250, and 300 μg/ml of AEPS also successfully increased HUVEC viability ($P < 0.05$) (**Figure 2D**). However, there was no significant difference in cell viability between these three doses of AEPS. In addition, Griess assay showed that treatment of TNF-α-induced HUVEC with 150, 250, and 300 μg/ml of AEPS increased NO production by HUVEC ($P < 0.05$) (**Figure 2E**). AEPS concentrations of 250 and 300 μg/ml stimulated more NO production compared to 150 μg/ml of AEPS ($P < 0.05$). However, there was no significant difference in the NO level between 250 and 300 μg/ml of AEPS. Based on the effects of AEPS on cell viability and NO production, 250 μg/ml of AEPS was selected as the dose for subsequent experiments. HUVEC exposed to 250 μg/ml of AEPS showed a normal cobblestone appearance and had a similar density as the control group (**Figure 2F**). TNF-α induced HUVEC had a striated appearance with less cell density compared to control. Treatment of TNF-α-induced HUVEC with AEPS improved the density, and the cells retained the cobblestone appearance.

DDAH1 mRNA Expression in HUVEC

There was no significant difference in *DDAH1* mRNA expression for the AEPS group compared to the control group ($P = 0.061$) (**Figure 3**). TNF-α decreased *DDAH1* mRNA expression by 0.52-fold compared to control ($P = 0.011$). Treatment of TNF-α-induced

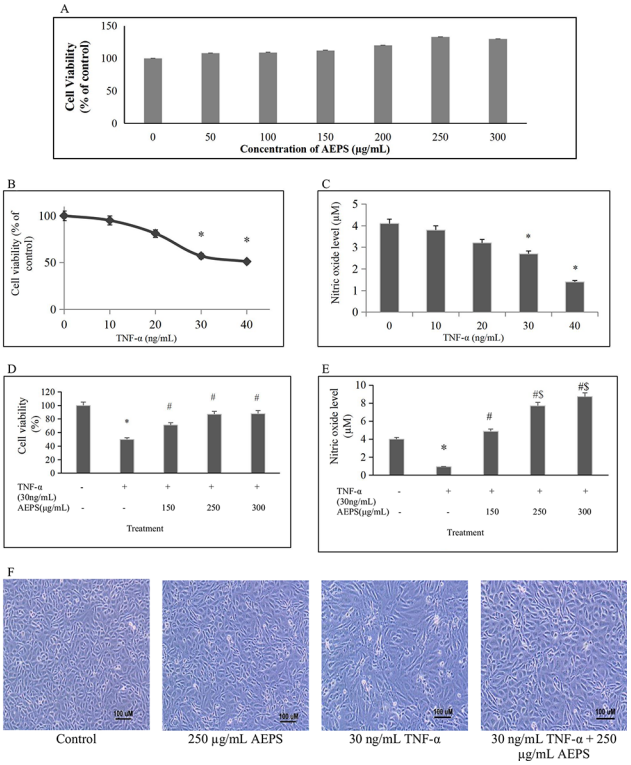

FIGURE 2 | Protective effect of aqueous extract of *P. sarmentosum* leaves (AEPS) against tumor necrosis factor (TNF)-α-induced toxicity in human umbilical vein endothelial cells (HUVEC). Toxicity of AEPS in HUVEC was determined by 3-(4,5-dimethylthiazol-2-yl)-2,5-diphenyltetrazolium bromide (MTT) assay after treatment with 50–300 μg/ ml of AEPS for 24 h **(A)**. Cells were exposed to 10–40 ng/ml TNF-α for 24 h, cell viability was measured by MTT assay **(B)**, and NO level was measured by Griess assay **(C)**. In addition, HUVEC were treated with 30 ng/ml of TNF-α in combination with different concentrations of AEPS (150, 250, and 300 μg/ ml) for 24 h, and then cell viability **(D)** and NO level **(E)** were measured. Cell density and morphology were observed under microscope at 100× magnification **(F)**. All data are shown as the mean ± SEM of at least three independent experiments (*$P < 0.05$ compared with the control group, #$P < 0.05$ compared with the TNF-α group, $$P < 0.05$ compared with the group treated with 150 μg/ml of AEPS).

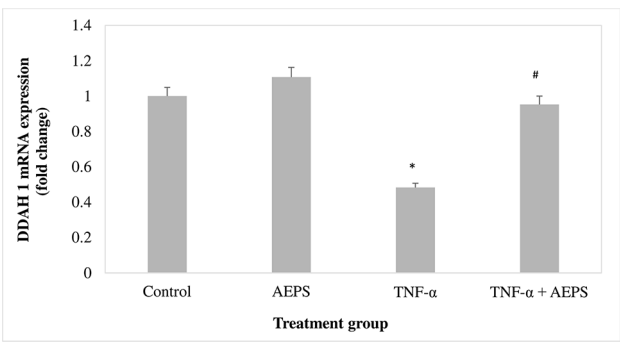

FIGURE 3 | *DDAH1* messenger RNA (mRNA) expression in human umbilical vein endothelial cells (HUVEC). Data shown as mean ± SEM, $n = 6$ [*$P < 0.05$ compared with the control group, #$P < 0.05$ compared with tumor necrosis factor (TNF)-α group].

HUVEC with AEPS increased *DDAH1* mRNA expression by 0.47-fold compared to the TNF-α group ($P = 0.033$).

DDAH1 Protein Level in HUVEC

AEPS increased DDAH1 protein level compared to control ($P = 0.001$) (**Figure 4**). TNF-α decreased DDAH1 protein level in HUVEC compared to control ($P = 0.004$). Treatment of TNF-α-induced HUVEC with AEPS increased DDAH1 protein level compared to the TNF-α group ($P = 0.002$).

DDAH Enzyme Activity in HUVEC

AEPS induced DDAH activity compared with control ($P = 0.023$) (**Figure 5**). TNF-α caused a reduction in DDAH activity compared to control ($P = 0.016$). Treatment of TNF-α-induced HUVEC with AEPS increased DDAH activity compared to the TNF-α group ($P = 0.039$).

ADMA Concentration in HUVEC

There was no significant difference in ADMA level between the AEPS and control groups ($P = 0.076$) (**Figure 6**). Treatment of HUVEC with TNF-α resulted in an increase in ADMA compared to control ($P = 0.0008$). Treatment of TNF-α-induced HUVEC with AEPS successfully reduced ADMA concentration compared to the TNF-α group ($P = 0.001$).

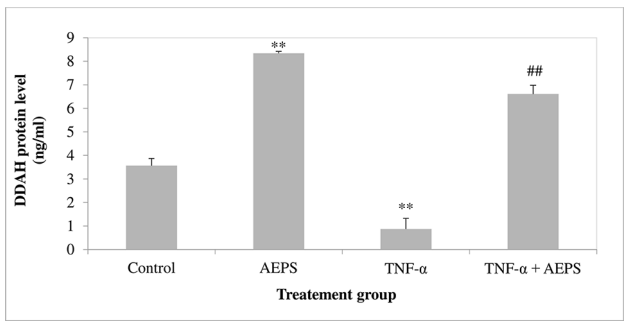

FIGURE 4 | DDAH1 protein level in human umbilical vein endothelial cells (HUVEC). Data shown as mean ± SEM, $n = 6$ [$^{**}P < 0.01$ compared with the control group, $^{\#\#}P < 0.01$ compared with the tumor necrosis factor (TNF)-α group].

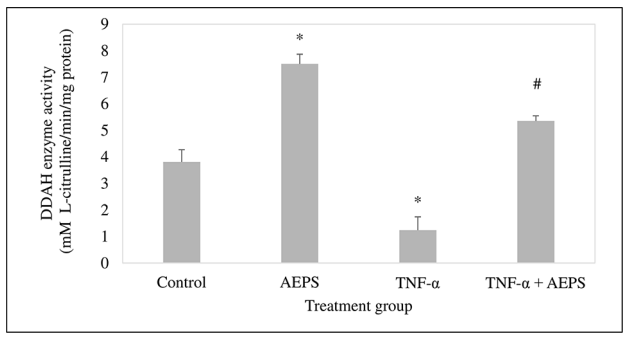

FIGURE 5 | Dimethylarginine dimethylaminohydrolase (DDAH) enzyme activity in human umbilical vein endothelial cells (HUVEC). Data shown as mean ± SEM, $n = 6$ [$^{*}P < 0.05$ compared with the control group, $^{\#}P < 0.05$ compared with the tumor necrosis factor (TNF)-α group].

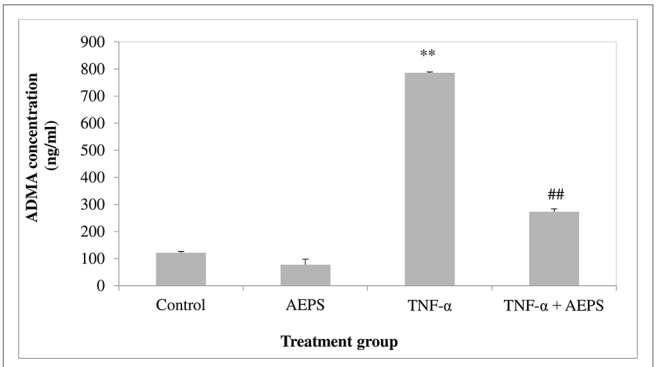

FIGURE 6 | Asymmetric dimethylarginine (ADMA) concentration in human umbilical vein endothelial cells (HUVEC). Data shown as mean ± SEM, $n = 6$ [$^{**}P < 0.01$ compared with THE control group, $^{\#\#}P < 0.01$ compared with the tumor necrosis factor (TNF)-α group].

NO Production in HUVEC

There was a significant increase in NO level produced by HUVEC treated with AEPS compared to the control group ($P = 0.0001$) (**Figure 7**). HUVEC induced by TNF-α showed a decrease in NO level compared to control ($P = 0.0007$). On the other hand, treatment of TNF-α-induced HUVEC with AEPS promoted NO production compared to the TNF-α group ($P = 0.0001$).

DISCUSSION

The main findings from this study were AEPS stimulated DDAH activity, thus decreasing ADMA level and increasing NO production in TNF-α-treated HUVEC. The results showed that TNF-α decreased *DDAH1* mRNA expression compared to control. This is in accordance with a previous study whereby mRNA expression of *DDAH1* is decreased in HUVEC treated

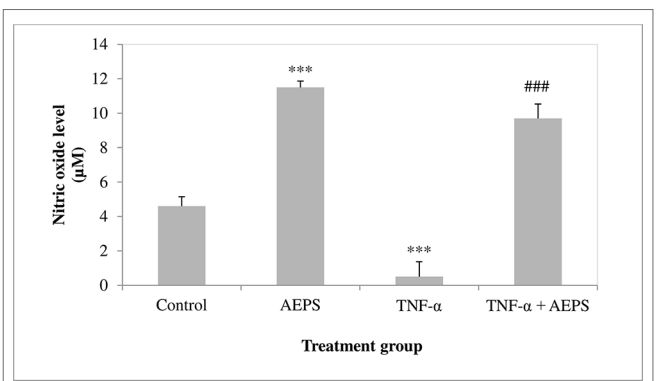

FIGURE 7 | Nitric oxide level in human umbilical vein endothelial cells (HUVEC). Data shown as mean ± SEM, $n = 6$ [$^{***}P < 0.001$ compared with the control group, $^{\#\#\#}P < 0.001$ compared with the tumor necrosis factor (TNF)-α group].

with TNF-α or oxidized low-density lipoprotein (ox-LDL) (Ito et al., 1999). Induction with TNF-α also caused reduction in DDAH1 protein level and DDAH activity. This study was in conformity with the previous study whereby 250 U/mol of TNF-α reduced 60% of DDAH activity in endothelial cells (Vairappan et al., 2009). AEPS was able to increase *DDAH1* mRNA expression in HUVEC treated with TNF-α. AEPS increased *DDAH1* mRNA expression, causing more DDAH1 protein to be synthesized and DDAH activity to be increased. AEPS was reported to have anti-inflammatory action whereby it suppressed nuclear factor-κβ (NF-κβ) activation and cellular adhesion molecule expression in HUVEC treated with TNF-α (Ismail et al., 2018). Anti-TNF therapy resulted in reduced NF-κβ-driven inflammation and improved DDAH and eNOS expression in cirrhotic rats (Balasubramanian et al., 2017). Therefore, in this study, the anti-inflammatory activity of AEPS could be a factor contributing to improved DDAH activity in TNF-α-induced HUVEC.

Since DDAH plays an important role in degrading ADMA, reduction in DDAH activity leads to an increase in ADMA, which in turn reduces eNOS activity and NO production. High ADMA concentration in the plasma is a risk factor for development of atherosclerosis and cardiovascular diseases (Jawalekar et al., 2013). This study showed that treatment of HUVEC with TNF-α for 24 h caused an increase in ADMA level. A previous study showed that TNF-α-treated HUVEC had higher level of ADMA after 24 and 48 h of incubation (Eid et al., 2007). Another *in vitro* study reported that HUVEC exposed to TNF-α for 48 h showed eight times increase in ADMA level (Ito et al., 1999) and DDAH activity decreased to 60% of baseline value.

Based on previous studies, intracellular DDAH plays an important role in controlling ADMA concentrations (Vairappan et al., 2009). Endothelial cells exposed to *S*-2-amino-4(3-methylguanidino) butanoic acid had reduced DDAH activity and increased ADMA formation (MacAllister et al., 1996). Similarly, in another study, exposure of endothelial cells to TNF-α caused a reduction in DDAH activity that leads to accumulation of intracellular ADMA (Eid et al., 2007). Treatment of TNF-α-induced HUVEC with AEPS successfully decreased ADMA level. Since AEPS stimulates DDAH activity, more ADMA will be degraded to L-citrulline and dimethylamine, thus decreasing ADMA level. On the other hand, there are several therapeutic ways to reduce ADMA. Previous studies have reported that L-arginine supplementation enhances endothelial function in hypercholesterolemic rabbits by reducing ADMA (Brinkmann et al., 2015). A clinical study on patients with rheumatoid arthritis showed a significant reduction in ADMA after 3 months of treatment with TNF-α inhibitors by increasing endothelial progenitor cells (Spinelli et al., 2013).

Endothelial NO is mainly synthesized by eNOS from L-arginine. Treatment of HUVEC with TNF-α reduced NO production. By inhibiting DDAH activity, TNF-α reduces ADMA degradation. ADMA inhibits eNOS competitively, thus reducing NO synthesis (Czarnecka et al., 2017). Furthermore, TNF-α reduces eNOS mRNA expression and the stability of eNOS mRNA, resulting in further reduction of NO production in HUVEC (Guijun et al., 2008). Treatment of TNF-α-induced HUVEC with AEPS promoted NO production. Since AEPS was able to stimulate DDAH activity, less ADMA was available to inhibit eNOS. This resulted in the increase in NO level. The results were in accordance with previous study whereby AEPS leaves stimulated eNOS activity and NO production in HUVEC (Ugusman et al., 2010).

The results also showed that AEPS promoted NO generation in both the absence and presence of TNF-α. In an earlier study, AEPS leaves had been shown to stimulate NO production in the absence and presence of hydrogen peroxide (H_2O_2) (Ugusman et al., 2010). Even in baseline culture condition without H_2O_2 treatment, AEPS alone was able to increase eNOS mRNA expression, eNOS protein level, and eNOS activity in HUVEC. This resulted in increased NO production by the cells (Ugusman et al., 2010). In this study, at baseline condition, AEPS alone promoted NO generation together with increased DDAH protein level and activity. Increased DDAH activity caused ADMA level to be maintained at a low baseline level, hence promoting eNOS activity and NO production. This result suggested that AEPS improved endothelial function by augmenting endothelial NO production in both healthy and diseased states.

Antioxidants are known to enhance NO by scavenging reactive oxygen species (ROS), hence protecting NO against oxidative destruction by ROS (Ignarro et al., 2006). As AEPS has an antioxidant effect, there may be a possibility that the increase in NO in this study is contributed by its ROS scavenging action too. However, this factor is beyond the scope of our study. It will be interesting to look at this factor in future experiments.

LC–MS Orbitrap full-scan analysis of AEPS leaves used in this study showed the presence of flavonoids such as naringenin, quercetin, and vitexin. Naringenin had been shown to stimulate eNOS and NO in endothelial cells exposed to high glucose (Qin et al., 2016). Quercetin caused an increase in plasma NO and eNOS activity in vascular tissues of hypertensive rats (Yamamoto and Oue, 2006). Besides, quercetin increased DDAH activity and decreased ADMA concentration in rat's liver (Trocha et al., 2012). Consumption of biscuits containing bioactive complex of quercetin, selenium, catechins, and curcumin reduced ADMA level in the plasma of healthy men (Madaric et al., 2013). Quercetin also inhibited ADMA-induced apoptosis in glomerular endothelial cells (Guo et al., 2014).

However, to date, there is no study done on the effect of vitexin on the DDAH–ADMA–NO pathway yet. Nevertheless, vitexin was proven to promote cell viability, suppressed apoptosis and reduced oxidative stress in HUVEC treated with ox-LDL (Zhang et al., 2017). Besides, vitexin inhibited overexpression of pro-inflammatory cytokines such as IL-1β, IL-6, TNF-α, and cellular adhesion molecules in ox-LDL-induced HUVEC by activating 5′-adenosine monophosphate-activated protein kinase (AMPK) signaling (Zhang et al., 2017). In lipopolysaccharide (LPS)-activated RAW 264.7 cells, vitexin was able to reduce pro-inflammatory mediators by inhibiting the expression of transcriptional factors such as p-p38, p-ERK1/2, and p-JNK (Rosa et al., 2016). Since anti-TNF therapy resulted in reduced inflammation and improved DDAH expression in rats (Balasubramanian et al., 2017), the anti-inflammatory activity of vitexin could also be a contributing factor to the effects of AEPS on DDAH activity in this study.

Previous phytochemical analysis showed that *P. sarmentosum* contains other active compounds such as rutin, vitamin E,

carotenes, tannins, and xanthophyll (Miean and Mohamed, 2001). An *in vivo* study on ischemia/reperfusion rat models reported that rutin stimulated the DDAH/NOS pathway by upregulating both eNOS and *DDAH1* expression (Lanteri et al., 2007). Besides, high-dose vitamin E supplementation potentially reduced ADMA level in patients with chronic renal insufficiency by improving DDAH activity and NO bioavailability (Jiang et al., 2002). In a Japanese population, high serum carotenoid levels such as α-carotene and β-carotene were linked to low ADMA level (Watarai et al., 2014). As this study used crude extract of *P. sarmentosum* and not its purified active compound, this study was unable to identify the specific component of the extract that mediated the observed effects. However, it is suggested that the effects were likely due to the active compounds mentioned above.

STUDY LIMITATIONS

This study did not evaluate the detailed intracellular signaling pathway by which AEPS acts on the endothelial cells. Besides, the present study did not consider the possibility of the results to be related to the reduction of oxidative stress by the antioxidant effect of AEPS. Further studies incorporating endothelial response to shear stress as well as functional studies should be performed in order to extrapolate the findings from this *in vitro* study to what is observed physiologically.

CONCLUSION

The present study shows that AEPS promotes endothelial NO production by stimulating DDAH activity and thus decreases ADMA level in TNF-α-induced HUVEC. Based on the vasoprotective and anti-atherosclerotic effects of endothelial NO, AEPS has the potential to reduce the risk of endothelial dysfunction and atherosclerosis. However, further studies using isolated bioactive components from AEPS are required in order to support the therapeutic potential of AEPS for endothelial dysfunction and atherosclerosis.

DATA AVAILABILITY

All datasets generated for this study are included in the manuscript.

ETHICS STATEMENT

This study was approved by the Ethical Research Committee of Universiti Kebangsaan Malaysia Medical Centre and National Medical Research Registration (approval numbers: FF-2014-412 and NMRR-14-583-20729). Informed written consent was obtained from all participants.

AUTHOR CONTRIBUTIONS

AU and CH conceptualized the study and designed the experiment. US and JL performed the experiments and analyzed the data. AU, CH, AA, JL, and US analyzed and interpreted the data. AU, CH, AA, JL, and US wrote the manuscript and performed critical analysis and the necessary revisions of the work. All authors read and approved the final manuscript.

FUNDING

This study was supported by research grants from the Ministry of Higher Education, Malaysia (Grant No.: FRGS/1/2014/SKK03/UKM/02/1), and Universiti Kebangsaan Malaysia (Grant No: GGPM-2013-029). The funders had no role in study design, data collection and analysis, decision to publish, or preparation of the manuscript.

ACKNOWLEDGMENTS

We are grateful to the staff nurses from the labor rooms in the Department of Obstetrics and Gynaecology, Hospital Kuala Lumpur, for their assistance in umbilical cord sample collection.

REFERENCES

Adel, A., Zaiton, Z., Faizah, O., Srijit, D., Santhana, R., and Nor-Anita, N. (2010). Aqueous extract of *Piper sarmentosum* decreases atherosclerotic lesions in high cholesterolemic experimental rabbits. *Lipids Health Dis.* 9, 44. doi: 10.1186/1476-511X-9-44

Albuquerque, M. L. C., Waters, C. M., Savla, U., Schnaper, H. W., and Flozak, A. S. (2000). Shear stress enhances human endothelial cell wound closure *in vitro*. *Am. J. Physiol. Heart Circ. Physiol.* 279 (1), H293–H302. doi: 10.1152/ajpheart.2000.279.1.H293

Balasubramanian, V., Mehta, G., Jones, H., Sharma, V., Davies, N. A., Jalan, R., et al. (2017). Post-transcriptional regulation of hepatic DDAH1 with TNF blockade leads to improved eNOS function and reduced portal pressure in cirrhotic rats. *Sci. Rep.* 7 (1), 179000. doi: 10.1038/s41598-017-18094-3

Benjamin, E. J., Blaha, M. J., Chiuve, S. E., Cushman, M., Das, S. R., Deo, R., et al. (2017). American Heart Association Statistics Committee and Stroke Statistics Subcommittee. Heart disease and stroke statistics—2017 update: a report from the American Heart Association. *Circulation* 135 (10), e146–e603. doi: 10.1161/CIR.0000000000000485

Bradford, M. M. (1976). A rapid and sensitive method for the quantitation of microgram quantities of protein utilizing the principle of protein-dye binding. *Anal. Biochem.* 72, 248–254. doi: 10.1016/0003-2697(76)90527-3

Brinkmann, S. J. H., Worner, E. A., Buijs, N., Richir, M., Cynober, L., van Leeuwen, P. A., et al. (2015). The arginine/ADMA ratio is related to the prevention of atherosclerotic plaques in hypercholesterolemic rabbits when giving a combined therapy with atorvastatine and arginine. *Int. J. Mol. Sci.* 16 (6), 12230–12242. doi: 10.3390/ijms160612230

Bulau, P., Zakrzewicz, D., Kitowska, K., Leiper, J., Gunther, A., Grimminger, F., et al. (2007). Analysis of methylarginine metabolism in the cardiovascular system identifies the lung as a major source of ADMA. *Am. J. Physiol. Lung Cell Mol. Physiol.* 292, L18–L24. doi: 10.1152/ajplung.00076.2006

Chan, E. W. C., and Wong, S. K. (2014). Phytochemistry and pharmacology of three *Piper* species: an update. *IJP.* 1 (9), 534–544. doi: 10.13040/IJPSR.0975-8232.IJP

Chaveerach, A., Mokkamul, P., Sudmoon, R., and Tanee, T. (2008). Ethnobotany of the genus *Piper* (Piperaceae) in Thailand. *Ethnobot. Res. Appl.* 4, 223–231. doi: 10.17348/era.4.0.223-231

Csonka, C., Páli, T., Bencsik, P., Görbe, A., Ferdinandy, P., and Csont, T. (2015). Measurement of NO in biological samples. *Br. J. Pharmacol.* 172 (6), 1620–1632. doi: 10.1111/bph.12832

Czarnecka, A., Milewski, K., and Zielińska, M. (2017). Asymmetric dimethylarginine and hepatic encephalopathy: cause, effect or association? *Neurochem. Res.* 42 (3), 750–761. doi: 10.1007/s11064-016-2111-x

Eid, H. M. A., Lyberg, T., Arnesen, H., and Seljeflot, I. (2007). Insulin and adiponectin inhibit the TNF-α induced ADMA accumulation in human umbilical endothelial cells: the role of DDAH. *Atherosclerosis* 194 (2), 1–8. doi: 10.1016/j.atherosclerosis.2006.11.008

Guijun, Y., You, B., Chen, S. P., Liao, J. K., and Sun, J. (2008). Tumor necrosis factor-α downregulates endothelial nitric oxide synthase mRNA stability *via* translation elongation factor 1-α 1. *Circ. Res.* 103, 591–597. doi: 10.1161/CIRCRESAHA.108.173963

Guo, W., Ding, J., Zhang, A., Dai, W., Liu, S., Diao, Z., et al. (2014). The inhibitory effect of quercetin on asymmetric dimethylarginine-induced apoptosis is mediated by the endoplasmic reticulum stress pathway in glomerular endothelial cells. *Int. J. Mol. Sci.* 15 (1), 484–503. doi: 10.3390/ijms15010484

Hafizah, A. H., Zaiton, Z., Zulkhairi, A., Mohd Ilham, A., Nor Anita, M. M., and Zaleha, A. M. (2010). *Piper sarmentosum* as an antioxidant on oxidative stress in human umbilical vein endothelial cells induced by hydrogen peroxide. *J. Zhejiang Univ. Sci. B.* 11, 357–365. doi: 10.1631/jzus.B0900397

Ignarro, L. J., Byrns, R. E., Sumi, D., de Nigris, F., and Napoli, C. (2006). Pomegranate juice protects nitric oxide against oxidative destruction and enhances the biological actions of nitric oxide. *Nitric Oxide* 15 (2), 93–102. doi: 10.1016/j.niox.2006.03.001

Ishizaka, M., Nagai, K., Iwanaga, M., Imamura, M., and Azuma, H. (2007). Possible involvement of enhanced arginase activity due to up-regulated arginases and decreased hydroxyarginine in accelerating intimal hyperplasia with hyperglycemia. *Vascul. Pharmacol.* 47, 272–280. doi: 10.1016/j.vph.2007.08.001

Ismail, S. M., Sundar, U. M., Ugusman, A., Hui, C. K., and Aminuddin, A. (2018). *Piper sarmentosum* attenuates TNF-α-induced VCAM-1 and ICAM-1 expression in human umbilical vein endothelial cells. *J. Taibah. Univ. Med. Sci.* 13 (3), 225–231. doi: 10.1016/j.jtumed.2018.01.003

Ito, A., Tsao, P. S., Adimoolam, S., Kimoto, M., Ogawa, T., and Cooke, J. P. (1999). Novel mechanism for endothelial dysfunction: dysregulation of dimethylarginine dimethylaminohydrolase. *Circulation* 99, 3092–3095. doi: 10.1161/01.CIR.99.24.3092

Jawalekar, S. L., Karnik, A., and Bhutey, A. (2013). Risk of cardiovascular diseases in diabetes mellitus and serum concentration of asymmetrical dimethylarginine. *Biochem. Res. Int.* 1–6. doi: 10.1155/2013/189430

Jiang, L., Li, N. S., Li, Y. J., and Deng, H. W. (2002). Probucol preserves endothelial function by reduction of the endogenous nitric oxide synthase inhibitor level. *Br. J. Pharmacol.* 135, 1175–1182. doi: 10.1038/sj.bjp.0704563

Lanteri, R., Acquaviva, R., DiGiacomo, C., Sorrenti, V., Destri, G.L., Santangelo, M., et al. (2007). Rutin in rat liver ischemia/reperfusion injury: effect on DDAH/NOS pathway. *Microsurgery* 27 (4), 245–251. doi: 10.1002/micr.20345

Liu, X., Hou, L., Xu, D., Chen, A., Yang, L., Zhuang, Y., et al. (2016). Effect of asymmetric dimethylarginine (ADMA) on heart failure development. *Nitric Oxide* 54, 73–81. doi: 10.1016/j.niox.2016.02.006

MacAllister, R. J., Parry, H., Kimoto, M., Ogawa, T., Russel, R. J., Hodson, H., et al. (1996). Regulation of nitric oxide synthesis by dimethylarginine dimethylaminohydrolase. *Br. J. Pharmacol.* 119, 1533–1540. doi: 10.1111/j.1476-5381.1996.tb16069.x

Madaric, A., Kadrabova, J., Krajcovicova-Kudlackova, M., Valachovicova, M., Spustova, V., Mislanova, C., et al. (2013). The effect of bioactive complex of quercetin, selenium, catechins and curcumin on cardiovascular risk markers in healthy population after a two month consumption. *Bratisl. Lek. Listy.* 114 (2), 84–87. doi: 10.4149/BLL_2013_019

Miean, K. H., and Mohamed, S. (2001). Flavonoid (myricetin, quercetin, kaempferol, luteolin, and apigenin) content of edible tropical plants. *J. Agric. Food Chem.* 49, 3106–3112. doi: 10.1021/jf000892m

Pope, A. J., Karuppiah, K., and Cardounel, A. J. (2009). Role of the PRMT–DDAH–ADMA axis in the regulation of endothelial nitric oxide production. *Pharmacol. Res.* 60, 461–465. doi: 10.1016/j.phrs.2009.07.016

Prescott, L. M., and Jones, M. E. (1969). Modified methods for the determination of carbamyl aspartate. *Anal. Biochem.* 32, 408–419. doi: 10.1016/S0003-2697(69)80008-4

Qin, W., Ren, B., Wang, S., Liang, S., He, B., Shi, X., et al. (2016). Apigenin and naringenin ameliorate PKCβII-associated endothelial dysfunction *via* regulating ROS/caspase-3 and NO pathway in endothelial cells exposed to high glucose. *Vascul. Pharmacol.* 85, 39–49. doi: 10.1016/j.vph.2016.07.006

Rosa, S. I. G., Rios-Santos, F., Balogun, S. O., and de Oliveira Martins, D. T. (2016). Vitexin reduces neutrophil migration to inflammatory focus by down-regulating pro-inflammatory mediators *via* inhibition of p38, ERK1/2 and JNK pathway. *Phytomedicine.* 23 (1), 9–17. doi: 10.1016/j.phymed.2015.11.003

Spinelli, F. R., Metere, A., Barbati, C., Pierdominici, M., Iannuccelli, C., Lucchino, B., et al. (2013). Effect of therapeutic inhibition of TNF on circulating endothelial progenitor cells in patients with rheumatoid arthritis. *Mediators Inflamm.* 1–8. doi: 10.1155/2013/537539

Su, J. B. (2015). Vascular endothelial dysfunction and pharmacological treatment. *World J. Cardiol.* 7 (11), 719–741. doi: 10.4330/wjc.v7.i11.719

Sukhovershin, R. A., Yepuri, G., and Ghebremariam, Y. T. (2015). Endothelium-derived nitric oxide as an antiatherogenic mechanism: implications for therapy. *Methodist Debakey Cardiovasc. J.* 11 (3), 166–171. doi: 10.14797/mdcj-11-3-166

Trocha, M., Merwid-Lad, A., Szuba, A., Sozanski, T., Magdalan, J., Szelag, A., et al. (2012). Effect of quercetin-5′-sulfonic acid sodium salt on SOD activity and ADMA/DDAH pathway in extracorporeal liver perfusion in rats. *Adv. Clin. Exp. Med.* 21 (4), 423–431.

Ugusman, A., Zakaria, Z., Hui, C. K., and Nordin, N. (2011). *Piper sarmentosum* inhibits ICAM-1 and Nox4 gene expression in oxidative stress-induced human umbilical vein endothelial cells. *BMC Complement. Altern. Med.* 11, 31. doi: 10.1186/1472-6882-11-31

Ugusman, A., Zakaria, Z., Hui, C. K., Nordin, N. A. M. M., and Mahdy, Z. A. (2012). Flavonoids of Piper sarmentosum and its cytoprotective effects against oxidative stress. *EXCLI J.* 11, 705-714. doi: 10.17877/DE290R-10356

Ugusman, A., Zakaria, Z., Hui, C. K., and Nordin, N. (2010). *Piper sarmentosum* increases nitric oxide production in oxidative stress: a study on human umbilical vein endothelial cells. *Clinics* 65, 709–714. doi: 10.1590/S1807-59322010000700010

Vairappan, B. (2015). Endothelial dysfunction in cirrhosis: role of inflammation and oxidative stress. *World J. Hepatol.* 7 (3), 443–459. doi: 10.4254/wjh.v7.i3.443

Vairappan, B., Sharma, V., Winstanley, A., Davies, N., Shah, N., Jalan, R., et al. (2009). Modulation of the DDAH–ADMA pathway with the Farnesoid receptor (FXR) agonist INT-747 restores hepatic eNOS activity and lowers portal pressure in cirrhotic rats. *Hepatology* 50, 336A–337A.

Watarai, R., Suzuki, K., Ichino, N., Osakabe, K, Sugimoto, K., Yamada, H., et al. (2014). Association between serum levels of carotenoids and serum asymmetric dimethylarginine levels in Japanese subjects. *J. Epidemiol.* 24 (3), 250–257. doi: 10.2188/jea.JE20130137

Yamamoto, Y., and Oue, E. (2006). Antihypertensive effect of quercetin in rats fed with a high-fat high-sucrose diet. *Biosci. Biotechnol. Biochem.* 70 (4), 933–939. doi: 10.1271/bbb.70.933

Zainudin, M. M., Zakaria, Z., and Nordin, N. A. M. M. (2015). The use of *Piper sarmentosum* leaves aqueous extract (Kadukmy™) as antihypertensive agent in spontaneous hypertensive rats. *BMC Complement. Altern. Med.* 15, 54. doi: 10.1186/s12906-015-0565-z

Zainudin, M. M., Zakaria, Z., Nordin, N. A. M. M., and Othman, F. (2013). Does oral ingestion of *Piper sarmentosum* cause toxicity in experimental animals? *Evid. Based. Complement. Alternat. Med.* 1–9. doi: 10.1155/2013/705950

Zhang, P., Hu, X., Xu, X., Chen, Y., and Bache, R.J. (2011). Dimethylarginine dimethylaminohydrolase 1 modulates endothelial cell growth through NO and Akt. *Arterioscler. Thromb. Vasc. Biol.* 31 (4), 890–897. doi: 10.1161/ATVBAHA.110.215640

Zhang, S., Guo, C., Chen, Z., Zhang, P., Li, J., and Li, Y. (2017). Vitexin alleviates ox-LDL-mediated endothelial injury by inducing autophagy *via* AMPK signaling activation. *Mol. Immunol.* 85, 214–221. doi: 10.1016/j.molimm.2017.02.020

Conflict of Interest Statement: The authors declare that the research was conducted in the absence of any commercial or financial relationships that could be construed as a potential conflict of interest.

frontiers in Pharmacology

ORIGINAL RESEARCH
published: 18 September 2019
doi: 10.3389/fphar.2019.00990

Si-Miao-Yong-An Decoction Protects Against Cardiac Hypertrophy and Dysfunction by Inhibiting Platelet Aggregation and Activation

Congping Su[1], Qing Wang[1], Huimin Zhang[1], Wenchao Jiao[1], Hui Luo[1], Lin Li[1], Xiangyang Chen[2], Bin Liu[2], Xue Yu[1], Sen Li[3], Wei Wang[1]* and Shuzhen Guo[1]**

[1] School of Traditional Chinese Medicine, Beijing University of Chinese Medicine, Beijing, China, [2] School of Chinese Materia Medica, Beijing University of Chinese Medicine, Beijing, China, [3] School of Life Sciences, Beijing University of Chinese Medicine, Beijing, China

OPEN ACCESS

Edited by:
Jianxun Liu,
China Academy of Chinese Medical Sciences, China

Reviewed by:
Meiping Wu,
Shanghai University of Traditional Chinese Medicine, China
Qiyang Shou,
Zhejiang Chinese Medical University, China

***Correspondence:**
Sen Li
senli@bucm.edu.cn
Wei Wang
Wangwei26960@126.com
Shuzhen Guo
guoshz@bucm.edu.cn

Specialty section:
This article was submitted to Ethnopharmacology, a section of the journal Frontiers in Pharmacology

Received: 07 April 2019
Accepted: 05 August 2019
Published: 18 September 2019

Citation:
Su C, Wang Q, Zhang H, Jiao W, Luo H, Li L, Chen X, Liu B, Yu X, Li S, Wang W and Guo S (2019) Si-Miao-Yong-An Decoction Protects Against Cardiac Hypertrophy and Dysfunction by Inhibiting Platelet Aggregation and Activation. Front. Pharmacol. 10:990. doi: 10.3389/fphar.2019.00990

Objective: The aim of this study was to determine whether Si-Miao-Yong-An decoction (SMYAD) could ameliorate pressure overload-induced heart hypertrophy and its mechanisms.

Methods: C57BL/6 mice were subjected to either sham or transverse aortic constriction (TAC) surgery to induce heart hypertrophy. SMYAD (14.85 g/kg/day, ig) or captopril (16.5 mg/kg/day, ig) was administered to the mice for 4 weeks. Cardiac function was evaluated based on echocardiography. Heart hypertrophy was detected using hematoxylin and eosin or wheat germ agglutinin staining. Protein expression of CD41, CD61, and P-selectin were measured with Western blot and immunohistochemistry. The expression levels of atrial natriuretic peptide, brain natriuretic peptide, β-myosin heavy chain, β-thromboglobulin, and von Willebrand factor were evaluated by quantitative polymerase chain reaction.

Results: Four weeks after TAC, mice developed exaggerated cardiac hypertrophy and demonstrated a strong decrease in left ventricular ejection fraction compared with sham (29.9 ± 9.3% versus 66.0 ± 9.9%; $P < 0.001$). Conversely, SMYAD improved cardiac dysfunction with preserved left ventricular ejection fraction (66.5 ± 17.2%; $P < 0.001$). Shortening fraction was increased by SMYAD, while the left ventricular internal diameter and left ventricular volume were decreased in SMYAD group. SMYAD treatment significantly attenuated cardiac hypertrophy as reflected by the inhibition of atrial natriuretic peptide, brain natriuretic peptide, β-myosin heavy chain mRNA expression, and by the decreasing of cardiac myocyte cross-sectional area. Furthermore, Western blot and immunohistochemistry indicated that the protein expression of platelet aggregation markers (CD41 and CD61) and platelet activation marker (P-selectin) were significantly higher in model mice compared

with control. These pathological alterations in TAC-induced mice were significantly ameliorated or blocked by SMYAD administration.

Conclusions: Our results suggested that SMYAD exerted its effect by inhibiting platelet aggregation and activation as revealed by CD41/CD61/P-selectin downregulation. Inhibition the activation of the platelets might contribute to the therapeutic effect of SMYAD in failing heart.

Keywords: Si-Miao-Yong-An decoction, cardiac hypertrophy, heart failure, platelet activation, transverse aortic constriction

INTRODUCTION

Cardiac hypertrophy is a common pathophysiological component of cardiac remodeling in many kinds of cardiovascular diseases, such as valvular heart disease, hypertension, and hypertrophic cardiomyopathy (Pillai et al., 2015). This process is usually considered to be a compensatory response of the heart to an increased hemodynamic load, which could cause contractile depression, ventricular dilatation, interstitial cardiac fibrosis, and eventually heart failure (HF) (Ooi et al., 2015). Studies have shown that platelet activation played a critical role in several cardiovascular diseases, such as HF (Schafer et al., 2003), coronary artery disease (George et al., 2016), and atrial fibrillation (Lim et al., 2014). Platelet activation is followed by platelet adhesion that is characterized by expression of variety of glycoproteins on platelet surface. In platelet-related thrombogenesis, platelets adhere to injured endothelium undergoing a conformational transition followed by activation and degranulation. This activation results in the combination of fibrinogen with the platelet surface receptors and consequently leading to thrombus formation (Santhakumar et al., 2015), thereby leading to coronary artery disease and HF.

Si-Miao-Yong-An decoction (SMYAD) is a traditional Chinese medicine formula, which consists of *Lonicerae Japonicae Flos* (Jinyinhua), *Scrophulariae Radix* (Xuanshen), *Angelica Sinensis Radix* (Danggui), and *Glycyrrhizae Radix et Rhizoma* (Gancao). SMYAD was reported to reduce the atherosclerosis plaque area, promote the recruitment of vasa vasorum pericytes, and stabilize atherosclerosis vulnerable plaques in ApoE$^{-/-}$ mice (Qi et al., 2019). SMYAD has also been verified to ameliorate the stability of atherosclerotic plaque by lowering blood lipid in rabbit model (Peng et al., 2012). The formula was also reported to have anti-inflammatory and anti-oxidation properties (Wang and Tian, 2014). We previously demonstrated that SMYAD promoted isoprenaline-induced HF through antioxidant effects (Ren et al., 2019). However, the role of SMYAD in pressure overload-induced cardiac hypertrophy has yet not been explored.

In this study, we found that SMYAD attenuated pressure overload-induced cardiac dysfunction through inhibiting platelet aggregation and activation, suggesting SMYAD as a promising therapeutic agent for adverse cardiac remodeling.

MATERIALS AND METHODS

Animals

All the animal experiments were performed in accordance with the "Guide for the Care and Use of Laboratory Animals" by the National Institutes of Health. This study was approved by the Animal Research Ethics Committee of Beijing University of Chinese Medicine (BUCM-4-2018090701-3019). All studies were conducted in line with the approval of the Animal Care Committee of Beijing University of Chinese Medicine. Male C57BL/6 mice, weighing 20–22 g, were obtained from Vital River (Beijing, China, License number: SCXK 2016-0006) and maintained on a 12:12-hour light–dark cycle with free *ad libitum* access to food and water for a 1-week acclimatization period.

Sample Preparation and Constituents Identification of Si-Miao-Yong-An Decoction

SMYAD was provided by School of Chinese Materia Medica, Beijing University of Chinese Medicine. *Lonicerae Japonicae Flos*, *Scrophulariae Radix*, *Angelica Sinensis Radix*, and *Glycyrrhizae Radix et Rhizoma* were obtained from Anguo Wanlian Chinese Medicine Yinpian Co. Ltd (Hebei, China) and identified by Professor Yuan Zhang. Detailed information of the drug materials and the scan of the vouchers were given in **Supplementary Table 1.** The voucher specimens were deposited in School of Chinese Materia Medica, Beijing University of Chinese Medicine. The SMYAD was prepared with *Lonicerae Japonicae Flos*, *Scrophulariae Radix*, *Angelica Sinensis Radix*, and *Glycyrrhizae Radix et Rhizoma* at a weight ratio of 3:3:2:1 according to the ancient documents. The herbs were extracted twice by refluxing with 10 times of water (volume/weight) for 2 h each time. Then, the extracted solution was filtered. The filtered extracts were mixed together and then concentrated to the relative density for 1.5 g/ml.

The high-performance liquid chromatography characteristic chromatogram of SMYAD has been previously established and used for its quality control (Li et al., 2018). On the basis of macroporous adsorption resin column chromatography, nuclear magnetic resonance, and mass spectrometry (MS), we have isolated and identified 22 compounds from SMYAD, which were 5(*S*)-5-carboxystrictosidine (1), harpagoside (2), geniposide (3), glycyrrhetinic acid (4), glycyrrhizic acid (5),

hyperoside (6), liquiritin (7), isoliquiritoside (8), liquiritigenin (9), isoliquiritigenin (10), luteolin (11), quercetin (12), 2-(3-hydroxy-4-methoxyphenyl)ethyl *O*-α-arabinopyranosyl-(1→6)-*O*-α- rhamnopyranosyl-(1→3)-*O*-β-glucopyranoside (13), angoroside C (14), acteoside (15), cinnamic acid (16), ferulic acid (17), (E)-aldosecologanin (18), protocatechuic acid (19), stigmasterol (20), hentriacontanol (21), and daucosterol (22), and 13 compounds were isolated from SMYAD for the first time (Liu et al., 2018).

To further investigate the pharmacokinetic change of SMYAD, we explored the absorbed constituents of water extract of SMYAD in rat plasma using liquid chromatography–MS-ion trap–time of flight method. As a result, 14 compounds were preliminary identified, of which 10 compounds were prototypes of SMYAD, and four were metabolites (Chi et al., 2016). In addition, seven major active ingredients of SMYAD extract (i.e., harpagide, chlorogenic acid, sweroside, loganin, liquiritin, angoroside C, harpagoside) in rat plasma were detected simultaneously by a sensitive ultra-performance liquid chromatography–tandem mass spectrometry method (Liu et al., 2017a).

Reagents

Captopril was obtained from Beijing Jingfeng Pharmaceutical Group Co. Ltd. (Drug Production Approval Number H20084569). Pentobarbital sodium was purchased from Sigma (St. Louis, USA).

Groups and Treatment

Mice were randomly assigned to four groups: sham with vehicle (sham), TAC with vehicle (TAC), TAC with captopril (TAC + captopril), and TAC with SMYAD (TAC + SMYAD). Mice in the latter three groups underwent TAC surgery. On day 3 post-surgery, SMYAD was administered at a dose of 14.85 g/kg/day *via* oral gavage administration for 28 days. Captopril, which was used as a positive control, was administered intragastrically at a dose of 16.5 mg/kg/day for 28 days. The sham and TAC groups were fed intragastrically with equal volumes of double distilled water once daily for 4 weeks.

Transverse Aortic Constriction

Mice were subjected to TAC-induced pressure overload as previously described (Ren et al., 2018). Briefly, the mice were anesthetized with 0.5% pentobarbital sodium (50 mg/kg), then they were orally intubated and placed on a ventilator to maintain respiration. TAC was created using a 6-0 suture banded between the carotid arteries over a 26-gauge needle. The needle was immediately removed after ligation. Sham group animals underwent the carotid arteries separation procedure but without aortic ligation.

Echocardiography

Four weeks after the TAC surgery, the cardiac function was assessed by the Vevo2100 imaging system (VisualSonics, Canada). Echocardiography was performed with a 30-MHz linear transducer probe (MS500). Images were captured in M-mode using pulse-wave Doppler and tissue Doppler imaging. Offline image analyses were performed using dedicated Visual Sonics Vevo2100 1.6.0 software.

Histochemical and Immunohistochemical Analyses

The hearts were fixed in 4% paraformaldehyde, embedded in paraffin, and then stained with hematoxylin and eosin (HE). Pictures were acquired by Aperio VERSA scanning system (Leica Biosystems Richmond, Inc.). For immunohistochemistry, the slides were incubated with primary antibodies against CD41 (Glycoprotein IIb) (1:100, Abcam, ab33661, UK), CD61 (Glycoprotein IIIa) (1:100, Abcam, ab210515, UK), P-selectin (1:100, Abcam, ab54427, UK) overnight at 4°C. After the slides were washed with phosphate-buffered saline, they were incubated with the corresponding secondary antibodies for 1 h at 37°C. Photomicrographs of stained sections were digitalized and analyzed by an automated image analysis system (Image-Pro Plus 6.0 software, Media Cybernetics, Silver Spring, USA).

Immunofluorescent Staining

Immunofluorescent staining was performed using fluorescein isothiocyanate-conjugated wheat germ agglutinin (WGA) (1:200, Sigma-Aldrich, L4895, USA), and cell nuclei were counterstained with 4',6-diamidino-2-phenylindole (DAPI) (ZLI-9557, ZSGB-BIO, China). For determination of cardiac myocyte cross-sectional areas, 6-μm thick paraffin-embedded sections were stained for membranes with WGA for 30 min and then sealed with DAPI. Images were taken from areas of transversely cut muscle fibers by microscopy under a 400× field.

Quantitative Polymerase Chain Reaction

SYBR Green quantitative polymerase chain reaction was performed with Bio-Rad CFX96 Real-Time System. Target-specific primers were designed, and their sequences are listed later (each gene symbol is followed by the forward and reverse primers). Forward and reverse primers, complementary DNA template, and the FastStart universal SYBR Green Master Mix (Roche, USA) were mixed to a final volume of 20 μl. The following programm was used: 95°C for 10 min, followed by 40 cycles of 95°C for 15 s and 60°C for 1 min.

β-actin mouse: F:GGCTGTATTCCCCTCCATCG, R:CCAGTTGGTAACAATGCCATGT;
ANP mouse: F: GCTTCCAGGCCATATTGGAG, R: GGGGGCATGACCTCATCTT;
BNP mouse: F: GAGGTCACTCCTATCCTCTGG, R: GCCATTTCCTCCGACTTTTCTC;
β-*MHC* mouse*:* F: ACTGTCAACACTAAGAGGGTCA, R: TTGGATGATTTGATCTTCCAGGG;
β-*TG* mouse*:* F: CTCAGACCTACATCGTCCTGC, R: GTGGCTATCACTTCCACATCAG;
vWF mouse*:* F: GCTGGCATGGAATATAAGGAGTG, R: CCAAGCCTACCTGGGCATT.

Western Blot Analysis

Total protein from heart tissues was extracted using radioimmunoprecipitation assay lysis buffer, and protein concentrations were evaluated using bicinchoninic acid protein assay kit (Applygen, China). The protein was separated using sodium dodecyl sulfate polyacrylamide gel electrophoresis and then transferred onto polyvinylidene difluoride membranes using a wet transfer apparatus (Bio-Rad, USA). The membranes were blocked in 5% nonfat milk incubated with dilutions of anti-CD41 (1:1,000, Proteintech, 24552-1-AP, China), anti-CD62P (1:1,000, Abcam, ab54427, UK), and anti-CD61 (1:1,000, Abcam, ab210515, UK) antibodies overnight at 4°C. The membranes were then incubated for 1 h at room temperature with secondary antibodies (1:5,000, BioDee Biotechnology, DE0601 and DE0602, China). The membranes were detected using an ECL Western-blotting Detection Reagent kit (catalogue RPN2106, GE Healthcare USA), with the LAS-3000 detection system. Protein levels were analyzed using Image Lab software.

Statistical Analysis

The statistical analysis was performed using SPSS 22.0 statistical software (IBM, Armonk, NY), and the results were presented as mean ± standard error of the mean. Differences between groups were compared by one-way analysis of variance. $P < 0.05$ was considered statistically significant.

RESULTS

Si-Miao-Yong-An Decoction Ameliorated Transverse Aortic Constriction-Induced Cardiac Dysfunction

To investigate the effect of SMYAD on the cardiac function, transthoracic echocardiography was performed on the day before the animals were sacrificed (**Figure 1B**). As previously described, the aortic blood flow rate at the constriction point was greater than 2,400 mm/s in TAC-proceeded mice, whereas in the sham group, it was less than 900 mm/s (**Figure 1A**) (Ren et al., 2018). According to echocardiographic evaluation, left ventricular ejection fraction and left ventricular fractional shortening in the TAC group were markedly decreased as compared with those in the sham group, but these two parameters were significantly improved in the TAC + SMYAD group as compared with those in the TAC group (**Figure 1C**). In addition, TAC mice displayed a remarkable increase in left ventricular internal diameter (LVID) compared with the sham-operated mice ($P < 0.05$ and $P < 0.001$ for LVID; d and LVID; s, respectively). In contrast, SMYAD administration effectively reduced the TAC-induced increase in LVID; d and LVID; s by 17.7% ($P < 0.05$) and 34.4% ($P < 0.01$), respectively. Left ventricular volume at end systole (LV Vol; s) was increased after 4 weeks of pressure overload ($P < 0.001$), and SMYAD administration prevented the TAC-induced decrease in LV Vol; s ($P < 0.001$) (**Figure 1C**).

Si-Miao-Yong-An Decoction Prevented Pressure Overload-Induced Cardiac Hypertrophy

Next, we determined whether SMYAD administration attenuated cardiac hypertrophy and HF. The samples shown in **Figure 2A** and HE staining of whole heart (**Figure 2B**) demonstrated that TAC mice have dilated hearts and SMYAD administration prevented left ventricle dilation. Histological analysis indicated that TAC caused significant increase of cardiac myocyte cross-sectional area. WGA staining of histological sections further confirmed the inhibitory effect of SMYAD on cardiac hypertrophy induced by TAC (**Figures 2E**, **F**). As shown in **Figure 2G**, pressure overload induced by TAC remarkably increased the ratio of heart weight to body weight (HW/BW) and the ratio of heart weight to tibia length compared by the sham group ($P < 0.001$). In contrast, SMYAD administration effectively reduced the ratio of HW/BW by 22.2% compared with the TAC group ($P < 0.01$). Consistently, real-time polymerase chain reaction analysis of cardiac hypertrophy markers, such as atrial natriuretic peptide, brain natriuretic peptide, and β-myosin heavy chain, manifested a significant alleviation in the presence of SMYAD compared with that in TAC-treated mice (**Figure 2H**). Together, these data indicated that SMYAD prevented the development of cardiac hypertrophy *in vivo*.

Si-Miao-Yong-An Decoction Attenuated Histological Changes Following Transverse Aortic Constriction Surgery

According to HE staining, the heart tissues of the sham group displayed normal myofibrils with neatly arrangement. In the TAC group, a dense inflammatory infiltration, necrosis of a large number of cardiomyocytes, muscle fiber dissolution, and the disappearance of the normal structure of the myofibrils were observed. Heart tissues in the SMYAD and captopril groups showed less necrosis of myocardial cell than that in the TAC group. In addition, we found that necrosis of cardiomyocytes were induced both interstitial and perivascular in TAC hearts and attenuated in SMYAD-treated hearts (**Figures 2C, D**).

Si-Miao-Yong-An Decoction Inhibited CD41- and CD61-Mediated Platelet Aggregation in TAC-Induced Heart Failure

To confirm that platelet aggregation is altered in hearts after TAC surgery, we examined CD41 and CD61 levels in hearts at 4 weeks after TAC surgery. **Figures 3A**, **B** and **4A**, **B** exhibited that CD41 and CD61 expressions were increased in TAC mice compared with those in the control mice. However, both CD41 and CD61 were significantly reduced in the SMYAD-treated mice. Furthermore, immunohistochemistry staining of heart tissues illustrated that TAC treatment significantly increased the accumulation of CD41 and CD61 ($P < 0.001$) (**Figures 3C**, **D** and **4C**, **D**). Compared with those in the TAC group,

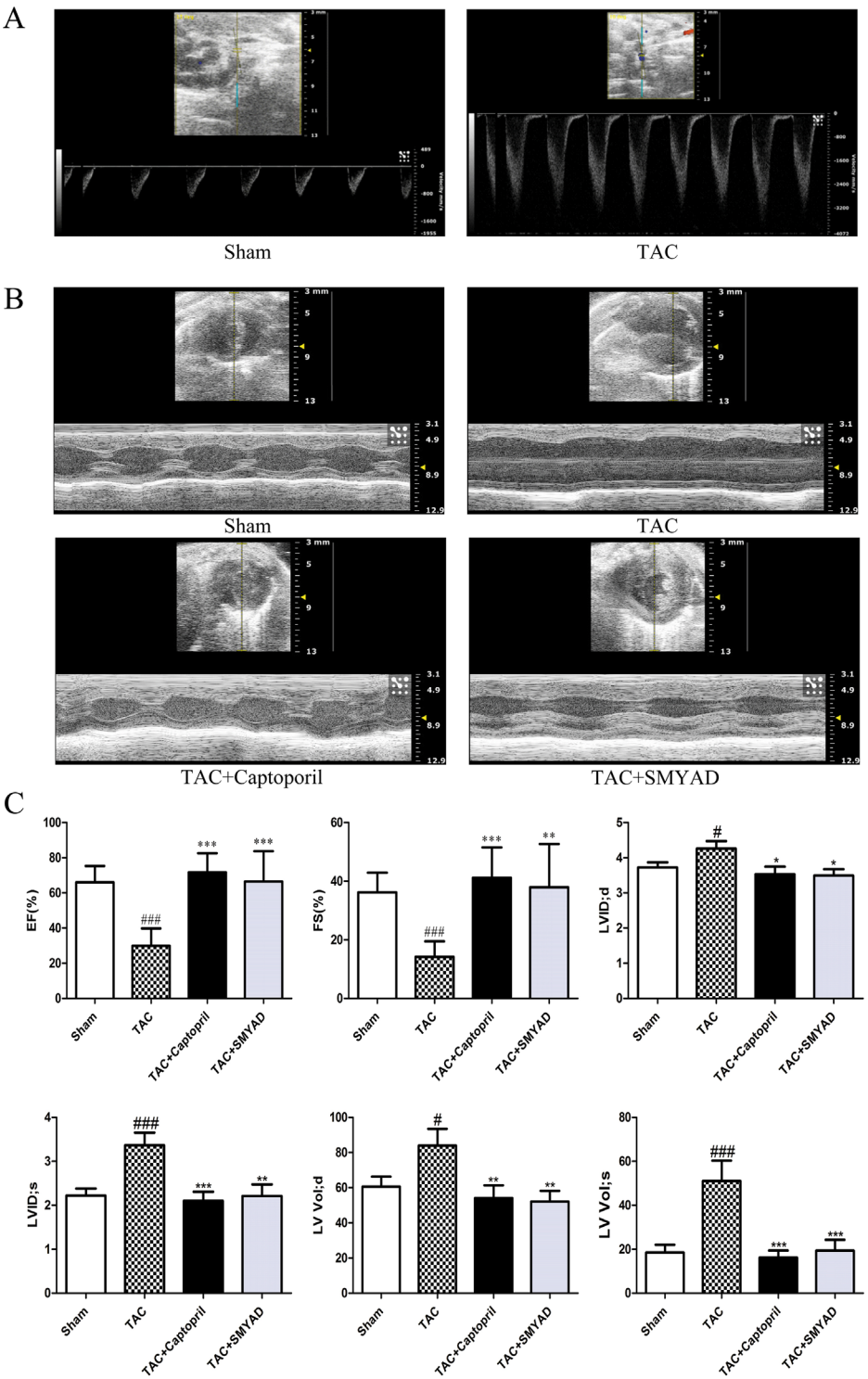

FIGURE 1 | SMYAD improved cardiac dysfunction 4 weeks after TAC. **(A)** Illustrating the transthoracic echo Doppler findings of velocity of blood flow in ascending aorta after TAC procedure. The aortic blood flow rate at the constriction point was greater than 2,400 mm/s in TAC-proceeded mice, while less than 900 mm/s in the sham group. **(B)** Representative M-Mode images. **(C)** Echocardiographic parameter analysis. EF, left ventricular ejection fraction; FS, left ventricular fractional shortening; LVID; d, left ventricular internal diameter at end diastole; LVID; s, left ventricular internal diameter at end systole; LV Vol; d, left ventricular volume at end diastole; LV Vol; s, left ventricular volume at end systole. Sham (n = 12), TAC (n = 8), TAC + captopril (n = 7), TAC + SMYAD (n = 9). $^{\#\#\#}P < 0.001$ compared with sham, $^{\#}P < 0.05$ compared with sham; $^{***}P < 0.001$ compared with TAC, $^{**}P < 0.01$ compared with TAC, $^{*}P < 0.05$ compared with TAC.

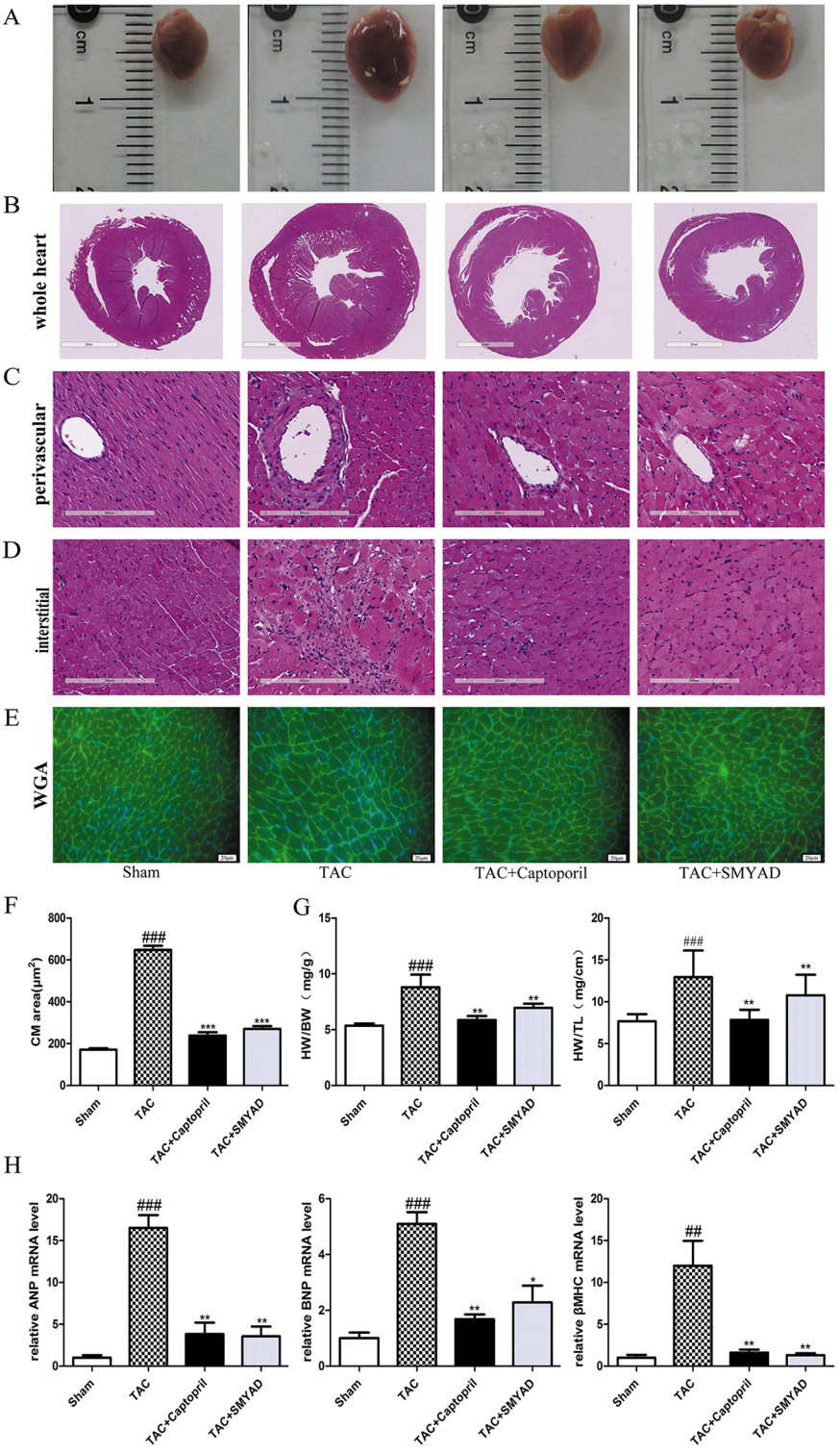

FIGURE 2 | SMYAD reversed cardiac hypertrophy in mice with TAC. **(A)** Representative image of whole heart. **(B**, **C**, and **D)** Representative images of HE staining in whole heart, perivascular, and interstitial. **(E)** WGA staining (green) of histological sections confirmed the inhibitory effect of SMYAD on hypertrophy, and nuclei were counterstained with DAPI (blue). **(F)** Quantification of cell cross-sectional area by measuring 100 random cells. **(G)** HW/BW and heart weight-to-tibia length ratios in each group. **(H)** The mRNA expression of hypertrophy-associated genes. β-actin was used as the internal control. ANP, atrial natriuretic peptide. BNP, brain natriuretic peptide. β-MHC, β-myosin heavy chain. $^{###}P < 0.001$ compared with sham, $^{##}P < 0.01$ compared with sham; $^{***}P < 0.001$ compared with TAC, $^{**}P < 0.01$ compared with TAC, $^{*}P < 0.05$ compared with TAC.

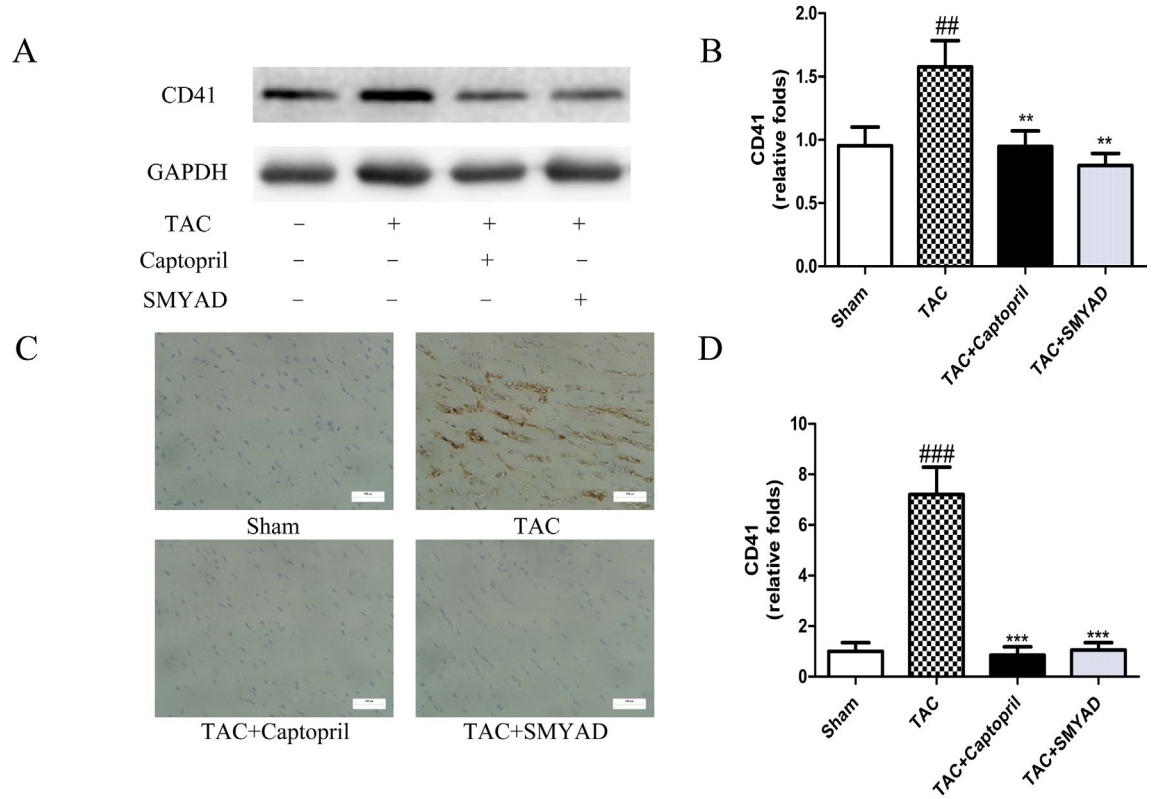

FIGURE 3 | SMYAD suppressed CD41 expression in mice with TAC. **(A** and **B)** Protein level of CD41 in sham, TAC, TAC + captopril, and TAC + SMYAD was verified by western blot. **(C** and **D)** Expression of CD41 in each group was verified by immunohistochemistry examination. $^{###}P < 0.001$, $^{##}P < 0.01$ vs the sham group; $^{***}P < 0.001$, $^{**}P < 0.01$ vs the TAC group.

CD41 and CD61 expressions were significantly decreased in the TAC + SMYAD group (**Figures 3C and 4C**).

Si-Miao-Yong-An Decoction Reduced Platelet Activation in Heart Tissue

β-thromboglobulin (β-TG) is a specific protein that secreted from the α-granules of platelet during the release reaction. von Willebrand factor (vWF) is critical for normal platelet tethering during hemostasis. vWF unfolds from its inactive globular conformation into an active string-like form that can specifically recruit platelets in response to blood shear forces. In our study, β-TG and vWF messenger RNA (mRNA) expression levels were increased by 3-fold and 1.3-fold, respectively, in TAC mice compared with those in sham, which were both reduced in SMYAD group (**Figures 5A**, **B**). P-selectin is a marker of activated platelet following heart injury. Thus, we investigated the possible involvement of P-selectin in the cardioprotective activity of SMYAD against cardiac hypertrophy by immunohistochemical staining and Western blot. In accordance to previous reports, TAC treatment significantly increased the expression of P-selectin protein as compared with sham group. SMYAD significantly attenuated the upregulation of P-selectin protein in TAC-treated mice (**Figures 5C, D**). Meanwhile, we observed that the levels of P-selectin in the TAC group were significantly increased compared with those in the sham-operated group based on immunohistochemical staining (**Figures 5E, F**). SMYAD treatment significantly suppressed the expression of P-selectin compared with the TAC group. In conclusion, our results suggested that SMYAD mediated the inhibitory effects on cardiac hypertrophy by disrupting both platelet aggregation and platelet activation.

DISCUSSION

HF represents a heterogeneous condition characterized by vulnerabilities in the blood, vasculature, and impaired flow dynamics that predispose to both arterial and venous thrombosis. Despite the fact that treatment with angiotensin-converting enzyme inhibitors, angiotensin receptor blockers, beta adrenergic antagonists, and mineralocorticoid receptor antagonists in HF patients has improved long-term outcomes, morbidity or mortality remain high in patients with acute decompensated HF (Zannad et al., 2013). Furthermore, there has been little progress in preventing the adverse cardiac remodeling that initiates HF.

Immune activation, inflammation, oxidative stress, alterations in mitochondrial bioenergetics, and autophagy have been postulated as important pathophysiological events in HF (Ayoub et al., 2017). It is commonly recognized that platelet activation

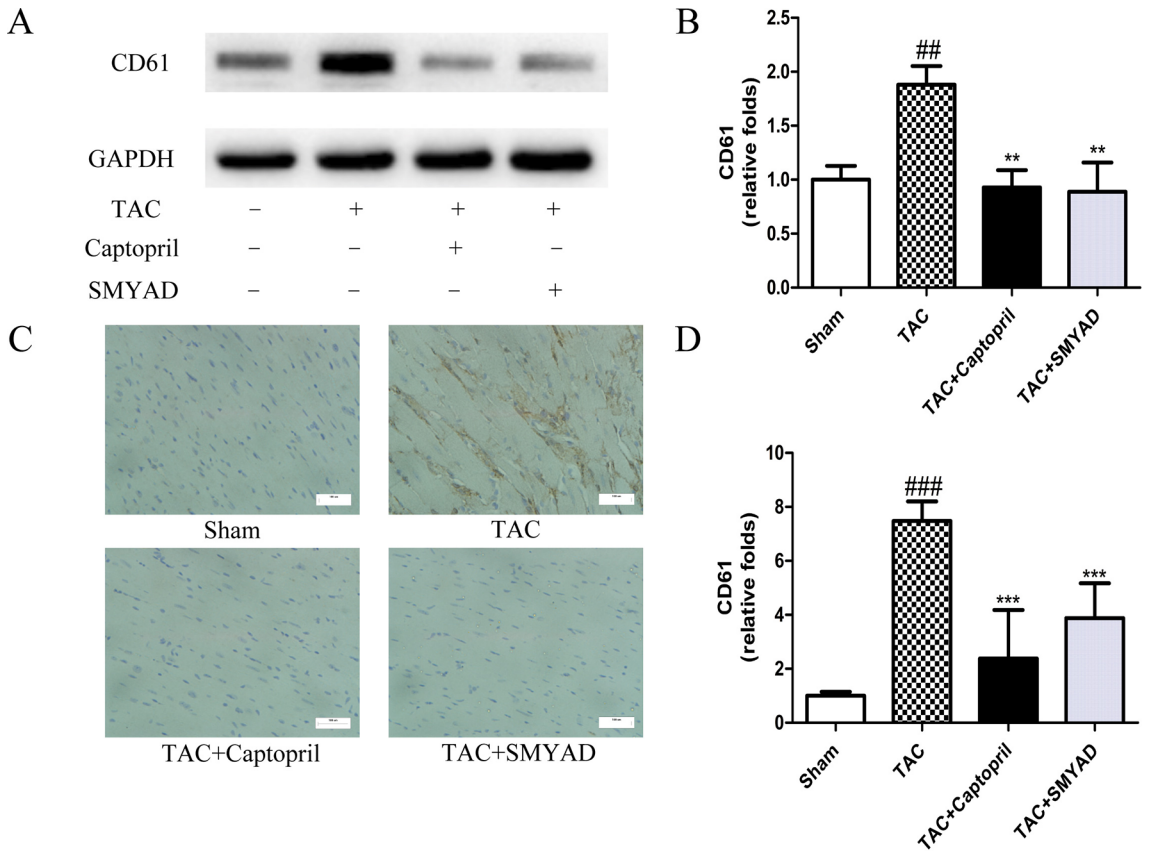

FIGURE 4 | SMYAD suppressed CD61 expression in mice with TAC. **(A** and **B)** Expression of CD61 protein in each group was verified by Western blot examination. **(C** and **D)** Representative immunostaining and quantification of CD61 by immunohistochemistry examination at 4 weeks post-surgery. $^{###}P < 0.001$, $^{##}P < 0.01$ vs the sham group; $^{***}P < 0.001$, $^{**}P < 0.01$ vs the TAC group.

plays a main role in cardiovascular disease. There is evidence that platelet activation and hypercoagulability present in HF, and stroke were reduced by warfarin therapy in the HF patient (Gurbel and Tantry, 2014). Platelets normally maintained a quiescent state and were sensitive to homeostasis changes resulting from endothelial cell damage, stress conditions, and hemodynamic abnormality (Hansen et al., 2015). A variety of adhesion molecules were prestored inside platelet granules and expressed on the platelet surface responding to activation. β-TG and platelet factor 4 represented specific platelet proteins of alpha-granules, which could be secreted into surrounding medium during cell activation. It was demonstrated that β-TG and P-selectin were significantly associated with the occurrence of atrial fibrillation and consequent stroke (Weymann et al., 2017). Thus, platelet activation contributes to the progress of cardiovascular disease.

SMYAD is a famous traditional Chinese medicine formula that was mainly applied to treat thromboangiitis obliterans in China for centuries and presented satisfactory curative effect. The main function of SMYAD is activation of blood circulation to dissipate blood stasis and promote vital energy regulation. Clinically, SMYAD was reported to improve myocardial infarction and HF (Zhou et al., 2012). Recently, SMYAD has been verified to improve liver function and reduce fat accumulation in hyperlipidemia rat by accelerated transformation of cholesterol into bile acids (Liu et al., 2017b). It has not been reported whether SMYAD had effect on cardiac dysfunction induced by TAC. Thus, our study is aimed to investigate the effects and mechanisms of SMYAD on cardiac hypertrophy.

We demonstrated that SMYAD improved systolic function in HF mice, as well as modestly reduced LVID and LV Vol. However, the molecular mechanism by which SMYAD mediates its anti-hypertrophic effects remains unclear, and the signaling pathways that interact to drive hypertrophy are very complicated. To understand the molecular mechanisms responsible for SMYAD's effects in HF, we investigated platelet, which has been shown to be activated in TAC-treated mice to induce cardiomyocyte hypertrophy and collagen synthesis (Wu et al., 2017a). We observed increased activation of cardiac CD41/61 and P-selectin in TAC-treated mice, as well as the reverse effect of SMYAD. P-selectin (CD62P) is a member of the selectin family of cell adhesion molecules and is stored on the membrane of platelet α-granules and endothelial Weibel–Palade bodies (Qi et al., 2015). It was the main platelet activation marker appearing

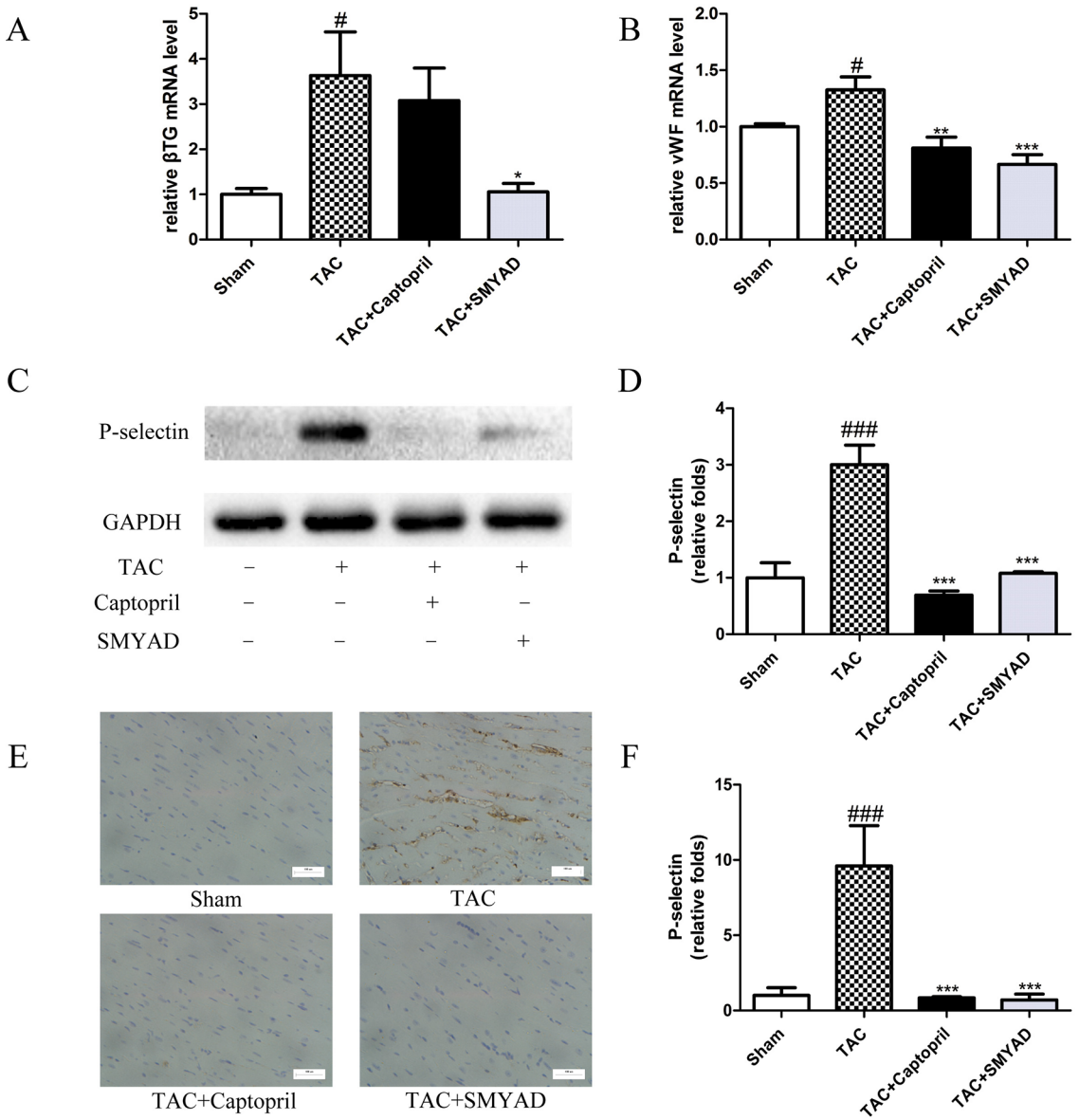

FIGURE 5 | SMYAD suppressed platelet activation in mice with TAC. **(A** and **B)** mRNA level of β-TG and vWF in each group. β-TG, β-thromboglobulin. vWF, von Willebrand factor. **(C** and **D)** Representative immunoblots and calculation of P-selectin levels in the sham, TAC, TAC + captopril, and TAC+ SMYAD. **(E** and **F)** Expression of P-selectin protein in the myocardium was detected by histopathological staining. $^{###}P < 0.001$ compared with sham, $^{#}P < 0.05$ compared with sham; $^{***}P < 0.001$ compared with TAC, $^{**}P < 0.01$ compared with TAC, $^{*}P < 0.05$ compared with TAC.

on the surface of platelet membrane (Xie et al., 2014). It was reported that the expression of platelet P-selectin was increased in hyperlipidemic patients after ischemic stroke (Pawelczyk et al., 2015). In our study, SMYAD reduced the activation of platelet by downregulating P-selectin. P-selectin is responsible for the adhesion of certain leukocytes and platelets to the endothelium when thrombosis develops and inflammation is caused. It rapidly translocated to the cell surfaces of platelets and endothelial cells upon activation (Qi et al., 2015). Platelets can induce cell survival and growth by secreting several sorts of growth factors, including vascular endothelial growth factors, fibroblast growth factors, and platelet-derived growth factors. The plasma concentration of soluble P-selectin is now recognized as a predictor of adverse cardiovascular events (Ishida et al., 2014).

CD41 and CD61 are the main receptors mediating platelet aggregation, and CD61 is the most abundant receptor expressed on the platelet surface. Increased expression of CD61 on platelet surfaces results in enhanced fibrinogen binding and, subsequently, platelets cross-linking and

thrombogenesis. SMYAD is suggested to inhibit platelet aggregation by CD41/61 expression and the elevation of vWF. CD41/61 and P-selectin significantly increased in atrial fibrillation patient with hypercoagulable state (Zhang et al., 2018). Besides, the prothrombotic state was characterized by the expression of CD41/61 and P-selectin mediating binding of vWF and fibrin interactions that led to different abnormalities in platelet function (Karmakar et al., 2015). In our study, inhibition of platelet activation by SMYAD reduced the infiltration of inflammatory cell into the heart.

Anticoagulants (e.g., warfarin) and antiplatelet agents (e.g. aspirin) are the principle antithrombotic agents. Many HF patients with sinus rhythm took aspirin because coronary artery disease was the leading cause of HF (Shantsila and Lip, 2016). The prescription of antiplatelet agents, such as clopidogrel and aspirin, has indeed become a stronghold of atherosclerotic cardiovascular disease and heart attack therapy. The therapeutic efficiency of clopidogrel is manipulated by the actions of hepatic cytochrome P450 (CYP) enzymes and influenced by individual genetic variations. The metabolism of clopidogrel into its active metabolites is affected by individual polymorphisms of CYP enzymes (Jarrar et al., 2016). Patients with high on-treatment platelet reactivity upon clopidogrel were at increased risk for thrombotic events, particularly for stent thrombosis and myocardial infarction, but cardiovascular mortality was also elevated in patients undergoing percutaneous coronary intervention (Gross et al., 2016). It was reported that aspirin use after discharge for HF hospitalization was associated with reduced risk of death, all-cause readmission, and HF readmission (Kim et al., 2016). However, data on aspirin in HF were inconclusive because of bleeding complications. There was evidence that a lower risk for death or stroke was associated with warfarin therapy in the HF patient (Hart et al., 2007). Warfarin (vitamin K antagonist) blocks multiple steps of coagulation by reducing the synthesis of vitamin K-dependent coagulation factors. As warfarin was metabolized by the CYP isoenzymes, the pharmacokinetics and pharmacodynamics of warfarin were influenced by interactions with other drugs that were metabolized by the same CYP isoenzymes (Gurbel and Tantry, 2014). Thus, it is of great urgency to find anti-platelet drugs with fewer adverse reaction.

Persistent hemodynamic overload will result in pathological cardiac hypertrophy, which is a leading predictor for the development of HF. In the present study, we used a TAC mice model to mimic pressure overload-induced stress. We demonstrated that SMYAD improved pressure overload-induced cardiac dysfunction and remodeling, and promoted histological changes in heart tissues. We also found that SMYAD decreased protein expressions of platelet aggregation markers (CD41, CD61) and platelet activation marker (P-selectin) in pressure overload-induced failing hearts. We have previously isolated and identified some chemical constituents, but the relationship between pharmacological effects and chemical constituents needs to be further studied.

The healthy endothelium in large vessels has multiple mechanisms that inhibit the adhesion or activation of platelets, either directly or by actively degrading platelet agonists. One of the earliest events in atherosclerosis is the loss of normal endothelial functions, including disruption of anti-platelet mechanisms. Endothelial cells respond to injury by releasing numerous factors, including vWF. vWF is an established marker of endothelial activation, and patients with elevated plasma levels of the ultra large vWF molecules are at high risk for future cardiovascular events (Warlo et al., 2017). vWF is a glycoprotein involved in both platelet activation and aggregation through its binding sites for GpIb and GpIIb/IIIa, respectively. High circulating levels of unusually large vWF multimers have strong procoagulant activity and facilitate platelet adhesion and aggregation by interacting with platelets after an acute event superimposed on coronary artery disease (Akyol et al., 2016). There was increasing evidence that platelet–endothelial interactions also contributed to early atherosclerotic plaque initiation and growth (Wu et al., 2017b). Platelets may also play a key role in neutrophil extracellular traps (Carestia et al., 2016).Through these interactions, platelet-derived factors can contribute to the pro-inflammatory and mitogenic status of resident mural cells. There was evidence that transendothelial migration of platelet monocyte complexes may result in dissociation and surface deposition of platelets (van Gils et al., 2008). In the next study, we will further investigate the interaction between platelet, endothelial cells, and neutrophil.

CONCLUSIONS

In this study, we characterized the property of SMYAD against cardiac hypertrophy. SMYAD inhibited pressure overload-induced platelet activation, cardiac hypertrophy, and dysfunction. It inhibited TAC-induced hypertrophy, myocardial necrosis, platelet aggregation, and platelet activation. CD41/CD61 served as a mediator of the platelet aggregation effect, while P-selectin/β-TG mediated the platelet activation effect. This study provided evidence that SMYAD may be a promising therapeutic agent for adverse cardiac remodeling.

DATA AVAILABILITY

All datasets generated for this study are included in the manuscript and/or the **Supplementary files**.

ETHICS STATEMENT

All the animal experiments were performed in accordance with the "Guide for the Care and Use of Laboratory Animals" by the National Institutes of Health. All studies were conducted in line with the approval of the Animal Care Committee of Beijing University of Chinese Medicine.

AUTHOR CONTRIBUTIONS

CS, SG, WW, and SL conceived and designed the experiments. CS, QW, HZ, WJ, and HL carried out the experiments, analyzed the data, and drafted the manuscript. BL, WW, XY,

LL, and XC participated in its design and prepared the paper. SL, SG, and QW revised the manuscript. All authors read and approved the final manuscript.

FUNDING

This study was funded by the National Nature Science Foundation of China (grant NO. 81874387, 81774101, and 81703942) and the Fundamental Research Funds for the Central Universities (2019-JYB-TD-002 and 2019-JYB-XS-012).

SUPPLEMENTARY MATERIAL

The Supplementary Material for this article can be found online at: https://www.frontiersin.org/articles/10.3389/fphar.2019.00990/full#supplementary-material

REFERENCES

Akyol, O., Akyol, S., and Chen, C. H. (2016). Update on ADAMTS13 and VWF in cardiovascular and hematological disorders. *Clin. Chim. Acta* 463, 109–118. doi: 10.1016/j.cca.2016.10.017

Ayoub, K. F., Pothineni, N. V. K., Rutland, J., Ding, Z., and Mehta, J. L. (2017). Immunity, inflammation, and oxidative stress in heart failure: emerging molecular targets. *Cardiovasc. Drugs Ther.* 31 (5–6), 593–608. doi: 10.1007/s10557-017-6752-z

Carestia, A., Kaufman, T., and Schattner, M. (2016). Platelets: new bricks in the building of neutrophil extracellular traps. *Front. Immunol.* 7, 271. doi: 10.3389/fimmu.2016.00271

Chi, S., Wang, W., and Liu, B. (2016). Absorbed constituents in rat serum after oral administration of water extract of Simiao Yong'an Decotion. *J. Beijing Univ. Tradit. Chin. Med.* 39 (11), 933–940. doi: 10.3969/j.issn.1006-2157.2016.11.009

George, R., Bhatt, A., Narayani, J., Thulaseedharan, J. V., Sivadasanpillai, H., and Tharakan, J. A. (2016). Enhanced P-selectin expression on platelet-a marker of platelet activation, in young patients with angiographically proven coronary artery disease. *Mol. Cell Biochem.* 419 (1–2), 125–133. doi: 10.1007/s11010-016-2756-4

Gross, L., Aradi, D., and Sibbing, D. (2016). Platelet function testing in patients on antiplatelet medications. *Semin. Thromb. Hemost.* 42 (3), 306–320. doi: 10.1055/s-0035-1570083

Gurbel, P. A., and Tantry, U. S. (2014). Antiplatelet and anticoagulant agents in heart failure: current status and future perspectives. *JACC Heart Fail.* 2 (1), 1–14. doi: 10.1016/j.jchf.2013.07.007

Hansen, K. B., Arzani, A., and Shadden, S. C. (2015). Mechanical platelet activation potential in abdominal aortic aneurysms. *J. Biomech. Eng.* 137 (4), 041005. doi: 10.1115/1.4029580

Hart, R. G., Pearce, L. A., and Aguilar, M. I. (2007). Meta-analysis: antithrombotic therapy to prevent stroke in patients who have nonvalvular atrial fibrillation. *Ann. Intern. Med.* 146 (12), 857–867. doi: 10.7326/0003-4819-146-12-200706190-00007

Ishida, K., Taguchi, K., Matsumoto, T., and Kobayashi, T. (2014). Activated platelets from diabetic rats cause endothelial dysfunction by decreasing akt/endothelial no synthase signaling pathway. *Plos One* 9 (7), e102310. doi: 10.1371/journal.pone.0102310

Jarrar, M., Behl, S., Manyam, G., Ganah, H., Nazir, M., Nasab, R., et al. (2016). Cytochrome allelic variants and clopidogrel metabolism in cardiovascular diseases therapy. *Mol. Biol. Rep.* 43 (6), 473–484. doi: 10.1007/s11033-016-3983-1

Karmakar, T., Mallick, S. K., Chakraborty, A., Maiti, A., Chowdhury, S., and Bhattacharyya, M. (2015). Signature biomarkers in diabetes mellitus and associated cardiovascular diseases. *Clin. Hemorheol. Microcirc.* 59 (1), 67–81. doi: 10.3233/CH-141818

Kim, J. H., Shah, P., Tantry, U. S., and Gurbel, P. A. (2016). Coagulation abnormalities in heart failure: pathophysiology and therapeutic implications. *Curr. Heart Fail. Rep.* 13 (6), 319–328. doi: 10.1007/s11897-016-0308-6

Li, C., Wang, C., Jiang, Y., and Liu, B. (2018). HPLC characteristic chromatogram of Simiao Yong'an Tang aqueous extract. *J. Beijing Univ. Tradit. Chin. Med.* 41 (4), 329–335. doi: 10.4103/wjtcm.wjtcm_13_18

Lim, H. S., Willoughby, S., Schultz, C., Chakrabarty, A., Alasady, M., Lau, D. H., et al. (2014). Successful catheter ablation decreases platelet activation and improves endothelial function in patients with atrial fibrillation. *Heart Rhythm* 11 (11), 1912–1918. doi: 10.1016/j.hrthm.2014.07.030

Liu, P., Zhang, W., Jiang, W., and Liu, B. (2018). Chemical constituents from Simiao Yongan decoction. *Chin. Tradit. Herb. Drugs* 49 (14), 3233–3239. doi: 10.7501/j.issn.0253-2670.2018.14.007

Liu, Y., Chi, S., Wang, W., Su, L., and Liu, B. (2017a). Simultaneous determination of seven components in RAT plasma by the UPLC-MS/MS method and application of pharmacokinetic studies to SimiaoYong'an decoction. *Molecules* 22 (11), 1937. doi: 10.3390/molecules22111937

Liu, Z. Y., Zhang, Y., Zhang, R. W., Gu, L. Q., and Chen, X. H. (2017b). Promotion of classic neutral bile acids synthesis pathway is responsible for cholesterol-lowing effect of Si-Miao-Yong-An decoction: application of LC-MS/MS method to determine 6 major bile acids in rat liver and plasma. *J. Pharmaceut. Biomed. Anal.* 135, 167–175. doi: 10.1016/j.jpba.2016.12.021

Ooi, J. Y., Tuano, N. K., Rafehi, H., Gao, X. M., Ziemann, M., Du, X. J., et al. (2015). HDAC inhibition attenuates cardiac hypertrophy by acetylation and deacetylation of target genes. *Epigenetics* 10 (5), 418–430. doi: 10.1080/15592294.2015.1024406

Pawelczyk, M., Chmielewski, H., Kaczorowska, B., Przybyla, M., and Baj, Z. (2015). The influence of statin therapy on platelet activity markers in hyperlipidemic patients after ischemic stroke. *Arch. Med. Sci.* 11 (1), 115–121. doi: 10.5114/aoms.2015.49216

Peng, L., Li, M., Xu, Y. Z., Zhang, G. Y., Yang, C., Zhou, Y. N., et al. (2012). Effect of Si-Miao-Yong-An on the stability of atherosclerotic plaque in a diet-induced rabbit model. *J. Ethnopharmacol.* 143 (1), 241–248. doi: 10.1016/j.jep.2012.06.030

Pillai, V. B., Samant, S., Sundaresan, N. R., Raghuraman, H., Kim, G., Bonner, M. Y., et al. (2015). Honokiol blocks and reverses cardiac hypertrophy in mice by activating mitochondrial Sirt3. *Nat. Commun.* 6, 6656. doi: 10.1038/ncomms7656

Qi, C. L., Li, B., Guo, S. M., Wei, B., Shao, C. K., Li, J. L., et al. (2015). P-selectin-mediated adhesion between platelets and tumor cells promotes intestinal tumorigenesis in Apc(Min/+) mice. *Int. J. Biol. Sci.* 11 (6), 679–687. doi: 10.7150/ijbs.11589

Qi, Z., Li, M., Zhu, K., and Zhang, J. (2019). Si-Miao-Yong-An on promoting the maturation of Vasa Vasorum and stabilizing atherosclerotic plaque in ApoE(-/-) mice an experimental study. *Biomed. Pharmacother.* 114, 108785. doi: 10.1016/j.biopha.2019.108785

Ren, W., Gao, S., Zhang, H., Ren, Y., Yu, X., Lin, W., et al. (2018). Decomposing the mechanism of Qishen granules in the treatment of heart failure by a quantitative pathway analysis method. *Molecules* 23 (7), 1829. doi: 10.3390/molecules23071829

Ren, Y., Chen, X., Li, P., Zhang, H., Su, C., Zeng, Z., et al. (2019). Si-Miao-Yong-An decoction ameliorates cardiac function through restoring the equilibrium of SOD and NOX2 in heart failure mice. *Pharmacol. Res.* 146, 104318. doi: 10.1016/j.phrs.2019.104318

Santhakumar, A. B., Stanley, R., and Singh, I. (2015). The ex vivo antiplatelet activation potential of fruit phenolic metabolite hippuric acid. *Food Funct.* 6 (8), 2679–2683. doi: 10.1039/C5FO00715A

Schafer, A., Fraccarollo, D., Hildemann, S., Christ, M., Eigenthaler, M., Kobsar, A., et al. (2003). Inhibition of platelet activation in congestive heart failure by aldosterone receptor antagonism and ACE inhibition. *Thromb. Haemost.* 89 (6), 1024–1030. doi: 10.1055/s-0037-1613404

Shantsila, E., and Lip, G. Y. (2016). Antiplatelet versus anticoagulation treatment for patients with heart failure in sinus rhythm. *Cochrane Database Syst. Rev.* 9, CD003333. doi: 10.1002/14651858.CD003333.pub3

van Gils, J. M., da Costa Martins, P. A., Mol, A., Hordijk, P. L., and Zwaginga, J. J. (2008). Transendothelial migration drives dissociation of plateletmonocyte complexes. *Thromb. Haemost.* 100 (2), 271–279. doi: 10.1160/TH08-03-0165

Wang, D. J., and Tian, H. (2014). Effect of Mailuoning injection on 8-iso-prostaglandin F2 alpha and superoxide dismutase in rabbits with extremity ischemia-reperfusion injury. *J. Surg. Res.* 192 (2), 464–470. doi: 10.1016/j.jss.2014.06.008

Warlo, E. M. K., Pettersen, A. R., Arnesen, H., and Seljeflot, I. (2017). vWF/ADAMTS13 is associated with on-aspirin residual platelet reactivity and clinical outcome in patients with stable coronary artery disease. *Thromb. J.* 15, 28. doi: 10.1186/s12959-017-0151-3

Weymann, A., Ali-Hasan-Al-Saegh, S., Sabashnikov, A., Popov, A. F., Mirhosseini, S. J., Nombela-Franco, L., et al. (2017). Platelets cellular and functional characteristics in patients with atrial fibrillation: a comprehensive meta-analysis and systematic review. *Med. Sci. Monit. Basic Res.* 23, 58–86. doi: 10.12659/MSMBR.902557

Wu, L., Zhao, F., Dai, M., Li, H., Chen, C., Nie, J., et al. (2017a). P2y12 receptor promotes pressure overload-induced cardiac remodeling *via* platelet-driven inflammation in mice. *Hypertension* 70 (4), 759–769. doi: 10.1161/HYPERTENSIONAHA.117.09262

Wu, M. D., Atkinson, T. M., and Lindner, J. R. (2017b). Platelets and von willebrand factor in atherogenesis. *Blood* 129 (11), 1415–1419. doi: 10.1182/blood-2016-07-692673

Xie, J. H., Yamniuk, A. P., Borowski, V., Kuhn, R., Susulic, V., Rex-Rabe, S., et al. (2014). Engineering of a novel anti-CD40L domain antibody for treatment of autoimmune diseases. *J. Immunol.* 192 (9), 4083–4092. doi: 10.4049/jimmunol.1303239

Zannad, F., Stough, W. G., Regnault, V., Gheorghiade, M., Deliargyris, E., Gibson, C. M., et al. (2013). Is thrombosis a contributor to heart failure pathophysiology? Possible mechanisms, therapeutic opportunities, and clinical investigation challenges. *Int. J. Cardiol.* 167 (5), 1772–1782. doi: 10.1016/j.ijcard.2012.12.018

Zhang, X. Z., Liu, A. G., Guo, M. L., Guan, J., Cai, S. L., Du, Q., et al. (2018). Relationship of platelet microparticle CD62P and activated GP IIb/IIIa with hypercoagulable state after atrial fibrillation radiofrequency catheter ablation. *Eur. Rev. Med. Pharmacol. Sci.* 22 (12), 3919–3924. doi: 10.26355/eurrev_201806_15277

Zhou, L. L., Lou, J. B., Hu, X. J., Xiang, Y. J., and Fu, R. (2012). Simiao Yongan decoction on Qi stagnancy and blood stasis in patients of 30 cases with chronic heart failure. *Chin. J. Exp. Tradit. Med. Formulae* 18 (15), 270–272. doi: 10.13422/j.cnki.syfjx.2012.15.009

Conflict of Interest Statement: The authors declare that the research was conducted in the absence of any commercial or financial relationships that could be construed as a potential conflict of interest.

frontiers in Pharmacology

ORIGINAL RESEARCH
published: 25 September 2019
doi: 10.3389/fphar.2019.01138

A Network Pharmacology Study of the Multi-Targeting Profile of an Antiarrhythmic Chinese Medicine Xin Su Ning

*Taiyi Wang[1,2], Hamish Streeter[1,2], Xuan Wang[1,2], Ujang Purnama[2], Ming Lyu[3], Carolyn Carr[2] and Yu-ling Ma[1,2]**

[1] Oxford Chinese Medicine Research Centre, University of Oxford, Oxford, United Kingdom, [2] Department of Physiology, Anatomy and Genetics, University of Oxford, Oxford, United Kingdom, [3] Institute of Chinese Materia Medica, China Academy of Chinese Medical Sciences, Beijing, China

Xin Su Ning (XSN) is a China patented and certified traditional Chinese herbal medicine used to treat premature ventricular contractions (PVCs) since 2005. XSN is formulated with 11 herbs, designed to treat arrhythmia with phlegm-heat heart-disturbed syndrome (PHHD) according to Chinese medicine theory. The rational compatibility of the 11 herbs decides the therapeutic outcome of XSN. Due to the multicomponent nature of traditional Chinese medicine, it is difficult to use conventional pharmacology to interpret the therapeutic mechanism of XSN in terms of clear-cut drug molecule and target interactions. Network pharmacology/systematic pharmacology usually consider all the components in a formula with the same weight; therefore, the proportion of the weight of the components has been ignored. In the present study, we introduced a novel coefficient to mimic the relative amount of all the components in relation with the weight of the corresponding herb in the formula. The coefficient is also used to weigh the pharmacological effect of XSN on all relative biological pathways. We also used the cellular electrophysiological data generated in our lab, such as the effect of liensinine and isoliquiritigenin on $Na_V1.5$ channels; we therefore set sodium channel as one of the targets of these two components, which would support the clinical efficacy of XSN in treating tachyarrhythmia. Combining the collected data and our discovery, a panoramagram of the pharmacological mechanism of XSN was established. Pathway enrichment and analysis showed that XSN treated PHHD arrhythmia through multiple ion channels regulation, protecting the heart from I/R injury, inhibiting the apoptosis of cardiomyocyte, and improving glucose and lipid metabolism.

Keywords: Xin Su Ning, network pharmacology, phlegm-heat heart-disturbance, weight coefficient, cardiac arrhythmia, electrophysiology

OPEN ACCESS

Edited by:
Xiu-Wei Yang,
Peking University,
Beijing,China

Reviewed by:
Yu-Ping Tang,
Shaanxi University of Chinese Medicine,China
Dan Yan,
Capital Medical University,
China

***Correspondence:**
Yu-ling Ma
yu-ling.ma@dpag.ox.ac.uk

Specialty section:
This article was submitted to Ethnopharmacology, a section of the journal Frontiers in Pharmacology

Received: *03 June 2019*
Accepted: *04 September 2019*
Published: *25 September 2019*

Citation:
Wang T, Streeter H, Wang X, Purnama U, Lyu M, Carr C and Ma Y-l (2019) A Network Pharmacology Study of the Multi-Targeting Profile of an Antiarrhythmic Chinese Medicine Xin Su Ning. Front. Pharmacol. 10:1138. doi: 10.3389/fphar.2019.01138

INTRODUCTION

Arrhythmia is a disease featuring the abnormalities of frequency or rhythm of heart excitement caused by abnormal cardiac electrophysiological activities generated by the electrical conduction system of the heart. Symptoms of arrhythmia often include dizziness, breathlessness, and palpitations (Barsky, 2001). The presence of cardiac arrhythmias may at times suggest a specific underlying heart disease

or even noncardiac pathological changes. The most common and important cause of cardiac arrhythmias is coronary artery disease (Atarashi and Hayakawa, 1996). In recent decades, even though plenty of non-chemical therapies have been developed, anti-arrhythmic drug is still the most common treatment. However, the proarrhythmic effect of the anti-arrhythmic drugs has been causing concerns on the safety of the arrhythmic patients.

As a complementary and alternative medicine, Chinese medicine plays an increasing role in the treatment of arrhythmias (Dong et al., 2017). Many proprietary Chinese medicines, such as Xin Su Ning capsule (Yuan and Zhou, 2000; Wang and Lu, 2008; Lin et al., 2011; Li and Zhang, 2015; Zhai et al., 2017), Wenxin Keli (Kalifa and Avula, 2012; Li and Guihua, 2018), and Shensong Yangxin capsule (Wang et al., 2011; Liu et al., 2014), have showed clear clinical antiarrhythmic efficacy comparable with the single chemical compound anti-arrhythmic drugs. However, the Chinese-patented antiarrhythmic medicines have rare adverse reactions being recorded.

Based on the theories of traditional Chinese medicine (TCM), a disease can be categorized from four fundamental dimensions, which is consisted of four pairs of relative concepts including yin–yang, exterior–interior, excess–deficiency, and cold–heat (Lu et al., 2004; Jiang et al., 2012). In terms of excess–deficiency categorization, arrhythmia can be divided into two main types of syndromes: excess syndrome and deficient syndrome (Chen and Ba, 2010). Deficiency syndrome is a TCM condition with weakness and lack of energy. Up to present, most of the marketed anti-arrhythmic Chinese medicines have been used to treat deficient syndrome, such as Wenxin Keli (Wang et al., 2016) and Shensong Yangxin capsule (Gu et al., 2005) for the deficiency of Qi and Yin, Xinbao Wan for the deficiency of Yang (Chen and Wu, 1996; Dong et al., 2005), and Tianwang Buxin Wan for the deficiency of Yin (Ni et al., 2019). Excess syndrome is a typical TCM syndrome caused by the accumulation of pathological phlegm and dampness in the body. Cardiac arrhythmia with typical clinical manifestation of phlegm-heat heart-disturbance (PHHD) syndrome takes a large proportion of the clinical treatment, and to the best of our knowledge, XSN is the only medicine for treating PHHD arrhythmia (Yuan and Zhou, 2000).

Xin Su Ning (XSN) is a multi-herbal medicine patented and launched in China since 2005 for treating cardiac ventricular arrhythmia, especially arrhythmias induced by cardiac ischemia and viral myocarditis (Zhai et al., 2017). XSN is comprised of 11 herbs: *Coptidis Rhizoma* (Huanglian, *Coptis chinensis* Franch.), *Pinelliae Rhizoma* (Banxia, *Pinellia ternata* [Thunb.] Makino), Poria (Fuling, *Poria cocos* [Schw.] Wolf), *Aurantii Fructus Immaturus* (Zhishi, *Citrus aurantium* L.), *Dichroae Radix* (Changshan, *Dichroa febrifuga* Lour.), *Nelumbinis Plumula* (Lianzixin, *Nelumbo nucifera* Gaertn.), *Sophorae flavescentis Radix* (Kushen, *Sophora flavescens* Ait.), *Artemisiae annuae Herba* (Qinghao, *Artemisia annua* L.), *Ginseng Radix et Rhizoma* (Renshen, *Panax ginseng* C. A. Mey.), *Ophiopogonis Radix* (Maidong, *Ophiopogon japonicus* (L. f) Ker Gawl.), and *Nardostachyos Radix et Rhizoma* (Gancao, *Glycyrrhiza uralensis* Fisch.).

However, the complexity of the chemical composition of multi-herbal TCM formula brings great difficulties to the pharmacological research. Network pharmacology has been one of the approaches to reveal the complex pharmacological mechanisms behind the multitargeting properties by the multicomponent medicines (Li et al., 2011). TCM formulas are well known by the characteristics of multi-herbal/component, which would exert its clinical efficacy through multiple targeting, hence multi-pharmacological actions (Leung et al., 2014). However, most of the studies were centered on attributing the edge between component and target and considering the weight values of all the components as the same (Shao and Zhang, 2013). A good TCM formula would be formed with the right herbs in an accurate proportion that would produce the best possible clinical efficacy with none or minimal toxicity. Therefore, each herb in a formula would be indispensable in evaluating the clinical efficacy of the formula as well as in a network pharmacological mechanism mapping. Furthermore, in terms of compound formula which consists of multiple herbs, the target spectrum (target distribution of all monomer components) determines the therapeutic range of the formula, and high-weight components may determine the therapeutic direction.

In this study, we tried to introduce a parameter, weight coefficient, to mimic the proportion of all the encompassed components and resort their effects on different targets and pathways. We used the data from multiple bioassay databases, combining with the results of pharmacological assays of high-weight coefficient components; a closer-to-the-fact pharmacological panorama was constructed.

MATERIALS AND METHODS

XSN Chemical Component Library Building

All of the chemical monomer components in the 11 herbs of XSN were retrieved from the book Chemical Components of Source Plants in Traditional Chinese Medicine (Zhou et al., 2009) and the database: TCM Systems Pharmacology Database and Analysis Platform (TcmSP™, http://lsp.nwu.edu.cn/tcmsp.php) (Ru et al., 2014). In addition, four important pharmacology-related properties of the collected components were also obtained from admetSAR (Cheng et al., 2012; Yang et al., 2018), including MW, ALogP, Hbond donor count, and Hbond acceptor count, Rotation bond count, and human oral bioavailability (HOB). The proportion of each herb in XSN formula was retrieved from the patent of XSN (Wang and Mao, 2018), and the contents of the main active components in all the 11 herbs were retrieved from published papers, and all the other components without quantitative data were set to be equal to the lowest quantity value of known components (details see **Supplement Table 1**).

Calculation of Weight Coefficients

Component weight coefficient:

$$w_{i,j} = \frac{m_i}{\Sigma_i^n m_i} \times \frac{C_{i,j}}{M_j} \times p_j(OB) \times 10^9$$

$w_{i,j}$ is the weight coefficient of component j in herb i, and m_i is the weight of herb i in XSN formula, n is the total count of herbs

in XSN, $C_{i,j}$ is the content of component j in herb i, and M_j is the molecular weight of component j, and $p_j(OB)$ is the predicted probability of positive human OB of component j.

The weight coefficient is the product of three elements: $\frac{m_i}{\sum_i^n m_i}$ is the proportion of each herb in the XSN formula, $\frac{c_{i,j}}{M_j}$ represented the molar concentration of each component in 1 gram of raw herb in XSN formula, and $pj(OB)$ is the probability of the bioavailability of each component reaching 30% of the total oral administration. Therefore, the coefficient $w_{i,j}$ is a relative quantity among all the components of the 11 herbs in XSN formula to reflect the proportional relationships of the components existed in the body.

Since the activity of the multiple herbal medicine involved in multiple targeting, and each target was usually bound by multiple components. Weight coefficient of one single target in this paper was represented by the sum of all the weight coefficients of the components interacting with this target. Furthermore, weight coefficient of each pathway was also represented by the sum of all the weight coefficients of all targets in this pathway.

Establishment of the Relationships Between Component-Target and Zheng Target

All the relative targets of each component in the 11 herbs of XSN were retrieved from BindingDB database (https://www.bindingdb.org/) as the component-target relationship library of XSN (Gilson et al., 2016). Since Zheng (TCM syndrome) is represented by the series of characteristics with clinical manifestations and symptoms (hereinafter referred to as TCM symptom), all the 10 TCM symptoms of PHHD arrhythmia referred in the indications of XSN capsule and the standard names of their corresponding modern medicine symptoms (MM symptom) were collected from SymMap database (https://www.symmap.org/) (Wu et al., 2018). All the target genes relative to each MM symptom above were obtained from the Human Phenotype Ontology Database (https://hpo.jax.org/app/) as the target-Zheng relationship library of PHHD arrhythmia.

Network Construction and Analysis

Two networks were constructed: the networks of PHHD target and XSN component targets. All the networks were visualized by Cytoscape 3.7.0 (http://www.cytoscape.org), which is an open-source project for complex network construction and visualizing and analyzing (Shannon et al., 2003). Pathway enrichment was carried out using Reactome pathway database (https://www.reactome.org) (Fabregat et al., 2017; Fabregat et al., 2018); the pathways with FDR < 0.05 were kept in the result.

Chemicals and Solutions

All the chemical agents were purchased from Sigma–Aldrich, and all high-weight coefficient components were obtained from Chengdu Herbpurify Co., Ltd. The intracellular buffer contained (in mM): KCl 120, $MgCl_2$ 2, $CaCl_2$ 1, Na_2ATP 3, EGTA 11, HEPES 10, and pH 7.2 corrected with 5M NaOH. The extracellular buffer contained (in mM): NaCl 112, $NaH_2PO_4 \bullet H_2O$ 1, KCl 5.4, HEPES 5, $NaHCO_3$ 24, glucose 10, $MgCl_2$ 1.2, $CaCl_2$ 1.8, and pH 7.4 corrected with 5M NaOH. Components experimented in this paper were dissolved in the external buffer, and for the dose–response research, the concentrations of the compounds studied were ranging from 1 to 100 μM in the external buffer solution.

Electrophysiological Research

CHL cells stably expressing the α-subunit of human $Na_V1.5$ (SCN5A) were used for electrophysiological assays. Patch clamp assays were carried out at room temperature (~ 22 to 24°C), and the cells were superfused with the extracellular buffer at a rate of 2 ml/min. Patch pipettes were pulled from borosilicate glass (Harvard Apparatus, UK) using a DMZ-Universal Puller (Zeitz-Instruments, Germany); the average pipette resistance was 3–5 MΩ. The control currents were recorded 5 minutes after the whole-cell configuration was achieved using an Axopatch™ 200B Amplifier (Molecular Devices, USA).

Data Analysis

Data was analyzed and illustrated using pCLAMP 10.3 software (Axon Instruments, Inc.) and Origin 9.1. For each protocol and condition, at least five cells were tested. Data values are presented as mean ± standard error of the mean (SEM). The difference between the control and the effect of a compound was statistically tested using Student's unpaired t-test. $P < 0.05$ was deemed to be statistically significant. Where results are not statistically significant, the actual p-value is provided.

RESULTS

XSN Component Library

Nine hundred sixty-three monomer components from 11 herbs of XSN were collected from Chemical Components of Source Plants in Traditional Chinese Medicine and TCMSP database (**Supplement Table 1**). Chemical properties including AlogP, Hbond donor and acceptor count, molecular weight (MW), human OB, and rotatable bond count were calculated by AdmetSar 2.0 as described above, analyzed and shown as **Figures 1A–F** (**Supplement Table 1**). The component accounts of each herb were analyzed and shown in **Figure 1G**. The content of monomer components was obtained from published chemical constituent research indexed by PubMed (https://www.ncbi.nlm.nih.gov/pubmed) and CNKI (http://www.cnki.net/) (**Supplement Table 1**). The contents of 47 of 963 components above were quantified in the reports, and the content values were abstracted from the references. The contents of the remaining 916 components were set as the lowest value of the content reported components. The most abundant component berberine was 2.82×10^6 times that of neohesperidin which was with the lowest content in the 47 reported components. The weight coefficients for all the components were calculated, and top 40 with references were listed and shown in **Figure 1H** with higher weight components.

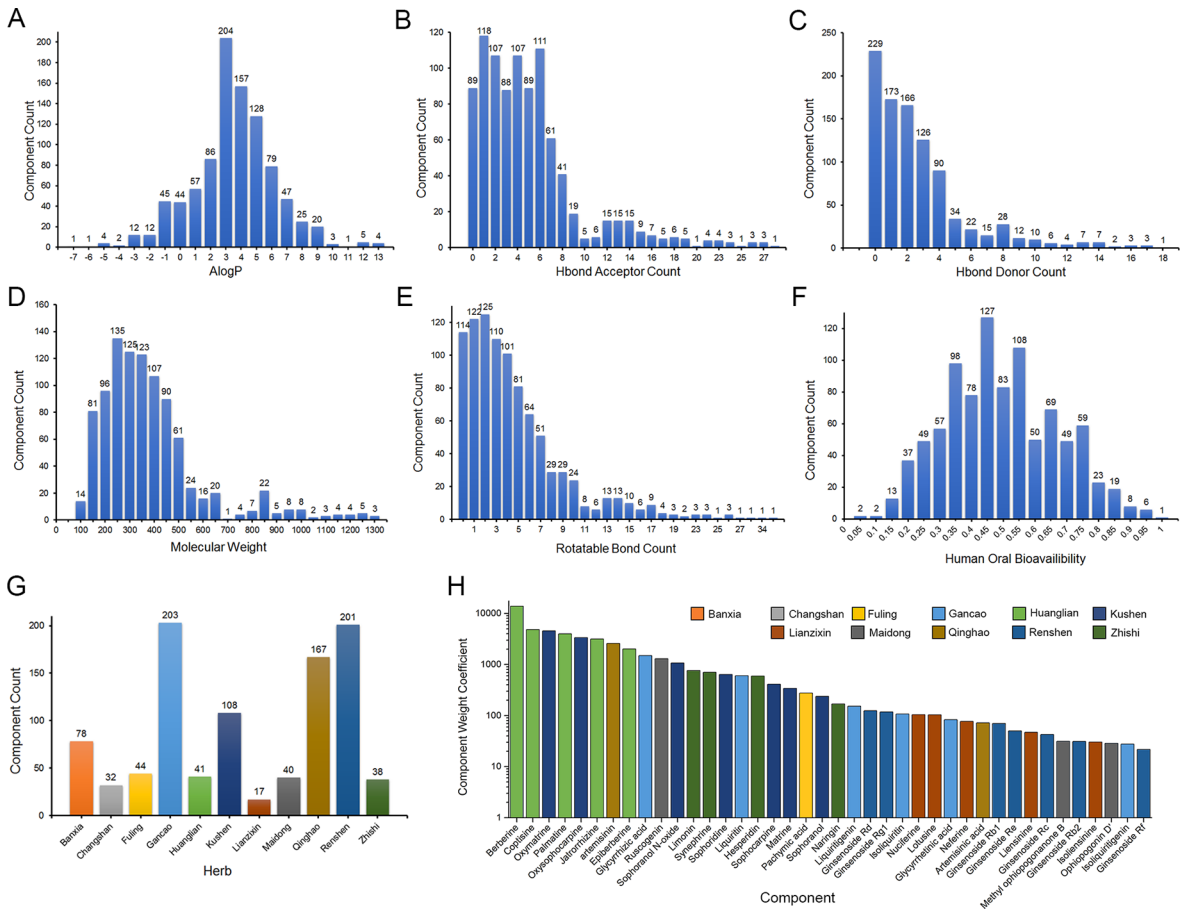

FIGURE 1 | Chemical properties statistics of components in the 11 herbs of XSN. **(A)** AlogP, **(B)** Hbond donor count, **(C)** Hbond acceptor count, **(D)** Molecular weight (MW), **(E)** human oral bioavailability, **(F)** rotatable bond count, **(G)** component count of each herb collected in XSN component library, and **(H)** weight coefficient of top 40 weight components in 11 herbs. The different colors means the source herb of components, which is same as **(G)**.

XSN Target Spectrum

Two thousand eight hundred thirty-five component-target relationship data were obtained, covering 487 monomer components and 618 targets (**Supplement Table 2**). The classification of targets was analyzed using the ChEMBL hierarchical target classification system (Bento et al., 2014), and the classification of enzymes were updated according to the ENZYME database (Bairoch et al., 2004). Major and secondary classifications of target spectrum were shown as **Figure 2** (**Supplement Table 3**). The proportion of targets were grouped by the means of target count in **Figure 2**, which shows the proportion of different target categories and also shows the differences between statistics by target count and weight coefficient, especially for cytochrome P450, hydrolase, nuclear receptor, enzymes, oxidoreductase, protease, protein kinase, and VGIC (proportion > 5% and fold change >3).

PHHD-Arrhythmia Target Spectrum

Since Zheng (TCM syndrome) is represented by the series of characteristics with clinical manifestations and symptoms (hereinafter referred to as TCM symptom); all the 10 TCM symptoms of PHHD arrhythmia and their relative modern medicine symptoms (MM symptom) were collected: Xin Ji (palpitations), Xiong Men (respiratory distress), Xin Fan (boredom), Yi Jing (panic attack), Kou Gan (xerostomia), Kou Ku (bitter taste in the mouth), Shi Mian (insomnia), Duo Meng (dreaminess), Xuan Yun (vertigo), and Mai Jie Dai (knotted or regularly intermittent pulse) (**Table 1**, **Supplement Table 4**).

TCM symptom Kou Ku means bitter taste in the mouth, but not bad breath in the mouth; therefore, the MM symptom halitosis retrieved from SymMap was replaced by another keyword: abnormality of taste sensation. Mai Jie Dai included two types of pulses: Jie Mai is knotted or bound pulse, which is slow, relaxed and stops at irregular intervals. Jie Mai represents an irregular beat or palpitation stemming from the heart. Dai Mai means the pulse is with regularly intermittent abnormality, which also suggests the patients with this pulse have advanced heart disease according to modern medicine. Therefore, an alternative keyword irregular heartbeat was used to represent the TCM symptom Mai Jie Dai.

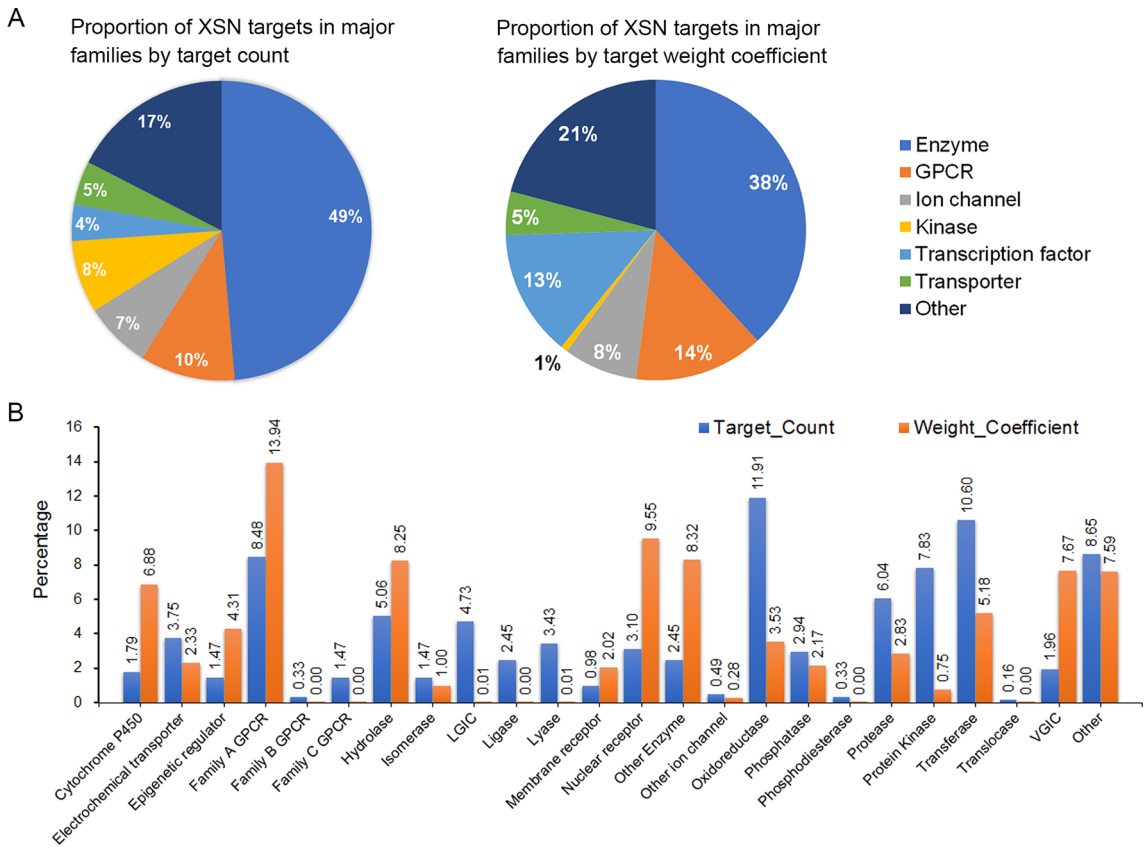

FIGURE 2 | The targeting spectrum of XSN. **(A)** Statistic and major classifications of XSN target spectrum by target count and **(B)** statistic and secondary classifications of XSN target spectrum. The X axis of **(B)** is labeled with targets including family A GPCR, rhodopsin-like GPCRs; family B GPCR, secretin-like GPCRs; family C GPCR, metabotropic glutamate receptor family; LGIC, ligand-gated ion channel; VGIC, voltage-gated ion channel.

TABLE 1 | The relative relationship between TCM symptoms and modern medicine symptom.

TCM symptom ID	TCM symptoms	MM symptom ID	MM symptoms	UMLS ID	Synonyms	UMLS ID	HPO ID	Target number
SMTS01333	*Xin Ji*	SMMS00282	Palpitations	C0030252			HP:0001962	52
SMTS01384	*Xiong Men*	SMMS00863	Chest Heaviness	C0742339	Respiratory distress	C0013404	HP:0002098	108
SMTS01324	*Xin Fan*	SMMS00381	Boredom	C0006019				
SMTS01567	*Yi Jing*	SMMS00119	Panic Attack	C0086769			HP:0025269	17
SMTS00573	*Kou Gan*	SMMS00144	Xerostomia	C0043352			HP:0000217	42
SMTS00580	*Kou Ku*	SMMS00585	Halitosis	C0018520	Abnormality of taste sensation	C4025879	HP:0000223	6
SMTS00970	*Shi Mian*	SMMS00033	Insomnia	C0917801			HP:0100785	12
SMTS00211	*Duo Meng*	SMMS00738	Nightmares	C0028084				
SMTS01439	*Xuan Yun*	SMMS00115	Vertigo	C0042571			HP:0002321	72
N/A	*Mai Jie Dai*				Irregular heart beat		0011675	317

TCM, traditional Chinese medicine; MM, modern medicine; UMLS, Unified Medical Language System; HPO, human phenotype ontology.

Five hundred two targets in total for PHHD arrhythmia were collected as PHHD-arrhythmia target spectrum; statistics of target count for each TCM symptom were shown in **Figure 3** (**Supplement Table 4**).

To obtain the pharmacological network of XSN on treating PHHD arrhythmia, 40 targets were obtained in the common set of XSN target spectrum and PHHD-arrhythmia target spectrum (**Table 2**). All the components interact with the 40 targets above consist of the panoramagram of the pharmacological mechanism of XSN for treating PHHD arrhythmia.

Pharmacodynamic Research of High-Weight Components in XSN

Based on our previous study, XSN is a class III anti-arrhythmic drug supported by the prolongation of the action potential of

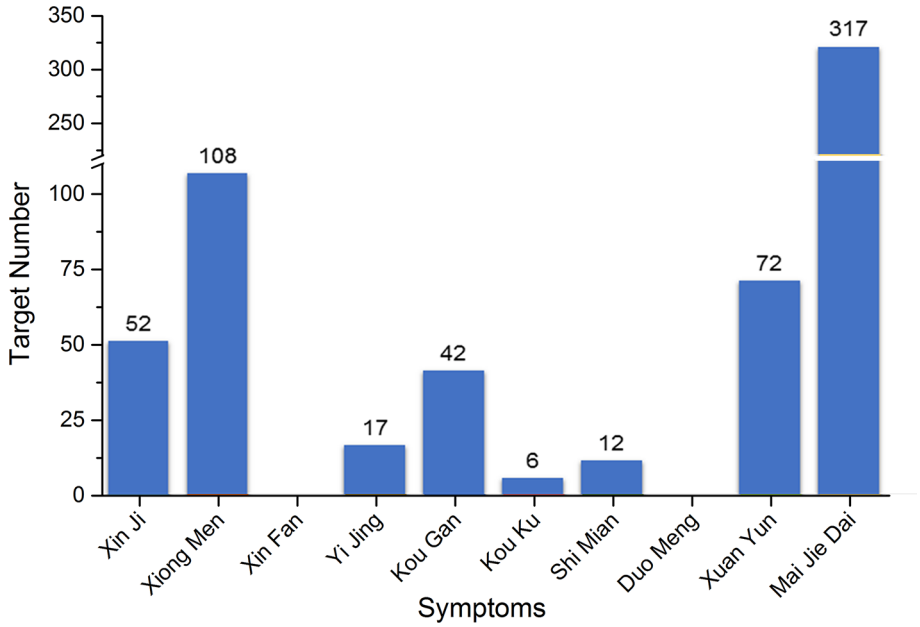

FIGURE 3 | Statistics of target count for each TCM symptom of PHHD arrhythmia.

cardiac myocytes through blocking hERG channel (Ma et al., 2016; Wang et al., 2017), and it also showed class I antiarrhythmic property of blocking sodium channels (Wang et al., 2019b). However, the available pharmacological research data of all the components in the 11 herbs of XSN reported and recorded in all the databases are not sufficient to correlate with the clinical antiarrhythmic efficacy and our discovery that inhibit human cardiac sodium current, $Na_V1.5$ channel (encoded by gene SCN5A) with total target weight coefficient of 1.32 (Wang et al., 2019b). Comparing with the effect of hERG channel (encoded by KCNH2), total target weight coefficient of hERG is 14838.89; both of them are with similar IC_{50} values generated by XSN, which can be considered as a combination of all the components. Thus, we screen the set of high-weight components with reported content in corresponding herbs on inhibiting $Na_V1.5$.

Two high-weight active components: liensinine (LSN, PubChem CID: 160644) and isoliquiritigenin (ISL, PubChem CID: 638278) were detected using electrophysiological approaches. LSN is the No. 35 high-weight component, which blocked human $Na_V1.5$ channel dose-dependently with an IC_{50} of 3.58 ± 0.36 μM (**Figure 4**). ISL reduced peak I_{Na} concentration dependently, with a median inhibitory concentration (IC_{50}) of 10.11 μM ± 1.12 μM. The positive control amiodarone (AMD) blocks $Na_V1.5$ channel with IC_{50} = 5.05 ± 0.55 μM.

Panoramagram of the Pharmacological Mechanism of XSN

Including the pharmacological effects of LSN and ISL, a panoramagram of the integrative pharmacological mechanism of XSN was interpreted (shown as **Figure 5**). The pharmacological network consisted of 963 components, 618 targets, and 10 symptoms. This panoramagram illustrated the network pharmacological relationships among the XSN formula, herbs, components, targets, symptoms, and PHHD arrhythmia.

Pathways Involved in the Pharmacological Mechanism of XSN on Treating PHHD Arrhythmia

All the 40 common targets between XSN target spectrum and PHHD-arrhythmia target spectrum were selected to carry out pathway enrichment with Reactome application in Cytoscape. 117 pathways with FDR less than 0.05 were obtained and resort by total weight coefficients (**Figure 6**, **Supplement Table 5**).

To better understand the antiarrhythmic therapeutic efficacy of XSN, cardiac conduction pathway is calculated to hold the highest total weight coefficient in the list of resorting pathway total weight coefficient. It was shown in **Figure 7** and all the components in XSN involved in regulating this pathway were marked in the figure.

DISCUSSION

Tan-Re-Rao-Xin Zheng is named as PHHD syndrome in English. Based on the traditional Chinese Medicine theories, PHHD is defined as that heat having existed in the body for a period of time without distributing leads to the body's fluids being concentrated as Phlegm. The concept *Heart* in the Chinese medicine mainly refers to the circulatory system and nervous system, and they are easily to be blocked or obstructed to cause malfunction (Jiao et al., 2015). This is why PHHD is classified as an "excess" syndrome; the heat and the phlegm must be cleared to treat the symptoms in circulatory system and neuronal system successfully.

TABLE 2 | The common genes between XSN target spectrum and PHHD-arrhythmia target spectrum.

Gene_Symbol	TCM_Symptom	Target_Weight_Coefficient	UniProt_ID	ChEMBL_ID	Target_Name	Classification_1	Classification_2
CALM1	Maijiedai, Xuanyun	790.2976034	P0DP23	CHEMBL6093	Calmodulin	Other	Unclassified protein
KCNH2	Maijiedai, Xinji	13942.14102	Q12809	CHEMBL240	HERG	Ion channel	VGIC
TP53	Yijing, Maijiedai, Xinji	13900.81344	P04637	CHEMBL4096	Cellular tumor antigen p53	Transcription factor	Other
ABCC8	Maijiedai	13817.52659	Q09428	CHEMBL2071	Sulfonylurea receptor 1	Transporter	Other
KCNJ11	Maijiedai	13817.40799	Q14654	CHEMBL1886	Potassium channel, inwardly rectifying, subfamily J, member 11	Ion channel	VGIC
KCNJ5	Maijiedai	169.079052	P48544	CHEMBL3038488	Kir3.1/Kir3.4	Ion channel	VGIC
CACNA1B	Maijiedai	593.6573686	Q00975	CHEMBL4478	Voltage-gated N-type calcium channel alpha-1B subunit	Ion channel	VGIC
TARDBP	Kougan	2584.201263	Q13148	CHEMBL2362981	TAR DNA-binding protein 43	Other	Unclassified protein
JAK2	Xuanyun	2032.705321	O60674	CHEMBL2971	Tyrosine-protein kinase JAK2	Kinase	Protein Kinase
TNNC1	Maijiedai	2017.925664	P63316	CHEMBL2095202	Troponin, cardiac muscle	Other	Other
TNNI3	Maijiedai	2017.925664	P19429	CHEMBL2095202	Troponin, cardiac muscle	Other	Other
TNNT2	Maijiedai	2017.925664	P45379	CHEMBL2095202	Troponin, cardiac muscle	Other	Other
GMNN	Xiongmen	95.88983101	O75496	CHEMBL1293278	Geminin	Other	Unclassified protein
SMAD3	Maijiedai	95.88983101	P84022	CHEMBL1293258	Mothers against decapentaplegic homolog 3	Other	Unclassified protein
PPARG	Maijiedai, Xinji	83.46168023	P37231	CHEMBL235	Peroxisome proliferator-activated receptor gamma	Transcription factor	Nuclear receptor
GJA1	Maijiedai	83.29977996	P17302		Gap junction alpha-1 protein	Other	Unclassified protein
PTPN11	Maijiedai	83.26574007	Q06124	CHEMBL3864	Protein-tyrosine phosphatase 2C	Enzyme	Phosphatase
LMNA	Maijiedai	83.14071435	P02545	CHEMBL1293235	Prelamin-A/C	Other	Unclassified protein
TSHR	Maijiedai	83.14071435	P16473	CHEMBL1963	Thyroid-stimulating hormone receptor	GPCR	Family A GPCR
ATXN2	Kougan	12.74911666	Q99700	CHEMBL1795085	Ataxin-2	Other	Unclassified protein
SOD1	Kougan	1.975815734	P00441	CHEMBL2354	Superoxide dismutase	Enzyme	Oxidoreductase
SDHA	Yijing, Maijiedai, Xinji, Xuanyun	1.990418899	P31040	CHEMBL5758	Succinate dehydrogenase (ubiquinone) flavoprotein subunit, mitochondrial	Enzyme	Oxidoreductase
PON1	Kougan	1.732079071	P27169	CHEMBL3167	Serum paraoxonase/arylesterase 1	Enzyme	Hydrolase
KYNU	Maijiedai	1.649920118	Q16719	CHEMBL5100	Kynureninase	Enzyme	Hydrolase
IFNG	Maijiedai	1.695300734	P01579	CHEMBL3286073	Interferon gamma	Other	Other
CHRM3	Kougan	0.769622544	P20309	CHEMBL245	Muscarinic acetylcholine receptor M3	GPCR	Family A GPCR
SCN5A	Maijiedai, Xinji	76.0137842	Q14524	CHEMBL1980	Sodium channel protein type V alpha subunit	Ion channel	VGIC
DAO	Kougan	1.396943488	P14920	CHEMBL5485	D-amino-acid oxidase	Enzyme	Oxidoreductase
CPT2	Maijiedai, Xiongmen	1.020829585	P23786	CHEMBL3238	Carnitine palmitoyltransferase 2	Enzyme	Transferase
CTNNB1	Xuanyun	1.020829585	P35222	CHEMBL5866	Catenin beta-1	Other	Unclassified protein
NAGS	Xiongmen	1.020829585	Q8N159		N-acetylglutamate synthase, mitochondrial	Enzyme	Transferase
TTR	Maijiedai	1.001902474	P02766	CHEMBL3194	Transthyretin	Other	Other
COL3A1	Xuanyun	0.45282272	P02461	CHEMBL2364188	Collagen	Other	Other
SLC1A3	Xuanyun	0.520835938	P43003	CHEMBL3085	Excitatory amino acid transporter 1	Transporter	Electrochemical transporter
HNF4A	Maijiedai	0.386540369	P41235	CHEMBL5398	Hepatocyte nuclear factor 4-alpha	Other	Unclassified protein
AKT1	Maijiedai	0.26386963	P31749	CHEMBL4282	Serine/threonine-protein kinase AKT	Kinase	Protein kinase

(Continued)

TABLE 2 | Continued

Gene_Symbol	TCM_Symptom	Target_Weight_Coefficient	UniProt_ID	ChEMBL_ID	Target_Name	Classification_1	Classification_2
GAA	Maijiedai	0.261304876	P10253	CHEMBL2608	Lysosomal alpha-glucosidase	Enzyme	Hydrolase
LDLR	Maijiedai	0.132692707	P01130	CHEMBL3311	LDL receptor	Other	Membrane receptor
EGF	Xuanyun	0.159065607	P01133	CHEMBL5734	Pro-epidermal growth factor	Other	Unclassified protein

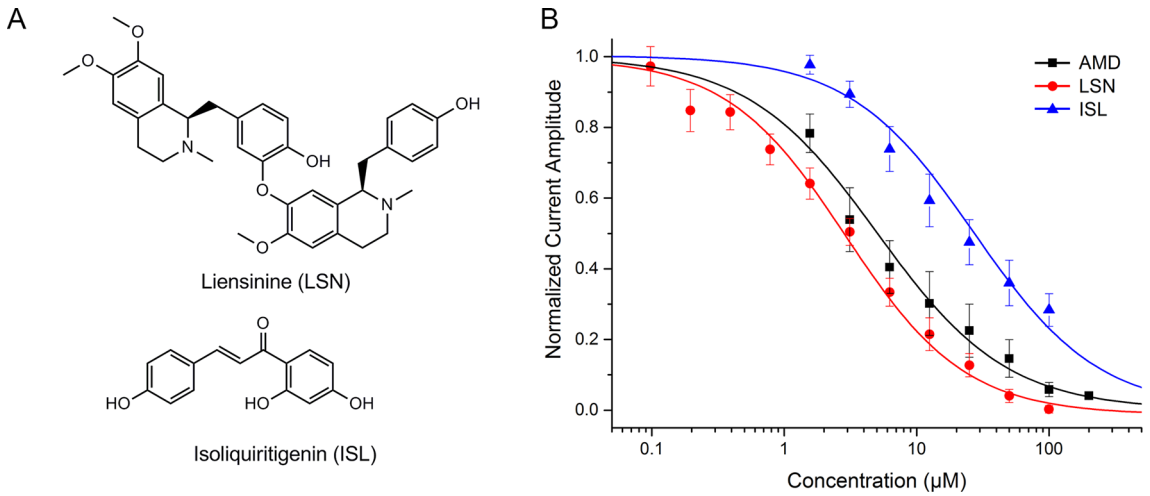

FIGURE 4 | (A) Chemical structure of liensinine (LSN) and isoliquiritigenin (ISL). **(B)** Dose–response curve of the inhibition on human $Na_v1.5$ channel by amiodarone (AMD, n=5), LSN (n=6), and ISL (n=8).

Physical symptoms of PHHD are usually consist of the followings (Yongdun et al., 2005; Ren et al., 2012; Xing et al., 2015): (1) insomnia, difficulty in falling asleep and frequent dream-disturbed waking. (2) Palpitations, the heart rhythm becomes out of control, e.g., PVCs or tachycardia. However, it depends on the severity of how much the heart had been disturbed by the phlegm fire; the clinical manifestation could range from incidental PVC to frequent PVC or from normal heart rate to tachycardia. In the region of the heart, there is often a sensation of heat or discomfort and oppressed chest, feeling difficult to breath. (3) Tongue, tongue body is red, especially at the tip, which is often swollen and painful. The tongue coating is yellow and thick. There is very often a mid-line crack extending to the tip, with yellow moss on it. Hypertension—high blood pressure—is often a feature of heart phlegm fire. (4) Pulse, slippery, and rapid and overflowing which means "excess"; it often appears after the first stage of infectious disease and shows excess heat. Complexion is red; eyes are bloodshot. Some mental symptoms could also happen, like boredom or even hypomania which also depends on the severity of phlegm-heat disturbing the neural system (which is also part of the *Heart* in TCM theory). Therefore, arrhythmia with obvious clinical signs of PHHD is a particular condition that the patient suffering from phlegm-heat, and the circulation system would be mostly influenced.

XSN capsule originated from the famous compound formula Huanglian Wendan (HLWD) Decoction recorded in 150 years ago, which has the effect of removing phlegm, blood stasis, and fire toxin. Huanglian, Banxia, Fuling, Gancao, and Zhishi are from the original formula HLWD decoction; Changshan, Lianzixin, Qinghao, and Kushen were added to make XSN formula more inclined to the circulation system. Therefore, XSN was not only a combination of anti-arrhythmic monomer components, but also a complex therapeutic system to regulate biological/pathological process relative to PHHD syndrome.

The compatibility principle of the herbs in XSN also reflects another key property of Chinese herbal medicine: amount/proportion of herbs in compound formula. For a better understanding of the pharmacological mechanism of XSN, we introduced a novel parameter, *weight coefficient*, to mimic the compatible combination of all the chemical components in the 11 herbs in XSN. As mentioned in methods section, weight coefficient is the product of proportion of herbs in the compound formula, content of each component in relative herb and the predicted probability of human OB of each component. Weight coefficient is not the absolute concentration of each chemical component but a relative content among them, which means the ranked order of weight coefficient of each component can be considered as the extent how much a component involved in the pharmacological mechanism of XSN. The weight coefficient of each component reflects its molar concentration in the blood; therefore, the higher the weight coefficient, the more molecules

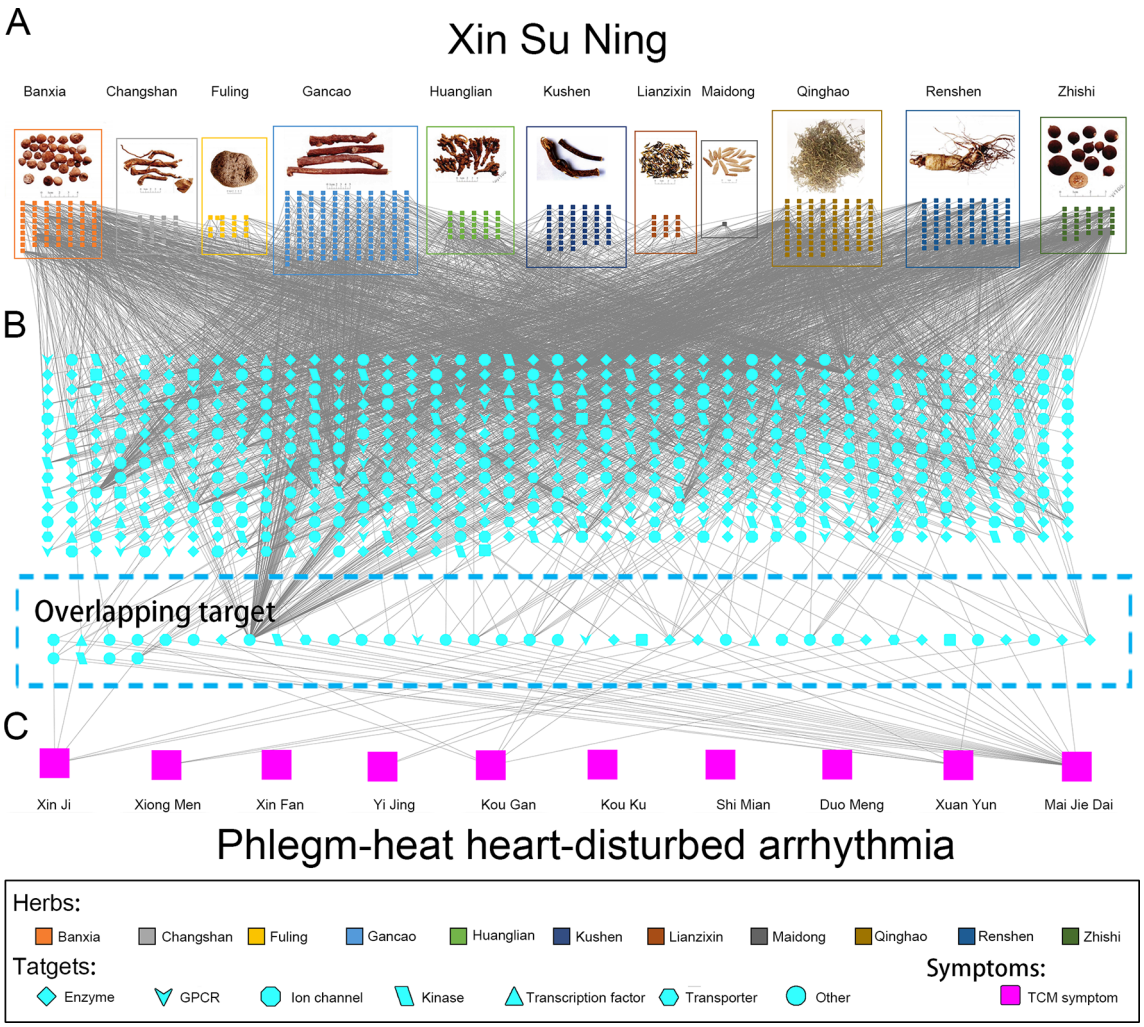

FIGURE 5 | Panoramagram of the pharmacological mechanism of XSN for treating PHHD arrhythmia. This panoramagram illustrated the connections among the XSN formula, herbs, components, targets, symptoms, and PHHD arrhythmia. **(A)** XSN formula and components. All the 11 herbs were shown as figures in the box with different colors, and the components of each herb were shown as small square with the same color as their source herb. **(B)** XSN target spectrum. All the targets were corresponding to the component in panel A; the 41 targets showed in the dash line box in the bottom is the overlapping target set between XSN target spectrum and PHHD-arrhythmia target spectrum. Targets were shown in different shapes according to the classifications as indicated in the keys. **(C)** Arrhythmia with PHHD Zheng and relative TCM symptoms. Ten TCM symptoms of PHHD arrhythmia were represented by large pink squares in the bottom panel.

will bind to the targets. However, the binding affinity of the component to the target remains to be tested pharmacologically.

In this study, we used network pharmacological approach to visualize the complex pharmacological mechanism of XSN on treating PHHD arrhythmia. All the data were collected from databases and books to assure the quality and reliability of all the relationships in the pharmacological network. Based on our previous study, XSN can be classified as class III antiarrhythmic drug, and with some pharmacological property of class I drug (Sweeney et al., 2019; Wang et al., 2019a; Wang et al., 2019b). The application of XSN resulted in significant morphological changes of the ECG trace of isolated rat heart featured by the suppression of the R wave amplitude. The QRS complex represents ventricular depolarization as a result of activation of $Na_V1.5$. Our previous study attributed the decrease in R wave amplitude to XSN dependent inhibition of I_{Na}; when whole-cell sodium currents were elicited using a depolarizing pulse protocol, it was evident that XSN inhibited I_{Na} concentration dependently and reversibly. However, the data from reported research recorded in the databases were not sufficient to support all the antiarrhythmic effect of XSN; we, therefore, carried out a small scale component screening on the target of class I antiarrhythmic drug, human $Na_V1.5$ channel. Given previous collected in this paper did not provide enough weight coefficient on $Na_V1.5$ channel, some unidentified high-content components should target $Na_V1.5$. Thus, we screened a series of high-content components listed in **Figure 1H**, to replenish the component-target information. LSN and ISL were identified as active components on $Na_V1.5$ channel in the present study. Briefly speaking, the pharmacologically defined inhibition of $Na_V1.5$ by the active components of the 11 herbs in XSN suggests that Lien and ISL bind to the channel in its inactivated state which reduces the I_{Na} amplitude. The total weight coefficient of $Na_V1.5$ is 76.013, which is still much lower than hERG 13942.141. The reason is understandable

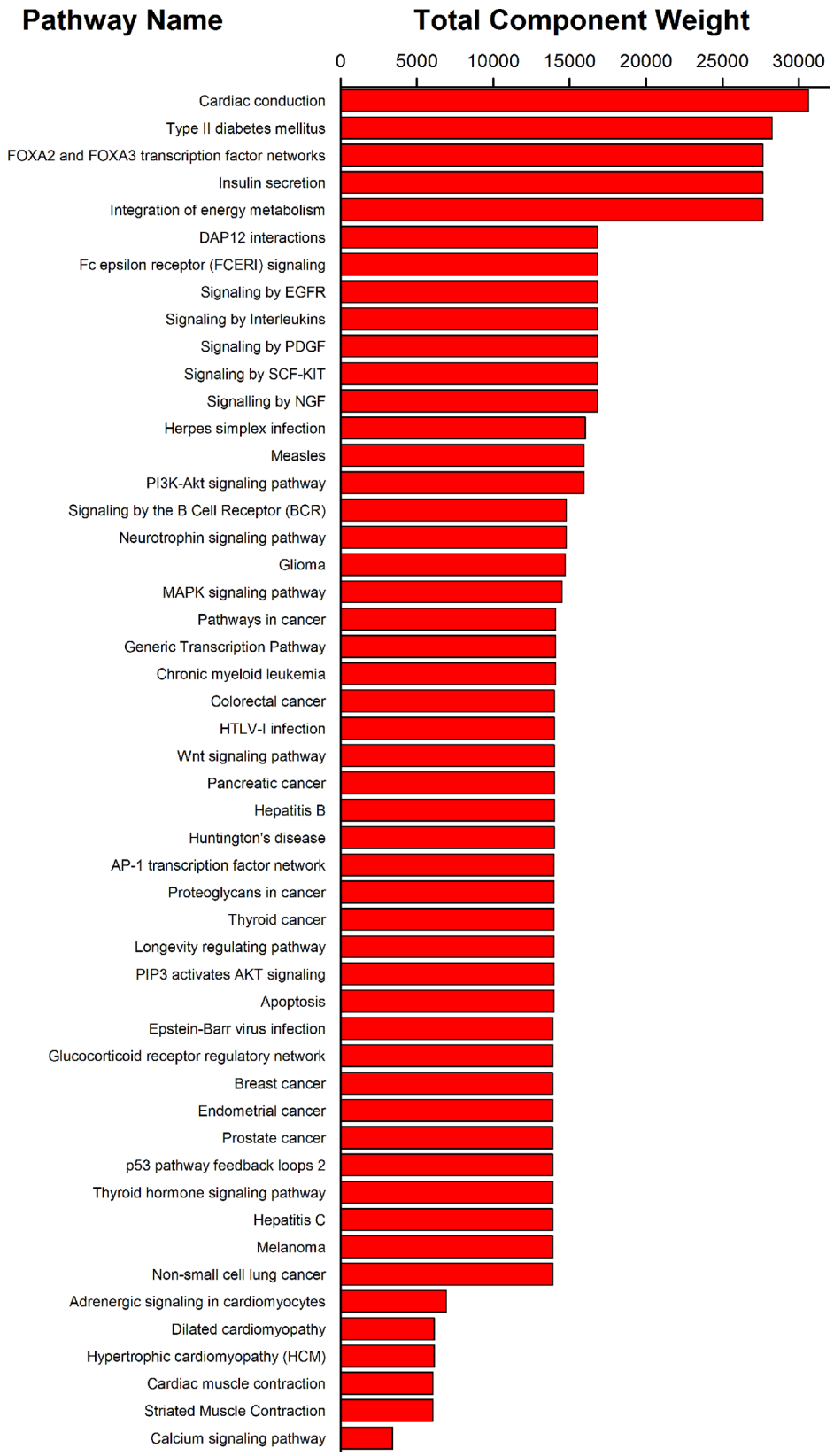

FIGURE 6 | Pathway enrichment results of 40 targets of XSN on treating PHHD arrhythmia. Top 50 pathways were shown here; and all were sorted by pathway weight coefficient.

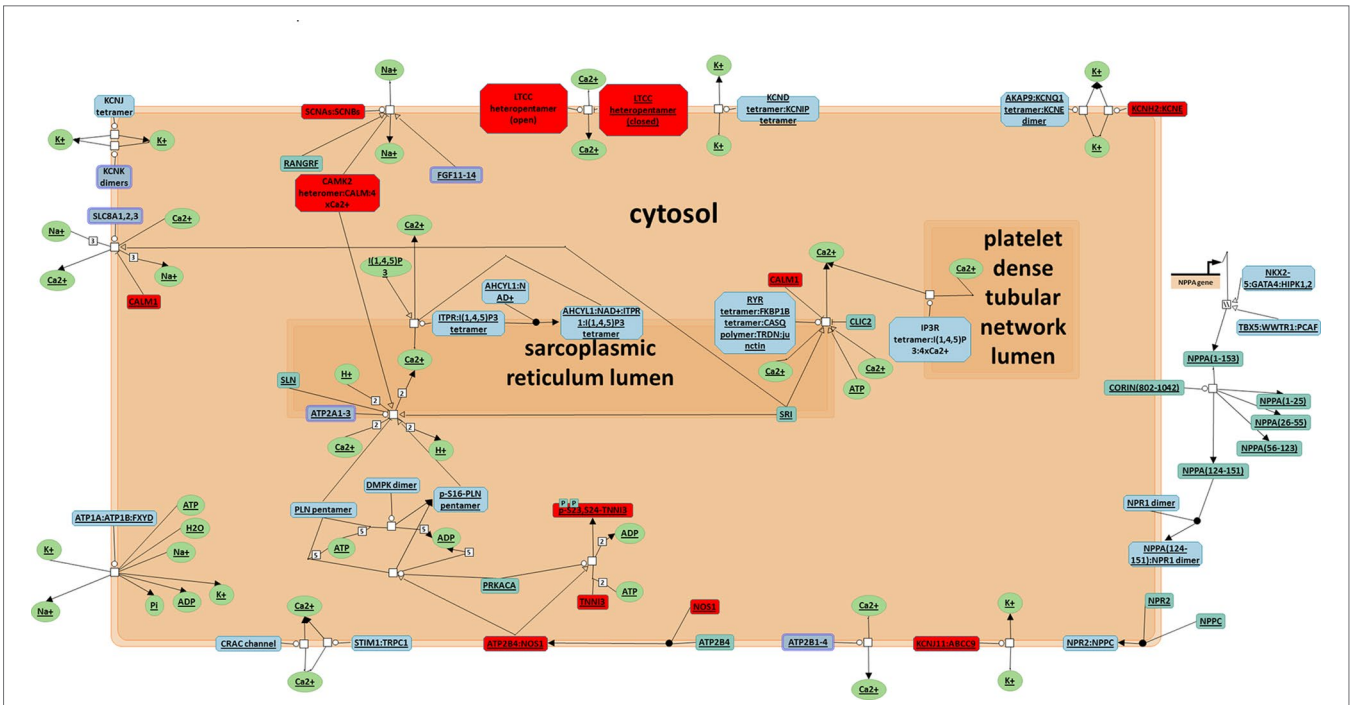

FIGURE 7 | Cardiac conduction pathway. Top 1 pathway in the rank of total target weight coefficient, all the target regulated in this pathway were marked in red (Jassal, 2014).

that, based on the content of components in the mixture of raw herbs of XSN, the weight of Huanglian (334g/2,377g mixture of raw herbs) is much more than Lianzixin (42g/2,377g mixture of raw herbs) and Gancao (167g/2,377g mixture of raw herbs); meanwhile, the concentration of berberine is much higher than LSN and ISL in relative herbs (details see **Supplement Table 1**). Secondly, the experimental inhibitory effect of $Na_V1.5$ by XSN was carried on directly on isolated heart or cell lines without influenced by absorption, distribution, metabolism, and excretion; the predicted oral bioavailability also lower down the weight coefficients of LSN and ISL. Technically, more active components inhibiting $Na_V1.5$ were still undiscovered, and further research on XSN is still needed.

Including the pharmacological effects of LSN and ISL, we drew a panoramagram of the integrative pharmacological mechanism of XSN with 475 components targeting 617 targets. Among the 617 targets, 40 targets were relative to PHHD arrhythmia. To explain the mechanism, we carried out pathway enrichment instead of subnetwork analysis, 116 pathways were obtained, and top 50 were shown as **Figure 6**.

As an antiarrhythmic drug, XSN showed multiple therapeutic effects. From the standpoint of TCM treatment, both tip and root causes can be reflected in the pathways, which can also be considered as quick-acting and long-acting mechanisms. First, ion channels play essential role in terminating abnormal electrical activity in arrhythmic heart. Based on the results from the analysis above, the mechanism on cardiac electronic activity may involve such targets: TNNI3, CACNA1S, SCN5A, KCNH2, KCNJ11, and CALM1. $Na_V1.5$, $Ca_V1.2$, and hERG are three key ion currents in cardiac electric conduction during depolarization and repolarization. Troponins I (encoded by TNNI3) is integral to cardiac muscle contraction, which is also used as diagnostic and prognostic indicators in the management of myocardial infarction and acute coronary syndrome. Calmodulin 1 (encoded by CALM1) mediates the regulation of plenty of enzymes, ion channels, aquaporins, and other proteins acting with calcium-binding. Secondary, as long-acting mechanism, XSN was used to treat arrhythmia caused by coronary heart disease and viral myocarditis. Protection of myocardium, such as protection of I/R injury, antithrombosis and anti-apoptotic effect should be the essential effects of XSN. Intracellular sodium accumulation is a key pathophysiological mechanism in myocardial ischaemia/reperfusion (I/R) injury. Furthermore, it is thought that, $Na_v1.5$, alongside NHE and other transporters, contributes to this sodium overload that can be reduced with application of lidocaine, suggesting that inhibition of I_{Na} may attenuate I/R injury. Previous work has shown XSN is cardioprotective in I/R injury induced in isolated rat hearts. Given the effect of ISL in inhibiting $Na_v1.5$, it is possible that LSN and ISL reported in the present study are responsible for some of XSN's cardioprotective actions in this way.

Besides of calcium overload, another reason of myocardium injury was caused by apoptosis of cardiomyocyte. The p53 tumor suppressor is one of the major apoptosis signaling pathways. It regulates a wide variety of genes involved in apoptosis, growth arrest, or senescence in response to genotoxic or cellular stress. The p53 can promote apoptosis through interactions with Bcl-2 family proteins in the cytoplasm. In addition, HIF1 alpha was also downregulated by the top1 component berberine (Mao et al., 2018). Berberine inhibits doxorubicin-induced cardiomyocyte apoptosis (Lv et al., 2012).

Inflammatory response is well recognized as a critical contributor for the development and complications of atherosclerosis

cardiovascular disease (ASCVD), including myocardial infarction (MI), heart failure, and stroke, which involve complex interactions between multiple biological processes.

Besides of cardiovascular pathways, several diabetic pathways were also obtained. In TCM system, disease with diabetes-related symptoms is called "*Xiaoke*," which is primarily caused by deficiency of Yin with dryness and heat syndromes as the secondary cause (Tong et al., 2012). As both PHHD and *Xiaoke* partially shared the pathogenesis of heat, it is understandable to share some biological pathways in common. In type II diabetes mellitus, insulin secretion, integration of energy metabolism pathways, KCNJ11, and ABCC8 were the common targets, which may be regulated by XSN. The beta-cell ATP-sensitive potassium (KATP) channel is a key component of stimulus-secretion coupling in the pancreatic beta-cell. The channel coupled metabolism to membrane electrical events bringing about insulin secretion. The channel consists of four subunits of the inwardly rectifying potassium channel Kir6.2 and four subunits of the sulfonylurea receptor 1 (SUR1).

Beyond of these targets, several targets including fatty acid synthase (FASN), pyruvate kinase L/R (PKLR), acetyl-CoA carboxylase (ACC, alpha unit encoded by ACACA), transketolase (TKT), free fatty acid receptor 1(FFAR1), glucagon-like peptide 1 receptor (GLP1R), and so on were also regulated by XSN. These targets are involved in the bioprocess of glycolysis, fatty acid synthesis, and pentose phosphate pathway, which are key steps of glucose and lipid metabolism. Through these mechanisms, XSN may improve fatty acid storage and convert it into glycogen. Lipid metabolism disorder has been reported being related to the TCM heat syndrome (Lv et al., 2012), which also suggest XSN regulate glucose and lipid metabolism to act as removing the extra heat based on the TCM theories.

In summary, the mechanism of XSN on treating PHHD arrhythmia may act as follows: on quick-acting aspect, XSN balanced the ion current of the heart by regulating multiple ion channels to terminate cardiac arrhythmia; on the long-acting aspect, XSN protects the heart from I/R injury, inhibits the apoptosis of cardiomyocyte, and improves glucose and lipid metabolism. Part of the mechanism of XSN on treating PHHD syndrome by sharing pathways with insulin secretion or glucose and lipid metabolism also suggest the potential therapeutic effect of diabetes and diabetic cardiopathy.

DATA AVAILABILITY STATEMENT

All datasets generated for this study are included in the manuscript/**Supplementary Files**.

AUTHOR CONTRIBUTIONS

Y-LM and TW conceived and designed the study; TW and HS performed the electrophysiological experiments; XW discussed, analyzed and standardized the TCM symptoms; UP and ML analyzed and discussed the biological functions of the pathways; CC provided experimental equipment and technical support for cell culturing; TW and Y-LM wrote the paper.

FUNDING

This work was supported by grants from the Chinese Medicine Research Fund, University of Oxford. The grant was funded by Shaanxi Momentum Pharmaceutical Co.,Ltd.

ACKNOWLEDGMENTS

We thank Prof. Yan Zhu (Tianjin University of Traditional Chinese Medicine) for providing the stable transfected cell lines and Dr. Hongbin Yang (East China University of Science and Technology) for technical support on AdmetSar 2.0 system.

SUPPLEMENTARY MATERIAL

The Supplementary Material for this article can be found online at: https://www.frontiersin.org/articles/10.3389/fphar.2019.01138/full#supplementary-material

TABLE S1 | XSN component library.

TABLE S2 | XSN component target relationships.

TABLE S3 | XSN Target Weight Coefficient type.

TABLE S4 | PHHD-arrhythmia target spectrum.

TABLE S5 | XSN PHHD Pathway.

REFERENCES

Atarashi, H., and Hayakawa, H. (1996). Etiology and classification of cardiac arrhythmias. *Nippon Rinsho* 54, 2023–2028.

Bairoch, A., Boeckmann, B., Ferro, S., & Gasteiger, E. (2004). Swiss-Prot: Juggling between evolution and stability. 5(1), 39–55. doi: 10.1093/bib/5.1.39

Barsky, A. J. (2001). Palpitations, arrhythmias, and awareness of cardiac activity. *Ann. Intern. Med.* 134, 832–837. doi: 10.7326/0003-4819-134-9_Part_2-200105011-00006

Bento, A.P., Gaulton, A., Hersey, A., Bellis, L.J., Chambers, J., Davies, M., et al. (2014). The ChEMBL bioactivity database: an update. *Nucleic Acids Res.*42(D1), D1083–D1090. doi: 10.1093/nar/gkt1031

Chen, G., and Wu, X. (1996). Treatment of refractory ventricular arrhythmia with the combined use of FDP, berberine, XinBaoWan and modified SMS. *J. Shantou Univ. Med. College* 2, 90–91.

Chen, W., and Ba, Z. (2010). Prof. ZHANG Yi's experience in treating severe arrhythmia. *J. Tradit. Chin. Med.* 30, 47–50. doi: 10.1016/S0254-6272(10)60012-X

Cheng, F., Li, W., Zhou, Y., Shen, J., Wu, Z., & Liu, G., et al. (2012). admetSAR: a comprehensive source and free tool for assessment of chemical admet properties. *J. Chem. Inf. Model.* 52 (11), 3099–3105. doi: 10.1021/ci300367a

Dong, S., Liu, J., Han, L., Zhao, W., and Luan, J. (2005). Contents of trace and constant elements and therapeutic effects of Chinese patent medicine on cardio-cerebral vascular disease: fuzzy classified principle. Chin. J. *Tissue Eng. Res.* 9, 254–256. doi: 10.3321/j.issn:1673–8225.2005.15.069

Dong, Y., Liao, J., Yao, K., Jiang, W., and Wang, J. (2017). Application of traditional Chinese medicine in treatment of atrial fibrillation. *Evid. Based Complement. Altern. Med.* 2017, 1–11. doi: 10.1155/2017/1381732

Fabregat, A., Jupe, S., Matthews, L., Sidiropoulos, K., Gillespie, M., Garapati, P., et al. (2018). The Reactome pathway knowledgebase. *Nucleic Acids Res.* 46, D649–d655. doi: 10.1093/nar/gkx1132

Fabregat, A., Sidiropoulos, K., Viteri, G., Forner, O., Marin-Garcia, P., Arnau, V., et al. (2017). Reactome pathway analysis: a high-performance in-memory approach. *BMC Bioinformatics* 18, 142. doi: 10.1186/s12859-017-1559-2

Gilson, M.K., Liu, T., Baitaluk, M., Nicola, G., Hwang, L., and Chong, J. (2016). BindingDB in 2015: A public database for medicinal chemistry, computational chemistry and systems pharmacology. *Nucleic Acids Res.* 44(D1), D1045–D1053. doi: 10.1093/nar/gkv107

Gu, C., Wu, Y., Tian, S., Gao, X., Qi, X., Jia, Z., et al. (2005). Effect of shensong yangxin capsule on ventricular premature beat and cardiovascular autonomic nervous function in patients with coronary heart disease. *Zhongguo Zhong Xi Yi Jie He Za Zhi* 25, 783–786. doi: 10.3321/j.issn:1003–5370.2005.09.004

Hong, Y., Huang, Y., Wu, H., Chen, Y., Li, F., and Mo, H. (2005). Clinical studies on relationship between TCM syndromes of coronary heart disease and inflammatory factors. *J. of Guangzhou Univ.* of *Tradit. Chin. Med.* 22(2), 81–86

Jassal, B. (2014). Image for "Cardiac conduction". Reactome: R-HSA-5576891.2, doi: 10.3180/R-HSA-5576891.1

Jiang, M., Lu, C., Zhang, C., Yang, J., Tan, Y., Lu, A., et al. (2012). Syndrome differentiation in modern research of traditional Chinese medicine. *J Ethnopharmacol* 140, 634–642. doi: 10.1016/j.jep.2012.01.033

Jiao, Y., Han, Y., Li, X., Fang, Y.-G., Liu, Z.-H., Zhou, W.-N., et al. (2015). Comparison of Body, Auricular, and Abdominal Acupuncture Treatments for Insomnia Differentiated as Internal Harassment of Phlegm-Heat Syndrome: An Orthogonal Design. *Evid. Based Complementary Altern. Med.* 2015, 1–9. doi: 10.1155/2015/578972.

Kalifa, J., and Avula, U. M. R. (2012). The Chinese herb extract Wenxin Keli: atrial selectivity from the far east. *Heart Rhythm* 9, 132–133. doi: 10.1016/j.hrthm.2011.11.030

Leung, E. L. H., Wong, V. K. W., Jiang, Z. H., Li, T., and Liu, L. (2014). Integrated network-based medicine: the role of traditional Chinese medicine in developing a new generation of medicine. *Science* 346, S16–S18.

Li, F., and Zhang, C. (2015). Clinical study of Xinsuning capsule in the treatment of paroxysmal atrial fibrillation. *Med. Front.* 5, 95–97. doi: 10.3969/j.issn.2095-1752.2015.26.077

Li, M., and Guihua, T. (2018). Therapeutic effects of Wenxin Keli in cardiovascular diseases: an experimental overview. *Front. Pharmacol.* 9, 1005. doi: 10.3389/fphar.2018.01005

Li, S., Zhang, B., and Zhang, N. (2011). Network target for screening synergistic drug combinations with application to traditional Chinese medicine. *BMC Syst. Biol.* 5, S10. doi: 10.1186/1752-0509-5-S1-S10

Lin, L., Liu, Y., and Lin, H. (2011). Observation on twenty-six cases of frequent premature ventricular contractions treated with Xinsuning capsules. *People's Mil. Surg.* 54, 512.

Liu, Y., Li, N., Jia, Z., Lu, F., and Pu, J. (2014). Chinese Medicine Shensongyangxin Is Effective for Patients with Bradycardia: Results of a Randomized, Double-Blind, Placebo-Controlled Multicenter Trial. *Evidence-Based Complementary and Alternative Medicine* 2014, 1–6. doi: 10.1155/2014/605714

Lu, A.-P., Jia, H.-W., Xiao, C., and Lu, Q.-P. (2004). Theory of traditional Chinese medicine and therapeutic method of diseases. *World J. Gastroenterol.* 10, 1854. doi: 10.3748/wjg.v10.i13.1854

Lv, X., Yu, X., Wang, Y., Wang, F., Li, H., Wang, Y., et al. (2012). Berberine inhibits doxorubicin-triggered cardiomyocyte apoptosis via attenuating mitochondrial dysfunction and increasing Bcl-2 expression. *PloS one* 7, e47351. doi: 10.1371/journal.pone.0047351

Ma, Y., Wang, T., Ellory, C., Wilkins, R., Carr, C., Mao, P., et al. (2016). Investigation of the active antiarrhythmic components of the multi-herbal medicine Xin Su Ning. *Proceedings of the British Pharmacological Society* http://www.pA2online.org/abstracts/Vol16Issue1abst093P.pdf

Mao, L., Chen, Q., Gong, K., Xu, X., Xie, Y., Zhang, W., et al. (2018). Berberine decelerates glucose metabolism via suppression of mTOR-dependent HIF-1α protein synthesis in colon cancer cells. *Oncol. Rep.* 39, 2436–2442. doi: 10.3892/or.2018.6318

Ni, X., Shergis, J. L., Zhang, A. L., Guo, X., Lu, C., Li, Y., et al. (2019). Traditional use of Chinese herbal medicine for insomnia and priorities setting of future clinical research. *J. Altern. Complement. Med.* 25, 8–15. doi: 10.1089/acm.2018.0249

Ren, Y., Zhang, M., Chen, K., You, S., Li, J., Guo, L., et al. (2012). Clinical and epidemiological investigation of TCM syndromes of patients with coronary heart disease in China. *Evid. Based Complementary Altern. Med.* 2012, 1–5. doi: 10.1155/2012/714517

Ru, J., Li, P., Wang, J., Zhou, W., Li, B., Huang, C., et al. (2014). TCMSP: a database of systems pharmacology for drug discovery from herbal medicines. *J. Cheminform* 6, 13. doi: 10.1186/1758-2946-6-13

Shannon, P., Markiel, A., Ozier, O., Baliga, N. S., Wang, J. T., Ramage, D., et al. (2003). Cytoscape: a software environment for integrated models of biomolecular interaction networks. *Genome Res.* 13, 2498–2504. doi: 10.1101/gr.1239303

Shao, L., and Zhang, B. (2013). Traditional Chinese medicine network pharmacology: theory, methodology and application. *J. Chin. J. Nat. Med.* 11, 110–120. doi: 10.1016/S1875-5364(13)60037-0

Sweeney, O., Wang, T., Ellory, C., Wilkins, R., and Ma, Y.-L. (2019). The effects of liquiritigenin on the activity of the hERG potassium channel. *Br. J. Pharmacol.* 176, 3067–3068.

Tong, X.-L., Dong, L., Chen, L., and Zhen, Z. (2012). Treatment of diabetes using traditional Chinese medicine: past, present and future. *Am. J. Chin. Med.* 40, 877–886. doi: 10.1142/S0192415X12500656

Wang, A., Pu, J., Qi, X., Miao, W., Hou, Z., Cong, H., et al. (2011). Evaluation of shensongyangxin capsules in the treatment of paroxysmal atrial fibrillation: a randomized, double-blind and controlled multicenter trial. *Zhonghua yi xue za zhi* 91, 1677–1681. doi: 10.3760/cma.j.issn.0376-2491.2011.24.006

Wang, B., and Mao, P. (2018). *Use of traditional chinese medicine composition in preparation of potassium ion channel modulator medicine*. US Patent App. 15/573, 583.

Wang, C., and Lu, J. (2008). Observation on thirty cases of viral myocarditis treated with Xinsuning capsules. *Shanxi Zhongyi* 29, 1362. doi: 10.3969/j.issn.1000-7369.2008.10.068

Wang, T., Ellory, C., Wilkins, R., and Ma, Y.-L. (2019a). Investigation on the mechanism and active component of sodium channel blockage effect of Xin Su Ning. *Br. J. Pharmacol.* 176, 3075–3076.

Wang, T., Xie, W., Ellory, C., Wilkins, R., Zhu, Y., and Ma, Y.-l. (2017). Investigation on the cardio-protective effect of Xin Su Ning on ischemia-reperfusion induced injury in isolated heart. *Proceedings of the British Pharmacological Society* http://www.pa2online.org/abstracts/vol18issue1abst171p.pdf

Wang, T., Xie, W., Yu, J., Zhu, Y., and Ma, Y.-L. (2019b). Ion channel targeted mechanisms of anti-arrhythmic Chinese herbal medicine Xin Su Ning. *Front. Pharmacol.* 10, 70. doi: 10.3389/fphar.2019.00070

Wang, X., Wang, Y., Feng, X., Lu, Y., Zhang, Y., Wang, W., et al. (2016). Systematic review and meta-analysis of randomized controlled trials on Wenxin keli. *Drug Des. Devel. Ther.* 10, 3725. doi: 10.2147/DDDT.S112333

Wu, Y., Zhang, F., Yang, K., Fang, S., Bu, D., Li, H., et al. (2018). SymMap: an integrative database of traditional Chinese medicine enhanced by symptom mapping. *Nucleic Acids Res.* 47, D1110–D1117. doi: 10.1093/nar/gky1021

Xing, Y., Hu, D., Zhang, T., and Antzelevitch, C. (2015). Traditional Chinese medicine and vascular disease. *Evid. Based Complementary Altern. Med.* 2015, 1–2. doi: 10.1155/2015/430818

Yang, H., Lou, C., Sun, L., Li, J., Cai, Y., Wang, Z., et al. (2018). admetSAR 2.0: web-service for prediction and optimization of chemical ADMET properties. *Bioinformatics* 35(6), 1067-1069. doi: 10.1093/bioinformatics/bty707

Yuan, S., and Zhou, C. (2000). Observation on sixty cases of rapid arrhythmia treated with Xinsuning capsules. *J. Shandong Univ. TCM* 24 (04), 290–293. doi: 10.3969/j.issn.1007-659X.2000.04.027

Zhai, J., Yin, X., Yang, X., and Zhang, J. (2017). Xinsuning capsule for the treatment of premature ventricualr contraction: a multicenter randomised clinical trial. *Lancet* 390, S61. doi: 10.1016/S0140-6736(17)33199-9

Zhou, J., Xie, G., and Yan, X., (2009). *Chemical components of source plants in traditional Chinese medicine*. Beijing: Science Press.

Conflict of Interest: The authors declare that this study received funding from Shaanxi Momentum Pharmaceutical Co., Ltd. The funder was not involved in the study design, collection, analysis, interpretation of data, the writing of this article or the decision to submit it for publication.

frontiers in Pharmacology

SYSTEMATIC REVIEW
published: 10 October 2019
doi: 10.3389/fphar.2019.01139

Efficacy and Safety of Chinese Herbal Medicine for Primary Intracerebral Hemorrhage: A Systematic Review of Randomized Controlled Trials

Hui-Lin Wang[1†], Hua Zeng[2†], Meng-Bei Xu[1], Xiao-Li Zhou[1], Pei-Qing Rong[1], Ting-Yu Jin[1], Qi Wang[2] and Guo-Qing Zheng[1*]*

[1] Department of Neurology, The Second Affiliated Hospital and Yuying Children's Hospital of Wenzhou Medical University, Wenzhou, China, [2] Institute of Clinical Pharmacology, Guangzhou University of Chinese Medicine, Guangzhou, China

OPEN ACCESS

Edited by:
Jianxun Liu,
China Academy of Chinese Medical Sciences, China

Reviewed by:
Jia Liu,
National Cancer Institute at Frederick, United States
Yi Sui,
Shenyang Medical College Affiliated Brain Hospital, China

***Correspondence:**
Qi Wang
wangqi@gzucm.edu.cn
Guo-Qing Zheng
gq_zheng@sohu.com

[†]These authors have contributed equally to this work

Specialty section:
This article was submitted to Ethnopharmacology, a section of the journal Frontiers in Pharmacology

Received: 14 May 2019
Accepted: 04 September 2019
Published: 10 October 2019

Citation:
Wang H-L, Zeng H, Xu M-B, Zhou X-L, Rong P-Q, Jin T-Y, Wang Q and Zheng G-Q (2019) Efficacy and Safety of Chinese Herbal Medicine for Primary Intracerebral Hemorrhage: A Systematic Review of Randomized Controlled Trials. Front. Pharmacol. 10:1139. doi: 10.3389/fphar.2019.01139

Background: Primary intracerebral hemorrhage (ICH) is the most harmful subtype of stroke, but there have yet been no specific proven therapies. Chinese herbal medicine (CHM) has been used for ICH for more than a thousand years; however, currently it is still lacking of available evidence. The objective of this study is to assess the current available evidence of CHM for acute ICH according to randomized controlled trials.

Methods: Eight databases were searched from the year of their respective inception to November 2017. Only the studies that assessed at least four domains with "yes" according to the Cochrane risk of bias tool were selected for analysis. All the data were analyzed by using Review Manager 5.3 software. $P < 0.05$ was considered to be statistically significant.

Results: Forty-five studies with 4,517 individuals were identified. CHM paratherapy can improve dependency, neurological function deficit, volume of hematoma, clinical effective rate, and volume of perihematomal edema compared with CHM alone or placebo (all $P < 0.05$). By contrast, it was not significant for improving the mortality rate of ICH patients ($P > 0.05$). In addition, adverse events were reported in 16 studies, whereas 29 studies did not mention it. The frequency of adverse events was 70/972 in the trial group and 48/944 in the control group.

Conclusion: The present study provided supportive evidence of CHM for improving dependency of ICH and showed generally safety; however, there is still lack of evidence for improving mortality rate, and it opens for further study.

Keywords: primary intracerebral hemorrhage, Chinese herbal medicine, systematic review, meta-analysis, randomized controlled trials

INTRODUCTION

Primary intracerebral hemorrhage (ICH), known as the irruption of blood in the brain parenchyma, is the most harmful subtype of stroke. It accounts for 10–15% of all strokes and is a devastating stroke with a higher mortality and disability rate compared to ischemic stroke (Liu et al., 2012). There is approximately 40% of case fatality at 1 month with an increase of 54% at 1 year (van Asch et al., 2010; Poon et al., 2014). However, currently no clinically proven specific therapy or treatment is available

(Morgenstern et al., 2015). The currently available evidences for the management of ICH recommended by the guidelines remain multifaceted and symptomatic (Steiner et al., 2014; Morgenstern et al., 2015).

Traditional Chinese medicine (TCM) that includes Chinese herbal medicine (CHM), acupuncture, and other non-drug therapies has been used for stroke for thousands of years, but it was difficult to differentiate the ischemic and hemorrhagic stroke. As for Western medicine, during the first half of the 20th century, clinicopathological studies have been concentrated on the clinical symptoms of patients who died after stoke. In 1935, cerebrovascular diseases began to be classified into thrombosis and hemorrhage (intracerebral or subarachnoid) by analyzing stroke patients studied clinically and at necropsy (Caplan, 2011). By the end of the 1980s and the 1990s, computed tomography (CT) and magnetic resonance imaging (MRI) scans became generally available so that brain hemorrhages were readily diagnosed by imaging. Patients could be recognized of accurate classification and differential diagnosis of brain hemorrhages or infarcts when they were alive through CT or MRI. With the introduction of modern Western medicine into China during the Early Republic of China (1912–1949), some doctors recognized that stroke can be either hemorrhagic or ischemic (Zheng and Huang, 2005). In 1978, the Chinese Medical Association approved the classification of cerebrovascular diseases on the Second National Conference on Neuropsychiatry, which clearly divided the stroke into hemorrhagic and ischemic (The Second National Conference on Neuropsychiatry, 1978). Since then, it became the most widely used classification method of cerebrovascular diseases in China. In 1997, stroke in TCM has its national classification standard that exactly same as western medicine. The *National standard of TCM*, section of *Clinical terminology of diagnosis and treatment on TCM* clearly divided it into ischemic and hemorrhagic stroke (China State Bureau of Quality and Technical Supervision, 1997; Zheng and Huang, 2005). Actually, TCM has been the dominantly medical modalities in China before Western medical healthcare was introduced into the regions (Zheng, 2009). It was also the only available medical care of stroke patients in ancient time and now still plays an important role in China and elsewhere worldwide. With the deepening of basic and clinical studies on stroke, TCM has shown its unique academic advantages in the prevention and treatment of stroke, and has gradually exerted a certain influence in the world (Wang, 1997; Wu et al., 2007). At present, there are great differences in the treatment of stroke between China and the West, the most remarkable difference is the use of TCM (Sze et al., 2005). CHM is the main pharmacological therapeutic method in TCM. In addition, systematic review of the rigorous randomized controlled trials (RCTs) has been recognized the highest level of evidence (Parnianfard et al., 2017). The validity of a conclusion of systematic review is highly dependent on the quality of RCTs included. Conversely, the low-quality RCTs with high risk of bias and high heterogenicity have the positive conclusions, which are not scientifically sound and misleading attribute to methodological flaws (Wang et al., 2019). Correspondingly, the Cochrane group guidelines for clinical reviews have developed a strict process to exclude such not-so-good studies when conducted a systematic review (Chan et al., 2012). Thus, the objective of the present systematic review is to assess the existing evidence of CHM for ICH after the exclusion of not-so-good RCTs.

METHODS

Ethical approval was not needed because of literature research. The systematic review was conducted according to the Preferred Reporting Items for Systematic Reviews and Meta-analyses: The PRISMA Statement (Moher et al., 2009).

Database and Search Strategies

Electronic searches were performed in eight databases from their respective inception to November 2017: PubMed, EMBASE, Web of Science, Cochrane Library, Chinese National Knowledge Infrastructure, Chinese Biomedical Literature Database, Chinese VIP Database, and Wanfang Database. We also manually searched the additional relevant studies using the references of the systematic reviews published previously. No language restrictions were applied. The following search strategy was used for PubMed and was modified to suit other databases.

1. Chinese medicine*
2. Chinese herbal*
3. integrative medicine
4. OR/1–3
4. intracerebral hemorrhage*
5. hemorrhagic stroke*
6. OR/4–5
7. 4 AND 6

Eligibility Criteria

Types of Studies

Only RCTs that assessed the efficacy and safety of CHM for acute ICH were included, regardless of publication status or language. If the study had a three-arm design, we extracted data only for the group(s) involving CHM and the control group(s). Quasi-randomized trials, such as those in which patients were allocated according to date of birth and order of admission number, were excluded.

Types of Participants

We included participants with a diagnosis of ICH within 7 days of stroke onset in accordance with the diagnostic criteria of Chinese Cerebrovascular Disease Diagnosis Standard (CCDDS) made by the Chinese Medical Association at the Fourth National Conference on cerebrovascular disease in 1995 (The Fourth National Conference on Cerebrovascular Disease, 1996), CCDDS in 1998 (Wang, 1998), and guidelines for prevention and treatment of cerebrovascular diseases issued by the Neurology Branch of Chinese Medical Association in 2007 (Rao, 2007), regardless of gender, age, or race. All participants were confirmed with CT/MRI scan.

Types of Interventions

The analyzed intervention was CHM adjunct western conventional medication (WCM), regardless of dosage, duration, administrated methods, administration route, or administration time of treatment. The comparator was given WCM alone or plus CHM placebo. WCM refers to the combination of needed therapies of the following aspects (Morgenstern et al., 2015): 1) general supportive care; 2) blood pressure management; 3) glucose management; 4) hemostasis and coagulopathy; patients with a severe coagulation factor deficiency or severe thrombocytopenia should receive appropriate factor replacement therapy or platelets, respectively; 5) surgical treatment; 6) management of medical complications; and 7) rehabilitation and recovery. Studies comparing one kind of CHM with another CHM were excluded.

Types of Outcomes

Mortality and dependency as primary outcomes were measured at the end of the treatment course and the follow-up period. Dependency has the definition of needing the aid of activity of daily living (ADL), which was measured by a standard rating scale such as the Barthel Index (BI), modified Rankin Standard (mRS), ADL Scale, Glasgow Outcome Scale (GOS), and the degree of disability. The degree of disability was recorded in the standard of the degree of clinical neurological deficit in stroke patients (SDCNFS1995) (Chen, 1996). The secondary outcomes were the neurological deficit improvement (Li et al., 2015), volume of hematoma (VH), the clinical effective rate, volume of perihematomal edema (VPE), and adverse events. The neurological deficit improvement was measured after treatment using National Institutes of Health Stroke Scale (NIHSS) score and Chinese Clinical Neurological Deficit Scale (CCNDS). A serious adverse event (SAE) is defined as "any untoward medical occurrence at any dose": a) results in death; b) is life-threatening; c) requires inpatient hospitalization or prolongation of an existing hospitalization; d) results in persistent or significant disability/incapacity; or e) is a congenital anomaly/birth defect (ICH Expert Working Group, 1996).

Data Extraction and Management

We extracted data that included first author's name; publication year; diagnosis standard of ICH; study design; patients' total number and characteristics (age, gender, belong to control or treatment group); inclusion of patient-based VH; intervention schedule and intervention time for treatment group and control group; follow-up time; change of outcome index; the reports of adverse reaction. The outcome information of the last evaluation would be extracted if there were multiple time-point outcome indicators. Reasons for the exclusion of studies were also recorded. For eligible studies, two authors extracted data independently and resolved all discrepancies by discussing with each other or with a third author.

Assessment of Risk of Bias

The Cochrane's Collaboration tool was used to assess the risk of bias by the 7-item criteria (Higgins et al., 2008). Two authors valued the eligible studies independently and a discussion with the corresponding author was conducted to solve any discrepancies. RCTs that received at least four out of seven domains "yes" were selected for analysis (Li et al., 2015; Yang et al., 2017)

CHM Composition

The main compositions of the CHM formulae were recorded. We calculated the frequency of use of all Chinese herbs, and analyzed and described in detail those used at high frequency.

The Quality of the Clinical Studies

In order to assess the quality of the clinical studies, we used a rating system (Wang et al., 2019) as follows: 1) high quality—full information about the botanical material is provided, including a voucher specimen; 2) moderate quality—only partial information about the botanical material is provided and a voucher specimen is missed; there are taxonomic inaccuracies; 3) low quality—inadequate information and overall taxonomically inadequate.

Statistical Analysis

Data were analyzed by using Review Manager (version 5.3). $P < 0.05$ was considered statistically significant. Dichotomous outcomes were calculated by the risk ratio (RR), with a 95% confidence interval (CI), whereas continuous outcomes were calculated by weighted mean differences (WMD) or standardized mean differences (SMD). The Cochrane Q-statistic test and the I^2-statistic were used to test the heterogeneity among studies. When no obvious heterogeneity exists ($P > 0.1$, $I^2 < 50\%$), we used a fixed effect model. Otherwise, the random effect model is a more plausible match. However, all meta-analyses were carried out through a random-effect model because of the clinical heterogeneity. Publication bias was visually estimated using funnel plots.

RESULTS

Description of Studies

We identified 14,596 potentially relevant hints from eight databases. Removing duplication of literature, there were 8,279 articles left. We excluded 7,514 studies that are not related to this study after reading the titles and abstracts in detail. Through reading the full text of 742 articles, 697 articles were excluded for at least one of the following reasons: 1) non-randomized or quasi-RCTs; 2) no clear ICH diagnostic criteria; 3) combined Chinese herbs with other TCM treatment modalities; 4) published by repeated data; and 5) unavailable data. Finally, 45 articles were included for analysis (**Figure 1**).

Characteristics of Included Studies

The sample sizes of the 45 studies ranged from 51 to 404. All studies were published between 2000 and 2017. There were 4,517 participants of Chinese ethnicity that were included in the 45 studies, of which 2,267 patients were treatment groups and 2,250 patients served as controls. Forty-two studies (Fan et al., 2000; Jia et al., 2000; Dai et al., 2002; Ma and Gong,

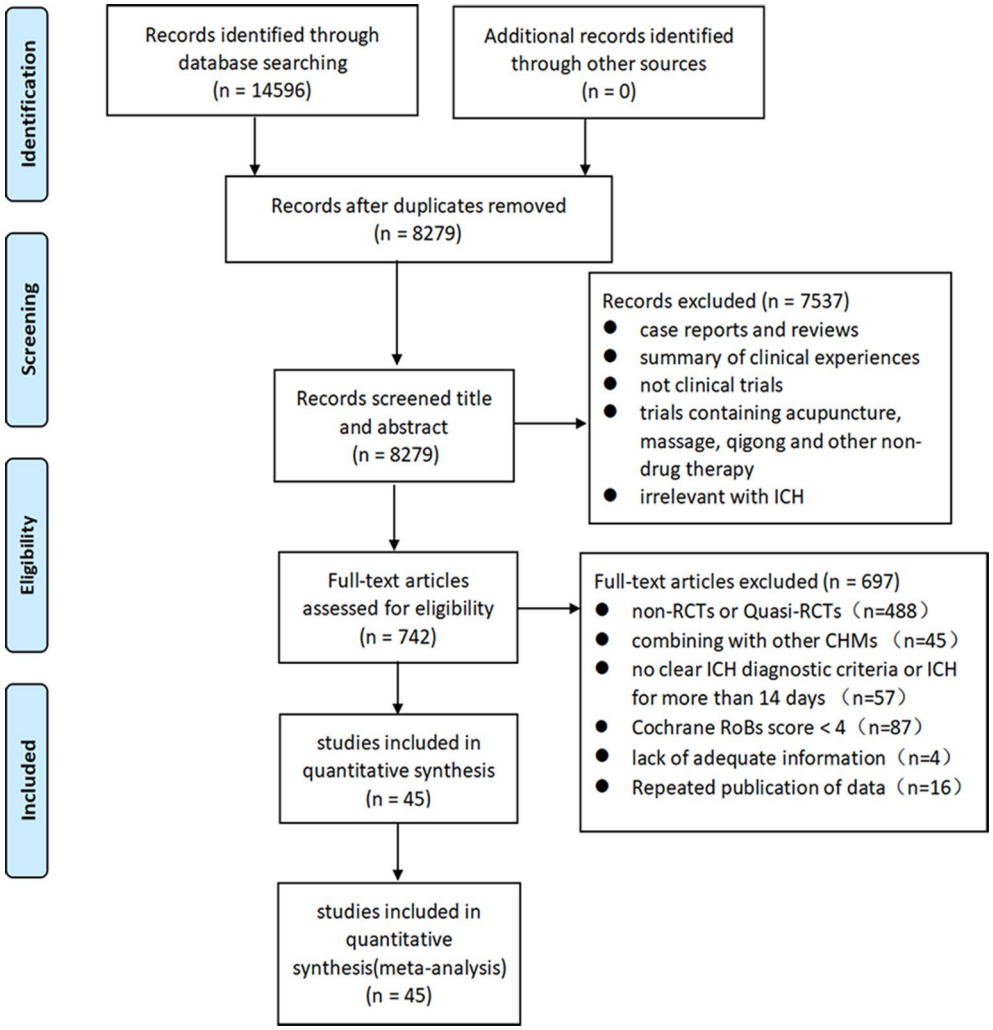

FIGURE 1 | Flowchart of study screening.

2005; Yang and Liu, 2006; Fan et al., 2008; Sun and Chen, 2008; Huang et al., 2010; Liao et al., 2010; Ming et al., 2010; Chen, 2011; Li et al., 2011; Peng et al., 2011; Wang and Wang, 2011; Li et al., 2012; Shen et al., 2012; Zhang et al., 2012; Ming et al., 2013; Wang et al., 2013; Bi and Hu, 2014; Gu et al., 2014; Guo et al., 2014; Li, 2014; Ye, 2014; Guan et al., 2015; Li et al., 2015; Luo et al., 2015; Peng and Feng, 2015; Shen and Luo, 2015; Guo et al., 2016; Jiang et al., 2016; Li et al., 2016; Liu and Wu, 2016; Liu and Zhang, 2016; Long et al., 2016; Shang and Yang, 2016; Xia et al., 2016; Zhou et al., 2016; Lei and Qiao, 2017; Ma and Zhang, 2017; Sun et al., 2017; Zhang et al., 2017) compared CHM plus WCM with WCM alone, and three studies (Huang et al., 2006; Chen et al., 2010; Liu et al., 2012) compared CHM plus WCM with CHM placebo plus WCM. The CHM treatment course varied from 7 to 90 days. Nineteen studies reported follow-up from 7 days to 1 year. The follow-up time over 3 months was reported in 18 studies (Jia et al., 2000; Dai et al., 2002; Huang et al., 2006; Chen et al., 2010; Huang et al., 2010; Wang and Wang, 2011; Li et al., 2012; Shen et al., 2012; Zhang et al., 2012; Ming et al., 2013; Wang et al., 2013; Ye, 2014; Li et al., 2015; Li and Wu, 2016; Liu and Zhang, 2016; Xia et al., 2016; Ma and Zhang, 2017). Mortality rate was observed in 14 studies; dependence in 10 studies; clinical effective rate in 28 studies; neurological deficit score in 37 studies; VH in 23 studies; VPE in 7 studies; and adverse events in 16 studies. The detailed characteristics are listed in **Supplementary Table 1**.

Risk of Bias in Included Studies

The total scores according to Cochrane risk of bias (**Table 1**) are as follows: Xia et al. (2016) with 7 points; Chen et al. (2010) and Li et al.(2016) with 6 points; Huang et al. (2006) and Luo et al. (2015) with 5 points; the other 40 RCTs with 4 points. The method of random distribution was clearly proposed in all included documents. In addition, three studies (Chen et al., 2010; Li et al., 2016; Xia et al., 2016) explicitly proposed the method of distribution concealment; two studies (Chen et al., 2010; Xia et al., 2016) had double blinding for the implementers and

TABLE 1 | Assessment of study quality and risk of bias.

First author, year	7-item criteria							
	A	B	C	D	E	F	G	Total
Fan et al., 2000	+	−	−	−	+	+	+	4
Jia et al., 2000	+	−	−	−	+	+	+	4
Dai et al., 2002	+	−	−	−	+	+	+	4
Ma and Gong, 2005	+	−	−	−	+	+	+	4
Huang et al., 2006	+	−	−	+	+	+	+	5
Yang and Liu, 2006	+	−	−	−	+	+	+	4
Fan et al., 2008	+	−	−	−	+	+	+	4
Sun and Chen, 2008	+	−	−	−	+	+	+	4
Liao et al., 2010	+	−	−	−	+	+	+	4
Chen et al., 2010	+	+	+	−	+	+	+	6
Huang et al., 2010	+	−	−	−	+	+	+	4
Ming et al., 2010	+	−	−	−	+	+	+	4
Chen, 2011	+	−	−	−	+	+	+	4
Li et al., 2011	+	−	−	−	+	+	+	4
Peng et al., 2011	+	−	−	−	+	+	+	4
Wang and Wang, 2011	+	−	−	−	+	+	+	4
Li et al., 2012	+	−	−	−	+	+	+	4
Liu et al., 2012	+	−	−	−	+	+	+	4
Shen et al., 2012	+	−	−	−	+	+	+	4
Zhang et al., 2012	+	−	−	−	+	+	+	4
Ming et al., 2013	+	−	−	−	+	+	+	4
Wang et al., 2013	+	−	−	−	+	+	+	4
Bi and Hu, 2014	+	−	−	−	+	+	+	4
Gu et al., 2014	+	−	−	−	+	+	+	4
Guo et al., 2014	+	−	−	−	+	+	+	4
Li, 2014	+	−	−	−	+	+	+	4
Ye, 2014	+	−	−	−	+	+	+	4
Guan et al., 2015	+	−	−	−	+	+	+	4
Li et al., 2015	+	−	−	−	+	+	+	4
Luo et al., 2015	+	−	−	+	+	+	+	5
Peng and Feng, 2015	+	−	−	−	+	+	+	4
Shen and Luo, 2015	+	−	−	−	+	+	+	4
Li et al., 2016	+	+	−	+	+	+	+	6
Guo et al., 2016	+	−	−	−	+	+	+	4
Jiang et al., 2016	+	−	−	−	+	+	+	4
Liu and Wu, 2016	+	−	−	−	+	+	+	4
Liu and Zhang, 2016	+	−	−	−	+	+	+	4
Long et al., 2016	+	−	−	−	+	+	+	4
Shang and Yang, 2016	+	−	−	−	+	+	+	4
Xia et al., 2016	+	+	+	+	+	+	+	7
Zhou et al., 2016	+	−	−	−	+	+	+	4
Lei and Qiao, 2017	+	−	−	−	+	+	+	4
Ma and Zhang, 2017	+	−	−	−	+	+	+	4
Sun et al., 2017	+	−	−	−	+	+	+	4
Zhang et al., 2017	+	−	−	−	+	+	+	4

A to G, the 7-Item criteria. A, adequate sequence generation; B, concealment of allocation; C, blinding of participants and personnel; D, blinding of outcome assessment; E, incomplete out-come data; F, selective reporting; G, other bias; +: low risk of bias, –: high risk of bias.

participants; and four studies (Huang et al., 2006; Luo et al., 2015; Li et al., 2016; Xia et al., 2016) evaluated the outcome indexes by blind method.

The Quality of the Clinical Studies

We accessed the quality of the included clinical studies with a rating system, which is related to the information about the botanical material and voucher specimens. All studies are low quality with inadequate information and overall taxonomically inadequate. The quality for each included clinical study is summarized in **Table 2**.

Effectiveness

Mortality

Fourteen studies (Fan et al., 2000; Jia et al., 2000; Dai et al., 2002; Huang et al., 2006; Sun and Chen, 2008; Chen et al., 2010; Huang et al., 2010; Wang and Wang, 2011; Liu et al., 2012; Guo et al., 2016; Liu and Zhang, 2016; Zhou et al., 2016; Lei and Qiao, 2017; Zhang et al., 2017) reported the mortality rate as outcome measure. Three studies (Huang et al., 2006; Chen et al., 2010; Liu et al., 2012) showed CHM plus WCM was not significant for improving mortality rate compared with CHM placebo plus WCM ($p > 0.05$). Meta-analysis of 11 studies

TABLE 2 | The quality of the clinical studies.

First author, year	Botanical material information	Voucher specimen	Quality
Fan et al., 2000	I	–	Low
Jia et al., 2000	I	–	Low
Dai et al., 2002	I	–	Low
Ma and Gong, 2005	I	–	Low
Huang et al., 2006	I	–	Low
Yang and Liu, 2006	I	–	Low
Fan et al., 2008	I	–	Low
Sun and Chen, 2008	I	–	Low
Liao et al., 2010	I	–	Low
Chen et al., 2010	I	–	Low
Huang et al., 2010	I	–	Low
Ming et al., 2010	I	–	Low
Chen, 2011	I	–	Low
Li et al., 2011	I	–	Low
Peng et al., 2011	I	–	Low
Wang and Wang, 2011	I	–	Low
Li et al., 2012	I	–	Low
Liu et al., 2012	I	–	Low
Shen et al., 2012	I	–	Low
Zhang et al., 2012	I	–	Low
Ming et al., 2013	I	–	Low
Wang et al., 2013	I	–	Low
Bi and Hu, 2014	I	–	Low
Gu et al., 2014	I	–	Low
Guo et al., 2014	I	–	Low
Li, 2014	I	–	Low
Ye, 2014	I	–	Low
Guan et al., 2015	I	–	Low
Li et al., 2015	I	–	Low
Luo et al., 2015	I	–	Low
Peng and Feng, 2015	I	–	Low
Shen and Luo, 2015	I	–	Low
Li et al., 2016	I	–	Low
Guo et al., 2016	I	–	Low
Jiang et al., 2016	I	–	Low
Liu and Wu, 2016	I	–	Low
Liu and Zhang, 2016	I	–	Low
Long et al., 2016	I	–	Low
Shang and Yang, 2016	I	–	Low
Xia et al., 2016	I	–	Low
Zhou et al., 2016	I	–	Low
Lei and Qiao, 2017	I	–	Low
Ma and Zhang, 2017	I	–	Low
Sun et al., 2017	I	–	Low
Zhang et al., 2017	I	–	Low

F, Full information about the botanical material is provided; P, Partial information about the botanical material is provided; I, Inadequate information about the botanical material is provided; +, includes a voucher specimen; -, a voucher specimen is missing.

(Fan et al., 2000; Jia et al., 2000; Dai et al., 2002; Sun and Chen, 2008; Huang et al., 2010; Wang and Wang, 2011; Guo et al., 2016; Liu and Zhang, 2016; Zhou et al., 2016; Lei and Qiao, 2017; Zhang et al., 2017) showed that CHM plus WCM was not significant for improving the mortality rate in acute ICH patients compared with WCM alone (n = 1006, nT/nC = 512/494, RR 0.69, 95%CI: 0.48~1.00, P = 0.05, heterogeneity χ^2 = 6.57, df = 10, p = 0.94, I^2 = 0%) (**Figure 2A**); meta-analysis of five studies (Jia et al., 2000; Dai et al., 2002; Huang et al., 2010; Wang and Wang, 2011; Liu and Zhang, 2016) that followed up for more than 3 months showed similar results (n = 492, nT/nC = 250/242, RR 0.71, 95% CI: 0.46~1.11, P = 0.13, heterogeneity χ^2 = 2.88, df = 4, p = 0.58, I^2 = 0%) (**Figure 2B**).

Dependency

Ten studies (Jia et al., 2000; Dai et al., 2002; Huang et al., 2006; Chen et al., 2010; Wang and Wang, 2011; Li et al., 2012; Liu et al., 2012; Li et al., 2016; Xia et al., 2016; Ma and Zhang, 2017) used the dependency as outcome measure. Three studies showed that CHM plus WCM was significant for reducing the dependence according to BI (Huang et al., 2006); combined use of mRS and BI (Chen et al., 2010) and home-made comparable scale (Liu et al., 2012) compared with CHM placebo plus WCM (P < 0.05). Seven studies (Jia et al., 2000; Dai et al., 2002; Wang and Wang, 2011; Li et al., 2012; Li et al., 2016; Xia et al., 2016; Ma and Zhang, 2017) compared the CHM plus WCM with WCM alone, and all showed that CHM plus WCM was significant for improving dependency at the end of the treatment and follow-up more than 3 months according to BI (Li et al., 2012), mRS (Li et al., 2016; Xia et al., 2016), GOS (Ma and Zhang, 2017), ADL (Wang and Wang, 2011), and degree of disability (Jia et al., 2000; Dai et al., 2002) (P < 0.05). Meta-analysis of two studies (Jia et al., 2000; Dai et al., 2002) showed CHM plus WCM was significant for improving degree of disability (n = 131, nT/nC = 66/65, RR 2.01, 95% CI: 1.40~2.89, P < 0.0001, heterogeneity χ^2 = 0.00, df = 1, p = 0.97, I^2 = 0%) at the end of the treatment compared with WCM (**Figure 3**).

Clinical Effective Rate

The clinical efficacy was reported in 28 studies (Fan et al., 2000; Jia et al., 2000; Dai et al., 2002; Ma and Gong, 2005; Huang et al., 2006; Yang and Liu, 2006; Huang et al., 2010; Chen, 2011; Li et al., 2012; Liu et al., 2012; Zhang et al., 2012; Guo et al., 2014; Li, 2014; Ye, 2014; Guan et al., 2015; Li et al., 2015; Peng and Feng, 2015; Shen and Luo, 2015; Guo et al., 2016; Jiang et al., 2016; Li et al., 2016; Liu and Wu, 2016; Long et al., 2016; Shang and Yang, 2016; Zhou et al., 2016; Lei and Qiao, 2017; Sun et al., 2017; Zhang et al., 2017). Meta-analysis of two studies (Huang et al., 2006; Liu et al., 2012) showed CHM plus WCM was significant for increasing clinical effective rate compared with CHM placebo plus WCM (P < 0.05). Meta-analysis of 20 studies (Dai et al., 2002; Ma and Gong, 2005; Yang and Liu, 2006; Huang et al., 2010; Chen, 2011; Li et al., 2012; Zhang et al., 2012; Guo et al., 2014; Li, 2014; Ye, 2014; Li et al., 2015; Peng and Feng, 2015; Shen and Luo, 2015; Guo et al., 2016; Jiang et al., 2016; Li et al., 2016; Liu and Wu., 2016; Long et al., 2016; Lei and Qiao, 2017; Zhang et al., 2017) showed CHM plus WCM was significant for increasing clinical effective rate compared with WCM alone according to SDCNFS 1995 (n = 1853, nT/nC = 935/918, RR 1.40, 95%CI: 1.30~1.51, P < 0.00001, heterogeneity χ^2 = 17.27, df = 19, p = 0.57, I^2 = 0%) (**Figure 4A**). The funnel graph is basically symmetrical, indicating that there is no obvious publication bias (**Figure 4B**). Owing to the different evaluation criteria of clinical efficiency, the other six studies (Fan et al., 2000; Jia et al., 2000; Guan et al., 2015; Shang and Yang, 2016; Zhou et al., 2016; Sun et al., 2017) failed to conduct meta-analysis, but they showed positive results (P < 0.05).

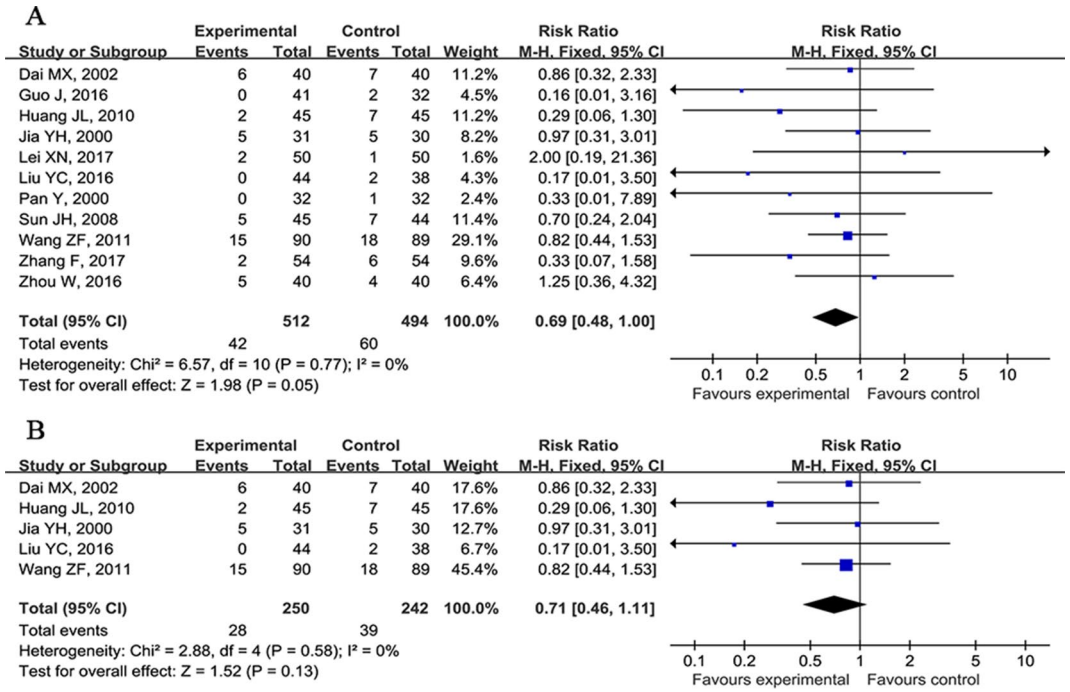

FIGURE 2 | Forest plots of meta-analysis of mortality rate. **(A)** Eleven studies compared CHM plus WCM with WCM alone. **(B)** Five studies that followed up for more than 3 months compared CHM plus WCM versus WCM alone in acute ICH patients.

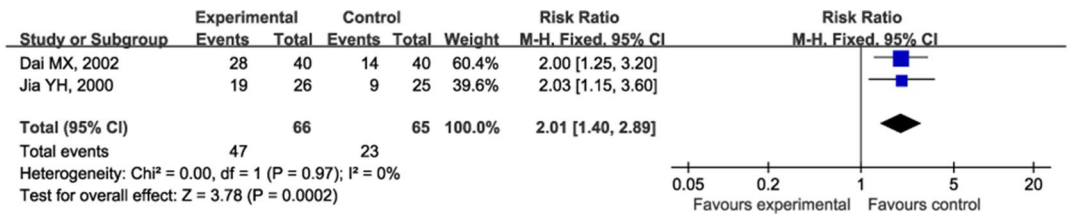

FIGURE 3 | Forest plot of meta-analysis of acute ICH patients' dependency (≥3 months follow-up) among two studies compared CHM plus WCM with WCM alone.

CCNDS Score

The CCNDS score as outcome measure was used in 12 studies (Jia et al., 2000; Dai et al., 2002; Ma and Gong, 2005; Yang and Liu, 2006; Huang et al., 2010; Chen, 2011; Wang and Wang, 2011; Li et al., 2012; Liu et al., 2012; Wang et al., 2013; Peng and Feng, 2015; Long et al., 2016). One study (Liu et al., 2012) showed that CHM plus WCM was significant for reducing the CCNDS score at 48 days compared with CHM placebo plus WCM ($P < 0.05$). Eleven studies compared CHM plus WCM with WCM alone at 14, 90, or 180 days. Meta-analysis of three studies (Ma and Gong, 2005; Yang and Liu, 2006; Long et al., 2016) showed CHM plus WCM was significant for reducing the CCNDS score at 14 days compared with WCM (n = 238, nT/nC = 120/118, WMD −5.05, 95%CI: −6.20∼−3.91, $P < 0.00001$, heterogeneity $\chi^2 = 2.59$, $df = 2$, $p = 0.27$, $I^2 = 23\%$; **Figure 5A**); three studies (Huang et al., 2010; Chen, 2011; Li et al., 2012) at 90 days (n = 254, nT/nC = 131/123, WMD −7.66, 95%CI: −9.09∼−6.23, $P < 0.00001$, heterogeneity $\chi^2 = 0.00$, $df = 2$, $p = 1.00$, $I^2 = 0\%$; **Figure 5B**); and two studies (Jia et al., 2000; Dai et al., 2002) at 180 days (n = 122, nT/nC = 60/62, WMD −6.42, 95%CI: −9.51∼−3.33, $P < 0.00001$, heterogeneity $\chi^2 = 0.00$, $df = 1$, $p = 1.00$, $I^2 = 0\%$; **Figure 5C**). Due to the inconsistent time points of evaluation, the other three studies (Wang and Wang, 2011; Wang et al., 2013; Peng and Feng, 2015) failed to conduct meta-analysis, but they reported positive results.

NIHSS Score

Nineteen studies (Huang et al., 2006; Fan et al., 2008; Sun and Chen, 2008; Liao et al., 2010; Shen et al., 2012; Zhang et al., 2012; Gu et al., 2014; Li, 2014; Guan et al., 2015; Luo et al., 2015; Jiang et al., 2016; Li et al., 2016; Liu and Wu, 2016; Liu and Zhang, 2016; Shang and Yang, 2016; Zhou et al., 2016; Lei and Qiao, 2017; Ma and Zhang, 2017; Sun et al., 2017) used NIHSS scores as outcome. Huang et al. (2006) showed that CHM plus WCM was significant for improving the NIHSS score compared with CHM placebo plus WCM at 90 days ($P < 0.05$). Eighteen studies (Fan et al., 2008; Sun and Chen, 2008; Liao et al., 2010; Shen et al., 2012;

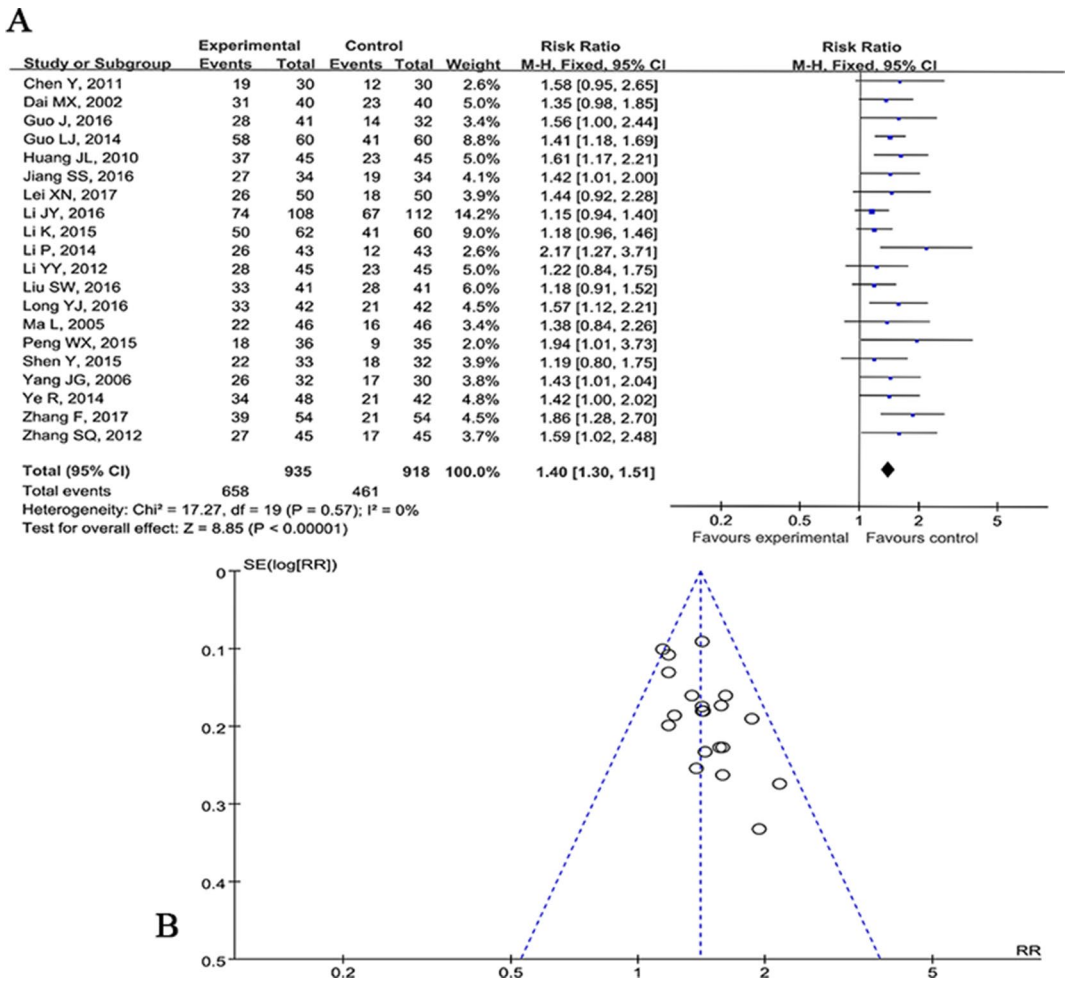

FIGURE 4 | (A) Forest plot of meta-analysis of clinical effective rate among 20 studies compared CHM plus WCM versus WCM alone. **(B)** Funnel graph of publication bias.

Zhang et al., 2012; Gu et al., 2014; Li, 2014; Guan et al., 2015; Luo et al., 2015; Jiang et al., 2016; Li et al., 2016; Liu and Wu, 2016; Liu and Zhang, 2016; Shang and Yang, 2016; Zhou et al., 2016; Lei and Qiao, 2017; Ma and Zhang, 2017; Sun et al., 2017) showed CHM plus WCM exerted a significantly better recovery of lost neurological functions than that of WCM alone ($P < 0.05$). We failed to conduct meta-analysis because of the various assessment time points from 7 to 90 days after CHM treatment.

VH

It was reported as an outcome measure in 23 studies (Fan et al., 2000; Jia et al., 2000; Ma and Gong, 2005; Yang and Liu, 2006; Liao et al., 2010; Ming et al., 2010; Chen, 2011; Li et al., 2011; Peng et al., 2011; Shen et al., 2012; Zhang et al., 2012; Wang et al., 2013; Bi and Hu, 2014; Guo et al., 2014; Li, 2014; Ye, 2014; Luo et al., 2015; Peng and Feng, 2015; Jiang et al., 2016; Li et al., 2016; Lei and Qiao, 2017; Sun et al., 2017) assessed at 7, 21, and 28 days after CHM treatment. Meta-analysis of eight studies (Jia et al., 2000; Ma and Gong, 2005; Yang and Liu, 2006; Liao et al., 2010; Chen, 2011; Shen et al., 2012; Guo et al., 2014; Li, 2014) showed that CHM plus WCM significantly reduced the VH at 7 days compared with WCM alone (n = 611, nT/nC = 307/304, WMD −3.96, 95%CI: −4.68~−3.25, $P < 0.00001$, heterogeneity $\chi^2 = 14.77$, df = 7, $p = 0.04$, $I^2 = 53\%$; **Figure 6A**); two studies (Jiang et al., 2016; Sun et al., 2017) at 21 days (n = 124, nT/nC = 68/68, WMD -5.66, 95%CI: −6.18~−5.15, $P < 0.00001$, heterogeneity $\chi^2 = 0.14$, df = 1, $p = 0.71$, $I^2 = 0\%$; **Figure 6B**); and six studies (Fan et al., 2000; Peng et al., 2011; Zhang et al., 2012; Ming et al., 2013; Li, 2014; Ye, 2014; Long et al., 2016) at 28 days (n = 465, nT/nC = 233/232, WMD −2.37, 95%CI: −3.03~−1.71, $P < 0.00001$, heterogeneity $\chi^2 = 6.63$, df = 5, $p = 0.25$, $I^2 = 25\%$; **Figure 6C**). Seven studies (Ming et al., 2010; Li et al., 2011; Wang et al., 2013; Bi and Hu, 2014; Ye, 2014; Luo et al., 2015; Li et al., 2016) failed to carry out meta-analysis because of the inconsistent time points of evaluation, but they reported positive results ($P < 0.05$).

VPE

It was reported in 7 studies at 14 days (Li, 2014; Long et al., 2016), 21 days (Sun and Chen, 2008; Ming et al., 2013; Ye, 2014), and 28 days (Peng et al., 2011; Zhang et al., 2012) after CHM treatment.

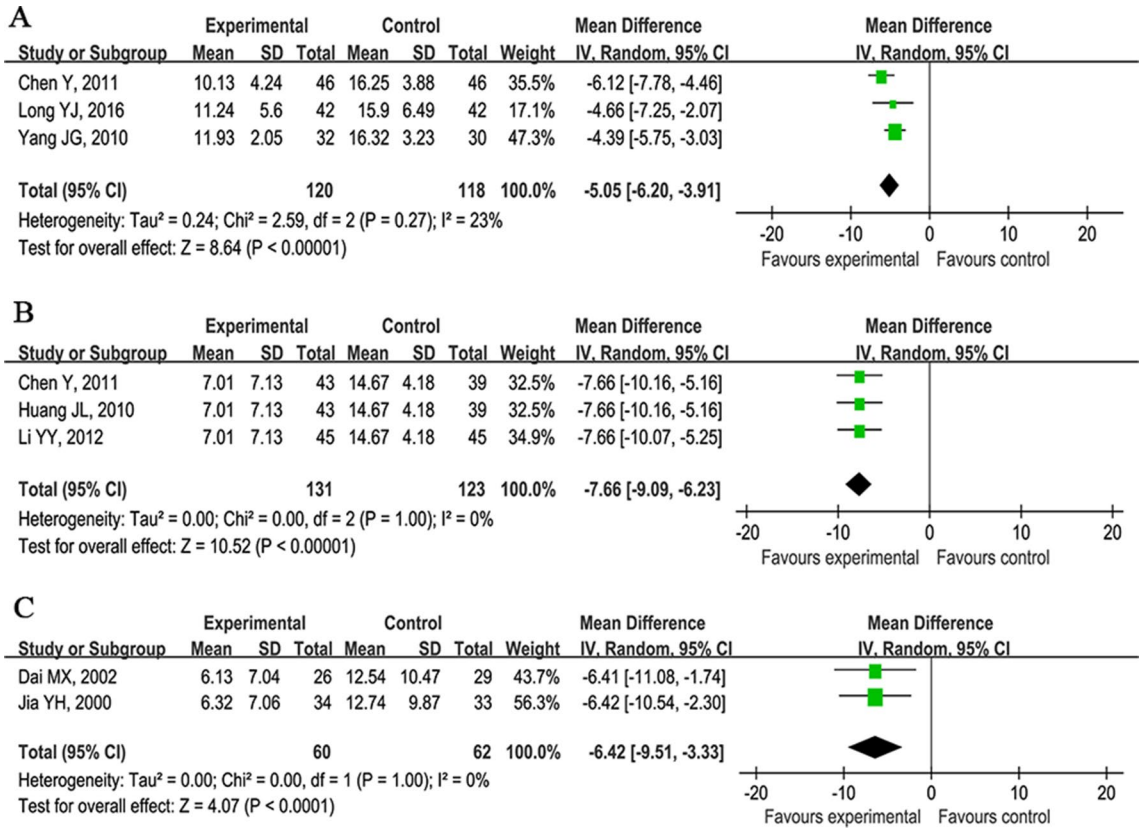

FIGURE 5 | Forest plots of meta-analysis of Chinese clinical neurological deficit scale score. **(A)** Three studies compared CHM plus WCM with WCM alone at 14 days. **(B)** Three studies at 90 days and **(C)** two studies at 180 days.

These studies showed CHM plus WCM significantly lessened VPE compared with WCM alone ($P < 0.05$).

Adverse Events

They were reported in 16 studies (Fan et al., 2000; Huang et al., 2006; Chen et al., 2010; Li et al., 2011; Peng et al., 2011; Gu et al., 2014; Li, 2014; Guan et al., 2015; Luo et al., 2015; Peng and Feng, 2015; Li et al., 2016; Liu and Wu, 2016; Xia et al., 2016; Zhou et al., 2016; Lei and Qiao, 2017), whereas 29 studies did not mention it. The frequency of adverse events was 70/972 in the trial group and 48/944 in the control group. Adverse events were as follows: diarrhea (n = 22); skin itching (n = 3); transient aminotransferase mild elevation (n = 3); two cases of rash; nausea (n = 2); and skin allergy (n = 1); all of them were relieved after drug withdrawal, decrement, or symptomatic treatment. Three studies (Peng et al., 2011; Gu et al., 2014; Li, 2014) reported no obvious adverse events. There was only one study (Chen et al., 2010) that reported two cases of SAEs in the treatment group and six SAEs in the control group, but it did not mention the SAEs exactly.

Ingredients of CHM Formulae and Frequently Used Herbs

The ingredients of CHM in each RCT are listed in **Supplementary Table 2**. The most frequently used herbs across all formulae were Dahuang (*Radix et Rhizoma Rhei,* rhubarb root and rhizome), Sanqi (*Radix Notoginseng,* Panax notoginseng), Chuanxiong (*Rhizoma Ligustici Chuanxiong,* Ligusticum chuanxiong Hort), Chishao (*Radix Paeoniae Rubra,* Paeonia veitchii Lynch), Shichangpu (*Rhizoma Acori Tatarinowii,* Acorus tatarinowii Schott), Yujin (*Radix Curcumae,* turmeric root tuber), Zhizi (*Fructus Gardeniae,* cape jasmine fruit), Taoren (*Semen Persicae,* peach seed), Shuizhi (*Hirudo,* leech), Honghua (*Flos Carthami,* safflower), Gancao (*Radix Glycyrrhizae,* liquorice root), Danggui (*Radix Angelicae Sinensis,*Angelica sinensis), Niuxi (*Radix Achyranthis Bidentatae,* twotoothed achyranthes root), and Huangqin (*Radix Scutellariae,* baical skullcap root) (**Table 3**).

DISCUSSION

Summary of Evidence

This study is an updated systematic review of the efficacy and safety of CHM for ICH. Forty-five low risk of bias RCTs with 4,517 subjects received at least four domains with "yes" according to the Cochrane Risk of Bias tool. The main findings of present systematic review demonstrated that CHM paratherapy can improve dependency, VH, VPE, clinical effective rate, and neurological function deficit; however, it was not significant for improving the mortality rate of ICH patients. In addition, CHM paratherapy had fewer side effects and was generally safe.

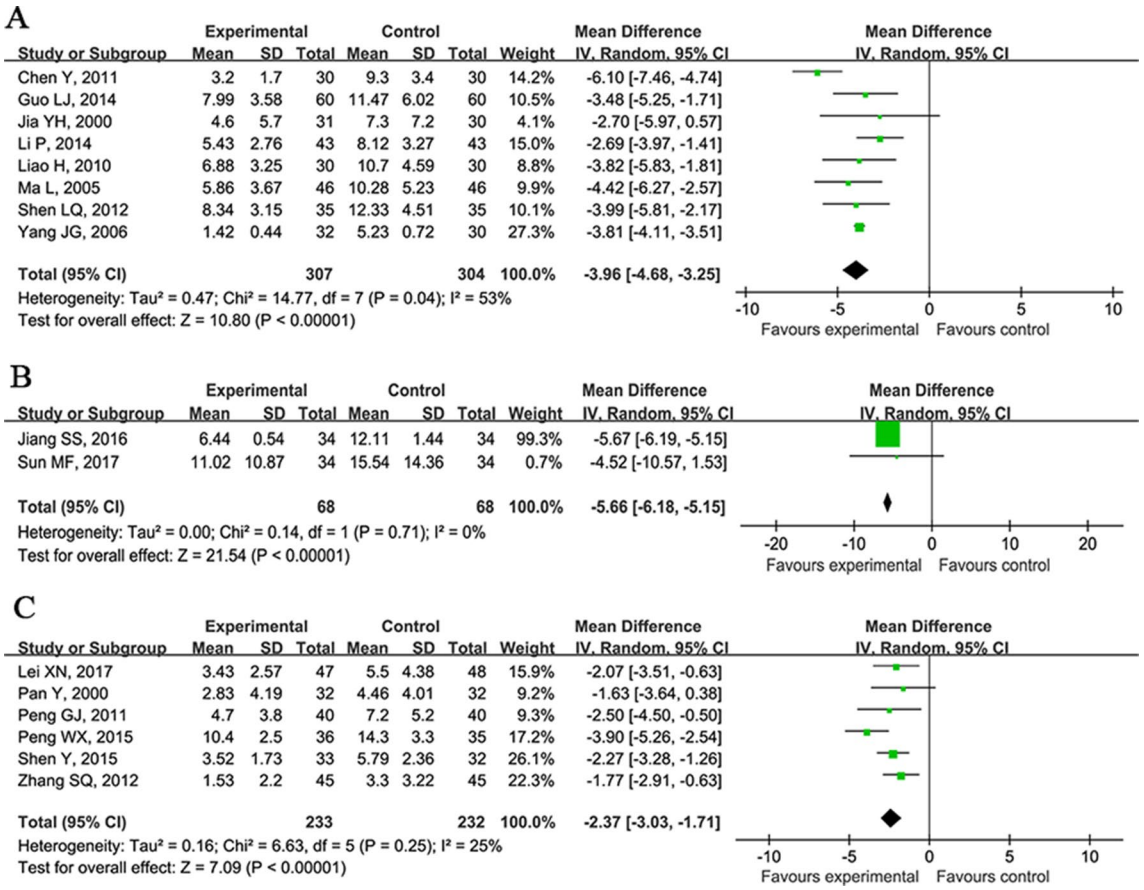

FIGURE 6 | Forest plots of meta-analysis of volume of hematoma. **(A)** Eight studies compared CHM plus WCM with WCM alone at 7 days. **(B)** Two studies at 21 days and **(C)** six studies at 28 days.

Although the present study provided supportive evidence of the efficacy and safety of CHM for dependency of ICH, we should treat the results cautiously because the included studies were of high clinical heterogeneity.

Limitations

First, none of the included studies had been formally registered. Thus, protocols were not available to confirm free of selective reporting (De Angelis et al., 2004). Second, the primary studies existed in some methodological flaws such as distribution concealment and blindness. The selection bias or observer bias may affect the results. Third, only three studies (Huang et al., 2006; Chen et al., 2010; Liu et al., 2012) used CHM placebo in the control group, and thus caution should be given to the interpretation of the positive findings. Fourth, most of the included studies did not carry out formal sample size estimates. Trials with inadequate sample sizes often run the risk of overestimating intervention benefits (Kjaergard et al., 2001). Fifth, the composition of a formula, dosage, administration methods, and duration of CHM treatments varied considerably in the primary RCTs. These clinical heterogeneities may compromise validity of the results of the present study. Sixth, only 18 studies (Jia et al., 2000; Dai et al., 2002; Huang et al., 2006; Chen et al., 2010; Huang et al., 2010; Wang and Wang, 2011; Li et al., 2012; Shen et al., 2012; Zhang et al., 2012; Ming et al., 2013; Wang et al., 2013; Ye, 2014; Li et al., 2015; Li et al., 2016; Liu and Wu, 2016; Liu and Zhang, 2016; Xia et al., 2016; Ma and Zhang, 2017) have more than 3 months' follow-up. The long prognosis of ICH of CMH treatment at least 6 months needed further clarifying.

Implications for Practice

The use of CHM in the treatment of ICH has increased in the past decades. The available evidence from the present study is supportive. We summarized the most frequently used 14 herbs: *Radix et Rhizoma Rhei, Radix Notoginseng, Rhizoma Ligustici Chuanxiong, Radix Paeoniae Rubra, Rhizoma Acori Tatarinowii, Radix Curcumae, Fructus Gardeniae, Semen Persicae, Hirudo, FlosCarthami, Radix Glycyrrhizae, Radix Angelicae Sinensis, Radix Achyranthis Bidentatae,* and *Radix Scutellariae*. These selected herbs have far-reaching clinical applications for the treatment based on syndrome differentiation of ICH patients according to the therapeutic functions of herbal medicine. *Radix et Rhizoma Rhei, Radix Notoginseng, Rhizoma Ligustici, Radix Curcumae, Semen Persicae, Hirudo, Flos Carthami, Radix Paeoniae Rubra, Radix*

TABLE 3 | Frequently used herbs in included studies.

Chinese name	Pharmaceutical name	Species	Family	Record	Number of studies(%)
Dahuang	*Radix et Rhizoma Rhei*	*Rheum palmatum* L.	*Polygonaceae*	–	25(0.56)
Sanqi	*Radix Notoginseng*	*Panax notoginseng* (Burkill) F.H.Chen	*Araliaceae*	146751	17(0.38)
Chuanxiong	*Rhizoma Ligustici Chuanxiong*	*Ligusticum striatum* DC.	*Apiaceae*	–	16(0.36)
Chishao	*Radix Paeoniae Rubra*	*Paeonia lactiflora* Pall.	*Paeoniaceae*	–	15(0.33)
Shichangpu	*Rhizoma Acori Tatarinowii*	*Acorus calamus* var. *angustatus* Besser	*Acoraceae*	2306	23(0.51)
Yujin	*Radix Curcumae*	*Curcuma aromatica* Salisb. *Curcuma wenyujin* Y.H.Chen & C.Ling	*Zingiberaceae*	235193 235308	11(0.24)
Zhizi	*Fructus Gardeniae*	*Gardenia jasminoides* J.Ellis	*Rubiaceae*	88270	10(0.22)
Taoren	*Semen Persicae*	*Prunus persica* (L.) Batsch	*Rosaceae*	376	10(0.22)
Shuizhi	*Hirudo*	–	*Hirudinidae*	–	9(0.2)
Honghua	*Flos Carthami*	*Crocus sativus* L.	*Iridaceae*	327454	9(0.2)
Gancao	*Radix Glycyrrhizae*	*Glycyrrhiza uralensis* Fisch.	*Leguminosae*	32406	9(0.2)
Danggui	*Radix Angelicae Sinensis*	*Angelica sinensis* (Oliv.) Diels	*Apiaceae*	–	8(0.18)
Niuxi	*Radix Achyranthis Bidentatae*	*Achyranthes bidentata* Blume	*Amaranthaceae*	–	8(0.18)
Huangqin	*Radix Scutellariae*	*Scutellaria baicalensis* Georgi	*Lamiaceae*	188938	8(0.18)

Angelicae Sinensis, and *Radix Achyranthis* have the function of promoting blood circulation for removing blood stasis; *Radix Notoginseng* and *Radix Scutellariae* have the function of hemostasis. Thus, we can deduce that the main pattern of primary ICH is the syndrome of blood stasis blocking brain. In addition, the selected high-frequency herbs can guide the prescribing of clinical treatment of primary ICH and can be used as candidate herbs for RCT.

Implications for Research

The present study identifies some key areas that contribute to further research. Firstly, the reasons why CHM cannot significantly improve the mortality rate are as follows: A) Sample size: Mortality rate was observed in 14 studies with 106/863 subjects in the treatment group and 179/850 subjects in the control group. There is no statistical difference between the two groups in spite of a presenting trend efficacy. It is difficult to draw conclusions and easy to get false negative results when the sample size is too small (Zhong, 2009). B) Types of participants: The participants' condition in the included studies was not severe, and some participants with milder conditions were less likely to die. C) Follow-up time: The follow-up time was from 7 days to 1 year, so that we cannot predict the long-term effects of CHM for ICH patients. However, it does not mean that CHM has no significance for improving the mortality rate for ICH patients. The significance of CHM for improving the mortality rate may be undervalued due to the above reasons. Thus, whether CHM can significantly improve the mortality rate of ICH deserves further study. Secondly, it is crucial to improve the methodological quality of RCTs. We recommend that specific guidelines, such as the CONSORT 2010 statement (Schulz et al., 2010), guidelines for RCTs investigating CHM (Flower et al., 2012), and CONSORT Extension for Chinese Herbal Medicine Formulas 2017 (Cheng et al., 2017), should be further used to design and report RCTs for CHM. Thirdly, although the CHM treatment in the included studies was generally safe in ICH patients, the safety of CHM for ICH still needs further confirmation. In addition, the safety of herbal patent injection itself has become a major concern to both national health authorities and the general public (Wang et al., 2010). A standard reporting format for adverse drug reactions (ADR) has been developed (Bian et al., 2010), and we suggest that we should pay close attention to improving the reporting of ADRs of CHM. Fourthly, a longer follow-up period with serial measurements of outcomes is important to determine the genuine effectiveness and long-term effect of ICH. Thus, a longer follow-up period for ICH patients in the design of further clinical trials is needed. Fifthly, disease-syndrome combination is the recognized trend in integrative medicine. Syndrome differentiation is the core of TCM practice, which can establish a TCM treatment principle and enable us to prescribe the herbal formula. Thus, syndrome differentiation is the bridge to prescription corresponding to syndrome (Wang and Xiong, 2012). Thus, when evaluating the efficacy and safety of CHM treatment, the syndrome differentiation of ICH should be considered to further stratify. A precisely tailor-made TCM prescription based on individual differences can help to improve the efficacy of the selected Chinese herbs (Jiang et al., 2012). For instance, one high-quality study published in JAMA (Bensoussan et al., 1998) indicated that using individualized CHM for the treatment of irritable bowel syndrome is more effective than prescribing a common hypnotic prescription. Therefore, based on the syndrome differentiation of patients, we can select the appropriate medicine from the most frequently used 14 herbs in this study in the future clinic treatment, so as to improve the therapeutic effect of CHM for the acute period of ICH. Last but not least, some new sensitive scales can be introduced into future trials, such as the ICH grading scale (Ruiz-Sandoval et al., 2007) and the FUNC score (Rost et al., 2008).

CONCLUSION

The present study provided supportive evidence of CHM for improving dependency of ICH and showed general safety;

however, there is still lack of evidence for improving mortality rate, and it opens for further study.

DATA AVAILABILITY STATEMENT

All datasets generated for this study are included in the manuscript/supplementary files.

AUTHOR CONTRIBUTIONS

H-LW and HZ contributed as the senior author and the principal investigator of this study, refined the study, and wrote the first draft of the manuscript. G-QZ and QW contributed to the overall design. M-BX and X-LZ identified and reviewed the studies for eligibility. P-QR and T-YJ performed the meta-analysis of the data. All authors read, critically reviewed, and approved the final manuscript.

FUNDING

This study was supported by grants from the National Natural Science Foundation of China (81573750/81473491/81173395/H2902), the Young and Middle-Aged University Discipline Leaders of Zhejiang Province, China (2013277), the Zhejiang Provincial Program for the Cultivation of High-level Innovative Health Talents (2015), the National Natural Science Foundation of China (81673627), and Guangzhou Science Technology and Innovation Commission Technology Research Projects (201805010005).

SUPPLEMENTARY MATERIAL

The Supplementary Material for this article can be found online at: https://www.frontiersin.org/articles/10.3389/fphar.2019.01139/full#supplementary-material

REFERENCES

Bensoussan, A., Talley, N. J., Hing, M., Menzies, R., Guo, A., and Ngu, M. (1998). Treatment of irritable bowel syndrome with Chinese herbal medicine: a randomized controlled trial. *JAMA* 280, 1585–1589. doi: 10.1001/jama.280.18.1585

Bi, X., and Hu, J. (2014). Effects of low dose Xueshuantong injection on hematoma absorption and clinical prognosis in patients with intracerebral hemorrhage. *Chin. Pract. J. Rural. Doc.* 11, 54–55. doi: 10.3969/j.issn.16727185.2014.11.031

Bian, Z. X., Tian, H. Y., Gao, L., Shang, H. C., Wu, T. X., Li, Y. P., et al. (2010). Improving reporting of adverse events and adverse drug reactions following injections of Chinese Materia Medica. *J. Evid. Based. Med.* 3, 5–10. doi: 10.1111/j.1756-5391.2010.01055.x

van Asch, C. J., Luitse, M. J., Rinkel, G. J., Van, d. T. I., Algra, A., and Klijn, C. J. (2010). Incidence, case fatality, and functional outcome of intracerebral haemorrhage over time, according to age, sex, and ethnic origin: a systematic review and meta-analysis. *Lancet Neurol.* 9, 167–176. doi: 10.1016/S1474-4422(09)70340-0

Caplan, L. R. (2011). Stroke classification: a personal view. *Stroke* 42, S3–S6. doi: 10.1161/STROKEAHA.110.594630

China State Bureau of Quality and Technical Supervision. (1997). *The National standard of TCM, section of Clinical terminology of diagnosis and treatment on TCM*. Beijing: China Standard Press, 52.

Chan, K., Shaw, D., Simmonds, M. S., Leon, C. J., Xu, Q., Lu, A., et al. (2012). Good practice in reviewing and publishing studies on herbal medicine, with special emphasis on traditional Chinese medicine and Chinese Materia Medica. *J. Ethnopharmacol.* 140, 469–475. doi: 10.1016/j.jep.2012.01.038

Chen, Q. T. (1996). Standard of the degree of clinical nerve function defect in stroke patients 1995. *Chin. J. Neurol.* 29, 381–383.

Chen, S., Zhang, X., Li, X., Wang, J., Long, C., Xiong, Y., et al. (2010). A randomized, double-blind, placebo-controlled clinical trial of Zhongfeng Xingnao oral liquid for acute cerebral hemorrhage. *China. Association Chin. Med.* 18, 572–573. doi: 10.3969/j.issn.1008-0805.2007.03.031

Chen, Y. (2011). Clinical observation of Xingnao Kaiqiao decoction in treating hypertensive cerebral hemorrhage. *Med. Innovat. Chin.* 8, 77–78. doi: 10.3969/j.issn.1674-4985.2011.18.045

Cheng, C. W., Wu, T. X., Shang, H. C., Li, Y. P., Altman, D. G., Moher, D., et al. (2017). Consort extension for Chinese herbal medicine formulas 2017: recommendations, explanation, and elaboration (simplified Chinese version). *Annals. Internal. Med.* 167, W7–W20. doi: 10.7326/M16-2977

Dai, M., Liu, J., Xiao, Y., Liu, M., Wang, J., Xiao, H., et al. (2002). Curative effect of Zhuyu Xiaozhong decoction combined with drilling urokinase dissolution by trephintion and drainage for hypertensive cerebral hemorrhage. *New. J. Trad. Chin. Med.* 34, 40–42. doi: 10.3969/j.issn.0256-7415.2002.03.017

De Angelis, C., Drazen, J. M., Frizelle, F. A., Haug, C., Hoey, J., Horton, R., et al. (2004). Clinical trial registration: a statement from the International Committee of Medical Journal Editors. *N. Engl. J. Med.* 351, 1250–1251. doi: 10.1056/NEJMe048225

Fan, Y., Hu, L., Zhou, Y., and Zhao, X. (2008). Effect of ß-aescinate on changes of cerebral edema after intracerebral hemorrhage. *Chin. J. Trad. Chin. Med. Pharm.* 23, 353–357.

Fan, Y., Zhou, Z., Jin, M., Li, J., Gu, X., Shen, W., et al. (2000). Effect of Liangxue Tongyu oral liquid on early rehabilitation of patients with primary hypertensive intracerebral hemorrhage. *Chin. J. Integr. Trad. West. Med.* 20, 59–61. doi: 10.7661/CJIM.2000.2.138

Flower, A., Witt, C., Liu, J. P., Ulrich-Merzenich, G., Yu, H., and Lewith, G. (2012). Guidelines for randomised controlled trials investigating Chinese herbal medicine. *J. Ethnopharmacol.* 140, 550–554. doi: 10.1016/j.jep.2011.12.017

Gu, H., Li, G., and Wan, D. (2014). Clinical observation of Xingnaojing injection for acute intracerebral hemorrhage and its effects on levels of Hs-Crp and Nse in serum of patients. *Chin. J. Exper. Tradit. Med. Form.* 20, 178–182. doi: 10.13422/j.cnki.syfjx.2014140178

Guan, J., Zhao, G., Zhang, X., Wang, S., and Wu, C. (2015). Clinical observation of the effects of Yinxing Damo injection on recovery of neural function after hypertensive intracerebral hemorrhage minimally invasive surgery. *Chin. Pharm.* 26, 4526–4528. doi: 10.6039/j.issn.1001-0408.2015.32.22

Guo, J., Wei, L., and Chang, X. (2016). Clinical observation on minimally invasive combined with refreshing enema in the treatment of hypertensive cerebral hemorrhage. *Chin. Med. Modern. Distance Edu. Chin.* 14, 74–75. doi: 10.3969/j.issn.1672-2779.2016.06.034

Guo, L., Hou, X., Hao, L., Wang, R., and Song, Z. (2014). Effect of Shuizhi Huoxue Sanzhong oral liquid on absorption of hematoma in intracerebral hemorrhage. *Chin. J. Inform. Trad. Chin. Med.* 21, 103–104. doi: 10.3969/j.issn.1005-5304.2014.02.032

Higgins, J. P. and Altman, D. G. (2008). Assessing Risk of Bias in Included Studies. In *Cochrane Handbook for Systematic Reviews of Interventions*. Eds. J. P. Higgins and S. Green. doi: 10.1002/9780470712184.ch8

Huang, J., Li, Y., and Lin, Z. (2010). Therapeutic efficacy of Dahuangzhidan decoction in hypertensive cerebral hemorrhage after operated. *Chin. Arch. Trad. Chin. Med.* 28, 1783–1785.

Huang, P., Huang, Y., Lu, M., Du, B., Liang, W., Ou, A., et al. (2006). Treatment of acute intracerebral hemorrhage with a comprehensive protocol of integrated Chinese and Western medicine. *Chin. J. Integr. Trad. West Med.* 26, 590–593. doi: 10.7661/CJIM.2006.7.590

ICH Expert Working Group (1996). "Guideline for Good Clinical Practice," in *ICH Harmonised Tripartite Guideline.* 1–53. Available from: http://www.ich.

org/fileadmin/Public_Web_?Site/ICH_Products/Guidelines/Efficacy/E6?_R1/Step4/E6_R1__Guideline.pdf

Jia, Y., Zhong, X., Liu, J., Liu, J., Cai, D., Wang, X., et al. (2000). Clinical study of Zhuyu Xiao Zhong mixture combined with stereotactic drainage in treating of hypertensive cerebral hemorrhage. *Chin. J. Integr. Trad. West Med.* 20, 498–500. doi: 10.7661/CJIM.2000.7.498

Jiang, M., Lu, C., Zhang, C., Yang, J., Tan, Y., Lu, A., et al. (2012). Syndrome differentiation in modern research of traditional Chinese medicine. *J. Ethnopharmacol.* 140, 634–642. doi: 10.1016/j.jep.2012.01.033

Jiang, S., Fu, Z., and Chen, L. (2016). Neurological recovery effect of blood activating and phlegm removing decoction in treatment of the patients with hypertensive cerebral hemorrhage. *Chin. J. Prim. Med. Pharm.* 8, 1252–1255. doi: 10.3760/cma.j.issn.1008-6706.2016.08.036

Kjaergard, L. L., Villumsen, J., and Gluud, C. (2001). Reported methodologic quality and discrepancies between large and small randomized trials in meta-analyse. *Annals. Internal. Med.* 135, 982–989. doi: 10.7326/0003-4819-135-11-200112040-00010

Lei, X., and Qiao, L. (2017). Clinical observation of Qingre Huotan Tongfu prescription for cerebral hemorrhage in acute stage of phlegm-heat fu-organ sthenia syndrome. *J. New Chin. Med.* 49, 24–27. doi: CNKI:SUN:REND.0.2017-09-007

Li, H. Q., Wei, J. J., Xia, W., Li, J. H., Liu, A. J., Yin, S. B., et al. (2015). Promoting blood circulation for removing blood stasis therapy for acute intracerebral hemorrhage: a systematic review and meta-analysis. *Acta Pharmacol. Sin.* 36, 659–675. doi: 10.1038/aps.2014.139

Li, J., Yuan, L., Zhang, G., Zhou, L., Gao, Y., Li, Q., et al. (2016). Activating blood circulation to remove stasis treatment of hypertensive intracerebral hemorrhage: a multi-center prospective randomized open-label blinded-endpoint trial. *Chin. J. Integr. Med.* 22, 328–334. doi: 10.1007/s11655-016-2467-7

Li, K., Xiang, Z., and Zhang, X. (2015). Observation of curative effect of Zhongfeng Xingnao oral liquid on improving neurological deficit in patients with acute intracerebral hemorrhage. *J. Milit. Surg. Southwest Chin.* 17, 640–641. doi: 10.3969/j.issn.1672-7193.2015.06.016

Li, P. (2014). Clinical observation of *Salvia miltiorrhiza* freeze-dried powder in treating hypertensive intracerebral hemorrhage. *J. Guangxi Univ. Chin. Med.* 17, 47–48.

Li, W., Gao, Y., Guo, W., and Wang, X. (2011). Clinical observation of integrated traditional Chinese and Western medicine in treating hypertensive cerebral hemorrhage. *Gansu Med. J.* 30, 348–350.

Li, Y., Dong, H., Dou, Y., Yang, R., Liu, Z., Zhang, Q., et al. (2012). Zhongfeng Gao for 45 cases of acute intracerebral hemorrhage. *Trad. Chin. Med. Res.* 25, 6–9. doi: 10.3969/j.issn.1001-6910.2012.02.004

Liao, H., Xu, J., Lin, Z., Yang, J., and Chen, Q. (2010). Effect of Tianhuang granule on intracranial pressure and serum matrix metalloproteinase-9 in patients with acute cerebral hemorrhage. *Chin. J. Integr. Med.* 16, 304–308. doi: 10.1007/s11655-010-0514-0

Liu, Z., Guan, L., Wang, Y., Xie, C. L., Lin, X. M., and Zheng, G. Q. (2012). History and mechanism for treatment of intracerebral hemorrhage with scalp acupuncture. *Evid.-Based Compl. Alt.* 2012, 895032. doi: 10.1155/2012/895032

Liu, J., Huang, L., Dai, X., and Zhu, W. (2012). Effect of Tongfu Xiere Huoxue method on vasoactive peptides in hypertensive intracerebral hemorrhage. *J. New Chin. Med.* 44, 29–31.

Liu, S., and Wu, R. (2016). Observation of curative effect of activating blood circulation to dissipate blood stasis on acute intracerebral hemorrhage. *J. Liaoning Univ. Trad. Chin. Med.* 18, 189–191.

Liu, Y., and Zhang, Y. (2016). Effect of Qingre Huayu decoction on neurological function and prognosis in patients with acute intracerebral hemorrhage. *Shandong Med. J.* 56, 76–78. doi: 10.3969/j.issn.1002-266X.2016.29.027

Long, Y., Wu, B., Zhou, D., Hu, H., Chen, Y., and Li, Z. (2016). Effects of Annao Pingchong pill on recovery of neural nerve function, cerebral edema and aquaporin after minimally invasive surgery for intracerebral hemorrhage. *Chin. J. Integr. Trad. West Med. Intens. Crit. Care* 4, 356–359. doi: 10.3969/j.issn.1008-9691.2016.04.005

Luo, Z., Xiong, N., Wang, T., Xiang, M., Tu, Q., Huang, Y., et al. (2015). Effects of Panax notoginseng saponins (Pns) on absorption of hematoma and neurological function recovery in patients with hypertensive intracerebral hemorrhage. *Stroke Nerv. Dis.* 22, 234–237. doi: 10.3969/j.issn.1007-0478.2015.04.011

Ma, H., and Zhang, R. (2017). Clinical effect of salvia ligustrazine injection in the treatment of hypertensive intracerebral hemorrhage. *Chin. J. Biochem. Pharmaceut.* 5, 179–181. doi: 10.3969/j.issn.1005-1678.2017.05.059

Ma, L., and Gong, J. (2005). Xuesaitong injection paratherapy for 46 cases of intracerebral hemorrhage. *Stud. J. Trad. Chin. Med.* 23, 612. doi: 10.3969/j.issn.1673-7717.2005.04.016

Ming, S., Dong, M., and Kong, H. (2010). Clinical study of Xingnaojing for intracerebral hemorrhage. *Chin. J. Clin. Neurosurg.* 15, 620–622. doi: 10.3969/j.issn.1009-153X.2010.10.016

Ming, S., Liu, Q., and Chen, K. (2013). Rhubarb in treating 40 cases of acute hypertensive intracerebral hemorrhage. *Chin. Med. Modern. Distan. Edu. Chin.* 11, 13–14. doi: 10.3969/j.issn.1672-2779.2013.05.006

Moher, D., Liberati, A., Tetzlaff, J., and Altman, D. G. (2009). Preferred reporting items for systematic reviews and meta-analyses: the prisma statement. *BMJ* 339, b2535. doi: 10.1136/bmj.b2535

Morgenstern, L. B., Hemphill Rd, J. C., Anderson, C., Becker, K., Broderick, J. P., Connolly, E. S., et al. (2015). Guidelines for the management of primary intracerebral hemorrhage: a guideline for healthcare professionals from the American heart association/American stroke association. *Stroke* 46, 2032. doi: 10.1161/STR.0000000000000069

Parnianfard, N., Eskandariyan, I., Parvan, R. and Azizi, H. (2017). 6: a systematic review of quality assessment of randomized controlled trials in cochrane arrhythmias systematic reviews. *BMJ Open 7 (Suppl 1)*. doi: 10.1136/bmjopen-2016-015415.6

Peng, G., Liang, L., and Yang, G. (2011). Observation of curative efficacy of Tianlong Tongjing prescription in treating cerebral hemorrhage. *Chin. Pract. Med.* 6, 128–129. doi: 10.3969/j.issn.1673-7555.2011.17.094

Peng, W., and Feng, W. (2015). Clinical observation of Liuwei Naoxue an decoction in treating hypertensive; intracerebral hemorrhage. *Chin. J. Trad. Med. Sci. Tech.* 22, 191–192.

Poon, M. T. C., Fonville, A. F., and Al-Shahi Salman, R. (2014). Long-term prognosis after intracerebral hemorrhage: systematic review and meta-analysis. *J. Neurol. Neurosurg. Psychiat.* 85, 660–667. doi: 10.1136/jnnp-2013-306476

Rao, M. (2007). *Guidelines for prevention and treatment of cerebrovascular diseases*. (Beijing: People's Medical Press), 36–42.

Rost, N. S., Smith, E. E., Chang, Y., Snider, R. W., Chanderraj, R., Schwab, K., et al. (2008). Prediction of functional outcome in patients with primary intracerebral hemorrhage: the func score. *Stroke* 39, 2304–2309. doi: 10.1161/STROKEAHA.107.512202

Ruiz-Sandoval, J. L., Chiquete, E., Romero-Vargas, S., Padilla-Martinez, J. J., and Gonzalez-Cornejo, S. (2007). Grading scale for prediction of outcome in primary intracerebral hemorrhages. *Stroke* 38, 1641–1644. doi: 10.1161/STROKEAHA.106.478222

Sze, F.K-h., Yeung, F. F., Wong, E., and Lau, J. (2005). Does Danshen improve disability after acute ischaemic stroke? *Acta Neurol. Scand.* 111, 118–125. doi: 10.1111/j.1600-0404.2004.00369.x

Schulz, K. F., Altman, D. G., Moher, D., and Group, C. (2010). Consort 2010 Statement: updated guidelines for reporting parallel group randomized trials. *J. Clin. Epidemiol.* 63, 834–840. doi: 10.1016/j.jclinepi.2010.02.005

Shang, Q., and Yang, Q. (2016). Clinical observation of integrated traditional Chinese and Western medicine in treatment of intracerebral hemorrhage. *Shangqing* 25, 201–202.

Shen, L., Huang, H., and Chen, Q. (2012). Interventional effect of Xuesaitong injection on neurological function in patients with intracerebral hemorrhage. *Prevent. Treat. Cardio-Cereb. Vasc. Dis.* 12, 396–398. doi: 10.3969/j.issn.1009-816X.2012.05.19

Shen, Y., and Luo, L. (2015). Clinical observation of Xuefu Zhuyu decoction combined with western medicine in treating hypertensive intracerebral hemorrhage. *J. Emerg. Trad. Chin. Med.* 24, 337–339. doi: 10.3969/j.issn.1004-745X.2015.02.059

Sun, J., and Chen, W. (2008). Clinical study of minimally traumatic puncture drainage of hematoma combined with *Salviae miltiorrhizae* injection in treatment of hypertensive cerebral hemorrhage. *Chin. J. Integr. Trad. West Med. Intens. Critic. Care* 15, 28–30. doi: 10.3321/j.issn:1008-9691.2008.01.008

Sun, M., Wang, F., Meng, H., Wu, T., and Xu, Q. (2017). Clinical analysis of Xingnao Kaiqiao Zhuyu decoction in treating acute intracerebral hemorrhage. *Chin. J. Trad. Med. Sci. Technol.* 5, 626–627.

Steiner, T., Al-Shahi Salman, R., Beer, R., Christensen, H., Cordonnier, C., Csiba, L., et al. (2014). European Stroke Organization (ESO) guidelines for the management of primary intracerebral hemorrhage. *Int. J. Stroke* 9, 840–855. doi: 10.1111/ijs.12309

The Second National Conference on Neuropsychiatry. (1978). Classification of acute cerebrovascular diseases (trial draft). *Chin. J. Psychiatry* 11 (2), 127–128.

The Fourth National Conference on Cerebrovascular Disease. (1996). Chinese national criteria in diagnostic essentials of various cerebrovascular diseases. *Chin. J. Neurosci.* 29 (6), 379–381.

Wang, Y. Y. (1997). Thinking on how to improve the curative effect of cerebrovascular diseases. *Chin. J. Integr. Tradit. West Med.* 17 (4), 195–196.

Wang, Y., Lou, X. T., Shi, Y. H., Tong, Q., and Zheng, G. Q. (2019). Erxian decoction, a Chinese herbal formula, for menopausal syndrome: an updated systematic review. *J. Ethnopharmacol.* 234, 8–20. doi: 10.1016/j.jep.2019.01.010

Wang, J., and Xiong, X. (2012). Current situation and perspectives of clinical study in integrative medicine in China. *Evid. Based. Compl. Alt.* 2012, 268542. doi: 10.1155/2012/268542

Wang, L., Yuan, Q., Marshall, G., Cui, X., Cheng, L., Li, Y., et al. (2010). Adverse drug reactions and adverse events of 33 varieties of traditional CHINESE medicine injections on national essential medicines list (2004 Edition) of China: an overview on published literatures. *J. Evid. Based. Med.* 3, 95–104. doi: 10.1111/j.1756-5391.2010.01073.x

Wang, X. D. (1998). Diagnostic essentials of various cerebrovascular diseases. *Chin. J. Neurol.* 21, 60.

Wang, Y., Shi, Q., and Wang, W. (2013). Clinical study of Xuefuzhuyu decoction on hypertensive intracerebral hemorrhage. *J. Emerg. Trad. Chin. Med.* 22, 1686–1687, 1689. doi: 10.3969/j.issn.1004-745X.2013.10.018

Wang, Z., and Wang, J. (2011). Efficacy observation of the sequential therapy of traditional Chinese medicine for hypertensive cerebral hemorrhage. *Chin. Pharm.* 22, 263–265.

Wu, B., Liu, M., Liu, H., Li, W., Tan, S., Zhang, S ., et al. (2007). Meta-analysis of traditional Chinese patent medicine for ischemic stroke. *Stroke* 38, 1973–1979. doi: 10.1161/STROKEAHA.106.473165

Xia, Z., Wang, J., Guo, J., Zhang, R., Li, J., Zhong, J., et al. (2016). Effect of Chinese drugs for breaking blood and expelling stasis on acute intracerebral hemorrhage: a prospective randomized double-blind controlled study. *Chin. J. Integr. Trad. West Med.* 36, 821–826.

Yang, J., and Liu, E. (2006). Clinical observation of integrated traditional Chinese and Western medicine for intracerebral hemorrhage. *J. Sichuan Trad. Chin. Med.* 24, 56–57. doi: 10.3969/j.issn.1000-3649.2006.10.032

Yang, W. T., Zheng, X. W., Chen, S., Shan, C. S., Xu, Q. Q., Zhu, J. Z., et al. (2017). Chinese herbal medicine for Alzheimer's disease: clinical evidence and possible mechanism of neurogenesis. *Biochem. Pharmacol.* 141, 143–155. doi: 10.1016/j.bcp.2017.07.002

Ye, R. (2014). Clinical study of minimally invasive puncture drainage combined with traditional Chinese medicine differentiation treating moderate and severe hypertensive intracerebral hemorrhage. *Chin. J. Chin. Med.* 29, 1135–1137.

Zhang, F., Li, W., and Hou, T. (2017). Influence of activating blood to remove stasis and refreshment decoction for plasma Mmp-9 and neural function of cerebral hemorrhage patients with microinvasive evacuation of hematoma. *Chin. Arch. Trad. Chin. Med.* 35, 1254–1256. doi: CNKI:SUN:ZYHS.0.2017-05-055

Zhang, S., Zhang, C., Chen, M., Xu, X., and Hou, B. (2012). Clinical study of Bushenhuoxuehuatan decoction on acute cerebral hemorrhage. *J. Emerg. Trad. Chin. Med.* 21, 529–530, 557. doi: 10.3969/j.issn.1004-745X.2012.04.008

Zheng, G. Q. (2009). Therapeutic history of Parkinson's disease in Chinese medical treatises. *J. Altern. Complem. Med.* 15, 1223–1230. doi: 10.1089/acm.2009.0101

Zheng, G. Q., and Huang, P. X. (2005). Origin and development of hemorrhagic stroke. *Chin. J. Med. History* 35, 25–28.

Zhou, W., Dong, M., Sun, X., and Li, H. (2016). Buyang Huanwu decoction with Western medicine in the treatment of acute hypertensive cerebral hemorrhage. *Shanxi J. Trad. Chin. Med.* 37, 971–973. doi: 10.3969/j.issn.1000-7369.2016.08.015

Zhong, B. L. (2009). How to calculate sample size in randomized controlled trial? *J. Thorac. Dis.* 1 (1), 51–54.

Conflict of Interest: The authors declare that the research was conducted in the absence of any commercial or financial relationships that could be construed as a potential conflict of interest.

frontiers in Pharmacology

ORIGINAL RESEARCH
published: 11 October 2019
doi: 10.3389/fphar.2019.01135

Salsolinol Attenuates Doxorubicin-Induced Chronic Heart Failure in Rats and Improves Mitochondrial Function in H9c2 Cardiomyocytes

*Jianxia Wen[1,2†], Lu Zhang[3†], Honghong Liu[4], Jiabo Wang[4], Jianyu Li[4], Yuxue Yang[1,2], Yingying Wang[1,2], Huadan Cai[2], Ruisheng Li[5] and Yanling Zhao[2]**

[1] College of Pharmacy, Chengdu University of Traditional Chinese Medicine, Chengdu, China, [2] Department of Pharmacy, Fifth Medical Center, General Hospital of Chinese PLA, Beijing, China, [3] College of Pharmacy, Zhejiang Chinese Medical University, Hangzhou, China, [4] Integrative Medical Center, Fifth Medical Center, General Hospital of Chinese PLA, Beijing, China, [5] Research Center for Clinical and Translational Medicine, Fifth Medical Center, General Hospital of Chinese PLA, Beijing, China

OPEN ACCESS

Edited by:
Guanhua Du,
Chinese Academy of Medical Sciences and Peking Union Medical College, China

Reviewed by:
Sergej Ostojic,
University of Novi Sad, Serbia
Ki-Tae Ha,
Pusan National University, South Korea

***Correspondence:**
Yanling Zhao
zhaoyl2855@126.com

†These authors have contributed equally to this work

Specialty section:
This article was submitted to Ethnopharmacology, a section of the journal Frontiers in Pharmacology

Received: 07 May 2019
Accepted: 03 September 2019
Published: 11 October 2019

Citation:
Wen J, Zhang L, Liu H, Wang J, Li J, Yang Y, Wang Y, Cai H, Li R and Zhao Y (2019) Salsolinol Attenuates Doxorubicin-Induced Chronic Heart Failure in Rats and Improves Mitochondrial Function in H9c2 Cardiomyocytes. Front. Pharmacol. 10:1135. doi: 10.3389/fphar.2019.01135

Backgrounds: Salsolinol (SAL), a plant-based isoquinoline alkaloid, was initially isolated from Aconiti Lateralis Radix Praeparata (ALRP) and identified as the active cardiotonic component of ALRP. This study was aimed to explore the therapeutic effect and mechanism by which SAL attenuates doxorubicin (DOX)-induced chronic heart failure (CHF) in rats and improves mitochondrial function in H9c2 cardiomyocytes.

Methods: Rats were intraperitoneally injected with DOX to establish CHF model. Therapeutic effects of SAL on hemodynamic parameters, serum indices, and the histopathology of the heart were analyzed *in vivo*. Moreover, H9c2 cardiomyocytes were pretreated with SAL for 2 h before DOX treatment in all procedures *in vitro*. Cell viability, cardiomyocyte morphology, proliferation, and mitochondrial function were detected by a high-content screening (HCS) assay. In addition, a Seahorse Extracellular Flux (XFp) analyzer was used to evaluate the cell energy respiratory and energy metabolism function. To further investigate the potential mechanism of SAL, relative mRNA and protein expression of key enzymes in the tricarboxylic acid cycle *in vivo* and mitochondrial calcium uniporter (MCU) signaling pathway-related molecules *in vitro* were detected.

Results: The present data demonstrated the pharmacological effect of SAL on DOX-induced CHF, which was through ameliorating heart function, downregulating serum levels of myocardial injury markers, alleviating histological injury to the heart, increasing the relative mRNA expression levels of key enzymes downstream of the tricarboxylic acid cycle *in vivo*, and thus enhancing myocardial energy metabolism. In addition, SAL had effects on increasing cell viability, ameliorating DOX-induced mitochondrial dysfunction, and increasing mitochondrial oxygen consumption rate (OCR) and extracellular acidification rate (ECAR) in H9c2 cardiomyocyte. Moreover, we found that SAL might have an effect on improving mitochondrial respiratory function and energy metabolism *via* inhibiting excessive activation of MCU pathway in H9c2 cells. However, the protective effect could be ameliorated by ruthenium red (an MCU inhibitor) and abrogated by spermine (an MCU activator) *in vitro*.

Conclusion: The therapeutic effects of SAL on CHF are possibly related to ameliorating cardiomyocyte function resulting in promotion of mitochondrial respiratory and energy metabolism. Furthermore, the potential mechanism might be related to downregulating MCU pathway. These findings may provide a potential therapy for CHF.

Keywords: Salsolinol, doxorubicin, chronic heart failure, energy metabolism, mitochondrial calcium uniporter

INTRODUCTION

Chronic heart failure (CHF), the most common form of cardiovascular disease, is a serious health problem worldwide, with rising incidence and prevalence (Stephan et al., 2017; Zhang et al., 2018). According to the "Heart disease and stroke statistics—2018 update: a report from the American Heart Association" (Benjamin et al., 2018), the prevalence of CHF will increase at 46% from 2012 to 2030, resulting in more than 8 million people not less than 18 years of age with heart failure (HF). Prevention and treatment of CHF will effectively reduce morbidity and mortality rates in human beings. Currently, although various potential mechanisms have been investigated for the treatment of CHF, there is still a lack of satisfaction for the targeted therapy. The heart is the main energy-consuming organ of one's body, and sufficient energy supply is a normal guarantee for maintaining its own needs and pumping function. Clinically, the insufficient myocardial energy supply or metabolic imbalance will lead to the abnormal structure and function of the heart and eventually lead to the occurrence of HF (Watanabe et al., 2010). In 2004 (van Bilsen et al., 2004), Van Bilsen proposed the concept of energy "metabolic remodeling," that is, the failing heart suffers from chronic energy starvation. The changes in mitochondrial function can also cause changes in heart function. From a metabolic point of view, the hypertrophic heart is characterized by a significant change in matrix preference from fatty acids to glucose. As energy metabolism is affected during compensated hypertrophy and cardiac failure, compounds that can promote mitochondrial energy metabolism may be potential drugs for the treatment of HF (Neubauer et al., 1997; Kalsi et al., 1999).

In the prevention and treatment of HF, with the safety and multi-target advantages, traditional Chinese medicine (TCM) protects myocardial mitochondria during HF, thus providing a new idea for studying the pathogenesis and targeted treatment of CHF. Our previous study had shown that Aconiti Lateralis Radix Praeparata (ALRP, *Fuzi* in Chinese) had an effect on anti-acute HF by enhancing mitochondrial biogenesis *via* Sirt1/PGC-1a pathway (Lu et al., 2017) and anti-CHF by promoting energy metabolism *via* PPARα/PGC-1α/Sirt3 pathway (Wen et al., 2019). However, the active components of this herbal couple are still unclear. Salsolinol (6,7-dioxy-1-methyl-1,2,3,4-tetrahydroisochinoline, SAL), a plant-based isoquinoline alkaloid, was initially isolated from ALRP and identified as 1-methyl-6,7-dihydroxy-1,2,3,4-tetrahydroisoquinoline by Dihua Chen in 1982 (Chen and Liang, 1982). Due to the effect on the biosynthesis of catecholamines *in vivo*, SAL has gradually attracted the attention of researchers. Experiments have shown that SAL is a weak beta-adrenergic stimulant that excites the atrium of isolated guinea pigs and increases the frequency of contraction. It can also increase the blood pressure of normal and ruined spinal cord rats and demonstrate excitatory effects on both β- and γα-adrenergic bodies (Zhou, 2011). As a water-soluble active ingredient in aconite, SAL has a certain cardiotonic effect. However, whether SAL can promote mitochondrial energy metabolism remains to be studied.

Mitochondrial calcium ion (Ca^{2+}) homeostasis plays a vital role in cellular physiological functions, including energy metabolism of cardiomyocytes and oxygen phosphorylation process (Foskett and Philipson, 2015). Mitochondrial calcium uptake 1 (MICU1) is a mitochondrial inner membrane protein that regulates the transport of Ca^{2+} through the mitochondrial calcium uniporter (MCU) and plays a role in maintaining the homeostasis of Ca^{2+} in mitochondria, thus playing a vital role in influencing cardiovascular disease (Mallilankaraman et al., 2012). The uptake of mitochondrial Ca^{2+} is primarily achieved by MCU on the inner membrane, which has highly selective and low affinity for Ca^{2+} (Penna et al., 2018). There is an interaction relationship between MICU1 and MCU. These two combine other protein molecules to form mitochondria that can also be formed as a mitochondrial unidirectional transporter complex, among which MCU is the center of this complex. There are other regulatory proteins, including MICU1, mitochondrial calcium uptake 2 (MICU2), and essential MCU regulator (EMRE) (Foskett and Philipson, 2015). Among them, MICU1 has dual regulation of mitochondrial Ca^{2+} transport (Mallilankaraman et al., 2012). MICU2 plays a key role in maintaining cardiovascular homeostasis (Bick et al., 2017). EMRE is a necessary regulatory protein for MCU. The inhibition of EMRE will reduce the activity of MCU, which can interact with MCU, as well as MICU1 and MICU2 (Alevriadou et al., 2017; Penna et al., 2018). As the core channel of the MCU complex, MCU can mediate Ca^{2+} transport and participate in the regulation

Abbreviations: CHF, chronic heart failure; TCM, traditional Chinese medicine; ALRP, Aconiti Lateralis Radix Praeparata; SAL, salsolinol; HCS, high-content screening; MCU, mitochondrial calcium uniporter; MICU1, mitochondrial calcium uptake 1; MICU2, mitochondrial calcium uptake 2; EMRE, essential mitochondrial calcium uniporter regulator; DOX, doxorubicin; MMP, mitochondrial membrane potential; LVSP, left ventricular systolic pressure; LVEDP, left ventricle end diastolic pressure; ± LV dp/dt_{max}, ± left ventricle dp/dt_{max}; DH, dobutamine hydrochloride; TUNEL, terminal deoxynucleotidyl transferase (TdT)-mediated dUTP nick-end labeling; OCR, oxygen consumption rate; ECAR, extracellular acidification rate; PDH, pyruvate dehydrogenase; MDH, malate dehydrogenase; NNT, nicotinamide nucleotide transhydrogenase; BNP, brain natriuretic peptide; LDH, lactate dehydrogenase; ALD, aldosterone. RR, ruthenium red; SP, spermine.

of ATP production (Zaglia et al., 2017). Therefore, MCU and the regulatory protein MICU1 play an important role in cardiomyocyte function by regulating mitochondrial Ca^{2+} uptake. Our previous study had shown that ALRP had an effect on anti-acute HF by enhancing mitochondrial energy metabolism pathway mediated by MCU (Zhang et al., 2017). However, the active components of this herbal couple are still unclear. This study was designed to investigate whether the active ingredient SAL in ALRP can protect doxorubicin (DOX)-induced H9c2 cardiomyocyte injury by affecting mitochondrial respiratory function and energy metabolism and, further, to explore whether its potential mechanism of action is related to the regulation of MCU protein expression.

In this study, rats were intraperitoneally injected with DOX to establish CHF model. Therapeutic effects of SAL on hemodynamic parameters, serum indices, and the histopathology of the cardiac were analyzed *in vivo*. Moreover, the effect of SAL on cell viability, cardiomyocyte morphology, and mitochondrial membrane potential (MMP) of H9c2 cardiomyocytes were investigated by high-content screening (HCS) assay. Mitochondrial respiratory function and energy metabolism of H9c2 cardiomyocyte were measured by Seahorse Extracellular Flux (XFp) analyzer. To further investigate the potential mechanism of SAL, relative mRNA, and protein expression of key enzymes in the tricarboxylic acid cycle (TAC) *in vivo* were detected. Ultimately, mRNA and proteins expressions associated with the mitochondrial energy metabolism of H9c2 cells were explored. The results indicated that the therapeutic effects of SAL on CHF are possibly related to ameliorating cardiomyocyte function resulting in promotion of mitochondrial respiratory and energy metabolism. Furthermore, the potential mechanism might be related to downregulating MCU pathway. These findings may provide a potential therapy for CHF. The research process of this study is shown in **Figure 1**.

MATERIALS AND METHODS

Materials

Standards of DOX (purity ≥98%, Cat. No. CHB160921) and SAL (purity ≥98%, Cat. No. CHB160922) were obtained from Chroma Biotechnology Co. Ltd (Chengdu, China). Ruthenium red (CAS No. 11103-72-3) and spermine (purity ≥96%, CAS No. 71-44-3) were purchased from Sigma Aldrich. All drugs above were dissolved in dimethyl sulfoxide (DMSO) and then diluted to corresponding concentration when used. DOX hydrochloride for injection (Shenzhen, China, batch number: 1809E2) was purchased from Shenzhen Main Luck pharmaceutical Inc. Dobutamine hydrochloride (DH) injection (Shanghai, China, batch number: 1803203) was obtained from SPH NO.1 Biochemical & Pharmaceutical Co., Ltd.

Animal Handling

The experimental protocols were approved by the Ethics Committee of the Ethics of Animal Experiments of the Fifth Medical Center of PLA General Hospital (Approval ID: IACUC-2018-010). The present study was conducted according to the recommendations of the Guidelines for the Care and Use of Laboratory Animals of the Ministry of Science and Technology of China.

Male Sprague-Dawley rats (200 ± 20 g, $n = 50$) were obtained from Beijing Keyu Animal Breeding Center [Permission No. SYXK (Jing) 2018-0036]. As in our previous study (Wen et al., 2019), rats in the control groups ($n = 12$) were intraperitoneally injected with saline and in the model groups ($n = 38$) were intraperitoneally injected with DOX hydrochloride for injection to establish CHF model. The injection was not stopped until the accumulative doses of DOX were 15 mg/kg body weight (2.5 mg/

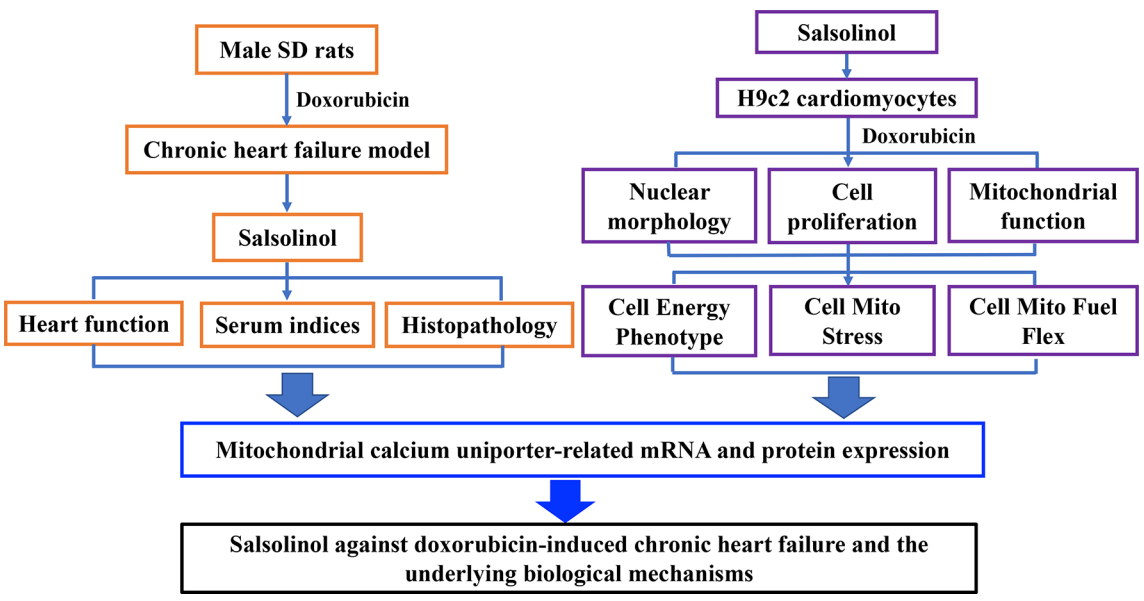

FIGURE 1 | Research framework of this study. SD, Sprague-Dawley.

kg body weight, twice a week for six times), which is a dose based on previous experiments (Siveski-Iliskovic et al., 1994; Bai et al., 2017). Notably, parameters, including left ventricular systolic pressure (LVSP), left ventricle end diastolic pressure (LVEDP), +left ventricle dp/dt_{max} (+LV dp/dt_{max}), and −left ventricle dp/dt_{max} (−LV dp/dt_{max}) in the control and model groups (three rats in each group) (Lu et al., 2017; Zhang et al., 2017), were comprehensively assessed using an RM6240 (Chengdu Instrument Factory, Sichuan, China) from the left ventricle *via* manometer after the last intraperitoneal treatment of DOX. The CHF model was successfully established when the values of +dp/dt_{max} decreased to less than 50% of the values of the control group.

The animals with successfully prepared CHF model were randomly divided into four different groups of eight rats in each, including the DOX group, DH (50 μg/kg), SAL low-dose group (5 mg/kg), and SAL high-dose group (10 mg/kg). The rats serving as a control and DOX group received an equal volume of normal saline. The other groups were intraperitoneally injected with corresponding drugs once a day for seven consecutive days. After the last treatment, heart function was assessed using a multi-channel physiological signal acquisition system. Finally, all the rats were sacrificed. The serum and heart tissue sample of each rats was collected and stored at −80°C for determining a series of indicators. Serum levels of brain natriuretic peptide (BNP), lactate dehydrogenase (LDH), renin, angiotensin (Ang)-II, and aldosterone (ALD) were measured on a Synergy H1 Hybrid Reader (Biotech, USA). The heart tissue was excised and fixed in 4% paraformaldehyde general tissue fixative. To detect apoptosis of myocardial cells, the paraffin-fixed heart sections were stained with the terminal deoxynucleotidyl transferase (TdT)-mediated dUTP nick-end labeling (TUNEL) technique.

Cell Culture and Cell Viability Assay

The H9c2 rat cardiomyocyte cell line was obtained from the Cell Resource Center, IBMS, CAMS/PUMC (CRC/PUMC, Beijing, China). Cells were cultivated with Dulbecco's modified Eagle's medium (DMEM) supplemented with 10% fetal bovine serum (FBS) and 1% penicillin/streptomycin in a humidified incubator containing 5% CO_2 at 37°C. Cell viability was detected using cell counting kit-8 (CCK-8; Cat. No. HY-K0301, MedChemExpress, USA). The optical density (OD) value was measured at 450 nm using a Synergy H1 Hybrid Reader (Biotech, USA).

High-Content Analysis Experiments

The Array Scan High-Content System (Thermo Scientific, Massachusetts, USA) was used to detect nuclear morphology, cell proliferation, and mitochondrial function of H9c2 cells. Fluorescent dyes, including Hoechst 33342 (H3570, Invitrogen), calcein AM (C3099, Invitrogen), and ethidium homodimer-1 (EthD-1) (L3224, Invitrogen) were used to confirm the position and cell morphology and make quantitative analysis of H9c2 cells. Tetramethylrhodamine, ethyl ester, perchlorate (TMRE, T669, Invitrogen), a $\Delta\psi_m$-dependent cationic dye, was used to monitor MMP. Cell health profiling assay module was selected in the HCS system, and several different wavelength channels were set to collect fluorescence images. The measured parameters and format are similar to those used previously (Chen et al., 2014). An Array Scan XTI (The Array Scan software algorithm was used to perform analysis) was used to quantify the mean fluorescence intensity of H9c2 cardiomyocytes.

Analysis of Mitochondrial Respiratory Function and Mitochondrial Energy Metabolism

Mitochondrial respiratory function and mitochondrial energy metabolism were performed according to the manufacturer's instructions. Briefly, H9c2 cells were plated at a density of 6×10^3 cells per well into 8-well plates and incubated for 24 h. Then, H9c2 cells were pretreated with SAL (20 μM) followed by 5 μM of DOX and routinely incubated for 24 h. Prior to the assay, DMEM was replaced by Agilent Seahorse XF Base Medium containing 1 mM of pyruvate, 2 mM of glutamine, and 10 mM of glucose (adjusted pH to 7.4 with 0.1 N NaOH). Then, the compounds were loaded into the appropriate ports of a hydrated sensor cartridge. Cellular oxygen consumption rate (OCR), extracellular acidification rate (ECAR), and different indices were determined using the Seahorse XFp analyzer (XFp, Seahorse Biosciences, MA) according to the different manufacturers' instructions. Among them, assay concentrations in the compound Seahorse XFp Cell Energy Phenotype Test were 10 μM of oligomycin and 10 μM of carbonyl cyanide-4-(trifluoromethoxy) phenylhydrazone (FCCP); the compounds in Seahorse XFp Cell Mito Stress Test were 10 μM of oligomycin, 10 μM of FCCP, and 5 μM of rotenone/antimycin; the compounds in Seahorse XFp Mito Fuel Flex Test were 4 μM of etomoxir, 3 μM of BPTES, and 2 μM of UK5099. Other relevant indicators were calculated according to the provided protocol. Cell counting was used for normalizing Seahorse XFp metabolic data to cellular parameters. H9c2 cells in each well were plated on cell counting slides, the dual chamber for cell counter (Bio-Rad, Cat. No. 145-0011), and counted using a TC10 automated cell counter (Bio-Rad, Singapore). Then, cell counting for normalization data was added to the normalized view for each assay result file using Wave 2.6.0 (Agilent Technologies, USA) before export. The normalization unit of the present study was 6×10^3 cells. Data were analyzed using Seahorse XF Cell Test Report data analysis. The complexes of the electron transport chain (ETC) and action targets of compounds in mitochondrial respiratory function, energy metabolism, and fuel oxidation are shown in **Figure 2**.

Reverse Transcription–Polymerase Chain Reaction (RT-PCR) Analysis *In Vivo* and *In Vitro*

Total mRNA was extracted from heart tissue and H9c2 cells using TRIzol reagent (Nordic Bioscience, Beijing, China) according to the manufacturer's protocol. Quantitative real-time PCR (RT-PCR) for pyruvate dehydrogenase (PDH), malate dehydrogenase (MDH), and nicotinamide nucleotide transhydrogenase (NNT) mRNA in rats, MCU, MICU1, and MICU2 mRNA in H9c2 cardiomyocytes was performed and analyzed using cDNA and SYBR Green PCR Master Mix (Nordic Bioscience, Beijing, China). Primers sequences are listed in **Table 1**. The relative amounts of mRNA were determined based on $2^{-\Delta\Delta Ct}$ calculations with β-actin as the endogenous reference.

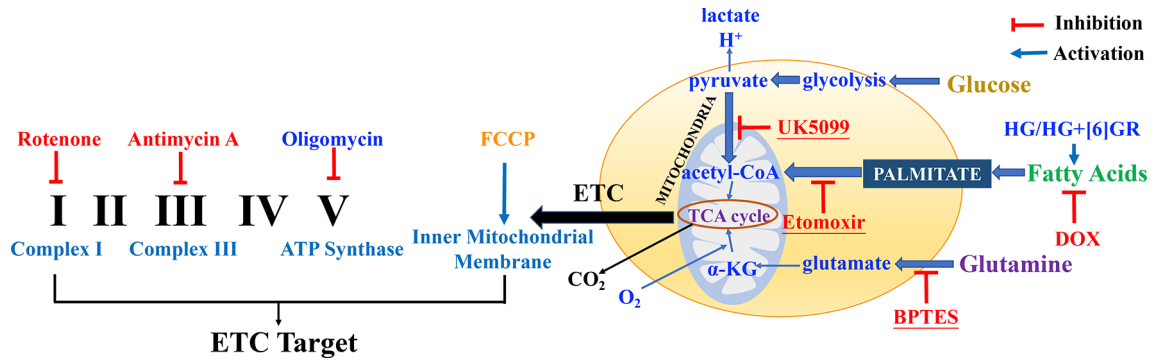

FIGURE 2 | The complexes of the electron transport chain (ETC) and action targets of compounds in the mitochondrial respiratory function, energy metabolism, and fuel oxidation.

TABLE 1 | Primers sequences used for real-time PCR analyses.

Gene	Forward (5′–3′)	Reverse (5′–3′)	prodSize
PDH	ACGAAGAGGAGGCTGTGCTAAGG	CGATACCGTTGCCGCCATAGAAG	80
MDH	CTGCTGTCATCAAGGCTCGGAAG	GGACACCATAGGAGTTGCCATCAG	147
NNT	GTTGCCTTGTCTCCTGCTGGTG	GCTTCGCCTGCTCCTGATTCC	80
MCU	ACGCTGCCAGTTCACACTCAAG	AAGTCATCGAGGAGCAGGAGGTC	162
MICU1	GACTGATGTTGGTGGCGTTCCTC	GTGGAGATTCTGCGTGAGCCTTC	87
MICU2	TGAGGCTGGCGGAGTTCAAGAG	CACACTCTGCTGCTGCGACAC	188
β-Actin	CACTATCGGCAATGAGCGGTTCC	CAGCACTGTGTTGGCATAGAGGTC	154

PCR, polymerase chain reaction.

Western Blot Analysis to Detect the Protein Expression in H9c2 Cardiomyocytes

Total protein was extracted from the H9c2 cardiomyocytes using ice-cold radioimmunoprecipitation assay (RIPA) buffer supplemented with phenylmethylsulfonyl fluoride (PMSF). Protein concentration was determined using a bicinchoninic acid assay (BCA) protein assay kit (Lot. No. 20190215, Solarbio, Beijing, China) according to the manufacturer's instructions. The polyvinylidene difluoride (PVDF) membranes were incubated with the primary antibodies, including rabbit anti-MCU antibody (D2Z3B, Cell Signaling Technology, dilution: 1:1,000), rabbit anti-CBARA1/MICU1 antibody (D4P8Q, Cell Signaling Technology, dilution: 1:1,000), rabbit anti-MICU2 antibody (A12198, ABclonal, dilution: 1:1,000), and anti-beta actin monoclonal antibody (ab115777, Abcam, dilution: 1:200). The antigen–antibody bands were detected using enhanced chemiluminescence (ECL) solution and visualized using X-ray film (Beyotime Institute of Biotechnology). Quantification of bands was performed by densitometric analysis using Bio-Rad Quantity One. β-Actin served as an internal control.

Statistical Analysis

All data were presented as mean ± standard deviation (SD) and analyzed with the SPSS software program (version 19.0; SPSS Inc., Chicago, IL, USA). Data were presented using one-way ANOVA followed by *t*-test. The differences were considered to be statistically significant when $P < 0.05$ and highly significant when $P < 0.01$.

RESULTS

DOX-Induced CHF in Rats in Terms of Cardiac Function

To identify whether CHF model had been successfully established, the role of DOX in rats was examined by hemodynamic parameters of cardiac function, including LVSP, LVEDP, and ± dp/dt_{max}. Hemodynamics results showed that administration of DOX decreased LVSP and ± dp/dt_{max} and increased LVEDP in rats in comparison with the control group ($P < 0.01$, $P < 0.01$, $P < 0.01$) (**Table 2**). The results indicated the dysfunction of left ventricle systolic and diastolic. To this point, the CHF model in rats had been successfully prepared.

Role of SAL on Cardiac Function

Next, the effects of SAL on DOX-induced CHF were evaluated by measurements of cardiac function, including LVSP, LVEDP, and ± dp/dt_{max}. As shown in **Figure 3**, the hemodynamic parameters of LVSP and ± dp/dt_{max} were markedly decreased in DOX-treated rats compared with the control group ($P < 0.01$, $P < 0.01$), which indicated left ventricle systolic and diastolic dysfunction.

TABLE 2 | DOX-induced myocardial injury in rats.

Group	n	LVSP (mmHg)	LVEDP (mmHg)	+dp/dt$_{max}$ (mmHg/s)	–dp/dt$_{max}$ (mmHg/s)
Control	3	121.65 ± 8.90	7.68 ± 0.94	5,865.51 ± 768.36	–5,040.13 ± 409.85
DOX	3	74.69 ± 8.80**	56.14 ± 8.11**	1,729.74 ± 158.23**	–1,524.40 ± 210.73**

*Data are presented as mean ± SD; n = 3 per group. **P < 0.01 versus control group. DOX, doxorubicin; LVSP, left ventricular systolic pressure; LVEDP, left ventricle end diastolic pressure.*

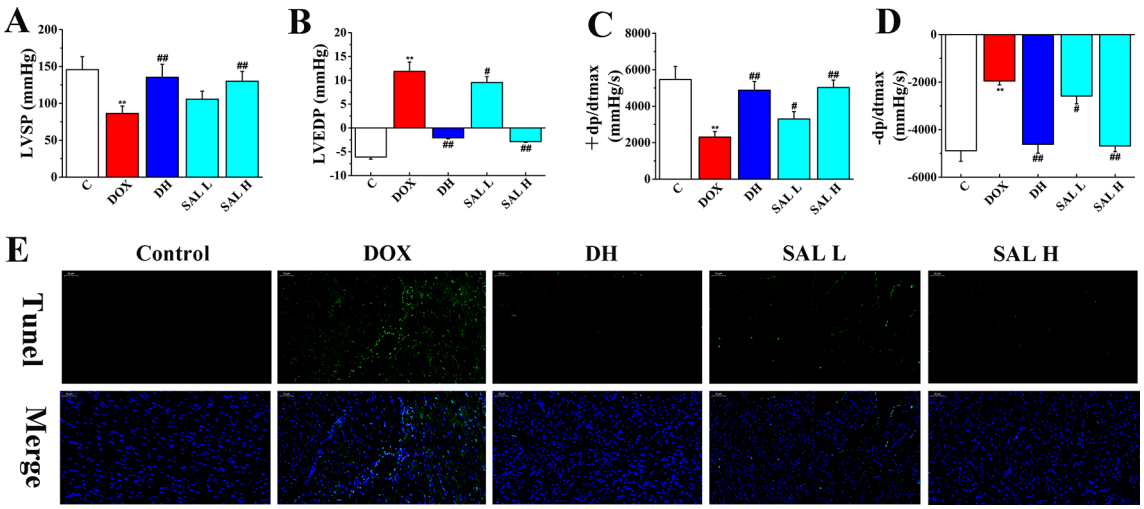

FIGURE 3 | Therapeutic effect of SAL on DOX-induced CHF in rats. **(A)** LVSP, **(B)** LVEDP, **(C)** +LV dp/dt$_{max}$, and **(D)** –LV dp/dt$_{max}$ were determined by multi-channel physiological signal acquisition and processing system. **(E)** TUNEL stain of heart tissue. $^{**}P < 0.01$ versus control group; $^{\#}P < 0.05$, $^{\#\#}P < 0.01$ versus DOX group. Data are presented as mean ± SD ($n = 6$). SAL, salsolinol; DOX, doxorubicin; CHF, chronic heart failure; LVSP, left ventricular systolic pressure; LVEDP, left ventricle end diastolic pressure.

However, DH efficiently increased the hemodynamic parameters of LVSP and ± dp/dt$_{max}$ and decreased LVEDP ($P < 0.01$, $P < 0.01$, $P < 0.01$). Similarly, the levels of LVSP and ± dp/dt$_{max}$ in rats with 5 and 10 mg/kg of SAL significantly increased, and 10 mg/kg of SAL was almost equal to that of DH, indicating the enhancement effect of SAL on heart function.

To have sufficient evidence to show cardiac cell damage and its recovery, TUNEL staining was used to examine the cytotoxicity and visually present the effect of SAL on cardiac apoptosis induced by DOX. As shown in **Figure 3E**, the ratio of TUNEL positive myocardial cells was significantly increased in DOX-treatment group, indicating vast apoptosis of myocardial cytotoxicity and the ratio of TUNEL positive myocardial cells. Contrastively, SAL had an effect on alleviating the cardiomyocyte from apoptosis especially in SAL high-dose group, which indicated the anti-apoptotic activity of SAL. These results indicated that 10 mg/kg of SAL continuously and significantly protected heart tissues from CHF.

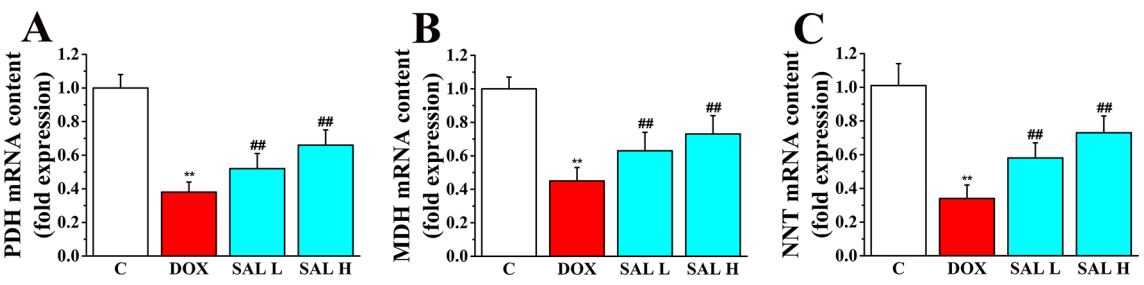

FIGURE 4 | Effects of SAL on the key enzymes of the TAC. Rats were treated with different doses of SAL. The following three enzymes in the cardiac tissue were assayed: **(A)** PDH, **(B)** MDH, and **(C)** NNT ($n = 6$ per group). $^{**}P < 0.01$ versus control group; $^{\#\#}P < 0.01$ versus DOX group. All data are presented as mean ± SD. SAL, salsolinol; TAC, tricarboxylic acid cycle; PDH, pyruvate dehydrogenase; MDH, malate dehydrogenase; NNT, nicotinamide nucleotide transhydrogenase; DOX, doxorubicin.

Therapeutic Effects of SAL on DOX-Induced CHF Rats

As shown in **Table 3**, rats given DOX displayed remarkable increases in the BNP and LDH levels ($P < 0.01$, $P < 0.01$). Conversely, the serum levels of these two indexes were significantly reduced when rats were treated with DH. The effect of 10 mg/kg of SAL was almost equal to that of DH. In addition, the level of LDH but not that of BNP was also altered by 5 mg/kg of SAL ($P < 0.05$, $P > 0.05$). In addition, the serum levels of renin, Ang-II, and ALD were markedly enhanced in DOX-treated rats compared with the control group ($P < 0.01$, $P < 0.01$, $P < 0.01$). DH (50 μg/kg) efficiently decreased the serum levels of renin, Ang-II, and ALD. Similarly, the levels of renin, Ang-II, and ALD in rats with 5 and 10 mg/kg of SAL significantly decreased ($P < 0.05$, $P < 0.01$).

Relative mRNA Expression of Key Enzymes in the TAC

Research has shown that stimulation of the activity of key enzymes in TAC, including PDH, MDH, and NNT, leads to the promotion of regeneration of NADH and NADPH, enhances ATP synthesis in mitochondrial energy metabolism, and maintains the stability of mitochondrial environment (Zhang et al., 2017; Wen et al., 2019). Thus, the three key enzymes in the cardiac tissue were assessed by RT-PCR to evaluate the potential mechanism of SAL on the mitochondrial energy metabolism. As shown in **Figure 4**, the relative mRNA levels of PDH, MDH, and NNT decreased significantly in DOX group ($P < 0.01$, $P < 0.01$, and $P < 0.01$, respectively) (**Figures 4A–C**). Conversely, SAL could significantly increase the mRNA levels of PDH, MDH, and NNT in the cardiac tissue ($P < 0.01$, $P < 0.01$, and $P < 0.01$, respectively).

SAL Suppressed DOX-Induced Cardiomyocyte Death in Cultured H9c2 Cells

Cell viability of H9c2 cardiomyocytes was detected using CCK-8 kit to determine the optimum concentrations of SAL for protecting H9c2 cells against DOX-induced cytotoxicity. The results showed that SAL treatment for 24 h potently suppressed cell viability in a concentration-dependent manner with the increased concentrations (0, 5, 10, 20, 40, and 80 μM), among which SAL in the concentrations of 40 and 80 μM could significantly inhibit the cell viability compared with the control groups ($P < 0.05$, $P < 0.01$) (**Figure 5A**). Thus, the optimal concentration was not more than 40 μM. Then, H9c2 cells were pretreated with different concentration of SAL (0, 5, 10, and 20 μM) for 2 h. Cell viability was significantly decreased to 56.85 ± 3.06% ($P < 0.01$) when treated with 5 μM of DOX, compared with the control group. Cell viability of H9c2 cells was dramatically increased to 65.59 ± 4.04%, 72.80 ± 3.82%, and 81.12 ± 5.64% ($P < 0.05$, $P < 0.01$, $P < 0.01$) (**Figure 5B**), respectively, when

TABLE 3 | Effects of SAL on serum BNP, LDH, renin, Ang-II, and ALD.

Group	n	BNP (ng/L)	LDH (ng/L)	Renin (pg/ml)	Ang-II (pg/ml)	ALD (pg/ml)
Control	6	55.66 ± 10.44	22.19 ± 5.29	57.77 ± 2.52	538.00 ± 52.84	118.79 ± 15.35
DOX	6	122.50 ± 18.98**	43.38 ± 6.01**	143.32 ± 17.15**	1,056.33 ± 94.49**	196.64 ± 33.29**
DH	6	63.81 ± 10.30##	28.49 ± 3.83##	66.14 ± 3.39##	615.50 ± 131.75##	128.99 ± 18.97##
SAL 5 mg/kg	6	113.99 ± 17.46	39.22 ± 5.69#	127.45 ± 14.28##	943.83 ± 100.00#	172.96 ± 15.63#
SAL 10 mg/kg	6	71.13 ± 11.79##	35.11 ± 4.16##	74.39 ± 9.03##	721.33 ± 130.66##	154.21 ± 32.61##

*Data are expressed as mean ± SD. **P < 0.01 compared with control group; #P < 0.05, ##P < 0.01 compared with DOX group. SAL, salsolinol; BNP, brain natriuretic peptide; LDH, lactate dehydrogenase; Ang-II, angiotensin-II; ALD, aldosterone; DOX, doxorubicin; DH, dobutamine hydrochloride.*

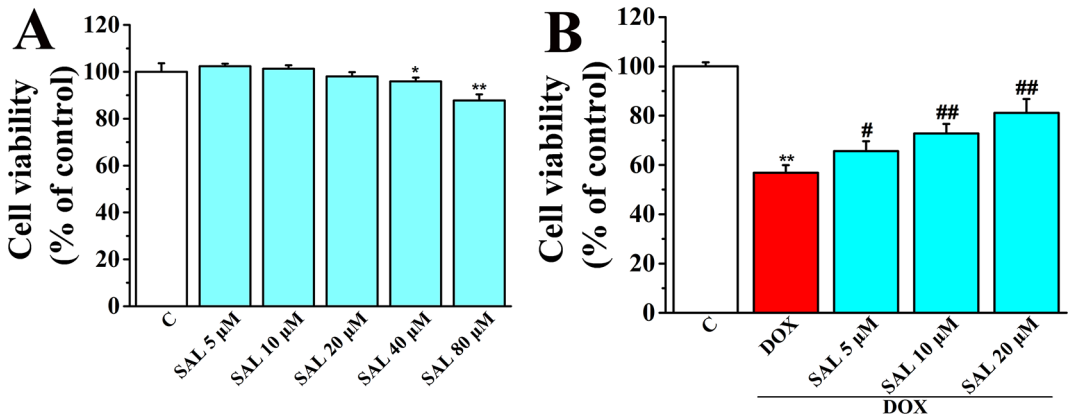

FIGURE 5 | Effect of SAL on cell viability of H9c2 cells in the absence and presence of DOX. **(A)** Cell viability of H9c2 cells in the absence of DOX. **(B)** Cell viability of H9c2 cells in the presence of DOX. *$P < 0.05$, **$P < 0.01$ versus control group, #$P < 0.05$, ##$P < 0.01$ versus DOX group ($n = 6$). Results were expressed as percentages of the control group. Data are shown as mean ± SD ($n = 6$). SAL, salsolinol; DOX, doxorubicin.

pretreated with 5, 10, and 20 μM SAL, compared with the DOX group. The results indicated that SAL could remarkably promote cell viability in a concentration-dependent manner in H9c2 cells, and 20 μM of SAL showed a relatively good protective effect. Therefore, 20 μM of SAL was used in this study to investigate the protective effect of SAL on H9c2 cardiomyocyte injury induced by DOX.

Effect of SAL on Nuclear Morphology and Cell Proliferation of H9c2 Cells

To more directly present the effect of SAL on cell morphological influence, high-content live-cell imaging assays were used to qualitatively and quantitatively assay cell count, morphology, and cell viability of H9c2 cells. Among them, nucleus staining (blue fluorescence), cell cytoplasm labeling (green fluorescence), and dead cells (red fluorescence) were marked by Hoechst 33342, calcein AM, and EthD-1, respectively. In the absence of the DOX group, including a control group and different concentrations of SAL, H9c2 cells possessed a homogenous Hoechst and calcein AM fluorescence in the nucleus and cytoplasm. However, there were alterations in morphological after treating cells with 5 μM of DOX, compared with the control group. Fortunately, SAL could mitigate H9c2 cells from cytotoxicity regarding morphological alterations, especially 20 μM (**Figure 6A**). As for cell count, it was significantly decreased after treated with DOX for 24 h ($P < 0.01$), compared with the control group. The reduction rate of cell number in the SAL group, compared with the model group, had significantly decreased ($P < 0.01$) (**Figure 6B**). In addition, the green fluorescence of the model group, compared with the control group, was significantly reduced ($P < 0.01$), and red fluorescence was significantly increased ($P < 0.01$), suggesting the decrease of live cells and increase of dead cells. SAL could certainly increase the green fluorescence and decrease the red fluorescence of H9c2 cells ($P < 0.01$) (**Figures 6C**, **D**). These results suggested that SAL could significantly ameliorate nuclear morphology and cell proliferation in DOX-induced cardiomyocyte injury and cytotoxicity in H9c2 cells.

Effects of SAL on DOX-Induced MMP Reduction on H9c2 Cells

To investigate the effects of SAL on mitochondrial functions of H9c2 cells, MMP was measured by HCS assay. As shown in **Figure 7**, fluorescent images of H9c2 cells stained with TMRE

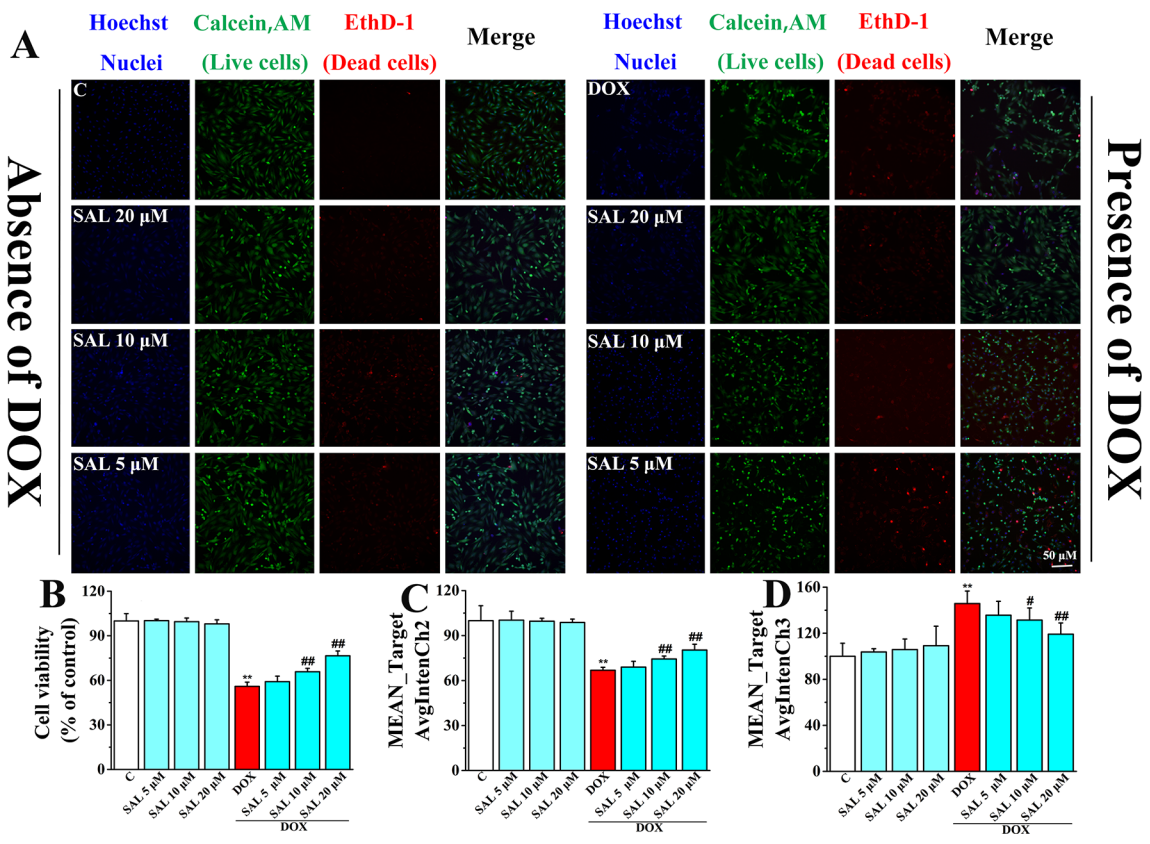

FIGURE 6 | Representative photomicrographs and summary data for HCS image analysis of H9c2 cells. **(A)** Representative photomicrographs for HCS analysis of H9c2 cells; scale bar = 50 μm. **(B)** Valid cell count for HCS analysis of H9c2 cells (% of control). **(C)** Live cell count (MEAN_TargetAvgIntenCh2). **(D)** Dead cells count (MEAN_TargetAvgIntenCh3). $^{*}P < 0.05$, $^{**}P < 0.01$ versus control group, $^{\#}P < 0.05$, $^{\#\#}P < 0.01$ versus DOX group. Results are expressed as percentages of control group. Data are shown as mean ± SD ($n = 6$). HCS, high-content screening; SAL, salsolinol; DOX, doxorubicin; EthD-1, ethidium homodimer-1.

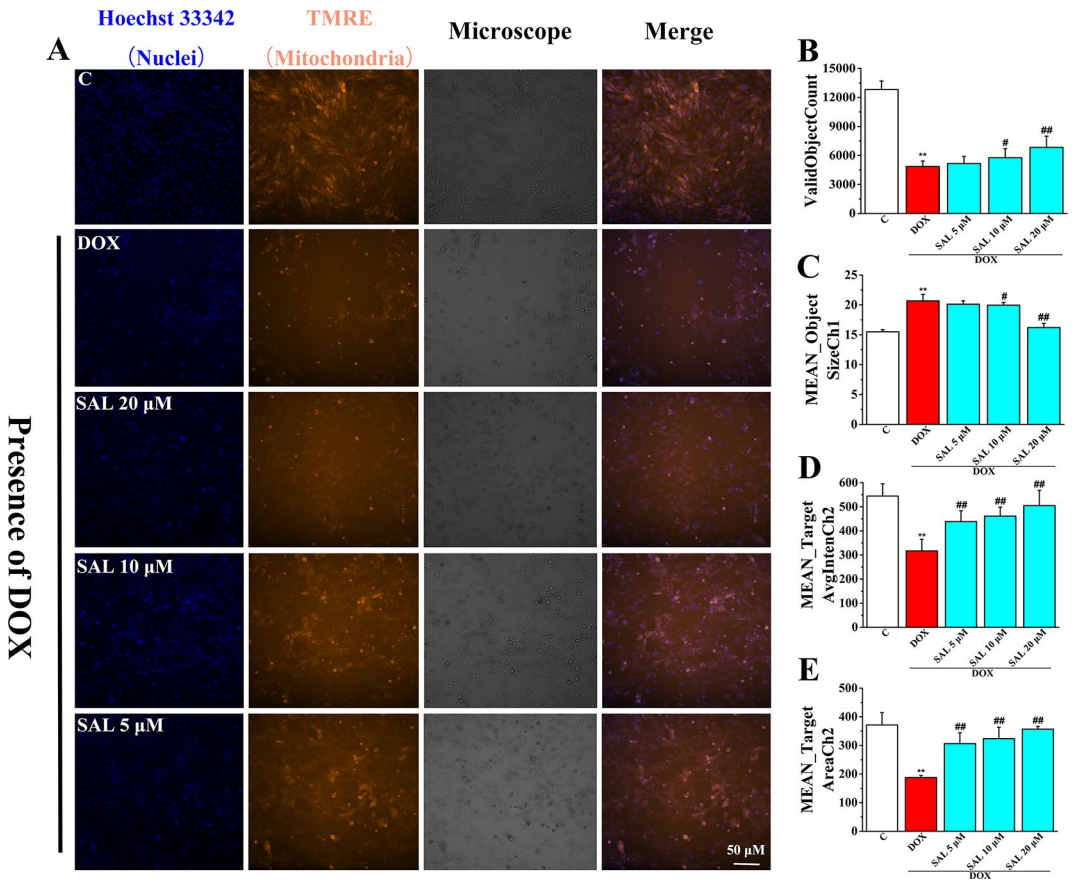

FIGURE 7 | Representative images and corresponding numerical data for some typical cytotoxic effects of SAL on H9c2 cells nuclei and mitochondria. **(A)** Representative photomicrographs and summary data for TMRE staining of H9c2 cells. Scale bar = 50 μm. **(B)** Effect of different drugs on valid object cell count of H9c2 cells. **(C)** Effect of different drugs on nuclear size of H9c2 cells (MEAN_ObjectSizeCh1). **(D)** Effect of different drugs on average brightness of functional mitochondrial mass (MEAN_TargetAvgIntenCh2). **(E)** Effect of different drugs on projected area occupied by functioning mitochondrial mass (MEAN_TargetAreaCh2). $^{**}P < 0.01$ versus control group, $^{\#}P < 0.05$, $^{\#\#}P < 0.01$ versus DOX group. All data are presented as mean ± SD ($n = 6$). SAL, salsolinol; DOX, doxorubicin.

showed that cells emitted red–orange fluorescence in the control group, suggesting that MMP stayed in a normal state. The fluorescence intensity of TMRE decreased significantly in the DOX group, compared with the control group, suggesting that DOX caused the decrease of MMP (**Figure 7A**). That is, DOX may have caused the opening of mitochondrial permeability transition pore. Conversely, pretreatment with SAL could significantly enhance the intensity of the orange–red fluorescence decreased by DOX. Moreover, we also found that cells treated with SAL increased DOX-induced decrease in cell count (ValidObjectCount) (**Figure 7B**), average brightness of functional mitochondrial mass (Mean_TargetAvgIntenCh2) (**Figure 7D**), and the projected area occupied by functioning mitochondrial mass (Mean_TargetAreaCh2) (**Figure 7E**). Simultaneously, SAL decreased nuclear size (Mean_ObjectSizeCh1) than did the DOX group (**Figure 7C**). These results suggested that DOX caused the decrease of MMP and TMRE brightness but increased nuclear size, indicating mitochondrial depolarization or a mitochondrial structural change. Thus, SAL may reduce DOX-induced mitochondrial dysfunction by affecting MMP.

SAL Promoted Mitochondrial Respiratory Function and Energy Metabolism

To assess whether the observed toxicity of DOX was correlated with mitochondrial respiration function, Seahorse XFp analyzer was used to determine the value of OCR and ECAR in H9c2 cells. The results indicated that treatment with DOX for 24 h specifically impaired both OCR and ECAR (**Figures 8A**, **B**). Interestingly, baseline OCR (**Figure 8C**), baseline ECAR (**Figure 8D**), stressed OCR (**Figure 8E**), and stressed ECAR (**Figure 8F**) were significantly promoted in H9c2 cells when pretreated with 20 μM of SAL, compared with the DOX group, for 2 h ($P < 0.01$, $P < 0.01$, $P < 0.01$, and $P < 0.01$). These results demonstrated that DOX treatment causes mitochondrial dysfunction and that pretreatment of SAL could partially prevent these effects.

To further understand the mechanism responsible for the protective effects of SAL, mitochondrial respiratory function and energy metabolism in H9c2 cells were measured using the Agilent Seahorse XFp Cell Mito Stress Test. Cells were treated with SAL (20 μM) for 2 h before DOX treatment. As expected, mitochondrial oxidative phosphorylation, as measured by OCR, was reduced in the DOX group compared with the

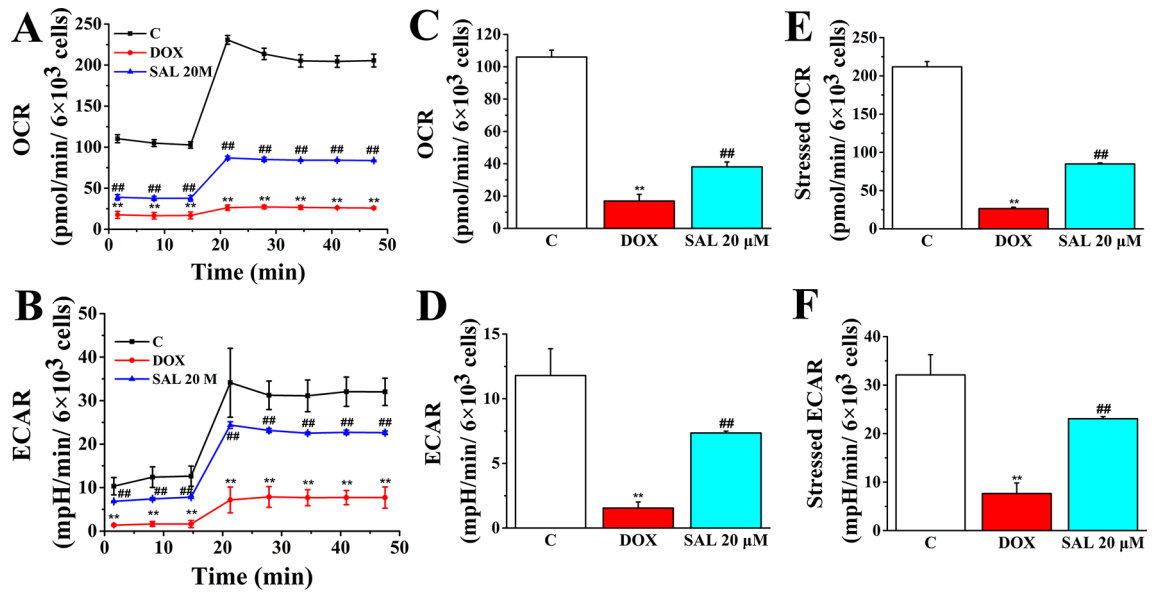

FIGURE 8 | Pretreatment with SAL could attenuate the inhibition effect of DOX in mitochondrial respiration. Mitochondrial respiration was measured by a Seahorse XFp apparatus detecting the basal OCR and ECAR. **(A)** OCR. **(B)** ECAR. **(C)** Baseline OCR. **(D)** Baseline ECAR. **(E)** Stressed OCR. **(F)** Stressed ECAR. $^{**}P < 0.01$, versus control group; $^{\#\#}P < 0.01$, versus DOX group. All data are presented as mean ± SD ($n = 3$). SAL, salsolinol; DOX, doxorubicin; OCR, oxygen consumption rate; ECAR, extracellular acidification rate.

control group. Impressively, OCR was significantly higher in the SAL group (**Figure 9**). Simultaneously, we observed that DOX could significantly decrease the basal respiration ($P < 0.01$) (**Figure 9B**), maximal respiration ($P < 0.01$) (**Figure 9C**), ATP production ($P < 0.01$) (**Figure 9D**), proton leak levels (**Figure 9E**), and spare respiratory capacity ($P < 0.01$) (**Figure 9F**) in H9c2 cells compared with control group. Notably, SAL could partially prevent these effects and significantly elevate basal respiration ($P < 0.01$) (**Figure 9B**), maximal respiration ($P < 0.01$) (**Figure 9C**), and proton leak (**Figure 9E**) levels, which were inhibited by DOX. In addition, SAL could significantly enhance ATP production ($P < 0.05$) (**Figure 9D**). The effects of

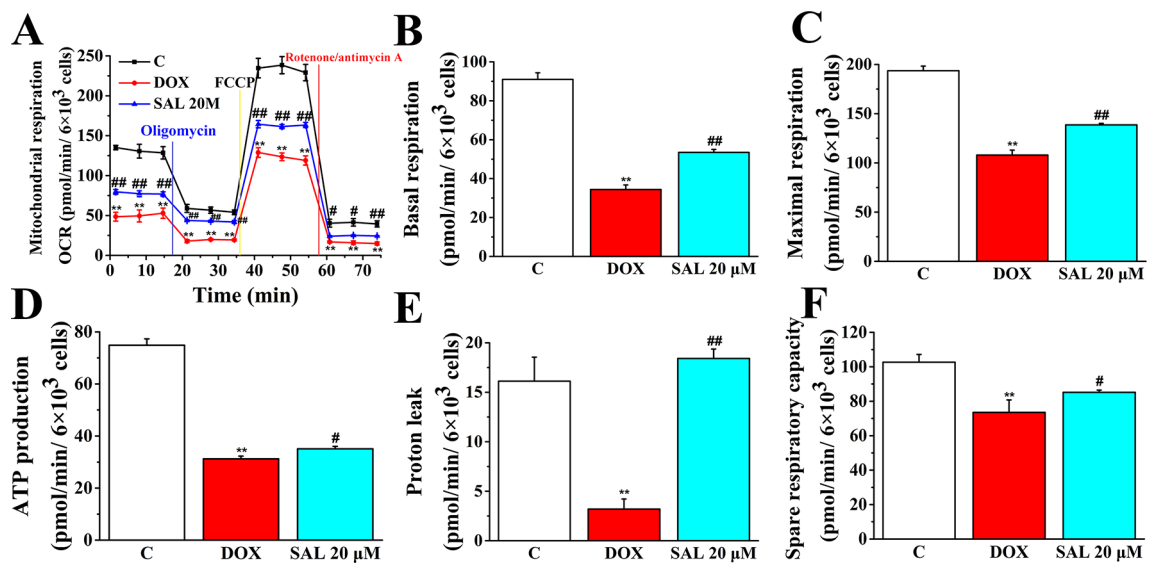

FIGURE 9 | SAL rescues mitochondrial respiration and energy metabolism in DOX-treated H9c2 cells. During testing, H9c2 cells were treated with 10 μM of oligomycin, 10 μM of FCCP, and 5 μM of rotenone/antimycin A. **(A)** OCR, **(B)** basal respiration, **(C)** maximal respiration, **(D)** ATP production, **(E)** proton leak, and **(F)** spare respiratory capacity were assessed using a Seahorse Bioscience XFp analyzer. $^{**}P < 0.01$ versus control group. $^{\#}P < 0.05$; $^{\#\#}P < 0.01$ versus DOX group. All data are presented as mean ± SD ($n = 3$). SAL, salsolinol; DOX, doxorubicin; FCCP, carbonyl cyanide-4-(trifluoromethoxy)phenylhydrazone; OCR, oxygen consumption rate; ECAR, extracellular acidification rate.

SAL on respiration were also reflected in the spare respiratory capacity of the mitochondria, as SAL increased spare oxidative capacity and attenuated the inhibition of spare capacity by DOX treatment ($P < 0.05$) (**Figure 9F**). These results support the finding that the potential protective effects of SAL against DOX-induced mitochondrial dysfunction in H9c2 cells may be related to the promotion of ATP production.

The rate of oxidation of each fuel (glutamine, glucose, and fatty acids) was determined by measuring OCR of H9c2 cells in the presence or absence of corresponding fuel pathway inhibitors. By blocking fatty acid metabolism with etomoxir (carnitine palmitoyltransferase-I inhibitor of fatty acid mitochondrial import) and subsequent inhibiting the glucose and glutamine pathways with UK5099 and BPTES, respectively, we found that DOX-treated H9c2 cells, compared with control groups, have a decreased OCR and dependency on fatty acids, while SAL-treated groups have an increased OCR and dependency to maintain baseline respiration (**Figures 10A**, **C**). In addition, by first inhibiting the glucose and glutamine pathway followed by blocking fatty acid metabolism, H9c2 cells show an increased capacity of fatty acid utilization to meet energy demand when other fuel pathways are inhibited (**Figures 10B**, **D**). This indicates that compared with blocking fatty acid first, H9c2 cells are able to maintain higher levels of ATP when energy production is primarily fatty acid dependent. There are still significant decreases in terms of flexibility of fatty acid in the DOX group ($P < 0.01$). Significant increase differences are observed in the flexibility of fatty acid oxidation in the SAL group ($P < 0.01$) (**Figure 10E**).

Relative Expression of MCU mRNA, MICU1 mRNA, and MICU2 mRNA in H9c2 Cells

Given that MCU can transfer Ca^{2+} from cytoplasm to mitochondrial matrix and controls its rate by electrochemical gradient, which has great significance in intracellular Ca^{2+} signal transduction, Ca^{2+} homeostasis, and mitochondrial energy metabolism (O'Brien et al., 2006), we next asked whether SAL could promote mitochondrial energy metabolism of H9c2 cells *via* regulating mRNA expression of MCU and its regulatory mRNA and whether the pharmacological inhibition of MCU could affect the effects of SAL. To this end, MCU inhibitor ruthenium red and MCU activator spermine were pretreated, and the expression of metabolism-related genes including MCU, MICU1, and MICU2 were determined by RT-PCR. Although the gene types of energy metabolism varied somewhat, all conditions showed similar results that DOX increased expression of MCU and its regulatory mRNA to values in H9c2 cells ($P < 0.01$). Furthermore, pretreatment with the MCU inhibitor ruthenium red (10 μM) following SAL (20 μM) resulted in lower expression of MCU, MICU1, and MICU2, but pretreatment with the MCU activator spermine (20 μM) following SAL (20 μM) resulted in higher expression in these genes (**Figure 11**).

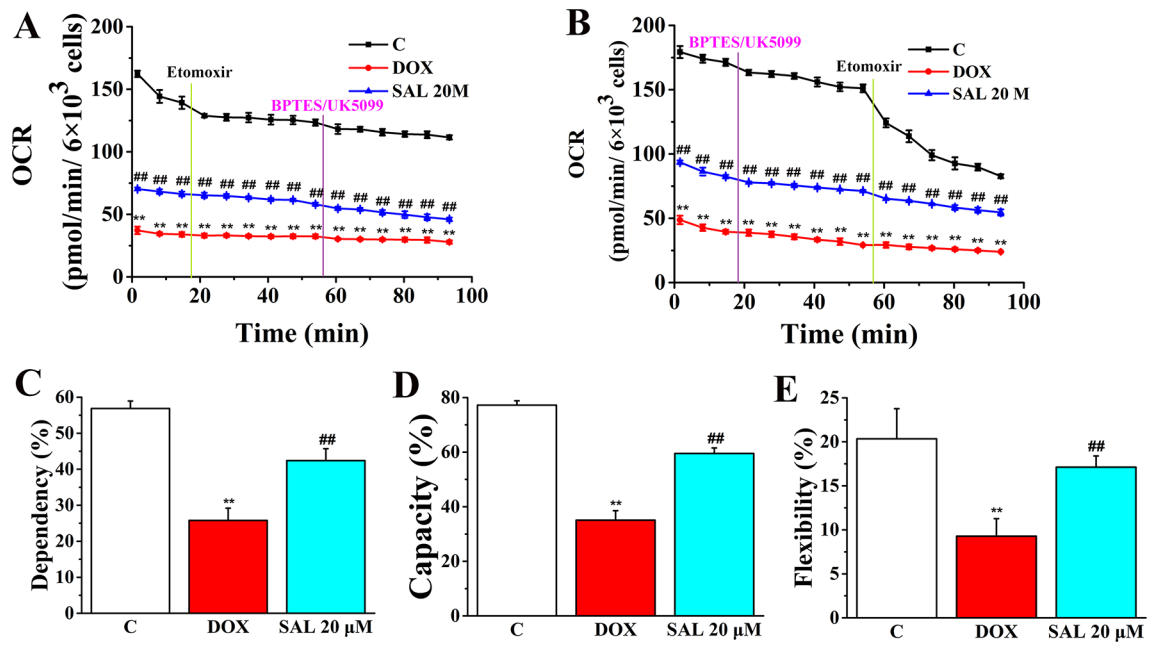

FIGURE 10 | SAL ameliorates H9c2 cells from DOX-induced decrease on mitochondrial fuel flex. Mitochondrial substrate analysis was determined. During testing, H9c2 cells were treated with 4 μM of etomoxir and 3 μM of BPTES/2 μM of UK5099 in succession. **(A)** Effects of SAL on fuel dependency in terms of the fatty acid oxidation pathway. **(B)** Effects of SAL on fuel capacity in terms of fatty acid oxidation pathway and oxidation rates of fatty acids expressed in dependency **(C)**, capacity **(D)**, and flexibility **(E)** to maintain baseline OCR levels determined with the Seahorse XFp respirometer. $^{**}P < 0.01$ versus control group. $^{\#\#}P < 0.01$ versus DOX group. All data are presented as mean ± SD ($n = 3$). SAL, salsolinol; DOX, doxorubicin; OCR, oxygen consumption rate.

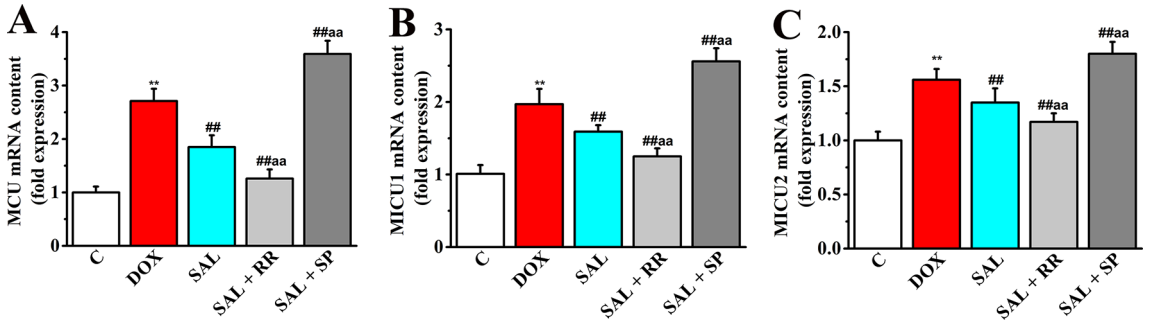

FIGURE 11 | Effects of SAL on the mRNA expression levels of MCU, MICU1, and MICU2 in H9c2 cells. The mRNA expression levels of MCU **(A)**, MICU1 **(B)**, and MICU2 **(C)** were detected by RT-PCR in different groups. $^{**}P < 0.01$ versus control group. $^{\#\#}P < 0.01$ versus DOX group. $^{aa}P < 0.01$ versus SAL group. All data are presented as mean ± SD ($n = 3$). SAL, salsolinol; DOX, doxorubicin; MCU, mitochondrial calcium uniporter; MICU1, mitochondrial calcium uptake 1; MICU2, mitochondrial calcium uptake 2; RT-PCR, reverse transcription–polymerase chain reaction.

Protein Expression of MCU, MICU1, and MICU2 in H9c2 Cells

To further confirm our speculation that MCU plays an important role in the energy metabolism-related signaling pathway in H9c2 cells, the protein expression of MCU and its regulatory protein, MICU1, and MICU2 in different groups with or without MCU inhibitors ruthenium red (10 μM) or MCU activator spermine (20 μM) were detected. The DOX group showed increased levels of MCU, MICU1 protein, and MICU2 protein compared with expression levels in the control group (**Figure 12**), consistent with the expression of mRNA. However, SAL treatment can significantly decrease these protein expressions. Conversely, the enhancement could be inhibited by MCU inhibitor ruthenium red. Interestingly, we found that in addition to MCU, the expressions of MICU1 and MICU2 were also decreased in the MCU inhibitors group

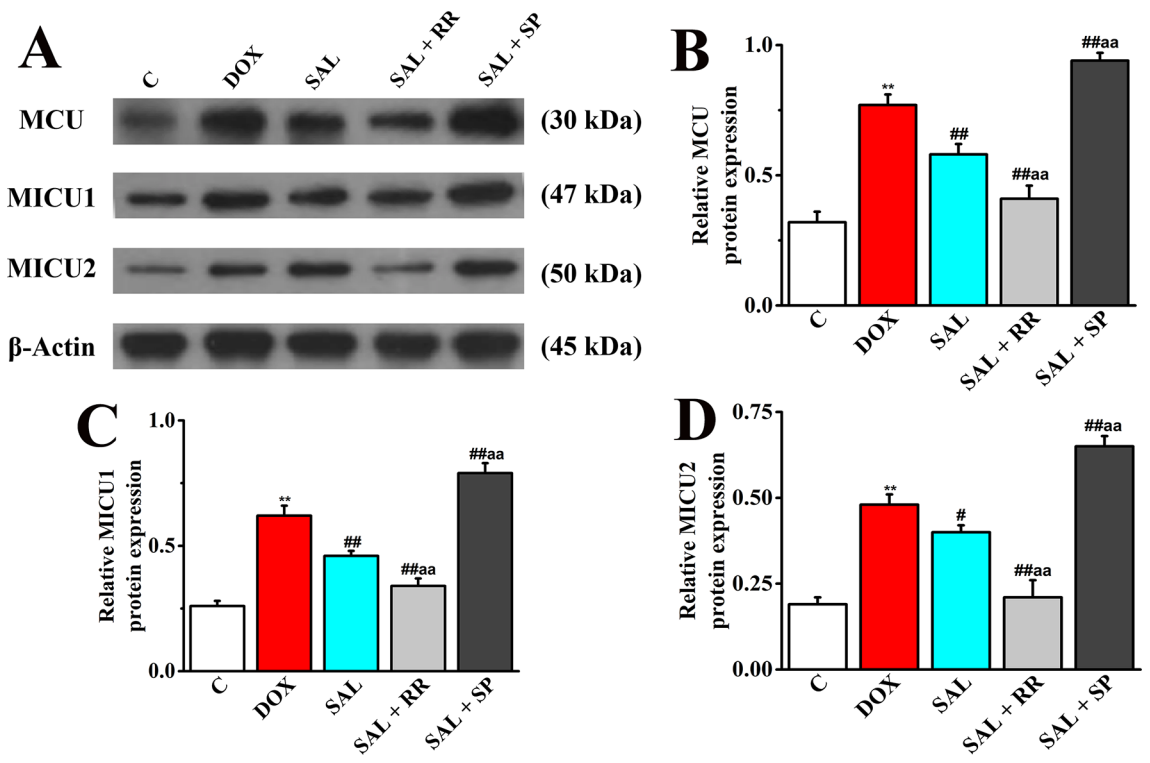

FIGURE 12 | Effects of SAL on the protein expression levels of MCU, MICU1, and MICU2, in H9c2 cells. **(A)** The Western blot images of MCU, MICU1, and MICU2. **(B)** Relative MCU protein level in H9c2 cells. **(C)** Relative MICU1 protein level in H9c2 cells. **(D)** Relative MICU2 protein level in H9c2 cells. $^{**}P < 0.01$ versus control group; $^{\#}P < 0.05$; $^{\#\#}P < 0.01$ versus DOX group. $^{aa}P < 0.01$ versus SAL group. All data are presented as mean ± SD ($n = 3$). SAL, salsolinol; MCU, mitochondrial calcium uniporter; MICU1, mitochondrial calcium uptake 1; MICU2, mitochondrial calcium uptake 2.

but increased in the MCU activator spermine group. This phenomenon provided further evidence that SAL may relieve H9c2 cells from DOX-induced cardiomyocyte injury *via* the downregulation of MCU activity.

DISCUSSION

The present study had provided the pharmacodynamics and mechanism evidence that SAL treatment attenuated the DOX-induced cardiac dysfunction *in vivo*, as well as mitochondrial respiratory function injury and energy metabolism dysfunction *in vitro*. Based on the positive inotropic and energy metabolism effects, these results suggested that SAL may be the active components of *Fuzi* in treatment CHF. To the best of our knowledge, this is the first report describing how SAL protects against DOX-induced CHF *in vivo* and *in vitro*.

DOX, also known as adriamycin, is widely used as one of the most effective anti-cancer therapeutics known to suppress mitochondrial function leading to mitochondrial toxicity. Thus, the clinical application of DOX is limited by these irreversible and cumulative side effects (Baughman et al., 2011). Currently, excessive mechanisms have been proposed to account for DOX-induced cardiotoxicities, such as cardiac energy homeostasis, intracellular calcium disturbance, oxidative stress, dysregulation of metabolites, inflammation, and apoptosis of cardiomyocytes (Jones et al., 2004; Cui et al., 2017). In addition, DOX is known to inhibit mitochondrial function and induce mitochondrial energy metabolism disorder in cardiomyocytes (Guo et al., 2018), which can lead to a dose-dependent, cumulative, and permanent degenerative cardiomyopathy (Hakuno et al., 2013; Hosseini et al., 2017). Although the relationship among the events of DOX-induced cytotoxicity, mitochondrial respiratory function injury, and energy metabolism disorder is not well defined, which can induce injury in cardiomyocyte function *in vitro*. Thus, DOX was used to establish a cardiomyocyte mitochondrial metabolism injury model. In the present study, the ability of SAL to increase cell viability, mitochondrial OCR and ECAR, basal respiration and maximal respiration, and ATP production may contribute to the protective role of reducing H9c2 cardiomyocyte mitochondrial energy metabolism disorder and respiratory function injury from DOX injury. Research also explains drugs that not only promote mitochondrial energy metabolism but also partially prevent the cell from DOX-induced mitochondrial function, which will benefit a lot in terms of cell metabolism and capacity of ATP production.

ALRP is a potent traditional herbal medicine extensively used in the treatment of cardiovascular diseases in many Asian countries (Yang et al., 2018). For several decades, researchers had paid more attention to investigate the cardioactive components of ALRP and verified the definite cardiac effects of ALRP (Liu et al., 2012; Zhou and Liu, 2013). Regarding the bidirectional effect of ALRP on cardiotoxicity and cardioprotection, researchers had found that the toxic component of ALRP is diester-type diterpene ester-soluble alkaloids represented by aconitine, and the cardiovascular active substance is heat-resistant water-soluble components (Yang et al., 2018). Among the cardioprotective components, SAL, a product of nonenzymatic condensation of dopamine and acetaldehyde, produces a dose-dependent positive chronotropic effect on the rat isolated perfused heart (Liu et al., 2012). Thus, SAL plays an important role in regulating heart performance. In addition, it is valued for playing a role in the biosynthesis of catecholamines in the body (Sokolova et al., 1990). SAL can be produced in the body and inhibits the activity of catechol-*O*-methyltransferase, which itself methylates the free hydroxy group under the action of the enzyme, thereby changing the metabolic rate of catecholamines such as dopamine *in vivo* (Melchior, 1979). Experiments have shown that SAL is a weak beta-adrenergic stimulant that excites the guinea pig's isolated atrium and increases the frequency of contraction and blood pressure in normal and ruined spinal cord rats and demonstrates excitatory effects on both β- and γα-adrenergic bodies (Melis et al., 2015). Although Chen and Liang (1982) isolated this compound from aconite in 1979, the cardiotonic effect of SAL is still not comprehensively evaluated and confirmed in current studies.

To investigate the therapeutic effects of SAL, Sprague-Dawley rats were intraperitoneally injected with DOX to induce CHF model. Then, hemodynamic indexes were performed to evaluate cardiac function in rats. Our results showed that the values of $\pm$ dp/dt_{max} in model groups were reduced to 50% those of the control group, indicating the CHF model was successfully prepared. Next, SAL was intraperitoneally administered to investigate whether it could produce a therapeutic effect on DOX-induced CHF. The results showed that compared with the DOX group, SAL could significantly improve heart function, reducing levels of myocardial injury markers and relieving cardiomyocyte apoptosis. Recent researches (Francesco et al., 2017; Ichiki et al., 2017; Vecchis and Ariano, 2018) have shown that RAAS plays a key role in CHF treatment. Therefore, serum levels of renin, Ang-II, and ALD were measured in this study. The serum levels of renin, Ang-II, and ALD in SAL group, compared with the model group, were decreased significantly, suggesting that SAL might play therapeutic effects by regulating the activity of RAAS to treat CHF *in vivo*. In addition, CCK-8 assay was used to assess the cell viability *in vitro*. The results indicated that SAL, compared with the control groups, could significantly inhibit the cell viability (more than 40 μM). Finally, 20, 10, and 5 μM of SAL was selected for the subsequent optimal concentration for further study. To directly demonstrate the protective effects of SAL on cell viability, HCS was used to qualitatively and quantitatively determine cell number, morphology, and cell viability of H9c2 cells. The results directly revealed that DOX, compared with the control group, could significantly increase the myocardial cell death, decrease the calcein AM fluorescence intensity, and increase the intensity of EthD-1 fluorescence. However, compared with the DOX group, SAL could reduce DOX-induced cardiomyocyte injury and cytotoxicity in varying degrees. Because MMP is a basic

prerequisite for maintaining oxidative phosphorylation of mitochondria to produce ATP, and the stability of MMP is conducive to maintaining the normal physiological function of cells (Jayaraman, 2005), the protective effects of SAL on MMP of H9c2 cells were identified by the use of TMRE and were detected by HCS. The results showed that SAL may reduce DOX-induced mitochondrial dysfunction by affecting MMP. Thus, the potential mechanism of SAL promoting cardiomyocyte energy metabolism may be related to affecting MMP *in vitro*.

As the ATP production of mitochondrial played a pivotal role in maintaining the energy supply of cardiomyocytes and DOX could cause myocardial cell energy metabolism disorders (Pillai et al., 2010), we investigated whether SAL plays an important role in DOX-induced ATP production deficiency in H9c2 cells. The cell energy phenotype was performed to measure the metabolic phenotypes and metabolic potential of H9c2 cells. In addition, the cell mitochondrial stress was implemented to measure mitochondrial respiration function. The cell mitochondrial fuel flex test was used to determine the oxidation rate of fatty acid by measuring mitochondrial respiration of H9c2 cells in the presence or absence of fatty acid pathway inhibitors, etomoxir. Our results identified new agents to the prevention of DOX-induced cardiomyocyte injury. The results showed that treatment with SAL attenuated the energy metabolism disorder and mitochondrial dysfunction in DOX-treated H9c2 cells in terms of baseline OCR, baseline ECAR, stressed OCR and stressed ECAR, and mitochondrial respiratory function reflected in basal respiration, maximal respiration, ATP production, and H^+ (proton) leak. Also, our results indicate that H9c2 cells' fatty acid mitochondrial fuel usage is decreased as a result of DOX treatment compared with control group and significantly increased OCR, dependency, capacity, and flexibility of fatty acids as observed for SAL in H9c2 cells compared with the DOX group. The results suggested that SAL could be a new therapeutic agent to ameliorate DOX-induced cardiomyocyte injury and, furthermore, for the treatment of HF.

To extend our results to cell energy metabolism signaling, potential mechanisms of SAL responsible for the mitochondrial respiration function and mitochondrial energy metabolism were investigated. Mitochondrial Ca^{2+} uptake plays a pivotal role both in cell energy balance and in cell fate determination (Cristina et al., 2017). Cardiac contractility is mediated by a variable flux in intracellular calcium Ca^{2+}, thought to be integrated into mitochondria *via* the MCU channel to match energetic demand. The MCU mediates high-capacity mitochondrial calcium uptake that stimulates energy production (Luongo et al., 2015). Recently, the identification of MCU and associated regulators has allowed the characterization of new physiological roles for calcium in both mitochondrial and cellular homeostasis in cytoskeletal remodeling through the modulation of ATP production (Nichols et al., 2018). In the present study, downregulation of MCU mRNA and protein expression markedly enhanced the generation of ATP decreased by DOX *in vitro*. It is noteworthy that MCU seems to have a critical role in promoting mitochondrial energy metabolism. To verify this hypothesis, we employed an MCU inhibitor ruthenium red and MCU activator spermine to specifically block or activate this pathway, to see whether the SAL still prevented H9c2 cells against DOX-induced downregulation of MCU, MICU1, and MICU2. Undoubtedly, ruthenium red cooperates with SAL to down-regulate the mRNA and protein expressions of MCU, MICU1, and MICU2 in H9c2 cells. These results verified our supposition that MCU is a critical regulatory protein in SAL-induced cardiac protection. SAL improves cardiomyocyte energy metabolism and has protective effects on mitochondrial respiratory function *via* the downregulation of MCU signaling pathway.

This study aimed to evaluate energy metabolism function and mechanism of SAL *in vivo* and *in vitro*. However, this study still has some limitations: (1) This study only tested the therapeutic effect of SAL on DOX-induced CHF model. Further studies are needed with pretreatment to determine whether SAL would be clinically useful before CHF. (2) Although several mitochondrial biomarkers were investigated in this study, the effects of SAL on the other parameters, such as real-time ATP rate, glycolytic rate, and glycolysis stress of DOX-treated H9c2 cells still need to be investigated in the future research. (3) The merit of this study is finding new active compound harboring the protective activity on cardiotoxicity. However, this study is not using positive control over the mechanism section to compare the efficacy of SAL. (4) This research tends to study the pharmacodynamics of SAL in the treatment of DOX-induced CHF. Nevertheless, the mechanism of SAL *in vivo* is insufficient. After the therapeutic effect has been confirmed, the mechanism of SAL in treating CHF should be further studied.

CONCLUSION

In conclusion, this study demonstrated that SAL may be the active component of ALRP, which can treat DOX-induced CHF and ameliorate H9c2 cells from DOX-induced cardiomyocyte toxicity. The molecular mechanism responsible for cardiomyocyte activity of SAL may involve the inhibition of MCU signaling pathway, which alleviates DOX-induced mitochondrial respiratory function impairment and energy metabolism disorders to improve H9c2 cells' dysfunction. This finding may provide evidence why ALRP has potential therapeutic effects on HF in the clinic.

DATA AVAILABILITY STATEMENT

The data used to support the findings of this study are available from the corresponding author upon reasonable request.

ETHICS STATEMENT

The experimental protocols were approved by the Ethics Committee of the Ethics of Animal Experiments of the Fifth Medical Center of PLA General Hospital (Approval ID: IACUC-2018-010). The present study was conducted according to the

recommendations of the Guidelines for the Care and Use of Laboratory Animals of the Ministry of Science and Technology of China.

AUTHOR CONTRIBUTIONS

J-XW and LZ performed the experiments, analyzed the data, and wrote the manuscript. H-HL, J-BW, and J-YL collected and prepared the samples. Y-XY, Y-YW, H-DC, and R-SL performed the analyses and amended the paper. Y-LZ designed the study and amended the paper.

FUNDING

This work was financially supported by grants from the National Key R&D Program of China (No. 2018YFC1704500) and National Natural Science Foundation of China (81573631 and 81874365).

REFERENCES

Alevriadou, B. R., Shanmughapriya, S., Patel, A., Stathopulos, P. B., and Madesh, M. (2017). Mitochondrial Ca^{2+} transport in the endothelium: regulation by ions, redox signalling and mechanical forces. *J. R. Soc. Interface* 14, 1–15. doi: 10.1098/rsif.2017.0672

Bai, Y., Chen, Q., Sun, Y. P., Wang, X., Lv, L., Zhang, L. P., et al. (2017). Sulforaphane protection against the development of doxorubicin-induced chronic heart failure is associated with Nrf2 upregulation. *Cardiovasc. Ther.* 35, 1–12. doi: 10.1111/1755-5922.12277

Baughman, J. M., Perocchi, F., Girgis, H. S., Plovanich, M., Belcher-Timme, C. A., Sancak, Y., et al. (2011). Integrative genomics identifies MCU as an essential component of the mitochondrial calcium uniporter. *Nature* 476, 341–345. doi: 10.1038/nature10234

Benjamin, E. J., Virani, S. S., Callaway, C. W., Chamberlain, A. M., Chang, A. R., Cheng, S., et al. (2018). Heart disease and stroke statistics—2018 update: a report from the American Heart Association. *Circulation* 137, e67–e492. doi: 10.1161/CIR.0000000000000558

Bick, A. G., Wakimoto, H., Kamer, K. J., Sancak, Y., Goldberger, O., Axelsson, A., et al. (2017). Cardiovascular homeostasis dependence on MICU2, a regulatory subunit of the mitochondrial calcium uniporter. *Proc. Nat. Acad. Sci. U.S.A.* 114, E9096–E9104. doi: 10.1073/pnas.1711303114

Chen, D. H., and Liang, X. T. (1982). Study on the constituents of lateral root of *Aconitum Carmichaeli Debx.* (FU-ZI): I. Isolation and structural determination of salsolinol. *Acta Pharmaceutica Sinica* 17, 792–794. doi: 10.16438/j.0513-4870.1982.10.011

Chen, M., Tung, C. W., Shi, Q., Guo, L., Shi, L., Fang, H., et al. (2014). A testing strategy to predict risk for drug-induced liver injury in humans using high-content screen assays and the 'rule-of-two' model. *Arch. Toxicol.* 88, 1439–1449. doi: 10.1007/s00204-014-1276-9

Cristina, M., Gherardi, G., and Rizzuto, R. (2017). Structure, activity regulation, and role of the mitochondrial calcium uniporter in health and disease. *Front. Oncol.* 7, 139. doi: 10.3389/fonc.2017.00139

Cui, L., Guo, J. B., Zhang, Q., Yin, J., Li, J., Zhou, W., et al. (2017). Erythropoietin activates SIRT1 to protect human cardiomyocytes against doxorubicin-induced mitochondrial dysfunction and toxicity. *Toxicol. Lett.* 275, 28–38. doi: 10.1016/j.toxlet.2017.04.018

Foskett, J. K., and Philipson, B. (2015). The mitochondrial Ca^{2+} uniporter complex. *J. Mol. Cell Cardiol.* 78, 3–8. doi: 10.1016/j.yjmcc.2014.11.015

Francesco, R., Annamaria, M., and Mollace, V. (2017). The pathophysiological role of natriuretic peptide–RAAS cross talk in heart failure. *Int. J. Cardiol.* 226, 121–125. doi: 10.1016/j.ijcard.2016.03.080

Guo, R., Hua, Y., Ren, J., Bornfeldt, K. E., and Nair, S. (2018). Cardiomyocyte-specific disruption of cathepsin K protects against doxorubicin-induced cardiotoxicity. *Cell Death Dis.* 9, 692. doi: 10.1038/s41419-018-0727-2

Hakuno, D., Toya, T., Hamba, Y., Shiraishi, Y., Kujiraoka, T., and Takeshi, A. (2013). Arginase inhibition improves left ventricular systolic dysfunction in murine doxorubicin-induced heart failure, and increased arginase activity correlates with cardiac dysfunction in patients with systolic heart failure. *Circulation* 128, A13526.

Hosseini, A., Bakhtiari, E., and Mousavi, S. H. (2017). Protective effect of *Hibiscus sabdariffa* on doxorubicin-induced cytotoxicity in H9c2 cardiomyoblast cells. *Iran. J. Pharm. Res.* 16, 708–713.

Ichiki, T., Burnett, J. C. J., Scott, C. G., Heublein, D. M., Miyata, M., Kinugawa, K., et al. (2017). Neurohumoral modulation during waon therapy in chronic heart failure—subanalysis of waon-CHF study. *Circ. J.* 81, 709–716. doi: 10.1253/circj.CJ-16-1117

Jayaraman, S. (2005). Flow cytometric determination of mitochondrial membrane potential changes during apoptosis of T lymphocytic and pancreatic beta cell lines: comparison of tetramethylrhodamineethylester (TMRE), chloromethyl-X-rosamine (H2-CMX-Ros) and MitoTracker Red 580 (MTR580). *J. Immunol. Methods* 306, 68–79. doi: 10.1016/j.jim.2005.07.024

Jones, R. L., Berry, G. J., Rubens, R. D., and Miles, D. W. (2004). Clinical and pathological absence of cardiotoxicity after liposomal doxorubicin. *Lancet Oncol.* 5, 575–577. doi: 10.1016/S1470-2045(04)01570-0

Kalsi, K. K., Smolenski, R. T., Pritchard, R. D., Khaghani, A., Seymour, A. M., and Yacoub, M. H. (1999). Energetics and function of the failing human heart with dilated or hypertrophic cardiomyopathy. *Eur. J. Clin. Invest.* 29, 469–477. doi: 10.1046/j.1365-2362.1999.00468.x

Liu, X. X., Jian, X. X., Cai, X. F., Chao, R. B., Chen, Q. H., and Chen, D. L. (2012). Cardioactive C_{19}-diterpenoid alkaloids from the lateral roots of aconitum carmichaeli "Fu Zi". *Chem. Pharm. Bull.* 60, 144–149. doi: 10.1248/cpb.60.144

Lu, X. H., Zhang, L., Li, P. Y., Wang, J. B., Li, R. S., Huang, Y. Q., et al. (2017). The protective effects of compatibility of Aconiti Lateralis Radix Praeparata and Zingiberis Rhizoma on rats with heart failure by enhancing mitochondrial biogenesis *via* Sirt1/PGC-1a pathway. *Biomed. Pharmacother.* 92, 651–660. doi: 10.1016/j.biopha.2017.05.117

Luongo, T. S., Lambert, J. P., Yuan, A., Zhang, X., Gross, P., Song, J., et al. (2015). The mitochondrial calcium uniporter matches energetic supply with cardiac workload during stress and modulates permeability transition. *Cell Rep.* 12, 23–34. doi: 10.1016/j.celrep.2015.06.017

Mallilankaraman, K., Doonan, P., Cardenas, C., Chandramoorthy, H. C., Müller, M., Miller, R., et al. (2012). MICU1 is an essential gatekeeper for MCU-mediated mitochondrial Ca^{2+} uptake that regulates cell survival. *Cell* 151, 630–644. doi: 10.1016/j.cell.2012.10.011

Melchior, C. L. (1979). Interaction of salsolinol and tetrahydropapaveroline with catecholamines. *Alcohol. Clin. Exp. Res.* 3, 364–367. doi: 10.1111/j.1530-0277.1979.tb05337.x

Melis, M., Carboni, E., Caboni, P., and Acquas, E. (2015). Key role of salsolinol in ethanol actions on dopamine neuronal activity of the posterior ventral tegmental area. *Addict. Biol.* 20, 182–193. doi: 10.1111/adb.12097

Neubauer, S., Horn, M., Cramer, M., Harre, K., Newell, J. B., Peters, W., et al. (1997). Myocardial phosphocreatineto-ATP ratio is a predictor of mortality in patients with dilated cardiomyopathy. *Circulation* 96, 2190–2196. doi: 10.1161/01.CIR.96.7.2190

Nichols, M., Pavlov, E. V., and Robertson, G. S. (2018). Tamoxifen-induced knockdown of the mitochondrial calcium uniporter in Thy1-expressing neurons protects mice from hypoxic/ischemic brain injury. *Cell Death Dis.* 9, 606. doi: 10.1038/s41419-018-0607-9

O'Brien, P. J., Irwin, W., Diaz, D., Howard-Cofield, E., Krejsa, C. M., Slaughter, M. R., et al. (2006). High concordance of drug-induced human hepatotoxicity with *in vitro* cytotoxicity measured in a novel cell-based model using high content screening. *Arch. Toxicol.* 80, 580–604. doi: 10.1007/s00204-006-0091-3

Penna, E., Espino, J., De, S. D., and Rizzuto, R. (2018). The MCU complex in cell death. *Cell Calcium* 69, 73–80. doi: 10.1016/j.ceca.2017.08.008

Pillai, V. B., Sundaresan, N. R., Jeevanandam, V., and Gupta, M. P. (2010). Mitochondrial SIRT3 and heart disease. *Cardiovasc. Res.* 88, 250–256. doi: 10.1093/cvr/cvq250

Siveski-Iliskovic, N., Kaul, N., and Singal, P. K. (1994). Probucol promotes endogenous antioxidants and provides protection against adriamycin-induced cardiomyopathy in rats. *Circulation* 89, 2829–2835. doi: 10.1161/01.CIR.89.6.2829

Sokolova, N. A., Chudakov, L. I., Ashmarin, I. P., Vinogradova, T. M., Volodin, N. D., Vlasov, G. P., et al. (1990). The positive chronotropic effects of salsolinol on the isolated rat heart. *Fiziol Zh SSSR Im I M Sechenova* 76, 1043–1047.

Stephan, H., Uwe, G., Michael, K., Frank, M., Schön, N., Jens, T., et al. (2017). Prevalence and clinical impact of iron deficiency and anaemia among outpatients with chronic heart failure: the PrEP registry. *Clin. Res. Cardiol.* 106, 436–443. doi: 10.1007/s00392-016-1073-y

van Bilsen, M., Smeets, P. J. H., Gilde, A. J., and Ger, J. V. (2004). Metabolic remodelling of the failing heart: the cardiac burn-out syndrome? *Cardiovasc. Res.* 61, 218–226. doi: 10.1016/j.cardiores.2003.11.014

Vecchis, R. D., and Ariano, C. (2018). Chronic antihypertensive therapy with thiazide diuretics in older women and risk of osteoporosis: a recently much-debated association. *Vascul. Pharmacol.* 53, 103–105. doi: 10.1016/j.vph.2017.12.017

Watanabe, S., Ono, K., Horie, T., Nishi, H., Kinoshita, M., Kuwabara, Y., et al. (2010). Ca^{2+}/calmodulin-dependent kinase kinase beta contributes to energy supply in adaptive phase of pressure-overload-induced heart failure. *Circulation* 122, A12639.

Wen, J. X., Zou, W. J., Wang, R. L., Liu, H. H., Yang, Y. X., Li, H. T., et al. (2019). Cardioprotective effects of Aconiti Lateralis Radix Praeparata combined with Zingiberis Rhizoma on doxorubicin-induced chronic heart failure in rats and potential mechanisms. *J. Ethnopharmacol.* 17, 111880. doi: 10.1016/j.jep.2019.111880

Yang, M., Ji, X., and Zuo, Z. (2018). Relationships between the toxicities of radix Aconiti Lateralis Preparata (Fuzi) and the toxicokinetics of its main diester-diterpenoid alkaloids. *Toxins (Basel).* 10, 391. doi: 10.3390/toxins10100391

Zaglia, T., Ceriotti, P., Campo., A., Borile, G., Armani, A., Carullo, P., et al. (2017). Content of mitochondrial calcium uniporter (MCU) in cardiomyocytes is regulated by microRNA-1 in physiologic and pathologic hypertrophy. *Proc. Nat. Acad. Sci. U.S.A.* 114, E9006–E9015. doi: 10.1073/pnas.1708772114

Zhang, L., Lu, X. H., Wang, J. B., Li, P. Y., Li, H. T., Wei, S. Z., et al. (2017). Zingiberis rhizoma mediated enhancement of the pharmacological effect of Aconiti Lateralis Radix Praeparata against acute heart failure and the underlying biological mechanisms. *Biomed. Pharmacother.* 96, 246–255. doi: 10.1016/j.biopha.2017.09.145

Zhang, X., Ji, R., Liao, X., Castillero, E., Kennel, P. J., Brunjes, D. L., et al. (2018). miR-195 regulates metabolism in failing myocardium *via* alterations in SIRT3 expression and mitochondrial protein acetylation. *Circulation* 137, 2052–2067. doi: 10.1161/CIRCULATIONAHA.117.030486

Zhou, Y. P. (2011). Review and evaluation of water-soluble active ingredients of aconite in the cardiovascular system. *Pharmacol. Clin. Chin. Mater. Med.* 27, 106–110. doi: 10.13412/j.cnki.zyyl.2011.06.038

Zhou, Y. P., and Liu, W. H. (2013). Review and re-evaluation of the study of the effects of aconite on cardiovascular system (1). *Pharmacol. Clin. Chin. Mater. Med.* 29, 198–205. doi: 10.13412/j.cnki.zyyl.2013.02.067

Conflict of Interest: The authors declare that the research was conducted in the absence of any commercial or financial relationships that could be construed as a potential conflict of interest.

frontiers in Pharmacology

ORIGINAL RESEARCH
published: 26 November 2019
doi: 10.3389/fphar.2019.01424

Pharmacodynamic Evaluation of Shenfu Injection in Rats With Ischemic Heart Failure and Its Effect on Small Molecules Using Matrix-Assisted Laser Desorption/Ionization–Mass Spectrometry Imaging

Hao Wu[1,2], *Zhenfeng Dai*[1,2], *Xi Liu*[1,2], *Ming Lin*[1,2], *Zeyu Gao*[1,2], *Fang Tian*[1,2], *Xin Zhao*[1,2], *Yi Sun*[1,2] *and Xiaoping Pu*[1,2]*

[1] National Key Research Laboratory of Natural and Biomimetic Drugs, Peking University, Beijing, China, [2] Department of Molecular and Cellular Pharmacology, School of Pharmaceutical Sciences, Peking University, Beijing, China

OPEN ACCESS

Edited by:
Jianxun Liu,
China Academy of Chinese Medical Sciences, China

Reviewed by:
Haibo Zhu,
Chinese Academy of Medical Sciences and Peking Union Medical College, China
Shuai Ji,
Xuzhou Medical University, China
Yin Lu,
Nanjing University of Chinese Medicine, China

***Correspondence:**
Xiaoping Pu
pxp123@bjmu.edu.cn

Specialty section:
This article was submitted to Ethnopharmacology, a section of the journal Frontiers in Pharmacology

Received: 09 April 2019
Accepted: 07 November 2019
Published: 26 November 2019

Citation:
Wu H, Dai Z, Liu X, Lin M, Gao Z, Tian F, Zhao X, Sun Y and Pu X (2019) Pharmacodynamic Evaluation of Shenfu Injection in Rats With Ischemic Heart Failure and Its Effect on Small Molecules Using Matrix-Assisted Laser Desorption/Ionization–Mass Spectrometry Imaging. Front. Pharmacol. 10:1424. doi: 10.3389/fphar.2019.01424

Objectives: We aimed to evaluate the effect of Shenfu injection in a rat model of ischemic heart failure and explore its mechanism.

Methods: A rat model of ischemic heart failure after myocardial infarction was established by ligating the left anterior descending coronary artery. Forty-eight hours after surgery, the rats were intraperitoneally administered Shenfu injection for 7 weeks. Then, left ventricular fractional shortening and left ventricular ejection fraction were measured using transthoracic echocardiography, whereas heart rate and left ventricular end-diastolic pressure were measured using a MD3000 biosignal acquisition and processing system. The hearts and lungs of the rats were excised and weighed to measure the heart and lung weight indexes. In addition, cardiac histopathological changes were observed *via* hematoxylin–eosin and Masson's trichrome staining, and serum cardiac troponin content was detected using a cardiac troponin ELISA kit. Furthermore, matrix-assisted laser desorption/ionization–mass spectrometry imaging was used to detect the levels and distribution of small molecules in the hearts of rats with ischemic heart failure.

Results: We found that Shenfu injection can significantly increase left ventricular fractional shortening and left ventricular ejection fraction in rats with ischemic heart failure and significantly reduce the left ventricular end-diastolic pressure, heart and lung weight indexes, and cardiac troponin content; improve cardiac tissue morphology; and reduce infarct size. In addition, the matrix-assisted laser desorption/ionization–mass spectrometry imaging results demonstrated that 22:6 phospholipids were predominately distributed in the non-infarct zone, whereas 20:4 phospholipids tended to concentrate in the infarct zone. Shenfu injection significantly reduced taurine, glutathione, and phospholipids levels in the hearts of rats with ischemic heart failure and primarily changed the distribution of these molecules in the non-infarct zone.

Conclusion: Shenfu injection induced obvious myocardial protective effects in rats with ischemic heart failure by stimulating antioxidation and changing the phospholipid levels and distribution.

Keywords: ischemic heart failure, left anterior descending artery, matrix-assisted laser desorption/ionization–mass spectrometry imaging, phospholipid, Shenfu injection

INTRODUCTION

Myocardial ischemia develops when coronary arteries, the major route of blood supply to the heart, are damaged. Recently, ischemic heart disease has become one of the most serious cardiovascular diseases worldwide, and ischemic heart failure (IHF) is an important cause of death (Liu et al., 2018). When ischemia develops in the heart, blood supply becomes limited, thereby accelerating the insufficiency of energy. Consequently, myocardial cells become dysfunctional and damaged (Liu et al., 2018), eventually leading to myocardial infarction (MI). In addition, myocardial remodeling after long-term MI leads to the deposition of fibrous tissue in the myocardium and impaired function, further leading to heart failure (Takemura et al., 2018). Left ventricular remodeling caused by MI accounts for approximately 70% of the 5 million cases of heart failure in the United States (Benjamin et al., 2018), and the mortality rate of heart failure after MI remains high in China and increases with increasing disease duration (Chen et al., 2017).

From short-term hemodynamic/pharmacological measures to long-term restorative strategies aimed at altering the biological properties of failing hearts, the treatment of IHF has undergone a noteworthy transformation since the 1990s (Yancy et al., 2013). Drugs targeting the renin–angiotensin–aldosterone system and the parasympathetic nervous system are attracting increasing attention, and positive inotropic drugs, beta-blockers [e.g., carvedilol (CAR)], angiotensin-converting enzyme inhibitors, and diuretics have become common treatments for IHF (Talameh and Lanfear, 2012; Yancy et al., 2013). Previous studies have confirmed that beta-blockers (such as CAR, etc.) can effectively treat heart disease, including IHF (Hjalmarson and Waagstein, 1994).

Shenfu injection is an injectable Chinese herbal medicine derived from Shenfu decoction. It is exclusively produced by Huarun Sanjiu Pharmaceutical Co., Ltd. (Sichuan, China). Shenfu injection is a refined suspension and mainly contains ginsenosides and aconitines; its primary effects include diuresis, reduction of myocardial oxygen consumption, alleviation of ischemia-reperfusion injury, and inhibition of inflammatory reactions (Wang et al., 2009; Guo and Li, 2013). Therefore, Shenfu injection can be used to treat IHF.

Matrix-assisted laser desorption/ionization–mass spectrometry imaging (MALDI–MSI) facilitates the *in situ* analysis of compounds without the need for labeling in two-dimensional biological tissue sections, thereby revealing the molecular information of compounds; the spatial coordinates and distribution of compounds in the tissue under study are linked. Using 1,5-diaminonaphthalene hydrochloride as a substrate, MALDI–MSI can detect various small molecules, including metal ions, tricarboxylic acid (TCA) cycle- and energy metabolism-related molecules, small endogenous antioxidants, and phospholipids, in heart tissue (Liu et al., 2014; Liu et al., 2017). These molecules have important implications for studying the effects of Shenfu injection on oxidative stress and myocardial remodeling in rats with IHF.

The present study confirmed the effects of Shenfu injection on myocardial injury in rats with IHF and elucidated its mechanism of action.

MATERIALS AND METHODS

Drug and Reagents

Shenfu injection (production batch no.: 17040401001) was provided by Huarun Sanjiu Pharmaceutical Co., Ltd. (Sichuan, China). Shenfu injection is extracted from two Chinese medicinal materials: red ginseng root (*Panax ginseng* C. A. Mey) and aconite tuber (*Aconitum carmichaeli* Debeaux). A flow chart of the Shenfu injection preparation process has been presented in **Supplementary Figure 1**. Briefly, red ginseng root and aconite tuber were separately soaked and concentrated into solutions and mixed in a ratio of 1:2 by volume to obtain Shenfu mixture. This mixture was then refined into Shenfu injection, followed by filling, sterilization, and quality evaluation. Shenfu injection was analyzed using high-performance liquid chromatography (HPLC) (**Supplementary Figure 2**) and was determined to mainly contain ginsenosides and aconitines [Ginsenoside Rg1 (0.13 mg/ml), ginsenoside Re (0.12 mg/ml), ginsenoside Rf (0.07 mg/ml), ginsenoside Rb1 (1.4 mg/ml), ginsenoside Rc (0.08 mg/ml), ginsenoside Rg2 (0.04 mg/ml), benzoylmesaconine (1.60 μg/ml), benzoylaconine (0.39 μg/ml), and benzoylhypacoitine (0.95 μg/ml)]. Of all these components, ginsenoside Rg1, ginsenoside Re, ginsenoside Rb1, and benzoylmesaconine were required to meet the quality standards of Shenfu injection (**Supplementary Table 1**), which was in line with the standards of the China Food and Drug Administration (Standard test nos.: WS3-B-3427-98-2013 and P. ZL. 205-001).

Ginsenosides were chromatographically analyzed using a Waters Symmetry Shield™ RP18 column (4.6 × 250 mm; 5.0 μm); the column temperature was maintained at 40°C. The mobile phases (A: Acetonitrile; B: H_2O) were 0%–10% A for 0–30 min, 10%–23% A for 30–40 min, 23% A for 40–50 min, and 23%–60% A for 50–80 min. Flow rate was maintained at 1.0 ml/min, and the detection wavelength for HPLC analysis was set at 203 nm. The analysis of aconitines was performed using a Thermo Hypersil BDS C18 column (4.6 × 250 mm; 5.0 μm) and column

temperature was maintained at 30°C. The mobile phases [A: 0.2% Triethylamine (adjust pH to 5.3 with glacial acetic acid); B:CH_3CN] were 70% A for 0–30 min and 45% A for 30–40 min. Flow rate was maintained at 1.0 ml/min, and the detection wavelength for the HPLC analysis was set at 235 nm.

CAR tablets were purchased from Qilu Pharmaceutical Co., Ltd. (Shandong, China). Heparin sodium was purchased from Beijing Suolaibao Technology Co., Ltd. (Beijing, China). Cardiac troponin T (cTnT) test kit was purchased from Wuhan Huamei Bioengineering Co., Ltd. (Wuhan, China). 1,5-Diaminonaphthalene was purchased from Sigma–Aldrich (St. Louis, Missouri, USA). Hematoxylin, eosin, Ponceau, and aniline blue were provided by Servicebio (Wuhan, China).

Animals

One hundred male age-matched Sprague–Dawley rats weighing 230–260 g were purchased from Beijing Vital River Laboratory Animal Technology Co., Ltd. [Beijing, China; license no.: SCXK (Beijing) 2016-0011]. The rats were labeled, weighed, caged, and permitted to eat and drink *ad libitum*. The temperature and humidity in the cage were maintained at 22°C–24°C and 50%–60%, respectively. The rats were maintained under a 12-h light/dark cycle and were allowed an acclimatization period of 1 week before surgery. All animal experiments were approved by the Peking University Biomedical Ethics Committee (Beijing, China; approval no.: LA2017282). The animal experimenters hold employment certificates from the Department of Laboratory Animal Science, Peking University Health Science Center, and have passed the laboratory entrance test held by Peking University School of Pharmaceutical Sciences.

IHF Model

The rats were intraperitoneally anesthetized with 0.5% pentobarbital sodium (1 ml/100 g), placed in the supine position, and provided positive-pressure ventilation using a small animal ventilator (frequency: 80 beats/min; respiratory ratio: 1:1; ventilation: 3 ml/100 g). Thereafter, the rats' limbs were connected to an electrocardiogram electrode and electrocardiography was performed (**Supplementary Figure 3A**). Next, thoracotomy was performed, exposing the heart, and the left anterior descending coronary artery was threaded and ligated, thereby producing a model of IHF. The procedure was considered successful when ST segment elevation was observed on the electrocardiogram (**Supplementary Figure 3B**). The normal (N) group received no treatment, whereas the sham (S) group underwent surgery without ligation of the left anterior descending coronary artery (Smith et al., 2003; Lv et al., 2016).

Grouping and Administration

The surviving rats with ligation of the left anterior descending artery were randomly divided into the model (MOD), CAR [10 mg/kg (Grandinetti et al., 2019), 6 ml/kg], and Shenfu injection groups [L, M, and H groups receiving Shenfu injection at concentrations of 3, 6, and 12 ml/kg, respectively (corresponding to clinical dosages of 36, 72, and 144 ml/70 kg, respectively)] 48 h after surgery. The CAR group (n = 9) received the drug intragastrically, whereas the L, M, and H groups received Shenfu injection intraperitoneally. The N, S, and MOD groups received normal saline intraperitoneally at 12 ml/kg/day. Then, body signs and survival of all rats were observed and recorded. A flow chart of the study workflow is illustrated in **Figure 1**.

Echocardiography and Hemodynamics

Seven weeks later, the rats were anesthetized with 2% isoflurane and echocardiographic examination was performed using a Vevo2010 ultra-high–resolution small animal imaging ultrasound system (Visual Sonics, Canada). Left ventricular end-diastolic diameter (LVEDD), left ventricular end-systolic diameter (LVESD), left ventricular fractional shortening (LVFS), and left ventricular ejection fraction (LVEF) were also measured. Thereafter, the right common carotid artery was used for catheter intubation, and the arterial catheter was then connected to a MD3000 biosignal acquisition and processing system for hemodynamic testing, including measurements of left ventricular end-diastolic pressure (LVEDP) and heart rate (HR).

Serum cTnT Measurement

After hemodynamic testing, blood (1 ml) was drawn from the abdominal aorta each rat and placed in a centrifuge tube. The blood samples were then centrifuged at 3,000 rpm for 15 min to obtain serum. The cTnT concentration in serum was determined using the cTnT test kit.

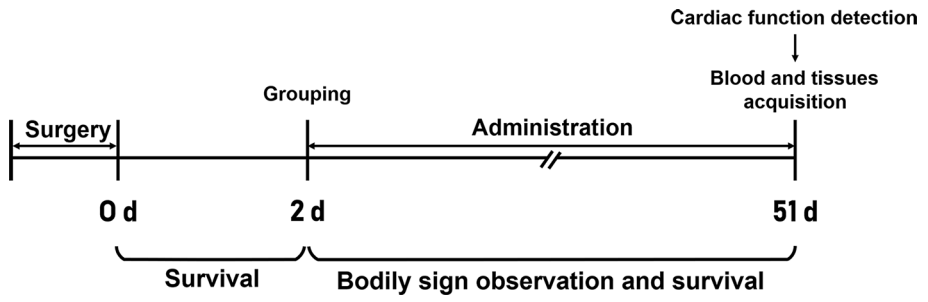

FIGURE 1 | Flow chart of the study workflow.

Histopathological Examination

After obtaining the blood, the hearts of four rats from each group were quickly separated, excised, and fixed in 4% paraformaldehyde for 48 h to prepare a 4-μm-thick paraffin section for hematoxylin–eosin (HE) and Masson's trichrome staining, which were performed to observe cardiac histopathological changes under a light microscope; myocardial infarct size (IS) was calculated using the following formula: IS (%) = midline infarct length/left ventricular midline circumference × 100% (Takagawa et al., 2007). In addition, the hearts and lungs of the other rats were obtained and cleaned. Heart weight index (HWI) and lung weight index (LWI) of the rats in each group were calculated using the following formula: organ index = organ wet weight (mg)/body weight of the rat on the day of sacrifice (g).

Matrix-Assisted Laser Desorption/Ionization–Mass Spectrometry Imaging

After obtaining the blood, the hearts of three rats each from the H, S, and MOD groups were quickly separated, excised, snap-frozen in liquid nitrogen and stored at −80°C for MALDI–MSI.

The snap-frozen hearts were fixed to the sample holder using ultrapure water, and 10-μm-thick transverse slices were prepared using a cryostat microtome (Scotsman Jencons, Germany) at −17°C. The distance from the slice position to the apex was 2/5th of the vertical length of the heart. The tissue slices were then transferred onto indium tin oxide slides (Bruker Daltonics, Germany) and dried in a vacuum pump for 30 min. Matrix spraying and MALDI–MSI were then conducted, as previously described (Liu et al., 2014; Liu et al., 2017). Molecular spectrum peaks were selected in the MALDI–MSI results, and statistical analysis was performed using the SCiLS Lab software based on the normalization of total ion chromatography.

Statistical Analysis

Data were expressed as mean ± standard error of the mean. Survival curve results were analyzed using Student's *t*-test (two-tailed), and the other results were compared using one-way analysis of variance. All statistical data were analyzed using the GraphPad Prism 6 software. $P < 0.05$ was considered statistically significant.

RESULTS

Effect of Shenfu Injection on Body Signs and Survival of the Rats With IHF

After treatment, the body signs and survival of rats were recorded. Compared with the rats in the S group, those in the MOD group consumed less food and water and exhibited less activity; moreover, some animals in the MOD group displayed dyspnea. After treatment, the rats were not easily scared and exhibited less dyspnea and more night activity.

Survival curves were drawn for the rats in each group, except for nine that died during surgery. Compared with that in the S group, the survival rate significantly decreased in the MOD group in the early phase of myocardial ischemia ($P < 0.05$) from post-surgery to pre-therapy (**Supplementary Figure 4A**). After treatment, the survival rate of the MOD group was significantly reduced (<60%; $P < 0.05$); in contrast, the L, M, and H groups had survival rates >80% (**Supplementary Figure 4B**).

Shenfu Injection Improves Left Ventricular Systolic Function of the Rats With IHF

Left ventricular systolic function, as assessed using LVFS and LVEF, was impaired in the rats with IHF, with the changes matched to elevations of LVESD and LVEDD (Smith et al., 2005; Xing et al., 2014). As shown in **Figure 2,** LVEDD and LVESD were higher in the MOD group than in the S group (both $P < 0.01$); in contrast, LVFS and LVEF were lower in the MOD group than in the S group ($P < 0.01$ and $P < 0.001$, respectively). After treatment with Shenfu injection, LVEDD and LVESD were significantly decreased in the H group ($P < 0.05$ and $P < 0.01$, respectively), whereas LVFS and LVEF were obviously increased (both $P < 0.05$). In addition, CAR obviously lowered LVEDD and LVESD ($P < 0.01$ and $P < 0.05$, respectively) and improved LVFS and LVEF (both $P < 0.05$).

Shenfu Injection Enhances Left Ventricular Diastolic Function of the Rats With IHF

Hemodynamic results indicating the changes of LVEDP and HR are shown in **Figure 3A**. L VEDP was inversely correlated with left ventricular diastolic function; moreover, LVEDP was significantly increased in the MOD group ($P < 0.001$) (**Figure 3B**), and 12 mg/kg Shenfu injection obviously reduced LVEDP ($P < 0.05$) (**Figure 3B**). In addition, CAR reduced LVEDP in the rats with IHF ($P < 0.05$) (**Figure 3B**). Thereafter, there was no significant difference in the HR among the S, MOD, and Shenfu injection groups (**Figure 3B**), consistent with prior findings (Smith et al., 2005).

Shenfu Injection Attenuates Abnormal Hypertrophy of the Heart and Lung of the Rats With IHF

HWI and LWI, which are associated with pathological conditions, such as cardiac hypertrophy and pulmonary blood stasis, are significantly greater in rats with IHF during the development of IHF (Smith et al., 2003). Compared with the S group, the MOD group exhibited decreased body weight ($P < 0.05$) (**Figure 4A**) and increased HWI and LWI (both $P < 0.001$) (**Figures 4B**, **C**). HWI (all $P < 0.01$) (**Figure 4B**) and LWI (all $P < 0.001$) (**Figure 4C**) were significantly improved in all Shenfu injection groups after treatment. In addition, treatment with CAR significantly improved HWI and LWI in the rats with IHF ($P < 0.01$ and $P < 0.001$, respectively) (**Figures 4B**, **C**).

Effect of Shenfu Injection on Heart Histopathology of the Rats With IHF

Shenfu Injection Inhibits Myocardial Damage

As demonstrated in **Figure 5**, myocardial tissue lesions of rats in the MOD group were primarily located in the middle of the

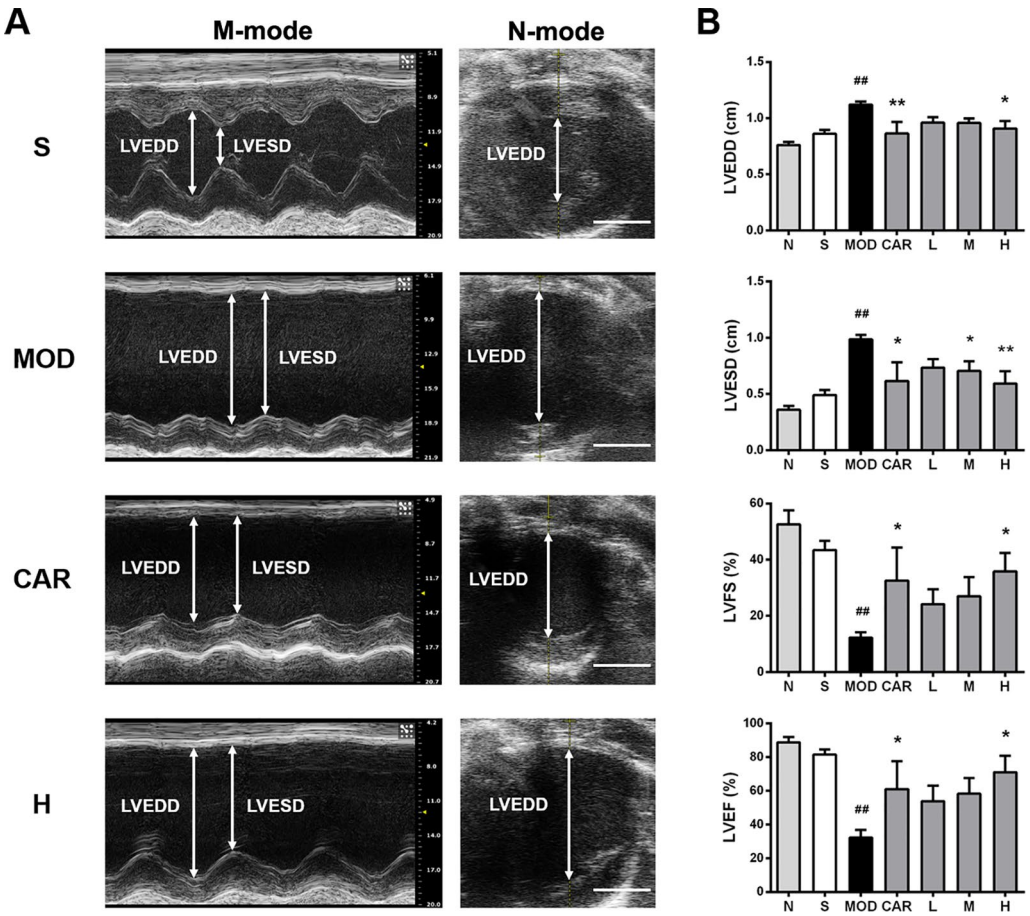

FIGURE 2 | Effect of Shenfu injection on the echocardiographic characteristics of the rats with ischemic heart failure. **(A)** M-mode and B-mode echocardiographic images of the hearts of rats in the S, MOD, CAR, and H groups. **(B)** Left ventricular end-diastolic diameter (LVEDD), left ventricular end-systolic diameter (LVESD), left ventricular fraction shortening, and left ventricular ejection fraction of the rats with IHF. Arrows demarcate the LVESD and LVEDD dimensions; scale bar, 5 mm. N, normal (n = 3); S, sham (n = 3); MOD, model (n = 4); CAR, carvedilol (n = 4); L, 3 ml/kg Shenfu injection (n = 5); M, 6 ml/kg Shenfu injection (n = 4); H, 12 ml/kg Shenfu injection (n = 4). Data are expressed as the mean ± standard error of the mean. $^{\#\#}P < 0.05$ vs. S group; $^{*}P < 0.05$, $^{**}P < 0.01$ vs. MOD group.

outer left ventricle wall wherein damaged myocardial fibers (yellow arrow), exaggerated nuclei with a deep color, and severe inflammatory cell infiltration (red arrow) were observed. After the administration of 12 mL/kg Shenfu injection, the extent of myocardial fiber damage and inflammatory cell infiltration was improved.

Shenfu Injection Decreases Myocardial IS

As shown in **Figure 6**, large amounts of blue collagen fibers appeared in the myocardial tissue lesions in the left ventricles (red arrow) of rats in the MOD group; compensatory hypertrophy and enlarged ventricular chamber were observed in the right ventricle (green arrow). After the administration of Shenfu injection or CAR, the amount of blue collagen fibers was reduced, and the left and right ventricular walls were more stable. Furthermore, 12 mg/kg Shenfu injection or CAR significantly decreased the size of the myocardial tissue lesions ($P < 0.01$ and $P < 0.05$, respectively).

Shenfu Injection Reduces Serum cTnT Levels of the Rats With IHF

In rats, myocardial ischemic injury leads to an increase in the serum cTnT levels (Wei et al., 2015). As shown in **Supplementary Figure 5**, compared with that in the S group, the increase in serum cTnT levels in the MOD group ($P < 0.01$) was significantly inhibited by 12 ml/kg Shenfu injection and CAR (both $P < 0.05$); however, 6 ml/kg Shenfu injection did not affect the serum cTnT levels.

Effect of Shenfu Injection on the Content and Distribution of 80–1000-Da Molecules in the Hearts of the Rats With IHF

Using MALDI–MSI, significant changes in the levels and distribution of some small molecules, including endogenous antioxidant molecules (taurine, glutathione, and ascorbic acid), phospholipids [phosphatidic acid (PA),

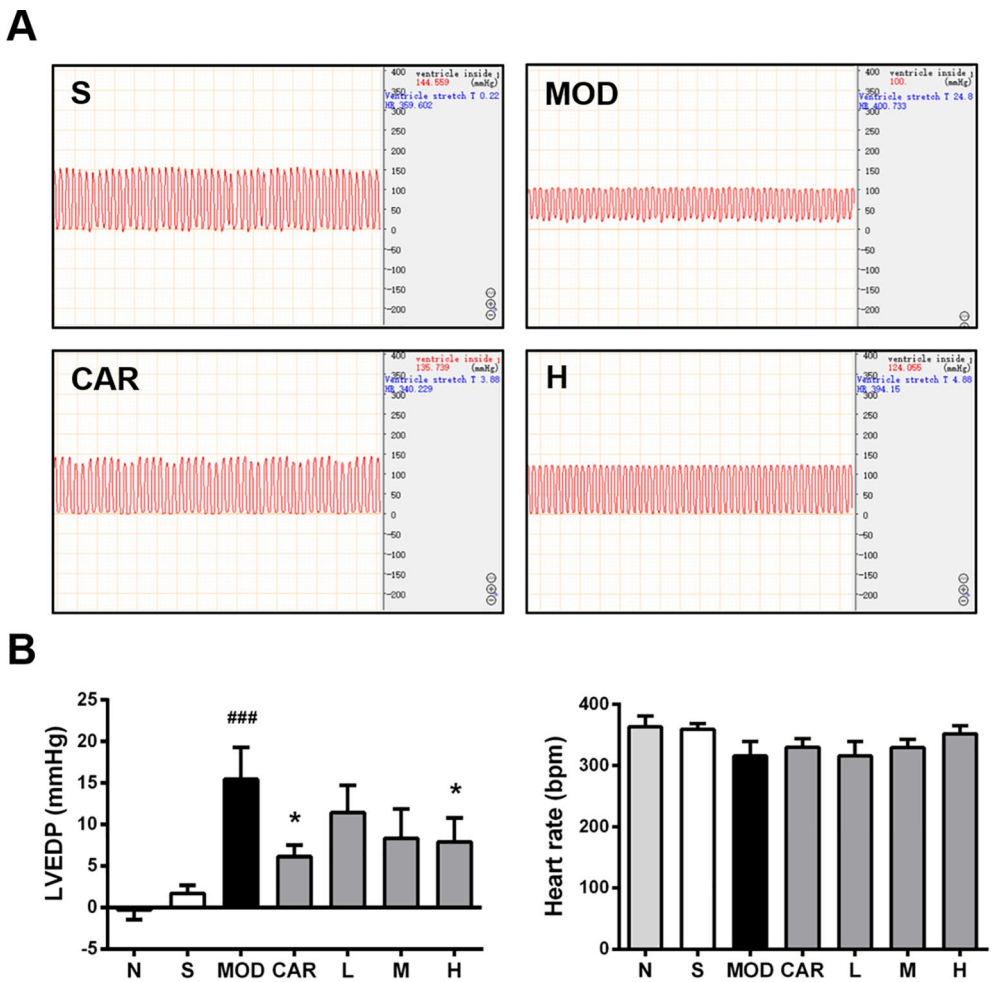

FIGURE 3 | Effect of Shenfu injection on the hemodynamics of the rats with ischemic heart failure. **(A)** Hemodynamic diagrams in the hearts of the rats in the S, MOD, CAR, and H groups. **(B)** Left ventricular end-diastolic pressure (LVEDP) and heart rate in the rats with IHF. N, normal (n = 7); S, sham (n = 11); MOD, model (n = 7); CAR, carvedilol (n = 7); L, 3 ml/kg Shenfu injection (n = 7); M, 6 ml/kg Shenfu injection (n = 7); H, 12 ml/kg Shenfu injection (n = 7). Data are expressed as the mean ± standard error of the mean. $^{###}P < 0.001$ vs. S group; $^{*}P < 0.05$ vs. MOD group.

phosphatidylethanolamine (PE), and phosphatidylinositol (PI)], and TCA cycle- and energy metabolism-related molecules (aspartate, N-acetyl--aspartate, and adenosine), were observed in the whole transverse heart tissue slices of the rats with IHF.

Based on the MALDI–MSI results of ascorbic acid and PE (16:0/22:6) in the heart slices and Masson's trichrome-stained images of the adjacent slices, the infarct zone was located using the MSI images and marked with red coils, as shown in **Figure 7**.

Shenfu Injection Changes Antioxidant Molecules Levels in the Rats With IHF

Taurine, ascorbic acid, and glutathione levels were significantly increased in the whole hearts of the rats in the MOD group than in the hearts of those in the S group ($P < 0.001$, $P < 0.001$, and $P < 0.01$, respectively). Shenfu injection reduced the glutathione and taurine levels (both $P < 0.05$) compared with those in the MOD group; however, it had no effect on ascorbic acid, as shown in **Figure 8**. In addition, in the MOD group, ascorbic acid was primarily distributed in the infarct zone, whereas taurine and glutamine were evenly distributed in the infarct as well as non-infarct zones; Shenfu injection primarily changed the distribution of taurine and glutamine in the non-infarct zone.

Shenfu Injection Regulates Phospholipids in the Rats With IHF

As shown in **Figure 9**, the PA (18:0/20:4), PA (18:0/22:6), PE (16:0/22:6), PE (P-18:0/22:6), and PI (18:0/20:4) levels were increased in the hearts of the rats in the MOD group than in the hearts of those in the S group ($P < 0.05$, $P < 0.01$, $P < 0.05$, $P < 0.01$, and $P < 0.01$, respectively); in contrast, Shenfu injection reduced the PA (18:0/22:6), PE (16:0/22:6), PE (P-18:0/22:6), and PI (18:0/20:4) levels ($P < 0.01$, $P < 0.01$, $P < 0.01$, and $P < 0.05$, respectively), with no significant impact on PA (18:0/20:4). Furthermore, PA (18:0/20:4), PE (16:0/22:6), and PE (P-18:0/22:6) in the hearts of the rats in the MOD group were observed to be primarily located in the non-infarct zone, and

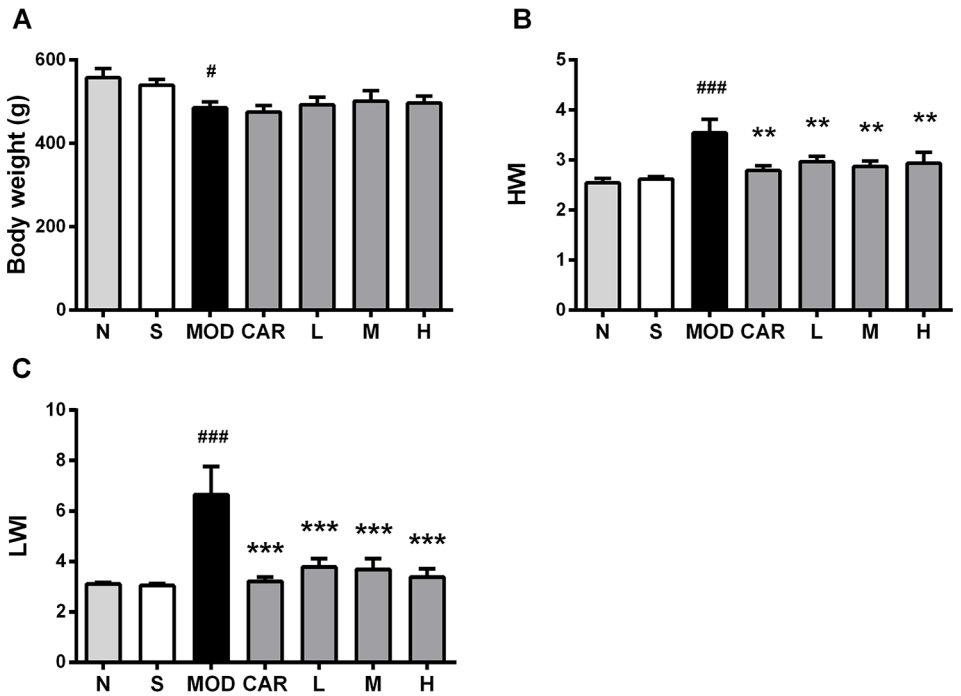

FIGURE 4 | Effect of Shenfu injection on body weight of the rats with ischemic heart failure. **(A–C)** Body weight, heart weight index, and lung weight index. N, normal (n = 7); S, sham (n = 11); MOD, model (n = 7); CAR, carvedilol (n = 7; L, 3 ml/kg Shenfu injection (n = 8); M, 6 ml/kg Shenfu injection (n = 7); H, 12 ml/kg Shenfu injection (n = 7). Data are expressed as mean ± standard error of the mean. $^{\#}P < 0.05$, $^{\#\#\#}P < 0.001$ vs. S group; $^{**}P < 0.01$, $^{***}P < 0.001$ vs. MOD group.

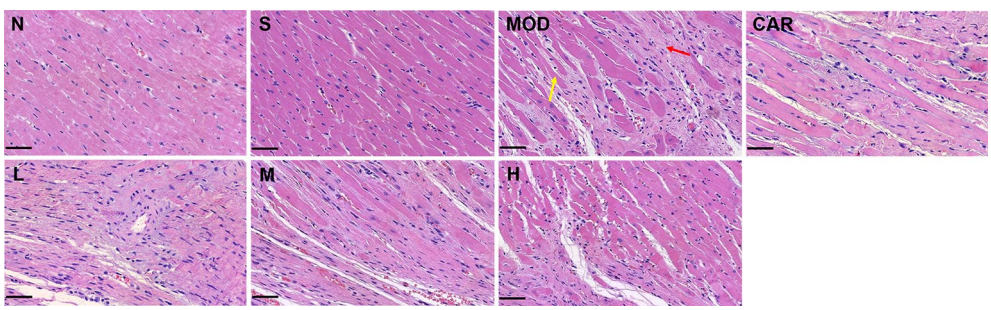

FIGURE 5 | Photomicrographs of heart sections stained with hematoxylin–eosin in each group after coronary artery ligation (close to the coronary vein, 200×). Scale bar, 50 μm in each panel. The yellow arrow denotes damaged myocardial fibers, whereas the red one indicates inflammatory cell infiltration. N, normal; S, sham; MOD, model; CAR, carvedilol; L, 3 ml/kg Shenfu injection; M, 6 ml/kg Shenfu injection; H, 12 ml/kg Shenfu injection.

PA (18:0/20:4) was located in the infarct zone. Shenfu injection predominately changed the distribution of phospholipids in the non-infarct zone.

Shenfu Injection has no Effect on TCA Cycle- and Energy Metabolism-Related Molecules in the Rats With IHF

As shown in **Supplementary Figure 6**, the aspartate and N-acetyl-aspartate levels were increased in the MOD group than in the S group (both $P < 0.05$); in contrast, adenosine levels were decreased in the MOD group than in the S group ($P < 0.01$). Shenfu injection did not reverse these abnormal changes. Further analysis revealed that in the MOD group, aspartic acid and N-acetyl-aspartate were primarily distributed around the infarct zone, and the distribution of adenosine as a downstream product of energy metabolism was changed in the infarct and non-infarct zones.

DISCUSSION

In the present study, Shenfu injection effectively improved myocardial ischemic injury, enhanced myocardial function, and reduced HWI and LWI levels in rats with IHF that underwent

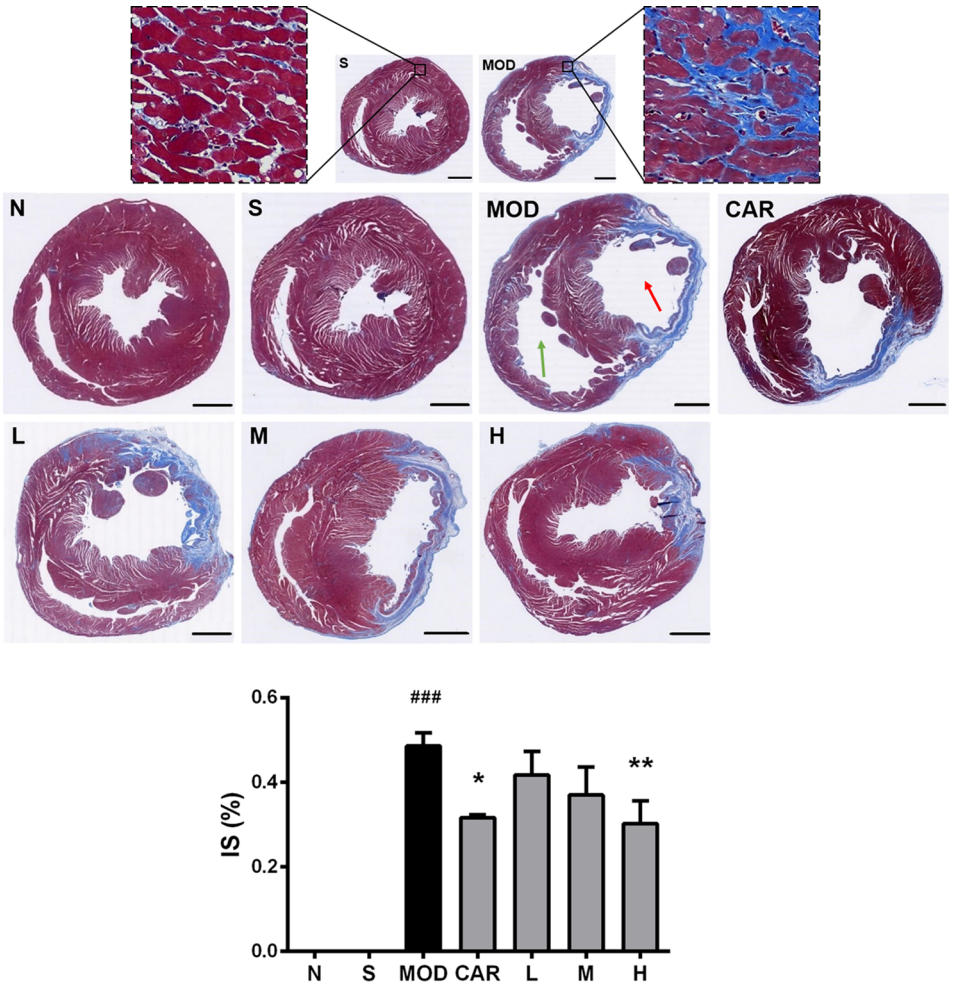

FIGURE 6 | Photomicrographs of Masson's trichrome-stained heart sections of rats from each group after coronary artery ligation. The magnification of the cross-sectional photomicrographs is 5.1× (scale bar, 2000 μm in each panel). The magnification of the local enlarged photomicrographs near the coronary vein is 200× (scale bar, 50 μm in each panel). The red arrow indicates the left ventricle, whereas the green one indicates the right ventricle. The infarct size was analyzed using Image-Pro Plus. N, normal (n = 4); S, sham (n = 4); MOD, model (n = 5); CAR, carvedilol (n = 4); L, 3 ml/kg Shenfu injection (n = 4); M, 6 ml/kg Shenfu injection (n = 4); H, 12 ml/kg Shenfu injection (n = 4). Data are expressed as mean ± standard error of the mean. $^{###}P < 0.001$ vs. S group; $^{*}P < 0.05$, $^{**}P < 0.01$ vs. MOD group.

left anterior descending coronary artery ligation. In addition, using MALDI–MSI, it was first discovered that Shenfu injection can reverse the abnormal levels and distribution changes of taurine, glutathione, PA, PE, and PI in the heart caused by IHF, thereby providing new opinions for studies on the links between PA-mediated signaling pathways and cardiac dysfunction in IHF.

The IHF rat model can well simulate clinical IHF caused by coronary artery stenosis (Haidara et al., 2015). The pathogenesis of IHF is extremely complex, involving a series of cell molecular biology, cardiac function, and morphological changes (Takemura et al., 2018). In our study, 12 ml/kg Shenfu injection exerted a cardiotonic effect by dramatically improving myocardial injury to enhance cardiac function and alleviating the occurrence of myocardial hypertrophy and pulmonary congestion; in contrast, 6 ml/kg Shenfu injection had less obvious effects. We subsequently found that Shenfu injection for the treatment of myocardial ischemia in rats was administered at concentrations >6 ml/kg or for periods >7 weeks (Wu et al., 2011; Zheng et al., 2015).

Indeed, previous studies have demonstrated that Shenfu injection could ameliorate cardiac injury by stabilizing cardiac hemodynamic parameters and improving left ventricular function in IHF (Zheng et al., 2015). Furthermore, using MALDI–MS, Zheng et al. (2015) demonstrated that haptoglobin and pentraxin 3 may be inflammatory markers of IHF. In contrast, our study involved a more comprehensive pharmacological evaluation of Shenfu injection and investigated small molecules that potentially play a role in suppressing oxidative stress to protect the myocardium using MALDI–MSI.

Both taurine and glutathione are endogenous antioxidant molecules present in the body and they induce significant effects on myocardial damage. Taurine can inhibit the abnormal

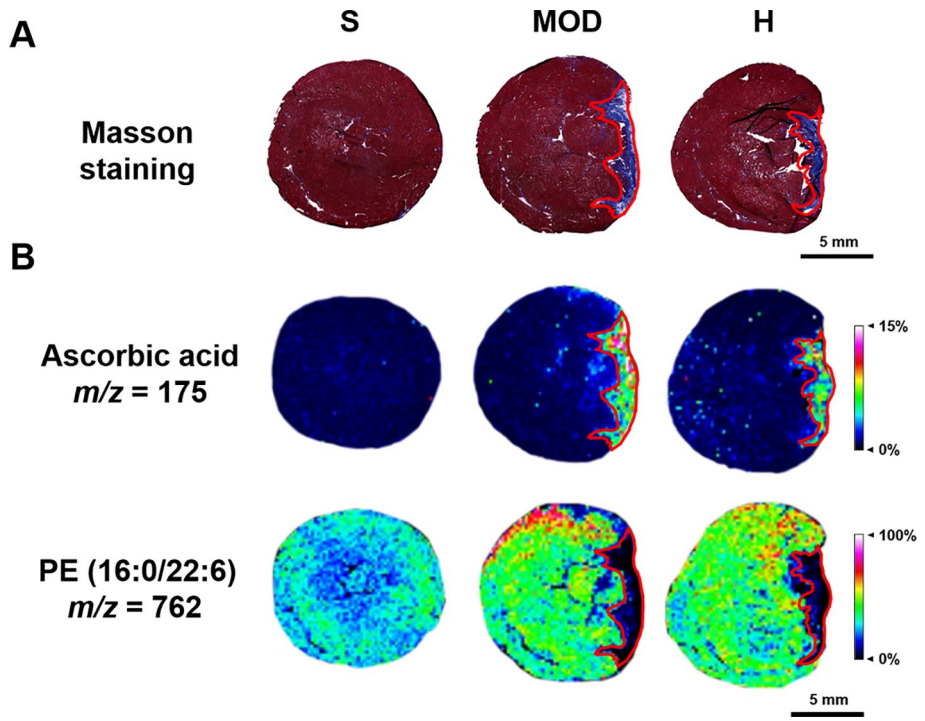

FIGURE 7 | Infarct zone of the matrix-assisted laser desorption/ionization–mass spectrometry imaging (MALDI–MSI) results (marked with red coils). **(A)** Masson staining of the adjacent heart slice. **(B)** The MALDI-MSI results of ascorbic acid and PE (16:0/22:6). The spatial resolution is 200 μm (scale bar, 5 mm). S, sham; MOD, model; H, 12 ml/kg Shenfu injection.

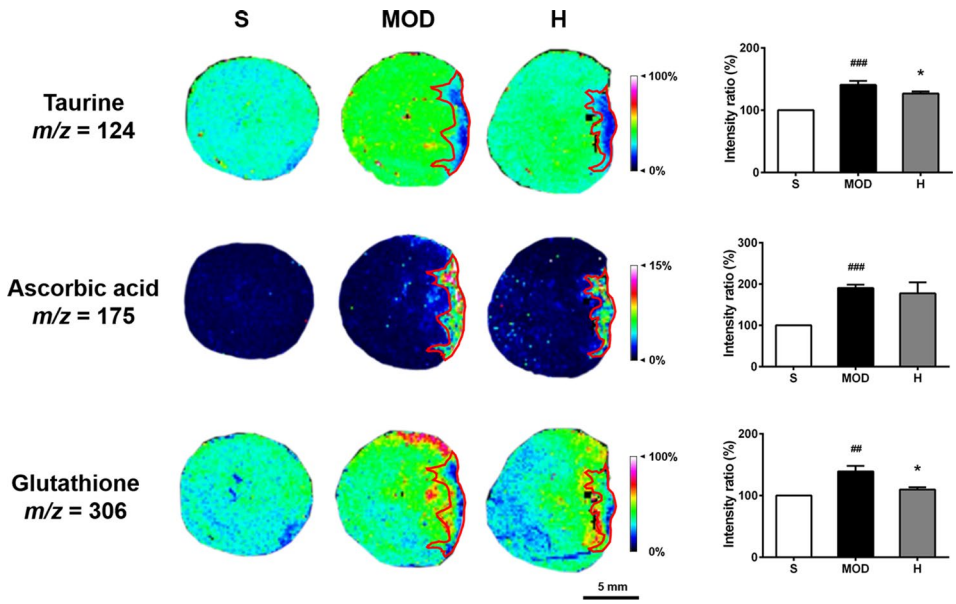

FIGURE 8 | Effect of Shenfu injection on antioxidant molecules in the hearts of rats with ischemic heart failure. Intensity ratios of molecules were analyzed using the SCiLS Lab software in a normalized manner. Spatial resolution is 200 μm (scale bar, 5 mm). S, sham; MOD, model; H, 12 ml/kg Shenfu injection. Data are presented as mean ± standard error of the mean; n = 3 per group. $^{\#\#}P < 0.01$, $^{\#\#\#}P < 0.001$ vs. S group; $^{*}P < 0.05$ vs. MOD group.

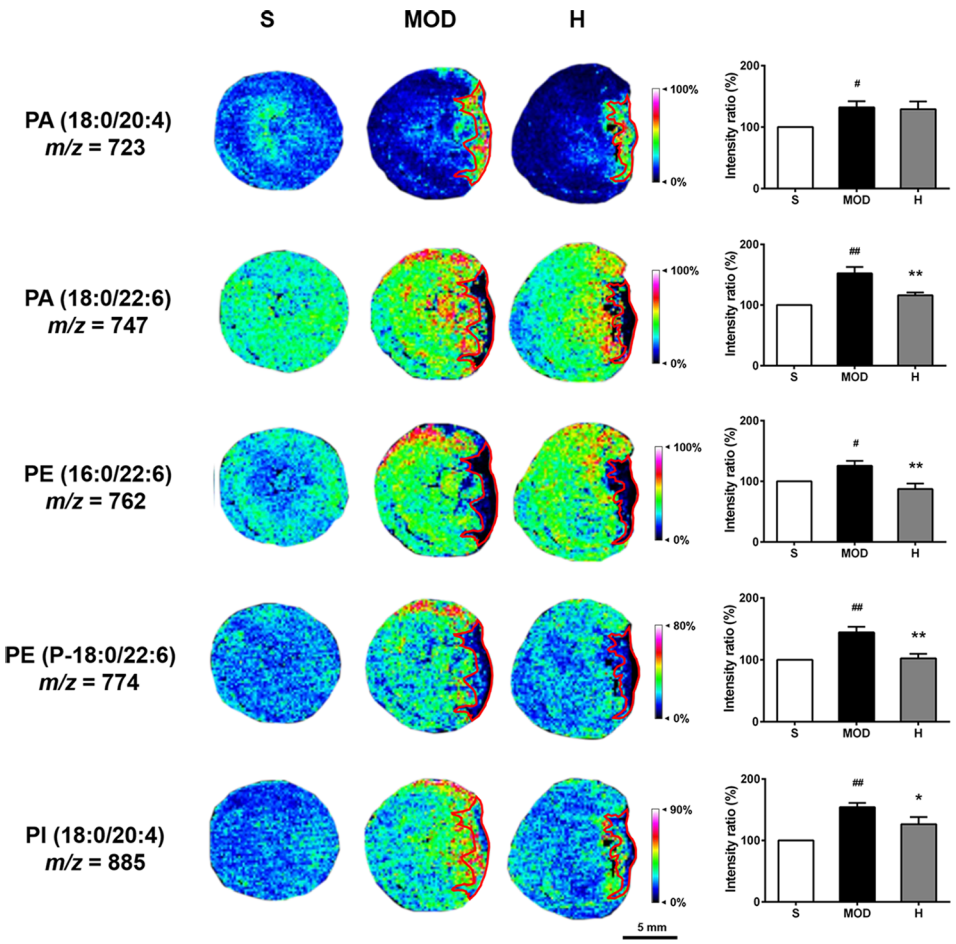

FIGURE 9 | Effect of Shenfu injection on phospholipids in the hearts of rats with ischemic heart failure. Intensity ratios of molecules were analyzed using SCiLS Lab software in a normalized manner. The spatial resolution is 200 μm (scale bar, 5 mm). S, sham; MOD, model; H, 12 ml/kg Shenfu injection. Data are presented as mean ± standard error of the mean; n = 3 per group. $^{\#}P < 0.05$, $^{\#\#}P < 0.01$ vs. S group; $^{*}P < 0.05$, $^{**}P < 0.01$ vs. MOD group.

increase in reactive oxygen species (ROS) caused by ischemic injury, enhance the activity of antioxidant enzymes, and reduce the levels of inflammatory markers (Shimada et al., 2015; Dallak, 2017). Glutathione directly scavenges ROS and antagonizes oxidative stress associated with excessive glutathionylation of cardiac myosin-binding protein C, which causes myocardial systolic and diastolic dysfunction (Stathopoulou et al., 2016). Based on our study findings, we hypothesize that the overall accumulation of taurine and glutathione in the MOD group is associated with antagonism of oxidative stress and that Shenfu injection can both reduce oxidative stress caused by myocardial ischemia and indirectly reduce glutathionylation to confer myocardial protection; this was predominately observed in the non-infarcted zone.

In addition, PA and PI play important roles as precursors of various glycerophospholipids and are also involved in the transmission of intracellular signals and cellular functions. PE is a neutral phospholipid present in the heart (Nishizuka, 1992; Ammar et al., 2014). Previous studies have revealed that cardiac non-infarct zones exhibit cardiac hypertrophy and imbalance of myocardial interstitial fibrillar collagen synthesis and that infarct zones exhibit apoptosis, necrosis, and scar formation (Liang et al., 2016; Takemura et al., 2018; Wang et al., 2018). The observed distribution of phospholipids in the non-infarct zone of our IHF rat model might be closely associated with myocardial remodeling in this area. Moreover, small amounts of PI (18:0/20:4) and the majority of PA (18:0/20:4) were distributed in the infarct and border zones (Pilla et al., 2015), which might be related to myocardial remodeling in the infarct zone and transition from the non-infarct zone to the infarct zone. In particular, phospholipids with a 22:6 fatty acyl chain were predominately distributed in the non-infarct zone, whereas phospholipids with a 20:4 fatty acyl chain tended to concentrate in the infarct zone. In addition, these phospholipids have many unsaturated fatty acids, which are susceptible to conversion to oxidized phospholipids (OxPLs) by ROS. OxPLs have proinflammatory effects and are associated with many inflammatory diseases, such as metabolic disorders, degenerative diseases, etc. (Freigang, 2016). Therefore, we consider that Shenfu injection can reverse the increase of the levels of various phospholipids caused by myocardial ischemia,

which may slow down the myocardial remodeling process in the non-infarct, border, and infarct zones; indirectly affect the overproduction of OxPLs; and inhibit the occurrence of oxidative stress and inflammatory responses. Furthermore, a previous study indicated that defects in PA-mediated signaling pathways might represent a novel mechanism of cardiac dysfunction in IHF (Tappia et al., 2001). Although our study can provide useful insights through the distribution of PA, further investigation is needed.

MALDI–MSI has an obvious advantage in detecting the levels and distribution of cardiac phospholipids. *In vitro* detection of phospholipids using the liquid chromatography–mass spectrometry or electrospray ionization tandem mass spectrometry technique can accurately quantify the level of a certain lipid but not reflect its distribution (Manickaraj et al., 2017; Tang et al., 2018). However, MALDI–MSI can facilitate the high-throughput detection of phospholipids and their distribution *in situ*. Because phospholipids are closely related to the structure and function of the heart, information regarding their distribution is extremely important.

It cannot be denied that this study had some limitations. Measurements were performed at only a single time point (i.e., at the seventh week), for which the results of phospholipids applied for only the seventh week. In addition, because the biochemical and biological functions of phospholipids are unclear, the effects of phospholipids in the course of IHF are uncertain. Therefore, our novel discoveries regarding phospholipids in IHF need to be confirmed through future studies. Furthermore, the adverse reactions of traditional Chinese medicine injections received recognition increasingly, and the causes of adverse reactions related to several factors such as clinical irrational drug use, the patient's allergic constitution, intravenous drip rate, and use of dosing. The most common adverse reaction of traditional Chinese medicine injections was the "allergic reaction", which strengthened the research on the clinical skin test of traditional Chinese medicine injections (Liang et al., 2015). If traditional Chinese medicine injections can be used to screen allergic people through skin tests like cephalosporins and penicillin, the safety will be greatly improved. And the State Food and Drug Administration has strengthened the supervision of Chinese medicine injections. In the new medical insurance catalogue 2017, 26 Chinese medicine injections were restricted.

To more clearly understand the relationship between the anomalous small molecules detected using MALDI–MSI, we identified ROS as important intermediaries in the abnormal changes of taurine, glutathione, ascorbic acid, aspartic acid, N-acetyl-aspartate, adenosine, and phospholipid levels (**Figure 10**); moreover, Shenfu injection effectively changed the taurine, glutathione, and phospholipid levels. In the past decade, the pharmaceutical industry has witnessed a shift from the pursuit of one active ingredient hitting a single target to seeking combination therapies that comprise several active ingredients, and given that Shenfu injection has been widely used in China for treating patients with septic shock, the present study suggests that Shenfu injection provides new treatment strategies of IHF in clinical settings.

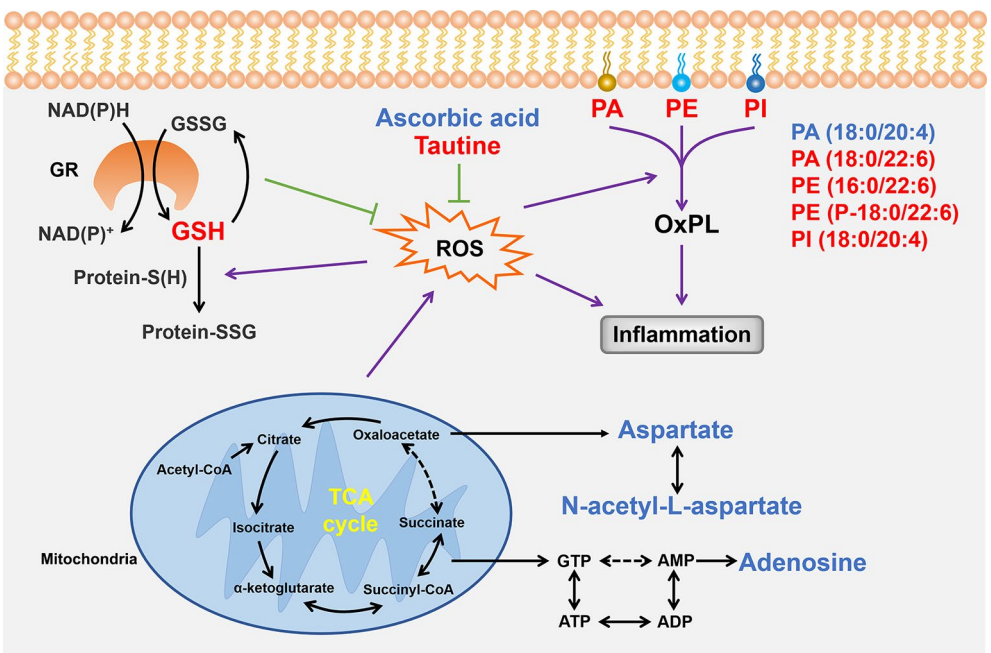

FIGURE 10 | Summary of the relationships between the small molecules found in the present study. Small molecules that Shenfu injection significantly affected are indicated by red font, whereas those that were significantly changed only in the model group are indicated by blue font. Black arrows indicate metabolic processes, whereas dashed arrows indicate omission of intermediates. Purple arrows indicate promotion, and the green T-shaped solid lines indicate inhibition. GR, glutathione reductase; GSH, glutathione.

DATA AVAILABILITY STATEMENT

The raw data supporting the conclusions of this manuscript will be made available by the authors, without undue resevation, to any qualified researcher.

ETHICS STATEMENT

This study was carried out in accordance with the recommendations of Peking University Biomedical Ethics Committee (Beijing, China; approval no.: LA2017282). The protocol was approved by Peking University Biomedical Ethics Committee. The animal experimenters hold employment certificates from the Department of Laboratory Animal Science, Peking University Health Science Center.

AUTHOR CONTRIBUTIONS

HW designed and performed the experiments, analyzed and interpreted the data, and wrote the manuscript. ZD participated in performing the experiments. XL, ML, and ZG assisted in data analysis. FT participated in material support. XZ and YS revised the paper. XP designed the study and revised the manuscript. All authors read and approved the final manuscript.

FUNDING

This study was supported by the following National Natural Science Foundation of China (Grant no.: U1603128), Science and Technology Major Projects: Significant New-Drugs Creation (Grant no.: 2018ZX09711001-009-006), and Sichuan Province Science and Technology Program (Grant no.: 2017JZ0036).

SUPPLEMENTARY MATERIAL

The Supplementary Material for this article can be found online at: https://www.frontiersin.org/articles/10.3389/fphar.2019.01424/full#supplementary-material

SUPPLEMENTARY TABLE 1 | Quality control of Shenfu injection.

SUPPLEMENTARY FIGURE 1 | Flow chart of the Shenfu injection preparation process.

SUPPLEMENTARY FIGURE 2 | Standardized analysis of Shenfu injection components using HPLC. **(A)** Six ginsenoside reference substances and **(B)** HPLC-fingerprint of Shenfu injection ginsenosides. **(C)** Three aconitine reference substances and **(D)** HPLC-fingerprint of Shenfu injection aconitines. **(E)** Chemical structure of the nine reference substances.

SUPPLEMENTARY FIGURE 3 | Electrocardiogram of rats. **(A)** Normal electrocardiogram (50 mm/s; 10 mm/mV). **(B)** Myocardial ischemia electrocardiogram (50 mm/s; 10 mm/mV).

SUPPLEMENTARY FIGURE 4 | Effect of Shenfu injection on the survival of the rats with ischemic heart failure. **(A)** Post-surgery to pre-therapy survival curve. **(B)** Post-therapy survival curve. N, normal; S, sham; All MOD and MOD, model; CAR, carvedilol; L, 3 ml/kg Shenfu injection; M, 6 ml/kg Shenfu injection; H, 12 ml/kg Shenfu injection. $^{\#}P < 0.05$ vs. sham group.

SUPPLEMENTARY FIGURE 5 | Effect of Shenfu injection on serum cardiac troponin T levels in the rats with ischemic heart failure. N, normal; S, sham; MOD, model; CAR, carvedilol; M, 6 ml/kg Shenfu injection; H, 12 ml/kg Shenfu injection. Data are expressed as mean ± standard error of the mean; n = 5 per group. $^{\#\#}P < 0.01$ vs. S group; $^{*}P < 0.05$ vs. MOD group.

SUPPLEMENTARY FIGURE 6 | Effect of Shenfu injection on TCA cycle- and energy metabolism-related molecules in the hearts of the rats with ischemic heart failure. Intensity ratios of molecules were analyzed using the SCiLS Lab software in a normalized manner. The spatial resolution is 200 μm (Scale bar, 5 mm). S, sham; MOD, model; H, 12 ml/kg Shenfu injection. Data are presented as the mean ± standard error of the mean; n = 3 per group. $^{\#}P < 0.05$, $^{\#\#}P < 0.01$ vs. S group.

REFERENCES

Ammar, M. R., Kassas, N., Bader, M. F., and Vitale, N. (2014). Phosphatidic acid in neuronal development: a node for membrane and cytoskeleton rearrangements. *Biochimie* 107 Pt A, 51–57. doi: 10.1016/j.biochi.2014.07.026

Benjamin, E. J., Virani, S. S., Callaway, C. W., Chamberlain, A. M., Chang, A. R., Cheng, S., et al. (2018). Heart disease and stroke statistics-2018 update: a report from the American Heart Association. *Circulation.* 137, e67–e492. doi: 10.1161/CIR.0000000000000558

Chen, W. W., Gao, R. L., Liu, L. S., Zhu, M. L., Wang, W., Wang, Y. J., et al. (2017). China cardiovascular diseases report 2015: a summary. *J. Geriatr. Cardiol.* 14, 1–10. doi: 10.11909/j.issn.1671-5411.2017.01.012

Dallak, M. (2017). A synergistic protective effect of selenium and taurine against experimentally induced myocardial infarction in rats. *Arch. Physiol. Biochem.* 123, 344–355. doi: 10.1080/13813455.2017.1347687

Freigang, S. (2016). The regulation of inflammation by oxidized phospholipids. *Eur. J. Immunol.* 46, 1818–1825. doi: 10.1002/eji.201545676

Grandinetti, V., Carlos, F. P., Antonio, E. L., De-Oliveira, H. A., Dos-Santos, L. F. N., Yoshizaki, A., et al. (2019). Photobiomodulation therapy combined with carvedilol attenuates post-infarction heart failure by suppressing excessive inflammation and oxidative stress in rats. *Sci. Rep.* 9, 9425. doi: 10.1038/s41598-019-46021-1

Guo, Z. J., and Li, C. S. (2013). Therapeutic effects of shenfu injection on post-cardiac arrest syndrome. *Chin. J. Integr. Med.* 19, 716–720. doi: 10.1007/s11655-013-1566-8

Haidara, M. A., Assiri, A. S., Yassin, H. Z., Ammar, H. I., Obradovic, M. M., and Isenovic, E. R. (2015). Heart failure models: traditional and novel therapy. *Curr. Vasc. Pharmacol.* 13, 658–669. doi: 10.2174/15701611136661502121 51506

Hjalmarson, A., and Waagstein, F. (1994). The role of beta-blockers in the treatment of cardiomyopathy and ischaemic heart failure. *Drugs.* 47 Suppl 4, 31–39. doi: 10.2165/00003495-199400474-00006

Liang, A. H., Yi, Y., Zhang, Y. S., Han, J. Y., Tian, J. Z., Lu, Y. T., et al. (2015). Pseudoallergic reactions of traditional Chinese medicine injections and the approaches for risk prevention and control. *Chin. Pharm. J.* 15, 1301–1308.

Liang, T., Zhang, Y., Yin, S., Gan, T., An, T., Zhang, R., et al. (2016). Cardio-protecteffect of qiliqiangxin capsule on left ventricular remodeling, dysfunction and apoptosis in heart failure rats after chronic myocardial infarction. *Am. J. Transl. Res.* 8, 2047–2058.

Liu, H., Chen, R., Wang, H., Chen, S., Xiong, C., Wang, J., et al. (2014). 1,5-Diaminonaphthalene hydrochloride assisted laser desorption/ionization mass spectrometry imaging of small molecules in tissues following focal cerebral ischemia. *Anal. Chem.* 86, 10114–10121. doi: 10.1021/ac5034566

Liu, H., Li, W., He, Q., Xue, J., Wang, J., Xiong, C., et al. (2017). Mass spectrometry imaging of kidney tissue sections of rat subjected to unilateral ureteral obstruction. *Sci. Rep.* 7, 41954. doi: 10.1038/srep41954

Liu, X., Xu, Y., Deng, Y., and Li, H. (2018). MicroRNA-223 regulates cardiac fibrosis after myocardial infarction by targeting RASA1. *Cell. Physiol. Biochem.* 46, 1439–1454. doi: 10.1159/000489185

Lv, F. H., Yin, H. L., He, Y. Q., Wu, H. M., Kong, J., Chai, X. Y., et al. (2016). Effects of curcumin on the apoptosis of cardiomyocytes and the expression of NF-kappaB, PPAR-gamma and Bcl-2 in rats with myocardial infarction injury. *Exp. Ther. Med.* 12, 3877–3884. doi: 10.3892/etm.2016.3858

Manickaraj, S., Thirumalai, D., Manjunath, P., Sekarbabu, V., Jeganathan, S., Sundaresan, L., et al. (2017). Oxidative environment causes molecular remodeling in embryonic heart-a metabolomic and lipidomic fingerprinting analysis. *Environ. Sci. Pollut. Res. Int.* 24, 23825–23833. doi: 10.1007/s11356-017-9997-y

Naghavi, M., Abajobir, A. A., Abbafati, C., Abbas, K. M., Abd-Allah, F., Abera, S. F., et al. (2017). Global, regional, and national age-sex specific mortality for 264 causes of death, 1980-2016: a systematic analysis for the Global Burden of Disease Study 2016. *Lancet.* 390, 1151–1210. doi: 10.1016/S0140-6736(17)32152-9

Nishizuka, Y. (1992). Intracellular signaling by hydrolysis of phospholipids and activation of protein kinase C. *Science.* 258, 607–614. doi: 10.1126/science.1411571

Pilla, J. J., Koomalsingh, K. J., Mcgarvey, J. R., Witschey, W. R., Dougherty, L., Gorman, J. H., et al. (2015). Regional myocardial three-dimensional principal strains during postinfarction remodeling. *Ann. Thorac. Surg.* 99, 770–778. doi: 10.1016/j.athoracsur.2014.10.067

Shimada, K., Jong, C. J., Takahashi, K., and Schaffer, S. W. (2015). Role of ROS production and turnover in the antioxidant activity of taurine. *Adv. Exp. Med. Biol.* 803, 581–596. doi: 10.1007/978-3-319-15126-7_47

Smith, S. A., Mammen, P. P., Mitchell, J. H., and Garry, M. G. (2003). Role of the exercise pressor reflex in rats with dilated cardiomyopathy. *Circulation.* 108, 1126–1132. doi: 10.1161/01.CIR.0000084538.40542.56

Smith, S. A., Williams, M. A., Mitchell, J. H., Mammen, P. P., and Garry, M. G. (2005). The capsaicin-sensitive afferent neuron in skeletal muscle is abnormal in heart failure. *Circulation.* 111, 2056–2065. doi: 10.1161/01.CIR.0000162473.10951.0A

Stathopoulou, K., Wittig, I., Heidler, J., Piasecki, A., Richter, F., Diering, S., et al. (2016). S-glutathiolation impairs phosphoregulation and function of cardiac myosin-binding protein C in human heart failure. *Faseb. J.* 30, 1849–1864. doi: 10.1096/fj.201500048

Takagawa, J., Zhang, Y., Wong, M. L., Sievers, R. E., Kapasi, N. K., Wang, Y., et al. (2007). Myocardial infarct size measurement in the mouse chronic infarction model: comparison of area- and length-based approaches. *J. Appl. Physiol.* 102, 2104–2111. doi: 10.1152/japplphysiol.00033.2007

Takemura, G., Kanamori, H., Okada, H., Miyazaki, N., Watanabe, T., Tsujimoto, A., et al. (2018). Anti-apoptosis in nonmyocytes and pro-autophagy in cardiomyocytes: two strategies against postinfarction heart failure through regulation of cell death/degeneration. *Heart. Fail. Rev.* 23, 759–772. doi: 10.1007/s10741-018-9708-x

Talameh, J. A., and Lanfear, D. E. (2012). Pharmacogenetics in chronic heart failure: new developments and current challenges. *Curr. Heart. Fail. Rep.* 9, 23–32. doi: 10.1007/s11897-011-0076-2

Tang, H. Y., Wang, C. H., Ho, H. Y., Wu, P. T., Hung, C. L., Huang, C. Y., et al. (2018). Lipidomics reveals accumulation of the oxidized cholesterol in erythrocytes of heart failure patients. *Redox Biol.* 14, 499–508. doi: 10.1016/j.redox.2017.10.020

Tappia, P. S., Yu, C. H., Di Nardo, P., Pasricha, A. K., Dhalla, N. S., and Panagia, V. (2001). Depressed responsiveness of phospholipase C isoenzymes to phosphatidic acid in congestive heart failure. *J. Mol. Cell. Cardiol.* 33, 431–440. doi: 10.1006/jmcc.2000.1315

Wang, Y. L., Wang, C. Y., Zhang, B. J., and Zhang, Z. Z. (2009). Shenfu injection suppresses apoptosis by regulation of Bcl-2 and caspase-3 during hypoxia/reoxygenation in neonatal rat cardiomyocytes in vitro. *Mol. Biol. Rep.* 36, 365–370. doi: 10.1007/s11033-007-9188-x

Wang, X., Guo, Z., Ding, Z., and Mehta, J. L. (2018). Inflammation, autophagy, and apoptosis after myocardial infarction. *J. Am. Heart. Assoc.* 7, e008024. doi: 10.1161/JAHA.117.008024

Wei, P., Yang, X. J., Fu, Q., Han, B., Ling, L., Bai, J., et al. (2015). Intermedin attenuates myocardial infarction through activation of autophagy in a rat model of ischemic heart failure via both cAMP and MAPK/ERK1/2 pathways. *Int. J. Clin. Exp. Pathol.* 8, 9836–9844.

Wu, Y., Xia, Z. Y., Meng, Q. T., Zhu, J., Lei, S., Xu, J., et al. (2011). Shen-Fu injection preconditioning inhibits myocardial ischemia-reperfusion injury in diabetic rats: activation of eNOS via the PI3K/Akt pathway. *J. Biomed. Biotechnol.* 2011, 384627. doi: 10.1155/2011/384627

Xing, J., Lu, J., and Li, J. (2014). Nerve growth factor decreases in sympathetic and sensory nerves of rats with chronic heart failure. *Neurochem. Res.* 39, 1564–1570. doi: 10.1007/s11064-014-1348-5

Yancy, C. W., Jessup, M., Bozkurt, B., Butler, J., Casey, D. E.Jr., Drazner, M. H., et al. (2013). 2013 ACCF/AHA guideline for the management of heart failure: a report of the American College of Cardiology Foundation/American Heart Association Task Force on Practice Guidelines. *J. Am. Coll. Cardiol.* 62, e147–e239.

Zheng, S., Wu, H., Yu, S., Ren, J., Duo, W., Ma, Z., et al. (2015). Shenfu Injection suppresses inflammation by targeting haptoglobin and pentraxin 3 in rats with chronic ischemic heart failure. *Chin. J. Integr. Med.* 21, 22–28. doi: 10.1007/s11655-013-1440-8

Conflict of Interest: The authors declare that the research was conducted in the absence of any commercial or financial relationships that could be construed as a potential conflict of interest.

frontiers in Pharmacology

SYSTEMATIC REVIEW
published: 24 December 2019
doi: 10.3389/fphar.2019.01542

Efficacy and Safety of Sodium Tanshinone IIA Sulfonate Injection on Hypertensive Nephropathy: A Systematic Review and Meta-Analysis

*Junyao Xu†, Chenghua Zhang†, Xiaoqing Shi, Jie Li, Ming Liu, Weimin Jiang and Zhuyuan Fang**

Institute of Hypertension, Affiliated Hospital of Nanjing University of Chinese Medicine, Nanjing, China

OPEN ACCESS

Edited by:
Xiu-Wei Yang,
Peking University, China

Reviewed by:
Manoj Gajanan Kulkarni,
University of KwaZulu-Natal, South Africa
Qiuwang Zhang,
St. Michael's Hospital, Canada

***Correspondence:**
Zhuyuan Fang
jsszyyfzy@163.com

†These authors have contributed equally to this work

Specialty section:
This article was submitted to Ethnopharmacology, a section of the journal Frontiers in Pharmacology

Received: *06 April 2019*
Accepted: *27 November 2019*
Published: *24 December 2019*

Citation:
Xu J, Zhang C, Shi X, Li J, Liu M, Jiang W and Fang Z (2019) Efficacy and Safety of Sodium Tanshinone IIA Sulfonate Injection on Hypertensive Nephropathy: A Systematic Review and Meta-Analysis. Front. Pharmacol. 10:1542. doi: 10.3389/fphar.2019.01542

Background: Sodium tanshinone IIA sulfonate (STS) injection, the extractive of traditional Chinese medicine Danshen, is supposed to be a supplementary treatment in hypertensive nephropathy.

Objectives: To evaluate the efficacy and safety of STS in treatment of hypertensive nephropathy.

Methods: We systematically searched China National Knowledge Infrastructure (CNKI), Chinese Scientific Journals Database (VIP), Wan-fang database, Chinese Biomedicine Database (CBM), PubMed, Embase, Web of Science, and Cochrane Library from their inception to December 2018. All studies were screened by two reviewers according to the inclusion and exclusion criteria independently. The Cochrane Collaboration's risk tool was used to assess the methodological quality of the included studies. Reviewer Manager 5.3 was employed for statistical analysis.

Results: Sixteen trials involving 1,696 patients were included. The meta-analysis results indicated a combination of STS and angiotensin receptor blockers (ARBs) was more effective than ARB monotherapy in modulating hypertensive nephropathy, as represented by improved estimated glomerular filtration rate (eGFR) [mean difference (MD) = 6.87, 95% CI (4.47, 9.28), $P < 0.00001$] and reduced 24 h urinary protein [MD = –0.23, 95% CI (–0.27, –0.19), $P < 0.00001$], serum creatinine (SCr) [MD = –21.74, 95% CI (–24.11, –19.38), $P < 0.00001$], cystatin-C [MD = –0.16, 95% CI (–0.24, –0.07), $P = 0.0003$], urinary immunoglobulin G (IgG) [MD = –0.85, 95% CI (–1.11, –0.59), $P < 0.00001$], and urinary transferrin [MD = –0.61, 95% CI (–1.04, –0.17), $P = 0.007$]. In addition, the combination therapy had better control in systolic blood pressure (SBP) [MD = –6.53, 95% CI (–8.19, –4.87), $P < 0.00001$] and diastolic blood pressure (DBP) [MD = –4.14, 95% CI (–5.69, –2.59), $P < 0.00001$]. Only three trials reported adverse events, and no adverse drug reactions were observed.

Conclusions: STS combined with ARBs had a stronger effect on improving renal function in patients with primary hypertensive nephropathy than ARB monotherapy. The combination therapy also provided auxiliary hypotensive effects. Further large-scale, multicenter, and rigorously designed randomized controlled trials (RCTs) should be conducted to confirm our findings.

Keywords: sodium tanshinone IIA sulfonate injection, hypertensive nephropathy, systematic review, meta-analysis, efficacy, safety

INTRODUCTION

The prevalence of primary hypertension (PH), a chronic disease, is increasing worldwide. It is estimated that approximately one of three people suffer from high blood pressure (BP) all over the world (Lim et al., 2012). PH has been one of the leading risk factors for global disease burden (Whelton et al., 2018). Although a system therapeutic regimen has been established, hypertension still remains undertreated and uncontrolled especially in developing countries like China (Lu et al., 2017). Patients with hypertension usually have a series of secondary lesions. The kidney, as a vital organ in balancing the volume load and the toxin level, is extremely vulnerable to high BP. It is known that structural damage to the renal unit, such as the barotrauma damage to the glomerular filtration barrier, can lead to compensatory but maladaptive increases in the reuptake of water and sodium by the renal tubule, further exacerbating BP abnormalities (Bidani et al., 2013; Hall et al., 2014). Nowadays, hypertensive kidney disease has been the second leading cause of end-stage renal disease (ESRD) after diabetes mellitus (Hart and Bakris, 2010). Approximately 30,000 individuals in the United States are diagnosed with hypertension-associated ESRD yearly, which exerts substantial adverse influence on public health and health-care financing (Suneel et al., 2011).

BP control is regarded as a vital target in patients of hypertensive nephropathy. Agents that inhibit the renin–angiotensin–aldosterone system (RAAS) are the first-line drugs of choice for those with hypertensive nephropathy since they can effectively reduce BP, proteinuria, and chronic kidney disease (CKD) progression as well as cardiovascular events associated with hypertension, diabetes, and vascular diseases (The GISEN Group, 1997; Lewis et al., 2001; Brenner et al., 2001). However, existing data have demonstrated that well controlled blood pressure (<130/80 mmHg) slows but does not stop progression of renal injury (Suneel et al., 2011). Furthermore, use of these drugs alone at the recommended dosages for BP control is usually unable to achieve enough renoprotective effect. Thus, in addition to BP control, nephropathy protection is necessary.

Traditional Chinese medicine is the most common form of both alternative and complementary medicine in Asia which has been used extensively for the treatment of CKD (Huang et al., 2018). Danshen, the dried root and rhizome of *Salvia miltiorrhiza Bge* (Labiatae), is a popular medicinal herb that has long been used for the treatment of various diseases. Studies have shown that Danshen is the top single herb prescribed for the treatment of CKD in outpatients in China (Huang et al., 2018). Sodium tanshinone IIA sulfonate (STS) injection, the extract of Danshen, has been widely used in current clinical practice for its activities in anti–free radical induced tissue damage, arteriolar vasodilation, lowering blood viscosity, and so on (Bai, 2012). It mainly contains STS (sodium 1,6,6-trimethyl-10, 11-dioxo-6,7,8,9,10,11- hexahydrophenanthro[1,2-b]furan-2-sulfonate) (Hao et al., 2007; Chen et al., 2013). The concentration of the commercial injection is 5 mg/ml, and the purity is more than 90% (STS: 90%–98%) (Wang et al., 2006; Liu, 2010; Chen et al., 2013; Dong et al., 2019). Quality control and chemical analyses of the material were also reported. (Wang et al., 2006; Hao et al., 2007; Liu, 2010; Chen et al., 2013; Dong et al., 2019). Procedures are fully reproducible.

In recent years, a large number of clinical trials suggested that STS and angiotensin receptor blocker (ARB) combination benefited patients with hypertensive nephropathy. However, no definite conclusion was drawn on this. Therefore, we conducted this systematic review and meta-analysis to investigate the efficacy of STS as an adjuvant agent in the management of hypertensive nephropathy.

MATERIALS AND METHODS

Readers can access the protocol of this systematic review in International Prospective Register of Systematic Reviews (PROSPERO) (CRD42018114511).

Database and Search Strategies

A literature search was carried out in the following eight databases from their inception to December 2018: China National Knowledge Infrastructure (CNKI), Chinese Scientific Journals Database (VIP), Wan-fang database, Chinese Biomedicine Database (CBM), PubMed, Embase, Web of Science, and Cochrane Library. The publishing language was restricted to Chinese and English. Search terms including "hypertension," "sodium tanshinone IIA sulfonate injection," "tanshinone IIA," "kidney diseases," "renal insufficiency," "kidney failure, chronic," "hypertensive nephropathy," "kidney injury," "kidney damage," "renal damage," "renal injury," "nephrosclerosis," "renal impairment," and "kidney impairment" were used individually or in combination. In addition, a filter for clinical trials was also employed.

Inclusion Criteria

Studies meeting the following criteria were included: (1) randomized controlled trials (RCTs), regardless of blinding or publication types; (2) patients with hypertensive nephropathy, (i) meeting the diagnostic criteria of hypertension, (ii) presenting with clinical features of renal injury like persistent proteinuria and increasing levels of serum creatinine (SCr), and (iii) without primary renal disease, secondary hypertension, or some other conditions such as diabetes mellitus causing renal injury; (3) intervention using STS combined with ARBs compared to ARB monotherapy; and (4) assessment of 24 h urinary protein as the primary outcome plus at least one additional outcome measure, which could be SCr, estimated glomerular filtration rate (eGFR), urinary immunoglobulin G (IgG), cystatin-C (Cys-C), urinary transferrin, systolic blood pressure (SBP) reduction, or diastolic blood pressure (DBP) reduction.

Exclusion Criteria

Studies were excluded if they met the following criteria: (1) duplicated publications; (2) non-clinical research, basic research, and review articles as well as case reports and theoretical discussions; (3) use of any other western medicines and/or herbal medicines during the research; or (4) outcome data of interest were unavailable for meta-analysis.

Data Extraction

Two investigators (JX, CZ) independently screened and extracted the data according to the inclusion and exclusion criteria. After the general details, patients' characteristics, interventions, and outcomes were extracted, a cross-check was then done. Any disagreements were resolved through discussion or the verification of a third investigator (XS).

Quality Assessment

Evaluation of methodological quality of the included studies was conducted by the same two investigators (JX, CZ), who used the Cochrane Collaboration's risk tool. Random sequence generation (selection bias), allocation concealment (selection bias), blinding of participants and personnel (performance bias), blinding of outcome assessment (detection bias), incomplete outcome date (attrition bias), selective reporting (reporting bias), and other bias were assessed. The grade of bias risk was classified as "low," "high," and "unclear." We also performed a funnel plot to evaluate publication bias.

Data Synthesis and Analysis

Revman 5.3 software was employed to pool the effect size. Mean difference (MD) or standardized mean difference (SMD) and 95% confidence intervals (CI) were used for continuous variables. Heterogeneity was evaluated statistically using the χ^2 test and inconsistency index statistic (I^2) (Higgins et al., 2003). If substantial heterogeneity existed ($I^2 > 50\%$ or $P < 0.05$), a random effect model was applied; otherwise, we adopted a fixed effect model (DerSimonian and Laird, 1986). We also performed subgroup analysis and sensitivity analysis to explore the potential sources of heterogeneity and inspect the stability of the result.

RESULTS

Search Results

A total of 1,029 articles were initially obtained through the search strategy. After excluding 548 duplications, the remaining articles were screened based on their titles and abstracts, and 459 records were removed. Out of the remaining 22 articles assessed for eligibility, 16 articles met the eligibility criteria of this systematic review and meta-analysis (Zhu et al., 2011; Yang et al., 2012; Wu, 2013; Zou et al., 2013; Cao et al., 2014; Li, 2014; Yu, 2014; Liu, 2015; Luo, 2015; Qiu, 2015; Zhu, 2015; Bi et al., 2016; Li, 2016; Wang et al., 2016; Li and Guo, 2017; Tusonguri, 2017). The flowchart for literature retrieval is shown in **Figure 1**.

Study Characteristics

All 16 included trials were conducted in China from 2011 to 2017 and involved a total of 1,696 participants. Sample size ranged from 50 to 230, and only seven trials included more than 100 participants (Li, 2014; Luo, 2015; Qiu, 2015; Bi et al., 2016; Li, 2016; Wang et al., 2016; Tusonguri, 2017). The average age of the enrolled participants was 63, with 55.5% male patients. The intervention used in all experimental groups was STS combined with ARBs (valsartan, V; irbesartan, Ir; losartan, L), and the control treatment was ARBs. The dose range of STS was from 40 to 60 mg/d. The duration of treatment was 2 or 4 weeks. More details of the included studies are presented in **Table 1**.

Quality Assessment of Included Studies

The methodological quality assessments of all included studies are shown in **Figures 2** and **3**. Only three trials described the randomization method used in their studies, while others did not report any specific randomization technique (Li, 2014; Qiu, 2015; Li and Guo, 2017). None of studies reported allocation concealment procedure and blinding. In general, most of the included studies had high risk of bias and low methodological quality.

META-ANALYSIS RESULTS

24 h Urinary Protein (g/d)

All 16 trials reported 24 h urinary protein measurement results. Following the test of heterogeneity ($P = 0.01$, $I^2 = 49\%$), we used a fixed effect model. The pooled analysis indicated that the intervention of STS combined with ARBs had better effect in decreasing 24 h urinary protein. The difference between two groups was statistically significant (MD = −0.23, 95% CI: −0.27 to −0.19; $P < 0.00001$, **Figure 4**). This result suggests that STS as an adjunct therapy to ARBs may alleviate renal injury more effectively than ARBs alone.

Serum Creatinine (μmol/L)

Eleven clinical trials reported SCr levels (Zhu et al., 2011; Wu, 2013; Zou et al., 2013; Li, 2014; Yu, 2014; Liu, 2015; Luo, 2015;

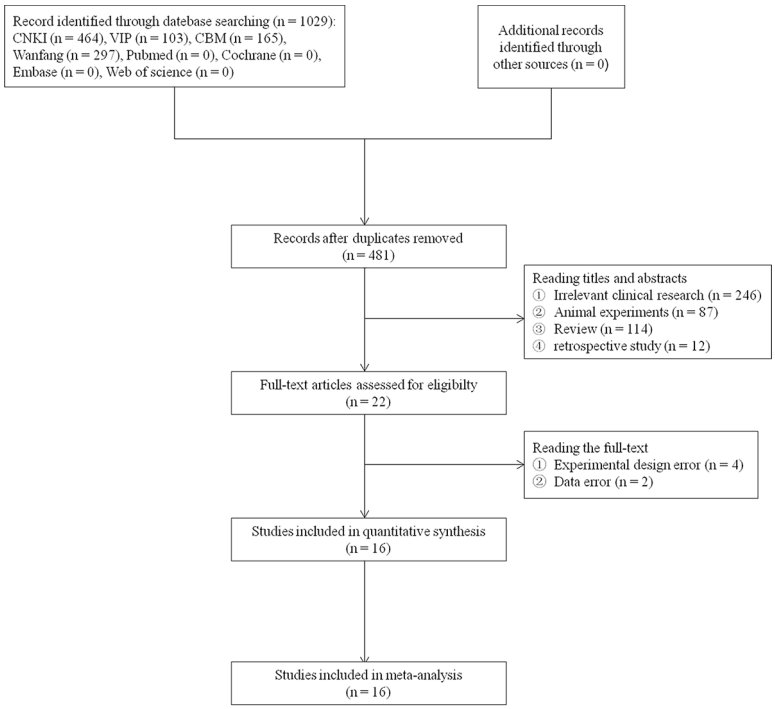

FIGURE 1 | Flow diagram of the literature selection.

TABLE 1 | Characteristics of included studies.

Study	Sex (M/F)	Case (E/C)	Age (E/C) (years)	Course of disease (E/C) (years)	Therapy of experiment group	Therapy of control group	Durance (weeks)	Outcomes
Tusonguri, 2017	68/60	64/64	39–81	3–22	Tl 60 mg q.d.+V 80 mg q.d.	V 80 mg q.d.	2	(1) (2) (3) (4) (7)
Li and Guo, 2017	104/96	100/100	63.5 ± 8/64.1 ± 8.1	5.1 ± 1.8/5.8 ± 1.9	Tl 60 mg q.d.+V 200 mg q.d.	V 200 mg q.d.	2	(1) (2) (3) (4) (7)
Wang et al., 2016	69/61	65/65	58.4 ± 2.9/57.4 ± 3.2	6.3 ± 1.4/6.4 ± 1.2	Tl 60 mg q.d.+V 80 mg q.d.	V 80 mg q.d.	2	(1) (2) (3) (7)
Li, 2016	35/25	30/30	23–70	Unclear	Tl 60 mg q.d.+V 80 mg q.d.	V 80 mg q.d.	4	(1) (2) (3) (4) (5) (6) (8)
Bi et al., 2016	Unclear	50/50	41–62	11.3 ± 5.1/12.6 ± 6.1	Tl 50 mg q.d.+Ir 150 mg q.d.	Ir 150 mg q.d.	4	(1) (2) (3) (6) (9) (10)
Zhu, 2015	55/43	49/49	40–75	1–8	Tl 60 mg q.d.+V 80 mg q.d.	V 80 mg q.d.	2	(1) (2) (3)
Qiu, 2015	62/46	54/54	43–71	5–20	Tl 60 mg q.d.+V 80 mg q.d.	V 80 mg q.d.	2	(1) (2) (3) (4) (6) (7) (8)
Luo, 2015	82/38	60/60	35–81	10 ± 8/10 ± 9	Tl 50 mg q.d.+V 80 mg q.d.	V 80 mg q.d.	2	(1) (2) (3) (4) (7)
Liu, 2015	53/37	45/45	27–65	1.5–12	Tl 50 mg q.d.+L 50 mg q.d.	L 50 mg q.d.	2	(1) (2) (3) (4) (5)
Yu, 2014	45/22	34/33	42–84	4–16	Tl 60 mg q.d.+V 80 mg q.d.	V 80 mg q.d.	2	(1) (2) (3) (4) (7)
Li, 2014	123/107	115/115	40–75	4–10	Tl 60 mg q.d.+V 80 mg q.d.	V 80 mg q.d.	2	(1) (2) (3) (4) (7)
Cao et al., 2014	44/45	45/44	63.1 ± 16.8/62.3 ± 17.6	12.4 ± 6.2/10.2 ± 8.0	Tl 60 mg q.d.+Ir 150 mg q.d.	Ir 150 mg q.d.	4	(1) (2) (3) (6) (11) (12)
Zou et al., 2013	45/35	40/40	62 ± 10/63 ± 8	10 ± 8/10 ± 6	Tl 60 mg q.d.+V 80 mg q.d.	V 80 mg q.d.	2	(1) (2) (3) (4) (7)
Wu, 2013	27/23	25/25	43.4 ± 7.3	91.3 ± 16.8 (months)	Tl 40 mg q.d.+L 50 mg q.d.	L 50 mg q.d.	2	(3) (4) (5) (15)
Yang et al., 2012	42/44	43/43	63.1 ± 16.8/62.3 ± 17.6	12.4 ± 6.2/10.2 ± 8.0	Tl 60 mg q.d.+V 80 mg q.d.	V 80 mg q.d.	4	(1) (2) (3) (6) (8) (12) (13)
Zhu et al., 2011	31/29	30/30	52.1 ± 8.6	89.1+17.3 (months)	Tl 40 mg q.d.+L 50 mg q.d.	L 50 mg q.d.	2	(1) (2) (3) (4) (5) (14) (15)

M, male; F, female; E, experimental group; C: control group; Tl, tanshinone injection; V, valsartan; Ir, irbesartan; L, losartan; q.d., once daily; (1) systolic blood pressure; (2) diastolic blood pressure; (3) 24 h urinary protein; (4) serum creatinine; (5) estimated glomerular filtration rate; (6) urinary IgG; (7) cystatin-C; (8) urinary transferrin; (9) podocalyxin; (10) carboxyterminal propeptide of type I procollagen; (11) urinary β2-microglobulin; (12) microalbuminuria; (13) urinary alpha1-microglobulin; (14) mean arterial pressure; (15) N-acetyl-beta-D-glucosaminidase.

Qiu, 2015; Li, 2016; Li and Guo, 2017; Tusonguri, 2017). Following the test of heterogeneity ($P < 0.00001$, $I^2 = 79\%$), a random effect model was used to estimate pooled effect size. The results showed that patients receiving the therapy of STS combined with ARBs had significantly decreased SCr compared with control groups. The difference between two groups was statistically significant (MD = −21.74, 95% CI: −24.11 to −19.38; $P < 0.00001$, **Figure 5**).

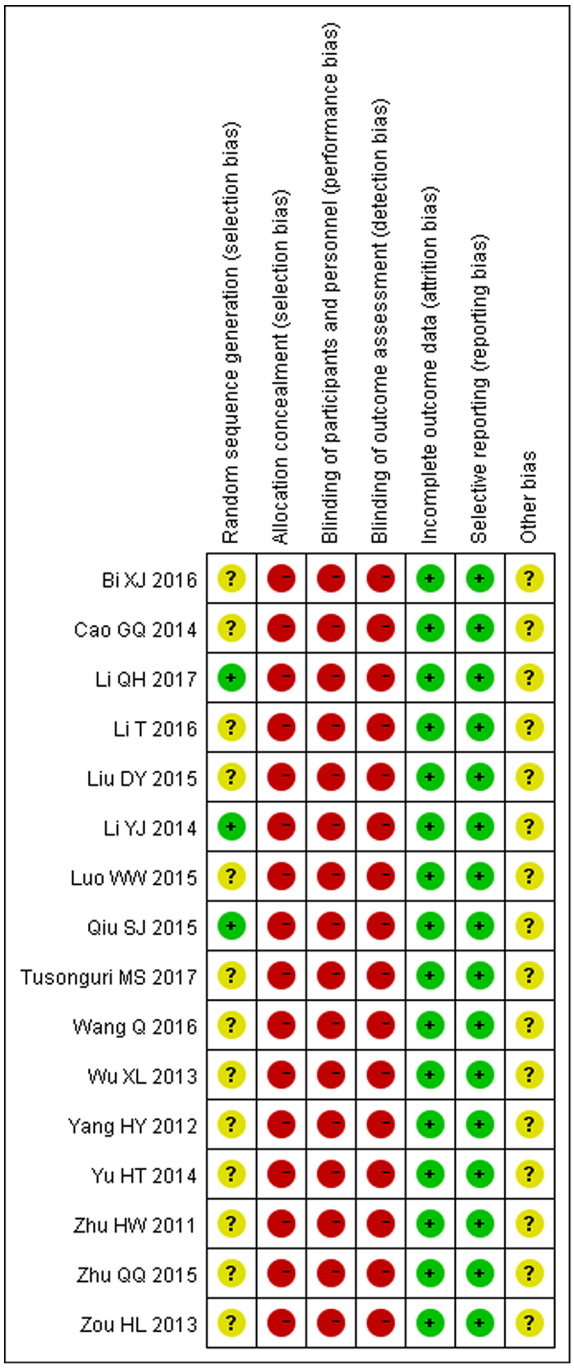

FIGURE 2 | Risk of bias summary.

Estimated Glomerular Filtration Rate (ml/Min·1.73m^2)

There were four studies that reported eGFR results (Zhu et al., 2011; Wu, 2013; Liu, 2015; Li, 2016). A fixed effect model was adopted to pool the data because of no heterogeneity found in these studies (P = 0.85, I^2 = 0%). The results showed that the therapy of STS combined with ARBs was more effective in maintaining eGFR (MD = 6.87, 95% CI: 4.47, 9.28, P < 0.00001, **Figure 6**).

Cystatin-C (mg/L)

There were 8 studies that showed Cys-C results (Zou et al., 2013; Li, 2014; Yu, 2014; Luo, 2015; Qiu, 2015; Wang et al., 2016; Li and Guo, 2017; Tusonguri, 2017). A fixed effect model was adopted to pool the data because of no heterogeneity found in these studies (P = 1.0, I^2 = 0%). The results revealed that STS plus ARBs was superior to ARBs alone in reducing Cys-C (MD = −0.16, 95% CI: −0.24 to −0.07; P = 0.0003, **Figure 7**).

Urinary Immunoglobulin G (mg/dl)

Five clinical trials reported urinary IgG levels (Yang et al., 2012; Cao et al., 2014; Qiu, 2015; Bi et al., 2016; Li, 2016). Following the test of heterogeneity (P = 0.22, I^2 = 31%), a fixed effect model was used to estimate pooled effect size. The results suggested that the level of urinary IgG in STS combined with ARBs was lower than that in the control group. The difference between two groups was statistically significant (MD = −0.85, 95% CI: −1.11 to −0.59; P < 0.00001, **Figure 8**).

Urinary Transferrin (mg/dl)

Only three clinical trials included urinary transferrin data (Yang et al., 2012; Qiu, 2015; Li, 2016). Following the test of heterogeneity (P = 0.09, I^2 = 58%), a random effect model was used to estimate pooled effect size. The results suggested that compared with control groups, patients treated with STS combined with ARBs had a significantly lower level of urinary transferrin (MD = −0.61, 95% CI: −1.04 to −0.17; P = 0.007, **Figure 9**).

Blood Pressure Reductions (mmHg)

There were 15 studies that reported SBP and DBP reductions (Zhu et al., 2011; Yang et al., 2012; Zou et al., 2013; Cao et al., 2014; Li, 2014; Yu, 2014; Liu, 2015; Luo, 2015; Qiu, 2015; Zhu, 2015; Bi et al., 2016; Li, 2016; Wang et al., 2016; Li and Guo, 2017; Tusonguri, 2017). Following the test of heterogeneity (P < 0.00001 for both SBP and DBP, I^2 = 72% and 88% for SBP and DBP, respectively), a random effect model was used to estimate pooled effect size. The results revealed that compared with ARB monotherapy, the combination treatment of STS and ARBs resulted in a significantly greater reduction in SBP (MD = −6.53, 95% CI: −8.19 to −4.87; P < 0.00001, **Figure 10**) and DBP (MD = −4.14, 95% CI: −5.69 to −2.59; P < 0.00001, **Figure 11**). In subgroup analysis, the hypotensive effect of combined STS and ARBs was better than ARB monotherapy in SBP (MD = −7.25, 95% CI: −8.92 to −5.58; P < 0.00001, **Figure 10**) and DBP (MD = −4.50, 95% CI: −6.38 to −2.61; P < 0.00001, **Figure 11**) at the 2-week follow-up time point. In addition, the combination treatment also had a significantly greater reduction in DBP (MD = −3.03, 95% CI: −4.55 to −1.52; P < 0.0001, **Figure 11**) at the 4-week follow-up time point. However, there were no differences in SBP reduction (MD = −4.25, 95% CI: −8.74 to 0.24; P = 0.06, **Figure 10**) at the 4-week follow-up time point.

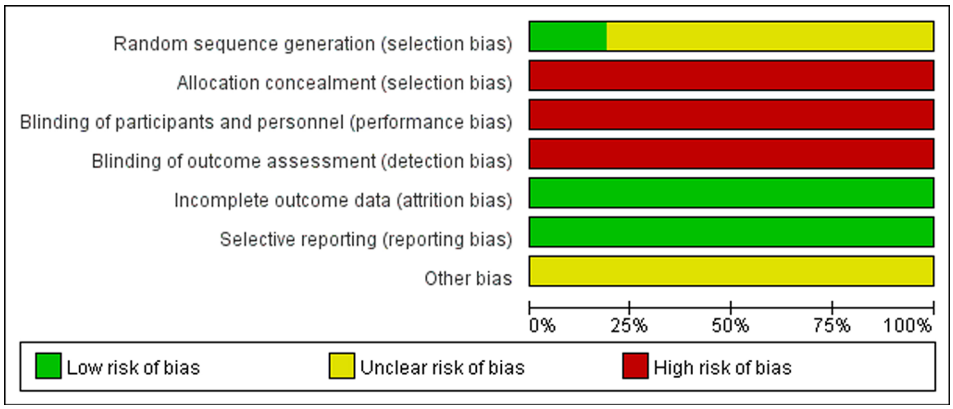

FIGURE 3 | Risk of bias graph of included trials.

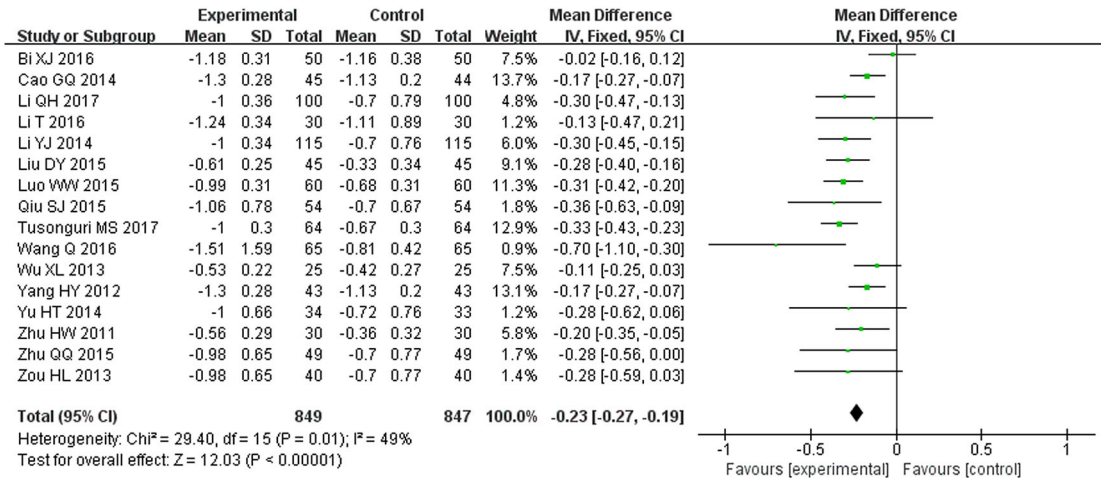

FIGURE 4 | Meta-analysis for comparison of 24 h urinary protein levels between the experimental and control groups.

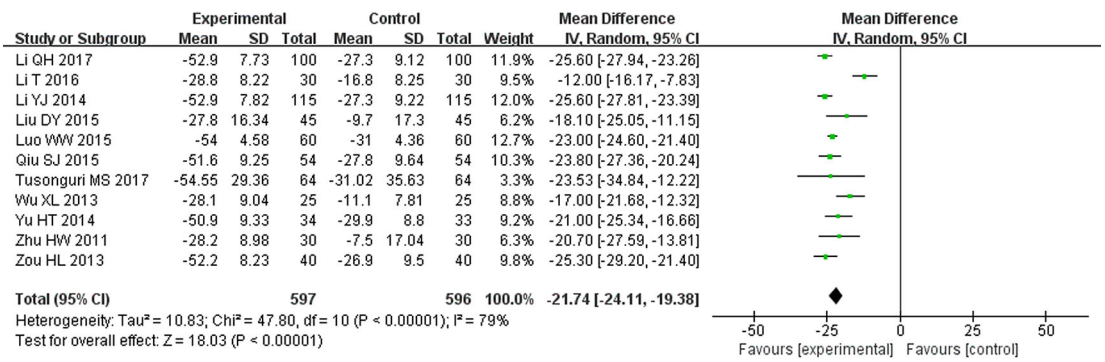

FIGURE 5 | Meta-analysis for comparison of serum creatinine (SCr) levels between the experimental and control groups.

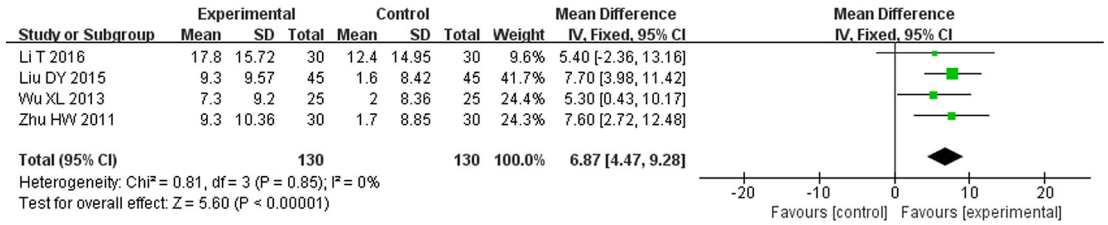

FIGURE 6 | Meta-analysis for comparison of estimated glomerular filtration rate (eGFR) levels between the experimental and control groups.

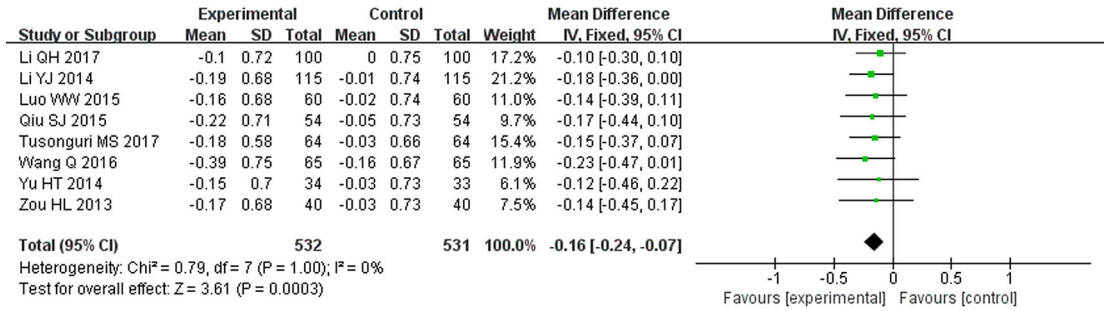

FIGURE 7 | Meta-analysis for comparison of cystatin-C (Cys-C) levels between the experimental and control groups.

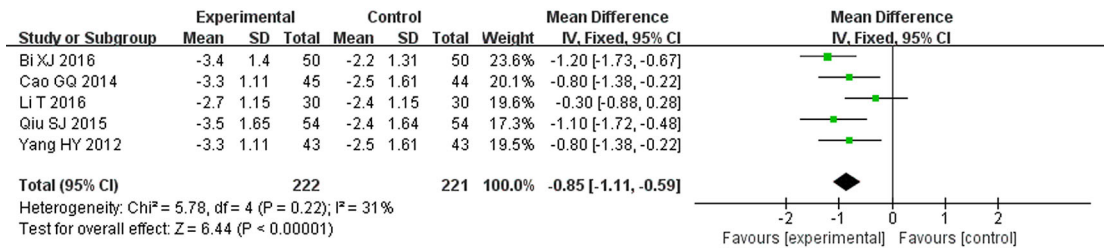

FIGURE 8 | Meta-analysis for comparison of urinary immunoglobulin G (IgG) levels between the experimental and control groups.

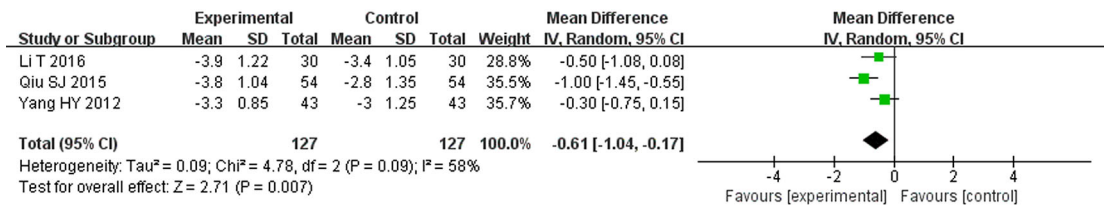

FIGURE 9 | Meta-analysis for comparison of urinary transferrin levels between the experimental and control groups.

Safety

Out of all included studies, only three trials examined adverse events (Zhu et al., 2011; Luo, 2015; Qiu, 2015). These studies all clearly reported that there were no adverse events associated with the STS/ARB combination therapy. However, because the remaining trials did not provide any details regarding adverse effects, it is difficult to draw a conclusion on the safety of STS.

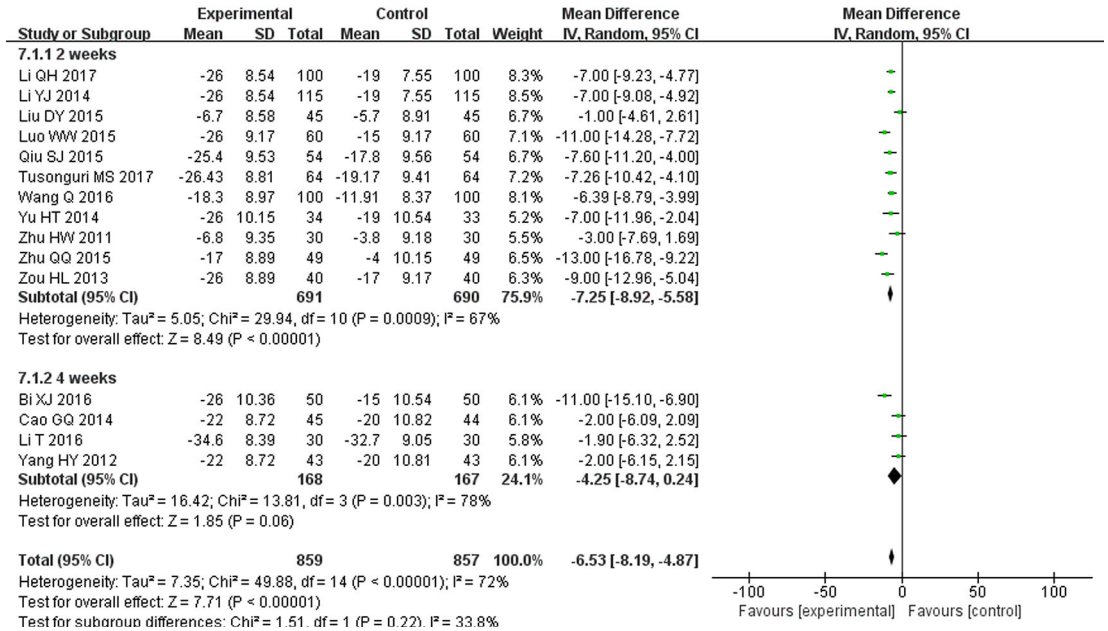

FIGURE 10 | Meta-analysis for comparison of systolic blood pressure (SBP) between the experimental and control groups.

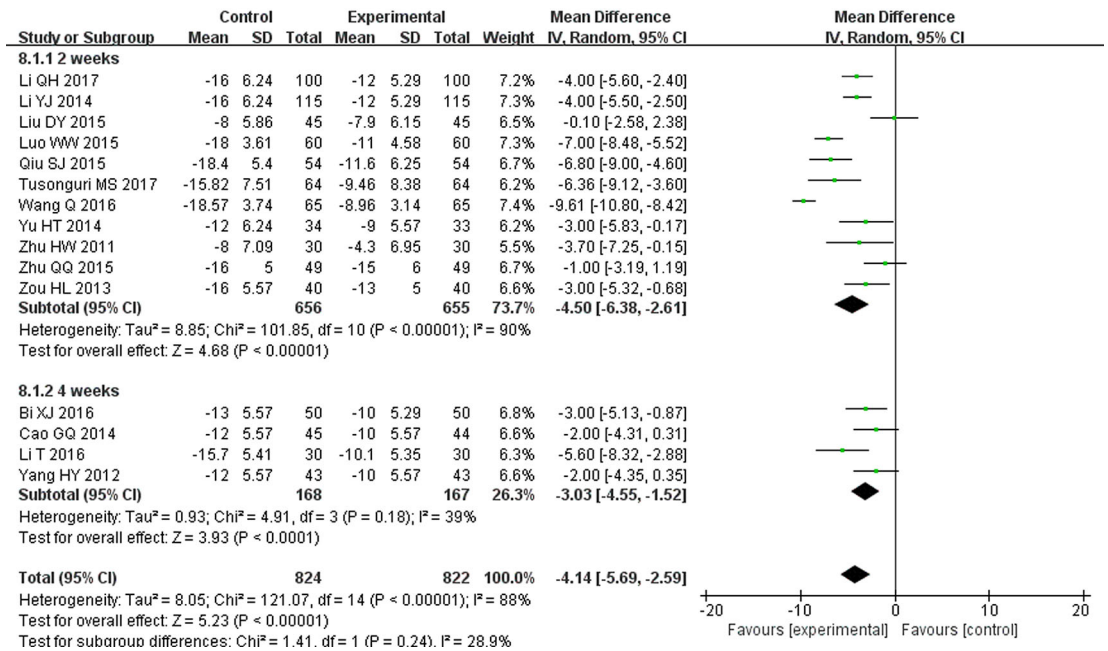

FIGURE 11 | Meta-analysis for comparison of diastolic blood pressure (DBP) between the experimental and control groups.

Subgroup Analysis

To explore the sources of heterogeneity and improve the persuasiveness of the evidence, we conducted a subgroup analysis based on the study characteristics for 24 h urinary protein and SCr, as both of these two biomarkers are crucial indicators that reflect the extent of the renal damage and predict the progression of diseases (Hillege et al., 2002; Lisowska-Myjak et al., 2011). The effect of the combination treatment with STS

and ARBs was consistent with the results described above for every subgroup regardless of the duration of treatment, the category of ARBs, the dose of STS, or the number of patients. However, the reduction in 24 h urinary protein did not show significant difference in irbesartan studies (MD = −0.10, 95% CI: −0.25 to −0.04; $P = 0.17$, **Table 2**). Meanwhile, the heterogeneity of each subgroup on 24 h urinary protein declined in various degrees, which indicates that these four factors may be the sources of heterogeneity, especially the intervention course and sample sizes. For SCr, unfortunately, we were not able to remove the heterogeneity from subgroup analysis. However, only Ting Li's study used 4 weeks as the cutoff for treatment duration, which might bias the heterogeneity (Li, 2016). Furthermore, removal of this study from SCr analysis resulted in a considerable reduced I^2 ($I^2 = 54\%$).

Sensitivity Analysis

To further confirm the stability of the results of the 24 h urinary protein and SCr, we respectively replaced fixed effect model with random effect model and excluded the most and least weighted trials. The results were not significantly different from those described above, suggesting our meta-analysis results are robust and reliable.

Publication Bias

We assessed the publication bias of 24 h urinary protein with the funnel plot. As shown in **Figure 12**, there was no obvious publication bias in our analysis. However, all the included studies were published in mainland China with positive results, potential publication bias still likely existed.

DISCUSSION

Although substantial efforts have been made in the prevention and combating of hypertension, it remains one of the most common chronic diseases, and its prevalence is increasing worldwide (Suneel et al., 2011). Hypertension is not only the direct cause of renal damage but can also contribute to the progression of kidney disease (Suneel et al., 2011). The rates of hypertension-associated CKD and ESRD continue to rise, which have a substantial negative influence on public health and health-care financing. BP-lowering therapy, especially the use of the RAAS blockers, has become the main strategy for nephroprotection for patients with renal damage. However, renoprotective effects cannot be achieved to a satisfying extent when these drugs are used alone at the dosages recommended for BP control (Ruggenenti et al., 2008). Thus, other treatments that synergize with RAAS inhibitors to further interfere with events leading to interstitial inflammation and structural damage are desirable (Remuzzi and Bertani, 1998).

Danshen, a popular Chinese herb from dried roots of *S. miltiorrhiza Bunge*, has been used for over 2,000 years for the treatment of cardiovascular diseases without obvious side effects (Yan et al., 2018). Tanshinone IIA, one of the major constituents extracted from Danshen, is officially regarded as a quality control marker as per Chinese Pharmacopoeia (Yan et al., 2018). Sodium tanshinone IIA sulfonate injection is a water-soluble derivative of tanshinone IIA and has become commercially available in China. Previous pharmacological studies have revealed that STS has various biological activities such as anti-atherosclerosis, anti-arrhythmia, improving myocardial blood supply, and cardiac remodeling (Gao et al., 2012). Therefore, STS has been widely used for the management of cardiovascular diseases including angina pectoris and myocardial infarction. Furthermore, intensive research has discovered the renoprotective effect of STS, which has drawn much significant attention and is becoming a research hot spot. Recent publications have demonstrated that tanshinone IIA can exert its renoprotective effects by fighting oxidative stress, attenuating renal fibrosis, regulating inflammation, counteracting ischemia-reperfusion injury, protecting podocytes and endothelial cells, and ameliorating microcirculatory disturbance (Han et al., 2008; Wang et al., 2015; Xu et al., 2016; Cao et al., 2017; Zhu et al., 2017). Increasing evidence indicates that STS combined with antihypertensive drugs like ARBs can additively alleviate the

TABLE 2 | Subgroup analyses on 24 h urinary protein and SCr.

Factor	24 h urinary protein				SCr			
	N	MD (95% CI)	*P*-value	I^2	N	MD (95% CI)	*P*-value	I^2
Duration								
2 weeks	12	−0.28 (−0.33, −0.23)	<0.00001	14%	10	−23.16 (−24.83, −21.50)	<0.00001	53%
4 weeks	4	−0.14 (−0.20, −0.07)	<0.0001	18%	1	−12 (−16.17, −7.83)	<0.00001	–
Category of ARBs								
Valsartan	11	−0.28 (−0.34, −0.23)	<0.00001	9%	8	−22.66 (−25.25, −20.06)	<0.00001	82%
Irbesartan	2	−0.10 (−0.25, 0.04)	0.17	67%	0	–	–	–
Losartan	3	−0.20 (−0.28, −0.12)	<0.00001	39%	3	−18.15 (−21.54, −14.77)	<0.00001	0%
Dose of STS								
40 mg q.d.	2	−0.15 (−0.25, −0.05)	0.004	0%	2	−18.17 (−22.04, −14.30)	<0.00001	0%
50 mg q.d.	3	−0.21 (−0.38, −0.03)	0.02	0%	2	−22.75 (−24.31, −21.19)	<0.00001	45%
60 mg q.d.	11	−0.25 (−0.30, −0.20)	<0.00001	53%	7	−22.51 (−25.92, −19.09)	<0.00001	84%
Number of patients								
≤100	10	−0.17 (−0.22, −0.12)	<0.00001	11%	6	−19.02 (−23.29, −14.75)	<0.00001	78%
>100	6	−0.33 (−0.39, −0.26)	<0.00001	0%	5	−24.24 (−25.32, −23.17)	<0.00001	22%

SCr, serum creatinine; MD, mean difference; CI, confidence interval; ARB, angiotensin receptor blocker; STS, sodium tanshinone IIA sulfonate; q.d., once daily.

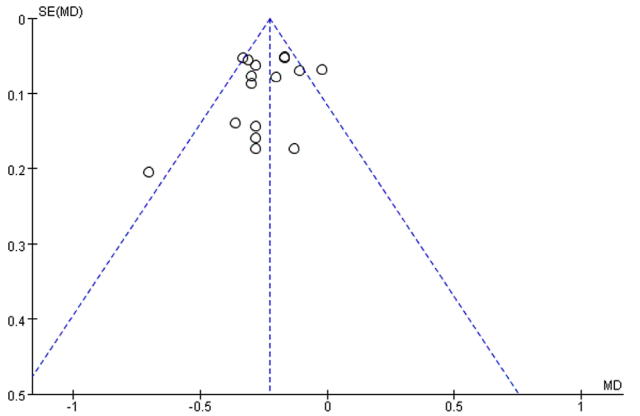

FIGURE 12 | Funnel plot of total 24 h urinary protein.

renal dysfunction induced by hypertension. However, the efficacy of STS injection as adjunctive therapy for ARBs on hypertensive nephropathy has not been systematically reviewed and analyzed.

To the best of our knowledge, this is the first systematic review and meta-analysis that assessed renoprotective effects of STS combined with ARBs. A total of 16 trials involving 1,696 patients were identified for this review. According to our analysis of currently available data, we concluded that STS combined with ARBs is more effective than ARB monotherapy in renoprotection, as our findings showed improved eGFR and reduced levels of 24 h urinary protein, SCr, Cys-C, urinary IgG, and urinary transferrin in patients receiving both STS and ARBs compared with those taking only ARBs.

In clinical trials, surrogate end points are often more frequently employed than clinical end points as they are practically measurable. Additionally, use of surrogate end points can reduce the sample size and shorten the duration of studies. Therefore, not surprisingly, we found that surrogate end points were used in all of the analyzed studies, while none of them mentioned primary end points (such as time to doubling of SCr, onset of ESRD, and death). There are a number of reasons for the universality of using surrogate end points in hypertensive nephropathy studies. Firstly, the course of hypertensive nephropathy is long. Clinical outcomes may take years to draw the scientific conclusion. Secondly, as the disease progresses, ARBs may not be suitable for further treatment (such as high creatinine levels and hyperkalemia). Lastly, the use of surrogate end points could aid our understanding of disease processes and mechanisms of action of therapies, directing our decision-making regarding the treatment (Lonn, 2001).

Among multiple surrogate biomarkers that reflect renal function, urinary protein, SCr, and eGFR are the most widely used indicators for the assessment of renoprotective effects of antihypertensive agents in clinical trials. After the pioneering Ramipril Efficacy In Nephropathy (REIN) trials found that short-term reduction in proteinuria slows the progression to ESRD in the long term, the reduction of proteinuria has been considered as a novel target of renoprotective therapy (The GISEN Group, 1997). Subsequent studies confirmed that proteinuria is a potent biomarker of renal dysfunction, and the slowest progression was observed in patients with the lowest residual proteinuria (Ruggenenti et al., 2003). Therefore, the 7th Report of the Joint National Committee on Prevention, Detection, Evaluation, and Treatment of High Blood Pressure (JNC 7) and the National Kidney Foundation (NKF) guidelines recommend that reduction of albuminuria and BP should be included as the cornerstone in a treatment strategy for hypertensive nephropathy (Ruggenenti et al., 2008; Hart and Bakris, 2010). Furthermore, albuminuria has also been identified as a risk factor for cardiovascular events. Consequently, special attention should be paid to the degree of proteinuria when evaluating the improvement of renal function. In our study, we chose the 24 h urinary protein as one of the major outcomes. Based on 16 trials, the combination treatment of STS and ARBs had better efficacy in terms of preventing the progression of proteinuria. However, subgroup analysis covering three different categories of ARBs found no difference in the irbesartan group. This might be attributable to the small number of patients in the irbesartan group. Thus, further trials in a large series are required to determine the efficacy of STS plus irbesartan. SCr, an accurate index for renal function, also reliably predicts the risk for renal injury (Spanaus et al., 2010; Yan et al., 2014). The results of our analysis indicated that STS combined with ARBs can significantly decrease serum levels of creatinine. However, it should be acknowledged that there was significant heterogeneity despite subgroup analysis. The fact that creatinine is influenced by various factors such as age, gender, and diet that may bias the result should also not be ignored. Thus, in recent clinical guidelines, eGFR, calculated based on the SCr level and other parameters, is recommended for the estimation of renal function because of its sensitivity and high specificity for one-time measures of renal damage or dysfunction (Qaseem et al., 2013; Stevens and Levin, 2013). Previous studies have demonstrated that angiotensin converting enzyme inhibitors (ACEIs) and ARBs could maintain eGFR during the progress of hypertension (Cheng et al., 2016). Similar to other outcomes, we found that STS and ARB combination is more effective than ARB monotherapy in improving eGFR. However, there is yet no consensus among different guidelines on which formula to use for calculating eGFR, possibly leading to enormous calculation difference due to the use of different formulas. Although our results showed no heterogeneity, none of the included studies in this review reported the equation used for eGFR calculation, which may increase the risk of bias.

Cys-C is another biomarker that detects renal damage, especially in the early stage of nephropathy. Unlike SCr, urinary IgG, or transferrin, Cys-C is not influenced by gender, race, and muscle mass, and thus has recently drawn considerable attention (Peralta et al., 2011). Cys-C also exhibits predictive value for the prognosis of renal and cardiovascular diseases (Peralta et al., 2011; Ozkok et al., 2014; Barr et al., 2017; Zhang et al., 2017). In our study, we found that STS plus ARBs therapy was better than ARBs alone in improving urinary protein, SCr,

and eGFR, which also suggested that STS could be beneficial as an "add-on" medication for hypertensive patients.

In addition, systolic and diastolic BP reductions were evaluated to detect the effects of STS in terms of BP control. The results revealed that STS/ARB combination decreased the average SBP and DBP by 6.53 and 4.14 mmHg, respectively, compared with ARB monotherapy. STS provided auxiliary hypotensive effects, thereby enabling hypertensive patients to better achieve their target BP goals. In the subgroup analysis according to the intervention course, SBP reductions were statistically significant when 2 weeks was used as the cutoff for intervention course. However, there were no statistical differences when 4 weeks was used in the analysis. Notably, the majority of patients enrolled in this systematic review had reached the target SBP and DBP by the end of 2 weeks. Therefore, according to above results, we speculate that STS as an adjuvant treatment may not have further effects on SBP when SBP is already under control. However, there were only four trials where combined therapy lasted for 4 weeks (Yang et al., 2012; Cao et al., 2014; Bi et al., 2016; Li, 2016). Although the results did not show significant differences, SBP had a tendency to be lower in the STS/ARB combination treatment group at 4 weeks. Conducting more trials may alter the statistical results. Meanwhile, we recognized that there was considerable heterogeneity. We attempted to address this heterogeneity by carefully checking all of the included studies and performing sensitivity analysis and several subgroup analyses. But, unfortunately, we were not able to figure out the origin of the heterogeneity. We believe it may be caused by several reasons, e.g., different timing of medication and BP measurement, different types of ARBs and dosages of STS used, etc., which might bias the results. Accordingly, these results should be interpreted cautiously.

LIMITATIONS

This study has several limitations. Firstly, all included trials were published in Chinese, and only three trials provided specific information of random sequence generation (Li, 2014; Qiu, 2015; Li and Guo, 2017). We tried to contact the authors by telephone, fax, or e-mail to confirm, but received no replies. Additionally, all included trials didn't provide details of allocation concealment, blinding of participants and personnel, and blinding of outcome assessment, which, as shown in **Figure 3**, can lead to high risk of selection, performance, and detection bias respectively. The absence of allocation concealment and blinding may subjectively influence participants and researchers as well, although objective outcomes are enrolled in all the included studies. In view of these methodological problems, in order to achieve more conclusive results, we suggest that future clinical trials in large series should adopt such methods as proper randomization, allocation concealment, participant and personnel blinding, and assessment blinding. Secondly, the treatment course in the 16 trials was short: either 2 or 4 weeks. Therefore, we were unable to assess the long-term efficacy of STS. Thirdly, the actual clinical evidence such as doubling of SCr, progression to dialysis, and death are lacking. Large-scale long-term studies should be conducted to evaluate renoprotective effects of STS. Lastly, special attention should be paid to adverse drug events or reactions. Safety is a fundamental principle in the provision of herbal products for health care. However, there is insufficient evidence to draw a conclusion on the issue of safety in this review. Because 13 trials did not report about adverse drug events or reactions. Current studies regarding the factors of adverse effect caused by STS often focus on allergic reactions. Although STS is extracted by *S. miltiorrhiza Bunge* with high purity, the composition is complex, which may lead to adverse events. Clinicians should dilute the injection according to the package insert strictly and avoid mixed application to prevent adverse events happening.

CONCLUSIONS

In conclusion, this meta-analysis included 16 RCTs in assessing the effect of STS plus ARBs on kidney-related outcomes in patients with hypertensive nephropathy compared to ARB monotherapy. The results illustrated that STS combined with ARBs not only exerts auxiliary antihypertensive effects but also protects renal function. These results, however, should be interpreted with caution due to the limitations described above. Further large-scale, multicenter, long-term, randomized, and double-blind clinical trials are needed. Meanwhile, the safety of STS should also be evaluated.

DATA AVAILABILITY STATEMENT

All datasets generated for this study are included in the article/ **Supplementary Material**.

AUTHOR CONTRIBUTIONS

JX and CZ conceived the study, conducted the database search, assessed included studies, extracted the data, and wrote the paper. XS checked the data with JX and CZ. JL, ML, and WJ conducted the data analysis. ML, WJ, and ZF revised the final manuscript.

FUNDING

This work was supported by the National Natural Science Foundation of China (grant 81573909), the Youth Natural Science Foundation of Jiangsu Province (grant BK20181095), and the Social Development Key Programs of Science and Technology Commission Foundation of Jiangsu Province (grant BE2015730).

SUPPLEMENTARY MATERIAL

The Supplementary Material for this article can be found online at: https://www.frontiersin.org/articles/10.3389/fphar.2019.01542/full#supplementary-material

REFERENCES

Bai, F. M. (2012). Advances in clinical application of sodium tanshinone IIA sulfonate. *Chin. Phaeam.*, 23, 2971–2973. doi: 10.6039/j.issn.1001-0408.2012.31.35

Barr, E. L., Reutens, A., Magliano, D. J., Wolfe, R., Lu, Z. X., Sikaris, K. A., et al. (2017). Cystatin C estimated glomerular filtration rate and all-cause and cardiovascular disease mortality risk in the general population: AusDiab study. *Nephrol. (Carlton)* 22, 243–250. doi: 10.1111/nep.12759

Bi, X. J., Wang, L. N., Xin, H. J., Wang, W., Zhang, Y. R., Qin, N., et al. (2016). Sodium tanshinon IIA silate sodium combined with irbesartan in the treatment of hypertension with renal damage and its effect on serum levels of PCX and PICP. *J. Northwest Pharm.* 31, 403–405. doi: 10.3969/j.issn.1004-2407.2016.04.023

Bidani, A. K., Polichnowski, A. J., Loutzenhiser, R., and Griffin, K. A. (2013). Renal microvascular dysfunction, hypertension and CKD progression. *Curr. Opin. Nephrol. Hypertens.* 22, 1–9. doi: 10.1097/MNH.0b013e32835b36c1

Brenner, B. M., Cooper, M. E., de Zeeuw, D., Keane, W. F., Mitch, W. E., Parving, H. H., et al. (2001). Effects of losarta Randomised placebo-controlled trial of effect of ramipril on decline in glomerular filtration rate and risk of terminal renal failure in proteinuric, non-diabetic nephropathy n on renal and cardiovascular outcomes in patients with type 2 diabetes and nephropathy. *N Engl. J. Med.* 345, 861–869. doi: 10.1056/NEJMoa011161

Cao, G. Q., Xu, X. H., and Han, R. Q. (2014). Efficacy of irbesartan combined with tanshinone IIA sodium sulfonate in the treatment of hypertension with renal damage. *Chin. J. Clin. Ration. Drug Use* 7, 46–47. doi: 10.3969/j.issn.1674-3296.2014.30.034

Cao, L., Huang, B., Fu, X., Yang, J., Lin, Y., and Lin, F. (2017). Effects of tanshinone IIA on the regulation of renal proximal tubular fibrosis. *Mol. Med. Rep.* 15, 4247–4 52. doi: 10.3892/mmr.2017.6498

Chen, S., Zhao, X., Li, Y., Yang, D., Zhou, T., and Fan, G. (2013). Impurities preparation of sodium tanshinone IIA sulfonate by high-speed counter-current chromatography and identification by liquid chromatography/multistage tandem mass spectrometry. *J. Chromatogr. A.* 1288, 28–34. doi: 10.1016/j.chroma.2013.02.055

Cheng, Y., Huang, R., Kim, S., Zhao, Y., Li, Y., and Fu, P. (2016). Renoprotective effects of renin-angiotensin system inhibitor combined with calcium channel blocker or diuretic in hypertensive patients: A PRISMA-compliant meta-analysis. *Med. (Baltimore)* 95, e4167. doi: 10.1097/md.0000000000004167

DerSimonian, R., and Laird, N. (1986). Meta-analysis in clinical trials. *Control Clin. Trials* 7, 177–188. doi: 10.1016/0197-2456(86)90046-2

Dong, Y., Ding, J., and Huang, Z. (2019). Isolation and structure identifcation of sodium tanshinone IIA sulfonate. *Shanghai Med. Pharmaceutical J.* 40, 70–73. doi: 10.3969/j.issn.1006-1533.2019.01.021

Gao, S., Liu, Z., Li, H., Little, P. J., Liu, P., and Xu, S. (2012). Cardiovascular actions and therapeutic potential of tanshinone IIA. *Atherosclerosis* 220, 3–10. doi: 10.1016/j.atherosclerosis.2011.06.041

Hall, M. E., Do Carmo, J. M., Da Silva, A. A., Juncos, L. A., Wang, Z., and Hall, J. E. (2014). Obesity, hypertension, and chronic kidney disease. *Int. J. Nephrol. Renovasc Dis.* 7, 75–88. doi: 10.2147/ijnrd.s39739

Han, J. Y., Fan, J. Y., Horie, Y., Miura, S., Cui, D. H., Ishii, H., et al. (2008). Ameliorating effects of compounds derived from Salvia miltiorrhiza root extract on microcirculatory disturbance and target organ injury by ischemia and reperfusion. *Pharmacol. Ther.* 117, 280–295. doi: 10.1016/j.pharmthera.2007.09.008

Hao, H., Wang, G., Cui, N., Li, J., and Ding, Z. (2007). Determination of sodium tanshinone IIA sulfonate in plasma by liquid chromatography-electrospray ionisation-tandem mass spectrometry. *Biomed. Chromatogr.* 21, 1172–1179. doi: 10.1002/bmc.871

Hart, P. D., and Bakris, G. L. (2010). Hypertensive nephropathy: prevention and treatment recommendations. *Expert Opin. Pharmacother.* 11, 2675–2686. doi: 10.1517/14656566.2010.485612

Higgins, J. P. T., Thompson, S. G., Deeks, J. J., and Altman, D. G. (2003). Measuring inconsistency in meta-analyses. *Bmj.* 327, 557–560. doi: 10.1136/bmj.327.7414.557

Hillege, H. L., Fidler, V., Diercks, G. F., van Gilst, W. H., de Zeeuw, D., van Veldhuisen, D. J., et al. (2002). Urinary albumin excretion predicts cardiovascular and noncardiovascular mortality in general population. *Circulation* 106, 1777–1782. doi: 10.1161/01.cir.0000031732.78052.81

Huang, K. C., Su, Y. C., Sun, M. F., and Huang, S. T. (2018). Chinese herbal medicine improves the long-term survival rate of patients with chronic kidney disease in Taiwan: a nationwide retrospective population-based cohort study. *Front. Pharmacol.* 9, 1117. doi: 10.3389/fphar.2018.01117

Lewis, E. J., Hunsicker, L. G., Clarke, W. R., Berl, T., Pohl, M. A., Lewis, J. B., et al. (2001). Renoprotective effect of the angiotensin-receptor antagonist irbesartan in patients with nephropathy due to type 2 diabetes. *N Engl. J. Med.* 345, 851–860. doi: 10.1056/NEJMoa011303

Li, Q. H., and Guo, J. (2017). Effect of tanshinone injection combined with valsartan on patients with hypertensive renal damage. *Xinjiang J. Med.* 47, 1304–5+1308.

Li, T. (2014). Clinical observation of tanshinone injection combined with Valsartan in treating 115 cases of hypertensive Renal damage. *Chin. J. Ethnomed. Ethnopharm.* 23, 57–58.

Li, T. (2016). Effect of tanshinone combined with valsartan on hypertensive nephropathy. *World Clin. Med.* 10, 88.

Lim, S. S., Vos, T., Flaxman, A. D., Danaei, G., Shibuya, K., Adair-Rohani, H., et al. (2012). A comparative risk assessment of burden of disease and injury attributable to 67 risk factors and risk factor clusters in 21 regions, 1990-2010: a systematic analysis for the Global Burden of Disease Study 2010. *Lancet* 380, 2224–2260. doi: 10.1016/S0140-6736(12)61766-8

Lisowska-Myjak, B., Krych, A., Kolodziejczyk, A., Pachecka, J., and Gaciong, Z. (2011). Urinary proteins, N-acetyl-beta-D-glucosaminidase activity and estimated glomerular filtration rate in hypertensive patients with normoalbuminuria and microalbuminuria. *Nephrol. (Carlton)* 16, 403–409. doi: 10.1111/j.1440-1797.2011.01444.x

Liu, Y. (2010). Content Determination of sulfotanshinone sodium. *China Prac. Med.* 5, 65–66. doi: 10.3969/j.issn.1673-7555.2010.02.035

Liu, D. Y. (2015). Clinical study of tanshinone in the treatment of hypertensive nephropathy. *Med. Sci.* 11, 24.

Lonn, E. (2001). The use of surrogate endpoints in clinical trials: focus on clinical trials in cardiovascular diseases. *Pharmacoepidemiol Drug Saf.* 10, 497–508. doi: 10.1002/pds.654

Lu, J., Lu, Y., Wang, X., Li, X., Linderman, G. C., Wu, C., et al. (2017). Prevalence, awareness, treatment, and control of hypertension in China: data from 1.7 million adults in a population-based screening study (China PEACE Million Persons Project). *Lancet* 390, 2549–2558. doi: 10.1016/S0140-6736(17)32478-9

Luo, W. W. (2015). Efficacy of valsartan combined with tanshinone injection in the treatment of hypertensive nephropathy. *J. Nor. Pharm.* 12, 37–38.

Ozkok, A., Akpinar, T. S., Tufan, F., Kaya, O., Bozbey, H. U., Atas, R., et al. (2014). Cystatin C is better than albuminuria as a predictor of pulse wave velocity in hypertensive patients. *Clin. Exp. Hypertens.* 36, 222–226. doi: 10.3109/10641963.2013.804548

Peralta, C. A., Shlipak, M. G., Judd, S., Cushman, M., McClellan, W., Zakai, N. A., et al. (2011). Detection of chronic kidney disease with creatinine, cystatin C, and urine albumin-to-creatinine ratio and association with progression to end-stage renal disease and mortality. *JAMA* 305, 1545–1552. doi: 10.1001/jama.2011.468

Qaseem, A.Jr., Hopkins, R. H., Sweet, D. E., Starkey, M., and Shekelle, P. (2013). Screening, monitoring, and treatment of stage 1 to 3 chronic kidney disease: A clinical practice guideline from the American College of Physicians. *Ann. Intern. Med.* 159, 835–847. doi: 10.7326/0003-4819-159-12-201312170-00726

Qiu, S. J. (2015). Effect of tanshinone injection combined with valsartan in the treatment of hypertensive nephropathy. *Med. Sci. Monitor.* 7, 203.

Remuzzi, G., and Bertani, T. (1998). Pathophysiology of progressive nephropathies. *N Engl. J. Med.* 339, 1448–1456. doi: 10.1056/nejm199811123392007

Ruggenenti, P., Perna, A., and Remuzzi, G. (2003). Retarding progression of chronic renal disease: the neglected issue of residual proteinuria. *Kidney Int.* 63, 2254–2261. doi: 10.1046/j.1523-1755.2003.00033.x

Ruggenenti, P., Perticucci, E., Cravedi, P., Gambara, V., Costantini, M., Sharma, S. K., et al. (2008). Role of remission clinics in the longitudinal treatment of CKD. *J. Am. Soc Nephrol.* 19, 1213–1224. doi: 10.1681/asn.2007090970

Spanaus, K. S., Kollerits, B., Ritz, E., Hersberger, M., Kronenberg, F., and von Eckardstein, A. (2010). Serum creatinine, cystatin C, and beta-trace protein in

diagnostic staging and predicting progression of primary nondiabetic chronic kidney disease. *Clin. Chem.* 56, 740–749. doi: 10.1373/clinchem.2009.138826

Stevens, P. E., and Levin, A. (2013). Evaluation and management of chronic kidney disease: synopsis of the kidney disease: improving global outcomes 2012 clinical practice guideline. *Ann. Intern. Med.* 158, 825–830. doi: 10.7326/0003-4819-158-11-201306040-00007

Suneel, U., Ivana, L., and Bakris, G. L. (2011). Epidemiology of hypertensive kidney disease. *Nat. Rev. Nephrol.* 7, 11–21. doi: 10.1038/nrneph.2010.154

The GISEN Group (1997). Randomised placebo-controlled trial of effect of ramipril on decline in glomerular filtration rate and risk of terminal renal failure in proteinuric, non-diabetic nephropathy. The GISEN Group (Gruppo Italiano di Studi Epidemiologici in Nefrologia). *Lancet* 349, 1857–1863. doi: 10.1016/s0140-6736(96)11445-8

Tusonguri, M. (2017). Clinical observation of valsartan combined with tanshinone injection in the treatemnt of 64 cases of hypertensive renal damage. *Guid. Chin. Med.* 15, 3. doi: 10.15912/j.cnki.gocm.2017.02.003

Wang, C., Han, J., and Zhou, J. (2006). HPLC method to test the assay of sodium tanshinon IIA sulfonate injection. *Hebei J. Ind. Sci. Tech.* 23, 246–248.

Wang, D. T., Huang, R. H., Cheng, X., Zhang, Z. H., Yang, Y. J., and Lin, X. (2015). Tanshinone IIA attenuates renal fibrosis and inflammation *via* altering expression of TGF-beta/Smad and NF-kappaB signaling pathway in 5/6 nephrectomized rats. *Int. Immunopharmacol.* 26, 4–12. doi: 10.1016/j.intimp.2015.02.027

Wang, Q., Li, C., and Zhou, X. H. (2016). Analysis of therapeutic effect of tanshinone IIA sodium sulfonate injection combined with valsartan regimen in hypertensive nephropathy. *J. Today Health* 15, 136. doi: 10.3969/j.issn.1671-5160.2016.07.126

Whelton, P. K., Carey, R. M., Aronow, W. S.Jr., Casey, D. E., Collins, K. J., Dennison Himmelfarb, C., et al. (2018). 2017 ACC/AHA/AAPA/ABC/ACPM/AGS/APhA/ASH/ASPC/NMA/PCNA guideline for the prevention, detection, evaluation, and management of high blood pressure in adults: executive summary: a report of the american college of cardiology/american heart association task force on clinical practice guidelines. *Circulation* 138, e426–e483. doi: 10.1161/cir.0000000000000597

Wu, X. L. (2013). Clinical efficacy of tanshinone in the treatment of hypertensive nephropathy. *Chin. Rura. Heal.* 3Z, 209.

Xu, Y. M., Ding, G. H., Huang, J., and Xiong, Y. (2016). Tanshinone IIA pretreatment attenuates ischemia/reperfusion-induced renal injury. *Exp. Ther. Med.* 12, 2741–2746. doi: 10.3892/etm.2016.3674

Yan, L., Ma, J., Guo, X., Tang, J., Zhang, J., Lu, Z., et al. (2014). Urinary albumin excretion and prevalence of microalbuminuria in a general Chinese population: a cross-sectional study. *BMC Nephrol.* 15, 165. doi: 10.1186/1471-2369-15-165

Yan, S. H., Zhao, N. W., Geng, Z. R., Shen, J. Y., Liu, F. M., Yan, D., et al. (2018). Modulations of Keap1-Nrf2 signaling axis by TIIA ameliorated the oxidative stress-induced myocardial apoptosis. *Free Radic. Biol. Med.* 115, 191–201. doi: 10.1016/j.freeradbiomed.2017.12.001

Yang, H. Y., Zhan, H. P., and Chen, H. (2012). Therapeutic effect of tanshinone combined with valsartan on hypertensive nephropathy. *J. Prac. Med.* 28, 340–341. doi: 10.3969/j.issn.1006-5725.2012.2.075

Yu, H. T. (2014). Clinical treatment of tanshinone in hypertensive nephropathy. *Fam. Psycho. Doc.* 10, 237–239.

Zhang, J., Wu, X., Gao, P., and Yan, P. (2017). Correlations of serum cystatin C and glomerular filtration rate with vascular lesions and severity in acute coronary syndrome. *BMC Cardiovasc. Disord.* 17, 47. doi: 10.1186/s12872-017-0483-8

Zhu, H. W., Zhu, M., and Gao, J. D. (2011). Clinical study of hypertensive nephropathy treated with tanshinone. *J. Inter. Med. Conc. Prac.* 6, 204–207. doi: 10.16138/j.1673-6087.2011.03.007

Zhu, J., Xu, Y., Ren, G., Hu, X., Wang, C., Yang, Z., et al. (2017). Tanshinone IIA Sodium sulfonate regulates antioxidant system, inflammation, and endothelial dysfunction in atherosclerosis by downregulation of CLIC1. *Eur. J. Pharmacol.* 815, 427–436. doi: 10.1016/j.ejphar.2017.09.047

Zhu, Q. Q. (2015). Feasibility and value of tanshinone injection combined with valsartan in the treatment of hypertensive nephropathy. *Med. Sci.* 3, 192.

Zou, H. L., Zhan, J., Wang, Y. G., and Chen, R. G. (2013). Clinical observation on tanshinone and valsartan for treatment of hypertensive nephropathy. *Chin. J. Integr. Med. Cardio-Cerebrovas. Dis.* 11, 1303–1304. doi: 10.3969/j.issn.1672-1349.2013.11.014

Conflict of Interest: The authors declare that the research was conducted in the absence of any commercial or financial relationships that could be construed as a potential conflict of interest.

frontiers in Pharmacology

ORIGINAL RESEARCH
published: 09 January 2020
doi: 10.3389/fphar.2019.01523

The Incidence and Risk Factors for Adverse Drug Reactions Related to Tanreqing Injection: A Large Population-Based Study in China

Xiao-Xiao Li[1,2†], *Lin Zhuo*[3,4†], *Yan Zhang*[5], *Yi-Heng Yang*[1], *Hong Zhang*[5], *Si-Yan Zhan*[3,4*] *and Suo-Di Zhai*[1,2*]

[1] Department of Pharmacy, Peking University Third Hospital, Beijing, China, [2] Department of Pharmacy Administration and Clinical Pharmacy, School of Pharmaceutical Sciences, Peking University, Beijing, China, [3] Research Center of Clinical Epidemiology, Peking University Third Hospital, Beijing, China, [4] Department of Epidemiology and Biostatistics, School of Public Health, Peking University, Beijing, China, [5] Technology and Development Center for TCM of China, State Administration of Traditional Chinese Medicine of the People's Republic of China, Beijing, China

OPEN ACCESS

Edited by:
Jianxun Liu,
China Academy of Chinese Medical Sciences, China

Reviewed by:
Yanping Deng,
Peking University, China
Chao Zhang,
Capital Medical University, China

***Correspondence:**
Si-Yan Zhan
siyan-zhan@bjmu.edu.cn
Suo-Di Zhai
zhaisuodi@163.com

[†]*These authors have contributed equally to this work*

Specialty section:
This article was submitted to Ethnopharmacology, a section of the journal Frontiers in Pharmacology

Received: *11 June 2019*
Accepted: *25 November 2019*
Published: *09 January 2020*

Citation:
Li X-X, Zhuo L, Zhang Y, Yang Y-H, Zhang H, Zhan S-Y and Zhai S-D (2020) The Incidence and Risk Factors for Adverse Drug Reactions Related to Tanreqing Injection: A Large Population-Based Study in China. Front. Pharmacol. 10:1523. doi: 10.3389/fphar.2019.01523

Background: Tanreqing injection (TRQ) is a traditional Chinese medicine commonly used in China to treat pulmonary diseases presenting as phlegm-heat syndrome. Robust data on the safety of TRQ from real-world observational cohorts are currently lacking.

Objective: To evaluate as the incidence, type, and predictors of adverse events (AEs) and adverse drug reactions (ADRs) of TRQ in clinical practice in China.

Methods: We conducted a population-based cohort, multicenter study to evaluate the incidence, manifestation, outcomes, and risk factors of AEs and ADRs following TRQ use in China. Between April 2014 and May 2015 a total of 30,322 consecutive inpatients/emergency attendance patients from 90 hospitals across China administrated TRQ were followed-up for 7 days. Odds ratios (ORs) with 95% confidence intervals (CIs) were estimated using logistic regression to identify predictors of ADRs.

Results: The incidence of AEs and ADRs was 1.4 and 0.3%, respectively. Skin and subcutaneous tissue disorders were the most common ADRs. All ADRs were mild or moderate in severity, except for one serious case of anaphylactic reaction. The majority of ADRs (72.8%) occurred in the first 2 h after TRQ administration. Two-thirds of patients (66.1%) in the study were prescribed TRQ off-label, including infants aged ≤24 months. A history of food allergy (OR 4.50, 95% CI: 1.35–15.00), drug allergy (OR 2.77, 95% CI: 1.56–4.94), and fast infusion speed (off-label use) (OR 2.10, 95% CI: 1.27–3.50) were associated with an increased risk of ADRs.

Conclusion: TRQ is well tolerated in the general population, yet off-label use is prevalent. Efforts are required to educate prescribers to adhere to the drug label in order to minimize potential patient harm.

Keywords: drug safety, adverse drug reactions, pharmacovigilance, anaphylaxis, traditional Chinese medicine, off-label

INTRODUCTION

Tanreqing injection (TRQ) is a traditional Chinese medicine (TCM) consisting of five water-soluble herbals extracts: Radix *Scutellariae* [*Scutellaria baicalensis* Georgi (radix), 30%], bear bile powder (*Fel Ursi Selenarctos thibetanus* G. Cuvier *Ursus arctos* L., 9%), goral horn (*Naemorhedus goral* Hardwicke, 7%), *Flos Lonicerae* [*Lonicera japonica* Thunb (flos), 30%], and Fructus *Forsythiae* [*Forsythia suspense* (Thunb.) Vahl. (fructus), 24%], with baicalin, chlorogenic acid, ursodeoxycholic acid, and chenodeoxycholic acid as the major bioactive constituents (CFDA, 2012; Zhang et al., 2016; Li et al., 2019). Owing to its antibacterial, antiviral, and anti-inflammatory effects, it is widely used in China to treat diseases presenting as "phlegm-heart syndrome" (Li et al., 2010; Yang et al., 2018), including acute upper respiratory infections (Wang et al., 2016), pneumonia (Wang et al., 2011; Xiong et al., 2018), and acute exacerbation of chronic obstructive pulmonary disease (COPD) (Zhong et al., 2010). It was approved for use by the Chinese Food and drug Administration (CFDA) in 2003. Between 2009 and 2011, the National Centre of Adverse Drug Reaction (ADR) Monitoring, affiliated with the CFDA, received 4,899 ADR following use of TRQ, including 172 serious adverse events (SAEs) most of which were anaphylaxis. Forty five percent of SAEs occurred in children under 5 years of age or in adults aged over 60 years (the National Centre of ADR Monitoring, unpublished).

Plant based extracts and proteins from animal sources have been considered to be major allergens in TCM injections, and in 2010 an allergen-warning was added to the product label along with wording that the product is contraindicated in infants aged less than 24 months and pregnant women. Other contraindications stated on the label include hepatic, renal, or heart failure. In response to concerns that the multi-ingredient composition and low-quality standards in production may be factors related to TRQ ADRs (Ji et al., 2009; Zhang et al., 2014), in December 2011 the CFDA introduced a standardized process on active ingredient preparation to control the quality of TRQ production (Li et al., 2014; Yang, B. et al., 2017; Yang, Y. et al., 2017; Li, W. L. et al., 2017). As part of the post-marketing surveillance of TRQ, there is a need to gather safety data from large population-based observational cohorts, yet currently only a few small single-centered studies on this topic have been conducted (Zhong et al, 2010; Xie et al, 2014; Wang et al, 2018). Therefore we carried out a population-based study to evaluate the incidence, manifestation, outcomes and risk factors of ADRs and adverse events (AEs) following TRQ in clinical practice across China.

Abbreviations: ADRIC, ADR interpretation committee; ADRs, Adverse drug reactions; AEs, Adverse events; CRF, Case report forms; CFDA, China Food and Drug Administration; COPD, Chronic obstructive pulmonary disease; CRA, Clinical research associate; CIs, Confidence intervals; EDC, Electronic data capture; EVSE, *Enteroviral* vesicular stomatitis with exanthema; OR, Odds ratios; TReQS, Post-Marketing Surveillance of the Tanreqing Injection: a Real-World Study; SAEs, Serious adverse events; SATCM, State Administration of Traditional Chinese Medicine of the People's Republic of China; TRQ, Tanreqing injection; TCM, Traditional Chinese medicine. IQR, interquartile range; WHO-UMC, World Health Organization - Uppsala Monitoring Centre.

MATERIALS AND METHODS

Study Design

We carried out a cohort study with prospective and retrospective components (ClinicalTrials.gov, identifier NCT02094638; Chinacohort.bjmu.edu.cn, identifier CCC2018062701). The study was conducted at 90 hospitals (55 general hospitals, 12 district/country hospitals, 9 specialized hospitals including women's and children's hospitals, and 14 TCM hospitals) within 27 provincial level administrative regions across China (see **Supplementary Figure A** and **Tables A**, **B** for details). Participating centers were selected based on sales of TRQ, scientific research capacity, and willingness to take part. The study was supported by State Administration of TCM of the People's Republic of China (SATCM, project number: 2013ZX04) and approved by Peking University Third Hospital Ethics Committee with waiver informed consent (reference number: IRB00006761-2014009).

Study Population

A total of 30,322 consecutive patients, either inpatients or those attending a hospital emergency department, who were administered TRQ for the first time between January 2014 and May 2015 were identified. This included 2,743 patients who were newly prescribed TRQ from January to March of 2014 and who belonged to a retrospective cohort, and 27,579 patients identified between April and May 2015 that formed a prospective cohort. In view of the short half-live of TRQ (Liu et al., 2013; Li et al., 2018), every patient involved was followed up for 7 days after either TRQ was discontinued or the date of hospital discharged.

Data Sources, Collection, and Quality Control

The methods of data collection are summarized in **Figure 1**. Two local investigators (predominantly pharmacists) in each study site were responsible for the data collection, which included a details on all prescriptions written for TRQ issued from the central hospital pharmacy (data collected daily), demographics, medical history (including history of allergy), diagnoses (including Chinese medical diagnoses), laboratory test results, medication use, details of TRQ administration, and AEs. Historical records, including medical records and reported ADRs were collected for patients in the retrospective and prospective cohort, while data from follow-up investigations were collected in the prospective cohort. Adverse events were also identified from the medical records of patients who died or who had disease exacerbation or abnormal laboratory test results.

Local investigators submitted data *via* a secure and password-protected web-based electronic data capture system (EDC, http://182.92.8.232/commedc/). International Classification of Diseases-10, Medical Dictionary for Regulatory Activities, and World Health Organization-Anatomical Therapeutic Chemical

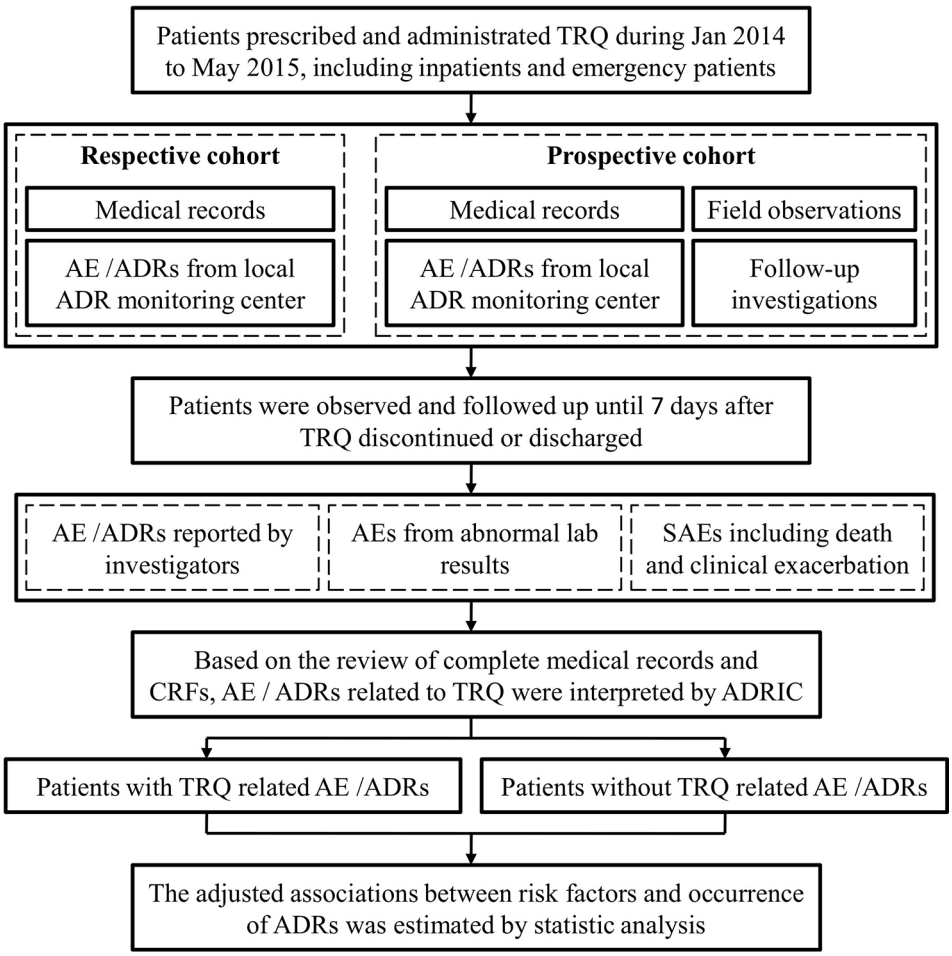

FIGURE 1 | Flow chart for adverse event (AE)/adverse drug reactions (ADRs) identification. The figure depicts the flow of AE/ADR identification from data collected from field observations and follow-up investigations in respective and prospective cohort. TRQ, Tanreqing injection; SAEs, serious adverse events; ADRIC, ADR interpretation committee.

codes were used as the data dictionary in the EDC for standardizing entries relating to medical history and diagnoses, AEs, and medications. To minimize transcription errors, local hospital information system (if authorized) was linked to the electronic data by matching on a series of identifiers for downloading basic information in the case report form (CRF), including demographics, laboratory test results, and economic outcomes. Each patient was assigned a unique ID and the submitted data were checked three times—by the second local investigator, by a clinical research associate, and by a data administrator. Any CRF with errors was returned to the first investigator inputting the data who subsequently revised the entry. The department of technology and development center for TCM, SATCM served as the point of data collection, coordination center, and de-identification. Data analysis was carried out at the Department of Epidemiology and Biostatistics, School of Public Health, Peking University.

Assessment of Adverse Events and Adverse Drug Reactions

A multidisciplinary ADR interpretation committee (ADRIC) assessed and interpreted all ADRs in accordance with the WHO Collaborating Centre for International Drug Monitoring (WHO-UMC) causality assessment system. The relationship between the reported ADRs and TRQ was categorized as certain, probable, possible, unlikely, conditional/unclassified, or unassessable/unclassifiable. Adverse events were graded as mild, moderate, and severe (Edwards and Aronson, 2000). A serious adverse event (SAE) was defined as any untoward medical occurrence that resulted in death, required hospital admission, prolonged an existing hospital stay, or was life threatening (Edwards and Aronson, 2000). A new ADR was described as either an unlabeled ADR or an ADR where severity is insufficiently described on the current drug label, as appropriate. Anaphylaxis was determined based on the criteria

recommended by the National Institute of Allergy and Infectious Diseases, the Food Allergy and Anaphylaxis Network, and the European Academy of Allergy and Clinical Immunology (Muraro et al., 2014; Sampson et al., 2016). The incidence of TRQ-related ADRs was the primary outcome measure. The incidence of AEs, outcomes of risk factors for TRQ-related ADRs were secondary outcomes. Indications for TRQ use and off-label prescribing were also described.

Statistics Analysis

PASS 11.0.7 was used to calculate the sample size. Based on an incidence of ADRs (0.14%) in the phase I to IV trials (Shanghai Kaibao Pharmaceutical Co., LTD, unpublished; Shen et al, 2007), and an expected 20% loss-to-follow-up, we estimated that 30,400 patients would be needed to observe an ADR incidence of less than 0.1% with a probability of 95%. Categorical variables were described using frequency counts and percentages, and continuous variables were described using medians with interquartile range (IQR). Multivariable non-conditional logistic regression model was then used to estimate the association between potential risk factors and occurrence of ADRs related to TRQ by calculating odds ratios (OR) with 95% confidence intervals (CIs). All p values were two-sided. SAS version 9.2 was used for all statistical analyses.

RESULTS

Baseline Characteristics

Of the 30,322 consecutive patients administrated TRQ between January 2014 and May 2015, 22,062 (72.8%) were from general hospitals and 3,475 (11.5%) were from TCM hospitals. Baseline characteristics of the study population are shown in **Table 1** and **Supplementary Figure B**. There were 11,621 (38.33%) females and the median age was 57 years (IQR 26, 72); 41% of patients were aged at least 60 years. A total of 2,326 (7.7%) patients had a history of food or drug allergy or other allergic disease. The median length of hospital stay was 11 days. TRQ-related costs accounted for 5.1% of the total medical costs with most covered by health insurance.

Overall, TRQ was administered for 32,883 different indications (a patient could have more than one different indication recorded). Infections and respiratory diseases were the most common accounting for 72.4% of indications, with acute upper respiratory tract pneumonia, COPD, bronchitis (acute or chronic), and hand, foot, and mouth disease being the most frequent indications. Most prescriptions for TRQ were made in accordance with the product label, including dosage (maximal dose being 20 ml for children, and 40 ml for adults), preparation concentration (≤10%), diluents (5% glucose or 0.9% normal saline), intravenous infusion mode of administration, and infusion rate (30–60 drops/min). However, a total of 20,058 (66.1%) patients were administered TRQ as off-label use (see **Supplementary Table C**). Of these, 1,851 (6.1%) patients were prescribed TRQ for pre-surgical infection prophylaxis, and 1,165 patients (3.8%) were aged ≤24 months, i.e., contraindicated.

TABLE 1 | Baseline characteristics of the study population. Data are n (%) unless otherwise stated.

Patient characteristic	Patients, N = 30,322
Demographics and lifestyle factors	
Median age (IQR), years	57 (26, 72)
<18	6,500 (21.4)
≥60	13,061 (41.1)
Female	11,621 (38.3)
Han ethnicity	29,589 (97.6)
History of allergy[a]	2,326 (7.7)
Food allergy	174 (0.6)
Drug allergy	1,969 (6.5)
Allergic disease	292 (1.0)
Lifestyle	
Current smoking	7,447 (24.6)
Current alcohol drinker	4,898 (16.2)
Hospitalization factors	
Median length of stay (IQR), days	11 (8, 18)
Death in hospital	239 (0.8)
Hospital department [c]	
Pneumology	7,461 (24.6)
Pediatrics	4,794 (15.8)
Infectious disease	1,613 (5.3)
General surgery	1,420 (4.7)
Emergency	963 (3.2)
TRQ related diagnosis (ICD-10 codes) [b,c]	
Pneumonia (J18)	9,760 (32.2)
Acute upper respiratory infections (J00-J06)	4,937 (16.3)
Chronic obstructive pulmonary disease (J44.9)	2,609 (8.6)
Acute bronchitis (J20)	2,500 (8.2)
Encounter for prophylactic surgery (Z40) [e]	1,851 (6.1)
Chronic bronchitis (J42)	1,244 (4.1)
Enteroviral vesicular stomatitis with exanthema (B08.4)	899 (3.0)
Combined diseases (ICD–10 codes) [b,d]	
Hypertensive diseases (I10–I16)	5,308 (17.5)
Atherosclerotic heart disease of native coronary artery (I25.1)	2,278 (7.5)
Type 2 diabetes mellitus (E11)	2,169 (7.2)
Cerebrovascular diseases (I60-I69)	1,442 (4.8)
Symptoms and signs involving the digestive system and abdomen (R10–R19)	1,307 (4.3)
Characteristic of TRQ administration [f]	
Median dosage (IQR), ml/d	20 (20, 30)
Median duration of therapy (IQR), days	6 (4, 9)
Median preparation concentration of TRQ (IQR), %	8 (8, 12)
Median duration from preparation to the administration of TRQ (IQR), minutes	30 (15, 30)
Median (Q1, Q3) infusion rate (IQR), drops/min [g]	40 (35, 50)

[a] *A patient could have ≥2 different allergy history.*
[b] *Only variables accounting for ≥2.9% patients are shown.*
[c] *A patient could have ≥2 different TRQ-related diagnoses.*
[d] *A patient could have ≥2 different types of combined disease.*
[e] *Z40 was applicable to describe infection prevention for surgery.*
[f] *The labeled recommended intravenous dosage of TRQ for adults is 20 ml for each dose once a day into 250~500 ml of 5% GS or 0.9% NS and doses up to a maximum of 40 ml for severe cases. The labeled recommendation for pediatric patients is 0.3~0.5 ml/kg up to a maximum of 20 ml per dose once a day through intravenous infusion.*
[g] *Median (IQR) infusion rate (ml/h) was 120 (105, 150) using needles of 0.55*19 mm or 0.7*24 mm. ICD, International Classification of Diseases; IQR, interquartile range; TRQ, Tanreqing injection.*

There were 459 patients (1.5%) with other contraindications as stated on the product label: hepatic failure (n = 138, 0.5%), renal failure (n = 292, 1.0%), both hepatic and renal failure (n = 17,

0.06%), and severe pulmonary heart disease with heart failure (n = 12, 0.04%). Also, 11,807 (38.9%) patients were administered TRQ with a preparation concentration of >10%, 2,058 (6.8%) patients were prescribed diluents beyond 5% glucose or 0.9% normal saline, and six patients (0.02%) were administered TRQ by aerosol inhalation. There were 30,055 (71.9%) patients who received TRQ concomitantly with other treatments such as systemic antibiotics, blood substitutes and perfusion solutions, and cough and cold preparations (see **Supplementary Table D**). A total of 173 (0.6%) patients were administered TRQ with other drugs within a same bottle/bag, which is another prohibition of use on the product label. In nine (0.03%) of these patients, the chemical reaction from co-administration was visually evident, showing up as cloudy white precipitate when TRQ was combined with doxofylline injection (three patients), levofloxacin lactate injection (three patients), moxifloxacin hydrochloride injection (two patients), or ornidazole and sodium chloride injection (one patient).

Incidence and Casualty Assessment of Adverse Events and Adverse Drug Reactions

A total of 434/30,322 patients (1.4%) experienced an AE, of whom 263 experienced a SAE. As shown in **Table 2**, according to the WHO-UMC causality criteria, 81 patients (0.3%) were classified to have a TRQ-related ADR (one was deemed as certain, 35 probable and 45 possible). The most common TRQ-related ADRs were rash (40.7%), chest discomfort (7.4%), and nausea (6.2%). Only one patient experienced a serious TRQ-ADR—a 65 years old female who presented with anaphylactic reaction with the involvement of laryngeal edema 13 min after the administration of TRQ alone, and who recovered following treatment with promethazine and dexamethasone. All other TRQ-related ADRs were either mild (n = 59, 72.8%) or moderate (n = 21 patients, 25.9%). Twelve new symptoms ("new ADRs") occurred among 22 patients, with chest discomfort accounting for just over a quarter (26.1%). There was little evidence of a difference in the incidence of ADRs between the patients in the prospective cohort (n = 76, 0.3%) and those in the retrospective cohort (n = 5, 0.2%, $p = 0.37$) or between patients in western medicine hospitals (n = 76, 0.3%) and those in TCM hospitals (n = 5, 0.1%, $p = 0.14$).

TABLE 2 | Casualty assessment of adverse events. Data are n (%).

Casualty assessment[a]	AEs N = 434	
	All AEs	SAEs
Certain	1 (0.003)	0
Probable	35 (0.1)	1 (0.003)
Possible	45 (0.1)	0
Unlikely	329 (1.1)	240 (0.8)
Conditional	9 (0.03)	9 (0.03)
Unassessable	15 (0.05)	13 (0.04)
Total	434 (1.4)	263 (0.9)

[a]*The estimation of relationship likelihood between AEs and TRQ were categorized based on WHO-UMC causality assessment system.*

AE, adverse event; SAE, serious adverse event; TRQ, Tanreqing injection; WHO-UMC, World Health Organization-Uppsala Monitoring Centre.

Characteristics of Adverse Drug Reactions

The frequency of TRQ-related ADRs according to the time of onset is shown in **Table 3**. The time interval between TRQ administration and ADR onset ranged between 5 min and 10 days. Among patients experiencing a TRQ-related ADR, the majority (n = 59, 72.8%) occurred within the first 2 h of drug administration. All patients who experienced an ADR saw their condition either improved (n = 45, 55.56%) or completely resolved (n = 36, 44.44%) after taking management measures (n = 79, 97.5%) or within time (n = 2, 2.5%). Management measures included TRQ withdrawal (n = 39, 48.1%), reintroducing of essential medicines (n = 22, 27.2%), both of these (n = 17, 21.0%), reduction in drip speed (n = 1, 1.2%). Recovery time varied from less than an hour (n = 27, 33.3%) to more than 24 h (n = 34, 42.0%).

The characteristics of ADRs among patients in the retrospective cohort were similar to those in the prospective cohort. Five ADRs occurred in five patients in the retrospective cohort: skin and subcutaneous tissue disorders such as rash (n = 2, 0.07%), pruritus (n = 1, 0.04%), urticaria (n = 1, 0.04%), and palpitations (n = 1, 0.04%). There was one patient in the retrospective cohort whose ADR (rash) that occurred in the first 2 h after TRQ administration, while three cases occurred between 2 and 24 h after TRQ administration. Only one ADR (pruritus) occurred 10 days after TRQ administration. All five patients in the retrospective cohort who experienced an ADR improved after TRQ withdrawal.

Risk Factors for Tanreqing Injection-Related Adverse Drug Reactions

As shown in **Figure 2**, factors associated with an increased risk of TRQ related ADRs were having history of food allergy (OR 4.50, 95% CI: 1.35–15.00), drug allergy (OR 2.77, 95% CI: 1.56–4.94), and an infusion speed of >60 drops/min [*vs.* 30–60 drops/min; OR 2.10, 95% CI (1.27– 3.50)].

DISCUSSION

Our study is the first large-scale population-based study to evaluate the safety of TRQ among patients in real-world clinical practice in China, providing valuable information for patients, physicians, and drug safety regulators. We found that the incidence of AEs and ADRs following TRQ was low at 1.4 and 0.3%, respectively, with most non-serious in severity and with the majority occurring within a couple of hours of drug administration. This suggests that TRQ is well-tolerated. However, we also found that two-thirds of patients administered TRQ received it not according to label, with nearly 6% of off-label use being in infants aged less than 24 months (1,165 in 20,058 patients). Other off-label use related to non-approved indications, dosage, preparation concentration, diluents, mode of administration way, or infusion rate. Off-

TABLE 3 | Frequency of Tanreqing injection-related adverse drug reactions according to the time of onset. Data are n (‰).

ADRs	The time interval between TRQ administration and the onset of ADRs (hours)				Total patients (*n* = 81)
	≤0.5 (n = 25)	0.5–2 (n = 34)	2–24 (n = 16)	>24 (*n* = 6)	
Cardiac disorders					
Palpitations	2 (0.07)	0	2 (0.07)	0	4 (0.1)
Eye disorders					
Periorbital edema[b]	0	1 (0.03)	0	0	1 (0.03)
Gastrointestinal disorders					
Abdominal distension	0	1 (0.03)	0	0	1 (0.03)
Diarrhea	0	0	2 (0.07)	0	2 (0.07)
Nausea	4 (0.01)	1 (0.03)	0	0	5 (0.2)
Vomiting	0	2 (0.07)	0	0	2 (0.07)
General disorders and administration site conditions					
Asthenia[b]	0	1 (0.03)	0	0	1 (0.03)
Chest discomfort[b]	3 (0.10)	2(0.07)	1 (0.03)	0	6 (0.2)
Chills	3 (0.10)	0	1 (0.03)	0	4 (0.1)
Edema[b]	0	0	1 (0.03)	0	1 (0.03)
Hyperpyrexia[b]	1(0.03)	1(0.03)	0	0	2 (0.07)
Infusion site discomfort	2 (0.07)	0	0	0	2 (0.07)
Pyrexia	1 (0.03)	2 (0.07)	0	0	3 (0.1)
Infections and infestations					
Laryngitis[b]	0	0	0	1 (0.03)	1 (0.03)
Investigations					
Blood pressure decrease [b]	1 (0.03)	0	0	0	1 (0.03)
Hepatic enzyme increased[b]	0	0	1 (0.03)	1 (0.03)	2 (0.07)
Nervous system disorders					
Dizziness	1 (0.03)	1 (0.03)	0	0	2 (0.07)
Renal and urinary disorders					
Hematuria [b]	0	0	2 (0.07)	0	2 (0.07)
Respiratory, thoracic, and mediastinal disorders					
Cough[b]	1 (0.03)	0	0	0	1 (0.03)
Dysphonia[b]	0	1 (0.03)	0	0	1 (0.03)
Dyspnoea[b]	2 (0.07)	2 (0.07)	0	0	4 (0.1)
Laryngeal edema [c]	1 (0.03)	0	0	0	1 (0.03)
Tachypnoea	0	1 (0.03)	0	0	1 (0.03)
Skin and subcutaneous tissue disorders					
Pruritus	0	1 (0.03)	0	1 (0.03)	3 (0.1)
Rash	10 (0.3)	16 (0.5)	4 (0.1)	3 (0.10)	33 (1.1)
Urticaria	0	1 (0.03)	2 (0.07)	0	3 (0.1)
Vascular disorders					
Flush	2 (0.07)	4 (0.01)	1 (0.03)	0	7 (0.02)
Phlebitis	0	3 (0.1)	1 (0.03)	0	4 (0.01)
Total	34 (1.1)	42 (1.4)	18 (0.6)	6 (0.2)	100 (3.3)

[a]*ADRs are presented as individual symptoms and system organ class, based on the MedDRA classification. Frequency was calculated as number/30,322*1,000‰.*
[b]*New ADRs.*
[c]*A 65 years old female who presented with anaphylactic reaction with the involvement of laryngeal edema 13 min after the administration of TRQ alone.*
ADR, adverse drug reaction; TRQ, Tanreqing injection; MedDRA, Medical Dictionary for Regulatory Activities.

label use has been reported in a previous literature review of small studies of TRQ use (Wang et al, 2019), including to children people with a history of drug allergy, and with an infusion speed of >60 drops/min also reported. As suspected, we found that a history of allergy, be it food or drug allergy, was found to be the strongest predictor of TRQ-ADRs in line with the caution on the product label for use in these patients. Fast infusion speed of >60 drops/min was also identified as a predictor or TRQ-related ADR, and the incidence of TRQ-ADRs among children reported in our previous literature (Li, X. X. et al., 2017) was higher incidence than in the general population (0.4 *vs.* 0.3%).

In our study, the most common TRQ-related ADRs related to the skin and appendages, and the majority ADRs occurred within the first 2 h of TRQ administration, being similar to the results reported in previous studies (Shen et al., 2007; Li et al, 2010; Zhong et al., 2010; Xie et al., 2014; Wang et al., 2016; Wang et al, 2019). However, it is important to note that the incidences of TRQ-related AEs and ADRs seen in our study are higher than those seen in TRQ clinical trials (0.3% *vs.* 0.1~0.14%) (Shen et al., 2007; Li et al, 2010; Zhong et al., 2010; Xie et al., 2014; Wang et al., 2016), highlighting the importance of post-marketing surveillance. Our study included a broad range of patients, including those with a history of allergy, infants, and the elderly who were excluded from the TRQ clinical trials (Shanghai Kaibao Pharmaceutical Co., LTD, unpublished; Shen et al., 2007). Although only one patient in our study suffered anaphylaxis, this suggests that prescribers should be aware that this severe adverse reaction is possible, and a management practices should be in place in case of this outcome.

Our study has several strengths. In addition to the large sample size, the broad study population was drawn from a large number of hospitals, including those of different specialties and with a wide geographical spread across China. Our results will therefore be more generalizable to the individuals prescribed TRQ in the general population of China than those from small single-centered studies. Investigators used multiple data source/lines of investigation to identify AEs, which were reviewed and interpreted by the ADRIC based on patients' complete patient medical records. Another strength of our study is the involvement of pharmacists as principle investigators at the study sites, which has been a feature of few other TCM post-marketing studies (Yan et al., 2017). Pharmacists are able to employ their expertise around prescribing issues and pharmacovigilance, and may have access to hospital pharmacy data unlike some other qualified health professionals.

Limitations of study should also be acknowledged. Firstly, our study population included patients in a retrospective cohort for whom some prospectively collected safety data, for example, patient self-reported AEs, could not be obtained. This may have lead to information bias and the possibility of underestimating AE incidence, although we found no evidence of a difference in the incidence of ADRs among patients in the retrospective and prospective cohorts. Secondly, our study included inpatient and emergency patients treated with TRQ and not individuals who were treated outside of this setting. A recent study reported that

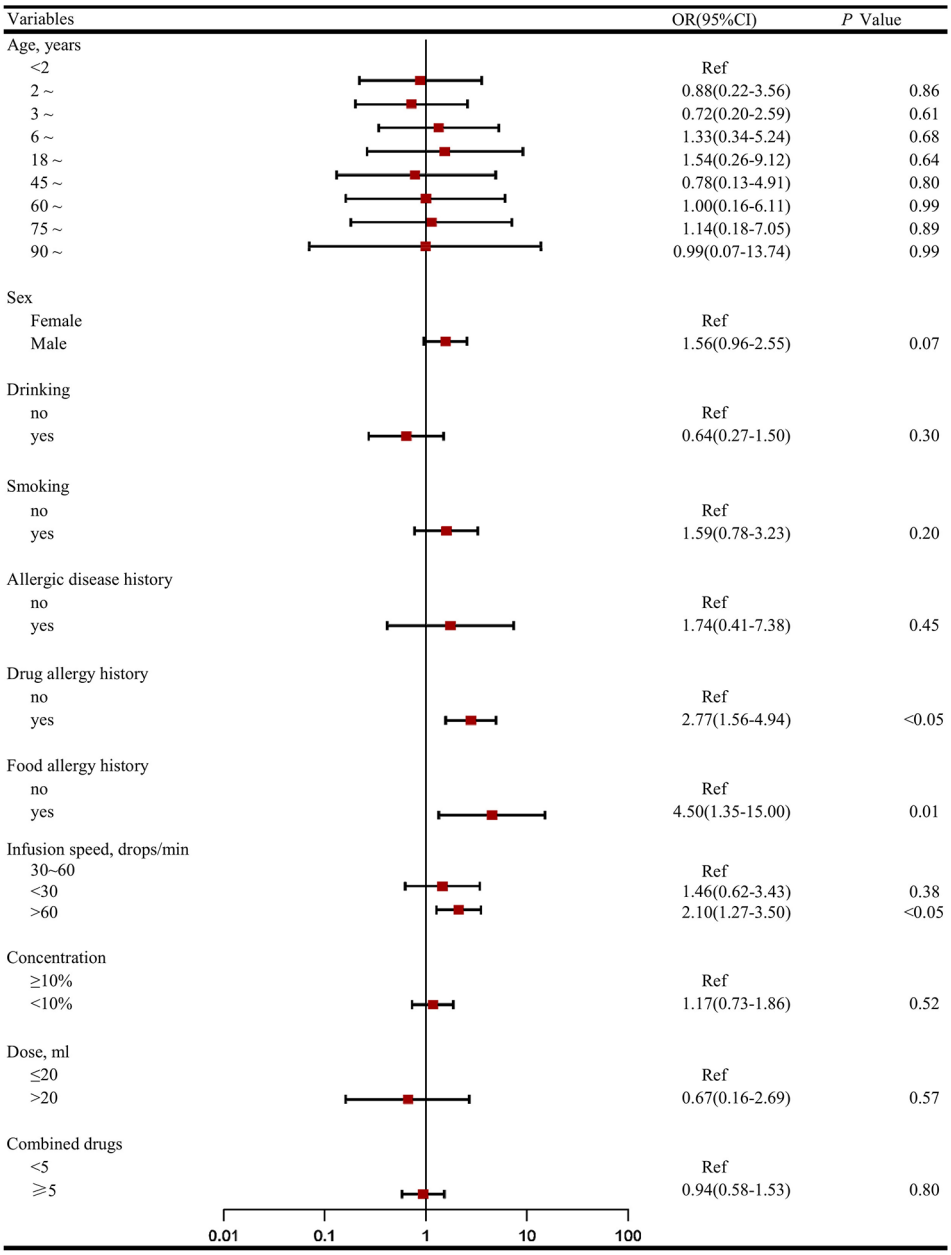

FIGURE 2 | Factors associated with the incidence of adverse drug reactions (ADRs)[a]. **(A)** The odds ratio (OR) for demographic characters (age, sex, food/drug allergy, allergic disease history, habit of smoking/drinking) and clinical characteristics characters (infusion speed, concentration, dose, combined drugs) were compared with patients aged <2 years, female, no food/drug allergy history, no allergic disease history, no habit of smoking/drinking, standard treatment (infusion speed 30~60 drops/min, concentration < 10%, dose < 20 ml) and combined drugs < 5. **(B)** Considering most ADRs occurred in the first 2 h after administration and almost half of them withdrawal Tanreqing injection, we dropped therapy duration as risk factor in logistic regression model.

over 50% of outpatients were prescribed with an injection-administered medication, other than oral medications, in rural township health centers in China (Jiang et al., 2012). There may therefore have been some selection bias toward a study population slightly less healthy than the true population prescribed TRQ, and this might lead to an overestimation of the true incidence of TRQ-related ADRs. Conversely, and thirdly, follow-up in our study was limited to 7 days and therefore later-onset AEs/ADRs will not have been documented, leading to an underestimation of AE/ADR incidence. Fourthly, AE data from laboratory investigations in our study were based on those included in the TRQ phase III and IV clinical trials (*Shanghai Kaibao Pharmaceutical Co., LTD, unpublished*; Shen et al., 2007), but focused on those from

routine blood, hepatic and renal function tests, hepatic and results from other clinical inspection were not investigated. This too may have led to an underestimation of AE/ADR incidence. Lastly, we were unable to report on the specific type of allergic AEs/ADRs TRQ based on the recorded data.

In conclusion, our results suggest that the incidence AEs and ADRs among patients treated with TRQ in clinical practice in China is higher than that seen previously in TRQ clinical trials and that off-label use is highly prevalent. Further data from other well-designed population-based studies in China are warranted to compare with findings from our study, and to help guide physicians and regulators as to whether a review of the current recommendations for TRQ is necessary. Efforts should be made to help TRQ prescribers adhere to the prescribing recommendations on the drug label in order to minimize avoidable patient harm.

AUTHOR'S NOTE

Findings from this study were presented in poster format at the 76th International Pharmaceutical Federation's World Congress of Pharmacy and Pharmaceutical Sciences, Buenos Aires, Argentina from August 28 -September 1, 2016, 32nd International Conference on Pharmacoepidemiology & Therapeutic Risk Management, Dublin, Ireland, August 25–28, 2016.

DATA AVAILABILITY STATEMENT

All datasets generated for this study are included in the article/ **Supplementary Material**.

ETHICS STATEMENT

The studies involving human participants were reviewed and approved by Peking University Third Hospital Ethics Committee with a waiver for informed consent (reference number: IRB00006761- 2014009). Written informed consent from the participants' legal guardian/next of kin was not required to participate in this study in accordance with the national legislation and the institutional requirements.

AUTHOR CONTRIBUTIONS

All authors took part in the final version for submission and accept overall accountability for the accuracy and integrity of the manuscript. S-DZ developed and conceptualized the topic. S-DZ, S-YZ, Y-HY, and HZ designed the methodology. X-XL, LZ, and YZ administrated the project, under supervision conducted by S-DZ and S-YZ. X-XL and YZ conducted the investigation, in cooperation with LZ, who carried out data curation and formal analysis. X-XL and LZ developed the visualization and writing of the original draft.

FUNDING

This work was supported by the State Administration of Traditional Chinese Medicine of the People's Republic of China (grant number: 2013ZX04).

ACKNOWLEDGMENTS

We thank all of the study investigators in the 90 hospitals. We are also grateful for all the members of the Scientific Committee and the Adverse Drug Events Interpretation Committee. We thank Susan Bromley, EpiMed Communications, Abingdon, Oxford, UK for the editorial assistance funded by Peking University.

SUPPLEMENTARY MATERIAL

The Supplementary Material for this article can be found online at: https://www.frontiersin.org/articles/10.3389/fphar.2019.01523/full#supplementary-material

REFERENCES

China Food and Drug Administration (CFDA). (2012). National Drug Standards: Tanreqing zhusheye (YBZ00912003-2007Z-2009). http://zy.yaozh.com/biaozhun/yaodianhui2012/185.pdf. (accessed 24 April 2018).

Edwards, I. R., and Aronson, J. K. (2000). Adverse drug reactions: definitions, diagnosis, and management. *Lancet.* 356 (9237), 1255–1259. doi: 10.1016/S0140-6736(00)02799-9

Ji, K. M., Li, M., Chen, J. J., Zhan, Z. K., and Liu, Z. G. (2009). Anaphylactic shock and lethal anaphylaxis cased by Houttuynia Cordata injection, a herbal treatment in China. *Allergy.* 64 (5), 816–817. doi: 10.1111/j.1398-9995.2009.01942.x

Jiang, H. L., Mao, B., Zhong, Y. Q., Yang, H. M., and Fu, J. J. (2009). Tanreqing Injection for community-acquired pneumonia: a systematic review of randomized evidence. *Zhong Xi Yi Jie He Xue Bao.* 7 (1), 9–19. doi: 10.3736/jcim20090102

Jiang, Q., Yu, B. N., Ying, G., Liao, J., Gan, H., Blanchard, J., et al. (2012). Outpatient prescription practices in rural township health centers in Sichuan Province, China. *BMC Health Serv. Res.* 12, 324. doi: 10.1186/1472-6963-12-324

Li, W., Mao, B., Wang, G., Wang, L., Chang, J., Zhang, Y., et al. (2010). Effect of Tanreqing Injection on treatment of acute exacerbation of chronic obstructive pulmonary disease with Chinese medicine syndrome of retention of phlegm and heat in Fei. *Chin. J. Integr. Med.* 16 (2), 131–137. doi: 10.1007/s11655-010-0131-y

Li, W. L., Liu, S. Y., Xue, D. S., and Qu, H. B. (2014). NIRS-based total quality control system construction of Tanreqing injection and relative thinking. *Zhongguo zhong yao za zhi.* 39 (17), 3409–3412. doi: 10.4268/cjcmm20141742

Li, W. L., Pan, J. C., Xue, D. S., Liu, S. Y., and Qu, H. B. (2017). Primary exploration of key influential factors recognization method of Tanreqing injection. *Zhongguo zhong yao za zhi.* 42 (6), 1062–1066. doi: 10.19540/j.cnki.cjcmm.20170223.019

Li, X. X., Zhuo, L., Yang, Y. H., Zhan, S. Y., and Zhai, S. D. (2017). Post-marketing surveillance of Tanreqing injection in children: a real world study. *Chin. J. Epidemiol.* 38 (2), 248–252. doi: 10.3760/cma.j.issn.0254-6450.2017.02.023

Li, C., Liu, S. Y., Luo, G., Wang, G. H., Zhang, B. X., and Nie, Q. X. (2018). Comparison of plasma pharmacokinetics of Tanreqing solution between intratracheal aerosolization and intravenous injection in rats. *Biomed. Chromatogr.* 32 (3), e4116. doi: 10.1002/bmc.4116

Li, C., Zang, C., Nie, Q., Yang, B., Zhang, B., and Duan, S. (2019). Simultaneous determination of seven flavonoids, two phenolic acids and two cholesterines in Tanreqing injection by UHPLC-MS/MS. *J. Pharm. BioMed. Anal.* 163, 105–112. doi: 10.1016/j.jpba.2018.08.058

Liu, S. Y., Zhang, X. L., Zhang, Z. H., Yi, Y., Zhang, J., Liu, L., et al. (2013). Pharmacokinetics of main active ingredients of Tanreqing injection in rats with LPS induced fever and its antifebrile effects. *Zhong Nan Yao Xue.* 11 (12), 881–884. doi: 10.7539/j.issn.1672-2981.2013.12.001

Muraro, A., Roberts, G., Worm, M., Bilò, M. B., Brockow, K., Fernández Rivas, M., et al. (2014). Anaphylaxis: guidelines from the European Academy of Allergy and Clinical Immunology. *Allergy.* 69 (8), 1026–1045. doi: 10.1111/all.12437

Sampson, H. A., Muñoz-Furlong, A., Campbell, R. L., Adkinson, N. F. Jr., Bock, S. A., Branum, A., et al. (2016). Second symposium on the definition and management of anaphylaxis: summary report–second National Institute of Allergy and Infectious Disease/Food Allergy and Anaphylaxis Network symposium. *J. Allergy Clin. Immunol.* 117 (2), 391–397. doi: 10.1016/j.jaci.2005.121303

Shen, X. H., Xiong, X. D., Shi, M. Y., Yan, H. P., Zhao, M., and Xie, M. (2007). The effective observation of Tanreqing injection on treating 1050 pneumonia patients with the type of phlegm thermal resistance lung. *Zhong Guo Zhong Yi Ji Zhen.* 16 (7), 772–773, 822. doi: 10.3969/j.issn.1004-745X.2007.07.003

Wang, Y., Wang, T., Hu, J. J., Ren, C. Y., Lei, H. T., Hou, Y. M., et al. (2011). Anti-biofilm activity of TanReQing, a Traditional Chinese Medicine used for the treatment of acute pneumonia. *J. Ethnopharmacol.* 134 (1), 165–170. doi: 10.1016/j.jep.2010.11.066

Wang, P., Liao, X., Xie, Y. M., Chai, Y., and Li, L. H. (2016). Tanreqing injection for acute bronchitis disease: a systematic review and meta-analysis of randomized controlled trials. *Complement. Ther. Med.* 25, 143–158. doi: 10.1016/j.ctim.2016.02.008

Wang, Y., Fan, Y. P., Song, J., Cai, Y. P., Jiang, T. T., Wang, Y. G., et al. (2018). Retrospective analysis and discussion on 74 cases of adverse reactions of traditional Chinese medicine injection. *Zhongguo zhong yao za zhi.* 43 (21), 4347–4351. doi: 10.19540/j.cnki.cjcmm.20180815.004.

Wang, L., Zhang, F., and Chen, W. S. (2019). Literature analysis of ADE induced by tanreqing injection. *Zhong Guo Yao Fang* 30 (5), 694–697. doi: 10.6039/j.issn.1001-0408.2019.05.24

WHO. Collaborating Centre for International Drug Monitoring, Uppsala. (2012). The use of the WHO-UMC system for standardised case causality assessment. http://www.who.int/medicines/areas/quality_safety/safety_efficacy/WHOcausality_assessment.pdf?ua=1. (Accessed 19 July 2019).

Xie, P. Y., Xie, Y. M., Wang, L. X., Chang, Y. P., and Liu, S. Y. (2014). Demonstration of nested case-control study design in mechanisms research of allergic reaction of tanreqing injection. *Zhongguo zhong yao za zhi.* 39 (18), 3567–3570. doi: 10.4268/cjcmm20141828

Xiong, L., Chen, L., Wang, C. Q., Yue, J. B., Li, Y. Q., Zhou, W. J., et al. (2018). Clinical efficacy and safety of tanreqing injection for pulmonary infection inpatients with tuberculosis: a meta-analysis.. *J. Altern. Complement. Med.* 24 (11), 1051–1062. doi: 10.1089/acm.2018.0020

Yan, Y. Y., Yang, Y. H., Wang, W. W., Pan, Y. T., Zhan, S. Y., Sun, M. Y., et al. (2017). Post-marketing safety surveillance of the salvia miltiorrhiza depsidesalt for infusion: a real world study.. *PloS One* 12 (1), e0170182. doi: 10.1371/journal.pone.0170182

Yang, B., Wang, Y., Shan, L. L., Zou, J. T., Wu, Y. Y., Yang, F. F., et al. (2017). A novel and practical chromatographic "Fingerprint-ROC-SVM" strategy applied to quality analysis of traditional chinese medicine injections: using KuDieZi injection as a case study. *Molecules* 22 (7), E1237. doi: 10.3390/molecules22071237

Yang, Y., Wang, L., Wu, Y. J., Liu, X. S., Bi, Y., Xiao, W., et al. (2017). On-line monitoring of extraction process of Flos Lonicerae Japonicae using near infrared spectroscopy combined with synergy interval PLS and genetic algorithm. *Spectrochim. Acta A. Mol. Biomol. Spectrosc.* 182, 73–80. doi: 10.1016/j.saa.2017.04.004

Yang, W. F., Liu, J. L., Blažeković, B., Sun, Y. N., Ma, S. H., Ren, C. Y., et al. (2018). *In vitro* antibacterial effects of Tanreqing injection combined with vancomycin or linezolid against methicillin-resistant Staphylococcus aureus. *BMC Complement. Altern. Med.* 18 (1), 1–10. doi: 10.1186/s12906-018-2231-8

Zhang, L., Wong, L. Y., He, Y., and Wong, I. C. (2014). Pharmacovigilance in China: current situation, successes and challenges. *Drug Saf.* 37 (10), 765–770. doi: 10.1007/s40264-014-0222-3

Zhang, F., Sun, L., Gao, S. H., Chen, W. S., and Chai, Y. F. (2016). LC-MS/MS analysis and pharmacokinetic study on five bioactive constituents of Tanreqing injection in rats. *Chin. J. Nat. Med.* 14 (10), 769–775. doi: 10.1016/S1875-5364(16)30091-7

Zhong, Y. Q., Mao, B., Wang, G., Fan, T., Liu, X. M., Diao, X., et al. (2010). Tanreqing injection combined with conventional Western medicine for acute exacerbations of chronic obstructive pulmonary disease: a systematic review. *J. Altern. Complement. Med.* 16 (12), 1309–1319. doi: 10.1089/acm.2009.0686

Conflict of Interest: X-XL is supported by National Key Clinical Specialty Discipline Construction Project 56495-04 and by Peking University Third Hospital, funded through State Administration of Traditional Chinese Medicine of the People's Republic of China 2013ZX04. LZ is supported by School of Public Health, Peking University, funded through State Administration of Traditional Chinese Medicine of the People's Republic of China 2013ZX04. YZ is supported by State Administration of Traditional Chinese Medicine of the People's Republic of China 2013ZX03 and 2013ZX04. Y-HY is supported by National Key Clinical Specialty Discipline Construction Project 56495-04 and by Peking University Third Hospital, funded through State Administration of Traditional Chinese Medicine of the People's Republic of China 2013ZX03 and 2013ZX04. HZ is supported by State Administration of Traditional Chinese Medicine of the People's Republic of China 2013ZX03 and 2013ZX04. S-YZ is supported by School of Public Health, Peking University, funded through State Administration of Traditional Chinese Medicine of the People's Republic of China 2013ZX03 and 2013ZX04. S-DZ is supported by National Key Clinical Specialty Discipline Construction Project 56495-04 and by Peking University Third Hospital, funded through SATCM 2013ZX03 and 2013ZX04.

frontiers in Pharmacology

ORIGINAL RESEARCH
published: 31 January 2020
doi: 10.3389/fphar.2019.01584

Anti-Atherosclerosis Effect of Angong Niuhuang Pill *via* Regulating Th17/Treg Immune Balance and Inhibiting Chronic Inflammatory on ApoE$^{-/-}$ Mice Model of Early and Mid-Term Atherosclerosis

*Qinghong Fan[1], Yujuan Liu[1], Jiaoyu Rao[1], Zhe Zhang[1], Wei Xiao[1], Tao Zhu[1], Xiaomeng Chai[1], Kaihe Ye[1], Na Ning[2], Zhen Yin[2], Yushuang Chai[2], Yimin Xu[2], Ruirui Lan[3], A Verkhratsky[4] and Hong Nie[1,5]**

[1] Guangdong Province Key Laboratory of Pharmacodynamic Constituents of Traditional Chinese Medicine and New Drugs Research, College of Pharmacy, Jinan University, Guangzhou, China, [2] Guangzhou Baiyunshan Zhongyi Pharmaceutical Co., Ltd, Guangzhou, China, [3] International Department, The Affiliated High School of SCNU, Guangzhou, China, [4] Faculty of Biology, Medicine and Health, The University of Manchester, Manchester, United Kingdom, [5] International Cooperative Laboratory of Traditional Chinese Medicine Modernization and Innovative Drug Development of Chinese Ministry of Education (MOE), College of Pharmacy, Jinan University, Guangzhou, China

OPEN ACCESS

Edited by:
Xiu-Wei Yang,
Peking University, China

Reviewed by:
Haolong Liu,
Peking University Health Science Centre, China
Dan Yan,
Capital Medical University, China

***Correspondence:**
Hong Nie
hongnie1970@163.com

Specialty section:
This article was submitted to Ethnopharmacology, a section of the journal Frontiers in Pharmacology

Received: 03 May 2019
Accepted: 06 December 2019
Published: 31 January 2020

Citation:
Fan Q, Liu Y, Rao J, Zhang Z, Xiao W, Zhu T, Chai X, Ye K, Ning N, Yin Z, Chai Y, Xu Y, Lan R, Verkhratsky A and Nie H (2020) Anti-Atherosclerosis Effect of Angong Niuhuang Pill via Regulating Th17/Treg Immune Balance and Inhibiting Chronic Inflammatory on ApoE$^{-/-}$ Mice Model of Early and Mid-Term Atherosclerosis. Front. Pharmacol. 10:1584. doi: 10.3389/fphar.2019.01584

Angong Niuhuang Pill (ANP) is a well-known patented Chinese medicine which is used for hundreds of years for treating the central nervous system diseases. Atherosclerosis is a poly-aetiological chronic inflammatory vascular disease. Preventing inflammation is fundamental for treating atherosclerosis in early stages. In this study, we investigated the protective effects and possible mechanisms of ANP action on a high-fat diet induced early and mid-term atherosclerosis ApoE$^{-/-}$ mice. The effects of ANP were compared with accepted drug simvastatin. Twelve male C57BL/6J mice were used as the control group, and 60 male ApoE$^{-/-}$ mice were randomly divided into five groups: Model group, Simvastatin group, Low-, Medium-, and High-dose ANP group these groups received, respectively, saline, simvastatin (3.0mg/kg), low-dose ANP (0.25 g/kg), medium-dose ANP (0.50 g/kg), and high-dose ANP (1.0 g/kg), once every other day for 10 weeks. After administration, serum biochemical indices were detected by the automatic biochemical analyzer, the concentrations of IL-6 and IL-10 in the serum were assayed by ELISA, expression levels of IL-1β, TNF-α, MMP-2, MMP-9, CCL2, and its receptor CCR2 in the full-length aorta, and expression levels of transcription factors Foxp3, RORγt in the spleen were assayed *via* western blotting and RT-qPCR. Flow cytometry was used to analyze Th17 cells and Treg cells. Pathological and histological analysis was completed on aortic root. ANP decreased LDL/HDL ratio, concentrations of IL-6 while increased IL-10 in serum. Moreover, ANP down-regulated the expression levels of IL-1β, TNF-α, MMP-2, MMP-9, CCL2, and CCR2 receptor in the full-length aorta. In addition, ANP decreased Th17 cells and expression levels of transcription factor RORγt, increased Treg cells and expression levels of transcription factor Foxp3. ANP decreased content of

collagen fibers and infiltration of inflammatory cells in the aortic root. In conclusion, we demonstrated that ANP has anti-atherosclerosis effects on a high-fat diet induced ApoE$^{-/-}$ mice early and mid-term AS model *via* regulating Th17/Treg balance, inhibiting chronic inflammation, reducing plaque collagen fibers, and reducing inflammatory cells infiltration, to exert its multi-channel multi-target anti-early and mid-term AS effects.

Keywords: Angong Niuhuang Pill, early and mid-term atherosclerosis, ApoE$^{-/-}$ mice, Th17/Treg balance, inflammation, plaque stability

INTRODUCTION

Cardiovascular diseases (CVD) and related chronic diseases are the number one cause of death. About 80% of CVD-related deaths occur in low-income and middle-income countries (Feigin et al., 2015). According to China Cardiovascular Disease Report 2017, the number of patients with CVD reached 290 million, and CVD deaths account for more than 40% of deaths. Since 2004, the average growth rate of CVD cost in China was much higher than the growth rate of GDP (Chen et al., 2018). The burden of China's CVD is increasing; it has become a major public health problem. It is well accepted that aterosclerosis (AS) is the primary cause of CVDs. Therefore, the search for effective therapy is of fundamental importance.

Pathogenesis of AS includes lipid infiltration, damage response, mononuclear macrophage invasion, and inflammation response. At present, it is generally accepted that AS is a chronic inflammatory disease (Ross, 1999), which involves cellular immune response, particularly of Th17 cells and $CD4^+CD25^+$ regulatory T (Treg) cells (Xie et al., 2010; Wu et al., 2017). Treg and Th17 cells have recently been described as two distinct subsets distinct from Th1 and Th2 cells, while Th17/Treg balance is different from balance of Th1/Th2 (Frostegard et al., 1999; Cheng et al., 2008). Treg cells expressing the forkhead/winged helix transcription factor (Foxp3) and Th17 cells expressing retinoic acid-related orphan receptorγt (RORγt) are two important immune cells for controlling anti-atherogenic cytokines such as interleukin (IL)-10, transforming growth factor (TGF)-β1, and pro-atherogenic cytokines such as IL-6, IL-17 (Shimon et al., 2006; Bettelli et al., 2007). Above cytokines play important roles in maintaining the number and function of Treg cells and Th17 cells and participate in the pathogenesis of human AS. In previous study (Chai et al., 2019), we reported that the Th17/Treg imbalance existed in the ApoE$^{-/-}$ mice AS model, which was induced by consecutive 8 weeks high-fat diet. Therefore, the Th17/Treg balance is critical for prevention of AS and autoimmune response.

Chronic inflammation represents the most basic pathogenetic factor of AS (Ross, 1999), Cytokines orchestrate the complex inflammatory response within the atherosclerotic plaque throughout the entire AS evolution (Tousoulis et al., 2016). At the early and middle stages of AS, endothelial dysfunction, secretion of chemokines and cytokines such as CCL2, IL-1β, TNF-α expression of intercellular adhesion molecule 1 (ICAM-1), vascular cell adhesion molecule 1 (VCAM-1), accumulation of immune cells such as T lymphocytes, dendritic cells, macrophages to the AS plaques, and migration and proliferation of vascular smooth muscle cells (VSMCs) to these plaques further aggravate inflammatory response (Ramji and Davies, 2015). Furthermore, activation of matrix metalloproteinases (MMPs) instigates expansion and instability of atherosclerotic plaques (Ramji and Davies, 2015; Tousoulis et al., 2016). The expanding plaque once ruptured may cause arterial thrombosis, stenosis or blockage of the lumen, affecting the arterial supply of blood to organs and tissues, eventually leading to cerebral infarction, acute coronary syndrome, myocardial infarction, and peripheral vascular disease (Weber and Noels, 2011). In the previous study (Chai et al., 2019), we found that ApoE$^{-/-}$ mice induced by 8 weeks high-fat diet demonstrate severe inflammatory response in the full-length aorta. Therefore, inhibiting this inflammatory response, reducing migration and adhesion of inflammatory cells, together with maintaining plaque stability are essential for the treatment of early and mid-stage AS.

Angong Niuhuang Pill (ANP) is a well-known patented Chinese medicine, used to treat stroke, encephalitis, and meningitis. Its main components include *Bovis Calculus*, *Powerdered Buffalo Horn Extract*, Artificial *Moschus*, *Cinnabaris*, *Coptis chinensis* Franch., *Hyriopsis cumingii*(Lea), *Scutellaria baicalensis* Georgi, *Realgar*, *Gardenia jasminoides* J.Ellis, *Curcuma aromatica* Salisb., and *Borneolum Syntheticum* (Editorial Committee of Pharmacopoeia of Ministry of Health PR China, 2015). The chemical structure of the known component in artificial Moschus were shown in **Supplementary Material (Table 1)**. Pharmacological effects of ANP include: hepatoprotection, anti-inflammation, anti-viral action, antipyresis, and anticonvulsive effects. Our previous study also found that ANP has anti-atherosclerosis and cardio-protective effect on high-fat diet combined with vitamin D3 induced AS rats (Fu et al., 2017). In the present study, we combine the studies of Th17/Treg balance and inflammatory pathways to attempt to investigate the possible mechanisms of ANP relevant for treating the early and middle AS in the ApoE$^{-/-}$ mice induced by 10-week high-fat diet (Nakashima et al., 1994; Gupta et al., 1997; Meir and Leitersdorf, 2004).

MATERIALS AND METHODS

Preparation of ANP

ANP was provided by Guangzhou Baiyunshan Zhongyi pharmaceutical co., Ltd (Guangzhou, China). It contains the following components: *Bovis Calculus* 100 g, *Powerdered Buffalo Horn Extract* 200 g, Artificial *Moschus* 25 g, *Hyriopsis cumingii* (Lea) 50 g, *Cinnabaris* 100g, *Realgar* 100 g, *Coptis chinensis* Franch. 100 g, *Scutellaria baicalensis* Georgi 100 g, *Gardenia*

jasminoides J. Ellis 100 g, *Curcuma aromatica* Salisb. 100 g, *Borneolum Syntheticum* 25 g (Editorial Committee of Pharmacopoeia of Ministry of Health PR China, 2015).

Cinnabaris, *Hyriopsis cumi-ngii* (Lea) and *Realg*ar were grounded or pulverized to the very fine powders (200 mesh). *Coptis chinensis* Franch., *Scutellaria baicalensis* Georgi, *Gardenia jasminoides* J. Ellis, and *Curcuma aromatica* Salisb. were pulverized to a fine powder (100 mesh). *Bovis Calculus*, *Powerdered Buffalo Horn Extract*, Artificial *Moschus,* and *Powerdered Buffalo Horn Extract* were triturated with the above powders, sifted and well mixed. Refined honey was mixed to make 600 big honeyed pills, or alternately coated with a gold film (Editorial Committee of Pharmacopoeia of Ministry of Health PR China, 2015). HLPC was used to verify the formulation to guarantee the quality of the ANP, fingerprint of ANP please see the **Supplementary Figure S1**. The UPLC Fingerprint of 24 ANP Batches was shown in **Supplementary Figure S3**.

Reagents

Main reagents used in the study were as follows: 1) ANP (Guangzhou Baiyunshan Zhongyi Pharmaceutical Co, Ltd, Lot: WA0076); 2) Simvastatin (Shangdong Xinqi Pharmaceutical Co., Ltd, Lot: 20170101); 3) High fat feed composed of 3% cholesterol, 0.5% sodium cholate, 0.2% propylthiouracil, 5% sugar, 10% lard, and 81.3% basic feed (Medical Science Experimental Animal Center, Guangdong, China, Lot: 201814); 4) Kits for IL-6, IL-10 (Wuhan Huamei Biological Co, Ltd, Lot: U23013173, U24018179), kit for reverse transcription, fluorescent dyes of SYBR (TAKARA, Lot: AI12361A, AK9304), kit for Masson staining (Sinopharm Chemical Reagent Co, Ltd, Lot: G1006), kit for BCA (Shanghai Beyotime biotechnology, Lot: 051018180514), and kit for ECL plus (Applygen, Lot: P1010); 5) Anti-αSMA, anti-CD11c, anti-CD68, fluorescent secondary antibody with FITC marker, and fluorescent secondary antibody with CY3 marker (Servicebio, Lot: GB130441, GB11058, GB11067, GB223011, GB21303); 6) β-actin, anti-MCP-1 (CST, Lot: 15,2), anti-CCR2, anti-Foxp3, anti-IL-1β, anti-TNF-α (Abcam, Lot: GR286626-10, GR239541-14, GR309542-2, GR235155-19), anti-RORγ (Santa, Lot: F3017), anti-MMP-2, and anti-MMP-9 (Wanleibio, Lot: WL03334, WL02141); 7) Horseradish peroxidase-conjugated goat anti-rabbit secondary antibody, horseradish peroxidase-conjugated goat anti-mouse secondary antibody (Shanghai Beyotime biotechnology, Lot: 040818180510, 040818184521); 8) PE anti-mouse CD25, APC anti-mouse CD127, PE/Cy7 anti-mouse CD4, Alexa Fluor® 488 anti-mouse IL-17A, APC Rat IgG2a κ Isotype Ctrl, PE Rat IgG2b κ Isotype Ctrl, Alexa Fluor® 488 Rat IgG1 κ Isotype Ctrl, PE/Cy7 Rat IgG2a κ Isotype Ctrl, Cell Activation Cocktail with Brefeldin A, 10×RBC Lysis Buffer, Fixation Buffer, 10×Intracellular Staining Permeabilization Wash Buffer (Biolegad, Lot: B247733, B232775, B249463, B259048, B238057, B255375, B236504, B236195, B248910, B250015, B252968, B252856).

Animals

Twelve 4-week old Specific Pathogen Free (SPF) male C57BL/6J mice (weight:18 ± 2.0g) and sixty 4-week old SPF male ApoE$^{-/-}$ mice (weight:18 ± 2.0g), were provided by the department of Laboratory Animal Science of the department of medicine, Peking University [Certificate No. SCXK (jing) 2011-0012]. Mice were housed in the Jinan University Medical School Laboratory Animal Management Center [Certificate No. SCXK (Guangdong) 2012-0117] and were maintained at 24°C and 65% humidity. Mice were maintained on a 12-h light/dark cycle, C57BL/6J mice were given free access to standard laboratory mouse chow and tap water, ApoE$^{-/-}$ mice were given free access to high fat feed and tap water. The experiments were approved by the Laboratory Animal Ethics Committee of Jinan University (No. 201812374), and were performed according to the instructions of the National Institute of Health (OLAW/NIH Revised 2015) (Office of Laboratory Animal Welfare/National Institutes of Health, 2015).

Model Establishment

After ten days of adaptive feeding, 60 SPF male ApoE$^{-/-}$ mice were randomly divided into five groups, i) model group, ii) simvastatin group (3.0 mg/kg), iii–v) low-, ledium-, and high-dose ANP groups (0.25 g/kg, 0.50 g/kg, 1.0g/kg, respectively) and given free access to high fat feed and tap water for 10 weeks. Each group contained twelve mice. Twelve SPF male C57BL/6J mice were used as controls and were given free access to standard laboratory mouse chow and tap water for 10 weeks. On the first day of high-fat diet administration, all experimental drug treatments (simvastatin and ANP) were administered intragastrically once every other day for 10 weeks. Drug dosages were titrated according to animal weight. Saline was given intragastrically in control group and model group. All drug treatments were prepared immediately before administration as a suspension by dissolving an appropriate amount of the drug in distilled water.

Sample Collection

After administration, serum was collected for biochemical analysis. The aortic root was separated for immunofluorescence staining and Masson staining. The full-length aorta was separated for Real-time quantitative polymerase chain reaction (RT-qPCR) and Western Blotting analysis. The liver, kidney, spleen, and thymus were separated for organ coefficient or organ index. Primary splenocytes were separated for flow cytometric analysis from the spleen.

Serum Biochemical Analysis

The cholesterol (CHOL), triglyceride (TG), low-density lipoprotein (LDL-C), and high-density lipoprotein (HDL-C) were measured using automatic biochemical analyzer. All protocols were followed in accordance to the manufacturer recommendations.

Organ Coefficient and Index Analysis

Liver coefficient, kidney coefficient, thymus index, and spleen index were calculated according to corresponded calculation formula separately. The formula of liver and kidney coefficient: weight of liver and kidney (mg)/weight of animal (g). The

formula of thymus and spleen index: weight of thymus and spleen (mg)/weight of animal (g)*10.

Flow Cytometric Analysis of Th17 and Treg Cells

The ratio of Th17 to Treg cells in splenocyte suspensions was analyzed by flow cytometry. The splenocyte suspensions were stimulated with 10 μl of Cell Activation Cocktail (with Brefeldin A) and mixed. After incubation at 37°C for 6 h, the sample was centrifuged, and the precipitate was suspended in 1 ml RBC. The suspensions were then centrifuged and the precipitate re-suspended in PBS twice. After antibody labeling of surface proteins, the sample was incubated in the dark for 20 min followed by centrifugation (1,500 rpm). The cells in the precipitate were then fixed with fixation buffer, followed by incubation in the dark for 20 min. The sample was again centrifuged and suspended in 1 mL Permeabilization Wash Buffer. The cells were then washed twice and labeled with an immunofluorescent antibody. After incubation in the dark for 20 min, the sample was washed using 1 ml Permeabilization Wash Buffer twice and suspended in PBS prior to flow cytometric detection.

Masson Staining

Masson staining was used to detect collagen fibers in the plaque of aortic root. According to kit for Masson staining manufacturer instructions, the aortic root fixed in 4% paraformaldehyde were dehydrated in alcohol, paraffin-embedded, sectioned and subjected to Masson staining. The stained sections were observed under the light microscope. Masson staining of the whole aorta was measured by Image Pro Plus 6.0. The area proportion of collagen fiber was calculated as the ratio of stained area to area of interest calculated by Image Pro Plus 6.0.

Immunofluorescence Staining

Immunofluorescence staining was used to detect inflammatory cells infiltration such as macrophages, DCs, and VSMCs in the plaque of aortic root. Anti-CD68, anti-CD11c, and anti-αSMA were respectively used as special marker in macrophages, DCs, and VSMCs. Frozen slices of aortic root were blocked in blocking buffer for 60 min, aspirated blocking solution, applied diluted primary antibody, incubated overnight at 4°C, rinsed three times in PBS for 5 min each, and then incubated specimen in fluorochrome-conjugated secondary antibody diluted in antibody dilution buffer for 1–2 h at room temperature in the dark, rinsed in PBS, thereafter, coverslips stained with DAPI. The stained sections were observed under fluorescence microscope, and Image J was used to semi-quantitatively analyze positive cells.

Cytokines Detection by ELISA

The serum concentrations of IL-6 and IL-10 were measured using the IL-6 and IL-10 ELISA kits. In line with the manufacturer's instructions, standard, or sample (100 μl) was added to each well and incubated for 2 h at 37°C. Then, the medium in each well was discarded, and biotin antibody (100 μl) was added to each well, followed by incubation for 1 h at 37°C. The medium in each well was aspirated and the wells were washed three times. Thereafter, HRP-avidin (100 μl) was added to each well and incubated for 1 h at 37°C. The medium in each well was aspirated and the wells were washed five times, followed by addition of tetramethylbenzidine substrate (90 μl) and incubation for 20 min at 37°C in the dark. Finally, the stop solution (50 ul) was added to each well, and the absorbance of the wells was read at 450 nm within 5 min.

Real-Time Quantitative Polymerase Chain Reaction

The mRNA levels of *Foxp3, RORγt* in the spleen, as well as *CCR2, CCL2, IL-1β, TNF-α, MMP-2,* and *MMP-9* in the full-length aorta, were analyzed by RT-qPCR. Total RNA was extracted with Trizol reagent according to the manufacturer instructions from full-length aorta and spleen. The concentration and purity of RNA was analyzed using a micro-detector. Reverse transcription kit was used for reverse transcription reaction to synthesize cDNA, RT-qPCR was performed to determine mRNA levels of inflammatory mediators with the SYBR Green real-time PCR master mix kit. Each sample was analyzed in triplicate, normalized to *GAPDH*. All the PCR primers used are listed in **Table 1**. RT-qPCR conditions were 95°C for 30 sec followed by 40 cycles of 95°C for 5 sec, 55°C for 30 sec, and 72°C for 60 sec.

Western Blotting Analysis

Protein levels of Foxp3, RORγt in the spleen, as well as CCR2, CCL2, IL-1β, TNF -α, MMP-9, and MMP-2 in the full-length aorta were detected by western blotting analysis. Total proteins were extracted from full-length aorta and spleen. The concentrations of protein were determined by BCA protein assay. Each sample containing 30 μg protein was separated, respectively, on 8%, 10%, and 15% SDS-PAGE gel electrophoresis and then transferred onto a polyvinylidene

TABLE 1 | Primers used for RT-qPCR.

Gene	Primer	Sequence 5′-3′
Foxp3	Forward primer	5'- TGGAACCACGGGCACTATCACA-3'
Foxp3	Reverse primer	5'- GAGGCTGCGTATGATCAGTTATGC-3'
RORγt	Forward primer	5'- TGCAAGACTCATCGACAAGG-3' 5'-
RORγt	Reverse primer	AGGGGATTCAACATCAGTGC-3'
CCR2	Forward primer	5'- AGAGAGCTGCAGCAAAAAGG-3'
CCR2	Reverse primer	5'- GGAAAGAGGCAGTTGCAAAG-3'
CCL2	Forward primer	5'- AGGTCCCTGTCATGCTTCTG-3'
CCL2	Reverse primer	5'- TCTGGACCCATTCCTTCTTG-3'
IL-1β	Forward primer	5'- ACTCATTGTGGCTGTGGAGA-3'
IL-1β	Reverse primer	5'- TTGTTCATCTCGGAGCCTGT-3'
TNF-α	Forward primer	5'- TCTACTGAACTTCGGGGTGATCG-3'
TNF-α	Reverse primer	5'- ACGTGGGCTACAGGCTTGTCA-3'
MMP-2	Forward primer	5'-CACACCAGGTGAAGGATGTG-3'
MMP-2	Reverse primer	5'-AGGGCTGCATTGCAAATATC-3'
MMP-9	Forward primer	5'-TGAATCAGCTGGCTTTTGTG-3'
MMP-9	Reverse primer	5'-GTGGATAGCTCGGTGGTGTT-3'
GAPDH	Forward primer	5'-CATCCATGACAACTTTGGCA-3'
GAPDH	Reverse primer	5'-CCTGCTTCACCACCTTCTTG-3'

difluoride membrane. Thereafter, membranes were incubated in a 5% (weight in volume) milk solution for 2 h and then incubated at 4°C overnight with one of the following primary antibodies: β-actin, IL-1β, TNF-α, CCL2, CCR2, Foxp3, RORγt, MMP-2 (1:1000 dilution each), and MMP-9 (1:500). After primary antibody incubation, membranes were washed and incubated with horseradish peroxidase-conjugated goat anti-rabbit secondary antibody (1:5000, 374°C, 2h) or horseradish peroxidase-conjugated goat anti-mouse secondary antibody (1:2000, 374°C, 2h). The blots were visualized using enhanced chemiluminescence reagent, and UVP BioSpectrum Imaging System was used to expose immune-positive bands. The bands were semi-quantitatively analyzed with Image J, and the results are expressed as ratios of IL-1β, TNF-α, CCL2, CCR2, Foxp3, RORγt, MMP-2, MMP-9 to β-actin densitometry readings.

Statistical Analysis

All data were performed as mean ± standard error of the mean (mean±SEM) and were analyzed by One-way ANOVA with Dunnett T3 test in SPSS Statistics 18.0. $p < 0.05$ were considered as statistically significant.

RESULTS

Body Weight, Liver and Kidney Coefficients

The body weight of ApoE$^{-/-}$ mice and C57BL/6J mice over a 10-week period was shown in **Figure 1A** and **Table 2**. The body weight of model group was higher than control group, and the body weight of model group was significantly increased at 3rd, 5th, and 10th week ($p < 0.05$ or $p < 0.01$) compared to the control group. The body weight of ANP groups and simvastatin group was lower than model group, and a significant difference was noted at 5th, 9th, and 10th week ($p < 0.05$ or $p < 0.01$), compared to the control group. Liver coefficient was significantly increased ($p < 0.05$) while kidney coefficient was significantly decreased ($p < 0.01$) in the model group. In medium- and high-dose ANP groups liver coefficient was significantly decreased ($p < 0.01$). Kidney coefficient was not altered in all ANP groups. These results were shown in**Figure 1B–C**.

Effect of ANP on Serum CHOL, TG, LDL-C, HDL-C, and LDL-C/HDL-C Ratio

LDL-C/HDL-C ratio and concentrations of CHOL, TG, LDL-C, HDL-C in model group were higher than in control group

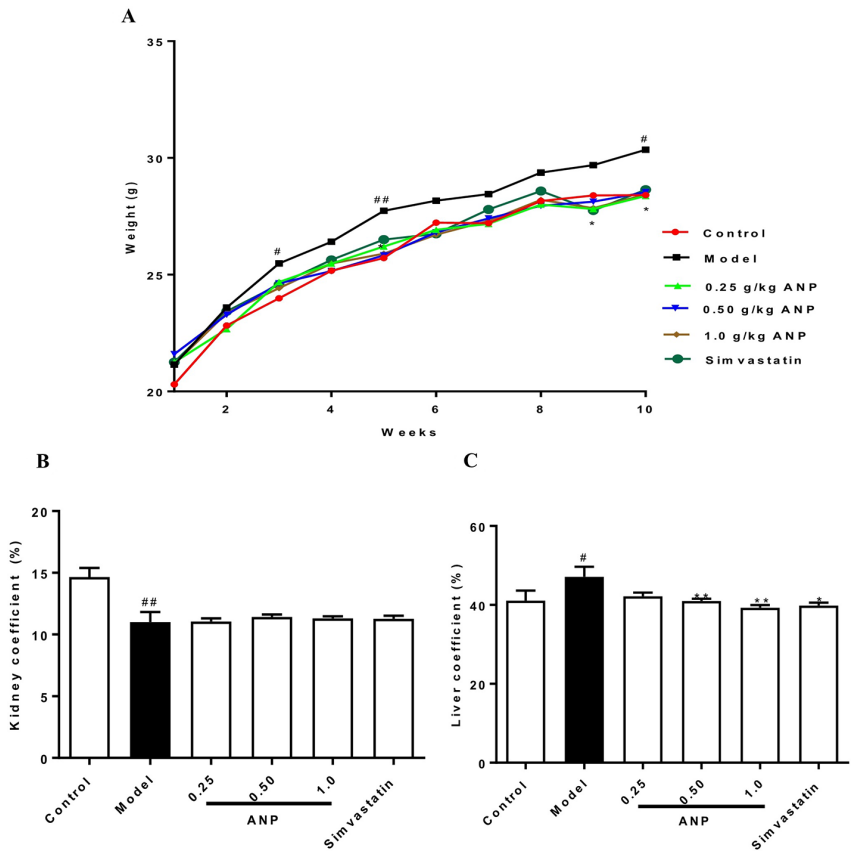

FIGURE 1 | The body weight, liver coefficient and kidney coefficient of ApoE$^{-/-}$ mice and C57BL/6J mice. **(A)** Average body weight curve. **(B)** Kidney coefficient. **(C)** Liver coefficient. Compared with control group, $^{\#}p < 0.05$, $^{\#\#}p < 0.01$; Compared with model group, $^{*}p < 0.05$, $^{**}p < 0.01$ (Mean ± SEM, liver and kidney coefficient n = 6). ANP, Angong Niuhuang Pill.

TABLE 2 | Body weight of C57BL/6 mice and ApoE$^{-/-}$mice in 10 weeks.

Weeks	Groups					
	Control	Model	Low-dose ANP	Medium-dose ANP	High-dose ANP	Simvastatin
1	20.3 ± 0.4	21.1 ± 0.2	21.2 ± 0.3	21.6 ± 0.4	21.2 ± 0.4	21.3 ± 0.3
2	22.8 ± 0.5	23.6 ± 0.3	22.7 ± 0.4	23.3 ± 0.5	23.4 ± 0.4	23.4 ± 0.4
3	24.0 ± 0.5	25.5 ± 0.4$^{\#}$	24.7 ± 0.5	24.6 ± 0.6	24.4 ± 0.4	24.6 ± 0.4
4	25.2 ± 0.6	26.4 ± 0.5	25.5 ± 0.5	25.2 ± 0.6	25.5 ± 0.4	25.6 ± 0.4
5	25.7 ± 0.6	27.7 ± 0.5$^{\#\#}$	26.2 ± 0.6*	25.8 ± 0.7*	25.9 ± 0.4	26.5 ± 0.3*
6	27.2 ± 0.5	28.2 ± 0.4	26.9 ± 0.7	26.8 ± 0.6	26.7 ± 0.5	26.8 ± 0.5
7	27.2 ± 0.5	28.4 ± 0.5	27.2 ± 0.7	27.4 ± 0.5	27.3 ± 0.4	27.8 ± 0.4
8	28.2 ± 0.6	29.4 ± 0.5	28.0 ± 0.6	28.0 ± 0.5	28.2 ± 0.4	28.6 ± 0.4
9	28.4 ± 0.6	29.4 ± 0.5	27.8 ± 0.7*	28.1 ± 0.5*	27.8 ± 0.5*	27.9 ± 0.5*
10	28.4 ± 0.7	30.3 ± 0.5$^{\#}$	28.4 ± 0.6*	28.5 ± 0.5*	28.4 ± 0.5*	28.4 ± 0.6*

Compared with Control, $^{\#}p < 0.05$, $^{\#\#}p < 0.01$; Compared with model group, $^{*}p < 0.05$, (mean ± SEM, n = 12).

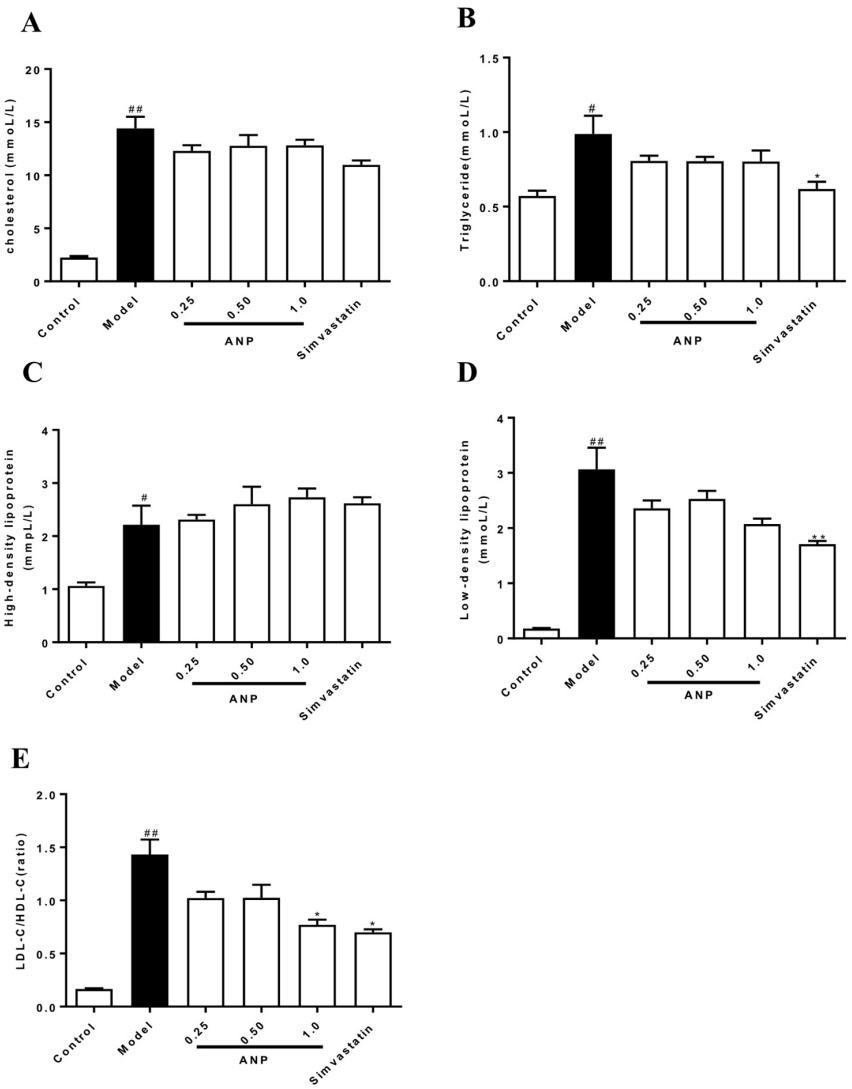

FIGURE 2 | Effect of ANP on concentrations of serum CHOL, TG, HDL-C, LDL-C and LDL-C/HDL-C ratio. **(A)** Serum concentrations of CHOL, **(B)**, Serum concentrations of TG, **(C)** Serum concentrations of HDL-C, **(D)** Serum concentrations of LDL-C, **(E)** Ratio of LDL-C/HDL-C. Compared with control group, $^{\#}p < 0.05$, $^{\#\#}p < 0.01$; Compared with model group, $^{*}p < 0.05$ (Mean ± SEM, n = 6). ANP, Angong Niuhuang Pill; CHOL, cholesterol; TG, triglyceride; LDL-C, low-density lipoprotein; HDL-C, high-density lipoprotein.

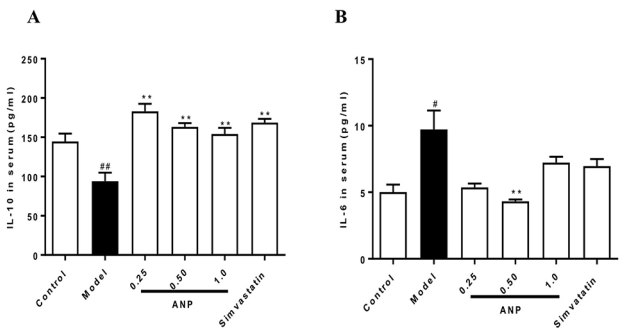

FIGURE 3 | Effect of ANP on serum concentrations of pro-inflammation IL-6 and anti-inflammation IL-10. **(A)** Serum concentrations of IL-10, **(B)** Serum concentrations of IL-6. Compared with control group, $^{\#}p < 0.05$, $^{\#\#}p < 0.01$; Compared with model group, $^{**}p < 0.01$ (Mean ± SEM, n = 6). ANP, Angong Niuhuang Pill.

($p < 0.05$ or 0.01). It should be noted that all ANP administrated groups showed no difference in serum CHOL, TG, LDL-C, HDL-C. However, when compared with model group, high-dose ANP significantly decreased LDL-C/HDL-C ratio ($p < 0.05$). These results were shown in **Figures 2A–E**.

Effect of ANP on Serum Concentrations of IL-6 and IL-10

Serum concentrations of IL-6 and IL-10 were shown in **Figures 3A, B**. When compared with control group, concentrations of pro-inflammation IL-6 were significantly increased ($p < 0.05$), and concentrations of anti-inflammation IL-10 were significantly decreased ($p < 0.01$). These data indicate indicated that ApoE$^{-/-}$ mice of model group had a chronic inflammation at the early and mid-term AS. When compared with model group, medium-dose ANP significantly decreased concentrations of serum IL-6 ($p < 0.01$), and all ANP administrated groups significantly increased concentrations of serum IL-10.

Effect of ANP on Th17/Treg Balance in the Spleen

According to results of thymus index and spleen index (**Figures 4A, B**), there was an upward trend in the ANP groups, and low-dose ANP significantly increased spleen index ($p < 0.05$). It suggests that ANP may affect the immune regulation of the spleen. In order to verify above results, splenocytes were used to analyze Th17/Treg balance in the spleen by flow cytometric analysis. In the model group, Th17/CD4^{+}T cells ratio, and Th17/Treg ratio were significantly increased, however, Treg/CD4^{+}T cells ratio was significantly decreased ($p < 0.05$ or 0.01). After ANP administration, when compared with model group, it was shown that medium-dose ANP significantly decreased Th17/CD4^{+}T cells ratio ($p < 0.01$), while low-dose and high-dose ANP significantly increased Treg/CD4^{+}T cells ratio ($p < 0.01$). It was also shown that all ANP administrated groups could decrease Th17/Treg ratio (**Figures 4C–G**).

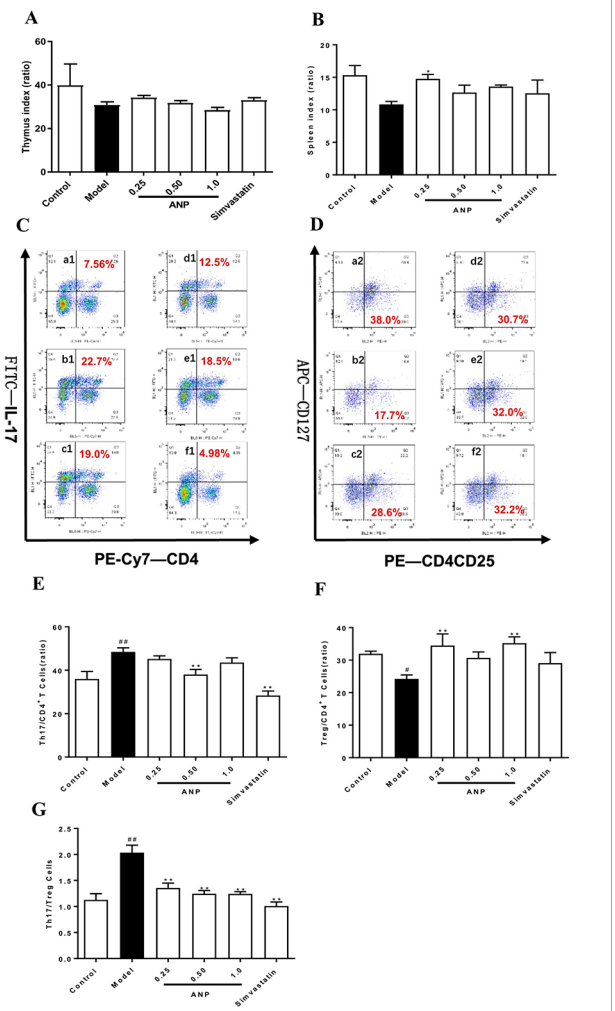

FIGURE 4 | Effect of ANP on Th17/Treg balance in the spleen. **(A)** Thymus index, **(B)** Spleen index, **(C)** Analysis of Th17 cells, **(D)** Analysis of Treg cells, **(E)** Th17/CD4+ T cells, **(F)** Treg/CD4+ T cells, **(G)** Th17/Treg cells. a1 and a2: Control group, b1 and b2: Model group, c1 and c2: Low-dose ANP group, d1 and d2: Medium-dose ANP group, e1 and e2: High-dose ANP group, f1 and f2: Simvastatin group. Compared with control group, $^{\#}p < 0.05$, $^{\#\#}p < 0.01$; Compared with model group, $^{**}p < 0.01$ (Mean ± SEM, n = 6). ANP, Angong Niuhuang Pill.

Effect of ANP on Expression of RORγt and Foxp3 in the Spleen

RORγt and Foxp3 are transcription factors for Th17 cells which regulate Th17/Treg balance. To evaluate effect of ANP on Th17/Treg balance, expression levels of RORγt, and Foxp3 were detected in the spleen. In the model group, mRNA and protein expression levels of RORγt was significantly up-regulated ($p < 0.05$ or 0.01), and Foxp3 was significantly down-regulated ($p < 0.05$ or 0.01). After ANP administration, when compared with model group, it was shown that low-dose and high-dose ANP significantly down-regulated protein expression of RORγt ($p < 0.05$). Moreover, low- and medium-dose ANP significantly up-

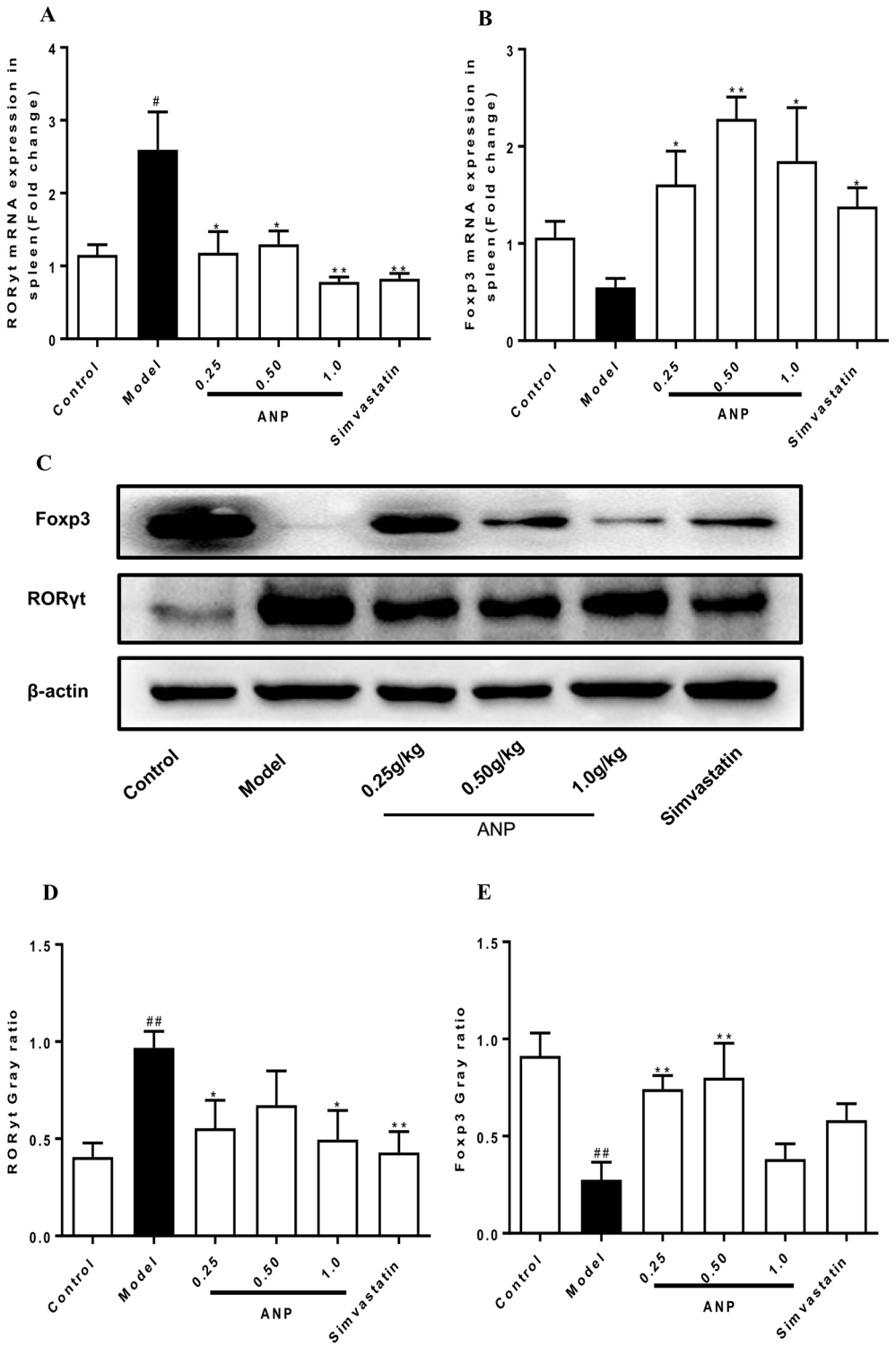

FIGURE 5 | Effect of ANP on expression of RORγt and Foxp3 in the spleen. **(A)** mRNA expression levels of RORγt, **(B)** mRNA expression levels of Foxp3, **(C)** Western blotting analysis of RORγt and Foxp3. The original blot image of Foxp3 was shown in **Supplementary Figure S4(a)**. **(D)** Semi-quantitative analysis of RORγt protein, **(E)** Semi-quantitative analysis of Foxp3 protein. Compared with control group, $^{\#}p < 0.05$, $^{\#\#}p < 0.01$; Compared with model group, $^{*}p < 0.05$, $^{**}p < 0.01$ (Mean ± SEM, RT-qPCR experiment n = 6; Western blotting experiment n = 3). ANP, Angong Niuhuang Pill.

regulated protein expression of Foxp3 ($p < 0.05$ or 0.01). Similarly, in all ANP groups mRNA expression levels of RORγt were down-regulated, while mRNA for Foxp3 was up-regulated ($p < 0.05$ or 0.01; **Figures 5A–E**).

Effect of ANP on Expression of Cytokines and Chemokines in the Aorta

Cytokines and chemokines play important roles in early and mid-term of AS and have a profound influence on the pathogenesis of AS. When compared to the control group, mRNA and protein expression levels of IL-1β, TNF-α, CCL2, CCR2 in the model group were significantly up-regulated ($p < 0.05$ or 0.01 or 0.001). In the medium-dose ANP mRNA and protein expression levels of IL-1β were significantly down-regulated ($p < 0.05$), while in low- and medium-dose ANP mRNA and protein expression levels of TNF-α, CCL2, and CCR2 were also significantly down-regulated ($p < 0.05$ or 0.01). At the mRNA level, the anti-inflammatory effect of the ANP was better than the positive drug simvastatin. It is worth noting that low- and medium-dose ANP had better anti-inflammatory effect, but there was no significantly difference in the high-dose ANP group. These results were shown in **Figures 6A–D** and **Figures 7A–E**.

Effect of ANP on Expression of MMP-2 and MMP-9 in the Aorta

MMPs are a group of proteases that degrade extracellular matrix, and they are mainly secreted by macrophages and VSMCs in atherosclerotic plaques. Overexpression of MMPs promotes the degradation of collagen and elastic fibers in plaque, destroying the stability of arterial plaque, which facilitate induction of cardiovascular risk events. As shown in **Figures 8 A–E**, both mRNA and protein expression levels of MMP-2 and MMP-9 in the model group were significantly up-regulated ($p < 0.01$ or 0.001). Administration of ANP significantly down-regulated mRNA and protein expression levels of MMP-2 and MMP-9 ($p < 0.05$ or 0.01).

Effect of ANP on Collagen Fibers in the Aortic Root

Masson staining was performed in the aortic root. The area of fibrosis which was stained blue covered a much larger area in the model group than in the control group ($p < 0.01$). Conversely, the area of collagen fiber in the medium-dose ANP were significantly lower than the model group ($p < 0.05$). These results were shown in **Figures 9A, B**.

Effect of ANP on Inflammatory Cells Infiltration in the Aortic Root

Immunofluorescence staining was performed in the aortic root. In the model group, the positive area of macrophages which were stained red was higher than in the control group ($p < 0.01$), and the positive area of VSMCs and dendritic cells, which was respectively stained green and red also was higher than that in the model group ($p < 0.001$). In low, or medium or high-dose ANP groups, the positive area of these inflammatory cells was significantly lower than in the model group ($p < 0.01$ or 0.001). These results were shown in **Figures 10A, B** and **Figures 11A–C**.

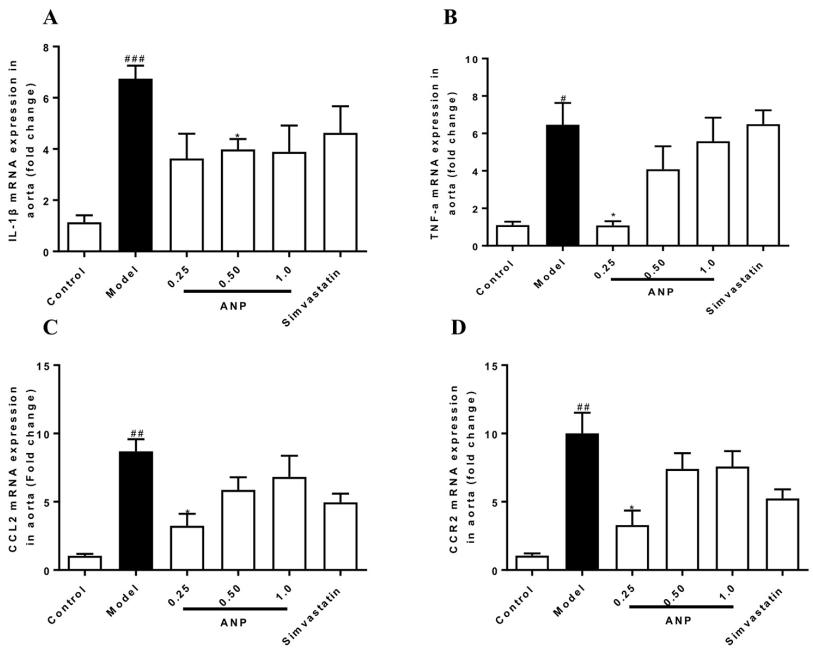

FIGURE 6 | Effect of ANP on mRNA expression levels of IL-1β, TNF-α, CCL2, and CCR2 in the aorta. **(A)** mRNA expression levels of IL-1β, **(B)** mRNA expression levels of TNF-α, **(C)** mRNA expression levels of CCL2, **(D)** mRNA expression levels of CCR2. Compared with control group, $^{\#}p < 0.05$, $^{\#\#}p < 0.01$, $^{\#\#\#}p < 0.001$; Compared with model group, $^{*}p < 0.05$. (Mean ± SEM, n = 6). ANP, Angong Niuhuang Pill.

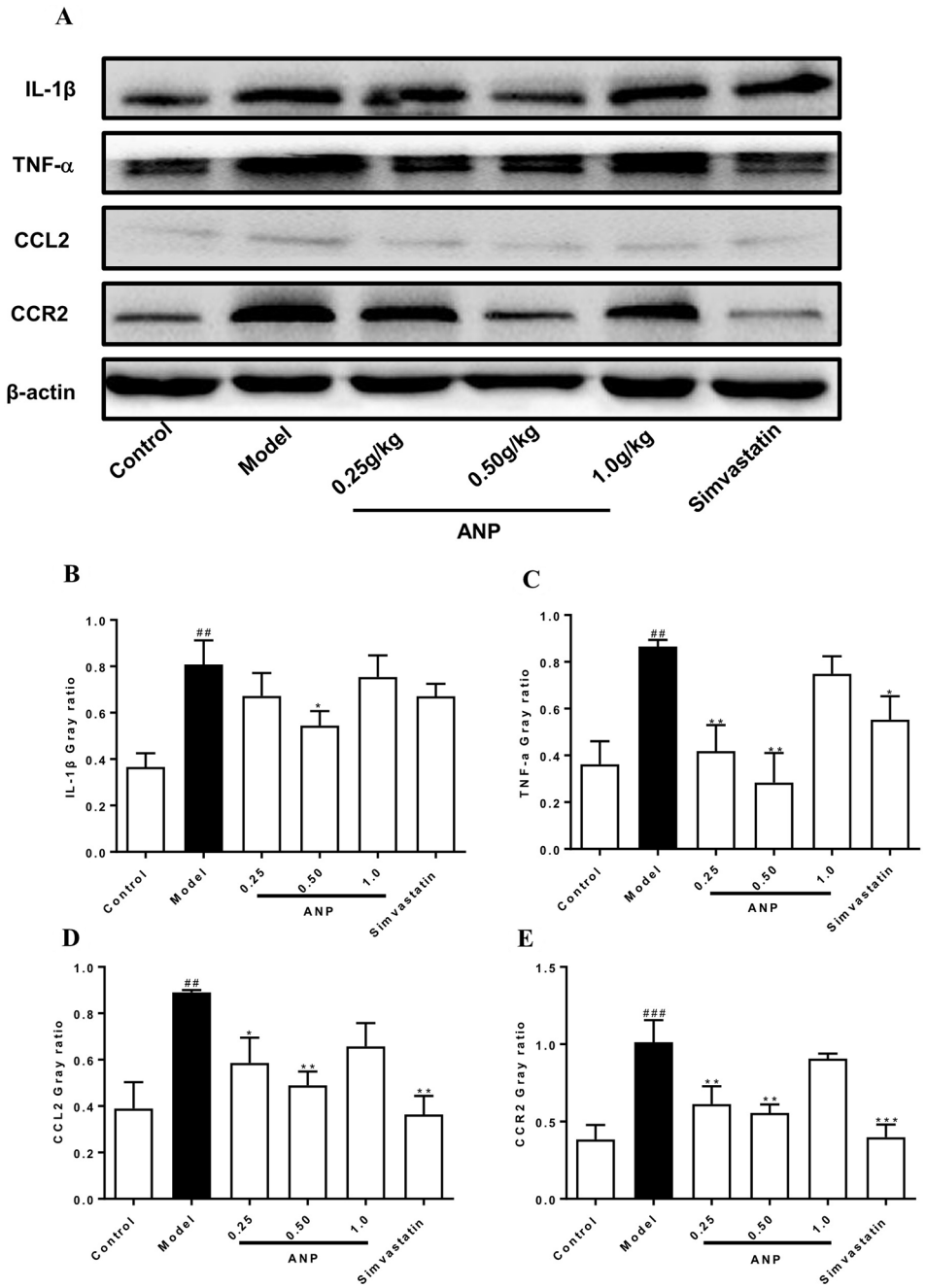

FIGURE 7 | Effect of ANP on protein expression of IL-1β, TNF-α, CCL2 and CCR2 in the aorta. **(A)** Western blotting analysis of IL-1β, TNF-α, CCL2, and CCR2. **(B)** Semi-quantitative analysis of IL-1β protein. The original blot images of IL-1β, TNF-α were shown in **Supplementary Figure S4(b)** and **Figure S4(c)**. **(C)** Semi-quantitative analysis of TNF-α protein, **(D)** Semi-quantitative analysis of CCL2 protein, **(E)** Semi-quantitative analysis of CCR2 protein. Compared with control group, $^{\#\#}p < 0.01$, $^{\#\#\#}p < 0.001$; Compared with model group, $^{*}p < 0.05$, $^{**}p < 0.01$, $^{***}p < 0.001$ (Mean ± SEM, n = 3). ANP, Angong Niuhuang Pill.

DISCUSSION

We found that treatment with ANP corrected the immune imbalance of Th17/Treg cells in the early AS ApoE$^{-/-}$ mice model by regulating RORγt and Foxp3 expression; ANP suppressed the release of pro-inflammatory mediators, promoted the release of anti-inflammatory factors, down-regulated the expression of chemokines and their receptors promoting thus an anti- inflammatory effects in the early AS. Furthermore, ANP down-regulated expression of MMP-2,

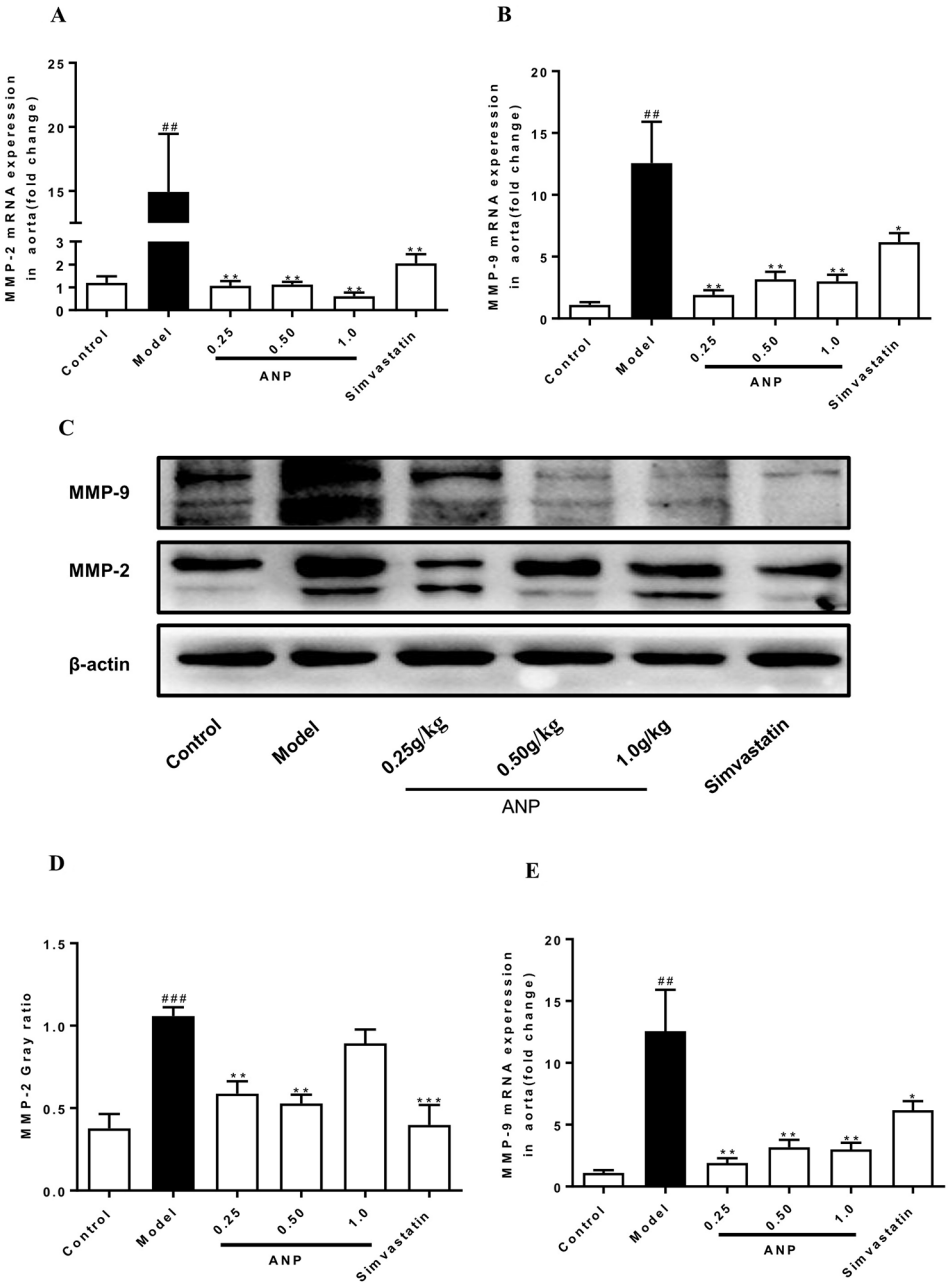

FIGURE 8 | Effect of ANP on mRNA and protein expression of MMP-2 and MMP-9 in the aorta. **(A)** mRNA expression levels of MMP-2, **(B)** mRNA expression levels of MMP-9, **(C)** Western blotting analysis of MMP-2 and MMP-9, **(D)** Semi-quantitative analysis of MMP-2 protein, **(E)** Semi-quantitative analysis of MMP-9 protein. Compared with control group, $^{\#\#}p < 0.01$, $^{\#\#\#}p < 0.001$; Compared with model group, $^{*}p < 0.05$, $^{**}p < 0.01$, $^{***}p < 0.001$ (Mean ± SEM, RT-qPCR experiment n = 6; Western blotting experiment n = 3). ANP, Angong Niuhuang Pill.

MMP-9, reduce collagen fibers and decreased infiltration of macrophages, dendritic cells, and vascular smooth muscle cells into plaques thus facilitating stability of the latter.

In this study, ANP was a kind of tawny powder, and distilled water was used as the solution medium. Due to the relatively complex composition of ANP, ANP was tawny suspension after dissolution. In order to maintain the stability of drug suspension, the ANP suspension was prepared before administration. In our next study, we will focus on the metabolic components of ANP in mice and the pharmacodynamic substance basis of ANP, and analyze the prescription.

It has been argued that increase in combined ratios (LDL-C/HDL-C) relates to the severity and prevalence of coronary artery disease (Enomoto et al., 2011; Acay et al., 2014). We demonstrated

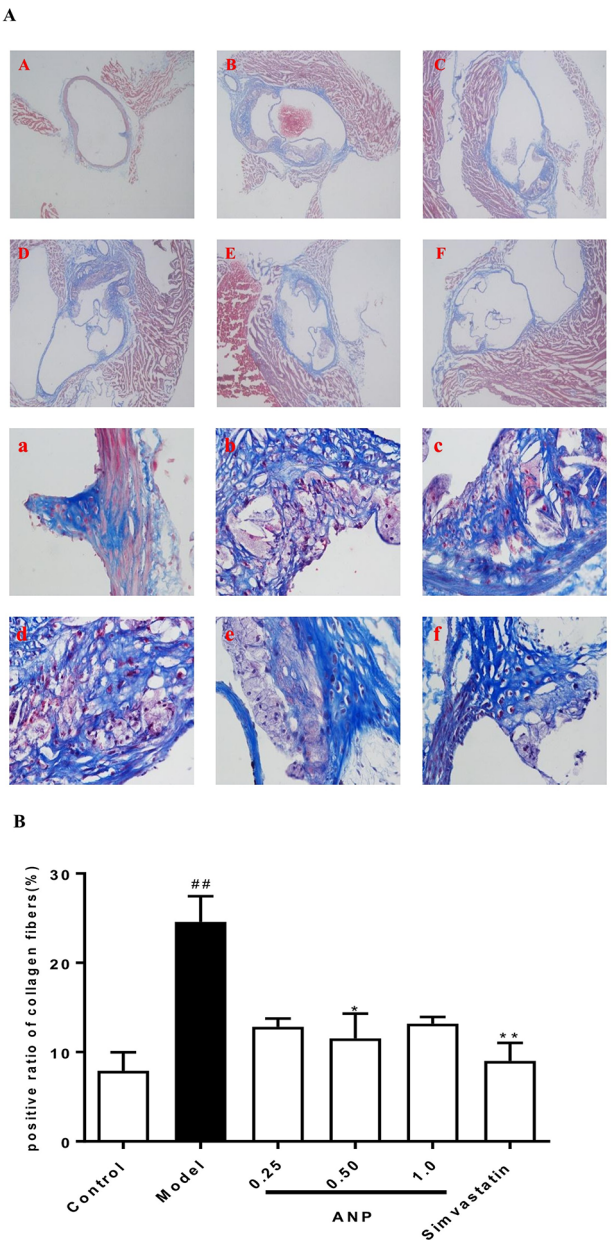

FIGURE 9 | Effect of ANP on collagen fibers in the aortic root. **(A)** Masson staining was performed in the aortic root, A and a: Control group, B and b: Model group, C and c: Low-dose ANP group, D and d: Medium-dose ANP group, E and e: High-dose ANP group, F and f: Simvastatin group. Picture A B C D E F ×40, Picture a b c d e f ×400. **(B)** Semi-quantitative analysis of collagen fibers. Compared with control group, $^{\#\#}p < 0.01$; compared with model group, $^{*}p < 0.05$, $^{**}p < 0.01$ (Mean ± SEM, n = 6). ANP, Angong Niuhuang Pill.

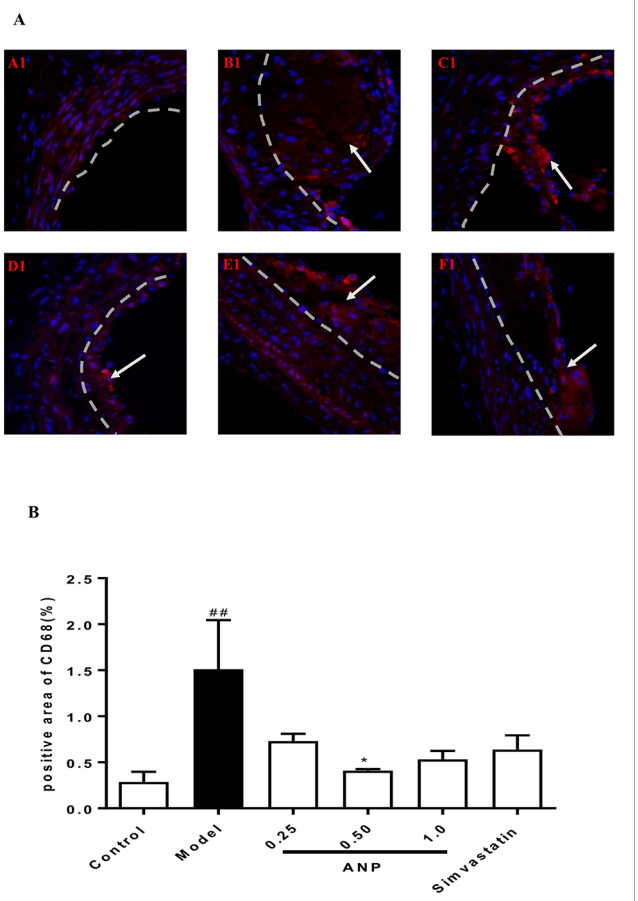

FIGURE 10 | Effect of ANP on macrophages infiltration in the aortic root. **(A)** Immunofluorescence staining of macrophages, white arrow represents the positive area of macrophages. A1: Control group, B1: Model group, C1: Low-dose ANP group, D1: Medium-dose ANP group, E1: High-dose ANP group, F1: Simvastatin (Picture A1 B1 C1 D1 E1 F1×400). **(B)** Semi-quantitative analysis of macrophages, positive area of CD68 for macrophages. Compared with control group, $^{\#\#}p < 0.01$; compared with model group, $^{*}p < 0.05$ (Mean ± SEM, n = 3). ANP, Angong Niuhuang Pill.

that LDL-C/HDL-C ratio in the high-dose ANP group (1.0 g/kg) was significantly lower than those in the model group. However, low-dose and medium-dose ANP groups did not show a decrease in LDL-C/HDL-C ratio, which indicates that only a high-dose ANP has a weak lipid-lowering effect.

The high-fat diet is a potential risk factor for the liver and kidney. Treatment with ANP significantly reduced the liver coefficient but did not improve the kidney coefficient; thus pointing on a certain hepatoprotective effect of ANP. This agreed with previous findings showing that ANP has a preventive and therapeutic effect on liver damage caused by bacterial toxins (He et al., 1992). The apparent changes of spleen index and thymus index suggest that ANP may have a regulatory effect on the immune system. The Th17/Treg is a pair of new balance which differs from Th1/Th2 balance in the immune system and plays an important role in the development of AS and plague rupture (Cheng et al., 2008; Xie et al., 2010). Many studies have confirmed that regulating Th17/Treg balance is a critical intervention target during development process of AS (Xie et al., 2010; Konstantinos et al., 2014; Tian et al., 2017; Wang et al., 2017). Treatment

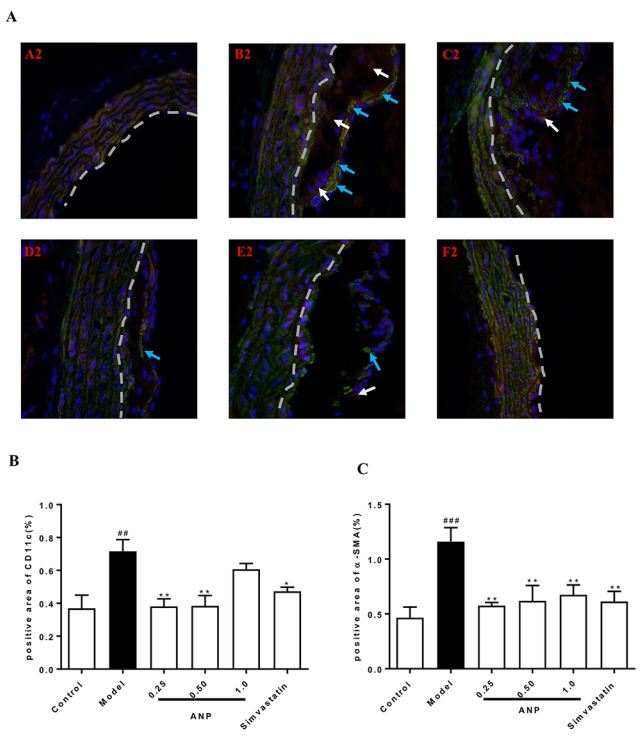

FIGURE 11 | Effect of ANP on VSMCs and dendritic cells infiltration in the aortic root. **(A)** Immunofluorescence staining of VSMCs and dendritic cells, white arrow represents the positive area of dendritic cells, and blue arrow represents the positive area of VSMCs. A2: Control group, B2: Model group, C2: Low-dose ANP group, D2: Medium-dose ANP group, E2: High-dose ANP group, F2: Simvastatin (Picture A2 B2 C2 D2 E2 F2×400), **(B)** Semi-quantitative analysis of dendritic cells, positive area of CD11c for dendritic cells, **(C)** Semi-quantitative analysis of VSMCs, positive area of α-SMA for VSMCs. Compared with control group, $^{\#\#}p < 0.01$, $^{\#\#\#}p < 0.001$; compared with model group, $^{*}p < 0.05$, $^{**}p < 0.01$ (Mean±SEM, n = 3). ANP, Angong Niuhuang Pill.

with ANP corrected the Th17/Treg cellular balance, with high doses of ANP having more pronounced immunomodulatory effect. The Th17/Treg balance is regulated by RORγt and Foxp3 respective transcription factors (Xie et al., 2010). We found that ANP significantly down-regulated expression of RORγt, while significantly up-regulating expression of Foxp3; indicating the underlying mechanisms.

Chronic inflammation is the key factor in AS pathogenesis, while inhibiting inflammatory response controls AS evolution (Tousoulis et al., 2016; Chistiakov et al., 2018). Inflammatory cells involved in the AS process can express different inflammatory factors, such as IL-1β, TNF-α, and IL-6, which are mainly secreted by macrophages, lymphocytes, and VSMCs (Tedgui and Mallat, 2006). Expression of IL-1β and TNF-α is regulated by the p38 MAPK/NF-κB pathway (Chan et al., 2000). Increased expression of IL-1β and TNF-α promotes overexpression of downstream ICAM-1 and VCAM-1, to further promote migration and adhesion of VSMCs and endothelial cells (Mackesy and Goalstone, 2014). Expression of IL-6 is regulated by IL-6 receptor and signal transducing protein gp130 (Ait-Oufella et al., 2011); IL-6 being a pro-atherogenic cytokine exacerbates the progression of atherosclerosis in ApoE$^{-/-}$ mice. Clinical studies revealed that high levels of serum IL-6 represent a risk factor for coronary artery disease (Biasucci, 1999). The anti-atherogenic cytokine IL-10 is secreted by Treg cells; IL-10 not only down-regulates expression of TNF-α, but also reduces expression of ICAM-1 in endothelial cells (Lisinski and Furie, 2002; Rajasingh et al., 2006). Treatment with ANP significantly reduced serum IL-6 and increased serum IL-10, although the dose-dependence was not obvious. Expression of TNF-α was significantly down-regulated in low-dose and medium-dose ANP groups, and expression of IL-1β was significantly down-regulated in low-dose ANP group. Thus ANP (especially at low and medium doses) exhibits anti-inflammatory capabilities.

Atherosclerotic plaque, the morphological substrate of AS, is induced by multiple factors, including accumulation of VSMCs, macrophages and T lymphocytes (Andrés et al., 2012; Moore et al., 2013); the proliferation of VSMCs and connective tissue matrix such as collagen fibers and elastic fibers; deposition of cholesterol crystals and free cholesterol. All these factors contribute to formation of fragile arterial plaques (Watson et al., 2018). Maintaining stability of plaques and arresting expansion of vulnerable plaques are in the focus of current treatment for AS which has already formed. It was reported that CCL2, CCR2, MMP-2, and MMP-9 are involved in impairing stability of arterial plaques, reduction in expression of plaques stability (Ishibashi et al., 2004; Krohn et al., 2007; Zhao, 2010; Cipriani et al., 2013). We found that ANP significantly down-regulated expression of CCL2, CCR2, MMP-2, and MMP-9. Masson staining showed that medium-dose ANP decreased plaques area in the aortic root when compared to the model group, similarly reduced was the content of collagen fibers. Treatment with ANP also reduced infiltration of macrophages, vascular smooth muscle cells and dendritic cells into the aortic root as evidenced by immunocytochemical analysis. These results indicate that ANP may improve the stability of arterial plaques and prevent their expansion, suppressing infiltration of inflammatory cells, and decreasing expression of CCL2, CCR2, MMP-2, and MMP-9. All these findings suggest that, ANP may exert an anti-atherosclerotic effect at the early and mid-term of AS.

CONCLUSION

In conclusion, ANP protects early and mid-term atherosclerotic ApoE$^{-/-}$ mice by regulating Th17/Treg balance, inhibiting chronic inflammation, reducing plaque collagen fibers, and reducing inflammatory cells infiltration. Moreover, ANP has anti-inflammatory effects in small doses, and ANP has immunoregulation effects on high doses. Possible mechanisms are shown in **Figure 12**.

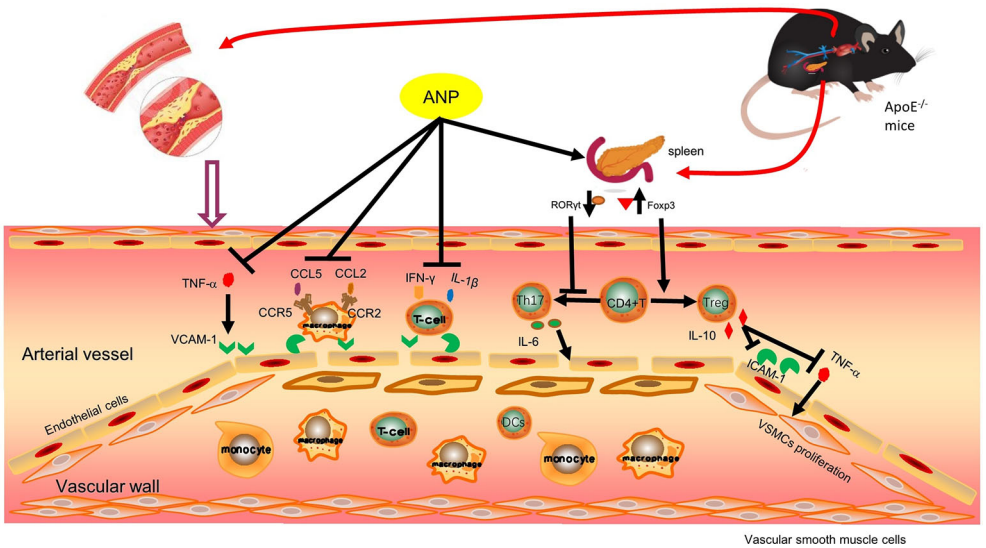

FIGURE 12 | Possible mechanism pathway of ANP. Previous research findings found that ANP could down-regulated mRNA expression levels of IFN-γ, CCL5 and CCR5, these results were shown in **Supplementary Material** (**Figure S2**). ANP, Angong Niuhuang Pill.

DATA AVAILABILITY STATEMENT

All datasets generated for this study are included in the article/ **Supplementary Material**.

ETHICS STATEMENT

The experiments were approved by the Laboratory Animal Ethics Committee of Jinan University (No. 201812374), and were performed according to the instructions of the National Institute of Health (OLAW/NIH Revised 2015).

AUTHOR CONTRIBUTIONS

HN supported and designed the experiments, and revised the manuscript. QF performed the experiments. YL, JR, ZZ, KY, WX, TZ, XC, NN, ZY, YC, and YX provided reagents/ materials. YL and JR analyzed the data. RL participated in checking data statistics and manuscript revision linguistically. AV gave guidance during the experimental design process, and revised the manuscript. QF and YL wrote the manuscript.

FUNDING

This work was supported by the National Natural Science Foundation of China (No. 81673634) and Guangzhou Baiyunshan Zhongyi Pharmaceutical Co., Ltd (No. 40116103).

SUPPLEMENTARY MATERIAL

The Supplementary Material for this article can be found online at: https://www.frontiersin.org/articles/10.3389/fphar.2019.01584/full#supplementary-material

REFERENCES

Acay, A., Ulu, M. S., Ahsen, A., Ozkececi, G., Demir, K., Ozuguz, U., et al. (2014). Atherogenic index as a predictor of atherosclerosis in subjects with familial Mediterranean fever. *Med. (Kaunas)* 50 (6), 329–333. doi: 10.1016/j.medici.2014.11.009

Ait-Oufella, H., Taleb, S., Mallat, Z., and Tedgui, A. (2011). Recent advances on the role of cytokines in atherosclerosis. *Arterioscler. Thromb. Vasc. Biol.* 31, 969–979. doi: 10.1161/atvbaha.110.207415

Andrés, V., Pello, O. M., and Silvestre-Roig, C. (2012). Macrophage proliferation and apoptosis in atherosclerosis. *Curr. Opin. Lipidol.* 23 (5), 429–438. doi: 10.1097/MOL.0b013e328357a379

Bettelli, E., Oukka, M., and Kuchroo, V. K. (2007). TH-17 cells in the circle of immunity and autoimmunity. *Nat. Immunol.* 8, 345. doi: 10.1038/ni0407-345

Biasucci, L. M. (1999). Increasing levels of interleukin (IL)-1Ra and IL-6 during the first 2 days of hospitalization in unstable angina are associated with increased risk of in-hospital coronary events. *Circ. (New York N.Y.)* 99 (16), 2079–2084. doi: 10.1161/circ.99.16.2079

Chai, Y. S., Yin, Z., Fan, Q. H., Zhang, Z., Ye, K. H., Xu, Y. M., et al. (2019). Protective effects of Angong Niuhuang Pill on early atherosclerosis in ApoE (-/-) mice by reducing the inflammatory response. *Evid.-Based Complement. Altern. Med.* 1–13. doi: 10.1155/2019/9747212

Chan, K., Siegel, M., and Lenardo, J. (2000). Signaling by the TNF receptor superfamily and T cell homeostasis. *Immunity* 13, 419–422. doi: 10.1016/S1074-7613(00)00041-8

Chen, W. W., Gao, R. L., Liu, L. S., Zhu, M.,. L., Wang, W., Wang, Y. J., et al. (2018). China cardiovascular disease report 2017 summary. *Chin. Circ. J.* 33 (1), 1–8. doi: 10.3969/j.issn.1000-3614.2018.01.001

Cheng, X., Yu, X., Ding, Y. J., Fu, Q. Q., Xie, J. J., Tang, T. T., et al. (2008). The Th17/Treg imbalance in patients with acute coronary syndrome. *Clin. Immunol.* 127 (1), 89–97. doi: 10.1016/j.clim.2008.01.009

Chistiakov, D. A., Melnichenko, A. A., Grechko, A. V., Myasoedova, V. A., and Orekhov, A. N. (2018). Potential of anti-inflammatory agents for treatment of atherosclerosis. *Exp. Mol. Pathol.* 104, 114–124. doi: 10.1016/j.yexmp.2018.01.008

Cipriani, S., Francisci, D., Mencarelli, A., Renga, B., Schiaroli, E., D'Amore, C., et al. (2013). Efficacy of the CCR5 antagonist maraviroc in reducing early, ritonavir-induced atherogenesis and advanced plaque progression in mice. *Circulation* 127 (21), 2114–2124. doi: 10.1161/CIRCULATIONAHA.113.001278

Editorial Committee of Pharmacopoeia of Ministry of Health PR China. (2015). *The Pharmacopoeia of Peoples Republic of China 2015* (Beijing: Chinese Medicial Science and Technology Press).

Enomoto, M., Adachi, H., Hirai, Y., Fukami, A., Satoh, A., Otsuka, M., et al. (2011). LDL-C/HDL-C ratio predicts carotid intima-media thickness progression better than HDL-C or LDL-C alone. *J. Lipids* 2011, 549137. doi: 10.1155/2011/549137

Feigin, V. L., Krishnamurthi, R. V., Parmar, P., Norrving, B., Mensah, G. A., Bennett, D. A., et al. (2015). Update on the global burden of ischemic and hemorrhagic stroke in 1990-2013: the GBD 2013 study. *Neuroepidemiology* 45 (3), 161–176. doi: 10.1159/000441085

Frostegard, J., Ulfgren, A. K., Nyberg, P., Hedin, U., Swedenborg, J., Anderson, U., et al. (1999). Cytokine expression in advanced human atherosclerotic plaques: dominance of pro-inflammatory (Th1) and macrophage-stimulating cytokines. *Atherosclerosis* 145, 33–43. doi: 10.1016/s0021-9150(99)00011-8

Fu, W. J., Lei, T., Yin, Z., Pan, J. H., Chai, Y. S., Xu, X. Y., et al. (2017). Anti-atherosclerosis and cardio-protective effects of the Angong Niuhuang Pill on a high fat and vitamin D3 induced rodent model of atherosclerosis. *J. Ethnopharmacol.* 195, 118–126. doi: 10.1016/j.jep.2016.11.015

Gupta, S., Pablo, A. M., Jiang, X.c., Wang, N., Tall, A. R., and Schindler, C. (1997). IFN-γ potentiates atherosclerosis in ApoE knock-out mice. *J. Clin. Invest.* 99, 2752–2761. doi: 10.1172/JCI119465

He, Y. H., Huang, Y. Y., Zheng, Q. N., Zhang, Y. Q., and Yuan, Z. R. (1992). Effect of Angong Niuhuang Pill on liver of experimental brain edema animals. *Jiangsu J. Trad. Chin. Med.* 12, 38–40.

Ishibashi, M., Egashira, K., Zhao, Q., Hiasa, K., Ohtani, K., Ihara, Y., et al. (2004). Bone marrow-derived monocyte chemoattractant protein-1 receptor CCR2 is critical in angiotensin II-induced acceleration of atherosclerosis and aneurysm formation in hypercholesterolemic mice. *Arterioscler. Thromb. Vasc. Biol.* 24 (11), e174–e178. doi: 10.1161/01.ATV.0000143384.69170.2d

Konstantinos, T., Alexandros, S., Ioannis, G., and Panagiota, B. (2014). T regulatory cells: a promising new target in atherosclerosis. *Crit. Rev. Immunol.* 34 (5), 389–397. doi: 10.1615/CritRevImmunol.2014010802

Krohn, R., Raffetseder, U., Bot, I., Zernecke, A., Shagdarsuren, E., Liehn, E. A., et al. (2007). Y-box binding protein-1 controls CC chemokine ligand-5 (CCL5) expression in smooth muscle cells and contributes to neointima formation in atherosclerosis-prone mice. *Circulation* 116 (16), 1812–1820. doi: 10.1161/CIRCULATIONAHA.107.708016

Lisinski, T. J., and Furie, M. B. (2002). Interleukin-10 inhibits proinflammatory activation of endothelium in response to Borrelia burgdorferi or lipopolysaccharide but not interleukin-1β or tumor necrosis factor. *J. Leukocyte Biol.* 72 (3), 503–511. doi: 10.1189/jlb.72.3.503

Mackesy, D., and Goalstone, M. (2014). ERK5: novel mediator of insulin and TNF-stimulated VCAM-1 expression in vascular cells. *J. Diabetes* 6, 595–602. doi: 10.1111/1753-0407.12132

Meir, K. S., and Leitersdorf, E. (2004). Atherosclerosis in the apolipoprotein-E-deficient mouse: a decade of progress. *Arterioscler. Thromb. Vasc. Biol.* 24 (6), 1006–1014. doi: 10.1161/01.ATV.0000128849.12617.f4

Moore, K. J., Sheedy, F. J., and Fisher, E. A. (2013). Macrophages in atherosclerosis: a dynamic balance. *Nat. Rev. Immunol.* 13, 709. doi: 10.1038/nri3520

Nakashima, Y., Plump, A. S., Raines, E. W., Breslow, J. L., and Ross, R. (1994). ApoE-deficient mice develop lesions of all phases of atherosclerosis throughout the arterial tree. *Arterioscler. Thromb.* 14 (1), 133–140. doi: 10.1161/01.atv.14.1.133

Office of Laboratory Animal Welfare/National Institutes of Health. (2015). *Public Health Service policy on human care and use of laboratory animals* (Bethesda, Maryland: National Institutes of Health). Available from: https://olaw.nih.gov/policies-laws/phs-policy.htm.

Rajasingh, J., Bord, E., Luedemann, C., Asai, J., Hamada, H., Thorne, T., et al. (2006). IL-10-induced TNF-alpha mRNA destabilization is mediated *via* IL-10 suppression of p38 MAP kinase activation and inhibition of HuR expression. *FASEB J.* 20 (12), 2112–2114. doi: 10.1096/fj.06-6084fje

Ramji, D. P., and Davies, T. S. (2015). Cytokines in atherosclerosis: key players in all stages of disease and promising therapeutic targets. *Cytokine Growth Factor Rev.* 26 (6), 673–685. doi: 10.1016/j.cytogfr.2015.04.003

Ross, R. (1999). Atherosclerosis — an inflammatory disease. *New Engl. J. Med.* 340 (2), 115–126. doi: 10.1056/nejm199901143400207

Shimon, S., Masahiro, O., Ruka, S., Haruhiko, Y., Shohei, H., Zoltan, F., et al. (2006). $Foxp3^{+}CD25^{+}CD4^{+}$ natural regulatory T cells in dominant self-tolerance and autoimmune disease. *Immunol. Rev.* 212, 8–27. doi: 10.1111/j.0105-2896.2006.00427.x

Tedgui, A., and Mallat, Z. (2006). Cytokines in atherosclerosis: pathogenic and regulatory pathways. *Physiol. Rev.* 86, 515–581. doi: 10.1152/physrev.00024.2005

Tian, Y. A.-O., Chen, T., Wu, Y., Yang, L., Wang, L., Fan, X., et al. (2017). Pioglitazone stabilizes atherosclerotic plaque by regulating the Th17/Treg balance in AMPK-dependent mechanisms. *Cardiovasc. Diabetol* 16 (140), 1–9. doi: 10.1186/s12933-017-0623-6

Tousoulis, D., Oikonomou, E., Economou, E. K., Crea, F., and Kaski, J. C. (2016). Inflammatory cytokines in atherosclerosis: current therapeutic approaches. *Eur. Heart J.* 37 (22), 1723–1732. doi: 10.1093/eurheartj/ehv759

Wang, B., Wang, X. P., Sun, H. F., Hu, L. L., and Gao, J. B. (2017). The effects of T helper 17 and regulatory T cells on patients with carotid atherosclerosis. *Pak. J. Pharm. Sci.* 30, 1923–1928.

Watson, M. G., Byrne, H. M., Macaskill, C., and Myerscough, M. R. (2018). A two-phase model of early fibrous cap formation in atherosclerosis. *J. Theor. Biol.* 456, 123–136. doi: 10.1016/j.jtbi.2018.08.010

Weber, C., and Noels, H. (2011). Atherosclerosis: current pathogenesis and therapeutic options. *Nat. Med.* 17 (11), 1410–1422. doi: 10.1038/nm.2538

Wu, M. Y., Li, C. J., Hou, M. F., and Chu, P. Y. (2017). New insights into the role of inflammation in the pathogenesis of atherosclerosis. *Int. J. Mol. Sci.* 18 (10), 1–18. doi: 10.3390/ijms18102034

Xie, J. J., Wang, J., Tang, T. T., Chen, J., Gao, X. L., Yuan, J., et al. (2010). The Th17/Treg functional imbalance during atherogenesis in ApoE(-/-) mice. *Cytokine* 49 (2), 185–193. doi: 10.1016/j.cyto.2009.09.007

Zhao, Q. (2010). Dual targeting of CCR2 and CCR5: therapeutic potential for immunologic and cardiovascular diseases. *J. Leukoc. Biol.* 88 (1), 41–55. doi: 10.1189/jlb.1009671

Conflict of Interest: Authors NN, ZY, YC and YX are employed by company Guangzhou Baiyunshan Zhongyi Pharmaceutical Co., Ltd. Author RL is a student of International Department, the Affiliated High School of SCNU. Author AV is a professor in the Faculty of Biology, Medicine and Health, The University of Manchester.

The authors declare that this study received funding from Guangzhou Baiyunshan Zhongyi Pharmaceutical Co., Ltd. The funders had no role in study design, data collection and analysis, decision to publish and preparation of the manuscript.

The remaining authors declare that the research was conducted in the absence of any commercial or financial relationships that could be construed as a potential conflict of interest.

frontiers in Pharmacology

ORIGINAL RESEARCH
published: 25 February 2020
doi: 10.3389/fphar.2020.00103

Ferulic Acid Attenuates Hypoxia/Reoxygenation Injury by Suppressing Mitophagy Through the PINK1/Parkin Signaling Pathway in H9c2 Cells

Chenxi Luo[1,2†], *Yehao Zhang*[2†], *Hao Guo*[2], *Xiao Han*[2], *Junguo Ren*[2] *and Jianxun Liu*[2*]

[1] Graduate School, Beijing University of Chinese Medicine, Beijing, China, [2] Beijing Key Laboratory of Pharmacology of Chinese Materia Region, Institute of Basic Medical Sciences, Xiyuan Hospital, China Academy of Chinese Medical Sciences, Beijing, China

OPEN ACCESS

Edited by:
Muriel Cuendet,
Université de Genève,
Switzerland

Reviewed by:
Sarra Djemil,
Georgetown University,
United States
Guibo Sun,
Chinese Academy of Medical Sciences and Peking Union Medical College, China

***Correspondence:**
Jianxun Liu
liujx0324@sina.com

[†]These authors have contributed equally to this work and share first authorship

Specialty section:
This article was submitted to Ethnopharmacology, a section of the journal Frontiers in Pharmacology

Received: 31 May 2019
Accepted: 28 January 2020
Published: 25 February 2020

Citation:
Luo C, Zhang Y, Guo H, Han X, Ren J and Liu J (2020) Ferulic Acid Attenuates Hypoxia/Reoxygenation Injury by Suppressing Mitophagy Through the PINK1/Parkin Signaling Pathway in H9c2 Cells. Front. Pharmacol. 11:103. doi: 10.3389/fphar.2020.00103

Ferulic acid protects against cardiac injury by scavenging free radicals. However, the role of mitophagy in ferulic acid-induced cardioprotection remains obscure. In the present study, H9c2 cells were exposed to hypoxia/reoxygenation and ferulic acid treatment during hypoxia. We illustrated the impact of ferulic acid on oxidative damage in H9c2 cells. Our results showed that ferulic acid significantly attenuated apoptosis induced by hypoxia/reoxygenation injury and reduced mitochondrial dysfunction, evidenced by a decline in the overproduction of reactive oxygen species and ATP depletion and recovery of the membrane potential. We also found that mitophagy, a selective form of autophagy, was excessively activated in H9c2 cells subjected to hypoxia/reoxygenation. Ferulic acid reduced the binding of mitochondria to lysosomes, down-regulated the PINK1/Parkin pathway, and was accompanied by increased p62 and decreased LC3-II/LC3-I levels. Ferulic acid also antagonistically reduced the activation of mitophagy by rapamycin. These findings suggest that ferulic acid may protect H9c2 cells against ischemia/reperfusion injury by suppressing PINK1/Parkin-dependent mitophagy. Accordingly, our findings may provide a potential target and powerful reference for ferulic acid in clinical prevention and treatment of hypoxia/reoxygenation injury.

Keywords: ferulic acid, hypoxia/reoxygenation, mitochondrial dysfunction, mitophagy, PINK1/Parkin

INTRODUCTION

Myocardial ischemia/reperfusion (I/R) injury is a complex process that causes damage to proteins, DNA, and plasma membranes, thereby promoting cell death and diminished cardiac output (Hausenloy and Yellon, 2013; Go et al., 2014). Mitochondrial dysfunction is a basic pathophysiological factor of I/R injury (Walters et al., 2012). Damaged mitochondria produce less ATP, generate greater amounts of reactive oxygen species (ROS), and activate mitochondria-

Abbreviations: FBS, fetal bovine serum; CCK8, cell counting kit-8; HSP60, Heat Shock Protein 60; SDS-PAGE, Sodium dodecyl sulfate-Polyacrylamide gel electrophoresis; TBST, Tris Buffered saline Tween; SQSTM1, Sequestosome 1; LC3B, Light Chain 3B.

dependent apoptosis (Ong and Gustafsson, 2012; Chen and Zweier, 2014). Cardiomyocytes, which depend heavily on energy generation by mitochondria, are more sensitive to mitochondrial dysfunction (Kasahara and Scorrano, 2014). Thus, preserving healthy mitochondria is imperative to cell survival in cardiomyocytes.

Autophagy is activated by energy consumption, oxidative stress, total protein, and damaged organelles (Tannous et al., 2008; Kim et al., 2013). It is a developmentally preserved process through which cytoplasmic components and organelles are digested and reused in lysosomes (Kroemer et al., 2010). Despite numerous evaluations illustrating the benefits of autophagy, excessive autophagy can induce cell death in myocardial I/R injury (Hamacher-Brady et al., 2006; Matsui et al., 2007). Mitochondrial autophagy (referred to as mitophagy), a selective form of autophagy, degrades dysfunctional mitochondria and regulates the mitochondrial population (Ashrafi and Schwarz, 2013; Hammerling and Gustafsson, 2014). Hypoxemia, starvation, and ROS can trigger mitophagy, which is associated with several forms of neurodegeneration and cardiovascular diseases (Youle and Narendra, 2011; Dorn and Kitsis, 2015). Recent studies suggest that PINK1 (phosphatase and tensin homolog-induced putative kinase 1) and the Parkin pathway play central roles in regulating mitophagy and mitochondrial quality control (Springer and Kahle, 2011). Furthermore, PINK1/Parkin-mediated mitophagy reportedly prevents cellular damage (Huang et al., 2011). Accordingly, mitophagy may have restorative potential for mitochondria-associated conditions such as I/R injury.

Ferulic acid (4-hydroxy-3-methoxy cinnamic acid, FA) is a kind of phenolic acid widely distributed in various plants (Pan et al., 2016). It is also an active ingredient of traditional Chinese medicines such as *Angelica sinensis* (Oliv.) Diels, *Ligusticum chuanxiong* Hort. and *Cimicifuga foetida* L. It has various biological activities, such as the scavenging of free radicals, anti-oxidation, anti-platelet aggregation, neuroprotection, and enhancement of immune function (Barone et al., 2009; Mancuso and Santangelo, 2014). Current research about the antioxidant mechanisms of FA have been focused on the scavenging of free radicals and inhibition of myocardial apoptosis (Alam et al., 2013). The potential role of FA in mitophagy has not yet been reported.

Therefore, we investigated the defensive impact of FA in cardiomyocytes against hypoxia/reoxygenation (H/R)-induced mitophagy, with a focus on the PINK1/Parkin pathway.

MATERIAL AND METHODS

Cell Culture and Treatment

Hypoxia/reoxygenation experiments were performed based on a previous method (Tang et al., 2013; Zhang et al., 2018). The H9c2 cells were cultured in Dulbecco′s Modified Eagle′s medium (DMEM) (Hyclone, China) supplemented with 10% (v/v) fetal bovine serum (FBS; Gibco, USA) and 1% penicillin/streptomycin (Sigma, St. Louis, MO) at 37°C in a culture box, with an atmosphere of 95% air and 5% CO_2. Then, the cells were placed in a pre-mixed gas (94% N_2, 5% CO_2, 1% O_2) culture box and cultured in deoxygenated DMEM without glucose and FBS for 2 hours. After 2 h, normal DMEM with 10% FBS serum was given, and cells were transferred to an atmosphere incubator for 2 h. The control group cells were cultured with normal DMEM. During hypoxia stimulation, cells were treated for 2 h with ferulic acid (FA, Beijing Laiyao Biotechnology Co., Ltd, China), with or without rapamycin (autophagy activator, Rapa, 100 nM, Beijing Laiyao Biotechnology Co., Ltd, China) (Hausenloy and Yellon, 2013; Sun et al., 2018).

Cell Viability Assay

After the hypoxia/reoxygenation stimulation, H9c2 cells were treated with the CCK-8 assay (10 μL/well, Dojindo, Kumamoto, Japan) for an additional 2 h. The absorbance was recorded at 450 nm using a microplate absorbance reader (BioTek, USA).

TUNEL Staining

After the indicated treatments, cells were fixed with 4% paraformaldehyde solution for 25 min at room temperature, and then washed with phosphate-buffered saline (PBS, Gibco, USA). The cells were then permeabilized with 0.2% Triton X-100 for 5 min. After washing with PBS, apoptosis was detected using a terminal deoxynucleotidyl transferase-mediated-dUTP nick end-labeling (TUNEL) kit (Roche, Indianapolis, IN, USA) according to the supplier′s instructions. DAPI counterstaining was performed to stain the nuclei. Cells were observed and photographed using a fluorescence microscope (Olympus, Tokyo, Japan). Quantitative analysis was presented as average counts of TUNEL-positive cells per field counted in five random fields with 350-400 total cells in each field and three independent experiments for each group.

ADP/ATP Ratio Measurements

The ATP/ADP level in cells was measured using a bioluminescent detection kit (ADP/ATP Ratio Assay Kit, Abcam) according to the manufacturer′s instructions. After the indicated treatments, the bioluminescent intensities were measured on a multi-mode microplate reader (Synergy H1 Hybrid, BioTek).

Mitochondrial Membrane Potentials Assay

The mitochondrial membrane potential was assessed using 5,5′,6,6′ -tetrachloro-1,1′,3,3′ -tetraethyl-benzimidazolecarbocyanide iodine (JC-1, Sigma, St. Louis, MO, USA). The H9c2 cells were incubated with JC-1 staining solution (10 μg/mL) for 20 min at 37°C in the dark and rinsed twice with PBS. The JC-1 fluorescence was measured by a fluorescence microplate reader at an excitation of 485 nm and emission of 535 nm (monomer form of JC-1, green), and excitation of 550 nm and emission of 600 nm (aggregate form of JC-1, red). The ratio of green and red fluorescence intensities reflected the changes in mitochondrial membrane potential.

Determination of ROS

After the indicated treatments, cells were collected, washed once with 1× wash buffer and stained with 20 μM 2′,7′-dichlorofluorescin diacetate (DCFDA) (Abcam, Cambridge, UK) for 30 min in the dark at 37°C, and then analyzed by flow

cytometry (FACS Calibur, Becton Dickinson Company, USA) at 485 nm excitation and 535 nm emission.

Detection of Mitophagy

Mitophagy was determined by the detection of lysosomes. The H9c2 cells were seeded at a density of 1×10^5 in 35-mm glass bottom Petri dishes. The cells were then incubated for 24 h. After the respective treatments, cells were harvested and washed twice. LysoTracker Red (Thermo Fisher Scientific, MA, USA) was then added to the growth medium to achieve a final concentration of 50 nM, and the cells were further incubated for 20 min. MitoTracker Green (Thermo Fisher Scientific, MA, USA) was added to achieve a final concentration of 50 nM, and the cells were again incubated for 15 min. Co-loaded cells were then washed and loaded with phenol red-free DMEM and immediately analyzed by confocal microscopy (Olympus FV1200, Tokyo, Japan). The green fluorescence of MitoTracker Green (excitation of 490 nm and emission of 516 nm) and the red fluorescence of LysoTracker Red (excitation of 647 nm and emission of 668 nm) were measured immediately. At least 50 cells from three independent experiments for each group were included; the counts were averaged.

Immunofluorescence Analysis

The H9c2 cells were cultured on a glass-bottom dish. After the respective treatments, cells were fixed with 100% methanol for 5 min at room temperature and then were blocked in 1% bovine serum albumin (BSA)/10% normal goat serum/0.3 M glycine in 0.1% PBS-Tween for 1 h at room temperature. The cells were then incubated with rabbit anti-PINK1 (1 μg/mL) and mouse anti-HSP60 (1 μg/mL) overnight at 4°C. The secondary antibodies, Alexa Fluor® 594 goat anti-rabbit IgG (1:200) and Alexa Fluor® 488 goat anti-mouse IgG (1:1000) were then added, and the cells were incubated for 1 h at 37°C. Furthermore, 4′,6-diamidino-2-phenylindole (DAPI) counterstaining wasperformed to stain the nuclei. Co-loaded cell images were obtained using a confocal laser microscope system (FV1000, Olympus, Tokyo, Japan).

Similarly, after the respective treatments, cells were fixed with 4% paraformaldehyde and permeabilized with 0.1% Triton X-100. The cells were then incubated with rabbit anti-Parkin (1:100) and mouse anti-HSP60 (1 μg/mL) overnight at 4°C. The secondary antibodies, Alexa Fluor® 488 goat anti-rabbit IgG (1:200) and goat anti-mouse IgG (1:1000), were added and the cells were further incubated for 1 h at 37°C. Counterstaining using DAPI was performed, and images were obtained as described above. All antibodies were purchased from Abcam.

Western Blot Analysis

Proteins were separated using 10% SDS-PAGE gel wells and electrotransferred onto polyvinylidene difluoride (PVDF) membranes. The TBST buffer was added and 5% BSA was used to block nonspecific sites for 60 min. After blocking, blots were probed overnight at 4°C with primary antibodies against SQSTM1/p62 (1:1000, CST, USA); LC3B (1:1000, ABclonal, USA); PINK1 (1:2000, Abcam, USA); Parkin (1:1000, Abcam, USA); Caspase3 (1:1000, Abcam, USA); and β-actin (1:2000, Abcam, China), followed by horseradish peroxidase-conjugated secondary antibody for 90 min at 37°C. The proteins were then visualized by chemiluminescence and exposure to X-ray film (Bio-Rad).

Statistical Analysis

Data management and analysis were performed using the GraphPad Prism software (San Diego, CA). All data were reported as mean ± SEM. Each experiment was repeated three times. Univariate analysis of variance (ANOVA) was used for multiple comparisons. The Student′s *t*-test was conducted to analyze intergroup comparisons. $P < 0.05$ were reported as statistically significant.

RESULTS

FA Attenuates H/R Injury in H9c2 Cells

The H9c2 cells were subjected to 2 h of hypoxia, followed by 2 h of reoxygenation. The CCK8 assay indicated that H/R treatment significantly reduces myocardial cell viability ($P < 0.01$, versus the control). FA (25~400 μM) displayed dose-dependent toxicity to H9C2 cells (**Figure S1**), yet the lower concentrations of FA (6.25~200 μM) reduced the damage caused by H/R injury. H9c2 cells were hypoxia for 2 h under different concentrations of FA (6.25, 12.5, 25, 50, 100, and 200 μM). The results showed that FA treatment attenuated the reduction in cell viability caused by H/R injury and reached the highest effective concentration at 12.5 μM ($P < 0.05$, versus H/R) (**Figure 1A**). Therefore, 12.5 μM FA was administered in the following tests.

Cardiomyocytes are sensitive to ischemia/reperfusion injury and undergo apoptosis due to an insufficient oxygen supply. We conducted the TUNEL assay to analyze the effect of FA on apoptosis during H/R treatment. Compared to the control group, the cells subjected to H/R injury showed a significant increase in apoptotic rate; however, this increase was attenuated by FA (**Figures 1B–C**). To further confirm the results, we used western blot analysis to detect the expression of cleaved caspase3, a key downstream effector protein of apoptosis. The expression of cleaved caspase3 in H9c2 cells was increased during H/R injury, and FA effectively reduced this expression (**Figures 1D–E**). The entire image of capase3 and cleaved caspase3 was shown in **Figure S2**. These data indicated that FA treatment could significantly increase cell viability and reduce apoptosis to attenuate H/R injury in H9c2 cells.

FA Protected Mitochondrial Function Against H/R Injury

Mitochondria are critical organelles associated with ATP production for cellular metabolism. Therefore, the level of ADP/ATP conversion is one marker of mitochondrial energy metabolism. The ADP/ATP ratio of cardiomyocytes was detected using an ATP bioluminescent kit. Our results showed that H/R injury led to a significant decline in the level of ATP production and FA treatment fully restored energy production in the H9c2 cells (**Figure 2A**).

Mitochondrial function was also assessed by examining changes in the membrane potential. When the mitochondrial

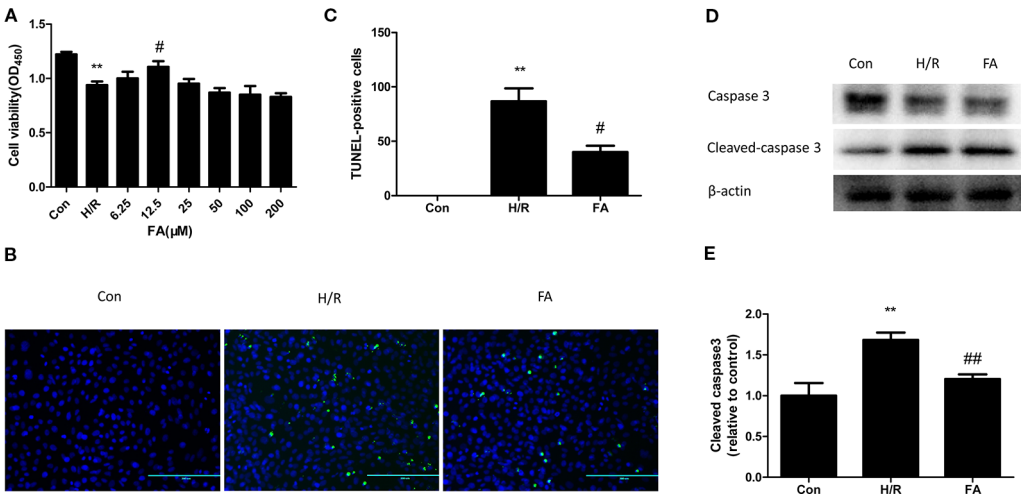

FIGURE 1 | Ferulic acid (FA) attenuated hypoxia/reoxygenation (H/R) injury in H9c2 Cells. **(A)** 12.5 μM FA increased cell viability. **(B, C)** FA inhibited the apoptosis levels tested by the TUNEL assay. **(D, E)** FA increased the level of cleaved caspase 3. Data were expressed as mean ± SEM (n = 6). **P < 0.01 versus control group; #P < 0.05 and ##P < 0.01 versus H/R groups.

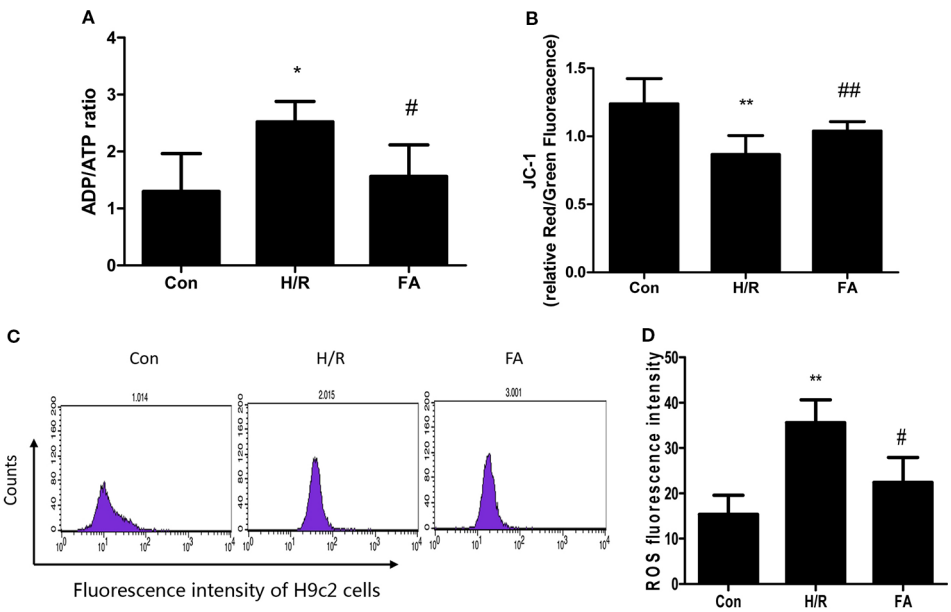

FIGURE 2 | Ferulic acid (FA) alleviated mitochondrial dysfunction following hypoxia/reoxygenation (H/R). **(A)** ADP/ATP ratio. **(B)** JC-1 staining. The ratio of Red/Green fluorescence reflected change in the mitochondrial membrane potential. **(C, D)** Cells were analyzed by flow cytometry after being stained with DCFDA to detect ROS. Data were expressed as mean ± SEM (n = 3). *P < 0.05 and **P < 0.01 versus the control group. #P < 0.05 and ##P < 0.01 versus the H/R group.

membrane potential is normal in H9c2 cells, JC-1 enters the mitochondria through the polarity of the mitochondrial membrane and forms a polymer that emits red fluorescence due to an increase in concentration. However, in damaged cells, the mitochondrial transmembrane is depolarized, and JC-1 is released from the mitochondria, thereby reducing its concentration, and is reversed to a monomeric form that emits green fluorescence. The relative proportion of commonly used green-red fluorescence is a measure of the ratio of changes in the mitochondrial membrane potential. Our results showed that mitochondrial depolarization was aggravated in H/R injury. Nevertheless, FA relieved the decline in membrane potential,

which appeared as a significant increase in the Red/Green ratio compared to that in H/R group (**Figure 2B**).

Significant ROS production results in mitochondrial dysfunction. As shown in **Figures 2C, D**, ROS levels were significantly elevated following H/R injury, and treatment with FA significantly reduced ROS generation compared with the untreated cells. Overall, these data indicate that FA treatment could alleviate mitochondrial dysfunction following H/R.

FA Inhibits Mitophagy in H/R Injury

Excessive autophagy induces cell death in myocardial I/R injury (Hamacher-Brady et al., 2006; Matsui et al., 2007). As FA protected mitochondrial function and attenuated H/R injury, we hypothesized that FA may confer mitochondrial protection by inhibiting mitophagy. Thus, rapamycin (Rapa, an autophagy activator) was co-administered with FA at the onset of hypoxia. We used MitoTracker Green and LysoTracker Red co-staining in H9c2 cells and then performed confocal microscopy analysis of co-localization of the mitochondria and lysosomes. Our results showed that H/R injury significantly activated mitophagy, and FA treatment effectively inhibited excessive mitophagy, as indicated by the fluorescence intensity of the red LysoTracker. Furthermore, rapamycin significantly promoted the increased number of lysosomes after H/R, and FA alleviated this increase (**Figure 3**).

FA Inhibits Mitophagy that was Dependent on PINK1/Parkin Signaling

Increasing evidence suggests that the PINK1/Parkin pathway is one of the most important ways by which mitophagy can be mediated (Mokranjac and Neupert, 2007; Matsuda et al., 2010; Moyzis et al., 2015). Therefore, we further investigated whether the inhibition of excessive mitophagy by FA is mediated through the PINK1/Parkin pathway. Autophagy is occurring accompanied with LC3-II (autophagosome membrane type) conversion from LC3-I (cytosolic LC3) and p62 degradation (Tanida et al., 2008). Western blotting analysis showed that compared with control cells, the H/R injury group showed a notable increase in the expression levels of PINK1 and Parkin, which occurred concurrently with the change in the levels of autophagy markers (increases in LC3-II/LC3-I and decline in p62 levels). The FA treatment significantly suppressed the activation of mitophagy in H9c2 cells, as evidenced by the decline in the expression levels of PINK1 and Parkin, with the reduction of LC3-II/LC3-I and accumulation of p62. Likewise, FA antagonistically reduced the activation of rapamycin (**Figures 4C–G**). In addition, co-immunofluorescence staining also demonstrated that the PINK1 and Parkin levels in H9c2 cells were markedly increased after H/R injury but were diminished by FA treatment. Thus, FA partially blocked the activation effects of rapamycin (**Figures 4A, B**).

DISCUSSION

To our knowledge, this study is the first to establish that FA exerts protective effects against H/R-induced injury in H9c2 cells by suppressing mitophagy. Moreover, FA may offer protection by alleviating H/R-induced apoptosis *via* the down-regulation of PINK1/Parkin-dependent mitophagy and reduction of

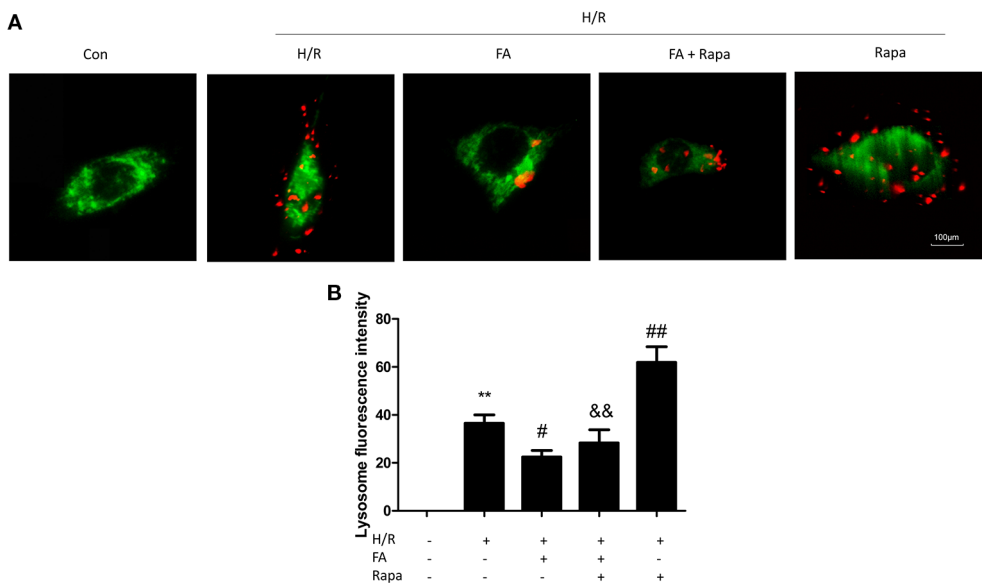

FIGURE 3 | Ferulic acid (FA) inhibited mitophagy. **(A)** Mitophagy was detected by using MitoTracker Green and LysoTracker Red staining. **(B)** Quantitative analysis of lysosome fluorescence intensity. At least 50 cells from three independent experiments for each group were included; the counts were averaged. Scale bar: 100 μm. Data were expressed as the mean ± SEM (n = 3). $^{**}P < 0.01$ versus the control group. $^{\#}P < 0.05$ and $^{\#\#}P < 0.01$ versus the hypoxia/reoxygenation (H/R) group. $^{\&\&}P < 0.01$ versus the rapamycin group.

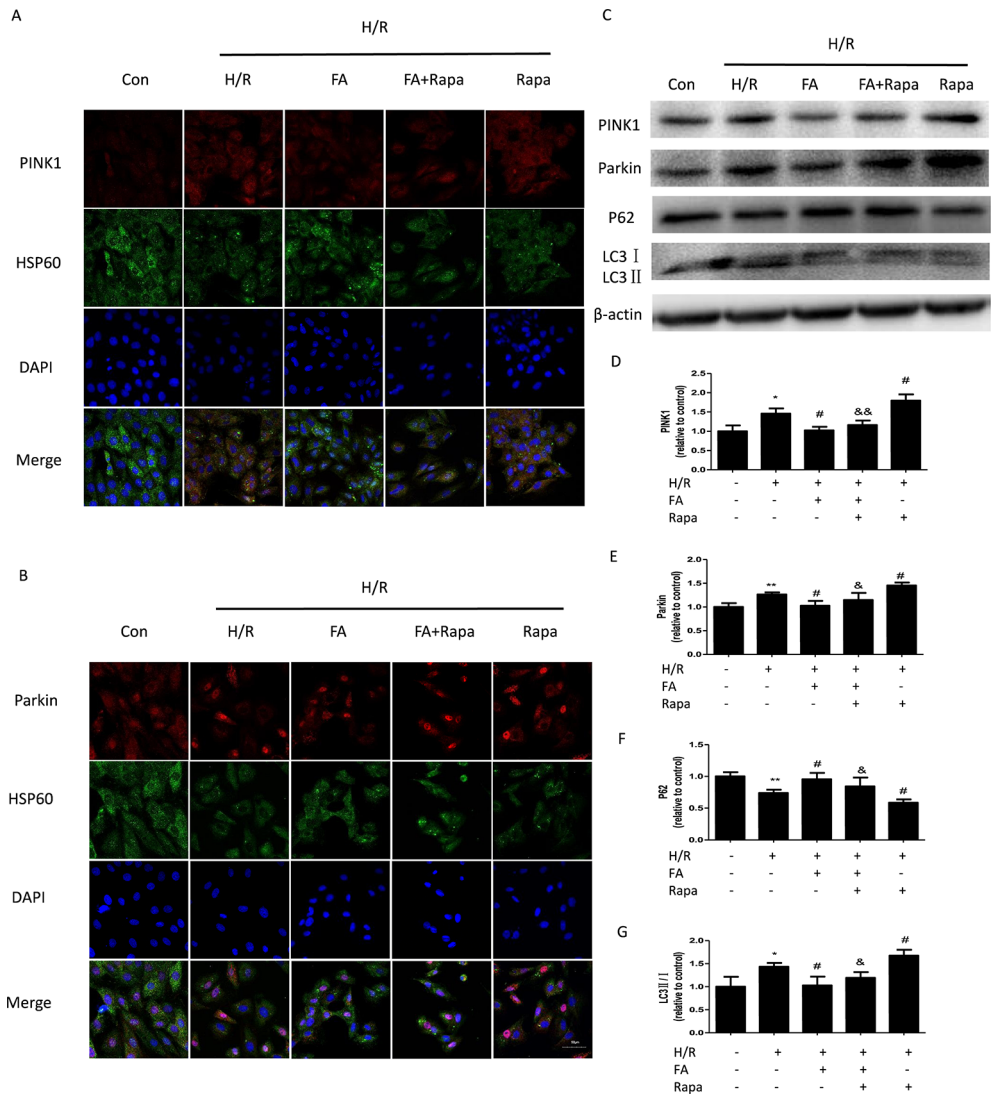

FIGURE 4 | Ferulic acid (FA) inhibited mitophagy that was dependent on PINK1/Parkin. **(A, B)** Co-immunofluorescence staining for PINK1/Parkin and HSP60-labeled mitochondria. Scale bar = 50 μm. **(C–G)** Expressions of mitophagy markers, including PINK1, Parkin, LC3, and P62. Data were expressed as the mean ± SEM (n = 3). *P < 0.05 and **P < 0.01 versus the control group. $^{\#}$P < 0.05 versus the H/R group. $^{\&}$P < 0.05 and $^{\&\&}$P < 0.01 versus the rapamycin group.

mitochondrial dysfunction. Overall, our findings showed the pivotal protective effects of FA in H9c2 cells subjected to H/R injury, which were achieved by regulating mitophagy.

Mitochondria perform a double role in the life and death of cardiomyocytes (Bourke et al., 2013). Normal mitochondria produce large quantities of ATP, which drives virtually all biological processes; however, damaged mitochondria produce pathological ROS. Excessive ROS generation attacks the bilayer lipid membrane of cells and subcellular organelles, decreases the mitochondrial membrane potential, and causes mitochondrial dysfunction (Cribbs and Strack, 2007; Detmer and Chan, 2007). Therefore, reducing the number of damaged mitochondria and ensuring mitochondrial quality is an important strategy against cell damage.

Autophagy is the only mechanism by which entire organelles are engulfed and recycled through the lysosomal pathway (Liu et al., 2013). Mitophagy refers to a specific autophagic phenomenon, in which cells are selectively cleared of damaged mitochondria through autophagy (Yang and Klionsky, 2010; Fimia et al., 2013). In general, normal mitophagy enables cells to degrade and remove damaged or dysfunctional mitochondria to maintain a balance of intracellular mitochondrial mass and quantity, and protect cell function (Hamacher-Brady et al., 2007; Kubli et al., 2013). Reducing mitophagy can reportedly lead to inflammation and cell death, which can lead to degenerative diseases (de Vries and Przedborski, 2013). In contrast, studies have shown that excessive mitophagy promotes the loss of cardiomyocytes (Lu et al., 2009; Ji et al., 2016). Recent reports showed that under acute mitochondrial stress, the cell

triggers program that result in the elimination of the defective mitochondria, first by promoting mitophagy, then by ensuring that the capacity for autophagosome degradation is increased by building more lysosomes (Deus et al., 2020). Our results suggested that H/R stimulation leads to defective mitophagy concurrently with cell injury and death, evidenced as reduced cell viability, increased expression of cleaved caspase 3, and apoptosis. Moreover, the binding of mitochondria and lysosomes was increased. These results showed that mitophagy was activated in H9c2 cells subjected to H/R. Thus, it was conceivable that inhibiting mitophagy might be beneficial to cardiomyocytes and represent a vital target for I/R injury.

Many studies have shown that FA can improve the clinical symptoms of patients with coronary heart disease and angina. It can also eliminate free radicals and reduce cardiomyocyte apoptosis (Alam et al., 2013). Moreover, new evidence shows that FA can alleviate cardiac injury caused by ischemia/reperfusion. Nevertheless, the exact mechanism of the protective effects of FA on H/R-induced myocardial injury is unclear. The present study demonstrated that FA can reserve mitochondrial function by decreasing ROS overproduction and ATP depletion and recovering the membrane potential. In addition, FA relieved the mitochondrial-based cell injury by inhibiting apoptosis. Moreover, FA administration during hypoxia reduced the binding of mitochondria and lysosomes in H/R cells and inhibited the process of mitophagy, which was activated by the autophagy activator, rapamycin. These findings suggested that mitophagy is an autophagy-related process.

Currently, PINK1/Parkin-directed mitophagy provided a mechanistic link between mitochondrial damage and autophagic clearance (Geisler et al., 2010). We further explored the signaling pathway mediated by FA in H9c2 cells. Upon mitochondrial damage, PINK1 aggregates abundantly on the outer membrane of the mitochondria and recruits Parkin from the cytoplasm to the mitochondria. Once recruited, Parkin ubiquitinates various substrates to induce and promote the autophagic removal of damaged mitochondria (Geisler et al., 2010). Studies have shown that the PINK1/Parkin pathway may be excessively activated in response to I/R injury to induce myocardial cell death (Wang et al., 2012; Ji et al., 2016). Consistent with these findings, we observed that in cultured H9c2 cells, H/R induced significant mitophagy, which was associated with activation of the PINK1/Parkin-mediated mitophagy signaling pathway. Furthermore, FA down-regulated the PINK1/Parkin pathway and suppressed subsequent mitophagy by reducing LC3-II/LC3-I levels and depleting P62 and antagonistically reducing the activation of mitophagy by rapamycin.

CONCLUSION

Generally, our findings offered compelling evidence that FA inhibited excessive mitophagy *via* the PINK1/Parkin pathway, thereby restoring mitochondrial function to counteract H/R-induced apoptosis and increase cardiomyocyte survival. This study might facilitate the development of a new application for FA in the prevention and treatment of ischemic heart disease.

DATA AVAILABILITY STATEMENT

All datasets generated for this study are included in the article/ **Supplementary Material**.

AUTHOR CONTRIBUTIONS

CL and YZ performed the research study. CL, YZ, and JL designed the research study. CL wrote the first draft of the manuscript. HG, XH, and JR contributed to the revision of the manuscript. All the authors reviewed and approved the submitted version.

FUNDING

This study was supported by grants from the National Basic Research Program (973 program) (China) (No.2015CB554405).

ACKNOWLEDGMENTS

The authors are grateful to Charlesworth Publishing Services Limited for their helpful suggestions and highly qualified English language editing.

SUPPLEMENTARY MATERIAL

The Supplementary Material for this article can be found online at: https://www.frontiersin.org/articles/10.3389/fphar.2020.00103/full#supplementary-material

REFERENCES

Alam, M. A., Sernia, C., and Brown, L. (2013). Ferulic acid improves cardiovascular and kidney structure and function in hypertensive rats. *J. Cardiovasc. Pharmacol.* 61, 240–249. doi: 10.1097/FJC.0b013e31827cb600

Ashrafi, G., and Schwarz, T. L. (2013). The pathways of mitophagy for quality control and clearance of mitochondria. *Cell Death Differ.* 20, 31–42. doi: 10.1038/cdd.2012.81

Barone, E., Calabrese, V., and Mancuso, C. (2009). Ferulic acid and its therapeutic potential as a hormetin for age-related diseases. *Biogerontology* 10, 97–108. doi: 10.1007/s10522-008-9160-8

Bourke, L. T., Knight, R. A., Latchman, D. S., Stephanou, A., and McCormick, J. (2013). Signal transducer and activator of transcription-1 localizes to the mitochondria and modulates mitophagy. *JAKSTAT* 2, e25666. doi: 10.4161/jkst.25666

Chen, Y. R., and Zweier, J. L. (2014). Cardiac mitochondria and reactive oxygen species generation. *Circ. Res.* 114, 524–537. doi: 10.1161/CIRCRESAHA.114.300559

Cribbs, J. T., and Strack, S. (2007). Reversible phosphorylation of Drp1 by cyclic AMP-dependent protein kinase and calcineurin regulates mitochondrial fission and cell death. *EMBO Rep.* 8, 939–944. doi: 10.1038/sj.embor.7401062

de Vries, R. L., and Przedborski, S. (2013). Mitophagy and Parkinson′s disease: be eaten to stay healthy. *Mol. Cell. Neurosci.* 55, 37–43. doi: 10.1016/j.mcn.2012.07.008

Detmer, S. A., and Chan, D. C. (2007). Functions and dysfunctions of mitochondrial dynamics. *Nat. Rev. Mol. Cell Biol.* 8, 870–879. doi: 10.1038/nrm2275

Deus, C. M., Yambire, K. F., Oliveira, P. J., and Raimundo, N. (2020). Mitochondria-Lysosome Crosstalk: From Physiology to Neurodegeneration. *Trends Mol. Med.* 26, 71–88. doi: 10.1016/j.molmed.2019.10.009

Dorn, G. W., and Kitsis, R. N. (2015). The mitochondrial dynamism-mitophagy-cell death interactome: multiple roles performed by members of a mitochondrial molecular ensemble. *Circ. Res.* 116, 167–182. doi: 10.1161/CIRCRESAHA.116.303554

Fimia, G. M., Kroemer, G., and Piacentini, M. (2013). Molecular mechanisms of selective autophagy. *Cell Death Differ.* 20, 1–2. doi: 10.1038/cdd.2012.97

Geisler, S., Holmström, K. M., Skujat, D., Fiesel, F. C., Rothfuss, O. C., Kahle, P. J., et al. (2010). PINK1/Parkin-mediated mitophagy is dependent on VDAC1 and p62/SQSTM1. *Nat. Cell Biol.* 12, 119–131. doi: 10.1038/ncb2012

Go, A. S., Mozaffarian, D., Roger, V. L., Benjamin, E. J., Berry, J. D., Blaha, M. J., et al. (2014). Executive summary: heart disease and stroke statistics–2014 update: a report from the American Heart Association. *Circulation* 129, 399–410. doi: 10.1161/01.cir.0000442015.53336.12

Hamacher-Brady, A., Brady, N. R., and Gottlieb, R. A. (2006). Enhancing macroautophagy protects against ischemia/reperfusion injury in cardiac myocytes. *J. Biol. Chem.* 281, 29776–29787. doi: 10.1074/jbc.M603783200

Hamacher-Brady, A., Brady, N. R., Logue, S. E., Sayen, M. R., Jinno, M., Kirshenbaum, L. A., et al. (2007). Response to myocardial ischemia/reperfusion injury involves Bnip3 and autophagy. *Cell Death Differ.* 14, 146–157. doi: 10.1038/sj.cdd.4401936

Hammerling, B. C., and Gustafsson, Å.B. (2014). Mitochondrial quality control in the myocardium: cooperation between protein degradation and mitophagy. *J. Mol. Cell. Cardiol.* 75, 122–130. doi: 10.1016/j.yjmcc.2014.07.013

Hausenloy, D. J., and Yellon, D. M. (2013). Myocardial ischemia-reperfusion injury: a neglected therapeutic target. *J. Clin. Invest.* 123, 92–100. doi: 10.1172/JCI62874

Huang, C., Andres, A. M., Ratliff, E. P., Hernandez, G., Lee, P., and Gottlieb, R. A. (2011). Preconditioning involves selective mitophagy mediated by Parkin and p62/SQSTM1. *PloS One* 6, e20975. doi: 10.1371/journal.pone.0020975

Ji, W., Wei, S., Hao, P., Xing, J., Yuan, Q., Wang, J., et al. (2016). Aldehyde dehydrogenase 2 has cardioprotective effects on myocardial ischaemia/reperfusion injury *via* Suppressing Mitophagy. *Front. Pharmacol.* 7, 101. doi: 10.3389/fphar.2016.00101

Kasahara, A., and Scorrano, L. (2014). Mitochondria: from cell death executioners to regulators of cell differentiation. *Trends Cell Biol.* 24, 761–770. doi: 10.1016/j.tcb.2014.08.005

Kim, J., Kim, Y. C., Fang, C., Russell, R. C., Kim, J. H., Fan, W., et al. (2013). Differential regulation of distinct Vps34 complexes by AMPK in nutrient stress and autophagy. *Cell* 152, 290–303. doi: 10.1016/j.cell.2012.12.016

Kroemer, G., Mariño, G., and Levine, B. (2010). Autophagy and the integrated stress response. *Mol. Cell* 40, 280–293. doi: 10.1016/j.molcel.2010.09.023

Kubli, D. A., Zhang, X., Lee, Y., Hanna, R. A., Quinsay, M. N., Nguyen, C. K., et al. (2013). Parkin protein deficiency exacerbates cardiac injury and reduces survival following myocardial infarction. *J. Biol. Chem.* 288, 915–926. doi: 10.1074/jbc.M112.411363

Liu, K., Sun, Y., Gu, Z., Shi, N., Zhang, T., and Sun, X. (2013). Mitophagy in ischaemia/reperfusion induced cerebral injury. *Neurochem. Res.* 38, 1295–1300. doi: 10.1007/s11064-013-1033-0

Lu, L., Wu, W., Yan, J., Li, X., Yu, H., and Yu, X. (2009). Adriamycin-induced autophagic cardiomyocyte death plays a pathogenic role in a rat model of heart failure. *Int. J. Cardiol.* 134, 82–90. doi: 10.1016/j.ijcard.2008.01.043

Mancuso, C., and Santangelo, R. (2014). Ferulic acid: pharmacological and toxicological aspects. *Food Chem. Toxicol.* 65, 185–195. doi: 10.1016/j.fct.2013.12.024

Matsuda, N., Sato, S., Shiba, K., Okatsu, K., Saisho, K., Gautier, C. A., et al. (2010). PINK1 stabilized by mitochondrial depolarization recruits Parkin to damaged mitochondria and activates latent Parkin for mitophagy. *J. Cell Biol.* 189, 211–221. doi: 10.1083/jcb.200910140

Matsui, Y., Takagi, H., Qu, X., Abdellatif, M., Sakoda, H., Asano, T., et al. (2007). Distinct roles of autophagy in the heart during ischemia and reperfusion: roles of AMP-activated protein kinase and Beclin 1 in mediating autophagy. *Circ. Res.* 100, 914–922. doi: 10.1161/01.RES.0000261924.76669.36

Mokranjac, D., and Neupert, W. (2007). Protein import into isolated mitochondria. *Methods Mol. Biol.* 372, 277–286. doi: 10.1007/978-1-59745-365-3_20

Moyzis, A. G., Sadoshima, J., and Gustafsson, Å.B. (2015). Mending a broken heart: the role of mitophagy in cardioprotection. *Am. J. Physiol. Heart Circ. Physiol.* 308, H183–H192. doi: 10.1152/ajpheart.00708.2014

Ong, S. B., and Gustafsson, A. B. (2012). New roles for mitochondria in cell death in the reperfused myocardium. *Cardiovasc. Res.* 94, 190–196. doi: 10.1093/cvr/cvr312

Pan, W., Hu, K., Bai, P., Yu, L., Ma, Q., Li, T., et al. (2016). Design, synthesis and evaluation of novel ferulic acid-memoquin hybrids as potential multifunctional agents for the treatment of Alzheimer′s disease. *Bioorg. Med. Chem. Lett.* 26, 2539–2543. doi: 10.1016/j.bmcl.2016.03.086

Springer, W., and Kahle, P. J. (2011). Regulation of PINK1-Parkin-mediated mitophagy. *Autophagy* 7, 266–278. doi: 10.4161/auto.7.3.14348

Sun, Y., Zheng, Y., Wang, C., and Liu, Y. (2018). Glutathione depletion induces ferroptosis, autophagy, and premature cell senescence in retinal pigment epithelial cells. *Cell Death Dis.* 9, 753. doi: 10.1038/s41419-018-0794-4

Tang, X., Liu, J., Dong, W., Li, P., Li, L., Lin, C., et al. (2013). The cardioprotective effects of citric Acid and L-malic Acid on myocardial ischemia/reperfusion injury. *Evid Based Complement Alternat. Med.* 2013, 820695. doi: 10.1155/2013/820695

Tanida, I., Ueno, T., and Kominami, E. (2008). LC3 and Autophagy. *Methods Mol. Biol.* 445, 77–88. doi: 10.1007/978-1-59745-157-4_4

Tannous, P., Zhu, H., Nemchenko, A., Berry, J. M., Johnstone, J. L., Shelton, J. M., et al. (2008). Intracellular protein aggregation is a proximal trigger of cardiomyocyte autophagy. *Circulation* 117, 3070–3078. doi: 10.1161/CIRCULATIONAHA.107.763870

Walters, A. M., Porter, G.A.Jr, and Brookes, P. S. (2012). Mitochondria as a drug target in ischemic heart disease and cardiomyopathy. *Circ. Res.* 111, 1222–1236. doi: 10.1161/CIRCRESAHA.112.265660

Wang, Y., Nartiss, Y., Steipe, B., McQuibban, G. A., and Kim, P. K. (2012). ROS-induced mitochondrial depolarization initiates PARK2/PARKIN-dependent mitochondrial degradation by autophagy. *Autophagy* 8, 1462–1476. doi: 10.4161/auto.21211

Yang, Z., and Klionsky, D. J. (2010). Eaten alive: a history of macroautophagy. *Nat. Cell Biol.* 12, 814–822. doi: 10.1038/ncb0910-814

Youle, R. J., and Narendra, D. P. (2011). Mechanisms of mitophagy. *Nat. Rev. Mol. Cell Biol.* 12, 9–14. doi: 10.1038/nrm3028

Zhang, Y., Liu, J., Yang, B., Zheng, Y., Yao, M., Sun, M., et al. (2018). Ginkgo biloba extract inhibits astrocytic lipocalin-2 expression and alleviates neuroinflammatory injury *via the* JAK2/STAT3 pathway after ischemic brain stroke. *Front. Pharmacol.* 9, 518. doi: 10.3389/fphar.2018.00518

Conflict of Interest: The authors declare that the research was conducted in the absence of any commercial or financial relationships that could be construed as a potential conflict of interest.

frontiers in Pharmacology

ORIGINAL RESEARCH
published: 06 March 2020
doi: 10.3389/fphar.2020.00134

Shenlian Extract Against Myocardial Injury Induced by Ischemia Through the Regulation of NF-κB/IκB Signaling Axis

Yuan Guo[1], Qing Yang[1], Xiao-Gang Weng[1], Ya-Jie Wang[1], Xue-Qi Hu[2], Xiao-Jun Zheng[3], Yu-Jie Li[1]* and Xiao-Xin Zhu[1]**

[1] Pharmacokinetics Laboratory, Institute of Chinese Materia Medica, China Academy of Chinese Medical Sciences, Beijing, China, [2] College of Pharmacy, Tianjin University of Traditional Chinese Medicine, Tianjin, China, [3] Pharmacy Department, First Hospital of Shanxi Medical University, Taiyuan, China

OPEN ACCESS

Edited by:
Jianxun Liu,
China Academy of Chinese Medical Sciences, China

Reviewed by:
Claire Elizabeth Robertson,
University of Westminster, United Kingdom
Nelson Chong,
University of Westminster, United Kingdom

***Correspondence:**
Xiao-Xin Zhu
xxzhu@icmm.ac.cn
Yu-Jie Li
yjli@icmm.ac.cn
Xiao-Jun Zheng
zhengxiaojun0525@163.com

Specialty section:
This article was submitted to Ethnopharmacology, a section of the journal Frontiers in Pharmacology

Received: 01 June 2019
Accepted: 31 January 2020
Published: 06 March 2020

Citation:
Guo Y, Yang Q, Weng X-G, Wang Y-J, Hu X-Q, Zheng X-J, Li Y-J and Zhu X-X (2020) Shenlian Extract Against Myocardial Injury Induced by Ischemia Through the Regulation of NF-κB/IκB Signaling Axis. Front. Pharmacol. 11:134. doi: 10.3389/fphar.2020.00134

Ischemic heart disease (IHD), caused predominantly by atherosclerosis, is a leading cause of global mortality. Our previous studies showed that Shenlian extract (SL) could prevent the formation of atherosclerosis and enhance the stability of atherosclerotic plaques. To further investigate the protective effects of SL on myocardial ischemic injury and its possible mechanisms, anesthetized dogs, *ex vivo* rat hearts, and H9c2 cardiomyocytes were used as models. The results showed that SL had a significant protective effect on the anesthetized dog ligating coronary artery model, reduced the degree of myocardial ischemia (Σ-ST), and reduced the scope of myocardial ischemia (N-ST). Meanwhile, SL alleviated ischemic reperfusion damage in *ex vivo* rat hearts with improved LVEDP and ± dp/dt_{max} values of the left ventricle. SL reduced the pathological changes of LDH, IL-1β, MDA, and NO contents, all of which are related to the expression of NF-κB. Further analysis by Bio-Plex array and signal pathway blocker revealed that the phosphorylation of IκB was a key factor for SL to inhibit myocardial ischemic injury, and the regulation of SL on IκB was primarily related to degradation of the IκB protein. These results provided dependable evidence that SL could protect against myocardial ischemic injury through the NF-κB signaling pathway.

Keywords: Shenlian extract (SL), ischemic heart disease (IHD), myocardial ischemic injury, NF-κB signaling pathway, inflammation

INTRODUCTION

Cardiovascular disease (CVD) remains the leading cause of global mortality. Ischemic heart disease (IHD), is the second leading cause of death for the Chinese population (Zhao et al., 2019), is one of the main clinical manifestations of CVD (Herrington et al., 2016). It has been reported that mortality caused by IHD is common in Eastern Europe and Asia (Moran et al., 2014; Akbalaeva et al., 2017). Myocardial ischemic disease has risen to a top cause of morbidity and mortality worldwide (Zhao et al., 2019). The development of atherosclerosis in the coronary artery is the underlying pathological mechanism of myocardial ischemia and myocardial

infarction (Foks and Bot, 2017). In the most serious situations, an advanced atherosclerotic plaque can rupture or erode, leading to the formation of an occluding thrombus and the subsequent incidence of an acute cardiovascular event. Simultaneously, inflammation, which is an emerging risk factor, leads to the accumulation of lipids and inflammatory cells in the vascular wall (Bertrand and Tardif, 2017). Many experimental and clinical studies support interleukin-1 beta (IL-1β) secretion, which targets vascular cells, as a promising research target to find new anti-atherosclerotic agents that better target inflammation (Hansson, 2017; Libby, 2017). Interventions targeting reductions in inflammation to prevent plaque instability are therefore required. Along with contemporary interventions and pharmacologic agents, traditional Chinese medicine (TCM) has been extensively prescribed in clinics in China and some Asian countries (Wang et al., 2017). TCM has attracted increasing attention around the world, because the treatment consists of significant bioactivity by multiple components (Xu et al., 2015; Zhang et al., 2015).

Shenlian extract (SL) is a combination of *Salvia miltiorrhiza Bunge* and *Andrographis paniculata* extract. Based on the clinical experience of TCM, SL can prevent and treat atherosclerosis and cardiovascular diseases (Zhou et al., 2013; Guo et al., 2016). The mechanism of action of *S. miltiorrhiza Bunge* includes promoting the circulation of blood, removing blood stasis, improving blood rheology by inhibiting platelet aggregation, and changing erythrocyte deformability or reducing plasma viscosity (Tang et al., 2002; Li et al., 2004). Via these mechanisms, it is shown to inhibit myocardial apoptosis after myocardial ischemic reperfusion injury in rats (Song et al., 2013). Furthermore, modern pharmacological studies have shown that *S. miltiorrhiza Bunge* also affects myocardial remodelling to improve myocardial infarction disease (Wang et al., 2018). The other ingredient, *A. paniculata,* has an anti-inflammation and detoxification effect (Pang et al., 2016; Zou et al., 2016), improving the hemodynamic and ventricular function against ischemic reperfusion injury (Ojha et al., 2012) and protecting endothelial cells (You et al., 2011).

Previous studies have demonstrated that SL has a protective effect on atherosclerosis plaque formation, significantly reducing the plaque area of atherosclerosis, reducing the severity of the pathological condition (Li et al., 2011), lowering the blood lipid levels by improving lipid metabolism, and reducing the infiltration and deposition of lipids in the blood vessel wall (Guo et al., 2016). Furthermore, SL has a protective effect by inhibiting the infiltration and adhesion of local inflammatory cells, improving the local blood flow of vessels, and inhibiting the cytoskeletal rearrangement after injury of vascular endothelium. Moreover, SL stabilized atherosclerosis plaques. Through an $ApoE^{-/-}$ mouse model with vulnerable plaques, which were induced by combined multi-factor induction, SL was reported to reduce the levels of macrophagocytes and lipids in plaque, decrease the expression levels of MMP-2 and MMP-9 in plaques, and up-regulate the contents of collagen fibers and expression of plaques (Guo et al., 2016). In addition, SL decreased the proliferation and degranulation of mast cells in extravascular mucosa induced by neuropeptide P, and reduced the inflammatory response and intraplaque hemorrhage of the plaque (Li Y. J. et al., 2016).

We propose that SL could synthetically affect the formation process of atherosclerosis through various pathways mainly inflammation responses. A primary goal of this report is to further explore the protective effect of SL on myocardial ischemic injury and its possible mechanism based on NF-κB signaling pathway.

MATERIALS AND METHODS

Materials and Reagents

Nitro blue tetrazolium chloride (N-BT) was purchased from the medicine supply station of the Academy of Military Medical Sciences (China). Lactate dehydrogenase (LDH), malondialdehyde (MDA), nitric oxide (NO), nitric oxide synthase (NOS), IL-1β, PI3K, and nuclear factor kB (NF-kB) kits were purchased from Nanjing Jiancheng Bioengineering Institute (China). High glucose Dulbecco's modified Eagle's medium (DMEM-H) and fetal bovine serum (FBS) were purchased from Gibco. MicroRotofor™ cell lysis kit and Bio-Plex Pro™ cell signaling MAPK panel were purchased from Bio-Rad (USA). Proteasome inhibitor, MG132, and IKK (inhibitor of nuclear factor kappa-B kinase, IκB) inhibitor, parthenolide, were purchased from Sigma.

Plant Materials

SL consisted of *S. miltiorrhiza Bunge* extract and *A. paniculata* extract at a ratio of 15:9. *S. miltiorrhiza Bunge* and *A. paniculata* originated from the Linyi, Shandong province and Guangxi province (China). The taxonomic authenticity was identified by Prof. Xirong He of the Institute of Chinese Materia Medica of the China Academy of Chinese Medical Sciences (Beijing, China). *S. miltiorrhiza Bunge* was identified as the dry rhizome of *S. miltiorrhiza Bge.,* and *A. paniculata* was identified as the herba of *A. paniculata* (Burm F.) Nees. The *S. miltiorrhiza Bunge* extract included two types of components. One component was extracted with ethanol under percolation and then concentrated under reduced pressure, and the other component was prepared by dilute ethanol soaking and purified by microporous resins SP825. The *A. paniculata* extract was prepared by dilute ethanol soaking, and purified by macroporous resins SP825. The extract of SL primarily contained tanshinone IIA (3%), salvianolic acid B (38%) and andrographolide (20%). The extraction rate of the water-soluble partial extract of *S. miltiorrhiza Bunge* was 2.27%, and that of the fat-soluble partial extract was 1.31%. The extraction rate of the partial extract of *A. paniculata* was 2.11%. (Guo et al., 2016).

High Performance Liquid Chromatography (HPLC) Analysis of SL

SL extract was detected using Waters HPLC. The conditions of the HPLC are shown in **Table 1**, and the HPLC chromatogram of SL can be found in the **Supplementary Material**.

TABLE 1 | High performance liquid chromatography (HPLC) conditions of Shenlian extract (SL).

	Andrographolide	Tanshinone IIA	Salvianolic acid B
Instrument Detector		Waters HPLC 2489 UV detector	
RP column	Phenomenex Synerigi Hydro-RP C18 (250×4.6mm, 4μm)	Phenomenex Gemini C18 (250×4.6mm, 5μm)	Phenomenex Gemini C18 (250×4.6mm, 5μm)
Column temperature		Indoor temperature	
Injection vol		10 μL	
UV wavelength	286 nm	228 nm	270 nm
Mobile phase	Methanol-Acetonitrile-Water (30/10/60, 0.1vol.% anhydrous formic acid)	Methanol-Water (45/55, v/v)	Methanol-Water (75/25, v/v)

Experimental Animals and Grouping

Healthy Beagle dogs (11.2 ± 2.5 kg), both male and female, were obtained from Beijing Shahe Tongli Experimental Animal Farm. The animal studies were approved in accordance with the recommendations in the Guidance for the Care and Use of Laboratory Animals issued by the Ministry of Science and Technology of China and the Use Committee of Institute of Basic Theory for Chinese Medicine, China Academy of Chinese Medicine Science. These dogs were randomly assigned into four groups (six dogs in each group): myocardial ischemia model group (MI, operated with ligating left anterior descending), positive control diltiazem treatment group (treated with at 5 mg/kg diltiazem), low dosage SL treatment group (66 mg/kg), and high dosage SL treatment group (132 mg/kg).

The adult male Wistar rats (250-300g) were obtained from Beijing Vital River Laboratory Animal Technology Co., Ltd. The animal studies were also performed in accordance with the Guidance for the Care and Use of Laboratory Animals issued by the Ministry of Science and Technology of China and the Use Committee of Institute of Basic Theory for Chinese Medicine, China Academy of Chinese Medicine Science. The rats were randomly assigned into the following five experimental groups (eight rats in each group): vehicle control group (control, operated with continuous perfusion); ischemia reperfusion control group (I/R, operated with at ischemia and reperfusion), positive control verapamil treatment group (150 ng/kg), low dosage SL treatment group (224 mg/kg), and high dosage SL treatment group (448 mg/kg).

All experimental procedures and animal management were approved and performed by Institute of Chinese Materia China Academy of Chinese Medical Science. All animals were maintained under controlled conditions of temperature (24 ± 2°C) and humidity (55 ± 5%), a 12-hour light/dark cycle, and allowed free access to food and water.

Procedure of Myocardial Ischemic Model

Dogs were maintained with free access to regular diet and distilled water for one week before surgery. The model of myocardial ischemia in anesthetized dogs was established as previously described (Berger et al., 1976; Fu et al., 2013). Briefly, Beagle dogs were anesthetized with 1% pentobarbital sodium 30 mg/kg by intravenous injection. After endotracheal intubation, the chest of the dog was opened by left thoracotomy to expose the heart, and the left anterior descending (LAD) coronary artery was ligated. Finally, 15 min after ligation, drugs were given by duodenal injection. Inclusion criteria for the study were that the ST segment increased more than 2 mV. After ligation, the multi-point epicardial electrode (30 landmarks) was sutured on the ventricular surface, and the epicardial electrocardiogram (EECG) was connected by the multi-channel physiological instrument (BIOPAC, USA). Myocardial ischemia degree (total mV of ST-segment elevation, Σ-ST) and the myocardial ischemia scope (total number of ST-segment elevation points, N-ST) were counted.

Measurement of Myocardial Infarction Area in Dogs by N-BT Staining

To detect myocardial infarction size, which is closely related to the left ventricular ejection fraction and cardiac function, N-BT staining was used. The N-BT non-stained area represents the infarcted area, and the N-BT stained area represents the non-infarcted area. The heart was removed and divided into five pieces. Next, the heart was cut parallel to the coronary sulcus and placed into the N-BT staining solution for 15 min at room temperature after EECG testing last 180 min. The medical image analysis system (HPIAS-1000, Beijing, China) was used to measure the infarcted area (N-BT non-stained area) and non-infarcted area (N-BT stained area) on each side. The percentage of infarcted area of the ventricle and total heart was calculated.

Procedure of Langendorff-Perfused Rat Hearts Model

Rats were anesthetized with 0.2% heparin sodium (1 mL, i.p.) and 20% urethane (0.5 mL/100g, i.p.) after 10 min. The hearts were quickly removed, and the aorta was cannulated and retrogradely perfused at constantly pressure (70–80 mmHg) on a Langendorff apparatus (LE3/42502002, Panlab, Spain) with a nutrient rich oxygenated KH (Krebs-Henseleit) solution maintained at 37 ± 1°C with a physiological pH of 7.4 (Ytrehus, 2000; Bell et al., 2011). A self-made latex balloon was inserted in the left ventricle of the heart, and a pressure transducer was placed on the other side of the balloon (DA100C, BIOPAC, USA). The experimental procedure of perfused the heart is summarized in **Figure 1**. The following parameters of myocardial function were measured during equilibration time and at 5, 10, 15, 20, 25, and 30 min during reperfusion by the MP150 multi-channel physiological instrument (BIOPAC, USA): the pressure curve of the left ventricle, the left ventricular systolic pressure (LVSP), the left ventricular end diastolic pressure (LVEDP), and the left ventricular internal pressure maximal rise and maximum decline rate ($\pm dp/dt_{max}$).

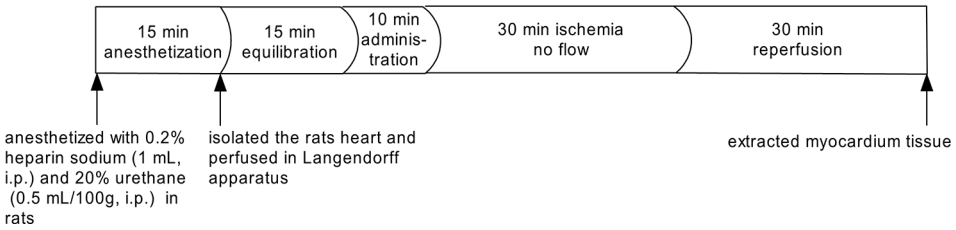

FIGURE 1 | Experimental protocol of ischemia–reperfusion *via* Langendorff.

Determination Biochemical Parameters of Myocardium Tissue of Rats

The myocardium tissue obtained from the re-perfused hearts were used for evaluating the concentration of LDH, MDA, NO, and NOS, which are routine indicators commonly used for diagnosing myocardial inflammation and acute myocardial infarction. After reperfusion for 30 min, the heart was immediately removed and contained approximately 0.4 g of apical tissue. Then, 10% (w/v) of fresh myocardial homogenate was prepared and centrifuged at 3,000 rpm for 15 min. The supernatant was collected to assay the levels of biochemical parameters using chemical colorimetry of kits, and specific operations was strictly followed by the manufacturer's instructions.

Measurement of Inflammatory Parameters by ELISA

The PI3K pathway plays an important role in regulating a variety of cellular functions including survival, transcription and protein synthesis. NF-κB is activated downstream of PI3K.The supernatant of fresh myocardial homogenate was acquired to measure the concentrations of IL-1β, PI3K and NF-κB by commercial enzyme linked immunosorbent assay (ELISA) kits, and the detection operations were performed according to the manufacturer's instructions.

H9c2 Cell Culture

H9c2 rat embryonic cardiomyocytes (from National Infrastructure of Cell Line Resource) were cultured in DMEM-H supplemented with 10% FBS. All cells were cultivated at 37°C in a humidified incubator maintained at 5% CO_2. Cells grown to sub-confluence were used to complete all the based cell experiments.

Measurement of H_2O_2-Induced Oxidative Cell Damage in H9c2 Cells

SL was mixed with the DMEM-H medium to make a stock solution with a concentration of 1 mg/mL. The dimethyl sulfoxide (DMSO) concentration in the stock solution was 0.1% v/v, and then the solution was stored in –20°C. The cells were treated with SL at a final concentration of 10, 25, or 50 μg/mL, diluted with with DMEM-H medium. The SL treatment groups were pre-treated with the corresponding drugs for 24 h before H_2O_2 induction, and the cells were exposed to H_2O_2 (500 μM) for 6 h to induce cells damage. The cells were divided into five groups: a untreated control group (untreated); a H_2O_2-induced group (500 μM H_2O_2 for 6 h); a 50 μg/mL SL treatment group (SL 50 μg/mL treatment for 24 h, then 500 μM H_2O_2 for 6 h); a 25 μg/mL SL treated group (SL 25 μg/mL treatment for 24 h, then 500 μM H_2O_2 for 6 h); a 10 μg/mL SL treated group (SL 10 μg/mL treatment for 24 h, then 500 μM H_2O_2 for 6 h). H9c2 cells seeded at 5×10^4 cells in 24 wells in DMEM-H and 10% FBS. The cells were cultured overnight, and then treated with SL extracts for 24 h and H_2O_2 (500 μM) for 6 h. The supernatant of the cell culture was collected. The concentrations of LDH and NO were determined by chemical colorimetry kits, and the concentrations of IL-1β was determined by ELISA. The instructions from the kit were strictly followed.

Bio-Plex Array Analysis in H9c2 Cells

H9c2 cells were lysed by MicroRotofor™ Cell Lysis Kit, and centrifuged at 15,000×g for 10 min at 4°C. The supernatant was collected, and its protein concentration was detected by the Bradford method. Following the kit's instruction, the Bio-Plex Pro™ Cell Signaling MAPK Panel was used to detect the following phosphorylated analytes from cell lysates: p-IκB-α, p-ERK1/2, p-p38 MAPK, p-Stat3, p-c-JUN, p-IGF-IR, p-MEK, p-Akt. The Bio-Plex cytokine assay buffer was used, the Bio-Plex array reader collects the data that were analyzed by the Bio-Plex® 200 Systems (Bio-Rad, USA).

Immunofluorescence Analysis in H9c2 Cells

In the SL treatment groups, the proteasome inhibitor, MG132 (5 μM), and IKK inhibitor, parthenolide (10 μM), were incubated in culture cells for 12 h before drug treatment to explore whether degradation or phosphorylation, respectively, modulated the IκB protein (Bergmann et al., 2001; Planavila et al., 2005). The function pathway was examined by comparing the expression of filamentous actin (F-actin) in the groups of H9c2 cells. Staining with fluorescently labeled phalloidin clearly showed the distribution of microfilaments in the cells (Lukinavičius et al., 2014). The expression of F-actin in the cells were observed by Laser Scanning Confocal Microscope (Olympus, Janpan) immediately after labelling, with excitation wavelength of 488 nm and emission wavelength of 530 nm, per instructions. The supernatant of cells was collected to detect the levels of NO by chemical colorimetry and IL-1β by ELISA to confirm the oxidative stress and inflammation levels in injured cells, respectively.

Statistical Analysis

All experimental data were analyzed by GraphPad Prism 5.0 and plotted as the mean ± standard error of the mean (SEM). Results were performed through one-way analysis of variance (ANOVA) and Dunnett's Multiple Comparison test to determine statistical significance; P-values less than 0.05 were defined as statistically significance.

RESULTS

SL Reduced the Degree and Scope of Myocardial Ischemia on Anesthetized Dogs

An EECG was performed to determine the real-time effect of SL on myocardial ischemic dog hearts. After ligation of LAD in the MI group, the ischemia degree (Σ-ST) increased markedly and continued to increase during the entire process (**Figure 2A**). Compared to the MI group, the Σ-ST significantly decreased after 66 mg/kg of SL ($P < 0.05$). At 180 min after administration, the ischemia degree of dogs treated with 66 mg/kg and 132 mg/kg of SL was reduced by 89% and 80%, respectively. Similarly, the ischemia scope (N-ST) significantly decreased after the administration with 66 mg/kg of SL at 15 and 30 min ($P < 0.05$, **Figure 2B**).

SL Reduced the Area of Myocardial Ischemia on Anesthetized Dogs

The myocardial infarction size was estimated by quantitative histological N-BT staining. Visually, the infarction size of the SL treatment groups was smaller than that of the MI group (**Figure 2C**). Compared to the MI group, the percentage of ventricular infract size in the SL 132mg/kg group was 11.4 ± 5.1%, which was significantly reduced ($P < 0.05$, **Figure 2D**), and that in the SL 66mg/kg group was significantly reduced to 12.0 ± 9.1% ($P < 0.05$). In contrast, the whole heart infarct size was 3.8 ± 1.8% in the SL 132mg/kg group and 3.5 ± 2.7% in the SL 66mg/kg group. Overall, these data suggest that SL treatment attenuated myocardial injury in anesthetized dogs.

SL Alleviated Myocardial Ischemia–Reperfusion Injury in Isolated Rat Hearts

A self-made latex balloon connected to a pressure transducer was inserted into the left ventricle. The left ventricular pressure curve was recorded to evaluate heart function in the dogs. During the process of ischemia–reperfusion injury, KH solution was injected into the balloon to make the LVEDP between 0-10 mmHg. The normal value of the LVSP was 50-60 mmHg when the heart was perfused and balanced for 15 min, but LVSP had no significant change of the SL treatment groups compared with the I/R group (**Figure 3A**). After 30 min of ischemia, 448 mg/kg of SL induced a significant increase in LVEDP compared with the I/R group

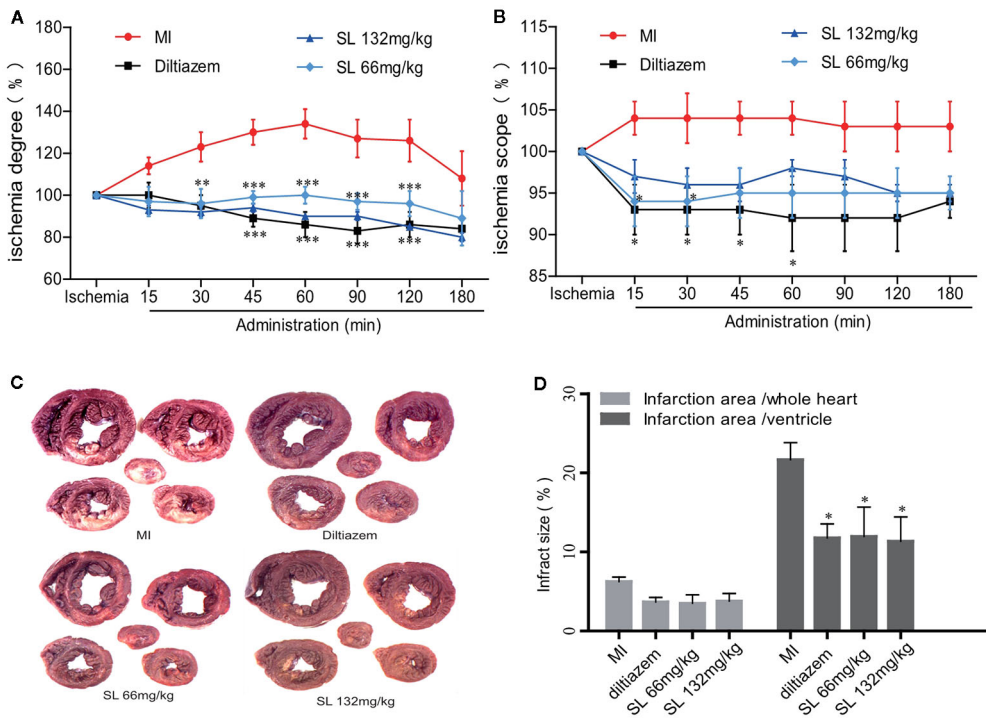

FIGURE 2 | Effects of Shenlian extract (SL) on myocardial ischemia in anesthetized dogs. **(A)** Effects of SL on the degree (Σ-ST) of myocardial ischemia indicated by epicardial electrocardiogram (EECG). **(B)** Effects of SL on the scope (N-ST) of myocardial ischemia as indicated by EECG. **(C)** Effects of SL on the area of myocardial infarction, represented by N-BT staining of the myocardial infarct. **(D)** Effects of SL on the infarction area, quantification of infarction area. Results represent mean ± SEM, n = 6. Statistical analysis was performed by one-way ANOVA, followed by Dunnett's Multiple Comparison test. *$P < 0.05$, *** $P < 0.001$ versus myocardial ischemia (MI) group.

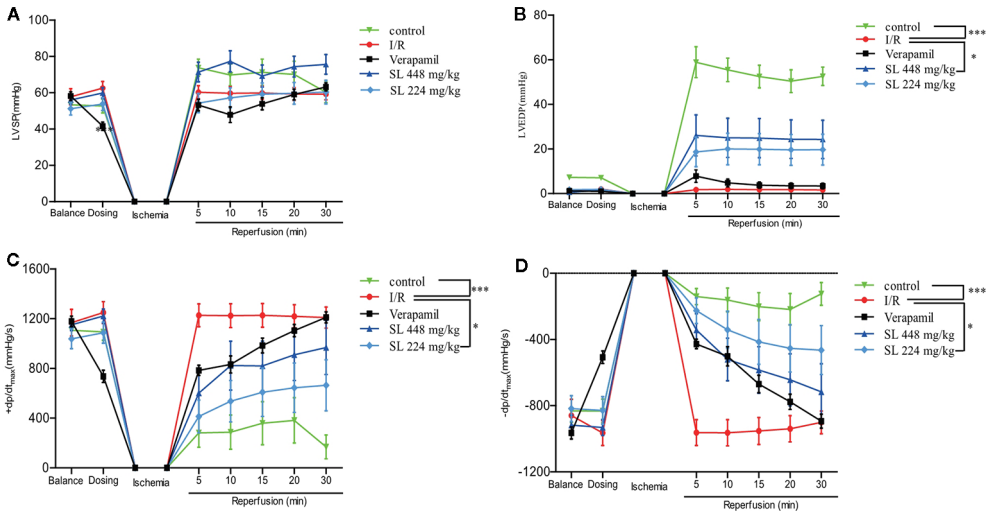

FIGURE 3 | Effects of Shenlian extract (SL) on left ventricular function in isolated rat hearts. **(A)** Changes in the left ventricular systolic pressure (LVSP) by myocardial ischemia and reperfusion by MP150 detection. **(B)** Changes in left ventricular end diastolic pressure (LVEDP) by myocardial ischemia and reperfusion by MP150 detection. **(C)** Changes in + dp/dt_{max} by myocardial ischemia and reperfusion calculated by left ventricular pressure curves. **(D)** Changes in -dp/dt_{max} by myocardial ischemia and reperfusion calculated by left ventricular pressure curves. Results represent mean ± SEM, n = 8. Statistical analysis was performed by one-way ANOVA, followed by Dunnett's Multiple Comparison test. * $P < 0.05$, *** $P < 0.001$ versus the ischemia reperfusion (I/R) group.

($P < 0.05$, **Figure 3B**). The myocardial diastolic function was reflected by ± dp/dt_{max} during the isovolumic contraction phase. The data suggest that there was a significant decreased in both in + dp/dt_{max} and – dp/dt_{max} in the SL 224 mg/kg group compared with the I/R group ($P < 0.05$, **Figures 3C, D**).

SL Protected the Myocardium From Ischemia–Reperfusion Injury by Elevating The Concentration of NF-κB in Isolated Rat Heart

After ischemia and 30 min of reperfusion, myocardial homogenate was made from the heart to detect the biochemical parameters. The levels of LDH, IL-1β and NO were markedly increased ($P < 0.001$, **Figures 4A, C, D**), indicating obvious myocardial injury after the myocardial ischemia–reperfusion. After SL administration, LDH, IL-1β and NO were markedly decreased compared with the I/R group ($P < 0.001$). No differences in MDA concentration between the groups (**Figure 4B**). Collectively, the above-mentioned results suggest that SL treatment protected the isolated heart.

NO regulates blood pressure and maintains blood flow distribution in tissues and organs through vasodilatation. Additionally, NO directly participates in the inflammatory response, and inhibits platelet aggregation and adherence of neutrophils. Some studies have found that the metabolites of NO have strong cytotoxicity and damage cells (Yamaoka et al., 2002). Our results displayed a marked decrease in NO ($P < 0.001$) compared with I/R after SL treatment (**Figure 4D**), evidencing effective control of the typical inflammatory response. Endothelial nitric oxide synthase (eNOS), as an isozyme of NOS, is one of key factors that regulates vascular function. Through production of. NO causes angiectasis and superoxide, which causes vasoconstriction (Lisakovska et al., 2017). Simultaneously, inducible NO synthase (iNOS), another isozyme of NO, is the primary rate-limiting enzyme of the inflammatory response. iNOS and eNOS were significantly decreased in the SL groups compared with the I/R group ($P < 0.05$, **Figures 4E, F**), indicating that SL protected the heart by regulated vascular function.

The PI3K/Akt signaling pathway regulates cardiac function through endothelial cells migration, angiogenesis, ventricular remodeling, and other mechanisms. Akt is phosphorylated after abnormal activation of PI3K pathway, which in turn activates the expression of NF-κB. As NF-κB is a key factor in regulation of the inflammatory signaling networks, the activation of NF-κB not only up-regulates the expression of many pro-inflammatory genes encoding inflammatory mediators and cytokines, including IL-1β, IL-1, and TNF-α, but also activates related enzymes, such as iNOS and vascular cells adhesion molecules, regulating the production of NO, and amplifying the cascade of the inflammatory responses. Our study showed that NF-κB expression was significantly decreased ($P < 0.05$) in the SL 448 mg/kg group compared with the I/R group (**Figure 4G**), but there was no change in the concentration of PI3K between groups (**Figure 4H**). Collectively, SL had a protective effect against NF-κB, similar to the effect against IL-1β. Therefore, SL likely protected against ischemia–reperfusion injury through NF-κB pathway.

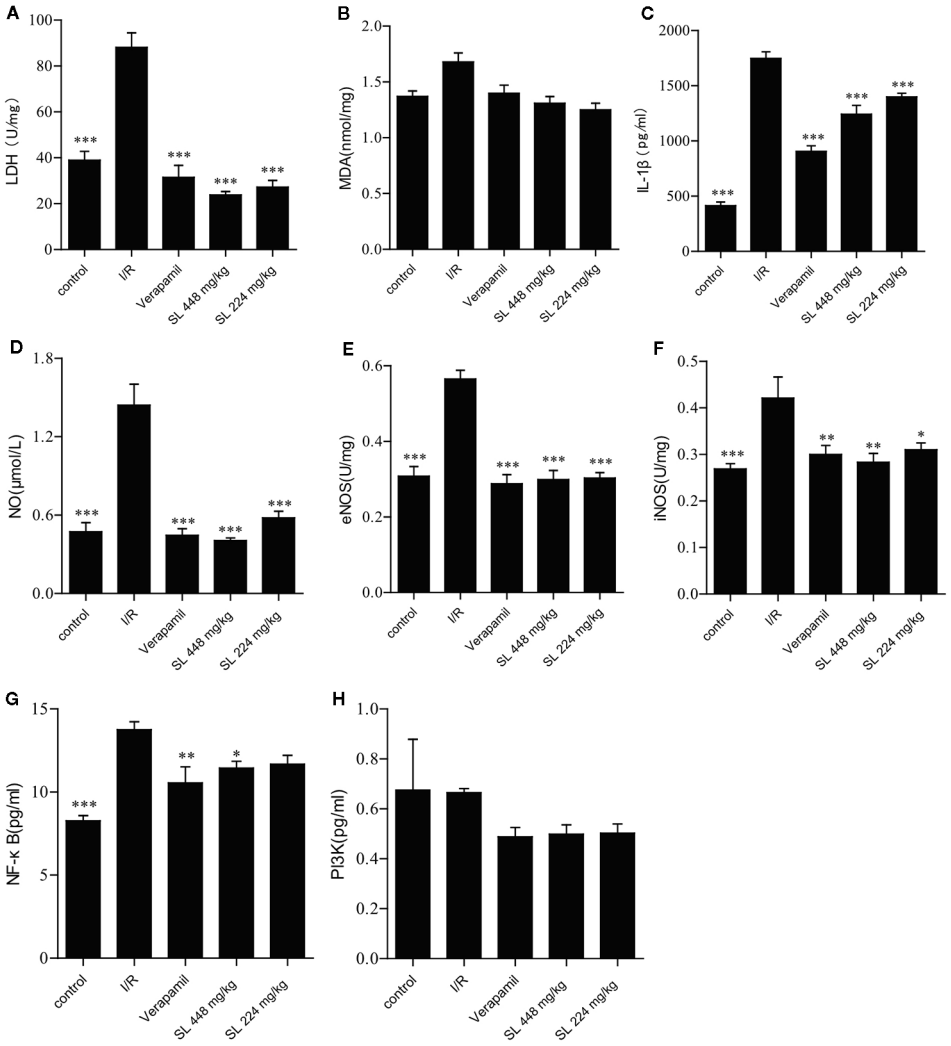

FIGURE 4 | Effects of Shenlian extract (SL) on biochemical parameters in isolated rat hearts. **(A)** Effect of SL on lactate dehydrogenase (LDH) contents in isolated rat hearts. **(B)** Effect of SL on malondialdehyde (MDA) contents in isolated rat hearts. **(C)** Effect of SL on interleukin (IL)-1β contents in isolated rat hearts. **(D)** Effect of SL on nitric oxide (NO) contents in isolated rat hearts. **(E)** Effect of SL on nitric oxide synthase e(NOS) contents in isolated rat hearts. **(F)** Effect of SL on iNOS contents in isolated rat hearts. **(G)** Effect of SL on NF-κB contents in isolated rat hearts. **(H)** Effect of SL on PI3K contents in isolated rat hearts. Results represent mean ± SEM, n = 8. Statistical analysis was performed by one-way ANOVA, followed by Dunnett's Multiple Comparison test. * $P < 0.05$, ** $P < 0.01$, *** $P < 0.001$ versus the ischemia reperfusion (I/R) group.

SL Protected H9c2 Cells From H_2O_2-Induced Damage

Based on the results in anesthetized dogs and isolated rat hearts, H9c2 cells induced by H_2O_2 were used to identify key targets responsible for the effect of SL. After H_2O_2-induction, LDH concentration increased significantly compared with the untreated group ($P < 0.001$, **Figure 5A**). After SL treatment, LDH significantly decreased in the SL 50 μg/mL ($P < 0.001$) and 25 μg/mL ($P < 0.01$) groups compared with the H_2O_2 group. Similar to the LDH contents, NO and IL-1β expression decreased significantly in the SL 50 μg/mL ($P < 0.001$) and 25 μg/mL ($P < 0.01$) groups compared with the H_2O_2 group (**Figures 5B, C**). These results revealed that SL could reduce the concentration of cellular damaged indicators, and effectively protect the cells from injury and inflammatory response.

NF-κB Was One of the Important Pathways for the Protective Effect of SL Against Myocardial Ischemic Injury

The phosphorylation levels of eight related signal transduction proteins were detected to explore the mechanism of SL treatment. The phosphorylation levels of IκB-α in H_2O_2 group were significantly increased compared with the untreated group, and 25 μg/mL of SL could reduce the expression of p-IκB-α compared with the H_2O_2 group ($P < 0.01$, **Figure 5D**). However, there were no significant changes in p-ERK1/2, p-p38 MAPK, p-c-JUN, p-

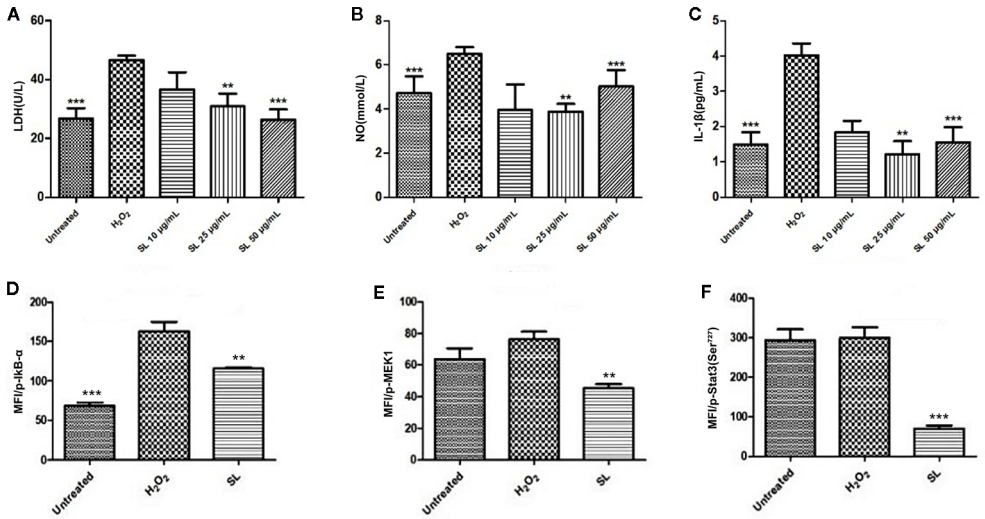

FIGURE 5 | Effect of Shenlian extract (SL) on H_2O_2-induced damage in H9c2 cells. **(A)** Effect of SL on lactate dehydrogenase (LDH) contents in H9c2 cells by H_2O_2-induction for 6 h. **(B)** Effect of SL on nitric oxide (NO) contents in H9c2 cells by H_2O_2-induction for 6 h. **(C)** Effect of SL on interleukin (IL)-1β contents in H9c2 cells by H_2O_2-induction for 6 h. **(D)** Effect of SL on p-IκB in H9c2 cells by H_2O_2-inductionfor 6 h by Bio-Plex array analysis. **(E)** Effect of SL on p-MEK1 in H9c2 cells by H_2O_2-induction for 6 h by Bio-Plex array analysis. **(F)** Effect of SL on p-Stat3 in H9c2 cells by H_2O_2-induced for 6 h by Bio-Plex array analysis. Results represent mean ± SEM of three independent experiments. Statistical analysis was performed by one-way ANOVA, followed by Dunnett's Multiple Comparison test. $^{**}P < 0.01$, $^{***}P < 0.001$ the H_2O_2-induced (H2O2) group.

IGF-IR, and p-Akt expression. And the expression of p-Stat3 ($P < 0.001$) and p-MEK ($P < 0.01$) were significantly decreased after 25 μg/mL of SL compared with H_2O_2 group (**Figures 5E, F**).

SL can reduce the expression of p-IκB-α in H_2O_2-induced cells *via* IKK kinase activity or protein degradation. Based on the SL-inhibited phosphorylation of IκB, further studies using the proteasome inhibitor, MG132, and IKK inhibitor, parthenolide, were conducted to observe the protective effect of SL in H_2O_2 stimulated H9c2 cells. The results suggest that 5 μM of MG132 partially reversed the inhibitory effect of SL on the expression of F-actin in H_2O_2-induced cells (**Figure 6A**), and increased NO and IL-1β in the cell supernatant. At a dose of 10 μM of MG132, SL completely reversed the effect of H_2O_2 induction, and significantly increased NO and IL-1β contents compared with 25 μg/mL of SL ($P < 0.05$, **Figures 6B, C**). In contrast, 5 μM and 10 μM of parthenolide had no significant effect on SL. These data suggest that the regulation of NF-κB by SL primarily affects the degradation of IκB by proteasome, leading to the inhibition of the nuclear translocation of NF-κB, which affects the activation of NF-κB pathway. This is independent of IKK kinase.

DISCUSSION

Previous studies have shown that SL inhibits and stabilizes atherosclerosis plaques through inflammatory reactions and plaque destabilization, which inhibits the expression of the inflammatory mediators, IL-10 and MCP-1, further increasing the expression of the metabolite of inflammatory dispersalin, LXA4 (Li et al., 2011). Furthermore, Guo Y (Guo et al., 2016) concluded that SL inhibits the formation of atherosclerotic plaques in the carotid artery and reduces the degree of lesions in $ApoE^{-/-}$ mice. SL regulates lipid metabolism by reducing the inflammatory biomarkers such as TC, TG and LDL. Meanwhile, by established an EC-SMC-MC co-culture system, the study showed that tanshinone IIA, an active ingredient of SL, exhibited significant efficacy against atherosclerosis and inhibited the inflammatory MMP-2 and NF-κB pathway (Li et al., 2015). SL plays a role in protecting against atherosclerosis by intervening against plaque formation and plaque instability.

This is the first report on the direct protection of SL against myocardial ischemic injury. This protective effect was observed, and its mechanism was preliminarily explored. In the animal models, SL treatment in anesthetized dogs and Langendorff-perfused rats had a significant protective effect on myocardial ischemia injury. Detection of markers of inflammation in isolated hearts highlights that SL protects against myocardial injury induced by ischemia via the NF-κB pathway. This result was further verified in H_2O_2-induced cells, which indicated that degradation of IκB was a core target for SL.

We successfully established a LAD coronary artery ligation model on anesthetized dogs, and data were gathered from an EECG to calculate the degree and scope of the ST segment. The ST segment increased a degree in the MI group and reduced in the N-ST scope. The myocardial tissue was collected to detect the myocardial infarction size by N-BT staining. The myocardial infarction size was significantly decreased after SL treatment with a 10% decreasing amplitude. As a whole, SL had a protective effect on the ischemic heart and could reduce myocardial infarct size.

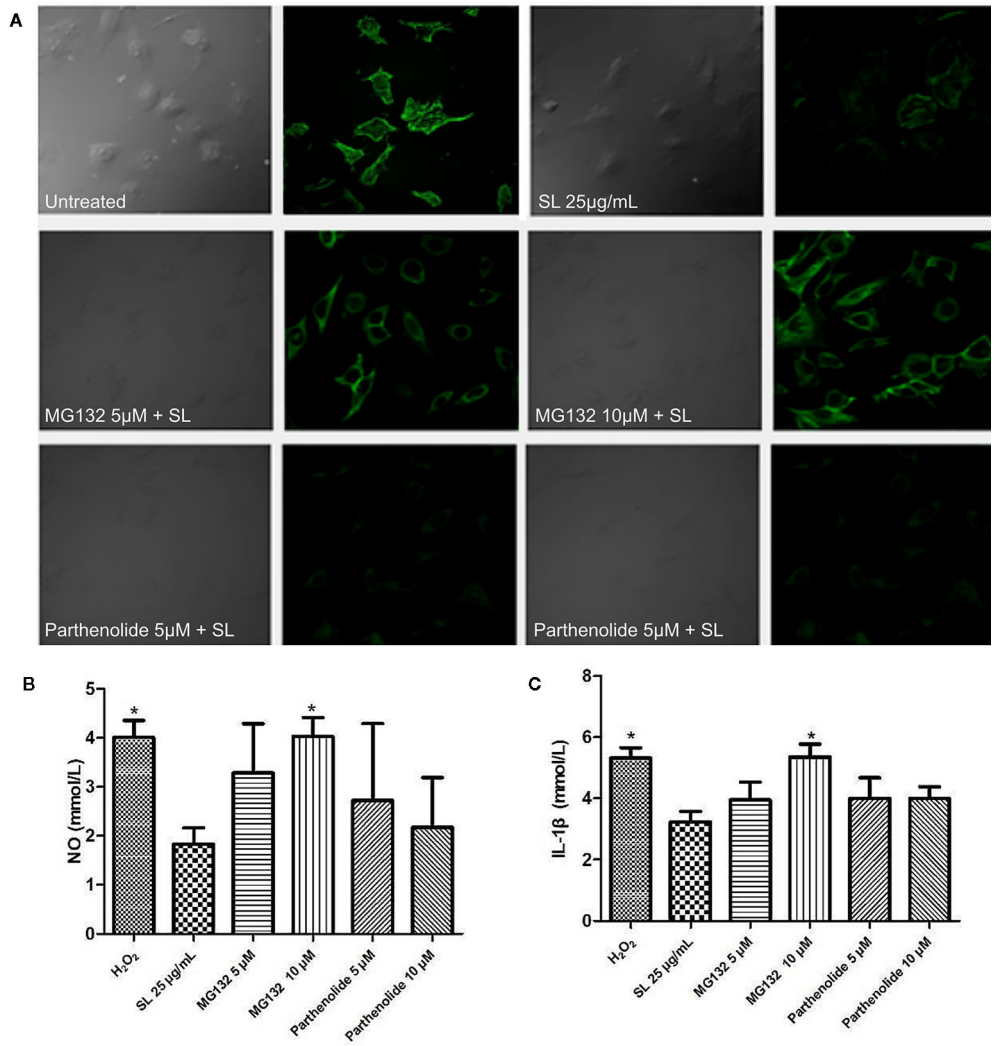

FIGURE 6 | Shenlian extract (SL) affects the degradation of IκB by the proteasome in the NF-κB pathway. **(A)** The expression of F-actin after the proteasome inhibitor, MG132 (5μM, 10μM), and IKK inhibitor, parthenolide (5μM, 10μM), were added to cultivate cells for 12 h before drug treatment. Staining with fluorescently labeled phalloidin, which is displayed in green, clearly shows the distribution of F-actin in the cells. Representative image chosen by 5 visual fields and photos by Laser Scanning Confocal Microscope. **(B)** Effect of SL on nitric oxide (NO) in by H_2O_2-induced cells with the added proteasome inhibitor and IKK inhibitor in H9c2 cells for 6 h. **(C)** Effect of SL on interleukin (IL)-1β contents in H_2O_2-induced H9c2 cells for 6 h with the added proteasome inhibitor 2 and IKK inhibitor. **(B, C)** represent the mean ± SEM of three independent experiments. Statistical analysis was performed by one-way ANOVA, followed by Dunnett's Multiple Comparison test. * $P < 0.05$ versus the SL 25 μg/mL group.

In another experiment, the Langendorff-perfused rat heart model was established, and we found that SL also had a same effect on isolated rat hearts by monitoring the parameters of the left ventricular function. As indicators of reflecting and evaluating left ventricular systolic and diastolic function, LVEDP and ± dp/dt_{max}, respectively, improved the heart function of the SL treatment after perfusion, which verified the protective effect of SL. In general, SL improved myocardial contractility to ensure well supplied blood to the heart.

Previous pathological studies have shown that IHD and acute myocardial infarction, as main clinical manifestations, have increasingly become a major cause of death (Zhao et al., 2019). IHD and acute myocardial infarctions are associated with atherosclerosis (Esper and Nordaby, 2019), a chronic inflammatory disease that is characterized by the development of cholesterol-rich arterial plaques (Stary et al., 1994) due to several factors, such as hyperlipidaemia, inflammation, oxidative stress, and immune cell infiltration (Viola and Soehnlein, 2015; Libby et al., 2016). Ischemia and necrotic cardiomyocytes would trigger early inflammation through IL-1β signaling and the NF-κB pathway (Latet et al., 2015; Sager et al., 2017; Michels et al., 2019). In the present study, inflammation markers were detected

by related kits in isolated hearts, and the results indicated that SL could interfere with myocardial injury under ischemia–reperfusion conditions. SL inhibited the increase in LDH and IL-1β, which may be related to the inflammatory response and lipid peroxidation. Additionally, when cells are stimulated by inflammatory factors, they can produce a large amount of NO. NO is a free radical that can react with a superoxide anion to form a highly oxidized peroxynitrite anion ($ONOO^-$), which causes lipid peroxidation and directly damages endothelial cells (Szabó et al., 1996). NO can also increase the expression of adhesion molecules and inflammation factors (Bonafede and Manucha, 2018). In addition, excessive peroxynitrite further leads to increased levels of nitrative tyrosine and decreased biological activity of NO, further causing DNA damage (Nowak et al., 2017). Our study showed that SL had a protective effect against increasing NO levels in myocardial ischemia injury, and had a significant improvement in nitrogen oxidative stress. Similarly, SL treatment groups had significantly decreased levels of eNOS and iNOS compared with the I/R group.

NF-κB is a key factor in the regulation of the inflammatory signaling networks, and the PI3K/Akt signaling pathway may activate NF-κB. For these reasons, our study detected the expression of related inflammatory factors on the PI3K pathway. NF-κB and IL-1β contents were significantly decreased in the SL treatment groups; however, there was no change in PI3K levels. These findings suggested that SL may protect against myocardial ischemia injury by affecting the NF-κB pathway, further regulating the level of the inflammatory response.

Large amounts of ROS, which is one of the main factors of myocardial cells death, can be produced during myocardial ischemia and reperfusion. H_2O_2 can simulate the pathological process to establish an ideal model for I/R *in vitro*. Our study used optimized H9c2 cell and stimulated oxidative stress by treating with H_2O_2. This H_2O_2-induced injury model has been shown in previous studies (Li Y. et al., 2016). H_2O_2, a source of ROS, can directly oxidize lipids and proteins on cell membranes. H_2O_2 can generate more active free radicals such as ·OH through reacting with iron ions, then induced cell apoptosis or necrosis. After H_2O_2-induction, the present study found that LDH, NO, and IL-1β contents had a significant decreased in the SL groups compared with the H_2O_2-induced group, which is consistent with the results found in the isolated heart. On this basis, Bio-Plex array analysis was used to further investigate the phosphorylation of related signal molecules and the intervention of SL, which explored eight phosphorylated signaling molecule: p-IκB, p-ERK1/2, p-p38 MAPK, p-Stat3, p-c-JUN, p-IGF-IR, p-MEK, and p-Akt. Twenty-five micrograms per millilitre of SL reduced p-IκB compared with the H_2O_2 group, which indicated that p-IκB was a core point for SL to inhibit myocardial ischemic injury.

Our study used the proteasome inhibitor, MG132, and the IKK kinase inhibitor, parthenolide, to observe NF-κB activation pathway. The results showed that MG132 at 5 μM partially reversed the inhibitory effect of SL on the expression of F-actin in H_2O_2-induced cells. The effect on NO and IL-1β also decreased; however, parthenolide had no significant effect on the SL-induced response. The results indicated that SL play its role may be mainly related to mechanism modulating degradation of IκB, and affected the activation of NF-κB pathway indirectly.

CONCLUSION

In conclusion, SL had a protective effect on myocardial ischemic injury. This conclusion was supported in three ways. First, SL effectively protected the degree and scope of myocardial ischemia and significantly decreased the area of myocardial infarction. SL maintained decent blood supply to the heart by improving myocardial contractility. Second, SL regulated the immune system by effectively reducing IL-1β, NO, iNOS, and eNOS contents. This result suggests modulation of the NF-κB pathway. Finally, SL primarily affected the degradation of IκB by proteasome, as shown through an inhibition study, in an IKK-independent manner. This reduction in IκB degradation caused by SL prevented the nuclear translocation of NF-κB, which affected the activation of the NF-κB pathway. As shown in the myocardial ischemia models of our study, the intervention of inflammatory response may be the core mechanism by which SL played its therapeutic effect. The present results showed that SL could protect against the common pathological cycle between the different stages of atherosclerosis and inflammation. These studies may provide new ideas and tools for intervention of myocardial ischemia cardiovascular disease, and be helpful in the prevention and treatment of cardiovascular diseases in the future.

DATA AVAILABILITY STATEMENT

All datasets generated for this study are included in the article/**Supplementary Material**.

ETHICS STATEMENT

The animal study was reviewed and approved by Guidance for the Care and Use of Laboratory Animals issued by the Ministry of Science and Technology of China and the Use Committee of Institute of Basic Theory for Chinese Medicine, China Academy of Chinese Medicine Science.

AUTHOR CONTRIBUTIONS

YG participated in most of the experiments, analyzed the data and wrote the manuscript. QY contributed to the experiment design and the experiments work. X-GW and Y-JW contributed to the experiment implementation. X-QH performed and analyzed the experiments. X-JZ and Y-JL reviewed the results and approved the version of the manuscript. X-XZ took charge of

the research design and coordinated the whole project. All authors contributed to reviewing the results, writing the manuscript, and approving the final version of the manuscript.

FUNDING

This work was supported by the National Natural Science Foundation of China (81573649, 81673640), and the experiment was funded by the Institute of Chinese Materia Medica, China Academy of Chinese Medical Sciences.

SUPPLEMENTARY MATERIAL

The Supplementary Material for this article can be found online at: https://www.frontiersin.org/articles/10.3389/fphar.2020.00134/full#supplementary-material

REFERENCES

Akbalaeva, B. A., Batyraliev., T. A., Fettzer, D. V., and Sidorenko, B. A. (2017). Ischemic heart disease: focus on acute infarction of the right ventricular myocardium. *Kardiologiia* (1), 90–94.

Bell, R. M., Mocanu, M. M., and Yellon, D. M. (2011). Retrograde heart perfusion: the Langendorff technique of isolated heart perfusion. *J. Mol. Cell Cardiol.* 50, 940–950. doi: 10.1016/j.yjmcc.2011.02.018

Berger, H. J., Zaret, B. L., Speroff, L., Cohen, L. S., and Wolfson, S. (1976). Regional cardiac prostaglandin release during myocardial ischemia in anesthetized dogs. *Circ. Res.* 38, 566–571. doi: 10.1161/01.res.38.6.566

Bergmann, M. W., Loser, P., Dietz, R., and von, Harsdorf, ,. R. (2001). Effect of NF-kappa B Inhibition on TNF-alpha-induced apoptosis and downstream pathways in cardiomyocytes. *J. Mol. Cell Cardiol.* 33, 1223–1232. doi: 10.1006/jmcc.2001.1385

Bertrand, M. J., and Tardif, J. C. (2017). Inflammation and beyond: new directions and emerging drugs for treating atherosclerosis. *Expert Opin. Emerg. Drugs* 22, 1–26. doi: 10.1080/14728214.2017.1269743

Bonafede, R., and Manucha, W. (2018). Nitric oxide and related factors linked to oxidation and inflammation as possible biomarkers of heart failure. *Clin. Invest. Arterioscler.* 30, 84–94. doi: 10.1016/j.arteri.2017.12.004

Esper, R. J., and Nordaby, R. A. (2019). Cardiovascular events, diabetes and guidelines: the virtue of simplicity. *Cardiovasc. Diabetol.* 18, 42. doi: 10.1186/s12933-019-0844-y

Foks, A. C., and Bot, I. (2017). Preface: pathology and pharmacology of atherosclerosis. *Eur. J. Pharmacol.* 816, 1–2. doi: 10.1016/j.ejphar.2017.10.052

Fu, J. H., Zheng, Y. Q., Li, P., Li, X. Z., Shang, X. H., and Liu, J. X. (2013). Hawthorn leaves flavonoids decreases inflammation related to acute myocardial ischemia/reperfusion in anesthetized dogs. *Chin. J. Integr. Med.* 19, 582–588. doi: 10.1007/s11655-012-1250-4

Guo, Y., Liu, X. C., Wang, Y. J., Li, Q., Yang, Q., Weng, X. G., et al. (2016). Effects of Shenlian extract on experimental atherosclerosis in ApoE-deficient mice based on ultrasound biomicroscopy. *BMC Complement Altern. Med.* 16, 469. doi: 10.1186/s12906-016-1449-6

Hansson, G. K. (2017). Inflammation and atherosclerosis: the end of a controversy. *Circulation* 136, 1875–1877. doi: 10.1161/CIRCULATIONAHA.117.030484

Herrington, W., Lacey, B., Sherliker, P., Armitage, J., and Lewington, S. (2016). Epidemiology of atherosclerosis and the potential to reduce the global burden of atherothrombotic disease. *Circ Res.* 118, 535–546. doi: 10.1161/CIRCRESAHA.115.307611

Latet, S. C., Hoymans, V. Y., Van Herck, P. L., and Vrints, C. J. (2015). The cellular immune system in the post-myocardial infarction repair process. *Int. J. Cardiol.* 179, 240–247. doi: 10.1016/j.ijcard.2014.11.006

Li, M., Zhao, C., Wong, R. N., Goto, S., Wang, Z., and Liao, F. (2004). Inhibition of shear-induced platelet aggregation in rat by tetramethylpyrazine and salvianolic acid B. *Clin. Hemorheol. Microcirc.* 31, 97–103.

Li, Y. J., Chen, Y., You, Y., Weng, X. G., Yang, Q., Ruan, C. X., et al. (2011). Effects of shenlian extracts on atherosclerosis by inhibition of the inflammatory response. *J. Tradit. Chin. Med.* 31, 344–348. doi: 10.1016/S0254-6272(12)60016-8

Li, Y., Guo, Y., Chen, Y., Wang, Y., You, Y., Yang, Q., et al. (2015). Establishment of an interleukin-1β-induced inflammation-activated endothelial cell-smooth muscle cell-mononuclear cell co-culture model and evaluation of the anti-inflammatory effects of tanshinone IIA on atherosclerosis. *Mol. Med. Rep.* 12, 1665–1676. doi: 10.3892/mmr.2015.3668

Li, Y., Bao, T., Li, Q., Chen, X., Wang, Y., Yang, Q., et al. (2016). Protective effect of compound ginkgo biloba granules on H_2O_2-induced H9c2 cell damage. *Chin. Herbal Med.* 47, 459–465. (in Chinese).

Li, Y. J., Ruan, C. X., Yang, Q., Weng, X. G., Chen, Y., Wang, Y. J., et al. (2016). Establishment of vulnerable plaque model by mast cell activation in adventitia and evaluation of effectiveness of intervention of Shenlian tablet. *Yao Xue Xue Bao.* 51, 1263–1270. (in Chinese). doi: 10.16438/j.0513-4870.2016-0156

Libby, P., Bornfeldt, K. E., and Tall, A. R. (2016). Atherosclerosis: successes, surprises, and future challenges. *Circ. Res.* 118, 531–534. doi: 10.1161/CIRCRESAHA.116.308334

Libby, P. (2017). Interleukin-1 beta as a target for atherosclerosis therapy: biological basis of CANTOS and beyond. *J. Am. Coll. Cardiol.* 70, 2278–2289. doi: 10.1016/j.jacc.2017.09.028

Lisakovska, O., Shymanskyy, I., Mazanova, A., Khomenko, A., and Veliky, M. (2017). Vitamin D3 protects against prednisolone-induced liver injury associated with the impairment of the hepatic NF-κB/iNOS/NO pathway. *Biochem. Cell Biol.* 95, 213–222. doi: 10.1139/bcb-2016-0070

Lukinavičius, G., Reymond, L., D'Este, E., Masharina, A., Göttfert, F., Ta, H., et al. (2014). Fluorogenic probes for live-cell imaging of the cytoskeleton. *Nat. Methods* 11, 731–733. doi: 10.1038/nmeth.2972

Michels, da S. D., Langer, H., and Graf, T. (2019). Inflammatory and molecular pathways in heart failure-ischemia, HFpEF and transthyretin cardiac amyloidosis. *Int. J. Mol. Sci.* 20, 1–28. doi: 10.3390/ijms20092322

Moran, A. E., Forouzanfar, M. H., Roth, G. A., Mensah, G. A., Ezzati, M., Murray, C. J., et al. (2014). Temporal trends in ischemic heart disease mortality in 21 world regions 1980 to 2010: the Global Burden of Disease 2010 study. *Circulation* 129, 1483–1492. doi: 10.1161/CIRCULATIONAHA.113.004042

Nowak, W. N., Deng, J., Ruan, X. Z., and Xu, Q. (2017). Reactive oxygen species generation and atherosclerosis. *Arterioscler. Thromb. Vasc. Biol.* 37, e41–e52. doi: 10.1161/ATVBAHA.117.309228

Ojha, S. K., Bharti, S., Joshi, S., Kumari, S., and Arya, D. S. (2012). Protective effect of hydroalcoholic extract of Andrographis paniculata on ischaemia-reperfusion induced myocardial injury in rats. *Indian J. Med. Res.* 135, 414–421.

Pang, H., Wu, L., Tang, Y., Zhou, G., Qu, C., and Duan, J. A. (2016). Chemical analysis of the herbal medicine Salviae miltiorrhizae Radix et Rhizoma (Danshen). *Molecules* 21, 51. doi: 10.3390/molecules21010051

Planavila, A., Sánchez, R. M., Merlos, M., Laguna, J. C., and Vázquez-Carrera, M. (2005). Atorvastatin prevents peroxisome proliferator-activated receptor gamma coactivator-1 (PGC-1) downregulation in lipopolysaccharide-stimulated H9c2 cells. *Biochim. Biophys. Acta* 1736, 120–127. doi: 10.1016/j.bbalip.2005.08.001,

Sager, H. B., Kessler, T., and Schunkert, H. (2017). Monocytes and macrophages in cardiac injury and repair. *J. Thorac. Dis.* 9, S30–S35. doi: 10.21037/jtd.2016.11.17

Song, M., Huang, L., Zhao, G., and Song, Y. (2013). Beneficial effects of a polysaccharide from Salvia miltiorrhiza on myocardial ischemia-reperfusion injury in rats. *Carbohydr. Polym.* 98, 1631–1636. doi: 10.1016/j.carbpol.2013.08.020

Stary, H. C., Chandler, A. B., Glagov, S., Guyton, J. R., Insull, W.Jr., Rosenfeld, M. E., et al. (1994). A definition of initial, fatty streak, and intermediate lesions of atherosclerosis. a report from the Committee on Vascular Lesions of the Council on Arteriosclerosis, *American Heart Association*. *Circulation* 89, 2462–2478. doi: 10.1161/01.CIR.89.5.2462

Szabó, C., Zingarelli, B., O'Connor, M., and Salzman, A. L. (1996). DNA strand breakage, activation of poly (ADP-ribose) synthetase, and cellular energy depletion are involved in the cytotoxicity of macrophages and smooth muscle cells exposed to peroxynitrite. *Proc. Natl. Acad. Sci. U. S. A.* 93, 1753–1758. doi: 10.1073/pnas.93.5.1753

Tang, M. K., Ren, D. C., Zhang, J. T., and Du, G. H. (2002). Effect of salvianolic acids from Radix Salviae miltiorrhizae on regional cerebral blood flow and platelet aggregation in rats. *Phytomedicine* 9, 405–409. doi: 10.1078/09447110260571634

Viola, J., and Soehnlein, O. (2015). Atherosclerosis - a matter of unresolved inflammation. *Semin. Immunol.* 27, 184–193. doi: 10.1016/j.smim.2015.03.013

Wang, M., Chen, L., Liu, D., Chen, H., Tang, D. D., and Zhao, Y. Y. (2017). Metabolomics highlights pharmacological bioactivity and biochemical mechanism of traditional Chinese medicine. *Chem. Biol. Interact.* 273, 133–141. doi: 10.1016/j.cbi.2017.06.011

Wang, L., Li, Y., Deng, W., Dong, Z., Li, X., and Liu, D. (2018). Cardio-protection of ultrafine granular powder for Salvia miltiorrhiza Bunge against myocardial infarction. *J. Ethnopharmacol.* 222, 99–106. doi: 10.1016/j.jep.2018.04.029

Xu, J., Lian, F., Zhao, L., Zhao, Y., Chen, X., Zhang, X., et al. (2015). Structural modulation of gut microbiota during alleviation of type 2 diabetes with a Chinese herbal formula. *ISME J.* 9, 552–562. doi: 10.1038/ismej.2014.177

Yamaoka, J., Kabashima, K., Kawanishi, M., Toda, K., and Miyachi, Y. (2002). Cytotoxicity of IFN-gamma and TNF-alpha for vascular endothelial cell is mediated by nitric oxide. *Biochem. Biophys. Res. Commun.* 291, 780–786. doi: 10.1006/bbrc.2002.6487

You, Y., Liu, W., Li, Y., Zhang, Y., Li, D., Li, W., et al. (2011). Joint preventive effects of swimming and Shenlian extract on rat atherosclerosis. *Clin. Hemorheol. Microcirc.* 47, 187–198. doi: 10.3233/CH-2010-1380

Ytrehus, K. (2000). The ischemic heart–experimental models. *Pharmacol. Res.* 42, 193–203. doi: 10.1006/phrs.2000.0669

Zhang, X., Zhao, Y., Xu, J., Xue, Z., Zhang, M., Pang, X., et al. (2015). Modulation of gut microbiota by berberine and metformin during the treatment of high-fat diet-induced obesity in rats. *Sci. Rep.* 14405, 1–10. doi: 10.1038/srep14405

Zhao, D., Liu, J., Wang, M., Zhang, X., and Zhou, M. (2019). Epidemiology of cardiovascular disease in China: current features and implications. *Nat. Rev. Cardiol.* 16, 203–212. doi: 10.1038/s41569-018-0119-4

Zhou, S. Y., Wang, Y. H., Li, Y. J., Yang, Q., Gong, Z. P., Ruan, C. X., et al. (2013). Effect of Shenlian extracts on blood flow and vessel pathological changes in rabbits carotid atherosclerosis model induced by low shear stress. *Zhongguo Zhong Yao Za Zhi.* 38, 1595–1600. (in Chinese).

Zou, W., Xiao, Z., Wen, X., Luo, J., Chen, S., Cheng, Z., et al. (2016). The anti-inflammatory effect of Andrographis paniculata (Burm. f.) Nees on pelvic inflammatory disease in rats through down-regulation of the NF-κB pathway. *BMC Complement Altern. Med.* 16, 483. doi: 10.1186/s12906-016-1466-5

Conflict of Interest: The authors declare that the research was conducted in the absence of any commercial or financial relationships that could be construed as a potential conflict of interest.

frontiers in Pharmacology

SYSTEMATIC REVIEW
published: 10 March 2020
doi: 10.3389/fphar.2020.00213

Dazhu Hongjingtian Preparation as Adjuvant Therapy for Unstable Angina Pectoris: A Meta-Analysis of Randomized Controlled Trials

*Changfeng Man, Zhe Dai and Yu Fan**

Institute of Molecular Biology and Translational Medicine, The Affiliated People's Hospital, Jiangsu University, Zhenjiang, China

OPEN ACCESS

Edited by:
Jianxun Liu,
China Academy of Chinese Medical Sciences, China

Reviewed by:
Fang Lu,
China Academy of Chinese Medical Sciences, China
Zhong Wang,
China Academy of Chinese Medical Sciences, China
Michael Heinrich,
UCL School of Pharmacy, United Kingdom

***Correspondence:**
Yu Fan
jszjfanyu@163.com

Specialty section:
This article was submitted to Ethnopharmacology, a section of the journal Frontiers in Pharmacology

Received: *11 February 2019*
Accepted: *14 February 2020*
Published: *10 March 2020*

Citation:
Man C, Dai Z and Fan Y (2020) Dazhu Hongjingtian Preparation as Adjuvant Therapy for Unstable Angina Pectoris: A Meta-Analysis of Randomized Controlled Trials. Front. Pharmacol. 11:213. doi: 10.3389/fphar.2020.00213

Objective: Dazhu hongjingtian [DZHJT, *Rhodiola wallichiana* var. *cholaensis* (Praeger) S.H. Fu] preparation as an add-on therapy has been applied to the treatment of angina pectoris. We aimed to evaluate the efficacy and safety of DZHJT as adjuvant therapy for the treatment of unstable angina pectoris (UAP).

Methods: An extensive literature search was conducted on PubMed, Emase, Cochrane Library, Wanfang, CNKI, and VIP databases from inception to January 2019. Randomized controlled trials (RCTs) comparing DZHJT in combination with Western medicine with Western medicine alone were included. Two authors independently performed the literature search, data extraction and risk of bias assessment of included studies, and conducted the statistical analysis.

Results: A total of 18 RCTs involving 1,679 patients were included in the meta-analysis. Adjuvant treatment with DZHJT significantly decreased ≥80% reduction in the frequency of angina attacks [risk ratio (RR) 1.57; 95% CI 1.36–1.81], weekly frequency of angina attacks [mean difference (MD) −1.03 times; 95% confidence interval (CI) −1.51 to −0.55], marked improved abnormal electrocardiogram (RR 1.46; 95% CI 1.23–1.74). In addition, DZHJT significantly reduced the whole-blood viscosity (MD −0.70 mPa.s; 95% CI −0.84 to −0.55), plasma viscosity (MD −0.28 mPa.s; 95% CI −0.38 to −0.19), serum level of fibrinogen (MD −0.67 g/L; 95% CI −0.79 to −0.54), thromboxanes B2 (MD −14.01 ng/L; 95% CI −20.86 to −7.15), and C-reactive protein (MD −1.48 mg/L; 95% CI −2.72 to −0.25). No significant differences in headache/dizziness (RR 0.72; 95% CI 0.31–1.67) were observed between two groups.

Conclusion: Adjuvant treatment with DZHJT has an add-on effect in reducing angina pectoris attacks in patients with UAP. The beneficial effect may be correlated with regulating whole-blood viscosity, plasma viscosity, fibrinogen, thromboxanes B2, and CRP level. However, future well-designed prospective, randomized, double-blind placebo-controlled trials with large sample sizes are required to evaluate the evidence.

Keywords: Dazhu hongjingtian, *Rhodiola wallichiana*, unstable angina pectoris, angina attacks, blood rheology, meta-analysis

INTRODUCTION

Angina pectoris is a symptomatic condition characterized by chest pain attacks. It is clinically classified into stable angina pectoris (SAP) and unstable angina pectoris (UAP). UAP is a type of acute coronary syndrome characterized by an attack at rest and severe, prolonged, and frequent or newly developed angina pectoris (Basra et al., 2016). The population weighted prevalence of UAP is 5.7% in men and 6.7% in women (Hemingway et al., 2008). UAP is associated with higher risk of acute myocardial infarction and sudden death. The current therapeutic strategy of angina pectoris mainly includes anti-ischemia, anti-thrombosis, and anti-platelet or revascularization procedures (Parikh and Kadowitz, 2014; Silva et al., 2015).

Dazhu hongjingtian (DZHJT)/*Rhodiola wallichiana* var. *cholaensis* [Praeger] S.H. Fu (R. wallichiana var.) has been frequently introduced to patients with angina pectoris in China (Fan et al., 2005). R. wallichiana var. is used for preparing DZHJT injection/capsule preparation, extracted from the root and rhizome. These preparations (detailed information of DZHJT is provided in **Supplemental Text S1**) have been approved by the Food and Drug Administration of China. Cardiovascular effects of DZHJT have been described in the dilation of cardiac vessels and reduction of myocardial oxygen consumption (Zhang et al., 2005). In addition, DZHJT also has anti-inflammatory activity (Choe et al., 2012), anti-diabetic effect (Gao et al., 2009), and sedative–hypnotic property (Li et al., 2007). Clinically, DZHJT is mainly used to treat angina pectoris (Jiang and Pan, 2012). A previous well-designed meta-analysis (Chu et al., 2014) has demonstrated the beneficial effects of DZHJT in SAP patients. Several clinical studies (Yu et al., 2011; Chen, 2013; Zhang, 2013; Cao et al., 2014; Jia and Wang, 2014; Li and Zhao, 2014; Shen et al., 2014) have investigated the add-on effects of the DZHJT in patients with UAP, but the findings were limited by small sample sizes and varying study quality. Therefore, we conducted this meta-analysis of randomized controlled trials (RCT) to assess the efficacy and safety of DZHJT as adjuvant therapy for patients with UAP.

MATERIALS AND METHODS

Literature Search

We conducted this meta-analysis following the checklists of the Preferred Reporting Items for Systematic Reviews and Meta-Analyses Guidelines (Liberati et al., 2009). This meta-analysis was registered in the PROSPERO international database of prospectively registered systematic reviews (PROSPERO CRD42018111885). Two authors systematically searched PubMed, Embase, Cochrane Library, China Science and Technology Journal Database (VIP), China National Knowledge Infrastructure (CNKI), and Wanfang Database and from inception to January 2019. The searching items for English medical literature were "unstable angina pectoris" OR "angina" OR "acute coronary syndrome" AND "rhodiola" OR "hong jing tian" OR "hongjingtian" AND "randomized controlled trial" OR "randomized" OR "randomized." Chinese searching terms included "bù wěn dìng xíng xin jiǎo tòng" OR "unstable angina pectoris" AND "hóng jing tiān" OR "rhodiola" AND "suí ji" AND "duìzhào." A manual search was performed using the reference lists of relevant articles.

Study Selection

Inclusion criteria were as follows: (1) study design was RCT; (2) patients diagnosed with UAP according to the guideline of the American College of Cardiology Foundation/American Heart Association (ACCF/AHA) (Braunwald et al., 2000), World Health Organization (Organization, 1979), European Society of Cardiology (ESC) (Fox et al., 2006) or Chinese Society of Cardiology (CSC) (Cardiology, 2000); (3) DZHJT in combination with conventional Western medicine vs. Western medicine alone; and (4) primary outcomes were $\geq$80% reduction in frequency of angina attacks weekly and marked improvement of abnormal electrocardiogram (restore normal or nearly normal defined by at least 0.05 mv restoration at ST segment). The secondary outcomes were the whole-blood viscosity, plasma viscosity, fibrinogen, thromboxanes B2, or C-reactive protein (CRP) and adverse events. Articles were excluded when: (1) diagnostic criteria for UAP were not specified; (2) patients have SAP; (3) combined application of DZHJT with other Chinese herbs as intervention.

Data Extraction and Quality Assessment

For the included trials, two authors independently extracted the data and assessed the methodological quality. Any disagreements in this process were resolved by discussion. The extracted data included the last name of the first author, year of publication, sample size, patients' age, diagnostic criteria, interventions (dose of DZHJT and course of treatment), outcome measures, and methodological information. We evaluated the methodological quality of the included trials according to the Cochrane risk of bias tool, which included selection bias, performance bias, detection bias, attrition bias, reporting bias, and other sources of bias. Each trial was categorized by "high," "unclear," or "low" risk of bias.

Statistical Analysis

The RevMan 5.2 software was used for the meta-analysis. We summarized as the risk ratio (RR) with 95% confidence intervals (CI) for dichotomous outcomes or mean difference (MD) with 95% CI for continuous outcomes. The Cochrane Q statistic and I^2 index were applied to the analysis of heterogeneity across the studies. A random effect meta-analysis was conducted when the p-value of Cochrane Q statistic test is <0.10 and $I^2 > 50\%$. Otherwise, we pooled the data by using a fixed-effect model. We used a funnel plot to examine the possible publication bias when the number of trials was sufficient. Leave-one-out sensitivity analysis was conducted to test the stability of the pooling results.

RESULTS

Search Results and Study Characteristics

In brief, our initial literature search yielded 615 potentially relevant articles. After screening the titles and abstracts, we retrieved 54 full-text articles for detailed evaluation. We further

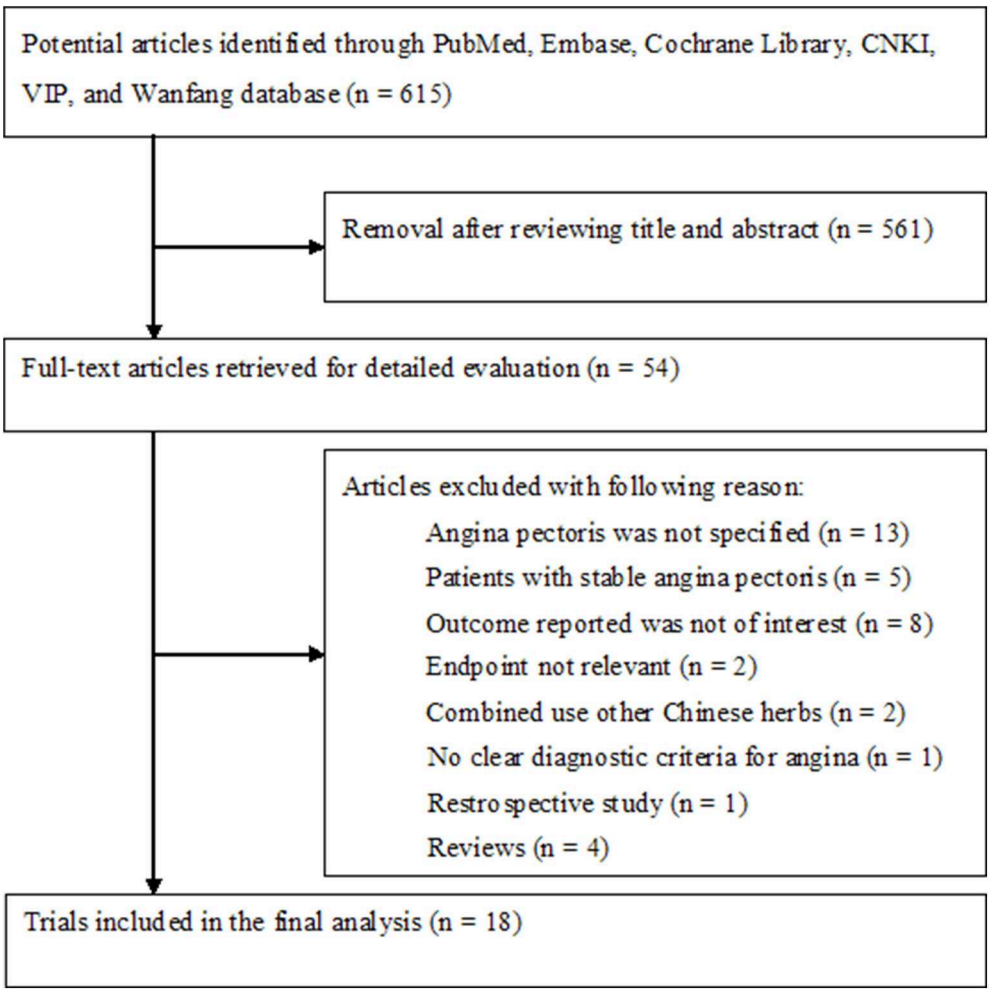

FIGURE 1 | Flow chart of studies selection process.

removed 36 articles on the basis of our predefined inclusion criteria. Thus, 18 articles (Yu et al., 2011; Chen, 2013; Zhang, 2013; Cao et al., 2014; Jia and Wang, 2014; Li and Zhao, 2014; Shen et al., 2014; Liu and Jiang, 2015; Wang et al., 2015; Weng et al., 2015; Zhai et al., 2015; Qin and Gao, 2016; Zhang and Lu, 2016; Du, 2017; Li, 2017; Li and Cheng, 2018; Wang and Yang, 2018; Zhang et al., 2018) were finally included in the meta-analysis (**Figure 1**).

The main characteristics of the included trials are summarized in **Table 1**. A total of 1,679 patients with UAP were identified with eligible trials. All of the selected trials were published in Chinese medical databases from 2011 to 2019. Two trials (Shen et al., 2014; Liu and Jiang, 2015) used DZHJT capsule as intervention, and the others used DZHJT injection. The duration of intervention ranged from 10 days to 8 weeks. Main conventional Western medicines referred to treatment included aspirin, nitrates, β-blockers, calcium channel blockers, angiotensin converting enzyme inhibitors, angiotensin receptor blockers, low molecular weight heparin, and lipid-lowering agents. All of the 18 trials indicated randomization, but only 4 trials (Chen, 2013; Liu and Jiang, 2015; Zhai et al., 2015; Zhang and Lu, 2016) described the detailed method of randomization. None of the trials reported the allocation concealment, dropout or withdrawal. **Figure S1** shows the detailed methodological quality of the included trials.

Frequency of Angina Attacks

A total of 13 trials (Yu et al., 2011; Chen, 2013; Zhang, 2013; Cao et al., 2014; Jia and Wang, 2014; Liu and Jiang, 2015; Wang et al., 2015; Zhai et al., 2015; Zhang and Lu, 2016; Du, 2017; Li, 2017; Li and Cheng, 2018; Wang and Yang, 2018) selected ≥80% reduction in frequency of angina attacks as an outcome. As shown in **Figure 2A**, a fixed-effect model was applied because no heterogeneity was observed across trials ($I^2 = 0\%$, $p = 0.63$). Meta-analysis showed that adjuvant treatment with DZHJT significantly reduced the ≥80% reduction in frequency of angina attacks (RR 1.57; 95% CI 1.36–1.81). When we removed one trial (Yu et al., 2011) enrolling patients with age of more than

TABLE 1 | Baseline characteristics of the included trials.

Study/year	No. patients DZHJT/Con	Age (years) DZHJT/Con	Diagnostic criteria	Main intervention		Treatment course	Outcome measures
				DZHJT group	Control group		
Yu et al. (2011)	34/30	80–92	2000 CBCMA	DZHJT 10 ml/d, iv drop + control	Aspirin, trimetazidine, isosorbide dinitrate, and symptomatic treatment.	10 days	① + ⑧
Zhang (2013)	42/41	58.72 ± 12.86/ 60.72 ± 11.56	ESC	DZHJT 10 ml/d, iv drop + control	Aspirin, rosuvastatin, β-blockers, CCBs, and nitrates.	10 days	① + ③ + ④ + ⑧ + ⑧
Chen (2013)	30/30	61–84	2000 CBCMA	DZHJT 10 ml/d, iv drop + control	Aspirin, atorvastatin, β-blockers, nitrates, and ACEIs.	14 days	① + ② + ③ + ⑧
Li and Zhao (2014)	40/40	57.5 ± 5.6/ 58.1 ± 5.2	CBCMA	DZHJT 10 ml/d, iv drop + control	β-blockers, ACEIs/ARBs, nitrates, CCBs, and LMWH	15 days	③ + ④ + ⑤ + ⑥
Cao et al. (2014)	46/46	62–80	1979 WHO	DZHJT 20 ml/d, iv drop + control	ACEIs, β-blockers, antiplatelet, and lipid-lowering agents	14 days	①
Shen et al. (2014)	46/46	57.2 ± 8.1/ 58.2 ± 8.8	CBCMA	DZHJT capsule 5.56 g/d, po + control	Aspirin, metoprolol, enalapril, atorvastatin, and nitrates	8 weeks	② + ③ + ⑤ + ⑥ + ⑦
Jia and Wang (2014)	45/42	35–76	2000 CBCMA	DZHJT 10 ml/d, iv drop + control	Aspirin, statins, β-blockers, nitrates	10 days	① + ③
Liu and Jiang (2015)	40/40	56 ± 3/ 56 ± 4	CBCMA	DZHJT capsule 2.28 g/d, po + gf control	Aspirin, isosorbide dinitrate, and clopidogrel	8 weeks	① + ④ + ⑥
Weng et al. (2015)	61/62	66 ± 6/ 66 ± 8	2007 ACC/AHA	DZHJT 10 ml/d, iv drop + control	Aspirin, clopidogrel, nitrates, statins, and creatine phosphate sodium	10 days	② + ③ + ⑤ + ⑧
Zhai et al. (2015)	40/40	64.8 ± 2.3/ 60.2 ± 3.2	WHO	DZHJT 10 ml/d, iv drop + control	Aspirin, β-blockers, nitrates, statins, and creatine phosphate sodium	10 days	① + ② + ⑧
Wang et al. (2015)	40/40	39–75	CBCMA	DZHJT 10 ml/d, iv drop + control	Aspirin, atorvastatin, clopidogrel, metoprolol, isosorbide dinitrate, LMWH	14 days	② + ③
Zhang and Lu (2016)	27/27	60 ± 7/ 60 ± 8	2000 CBCMA	DZHJT 10 ml/d, iv drop + control	Aspirin, β-blockers, nitrates, statins, and clopidogrel	14 days	① + ② + ④ + ⑥
Qin and Gao (2016)	42/42	52–82	CBCMA	DZHJT 10 ml/d, iv drop + control	Aspirin, β-blockers, ACEIs/ARBs, nitrates, CCBs, and LMWH	10 days	⑧
Du (2017)	40/40	70.45 ± 9.83/ 71.02 ± 9.79	2000 CBCMA	DZHJT 10 ml/d, iv drop + control	Aspirin, trimetazidine, isosorbide dinitrate, and symptomatic treatment.	10 days	①

(Continued)

TABLE 1 | Continued

Study/year	No. patients DZHJT/Con	Age (years) DZHJT/Con	Diagnostic criteria	Main intervention		Treatment course	Outcome measures
				DZHJT group	Control group		
Li (2017)	39/39	57.75 ± 6.21/ 57.83 ± 6.07	CBCMA	DZHJT 10 ml/d, iv drop + control	Isosorbide dinitrate, statins, clopidogrel	14 days	① + ② + ③ + ⑦
Zhang et al. (2018)	63/63	60.3 ± 6.7	CBCMA	DZHJT 10 ml/d, iv drop + control	Anticoagulation, antiplatelet, antiischemia, salvianolate	14 days	④ + ⑥ + ⑧
Li and Cheng (2018)	38/38	58.21 ± 7.61/ 57.90 ± 7.04	CBCMA	DZHJT 10 ml/d, iv drop + control	β-blockers, antiplatelet, nitrates, CCBs	28 days	① + ⑦
Wang and Yang (2018)	130/130	49.3 ± 11.9/ 52.6 ± 10.3	CBCMA	DZHJT 10 ml/d, iv drop +control	Isosorbide dinitrate, statins, antiplatelet, and symptomatic treatment.	14 days	① + ③

DZHJT, Dazhu Hongjingtian; Con, control; ACEIs, angiotensin converting enzyme inhibitors; CCBs, calcium channel blockers; ARBs, angiotensin receptor blockers; CBCMA, Cardiovascular branch of Chinese Medical Association; ESC, European Society of Cardiology; ACC/AHA, American College of Cardiology Foundation/American Heart Association; ESC, European Society of Cardiology; LMWH, low molecular weight heparin.

① ≥80% reduction in frequency of angina attacks; ② weekly frequency of angina attacks; ③ marked improvement of abnormal electrocardiogram; ④ whole-blood viscosity; ⑤ plasma viscosity; ⑥ fibrinogen; ⑦ Thromboxanes B2; ⑧ adverse events.

80 years, the pooled RR of ≥80% reduction in frequency of angina attacks was 1.52 (95% CI 1.31–1.76) in a fixed-effect model. Visual inspection of the funnel plot showed no evidence of publication bias (**Figure S2**). Five trials (Chen, 2013; Shen et al., 2014; Weng et al., 2015; Zhang and Lu, 2016; Li, 2017) reported the weekly frequency of angina attacks as an outcome measure. As shown in **Figure 2B**, a random effect model meta-analysis showed that adjuvant treatment with DZHJT was associated with a reduced weekly frequency of angina attacks [MD −1.03 times; 95% confidence interval (CI) −1.51 to −0.88; $I^2 = 84\%$, $p < 0.001$].

Abnormal Electrocardiogram

Nine trials (Chen, 2013; Zhang, 2013; Jia and Wang, 2014; Li and Zhao, 2014; Shen et al., 2014; Wang et al., 2015; Weng et al., 2015; Li, 2017; Wang and Yang, 2018) reported marked improvement of abnormal electrocardiogram as an outcome. As shown in **Figure 3**, a fixed-effect model meta-analysis indicated that adjuvant treatment with DZHJT was associated with marked improvement of abnormal electrocardiogram (RR 1.46; 95% CI 1.23–1.74; $I^2 = 0\%$, $p = 0.93$). No evidence of publication bias was observed based on the visual inspection of the funnel plot (**Figure S3**).

Serum Fibrinogen, Whole-Blood Viscosity, and Plasma Viscosity

As shown in **Figure 4A**, a fixed-effect model meta-analysis of five trials (Zhang, 2013; Li and Zhao, 2014; Liu and Jiang, 2015; Zhang and Lu, 2016; Zhang et al., 2018) indicated that adjuvant treatment with DZHJT significantly reduced serum fibrinogen level (MD −0.67 g/L; 95% CI −0.79 to−0.54; $I^2 = 26\%$, $p = 0.25$). As shown in **Figures 4B,C**, a random effect model meta-analysis showed that whole-blood viscosity (MD −0.78 mPa.s; 95% CI −1.14 to −0.41; $I^2 = 76\%$, $p = 0.006$); four trials (Zhang, 2013; Li and Zhao, 2014; Liu and Jiang, 2015; Zhang et al., 2018) and plasma viscosity (MD −0.28 mPa.s; 95% CI −0.38 to −0.19; $I^2 = 80\%$, $p = 0.002$); four trials (Zhang, 2013; Li and Zhao, 2014; Shen et al., 2014; Weng et al., 2015) were significantly reduced in the DZHJT combined with Western medicine group.

Serum Thromboxanes B2 and CRP Level

As shown in **Figure 5A**, a random effect model meta-analysis of three trials showed that DZHJT in combination with conventional Western medicine significantly decreased serum thromboxanes B2 level (MD −14.01 ng/L; 95% CI −20.86 to −7.15; $I^2 = 74\%$, $p = 0.02$); 3 trials (Shen et al., 2014; Li, 2017; Li and Cheng, 2018) compared with Western medicine alone. Moreover, **Figure 5B** shows that adjuvant treatment with DZHJT also significantly reduced serum CRP level (MD −1.48 mg/L; 95% CI −2.72 to −0.25; $I^2 = 94\%$, $p < 0.001$); three trials (Wang et al., 2015; Weng et al., 2015; Li, 2017) in a random effect model.

Adverse Events

Five trials (Yu et al., 2011; Weng et al., 2015; Zhai et al., 2015; Qin and Gao, 2016; Zhang et al., 2018) described the

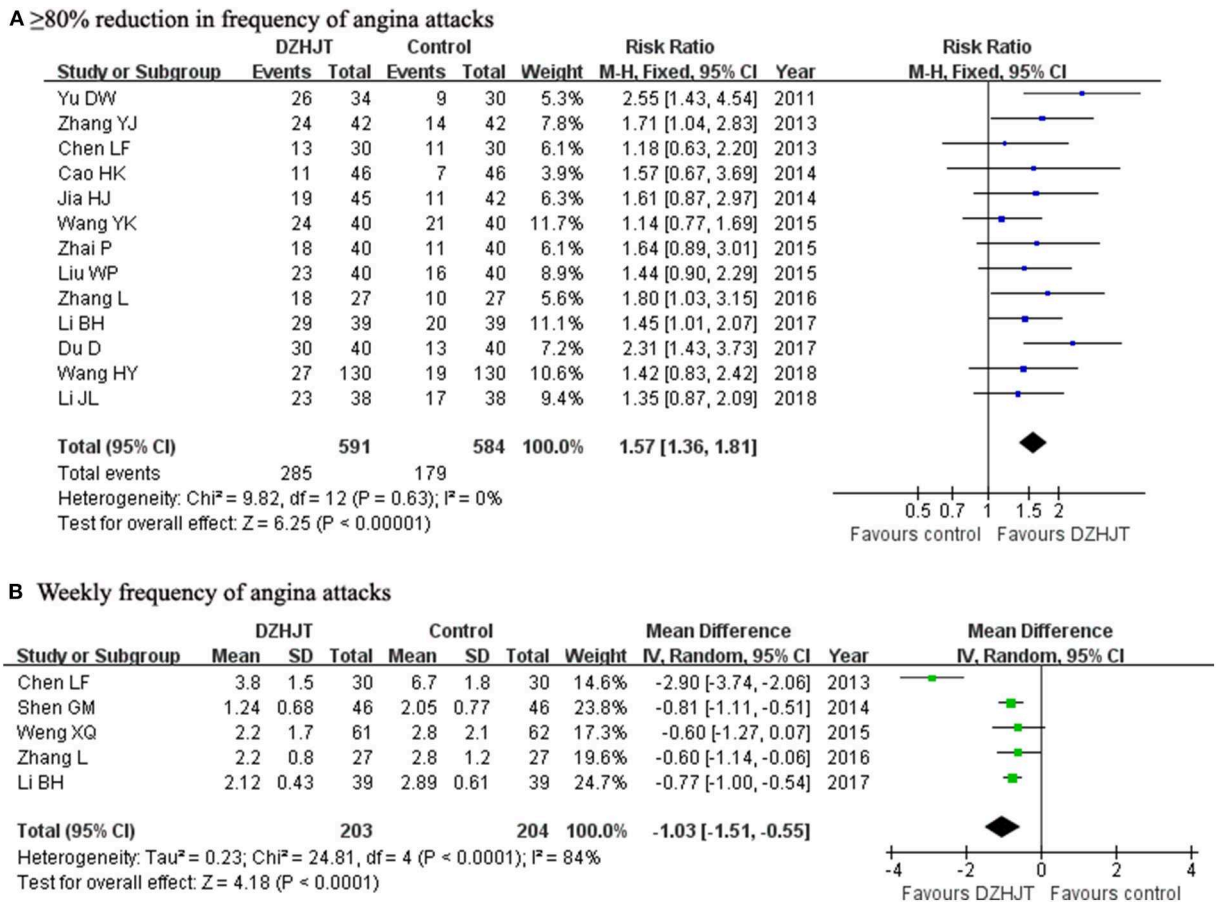

FIGURE 2 | Forest plots showing comparison of ≥80% reduction in frequency of angina attacks **(A)** and weekly frequency of angina attacks **(B)** in patients with or without DZHJT treatment.

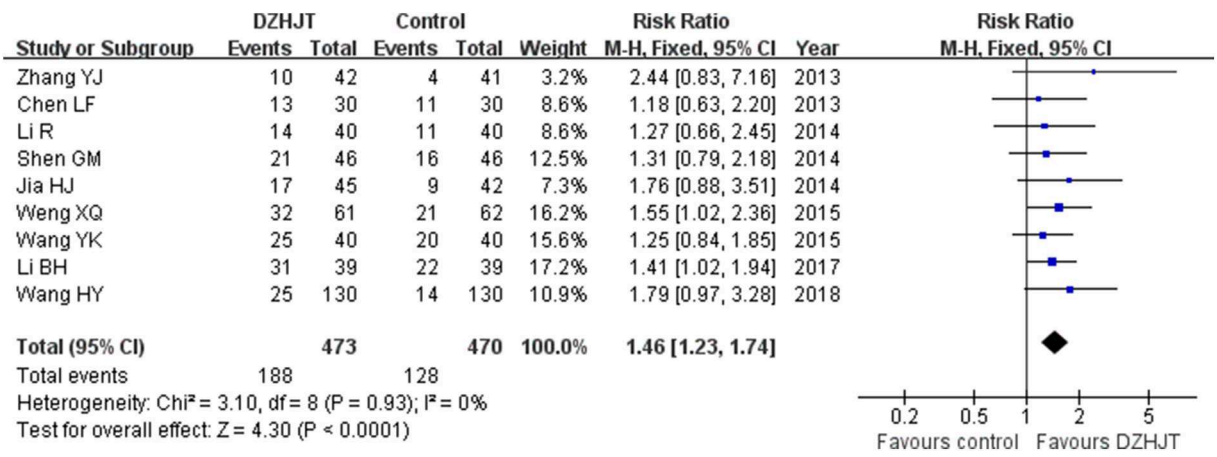

FIGURE 3 | Forest plots showing comparison of marked improvement of abnormal electrocardiogram in patients with or without DZHJT treatment.

adverse events. The common adverse events were headache and dizziness. No severe adverse events were reported. The incidences of headache and dizziness was 3.75 and 5.06%, respectively. As shown in **Figure 6**, no significant differences were found in headache and dizziness (RR 0.72; 95% CI 0.31–1.67; $I^2 = 0\%$, $p = 0.60$) between two groups. When

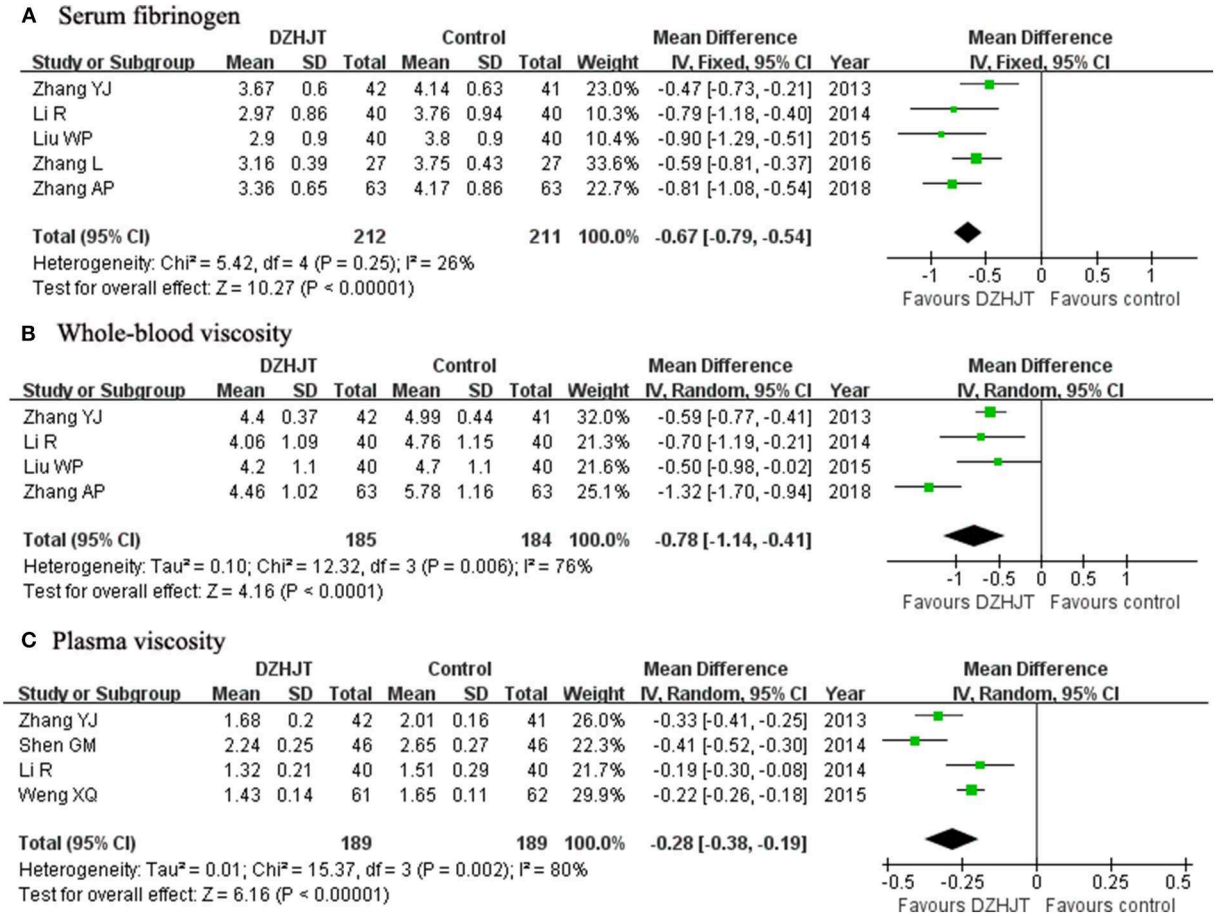

FIGURE 4 | Forest plots showing comparison of the serum fibrinogen **(A)**, whole-blood viscosity **(B)**, and plasma viscosity **(C)** in patients with or without DZHJT treatment.

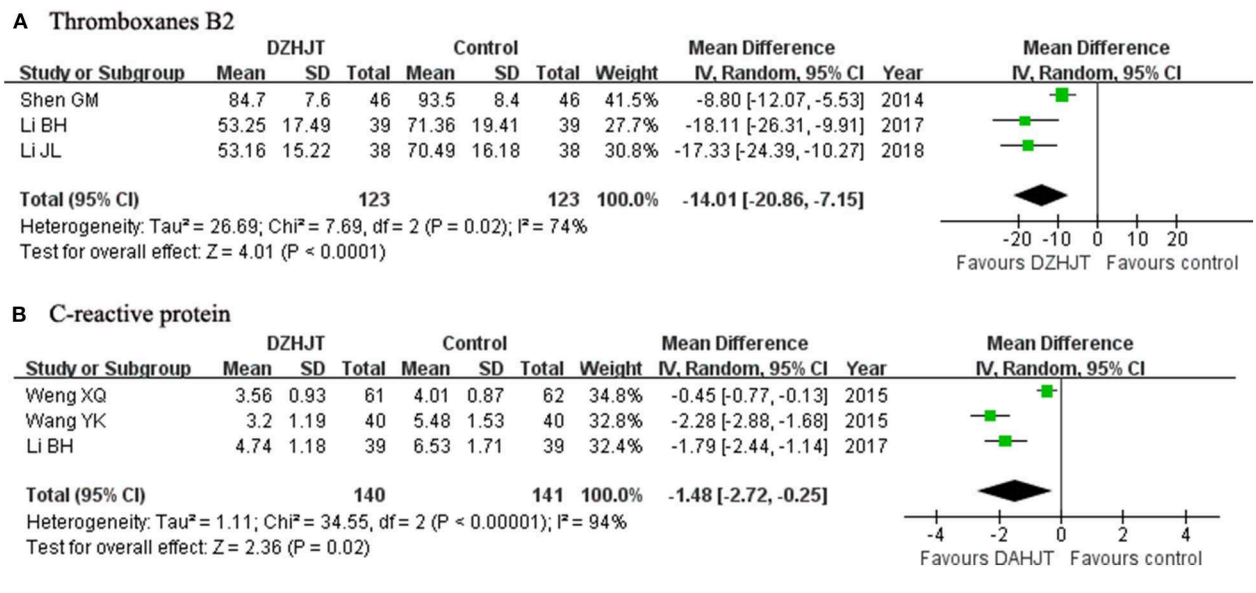

FIGURE 5 | Forest plots showing comparison of the serum thromboxanes B2 **(A)** and C-reactive protein **(B)** level in patients with or without DZHJT treatment.

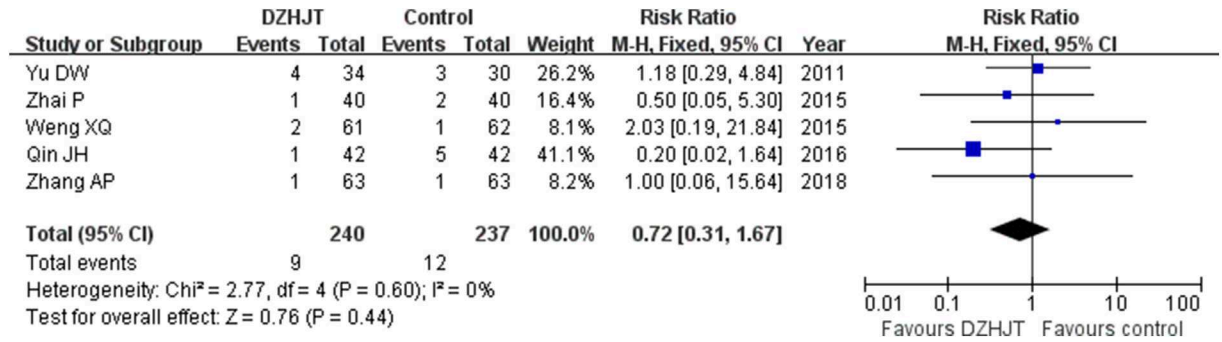

FIGURE 6 | Forest plots showing comparison of incidence of headache/dizziness in patients with or without DZHJT treatment.

we excluded one trial (Yu et al., 2011) enrolling patients with age of more than 80 years old, the pooled RR of headache and dizziness was 0.56 (95% CI 0.19–1.63) in a fixed-effect model.

DISCUSSION

The main findings of this meta-analysis suggested that adjuvant treatment with DZHJT significantly reduced the frequency of angina attacks and restored the abnormal electrocardiogram. Moreover, whole-blood viscosity, plasma viscosity, fibrinogen, thromboxanes B2, and CRP levels were significantly lower after DZHJT in combination with Western medicine treatment compared with conventional Western medicine alone.

Haemostatic parameters mainly include fibrinogen level, whole-blood viscosity, plasma viscosity, and hematocrit. These haemostatic parameters are elevated in patients with UAP (Neumann et al., 1991). Whole-blood viscosity represents the frictional resistance of blood flow on the intimal wall of blood vessels. Fibrinogen plays a major determinant in platelet aggregation and blood viscosity, whereas increased whole-blood viscosity may lead to high shear forces at the vascular endothelium, contributing to plaque instability (Cowan et al., 2012). Elevated haemorheological parameters correlate with the increased risk of cardiovascular events (Di Minno and Mancini, 1990; Lowe et al., 1997; Marton et al., 2003). DZHJT has the action of removing stasis and stopping bleeding. Therefore, it can reduce the high blood viscosity associated with blood stagnation. Our meta-analysis indicated that adjuvant treatment with DZHJT significantly decreased the whole-blood viscosity, plasma viscosity, fibrinogen, and thromboxanes B2 level. DZHJT significantly reduced serum CRP level. In summary, the beneficial effect of DZHJT in patients with UAP may correlate with the capability to normalize blood rheology and reduce the inflammatory reaction. However, whether DZHJT can decrease the development of coronary artery disease requires further investigation.

Most of the included trials did not select adverse events as outcome measures. None of the included trials reported severe adverse events. Headache and dizziness were the most frequently reported adverse events among these included trials. Headache may be more closely correlated with the use of nitrates (Thadani and Rodgers, 2006). Nevertheless, our pooled results revealed no significant differences in headache and dizziness between two groups. The possible adverse events associated with DZHJT use require further monitoring.

Several limitations in this meta-analysis must be noted. Firstly, the overall methodological quality of the included trials was suboptimal. All the included trials were generally of small sample size and none of the trials mentioned the sample size calculation, allocation concealment, and withdrawal/dropout or adopted the blinded, placebo controlled designs. Secondly, Traditional Chinese Medicine (TCM) is a holistic system of medicine. However, most of the included trials did not consider syndrome differentiation in patient selection. TCM syndrome differentiation must be incorporated into the diagnostic process and DZHJT is suitable for blood stagnation syndrome. Thirdly, generalizing the current findings to patients with SAP must be with caution. Finally, the included trials did not report the long-term follow-up results, and whether adjuvant treatment with DZHJT can reduce the risk of future cardiovascular events is unknown.

CONCLUSIONS

This meta-analysis suggests that adjuvant treatment with DZHJT has an add-on effect in reducing the frequency of angina pectoris attacks among patients with UAP. The beneficial effect of DZHJT may be correlated with its function to regulate whole-blood viscosity, plasma viscosity, fibrinogen, thromboxanes B2 and CRP level. However, based on the existing evidence, no conclusion about the therapeutic benefits, limitations of use and potential risks can be drawn. Future well-designed prospective, randomized, double-blind placebo-controlled trials with large sample sizes are required to evaluate the evidence.

AUTHOR CONTRIBUTIONS

CM and ZD made the literature search, extracted data, evaluated the study quality, and performed the statistical analysis. CM drafted the manuscript. YF designed the study, interpreted the results, and revised the manuscript.

FUNDING

This work was supported by Jiangsu Provincial Key&D Special Fund (BE2015666).

SUPPLEMENTARY MATERIAL

The Supplementary Material for this article can be found online at: https://www.frontiersin.org/articles/10.3389/fphar.2020.00213/full#supplementary-material

Supplemental Text S1 | The detailed information of DZHJT.

Figure S1 | Risk of bias graph **(A)** and risk of bias summary **(B)**.

Figure S2 | Funnel plots of trial reporting ≥80% reduction in frequency of angina attacks.

Figure S3 | Funnel plots of trial reporting marked improvement of abnormal electrocardiogram.

REFERENCES

Basra, S. S., Virani, S. S., Paniagua, D., Kar, B., and Jneid, H. (2016). Acute coronary syndromes: unstable angina and non-ST elevation myocardial infarction. *Heart Fail. Clin.* 12, 31–48. doi: 10.1016/j.hfc.2015.08.004

Braunwald, E., Antman, E. M., Beasley, J. W., Califf, R. M., Cheitlin, M. D., Hochman, J. S., et al. (2000). ACC/AHA guidelines for the management of patients with unstable angina and non-ST-segment elevation myocardial infarction: executive summary and recommendations. A report of the American college of cardiology/American heart association task force on practice guidelines (committee on the management of patients with unstable angina). *Circulation* 102, 1193–1209. doi: 10.1161/01.CIR.102.10.1193

Cao, H. K., Zhang, Y. K., Fu, W., and Yang, K. (2014). Effect of Dazhu hongjingtian Injection on unstable angina pectoris in the elderly patients. *Med. Infor.* 27, 272–273. doi: 10.3969/j.issn.1006-1959.2014.30.423

Cardiology, C. S. O. (2000). Recommendations for the diagnosis and treatment of unstable angina pectoris. *Chin. J. Cardiol.* 28, 409–412. doi: 10.3321/j.issn:1000-3614.2001.03.033

Chen, L. F. (2013). Treatment of 30 cases of elderly unstable angina pectoris by integrated traditional Chinese and Western medicine. *Fujian J. TCM* 44, 27–28. doi: 10.13260/j.cnki.jfjtcm.011391

Choe, K. I., Kwon, J. H., Park, K. H., Oh, M. H., Kim, M. H., Kim, H. H., et al. (2012). The antioxidant and anti-inflammatory effects of phenolic compounds isolated from the root of Rhodiola sachalinensis A. *BOR. Mol.* 17, 11484–11494. doi: 10.3390/molecules171011484

Chu, J. F., Wu, G. W., Zheng, G. H., Zheng, F., Xu, J. F., Peng, J., et al. (2014). A systematic review of randomized controlled trials on treating chronic stable angina pectoris by Rhodiola. *Chin. J. Integr. Trad. West Med.* 34, 940–946. doi: 10.7661/CJIM.2014.08.0940

Cowan, A. Q., Cho, D. J., and Rosenson, R. S. (2012). Importance of blood rheology in the pathophysiology of atherothrombosis. *Cardiovasc. Drugs Ther.* 26, 339–348. doi: 10.1007/s10557-012-6402-4

Di Minno, G., and Mancini, M. (1990). Measuring plasma fibrinogen to predict stroke and myocardial infarction. *Arteriosclerosis* 10, 1–7. doi: 10.1161/01.ATV.10.1.1

Du, D. (2017). Effects of dazhu hongjingtian injection on QT dispersion and heart rate variability in elderly patients with unstable angina pectoris. *Mod. J. Int. Trad. Chin. Western Med.* 26, 723–725. doi: 10.3969/j.issn.1008-8849.2017.07.013

Fan, J. M., Wang, S. F., Qing, H., Zhai, L. H., Mao, J. Y., and Sun, L. J. (2005). Efficacy of rhodiola injection treatment for 233 cases of coronary heart disease associated with angina pectoris (blood-stasis syndrome): a multicenter randomized, double- blind, positive controlled trial. *TCM Res.* 18, 26–28. doi: 10.3969/j.issn.1001-6910.2005.10.017

Fox, K., Garcia, M. A., Ardissino, D., Buszman, P., Camici, P. G., Crea, F., et al. (2006). Guidelines on the management of stable angina pectoris: executive summary: the task force on the management of stable angina pectoris of the European society of cardiology. *Eur. Heart J.* 27, 1341–1381. doi: 10.1093/eurheartj/ehl001

Gao, D., Li, Q., Liu, Z., Feng, J., Li, J., Han, Z., et al. (2009). Antidiabetic potential of *Rhodiola sachalinensis* root extract in streptozotocin-induced diabetic rats. *Methods Find. Exp. Clin. Pharmacol.* 31, 375–381. doi: 10.1358/mf.2009.31.6.1380457

Hemingway, H., Langenberg, C., Damant, J., Frost, C., Pyorala, K., and Barrett-Connor, E. (2008). Prevalence of angina in women versus men: a systematic review and meta-analysis of international variations across 31 countries. *Circulation* 117, 1526–1536. doi: 10.1161/CIRCULATIONAHA.107.720953

Jia, H. J., and Wang, G. T. (2014). Effect of dazhu hongjingtian injection on the treatment of unstable angina pectoris and serum level of SOD and MDA. *Heilongjiang Med. J.* 38, 640–641. doi: 10.3969/j.issn.1004-5775.2014.06.012

Jiang, H., and Pan, T. (2012). Research progress of Rhodiola in prevention and treatment of cardiovascular diseases. *Chin. J. Int. Med. Cardio-/Cerebrovascular Dis.* 10, 341–342. doi: 10.3969/j.issn.1672-1349.2012.03.045

Li, B. H. (2017). Therapeutic effect of dazhu hongjingtian injection combined with clopidogrel on unstable angina pectoris and its effect on platelet function. *Clin. Med.* 37, 99–100. doi: 10.19528/j.issn.1003-3548.2017.10.050

Li, J. L., and Cheng, H. T. (2018). Curative effect of sofren injection on unstable angina pectoris and its influence on platelet function. *Chin J. Heart. Heart Rhythm* 6, 65–67. doi: 10.1016/j.hrthm.2017.09.007

Li, R., and Zhao, L. (2014). Sofren injection for the treatment of unstable angina pectoris and its influence on hemorheology. *Mod. Dist. Educ. Chin. Med.* 12, 50–51. doi: 10.3969/j.issn.1672-2779.2014.21.028

Li, T., Xu, G., Wu, L., and Sun, C. (2007). Pharmacological studies on the sedative and hypnotic effect of salidroside from the Chinese medicinal plant rhodiola sachalinensis. *Phytomedicine* 14, 601–604. doi: 10.1016/j.phymed.2006.12.016

Liberati, A., Altman, D. G., Tetzlaff, J., Mulrow, C., Gotzsche, P. C., Ioannidis, J. P., et al. (2009). The PRISMA statement for reporting systematic reviews and meta-analyses of studies that evaluate health care interventions: explanation and elaboration. *J. Clin. Epidemiol.* 62, e1–34. doi: 10.1016/j.jclinepi.2009.06.006

Liu, W. P., and Jiang, C. H. (2015). Rhodiola crenulate capsule on thrombus formation in patients with unstable angina pectoris. *China J. Pharmaceutical Econ.* 10, 36–37.

Lowe, G. D., Lee, A. J., Rumley, A., Price, J. F., and Fowkes, F. G. (1997). Blood viscosity and risk of cardiovascular events: the Edinburgh artery study. *Br. J. Haematol.* 96, 168–173. doi: 10.1046/j.1365-2141.1997.8532481.x

Marton, Z., Horvath, B., Alexy, T., Kesmarky, G., Gyevnar, Z., Czopf, L., et al. (2003). Follow-up of hemorheological parameters and platelet aggregation in patients with acute coronary syndromes. *Clin. Hemorheol. Microcirc.* 29, 81–94.

Neumann, F. J., Katus, H. A., Hoberg, E., Roebruck, P., Braun, M., Haupt, H. M., et al. (1991). Increased plasma viscosity and erythrocyte aggregation: indicators of an unfavourable clinical outcome in patients with unstable angina pectoris. *Br. Heart J.* 66, 425–430. doi: 10.1136/hrt.66.6.425

Organization, W. H. (1979). Nomenclature and criteria for diagnosis of ischemic heart disease. Report of the joint international society and federation of cardiology/World Health Organization task force on standardization of clinical nomenclature. *Circulation* 59, 607–609. doi: 10.1161/01.CIR.59.3.607

Parikh, R., and Kadowitz, P. J. (2014). Angina pectoris: current therapy and future treatment options. *Expert Rev. Cardiovasc. Ther.* 12, 175–186. doi: 10.1586/14779072.2014.880339

Qin, J. H., and Gao, Y. (2016). Clinical efficacy of dazhu hongjingtian for treatment of unstable angina pectoris. *J. Med. Theor. Prac.* 29, 3345–3346. doi: 10.19381/j.issn.1001-7585.2016.24.019

Shen, G. M., Fan, S. M., and Tian, X. S. (2014). Influence of big plant rhodiola capsule treat on unstable angina patients. *Chin. J. Exp. Trad. Med. Form.* 20, 200–203. doi: 10.13422/j.cnki.syfjx.2014160200

Silva, F. M., Pesaro, A. E., Franken, M., and Wajngarten, M. (2015). Acute management of unstable angina and non-ST segment elevation myocardial infarction. *Einstein* 13, 454–461. doi: 10.1590/S1679-45082015RW3172

Thadani, U., and Rodgers, T. (2006). Side effects of using nitrates to treat angina. *Expert Opin. Drug Saf.* 5, 667–674. doi: 10.1517/14740338.5.5.667

Wang, H. Y., and Yang, S. Z. (2018). Clinical observation of dazhu hongjingtian injection in the treatment of unstable angina pectoris. *Chin. J. Int. Med. Cardio-/Cerebrovascular Dis.* 16, 1075–1077. doi: 10.12102/j.issn.1672-1349.2018.08.024

Wang, Y. K., Shang, S. Z., Gu, X., Zhang, Y. J., Ding, Z. X., Li, J. J., et al. (2015). Clinical observation on treating 80 cases of unstable angina with the dazhu hongjingtian injection. *Clin. J. Chin. Med.* 7, 62–64. doi: 10.3969/j.issn.1674-7860.2015.22.032

Weng, X. Q., Zhuang, C. W., Shi, X. L., Tu, C. L., and Jiang, H. (2015). Clinical analysis of the efficacy of creatine phosphate sodium combined with Dazhu Hongjingtian Injection for the treatment of unstable angina pectoris. *Clin. J. Med. Offic.* 43, 827–830. doi: 10.16680/j.1671-3826.2015.11.16

Yu, D. W., Su, Y., Yang, Y., Liang, Y., Liu, D., and Hua, P. H. (2011). Clinical analysis of Dazhu Hongjingtian in treatment of unstable angina pectoris in patients with advanced age. *Med. J. Nat. Defending Forces Southwest China* 21, 1309–1311. doi: 10.3969/j.issn.1004-0188.2011.12.011

Zhai, P., Zhu, G. B., and Liang, J. (2015). Efficacy of dazhu hongjingtian combined with creatine phosphate sodium for the treatment of 80 cases of unstable angina pectoris. *Chin. Rem. Clin.* 15, 556–557.

Zhang, A. P., Zhang, H. S., and Zhang, C. J. (2018). Clinical study on sofren injection combined with salvianolate in treatment of unstable angina pectoris. *Drugs Clin.* 33, 1594–1598.

Zhang, L., and Lu, G. X. (2016). Therapeutic effects of dazhu hongjingtian injection combined with clopidogrel on unstable angina pectoris. *Hebei Med. J.* 38, 2140–2142.

Zhang, Y. J. (2013). Clinical observation of sofren injection in treating patients with unstable angina. *Henan Med. Res.* 22, 348–350.

Zhang, Z. H., Liu, J. S., Chu, J. N., Shang, X. H., Lin, C. R., Ma, X. B., et al. (2005). The effect of hongjingtian (Gadol) injection on cardiac hemodynamics and myocardial oxygen consumption of dogs. *Zhongguo Zhong Yao Za Zhi* 30, 1001–1005. doi: 10.3321/j.issn:1001-5302.2005.13.012

Conflict of Interest: The authors declare that the research was conducted in the absence of any commercial or financial relationships that could be construed as a potential conflict of interest.

frontiers in Pharmacology

ORIGINAL RESEARCH
published: 27 March 2020
doi: 10.3389/fphar.2020.00375

Berberine Promotes OATP1B1 Expression and Rosuvastatin Uptake by Inducing Nuclear Translocation of FXR and LXRα

Mingyi Liu[1†], Dandan Zhu[1†], Jinhua Wen[2], Wei Ding[1], Shibo Huang[1], Chunhua Xia[1], Hong Zhang[1] and Yuqing Xiong[1]*

[1] Clinical Pharmacology Institute, Nanchang University, Nanchang, China, [2] Department of Pharmacy, First Affiliated Hospital of Nanchang University, Nanchang, China

OPEN ACCESS

Edited by:
Jianxun Liu,
China Academy of Chinese Medical Sciences, China

Reviewed by:
Suresh Kumar Mohankumar, JSS College of Pharmacy, India
Takeo Nakanishi, Takasaki University of Health and Welfare, Japan

***Correspondence:**
Yuqing Xiong
xyqncu@126.com

[†]These authors have contributed equally to this work

Specialty section:
This article was submitted to Ethnopharmacology, a section of the journal Frontiers in Pharmacology

Received: 22 June 2019
Accepted: 12 March 2020
Published: 27 March 2020

Citation:
Liu M, Zhu D, Wen J, Ding W, Huang S, Xia C, Zhang H and Xiong Y (2020) Berberine Promotes OATP1B1 Expression and Rosuvastatin Uptake by Inducing Nuclear Translocation of FXR and LXRα. Front. Pharmacol. 11:375. doi: 10.3389/fphar.2020.00375

Berberine, a quinoline alkaloid, can be used in combination with statins to enhance hypolipidemic effects and reduce the dose and side effects of statins. The hypolipidemic effects of statins in the liver are mainly regulated by organic anion transporting polypeptides (OATPs), and the expression of OATPs is regulated by nuclear receptors. Berberine has been reported to affect nuclear receptors. However, whether berberine affects the uptake of statins by regulating nuclear receptor-mediated expression of OATPs remains to be determined. The aim of this study was to investigate the effects of berberine on the expression of OATP1B1 in HepG2 and explore the underlying mechanism. In HepG2 cells, 10–50 μM berberine significantly increased the uptake of rosuvastatin by inducing the expression of OATP1B1 mRNA and protein. Dual-Luciferase reporter assay showed that luciferase activity of hFXR and hLXRα activated OATP1B1 promoter was increased by 2.5–50 μM berberine in a concentration-dependent manner, with half-maximal effective concentration (EC_{50}) of 12.19 ± 0.86 and 32.15 ± 2.32 μM, respectively. In addition, after silencing FXR or LXRα by small interfering RNA (siRNA), berberine-induced OATP1B1 expression was significantly attenuated. Western blot analysis of FXR and LXRα protein levels in the cytoplasm and nucleus of HepG2 cells after treatment with berberine showed that berberine induced nuclear translocation and activation of FXR and LXRα. In conclusion, berberine-induced nuclear translocation of FXR and LXRα could activate OATP1B1 promoter, resulting in enhanced expression of OATP1B1 and increased uptake of rosuvastatin.

Keywords: berberine, OATP1B1, FXR, LXRα, rosuvastatin

INTRODUCTION

Statins have been widely used as lipid-lowering drugs because they are inhibitors for hydroxyl methylglutaryl coenzyme A (HMG-CoA) reductase. The combination therapy of statins with bile acid sequestrants, niacin, or ezetimibine have significantly improved efficacy in the treatment of hyperlipidemia (Knapp et al., 2001; Wolfe et al., 2001; Robinson and Davidson, 2006; Huijgen et al.,

2010). However, combination therapy have the possibility to increase adverse effects such as muscle toxicity and myopathy, which may be associated with drug interactions mediated by organic anion transporting polypeptide (OATP) transporters (Staffa et al., 2002; Shitara and Sugiyama, 2006; Kitamura et al., 2008; Kunze et al., 2014).

Pregnane X receptor (PXR), constitutive androgen receptor (CAR), farnesoid X receptor (FXR), and liver X receptor α (LXRα) are members of constitutive and ligand-activated nuclear receptor superfamily and play a crucial role in regulating target genes involved in drug metabolism and transport (Urquhart et al., 2007; Staudinger et al., 2013). FXR and LXRα have been characterized as transcriptional factors which regulate the expression of OATP1B1 (Meyer Zu Schwabedissen et al., 2010). Rifampicin significantly increases the expression of OATP1B1 protein and mRNA in hepatocytes by activating PXR (Jigorel et al., 2006).

Berberine is a compound isolated from traditional Chinese medicines and exerts a variety of pharmacological effects such as anti-diabetes, immunoregulation, anti-hypertension, anti-arrhythmia, and lipid-lowering (Lau et al., 2001; Kong et al., 2004; Kong et al., 2009; Gu et al., 2015; Montes et al., 2019; Neag et al., 2018; Belwal et al., 2020;). In addition, berberine regulates metabolic enzymes and transporters to affect the absorption, distribution and metabolism of endogenous and exogenous substances *in vivo*. Berberine increased the blood concentration of cyclosporine A in renal transplanted patients by inhibiting CYP3A4 (Wu et al., 2005). Moreover, berberine can regulate the absorption and metabolism of dextromethorphan, losartan, and midazolam in healthy human by suppressing the activity of CYP2D6, 2C9, and 3A4 (Guo et al., 2012). Berberine-activated LXRα increased the expression of ABCA1 transporter and reduced the accumulation of low-density lipoprotein cholesterol (LDL-c) in macrophages to prevent the formation of foam cells (Lee et al., 2010). Berberine-disrupted STAT5 signaling promoted Ntcp/NTCP expression, resulting in enhanced bile acid uptake (Bu et al., 2017). In addition, berberine-activated RXRα/FXR and RXRα/LXR heterodimers enhanced luciferase activity of FXRE and LXRE (Ruan et al., 2017). Recently, combination of statins and berberine has been clinically used to treat hyperlipidemia. Kong *et al.* demonstrated that combined use of simvastatin and berberine significantly reduced LDL-c levels in rats and hyperlipidemia patients and adverse effects compared to monotherapy (Kong et al., 2008). The combination of berberine and simvastatin remarkably attenuated adverse effects such as rhabdomyolysis and improved the efficacy and safety of treatment (Bei-Bei et al., 2009; Li et al., 2019). Therefore, we speculated that berberine could induce the expression of OATP1B1 transporter through nuclear receptors and boosts the uptake of statins by hepatocytes, thereby improving the lipid-lowering efficacy in combination treatment. Notably, rosuvastatin is not metabolized by CYP450 but is transported by OATP (White, 2002). Therefore, in this study we used rosuvastatin to avoid the interference by CYP450 and used HepG2 cell as the model to investigate the effects of berberine on the expression of OATP1B1 and explore the underlying mechanisms.

MATERIALS AND METHODS

Chemicals

Berberine (purity 98.0%), atorvastatin [internal standard (IS) for rosuvastatin, purity 95.3%], and rosuvastatin (purity 97.6%) were obtained from the National Institutes for Food and Drug Control Products (Beijing, China). GW4064 (purity 99.80%) and GW3965 (purity 99.09%) were purchased from SelleckChem (Houston, TX, USA). Rifampicin (RIF, purity 97.0%) was purchased from Sigma-Aldrich (St. Louis, MO, USA). CITCO (purity 98.0%) was purchased from APExBIO (Beijing, China). FXR, LXRα, OATP1B1, and GAPDH oligonucleotide primers were synthesized by Sangon Biotech Co., Ltd (Shanghai, China). The Dual-Luciferase reporter assay system was purchased from Promega (Madison, WI, USA). Lipofectamine 3000 were purchased from Thermo Fisher Scientific (New York, USA). Rabbit polyclonal antibodies to OATP1B1 (catalog: DF4534), LXRα (catalog: DF6864) and GAPDH (catalog: AF0911) were purchased from Affinity Biosciences (Cincinnati, OH, USA). Rabbit polyclonal antibody to FXR (catalog: ab235094) was purchased from Abcam (Abcam, Cambridge, MA). HANK's balanced salt mixture (supplemented with Mg^{2+} and Ca^{2+}) and 1 mol/L HEPES were supplied by Solarbio (Beijing, China). All other chemicals were of analytical grade and were commercially available. Berberine, GW3964 and GW4064 were all dissolved in dimethylsulfoxide (DMSO) to prepare stock solutions of 10 mM. The working solutions were obtained by diluting the stock solutions with DMEM medium and final concentrations of DMSO were no more than 0.1%.

Plasmids and Small Interfering RNAs

The pTracer-hFXR, pTracer-hLXRα, and empty pTracer-CMV2 vector were purchased from Maijie Biotech (NanTong, China). The pGL3-OATP1B1 reporter plasmid containing LXRα response element(−128 to +53 bp) and FXR response element (−3040 to −4070 bp) fragment of the SLCO1B1 5′-UTR was constructed by Maijie Biotech (NanTong, China). (Meyer Zu Schwabedissen et al., 2010) The small interfering rnas (siRNAs) against hFXR (5′-GAGGAUGCCUCA-GGAAAUA-3′) and hLXRα (5′-AACTCAATGATGCTGAGTT-3′) and negative control scramble siRNA were purchased from Maijie Biotech (NanTong, China).

Cell Culture

The human liver carcinoma cell line HepG2 was provided by Novo Biotechnology (Shanghai, China) and cultured in Dulbecco's modified Eagle medium (DMEM, Solarbio Co., Ltd, Beijing, China) supplemented with 10% fetal bovine serum (FBS, Biological Industries, Israel) as described previously (Zhong et al., 2018). Cells were cultured to 70%–80% confluency and then treated with the chemicals for 24 h, and cells treated with

0.1% DMSO (generally considered noncytotoxic) were used as the blank control.

Real-Time PCR

Total RNA was isolated from HepG2 cells using EasySpin cell RNA extraction kit (Aidlab Biotechnologies Co., Ltd, Beijing, China) following the manufacturer's instruction. RNA (1.5 μg) was first reverse-transcribed into cDNA using Transcriptor First-strand cDNA Synthesis Kit (TransGen Biotech. Beijing, China), and real-time PCR was performed using Premix Ex Taq™ Probe qPCR (TaKaRa Biotech, Kyoto, Japan) following the manufacturer's instructions. The following primers were used: OATP1B1, 5′- ACCTGCTAGA CAGGGTGAGAT-3′ (forward) and 5′- ACCTGCTAGACAGGG-TGAGAT-3′ (reverse); FXR, 5′- TCAGCCAAC ATTCCCATC-3′ (forward) and 5′- CCTGTGACAAAGAAGCCG-3′ (reverse); LXRα, 5′- CCACTGCCCCATGGACA-CCT-3′ (forward) and 5′- TGTTCCTCCTCT TGCCGCTTC-3′ (reverse); GAPDH, 5′- CAGGGCTGCTTTTAACTCTGGT-3′ (forward) and 5′- GATTTTGGAGGGA-TCTCGCT-3′ (reverse). The data were calculated according to the comparative △△CT method and presented as relative fold of the control.

Western Blot Analysis

Cells were lysed with RIPA buffer (Applygen Gene Technology Co., Ltd. Beijing, China), and the nuclear and cytoplasmic proteins were separated and extracted using a nuclear and cytoplasmic extraction kit (Boster, Wuhan, China) according to the manufacturer's instructions. Protein concentrations were quantified with BCA protein assay kit (Vazyme Biotech, Nanjing, China). Proteins (20 μg/sample) were separated using 10% SDS–PAGE and transferred onto polyvinylidene fluoride (PVDF) membranes. Subsequently, the membranes were blocked for 2 h with 5% skim milk and then incubated overnight at 4°C with primary antibodies. The membranes were washed in TBS and then incubated with horseradish peroxidase-conjugated anti-rabbit or anti-rat IgG antibody (Santa Cruz, CA, USA) for 1 h at room temperature. GAPDH and Lamin B1 were used as loading controls. The bands were detected using a Bio-Rad ChemiDoc XRS imaging system (Bio-Rad Laboratories).

Rosuvastatin Uptake Assay

Rosuvastatin uptake assay in HepG 2 cells was performed as previously described (Li et al., 2012). Briefly, the cells were seeded at 2×10^5/well into 24-well plates and cultured for 24 h, and then treated with a medium containing berberine or a blank control (0.1% DMSO) at 37°C for 24 h. In the uptake experiments, cells were washed three times with HBS–HEPES (99:1) uptake buffer at 37°C, and then the cells were incubated for 10 min in uptake buffer containing 20 μM rosuvastatin. After the incubation, the buffer was quickly aspirated, the cells were washed three times with ice-cold HBSS–HEPES buffer, and repeatedly thawed three times at −80°C and room temperature. Finally, 100 μl cell lysate was spiked with 20 μl IS (10 ng/ml atorvastatin), and 200 μl methanol was added. The mixture was then vortexed for 1 min and centrifuged at 10,000*g* for 10 min, with an aliquot (10 μl) automatically injected into the LC-MS/MS system for analysis, and protein content was determined by BCA method. Three independent experiments were performed in triplicates.

Quantification of Rosuvastatin by LC-MS/MS

The concentration of rosuvastatin in cells was determined by LC-MS/MS system consisted of Shimadzu LC-20AB pumps (Shimadzu Corporation, Kyoto, Japan) and an AB SCIEX API 4000 mass spectrometer (Applied Biosystems/SCIEX, Foster, CA, USA). Data acquisition was performed using Analyst 1.6.1 software (AB SCIEX). Chromatographic separation was achieved on a Luna C18 column (50 × 2.0 mm i.d., 5 μm; Phenomenex Technologies). The mobile phase consisted of 10-mM ammonium formate (A) and acetonitrile (B) using a gradient elution of 40-90% B at 0.0–1.0 min, 90%–90% B at 1.0–2.5 min, and 40%–40% B at 2.51–3.5 min. The flow rate was 0.4 ml/min, the operating temperature was 25°C.

Samples were ionized utilizing an electrospray-ionization probe in the positive-ion mode, and quantification was performed using the multiple-reaction monitoring (MRM) method, with the precursor-to-product transition being m/z 482.3→258.2 for rosuvastatin and m/z 559.2→440.0 for atorvastatin (IS). Nitrogen was used as the curtain and auxiliary gas, and air was used as the nebulizer gas under the following conditions: curtain gas, 40 psi; ion-spray voltage, 5500 V; nebulizer gas, 50 psi; auxiliary gas, 50 psi; and turbo temperature, 500°C. The collision energy (CE) was 45 V for rosuvastatin and 28V for atorvastatin, and the declustering potential (DP) was 118 V for rosuvastatin and 100 V for atorvastatin.

Dual Luciferase Assay

pTracer-hFXR, pTracer-hLXRα, and empty pTracer-CMV2 vector were purchased from Maijie Biotech (NanTong, China). The pGL3-OATP1B1 vector was prepared as described (Meyer Zu Schwabedissen et al., 2010) containing LXRα response element (−128 to +53 bp) and FXR response element (−3,040 to −4,070 bp) fragment of the *SLCO1B1* 5′-UTR, and empty plasmid pGL3-Basic, internal reference Renilla luciferase plasmid pRL-TK were purchased from Maijie Biotech. Corresponding plasmids were transfected into HepG2 cells with Lipofectamine 3000 transfection reagent following the manufacturer's instructions. Finally, the cells were harvested and cell lysates were assayed for firefly activities normalized against the activities of co-transfected renilla luciferase using a dual-luciferase kit (Promega).

RNA Interference

The siRNA against hFXR or hLXRα and negative control scramble siRNA were purchased from Maijie Biotech (NanTong, China). siFXR (5′-GAGGAUGCCUCA-GGAAAUA-3′) or siLXRα (5′-AACTCAATGATGCTGAGTT-3′) was transfected into HepG2 cells at the final concentration of 50 nmol/L. The knockdown efficiency was detected by Western blot analysis.

Statistical Analysis

The data from three independent experiment were presented as mean ± standard deviation (mean ± SD), and one-way ANOVA was used to determine the differences among the groups using GraphPad Prism 5.0. $p < 0.05$ indicated that the differences were significant.

RESULTS

Effect of Berberine on OATP1B1 Expression in HepG2 Cells

To investigate the effects of berberine on the expression of OATP1B1, HepG2 cells were treated with a series of concentrations of berberine (5, 10, 25, and 50 μM) for 24 h, or treated with 25 μM berberine for a series of time (6, 12, 24, and 48 h). Real-time PCR showed that berberine significantly upregulated OATP1B1 mRNA levels in a concentration and time- dependent manner (**Figures 1A, B**). Western blot analysis showed that 10–50 μM berberine enhanced the expression of OATP1B1 protein in a concentration-dependent manner after 24-h treatment (**Figures 1C, D**).

Berberine Increased Rosuvastatin Uptake in HepG 2 Cells

To investigate the effects of berberine on OATP1B1 transport function, the time- and concentration-dependent uptake assays were conducted, and uptake kinetic parameters were examined in a series concentration or time point (data not shown). The HPLC-MS-MS method for the determination of rosuvastatin was validated with selectivity, precision, accuracy, extract recovery, and matrix effect (**Supplementary Figure 1**). The uptake of rosuvastatin was linear with time over the first 10 min, and the *Km* (Michaelis constant) was determined to be 21.50 ± 1.77 μM, thus we performed the specific rosuvastatin uptake test under the condition of 20 μM and 10 min. After treatment with increasing concentrations (2, 5, 10, 25, and 50 μM) of berberine for 24 h, the uptake of rosuvastatin was increased 1.24-fold (5 μM berberine-treated), 1.42-fold (10 μM berberine-treated), 1.78-fold (25 μM berberine-treated), and 1.93-fold (50 μM berberine-treated)

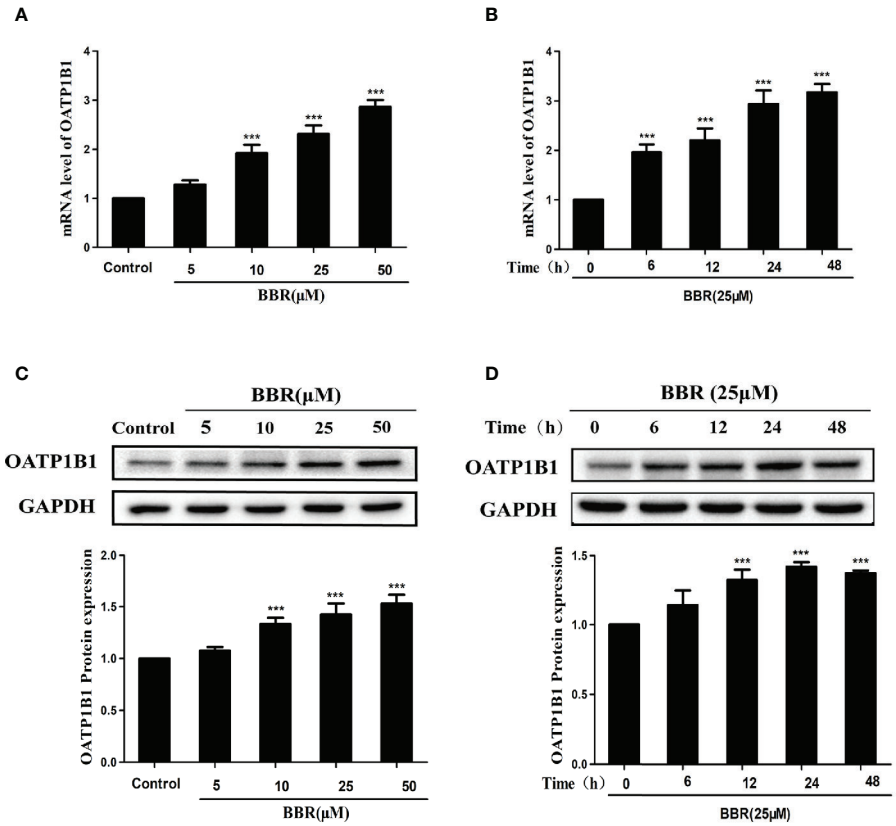

FIGURE 1 | Effects of berberine on OATP1B1 expression in HepG2 cells. **(A, B)**. *OATP1B1* mRNA expression was analyzed by real-time PCR in HepG2 cells after treatment with increasing concentrations of berberine (5, 10, 25, and 50 μM) for 24 h or treatment with 25 μM berberine at a series of time points (6, 12, 24, and 48 h). **(C, D)** OATP1B1 protein levels were determined by Western blotting in HepG2 cells after treatment with increasing concentrations of berberine (5, 10, 25, and 50 μM) for 24 h or treatment with 25 μM berberine at a series of time points (6, 12, 24, and 48 h). Data are represent as mean ± SD from triplicate independent experiments after being normalized to GAPDH, and 0.1% dimethylsulfoxide (DMSO) were used as the negative control. ***P < 0.001 compared to the control.

compared to control, respectively (**Figure 2A**). The half-maximal effective concentration (EC_{50}) value was measured to be 19.01 ± 1.21 μM (**Figure 2B**).

Berberine Enhanced FXR and LXRα Mediated Activation of OATP1B1 Promoter

HepG2 cells were treated with 10 μM of nuclear receptor ligands including rifampicin (PXR ligand), CITCO (CAR ligand), GW4064 (FXR ligand), or GW3965 (LXRα ligand) for 24 h. PCR and Western blot analysis showed that only GW3965 (a specific LXRα agonist) and GW4064 (a specific FXR agonist) markedly upregulated the expression of OATP1B1 mRNA and protein (**Figures 3A, B**).

Next we performed dual luciferase reporter assay to investigate the potency of berberine on activating transcriptional activity of LXRα and FXR on *OATP1B1* promoter. As shown in **Figure 4A**, luciferase activity significantly increased after treatment with 25 μM berberine or/and 10 μM corresponding ligands. Meanwhile, the EC_{50} value was 12.19 ± 0.86 μM in HepG2-hFXR-OATP1B1-luc cells (**Figure 4B**), and the EC_{50} value was 32.15 ± 2.32 μM in HepG2-hLXRα-OATP1B1-luc cells (**Figure 4C**), while the EC_{50} in the two cell lines were 2.56 ± 0.21 and 2.37 ± 0.36 μM, respectively, after GW4064 and GW3965 treatment. These data suggest that berberine could improve hFXR or hLXRα-mediated activation of OATP1B1 luciferase activity in a concentration-dependent manner,

Berberine Enhanced FXR and LXRα Induced Expression of OATP1B1 Protein and Transport Function

To further investigate the potency of LXRα and FXR activated by berberine on regulating OATP1B1 expression, HepG2 cell models with silenced or induced FXR and LXRα activities were

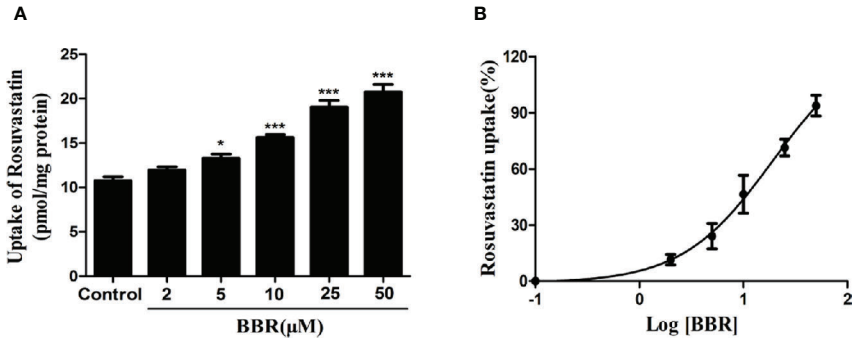

FIGURE 2 | Berberine enhanced rosuvastatin uptake in HepG2 cells. **(A, B)** Rosuvastatin uptake assay was conducted in HepG2 cells treated with increasing concentrations (2, 5, 10, 25, and 50 μM) of berberine for 24 h. The concentrations of rosuvastatin were determined by HPLC-MS/MS. DMSO (0.1%) was used as the negative control. Data are expressed as mean ± SD of triplicate independent experiments,*P < 0.05, ***P < 0.001 compared to the control.

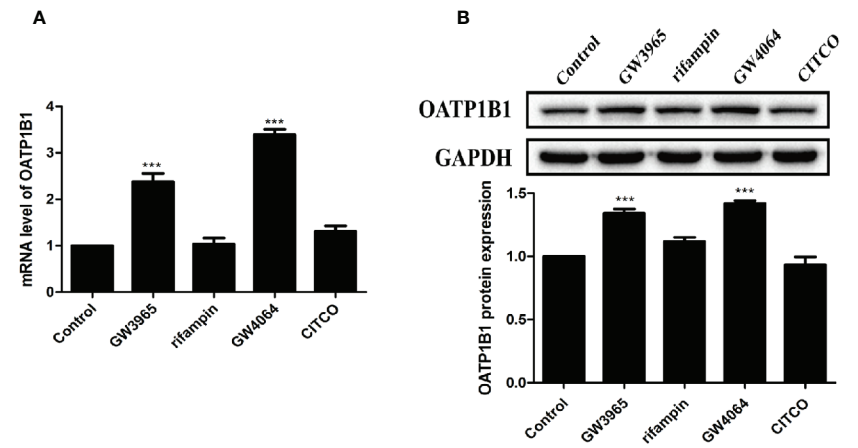

FIGURE 3 | Effects of diverse nuclear receptors activators on OATP1B1 expression in HepG2 cells. HepG2 cells were treated with 10 μM GW3965, 10 μM rifampin, 10 μM GW4064, or 10 μM CITCO for 24 h, OATP1B1 expression was determined by real-time PCR **(A)** and Western blot analysis **(B)**. DMSO (0.1%) was used as the negative control. Data are expressed as mean ± SD from triplicate independent experiments, ***P < 0.001 compared to the control.

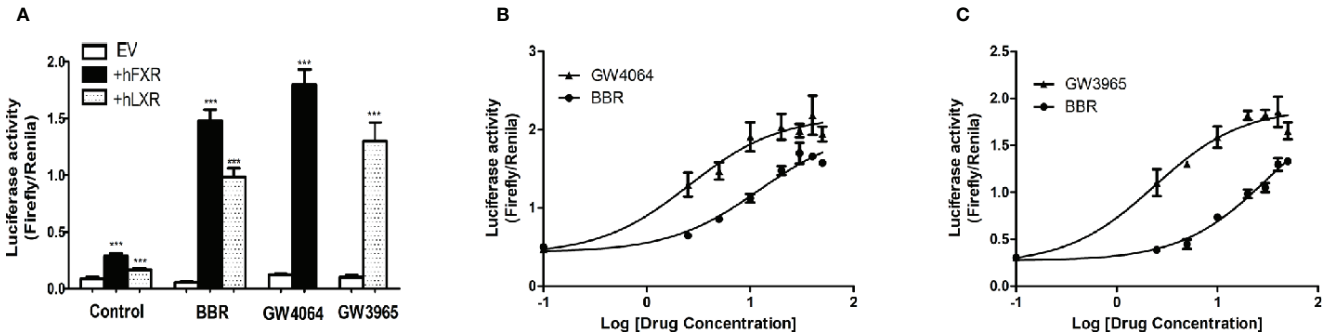

FIGURE 4 | Effect of berberine on OATP1B1 promoter in HepG2 cells transiently transfected with hFXR or hLXRα. HepG2 cells transiently co-transfected with pTracer-hFXR or pTracer-hLXRα and reporter vector pGL3-OATP1B1 were treated with berberine (25 μM), GW4064 (10 μM), or GW3965 (10 μM) **(A)**, and increasing concentrations of berberine (2.5, 5, 10, 20, 30, 40, 50 μM), GW4064 (2.5, 5, 10, 20, 30, 40, 50 μM), or GW3964 (2.5, 5, 10, 20, 30, 40, 50 μM) **(B, C)**. The fold induction of luciferase activity was determined using a Dual-Luciferase reporter assay system. DMSO (0.1%) was used as the negative control. Data are expressed as mean ± SD of triplicate independent experiments, ***P < 0.001 compared to the control.

constructed. First, Western blot analysis confirmed that transfection of siRNA-hFXR or siRNA-hLXRα into HepG2 cells significantly reduced FXR and LXRα protein levels compared to control group (**Figures 5A, C**). Subsequently, HepG2 cells were treated with berberine, GW4064, GW3965, or/and FXR/LXRα siRNAs. As shown in **Figures 5B, D**, the induction of OATP1B1 expression by GW4064 and GW3965 was significantly increased by berberine, while FXR or LXRα siRNA eliminated the upregulation of OATP1B1 by berberine. Furthermore, berberine, GW4064 and GW3965 significantly increased the uptake of rosuvastatin by OATP1B1, but knockdown of FXR or LXRα significantly reduced berberine stimulated rosuvastatin uptake by OATP1B1 (**Figure 5E**). These results indicate that FXR and LXRα participate in the upregulation of OATP1B1 expression by berberine.

Berberine Induced Nuclear Translocation of FXR and LXRα

Previous studies reported that nuclear receptors such as FXR and LXRα regulate the expression of target genes after ligand-induced nuclear translocation (Lee et al., 2010; Xu et al., 2016). Therefore, we investigated the effect of berberine on the expression and distribution of FXR and LXRα in HepG2 cells. PCR analysis showed that berberine significantly increased FXR mRNA expression in a concentration-dependent manner (**Figure 6A**). Consistently, Western blot analysis showed that berberine upregulated the expression of FXR protein in HepG2 cells, except that the induction of FXR protein by berberine was attenuated slightly at the highest dose of 50 μM (**Figure 6B**). However, berberine had no significantly effect on the expression of LXRα at both mRNA and protein levels (**Figures 6D, E**). Subsequently, cytoplasmic proteins and nuclear proteins were isolated and Western blot analysis showed that nuclear FXR and LXRα protein levels increased significantly after treatment with berberine for 24 h, while cytoplasmic FXR and LXRα protein levels decreased slightly (**Figures 6C, F**). These results indicate that berberine could promote nuclear translocation of FXR and LXRα.

DISCUSSION

In this study, we provide the first evidence that berberine enhanced FXR and LXRα mediated upregulation of OATP1B1 expression, resulting in enhanced uptake of the substrate rosuvastatin in HepG2 cells, which may be responsible for improved lipid-lowering efficacy in combination with statins.

Berberine is a new type of hypolipidemic drug widely used with favorable clinical efficacy and safety (Kong et al., 2004; Kong et al., 2009). Studies have reported that the combination of berberine with simvastatin can significantly enhance the hypolipidemic efficacy in patients and rats with hyperlipidemia, reduce the dose of statins, and lower the risk of adverse reactions (Bei-Bei et al., 2009; Kong et al., 2009; Li et al., 2019). Notably, we found that rosuvastatin had rapid uptake in HepG2 cells, this may be explained by that rosuvastatin is mainly transported by OATP1B1 and OATP1B3, which are highly expressed in the liver (Hagenbuch and Meier, 2003) Furthermore, we showed that berberine upregulated the expression of OATP1B1 transporter at both mRNA and protein levels in HepG2 cells, which could promote rosuvastatin uptake in HepG2 cells.

FXR and LXRα are widely involved in the regulation of transporters expression *in vivo*. Ligand-activated FXR can upregulate BSEP transcription, inhibit NTCP transcription or induce PLTP and CYP7A1 expression to promote bile acid secretion, suppress uptake of bile acid in the liver or increase cholesterol metabolism (Mak et al., 2002). LXRα regulates the metabolism of bile acids and cholesterol in the liver by regulating target genes such as CYP7, ABC transporter ABCA1, and lipoprotein lipase (Peet et al., 1998; Schmitz and Langmann, 2001). It has been reported that nuclear receptors FXR and LXRα

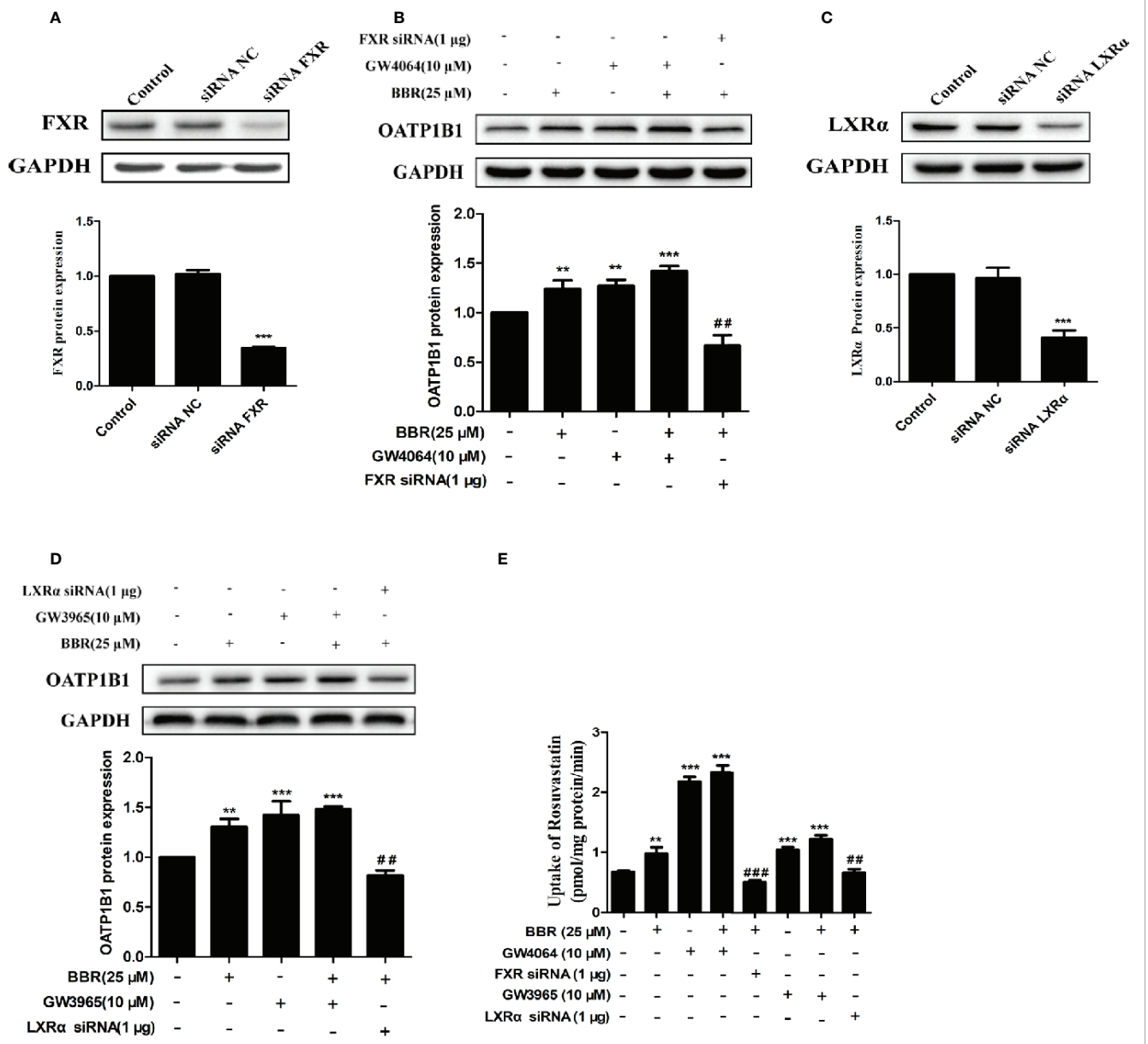

FIGURE 5 | Silencing *hFXR* and *hLXRα* expression abolished berberine-induced OATP1B1 expression in HepG2 cells. HepG2 cells were transiently transfected with small interfering RNA (siRNA)-hFXR or siRNA-hLXRα, and 48 h later protein levels of FXR **(A)** and LXRα **(C)** were examined by Western blot. HepG2 cells were then treated with berberine (25 μM), GW4064, or GW3965 (10 μM) for 24 h, OATP1B1 protein levels were analyzed by Western blot **(B, D)**. **(E)** Rosuvastatin uptake assay was conducted in HepG2 cells treated with berberine (25 μM), GW4064 or GW3965 (10 μM), or FXR siRNA or LXRα siRNA for 24 h. The concentrations of rosuvastatin were determined by HPLC-MS/MS. DMSO (0.1%) was used as negative control. Data are expressed as mean ± SD of triplicate independent experiments, $^{**}P < 0.01$, $^{***}P < 0.001$ compared to the control. $^{\#\#}P < 0.01$ and $^{\#\#\#}P < 0.001$ compared to 25 μM BBR group.

can act on OATP1B1 promoter to regulate the expression (Meyer Zu Schwabedissen et al., 2010). Our study demonstrated that berberine regulated the expression of OATP1B1 by activating FXR and LXRα. This finding was confirmed by Dual-Luciferase reporter assay. The results indicated that berberine had stronger induction on hFXR-mediated transcriptional activation of OATP1B1 than on hLXRα, but the effect was weaker than classical agonists GW4064 and GW3965. However, the combination of berberine and the corresponding agonists can further improve the expression of target proteins. Silencing FXR or LXRα by siRNA dramatically diminished the upregulation of OATP1B1expression by berberine. These results confirmed that FXR and LXRα mediate the effects of berberine on the upregulation of OATP1B1 expression.

However, the underlying mechanism by which berberine activates FXR and LXRα in HepG2 cells is unclear. LXRα and

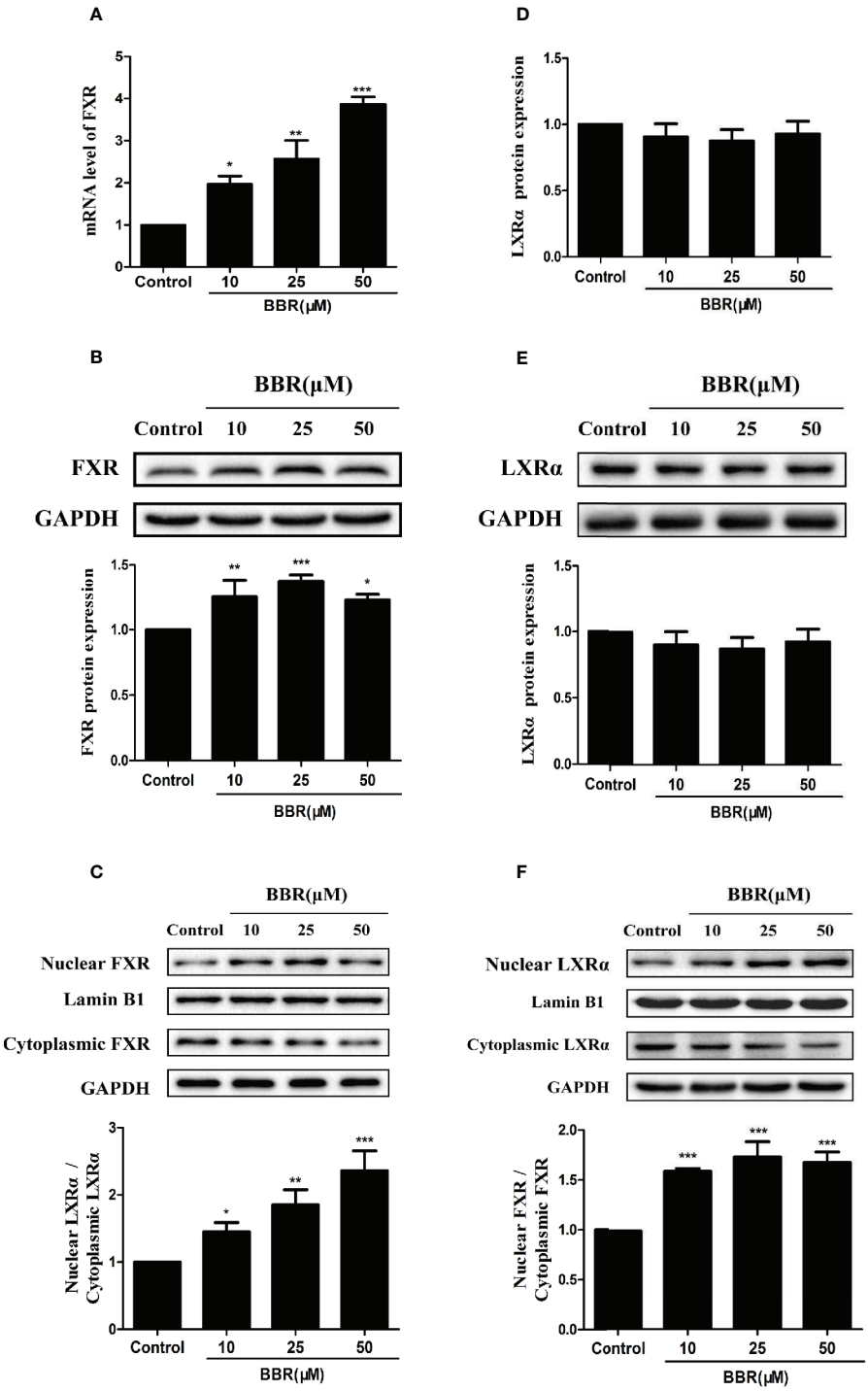

FIGURE 6 | Effects of berberine on FXR and LXRα expression and distribution in HepG2 cells. HepG2 cells were treated with increasing concentrations of berberine (10, 25, and 50 μM) for 24 h. FXR **(A)** and LXRα **(D)** mRNA levels were measured by PCR; protein levels were measured by Western blot **(B, E)**. The nuclear and cytoplasmic FXR **(C)** and LXRα **(F)** protein levels were quantified by Western blot. The determination of mRNA and protein were normalized to GAPDH, nuclear and cytoplasmic protein was normalized to Lamin B1 and GAPDH, respectively. DMSO (0.1%) was used as the negative control. Data are expressed as mean ± SD of triplicate independent experiments,*P < 0.05, **P < 0.01, ***P < 0.001 compared to the control.

FXR have been identified as critical nuclear receptors which bind to the promoters of target genes to regulate transcriptional activity of downstream target genes after ligand-activated nuclear translocation (Meyer Zu Schwabedissen et al., 2010; Xu et al., 2016; Zhou et al., 2016). In this study we found that berberine promoted nuclear translocation and activation of FXR and LXRα, similar to other Chinese herbal medicines such as ginkgolide b (Zhou et al., 2016) and dihydroartemisinin (Xu et al., 2016). In addition, berberine significantly increased the expression of FXR protein and mRNA at 10 and 25 μM, but only moderately upregulated the expression of FXR protein at 50 μM, while the mRNA expression was still significantly upregulated, suggesting that FXR may be subjected to a series of post-transcriptional regulations, such as phosphorylation, acetylation, and glycosylation (Chang, 2009; Sugatani et al., 2014).

Although statins are known as HMG-CoA reductase inhibitors, previous study suggested that berberine inhibited HMG-CoA reductase activity *via* increased phosphorylation of HMG-CoA reductase, leading to reduced hepatic cholesterol level (Wu et al., 2011). In addition, recent reports showed that berberine could inhibit lipogenesis by targeting sterol regulatory element-binding protein (SREBP) related signaling (Yunxin et al., 2019; Zhu et al., 2019). Therefore, furthers studies are needed to demonstrate that berberine and statins in combination can inhibit SREBP signaling and HMG-Co reductase activity to achieve enhanced hypolipidemic effects.

In summary, our results suggest that berberine upregulates the expression of OATP1B1 in HepG2 cells by inducing nuclear translocation of FXR and LXRα, which then activate the expression of OATP1B1 and increase the uptake of rosuvastatin.

DATA AVAILABILITY STATEMENT

All datasets generated for this study are included in the article/ **Supplementary Material**.

AUTHOR CONTRIBUTIONS

YX, HZ, and CX participated in study design. ML, DZ, and WD conducted the experiments and analyzed the data. JW and SH contributed to the writing of the manuscript.

FUNDING

This work was supported by the Natural Science Foundation of China (No. 81673506).

SUPPLEMENTARY MATERIAL

The Supplementary Material for this article can be found online at: https://www.frontiersin.org/articles/10.3389/fphar.2020.00375/full#supplementary-material

REFERENCES

Bei-Bei, Z., Jing, W. E. I., Jian-Dong, J., He-He, G., and Rui-Sheng, Z. (2009). The therapeutic effects of combination of simvastatin with berberine on the patients with hyperlipemia. *Acta Universitatis Med. Nanjing* 29, 1493–1497.

Belwal, T., Bisht, A., Devkota, H.P., Ullah, H., Khan, H., Bhatt, I.D., et al. (2020). hytopharmacology and clinical updates of Berberis species against diabetes and other metabolic diseases. *Front. Pharmacol.* 11, 41. doi: 10.3389/fphar.2020.00041

Bu, P., Le, Y., Zhang, Y., Zhang, Y., and Cheng, X. (2017). Berberine-induced inactivation of signal transducer and activator of transcription 5 signaling promotes male-specific expression of a bile acid uptake transporter. *J. Biol. Chem.* 292, 4602–4613. doi: 10.1074/jbc.M116.757567

Chang, T. K. H. (2009). Activation of pregnane x receptor (pxr) and constitutive androstane receptor (car) by herbal medicines. *AAPS J.* 11, 590–601. doi: 10.1208/s12248-009-9135-y

Gu, S., Cao, B., Sun, R., Tang, Y., Paletta, J. L., Wu, X.-L., et al. (2015). A metabolomic and pharmacokinetic study on the mechanism underlying the lipid-lowering effect of orally administered berberine. *Mol. Biosyst.* 11, 463–474. doi: 10.1039/c4mb00500g

Guo, Y., Chen, Y., Tan, Z.-R., Klaassen, C. D., and Zhou, H.-H. (2012). Repeated administration of berberine inhibits cytochromes p450 in humans. *Eur. J. Clin. Pharmacol.* 68, 213–217. doi: 10.1007/s00228-011-1108-2

Hagenbuch, B., and Meier, P. J. (2003). The superfamily of organic anion transporting polypeptides. *Biochim. Et Biophys. Acta-Biomembranes* 1609, 1–18. doi: 10.1016/s0005-2736(02)00633-8

Huijgen, R., Abbink, E. J., Bruckert, E., Stalenhoef, A. F. H., Imholz, B. P. M., Durrington, P. N., et al. (2010). Colesevelam added to combination therapy with a statin and ezetimibe in patients with familial hypercholesterolemia: A 12-week, multicenter, randomized, double-blind, controlled trial. *Clin. Ther.* 32, 615–625. doi: 10.1016/j.clinthera.2010.04.014

Jigorel, E., Le Vee, M., Boursier-Neyret, C., Parmentier, Y., and Fardel, O. (2006). Differential regulation of sinusoidal and canalicular hepatic drug transporter expression by xenobiotics activating drug-sensing receptors in primary human hepatocytes. *Drug Metab. Disposition* 34, 1756–1763. doi: 10.1124/dmd.106.010033

Kitamura, S., Maeda, K., Wang, Y., and Sugiyama, Y. (2008). Involvement of multiple transporters in the hepatobiliary transport of rosuvastatin. *Drug Metab. Disposition* 36, 2014–2023. doi: 10.1124/dmd.108.021410

Knapp, H. H., Schrott, H., Ma, P., Knopp, R., Chin, B., Gaziano, J. M., et al. (2001). Efficacy and safety of combination simvastatin and colesevelam in patients with primary hypercholesterolemia. *Am. J. Med.* 110, 352–360. doi: 10.1016/s0002-9343(01)00638-6

Kong, W. J., Wei, J., Abidi, P., Lin, M. H., Inaba, S., Li, C., et al. (2004). Berberine is a novel cholesterol-lowering drug working through a unique mechanism distinct from statins. *Nat. Med.* 10, 1344–1351. doi: 10.1038/nm1135

Kong, W., Wei, J., Zou, Z., Wang, Y., Song, D., You, X., et al. (2008). Combination of simvastatin with berberine improves the lipid-lowering efficacy. *Metabolism* 57, 1029–1037. doi: 10.1016/j.metabol.2008.01.037

Kong, W.-J., Zhang, H., Song, D.-Q., Xue, R., Zhao, W., Wei, J., et al. (2009). Berberine reduces insulin resistance through protein kinase c-dependent up-regulation of insulin. Receptor expression. *Metabolism-Clin. Exp.* 58, 109–119. doi: 10.1016/j.metabol.2008.08.013

Kunze, A., Huwyler, J., Camenisch, G., and Poller, B. (2014). Prediction of organic anion-transporting polypeptide 1b1-and 1b3-mediated hepatic uptake of statins based on transporter protein expression and activity data. *Drug Metab. Disposition* 42, 1514–1521. doi: 10.1124/dmd.114.058412

Lau, C. W., Yao, X. Q., Chen, Z. Y., Ko, W. H., and Huang, Y. (2001). Cardiovascular actions of berberine. *Cardiovasc. Drug Rev.* 19, 234–244. doi: 10.1111/j.1527-3466.2001.tb00068.x

Lee, T. S., Pan, C. C., Peng, C. C., Kou, Y. R., Chen, C. Y., Ching, L. C., et al. (2010). Anti-atherogenic effect of berberine on lxrα-abca1-dependent cholesterol efflux in macrophages. *J. Cell. Biochem.* 111, 104–110. doi: 10.1002/jcb.22667

Li, J., Wang, Y., Zhang, W., Huang, Y., Hein, K., and Hidalgo, I. J. (2012). The role of a basolateral transporter in rosuvastatin transport and its interplay with apical breast cancer resistance protein in polarized cell monolayer systems. *Drug Metab. Disposition* 40, 2102–2108. doi: 10.1124/dmd.112.045666

Li, G., Zhao, M., Qiu, F., Sun, Y., and Zhao, L. (2019). Pharmacokinetic interactions and tolerability of berberine chloride with simvastatin and fenofibrate: An open-label, randomized, parallel study in healthy chinese subjects. *Drug Design Dev. Ther.* 13, 129–139. doi: 10.2147/dddt.s185487

Mak, P. A., Kast-Woelbern, H. R., Anisfeld, A. M., and Edwards, P. A. (2002). Identification of pltp as an lxr target gene and apoe as an fxr target gene reveals overlapping targets for the two nuclear receptors. *J. Lipid Res.* 43, 2037–2041. doi: 10.1194/jlr.C200014-JLR200

Meyer Zu Schwabedissen, H. E., Böttcher, K., Chaudhry, A., Kroemer, H. K., Schuetz, E. G., and Kim, R. B. (2010). Liver x receptor α and farnesoid x receptor are major transcriptional regulators of oatp1b1. *Hepatology* 52, 1797–1807. doi: 10.1002/hep.23876

Montes, F. Q., Vázquez-Hernández, A., and Fenton-Navarro, B. (2019). Active compounds of medicinal plants, mechanism for antioxidant and beneficial effects. *Phyton Int. J. Exp. Bot.* 88, 1–10. doi: 10.32604/phyton.2019.04525

Neag, M. A., Mocan, A., Echeverría, J., Pop, R. M, Bocsan, C. I., Crişan, G., et al. (2018). Berberine: Botanical occurrence, traditional uses, extraction methods, and relevance in cardiovascular, metabolic, hepatic, and renal disorders. *Front. Pharmacol.* 9, 557. doi: 10.3389/fphar.2018.00557

Peet, D. J., Turley, S. D., Ma, W. Z., Janowski, B. A., Lobaccaro, J. M. A., Hammer, R. E., et al. (1998). Cholesterol and bile acid metabolism are impaired in mice lacking the nuclear oxysterol receptor lxr alpha. *Cell* 93, 693–704. doi: 10.1016/s0092-8674(00)81432-4

Robinson, J. G., and Davidson, M. H. (2006). Combination therapy with ezetimibe and simvastatin to achieve aggressive ldl reduction. *Expert Rev. Cardiovasc. Ther.* 4, 461–476. doi: 10.1586/14779072.4.4.461

Ruan, H., Zhan, Y., Hou, J., Xu, B., Chen, B., Tian, Y., et al. (2017). Berberine binds rxrα to suppress β-catenin signaling in colon cancer cells. *Oncogene* 36, 6906. doi: 10.1038/onc.2017.296

Schmitz, G., and Langmann, T. (2001). Structure, function and regulation of the abc1 gene product. *Curr. Opin. Lipidol.* 12, 129–140. doi: 10.1097/00041433-200104000-00006

Shitara, Y., and Sugiyama, Y. (2006). Pharmacokinetic and pharmacodynamic alterations of 3-hydroxy-3-methylglutaryl coenzyme a (hmg-coa) reductase inhibitors: Drug-drug interactions and interindividual differences in transporter and metabolic enzyme functions. *Pharmacol. Ther.* 112, 71–105. doi: 10.1016/j.pharmthera.2006.03.003

Staffa, J. A., Chang, J., and Green, L. (2002). Cerivastatin and reports of fatal rhabdomyolysis. *New Engl. J. Med.* 346, 539–540. doi: 10.1056/nejm200202143460721

Staudinger, J. L., Woody, S., Sun, M., and Cui, W. (2013). Nuclear-receptor-mediated regulation of drug- and bile-acid-transporter proteins in gut and liver. *Drug Metab. Rev.* 45, 48–59. doi: 10.3109/03602532.2012.748793

Sugatani, J., Hattori, Y., Noguchi, Y., Yamaguchi, M., Yamazaki, Y., and Ikari, A. (2014). Threonine-290 regulates nuclear translocation of the human pregnane x receptor through its phosphorylation/dephosphorylation by ca2+/calmodulin-dependent protein kinase ii and protein phosphatase 1. *Drug Metab. Disposition* 42, 1708–1718. doi: 10.1124/dmd.114.059139

Urquhart, B. L., Tirona, R. G., and Kim, R. B. (2007). Nuclear receptors and the regulation of drug-metabolizing enzymes and drug transporters: Implications for interindividual variability in response to drugs. *J. Clin. Pharmacol.* 47, 566–578. doi: 10.1177/0091270007299930

White, C. M. (2002). A review of the pharmacologic and pharmacokinetic aspects of rosuvastatin. *J. Clin. Pharmacol.* 42, 963–970. doi: 10.1177/009127002401102876

Wolfe, M. L., Vartanian, S. F., Ross, J. L., Bansavich, L. L., Mohler, E. R., Meagher, E., et al. (2001). Safely and effectiveness of niaspan when added sequentially to a statin for treatment of dyslipidemia. *Am. J. Cardiol.* 87, 476–47+. doi: 10.1016/s0002-9149(00)01410-7

Wu, X. C., Li, Q., Xin, H. W., Yu, A. R., and Zhong, M. Y. (2005). Effects of berberine on the blood concentration of cyclosporin a in renal transplanted recipients: Clinical and pharmacokinetic study. *Eur. J. Clin. Pharmacol.* 61, 567–572. doi: 10.1007/s00228-005-0952-3

Wu, N., Sarna, L. K., Siow, Y. L., and O, K. (2011). Regulation of hepatic cholesterol biosynthesis by berberine during hyperhomocysteinemia. *Am. J. Of Physiology-Regulatory Integr. Comp. Physiol.* 300, R635–R643. doi: 10.1152/ajpregu.00441.2010

Xu, W., Lu, C., Zhang, F., Shao, J., and Zheng, S. (2016). Dihydroartemisinin restricts hepatic stellate cell contraction via an fxr-s1pr2-dependent mechanism. *IUBMB Life* 68, 376–387. doi: 10.1002/iub.1492

Yunxin, L., Weiwei, H., Yao, L., Xirui, X., Zheng, Z., Chao, L., et al. (2019). Berberine suppresses colon cancer cell proliferation by inhibiting the scap/srebp-1 signaling pathway-mediated lipogenesis. *Biochem. Pharmacol.* 174. doi: 10.1016/j.bcp.2019.113776

Zhong, J., Deng, L., Jiang, Y., Zou, L., Yuan, H., and Tan, S.-X. (2018). Gene expression profiling of hepg(2) cells after treatment with black tea polyphenols. *Biocell* 42, 99–104. doi: 10.32604/biocell.2018.04915

Zhou, T., You, W.-T., Ma, Z.-C., Liang, Q.-D., Tan, H.-L., Xa, C.-R., et al. (2016). Ginkgolide b protects human umbilical vein endothelial cells against xenobiotic injuries via pxr activation. *Acta Pharmacol. Sin.* 37, 177–186. doi: 10.1038/aps.2015.124

Zhu, X. P., Bian, H., Wang, L., Sun, X. Y., Xu, X., Yan, H. M., et al. (2019). Berberine attenuates nonalcoholic hepatic steatosis through the ampk-srebp-1c-scd1 pathway. *Free Radical Biol. Med.* 141, 192–204. doi: 10.1016/j.freeradbiomed.2019.06.019

Conflict of Interest: The authors declare that the research was conducted in the absence of any commercial or financial relationships that could be construed as a potential conflict of interest.

frontiers in Pharmacology

ORIGINAL RESEARCH
published: 13 May 2020
doi: 10.3389/fphar.2020.00652

Network Pharmacology-Based Approach Uncovers the Mechanism of GuanXinNing Tablet for Treating Thrombus by MAPKs Signal Pathway

Mu-Lan Wang[1,2†], Qin-Qin Yang[1,3†], Xu-Hui Ying[2], Yuan-Yuan Li[1], Yang-Sheng Wu[1], Qi-Yang Shou[1], Quan-Xin Ma[1], Zi-Wei Zhu[2] and Min-Li Chen[1]*

[1] Academy of Chinese Medicine & Institute of Comparative Medicine, Zhejiang Chinese Medical University, Hangzhou, China, [2] The Department of Medicine, Chiatai Qingchunbao Pharmaceutical Co., Ltd., Hangzhou, China, [3] Department of Experimental Animals, Zhejiang Academy of Traditional Chinese Medicine, Hangzhou, China

OPEN ACCESS

Edited by:
Jianxun Liu,
China Academy of Chinese Medical Sciences, China

Reviewed by:
Songxiao Xu,
Artron BioResearch Inc., Canada
Yi Ding,
Fourth Military Medical University, China
Yunyao Jiang,
Tsinghua University, China

****Correspondence:***
Min-Li Chen
cmli991@zcmu.edu.cn

[†]These authors have contributed equally to this work

Specialty section:
This article was submitted to Ethnopharmacology, a section of the journal Frontiers in Pharmacology

Received: *31 May 2019*
Accepted: *22 April 2020*
Published: *13 May 2020*

Citation:
Wang M-L, Yang Q-Q, Ying X-H, Li Y-Y, Wu Y-S, Shou Q-Y, Ma Q-X, Zhu Z-W and Chen M-L (2020) Network Pharmacology-Based Approach Uncovers the Mechanism of GuanXinNing Tablet for Treating Thrombus by MAPKs Signal Pathway. Front. Pharmacol. 11:652. doi: 10.3389/fphar.2020.00652

Background: GuanXinNing tablet (GXNT), a traditional Chinese patent medicine, has been found to have remarkable antithrombotic effects and can effectively inhibit pro-thrombotic factors in previous studies. However, the mechanism of its antithrombotic effects remains little known.

Methods: In this study, we first determined and identified the sources of each main compound in GXNT using liquid chromatography-mass spectrometry (LC-MS). Through the approach of network pharmacology, we predicted the action targets of the active components, mapped the target genes related to thrombus, and obtained potential antithrombotic targets for active ingredients. We then performed gene ontology (GO) enrichment analyses and KEGG signaling pathway analyses for the action targets, and constructed networks of active component–target and active component–target–pathway for GXNT. Additionally, we evaluated the pharmacodynamic effects of GXNT on thrombus using the rat thrombus model induced by $FeCl_3$, observed the effects of antiplatelet aggregation *via* platelet assay, and further verified the results predicted by network pharmacology *via* Western blot.

Results: In total, 14 active ingredients were identified in GXNT, and 83 action targets were predicted, 17 of which are antithrombotic targets that potentially participate in processes including response to oxidative stress and positive regulation of blood vessel endothelial cell migration. KEGG pathway analyses revealed that the predicted action targets were involved in multiple signal pathways, such as MAPK, IL-17, and platelet activation. Pharmacodynamics study found that GXNT could significantly reduce the thrombus length and weight, lower platelet aggregation function, and decrease the levels of Fbg and PAI-1. In addition, GXNT could significantly increase 6-keto-PGF1α content and regulate the ratio of TXB_2/6-keto-PGF1α, while not having dramatic effects on TXB_2. GXNT was also observed to visibly inhibit maximum platelet aggregation. Herein, we further studied the thrombus-related MAPKs signaling pathway and found that GXNT could significantly reduce the phosphorylation levels of p38MAPK, ERK, and JNK proteins in platelet.

Conclusions: This study revealed the pharmacodynamic material basis of GXNT and its potential multicomponent–multitarget–multipath pharmacological effects, confirmed the antithrombotic effects of GXNT, and showed that its mechanism may be related to inhibiting phosphorylation of p38, ERK, and JNK proteins in MAPKs signaling pathway, partially verifying the results from network pharmacology. The results from this study could provide a theoretical basis for the development and clinical application of GXNT.

Keywords: GuanXinNing tablet, network pharmacology, thrombus, Danshen, Chuanxiong, MAPKs signal pathway

INTRODUCTION

Thrombus is a common pathophysiological basis for various cardiovascular diseases in the clinic, such as acute myocardial infarction, stroke, and coronary heart disease (Sadowski et al., 2014; Wang, 2018). Traditional Chinese medicine (TCM) believes that cold coagulation and blood stasis plays an important role in thrombotic diseases (Gu, 2010). Warming collaterals and activating blood circulation therapy is a general principle for treating cold coagulation and blood stasis syndrome, according to the Yellow Emperor's Internal Classic. As a consequence, Chinese medicine with the function of activating blood circulation and removing blood stasis is often used to prevent and cure thromboembolic diseases.

GuanXinNing is a classical Chinese herbal formula preparation, which is composed of two well-established Chinese herbs that activate blood circulation and remove blood stasis: *Salvia miltiorrhiza* Bge. (Chinese name Danshen, DS) and *Ligusticum chuanxiong* Hort. (Chinese name Chuanxiong, CX). This preparation has the effect of activating blood circulation, removing blood stasis, dredging arteries, and nourishing the heart. To improve patient convenience and compliance, GuanXinNing tablet (GXNT) is a novel preparation developed from the widely used GuanXinNing injection with an improved extraction process. GXNT consists of extracts from Danshen and Chuanxiong at the ratio of 1:1 (Chen et al., 2005), and has already been approved for listing by the China Food and Drug Administration (CFDA approval no. Z20150028). Danshen, the dry roots of *Salvia miltiorrhiza* Bge., is beneficial to heart and liver with a bitter taste and a slightly cold property. Studies have demonstrated that Danshen has significant anti-arrhythmia effects *via* reducing myocardial infarct size, protecting myocardial injury (Chang et al., 2016), and improving myocardial ischemia (Zhang et al., 2013). The second Chinese herb component, Chuanxiong, is the dry rhizome of *Ligusticum chuanxiong* Hort. Chuanxiong is known to protect the liver, gallbladder, and pericardium with a mild property and an acrid taste, and has the effects of activating blood circulation, moving qi, dispelling wind, and relieving pain (Chen et al., 2018b). Modern pharmacological studies have shown that Chuanxiong has antioxidation, anti-inflammation, neuroprotection, and anti-bacteria activities (Chen et al., 2018b; Shan et al., 2018). Moreover, our previous studies have found that GXNT could reduce platelet aggregation, scavenge free radicals, ameliorate blood coagulation in rats with qi stagnation and blood stasis, protect the vascular endothelium (Chen et al., 2005), and have antithrombotic activities with multiple-target effects (Wang et al., 2016). Nevertheless, TCM is a complex chemical composition system of multiple components, with multiple targets, multiple links, and multiple effects. Therefore, a holistic view of "multiple components-multiple targets-multiple pathways" is needed to study the material basis and action mechanism of GXNT on thrombus.

Network pharmacology uses high-throughput omics data analysis, virtual computing, and network database retrieval to construct an interaction network of "compound-gene-disease" and to provide a holistic understanding of the relationship between drugs and targets. Integrating with systems biology, multi-directional pharmacology and bioinformatics, and network pharmacology offers new approaches and strategies for designing and developing new drugs (Hopkins, 2008; Li, 2013). In particular, it has unique advantages and potential in predicting and identifying the active ingredient clusters and action targets of Chinese medicines, and in discovering new indications through active molecule screening, target prediction, network construction, and analysis. The systemic and holistic traits of network pharmacology are in line with the complexity of TCM, making it widely adopted in studying the pharmacodynamic material basis and action mechanism of TCM preparations, such as XinShengHua granule (Pang et al., 2018), MaZiRen wan (Huang et al., 2018), YinHuangQingFei capsule (Yu et al., 2017), YangXinShi tablet (Chen et al., 2018a), etc.

In this study, we used network pharmacology to predict the targets of active ingredients in GXNT and investigate its action mechanism. Firstly, the main active components of GXNT were identified and screened based on liquid chromatography-mass spectrometry (LC-MS) combined with traditional Chinese medicine system pharmacology technology platform (TCMSP). Then, active ingredient targets were predicted using Swiss Target Prediction web server to construct the active ingredient-target, protein interaction, and component–target–pathway network for analyzing the pharmacodynamic basis and action mechanism of GXNT. Next, the common carotid artery thrombus model in rats induced by $FeCl_3$ was adopted to further verify the antithrombotic effects of GXNT, followed by the antiplatelet study. Finally, we examined the protein expressions in the predicted thrombus-related signaling pathways *via* Western blot to verify the antithrombotic mechanism of GXNT. The results from this study provided a theoretical reference for the development and utilization of GXNT.

MATERIALS AND METHODS

Materials and Regents

GXNT (GXN extract powder, raw drug dosage of 12.8 g/g), Danshen and Chuanxiong were all provided by Chiatai Qinchunbao Pharmaceutical co., LTD. (Hangzhou, China). The herbal medicines of Danshen and Chuanxiong in GXNT were collected from Linyi City (Shandong Province, China) and Dujiangyan City (Sichuan Province, China) respectively, and were authenticated correspondingly by Prof. Yuqing Ye (Chinese Medicine Resource Research and Development Center, Shanghai Institute of Traditional Chinese Medicine) and Prof. Guihua Jiang (School of Pharmacy, Chengdu Chinese Medical University). The voucher specimens were deposited in the Quality Department of Chiatai Qinchunbao Pharmaceutical co., LTD. Reference standards of tanshinol sodium (110855-200809, purity=100%), protocatechualdehyde (110810-201608, purity=99.3%), chlorogenic acid (110753-200413, purity=100%), caffeic acid (110885-200102, purity=100%), ferulic acid (110773-201012, purity=100%), rosmarinic acid (111871-201505, purity=98.5%), and salvianolic acid B (111562-201514, purity=93.7%) were all purchased from National Institute for the Control of Pharmaceutical and Biological Products (Beijing, China). LC-MS grade acetonitrile and formic acid with ≥98.0% of the purity were purchased from Merck (Darmstadt, Germany). Other reagents were all of analytical grade. Ultrapure water purified by Millipore Ultra-pure Water Purifier (Millipore, Milford, MA, USA) was used. Clopidogrel bisulfate was purchased from Sanofi-Aventis Pharmaceutical Co., Ltd. (Hangzhou, China). Fibrinogen (Fbg) kit was purchased from Dade Behring Marburg GmbH (Marburg, Germany). Plasminogen activator inhibitors (PAI-1), 6-keto-prostaglandin F1α (6-keto-PGF1α), and thromboxane B_2 (TXB_2) assay kits were all purchased from Nanjing Jiancheng Bioengineering Research Institute Co., Ltd. (Nanjing, China). Aspirin enteric-coated tablets were purchased from Bayer healthcare Co., Ltd. (Leverkusen, Germany). Adenosine diphosphate (ADP) and albumin from bovine serum (BSA) were purchased from Sigma-Aldrich (St. Louis, Missouri, USA). KeyGEN total protein extraction kit, BCA protein assay kit and western stripping buffer were purchased from Beyotime Biosciences (Shanghai, China). Primary antibodies against Phospho-p44/42 MAPK (Erk1/2, #4370), Phospho-p38 MAPK (#4511), Phospho-SAPK/JNK (#9255), and GAPDH were all purchased from Cell Signaling Technology (Boston, MA, USA). All male Sprague-Dawley (Gfeller et al.) rats, weighing 300 to 350 g, were purchased from Shanghai SLAC Laboratory Animal Co., Ltd (Certification No: SCXK [Hu] 2012-002; Shanghai, China). Prior to the experiment, the animals were housed in individually ventilated cages (IVC) with two rats in each cage under a 12-h light/dark cycle, and were provided with food and water *ad libitum*. All experiments were carried out strictly according to the requirements of the Institutional Animal Care and Use Committee of Zhejiang Chinese Medical University, and was approved by the Laboratory Animal Research Center of Zhejiang Chinese Medical University (Certification No: SYXK [Zhe] 2013-184).

Preparation for the Control Sample

The appropriate amount of each standard sample was accurately weighed using 1/100,000 precision analytical balance (Sartorius Group, German), and was diluted with 50% methanol solution to a constant volume for preparing mother liquor. It was then diluted to a series of concentrations and filtered with a 0.45-μm needle filter, from which the filtrate was obtained finally.

Preparation for GXNT Testing Sample

We took a mixture of Danshen and Chuanxiong (10 kg each), added it with 160 L water, and boiled it for 2 h. Afterwards, the extracted solution was poured out, and the remaining residue was extracted twice, in which 120 L water was added each time and boiled for 1.5 h. The three extracts were merged to concentrate to 15 L at 60°C in a single-effect concentrator, and the solution after concentration was transferred to a rotary evaporator to concentrate to approximately 9 L at 60°C. About 35 L of 95% ethanol solution was added to the concentrated liquor, and was allowed to stand overnight. The supernatant was taken and concentrated to about 5 L at 60°C using a rotary evaporator. The concentrate was placed into a vacuum drying oven, dried thoroughly at 60°C, and powdered homogeneously with a powder machine to obtain solid powder of about 1.5 kg (raw dose of 12.85 g/g). Subsequently, 1.0 g of the powder was accurately weighed, brought to 20 mL with 50% methanol added, and sonicated for 10 min. It was then filtered through a 0.45-μm microporous filter column, from which an appropriate amount was injected into HPLC-MS instrument for analysis (Shimadzu LC-20A liquid chromatograph, Shimadzu, Japan; API 3200 LCMS/MS Mass Spectrometry System, American AB SCIEX, USA).

Preparation for Danshen Testing Sample

The preparation was performed in accordance with GXNT technology. We took 6 kg of Danshen and decocted it with water three times. In specific, 48 L was added and boiled for 2 h for the first time, and 36 L was added and boiled for 1.5 h for the second and third time. The three extracts were merged to concentrate to 3.2 L at 60°C in a single-effect concentrator. About 8.5 L of 95% ethanol solution was added into the concentrated liquor, and was allowed to stand overnight. The supernatant was taken and concentrated to about 1 L at 60°C using a rotary evaporator. The concentrate was placed into a vacuum drying oven, dried thoroughly at 60°C, and powdered evenly to obtain about 402 g of solid powder (raw dose of 15.0 g/g). Subsequently, 0.5 g of the powder was weighed accurately, brought to 20 mL with 50% methanol, and sonicated for 10 min. After that, it was filtered through a 0.45-μm microporous filter column, from which an appropriate amount was injected into HPLC-MS instrument for analysis.

Preparation for Chuanxiong Testing Sample

The preparation was conducted according to GXNT technology. We took 3.5 kg of Chuanxiong, and decocted it with water three times. In specific, 28 L was added and boiled for 2 h for the first

time, and 21 L was added and boiled for 1.5 h for the second and third time. The three extracts were merged to concentrate to 2 L at 60°C in a single-effect concentrator. About 7.5 L of 95% ethanol solution was added into the concentrate, and was allowed to stand overnight. The supernatant was taken and concentrated to about 1 L at 60°C using a rotary evaporator. The concentrate was placed into a vacuum drying oven, dried thoroughly at 60°C, and powdered evenly to obtain about 538 g of solid powder (raw dose of 6.5 g/g). Subsequently, 1.0 g of powder was weighed accurately, brought to 20 mL with 50% methanol, and sonicated for 10 min. After that, it was filtered through a 0.45-μm microporous filter column, from which an appropriate amount was taken to inject into HPLC-MS instrument for analysis.

LC-MS Analysis

LC-MS analysis of samples was carried out on a Shimadzu LC-20A liquid chromatograph (Shimadzu, Japan). An Agilent ZORBAX SB-C18 column (250×4.6 mm i.d., 5 μm, Agilent, USA) was used for column separation. The column temperature was maintained at 40°C, and the flow rate was kept at 1 mL/min, with acetonitrile as the mobile phase A and 0.1% formic acid in water as the mobile phase B. The gradient running procedure was programmed as follows: 0~5 min, 40~40% A; 5~25 min, 40~69% A; 25~30 min, 69~100% A. The injection volume was 5 μl. In addition, the mass spectrometer was an API 3200 LCMS/MS system. The detection mode was Q1 scan profile mode. The total scan time was 5 s per cycle with 599 cycles, and data was collected in the positive mode. The capillary voltage was 4500 V, and the mass range was from m/z 100 to 1000. Curtain Gas, Atomized Gas (Gas1), and Auxiliary Gas (Gas2) were nitrogen, and the pressure was set to 15 psi, 30 and 30 psi, respectively. We used 4500 V for the spray voltage, 450°C for the atomization temperature, 10 V for the collision chamber inlet voltage, and 70 V for the de-clustered voltage (DP). All data collection and processing were performed using Analyst software (version 1.6). The chemical structures of main compounds identified in GXNT were drawn with ChemDraw from CambridgeSoft. The chemical drawing software is capable of performing accurate mass analyses for LC/MS (electrospray), such as adducts and protonated molecules.

Establishment of SMILES Format File for Active Ingredients in GXNT

The molecular structure of the active compound was mapped with ChemBio Draw Ultra 14.0 software, and was saved in the MDL sdf. format. All chemical structures were converted to Mol2 format using ChemBio 3D Ultra software in order to establish an active molecular library. The active molecular Mol2 file was converted to a SMILES file using Open Babel GUI software for subsequent analyses.

Prediction of Potential Targets for Active Ingredients in GXNT

Swiss Target Prediction (http://www.swisstargetprediction.ch/) is a web server to accurately predict the action targets of bioactive molecules based on the similarity of two dimension and three dimension of known ligands, providing valuable insights into the action mechanism of active molecules (Gfeller et al., 2014). The SMILE format files of active ingredients identified by LC-MS were uploaded to the Swiss Target Prediction server, and "Homo sapiens" was selected as the species. Then, the potential drug targets were searched using the active small molecules as probes. The target prediction results were sorted from high to low according to "Probability", and the official names of drug targets were retrieved through the UniProtKB search function in the UniProt database (http://www.uniprot.org/).

Mapping of Thrombus-Related Targets

Reported genes, possibly related to thrombus, were searched by the keyword "thrombus" in CooLGeN (http://ci.smu.edu.cn/CooLGeN/) and in the GeneCards database. Comparing these with the targets obtained from Swiss Target Prediction server, we obtained the potential targets of the active ingredients in GXNT that are potentially involved in the antithrombotic mechanism.

Functional Enrichment Analysis of the Potential Action Targets

Bioscape Annotation Database Metascape (http://metascape.org) is a reliable, effective, and intuitive online bioinformatics annotation tool for understanding the biological functions of genes and protein lists on a large scale for biomedical researchers. Gene ontology (GO) enrichment and KEGG pathway annotation analyses of the basic ontology term were performed using Metascape for the potential targets of GuanXinNing, and "$P < 0.05$" was considered as the statistically significant screening condition.

Construction of Component–Target Network and Component–Target–Pathway Network

The action targets and related signaling pathways were predicted according to the active component candidates identified from GXNT, and were then imported into Cytoscape software for constructing compound-target networks, and compound-target-path networks to explore the overall pharmacological mechanisms of GXNT. The importance of every node in the network was determined by the degree of topological parameters. The degree of a node refers to the number of edges connected to that node, i.e. the higher the degree is, the more nodes it is directly connected to, and the more importance the node has in the network. Edges represent the interactions between the compounds and the targets in the network.

Thrombus Animal Experiment

Animal Administration and Modeling

After 3 to 5 days of adaptive breeding, 48 SD rats were randomly divided into six groups, namely, the control group, the model group, the GXNT low, medium, and high groups with doses of 75, 150, and 300 mg/kg, and the positive group (n = 8). Each GXNT group was given the corresponding dose of GXN extract powder solution by oral administration. The positive group was

given 12.5 mg/kg of clopidogrel solution orally, and the control group and the model group were intragastrically administrated with 10 mL/kg of distilled water. After 1 h of administration, thrombus model operation induced by $FeCl_3$ was conducted in SD rats. Briefly, rats were anesthetized by intraperitoneal injection of 3% sodium pentobarbital solution (0.15 mL/kg). The rats were fixed on a 37°C insulated operating platform with neck hair shaved and neck skin disinfected. Next, the right common carotid artery was carefully separated, and a plastic paper with a width of 1 cm was placed on the bottom of the right common carotid artery. Then, the 1 ×1 cm filter paper, added with 10 μl of 35% $FeCl_3$, was wrapped around the common carotid artery rapidly for 15 min of external application. Afterwards, we removed the plastic paper and the filter paper, ligated both ends of the thrombus, and cut the embolus.

Measurement of Thrombus Length and Weight

Before SD rats were sacrificed, the emboli of the rats were quickly cut, and the redundant blood was absorbed by clean filter paper. The length of the thrombus was accurately measured using vernier caliper and recorded as L_{right}. The weight of the thrombus was also accurately weighed with an analytical balance and recorded as M_{right}. Then, a proper length of the left common carotid artery of SD rats was taken, with the blood in the vessels absorbed by filter paper. The length of the blood vessel was precisely measured by the vernier caliper and recorded as L_{left}. The weight of the thrombus was weighed using an analytical balance and recorded as M_{left}. The weight of the thrombus was calculated with the following formula:

$$\frac{L(left)}{M(left)} = \frac{L(right)}{M(right) - M(thrombus)}, M(thrombus)$$

$$= M(right) - \left(\frac{M(left)}{L(left)}\right) \times L(right)$$

Preparation of Platelet-Rich Plasma and Platelet-Poor Plasma

Blood of rats in each group was taken from the abdominal aorta, transfused into PE tubes containing 3.8% sodium citrate anticoagulant (9:1, v/v), and then repeatedly inverted several times to fully mix the blood and anticoagulant. Part of the anticoagulant blood in the PE tube was centrifuged at 3,500 rpm for 15 min, and plasma was taken and stored at −80°C for further usage. The rest of the anticoagulant blood was taken and centrifuged at 1000 rpm for 10 min at room temperature, and the supernatant, namely platelet-rich plasma (PRP), was obtained to detect platelet aggregation rates and protein expressions. The remaining part was further centrifuged at 3000 rpm for 10 min, and the resulting supernatant, namely platelet-poor plasma (PPP), was taken.

Determination of Fbg, PAI-1, 6-keto-PGF1α, and TXB_2 in the Blood

Anti-coagulated plasma at −80°C was taken and thawed. Fbg was measured using CA500 automatic blood coagulation analyzer (Sysmex, Japan). The specific procedures were carried out in strict accordance with the commercially available kit. The PAI-1, 6- 6-keto-PGF1α, and TXB_2 assay kits were used to detect the expression levels of PAI-1, 6-keto-PGF1α, and TXB_2 in samples by the enzyme linked immunosorbent assay (ELISA) method under the guidance of corresponding kit instructions.

Platelet Aggregation Assay

According to optical principles, the platelet aggregation rate was measured using Chrono-log platelet aggregation instrument (CHRONO-LOG, USA). We took PRP and PPP into turbidity tubes, and placed them in preheating holes. Platelet aggregation assay was performed after incubation at 37°C for 5 min, and PPP was applied to zero setting during measurement. Then, ADP (10 μM) as the agonist was added to PRP with magnetic stirrer stirring, and the aggregation curve was traced. The inhibition rate of platelet aggregation was calculated by the following formula:

$$\begin{aligned} &Inhibition\ rate\ (\%) \\ &= \{(aggregation\ rate\ of\ the\ control\ group \\ &\quad - aggregation\ rate\ of\ the\ administration\ group)/ \\ &\quad aggregation\ rate\ of\ \ the\ control\ group\} \times 100\,\% \end{aligned}$$

Determination of MAPKs Signaling Pathway-Related Protein Expressions in Platelets by Western Blot

Prepared PRP was taken, induced with ADP, incubated for 20 min at 37°C, and centrifuged at 3000 rpm for 5 min. The supernatant was discarded, and the precipitated fraction was used for the extraction of total platelet protein, which was carried out according to the instructions of the KeyGEN total protein extraction kit. Then, protein concentrations were quantified using the BCA protein assay kit. After protein samples were mixed with sample loading buffer (4:1, v/v), they were boiled for 5 min. Next, proteins (10 μg) were separated by SDS-PAGE electrophoresis, and transferred to PVDF membranes. The membranes were blocked with 3% albumin from bovine serum at room temperature and then incubated overnight with primary antibodies (p-P38, p-ERK1/2, and p-JNK of 1:1000 dilution; GAPDH of 1:200 dilution; all diluted with 3% BSA) at 4°C. After 48 h, the membranes were washed with TBST for 4 times, and were incubated with the secondary antibodies at 37°C for 2 h. Finally, the membranes were washed with TBST for four times and with TBS for 1 min, and were scanned in the odyssey infrared fluorescence scanner (Thermo company, USA). Afterwards, the membranes containing p-P38, p-ERK1/2, p-JNK proteins were washed with western stripping buffer to further detect P38, ERK1/2, and JNK proteins by the procedures as mentioned above.

Statistical Analysis

All data were statistically analyzed using SPSS 22.0 software, and expressed as mean ± standard error ($\bar{\chi}$± SEM). Statistical analysis was conducted *via* one-way analysis of variance (ANOVA) for comparison between groups and *via* L-S-D test

for pairwise comparison. Drawings of statistical graph were done using GraphPad Prism 6.0 software. $P < 0.05$ indicates statistical significance.

RESULTS

Optimization of Fingerprint of GXNT

Non-volatile phosphoric acid was used as the mobile phase additive in the fingerprint of GXNT, which was established by the institute previously (Lin et al., 2017). Since this condition is not suitable for LC-MS system, the analytical method needs to be properly optimized. When no additive was used (i.e. pure water was used as the water phase), the compound had a wider peak shape, poor symmetry, and a certain degree of tailing. After a certain amount of formic acid was added, the peak shape could be visibly improved, and the mass spectral response was also enhanced. Hence, 0.1% formic acid was used as the aqueous phase. The optimized analysis conditions were used to analyze the GXNT samples. The mass spectrum TIC map (in positive and negative modes) and the ultraviolet chromatogram at 280 nm are both shown in **Figure 1**. Since the mass spectrometry detector was a broad-spectrum detector, many compounds that were limited to ultraviolet response could be detected, and thus more complete material information could be obtained. It was observed that the main ion peaks of TIC images under the positive and negative modes of the mass spectrum were all reflected in the fingerprint, indicating that the currently established fingerprint map basically satisfied the principle of compound information maximization.

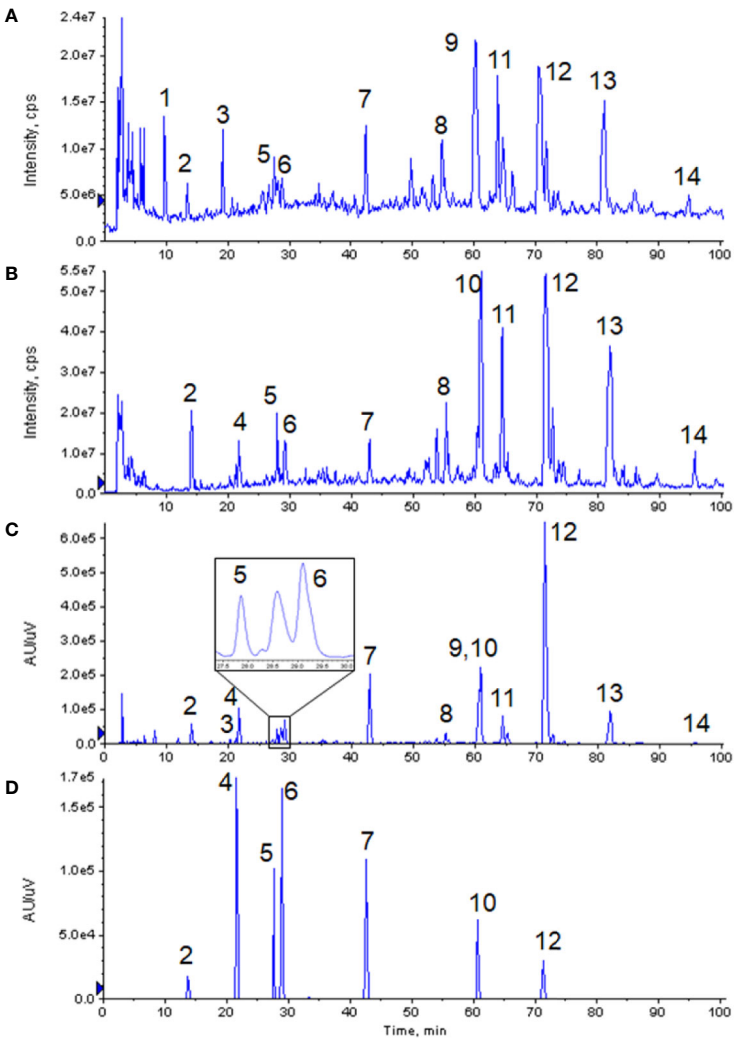

FIGURE 1 | Chromatograms of GXNT and mixed standard. **(A)** TIC diagram of GXNT mass spectrometry in the positive mode. **(B)** TIC diagram of GXNT mass spectrometry in the negative mode. **(C)** Chromatogram of GXNT at 280 nm. **(D)** Chromatogram of mixed standard at 280 nm. (1) Phenylalanine; (2) Tanshinol; (3) Senkyunolide B; (4) Protocatechualdehyde; (5) Chlorogenic acid; (6) Caffeic acid; (7) Ferulic acid; (8) Salvianolic acid D; (9) Senkyunolide I; (10) Rosemary acid; (11) Isosalvianolic acid A; (12) Salvianolic acid B; (13) Salvianolic acid A; (14) Isosalvianolic acid C.

Maps of GXNT and Single Chinese Herb

From the chromatographic comparative map at 280 nm (as shown in **Figure 2**), it could be seen that most compounds in GXNT were from Danshen, while a small amount came from Chuanxiong, since most components in Chuanxiong were volatile oils and the extraction rate of the water extraction process was lower. Among all the compounds, peaks 1 and 6 were the common peaks of the two drugs. Though the fingerprint had only one peak at 60 min, we can see from the mass spectrometry of Danshen (peak 10) and Chuanxiong (peak 9) separately that both compounds had peaks at the same retention time, meaning that the single peak consists of two superimposed peaks from Danshen and Chuanxiong and that these two compounds are not the same substance. This is difficult to see in the ultraviolet chromatogram alone. However, it could be effectively identified in the mass spectrum, and distinguished and quantified separately by extracting ion peaks.

Identification of Active Ingredients in GXNT

The mass spectrometry information of the materials obtained from the experiment was compared with the related literature reports. As a result, 14 compounds were identified in GXNT, of which 7 major compounds were verified by standard products. The specific identification results were summarized in **Table 1**, and the mass spectrum and the structure of each compound are shown in **Figure 3**. In specific, peak 1 was identified as phenylalanine, in which one molecule of NH_3 and/or HCOOH was removed to form a responsive fragment ion in the mass spectrum (Ying et al., 2013b). Peak 2 was identified as tanshinol, which responded weakly in the positive mode, with one molecule of H_2O as well as HCOOH removed to form the major fragment ion in the negative mode (Chen et al., 2011). Peak 3 only responded in the positive mode of mass spectrometry, mainly forming a dehydrated ion peak. Senkyunolide B and C, corresponding to molecular weights and compounds that could form dehydrated ion peaks in Chuanxiong, were mainly obtained *via* searching the literature. Given the polarity according to the peak time and the structure of the compound, it was preliminarily presumed to be senkyunolide B (Hu et al., 2012). Peak 4 was identified as protocatechuic aldehyde, which responded only in the negative mode, where one molecule of CO was removed to form the major fragment ion of *m/z* 109 (Chen et al., 2011). Peak 5 was identified as chlorogenic acid, which mainly formed [M+H-192]+ by removing one molecule of quinic acid in the positive mode and fragment ions of quinic acid (*m/z* 191) in the negative mode (Ying et al., 2013a). Peak 6 was identified as caffeic acid, where molecule of H_2O was removed in the positive mode of mass spectrometry and one molecule of CO_2 was removed in the negative mode, corresponding to the carboxyl group of structure (Chen et al., 2011). Peak 7 was identified as ferulic acid, which

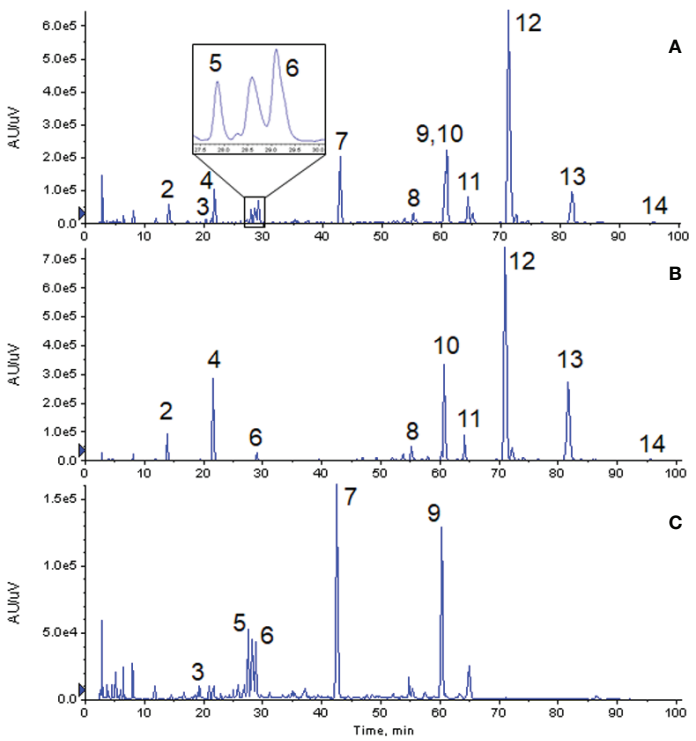

FIGURE 2 | Comparison of chromatogram of each extract at 280 nm. **(A)** Ultraviolet chromatogram of GXNT. **(B)** Ultraviolet chromatogram of Danshen. **(C)** Ultraviolet chromatogram of Chuanxiong. (2) Tanshinol; (3) Senkyunolide B; (4) Protocatechualdehyde; (5) Chlorogenic acid; (6) Caffeic acid; (7) Ferulic acid; (8) Salvianolic acid D; (9) Senkyunolide I; (10) Rosemary acid; (11) Isosalvianolic acid A; (12) Salvianolic acid B; (13) Salvianolic acid A; (14) Isosalvianolic acid C.

TABLE 1 | Identification results of main compounds in GXNT.

Peak No.[a]	RT (min)	Main ions in the positive mode	Main ions in the negative mode	Molecular weight	Identification result	Source
1	9.7	166[M+H]+;149[M+H-NH3]+;120[M+H-HCOOH]+;103[M+H-HCOOH-NH3]+	164[M-H]−;147[M-H-NH3]−	165	Phenylalanine	Common
2	14.1	199[M+H]+	197[M-H]-;179[M-H-H2O]-;133[M-H-H2O-HCOOH]-	198	Tanshinol[c]	Danshen
3	19.2	205[M+H]+;187[M+H-H2O]+	n.d.[b]	204	Senkyunolide B	Chuanxiong
4	21.7	n.d.	137[M-H]-;109[M-H-CO]-	138	Protocatechualdehyde[c]	Danshen
5	27.9	355[M+H]+、163[M+H-192]+	707[2M-H]-;353[M-H]-;191[M-H-162]-	354	Chlorogenic acid[c]	Chuanxiong
6	29.1	181[M+H]+;163[M+H-H2O]+	179[M-H]-;135[M-H-CO2]-	180	Caffeic acid[c]	Common
7	42.9	195[M+H]+;177[M+H-H2O]+;149[M+H-H2O-CO]+;117[M+H-H2O-CO-CH3OH]+	193[M-H]-;178[M-H-CH3·]-•;134[M-H-CH3··CO2]-•	194	Ferulic acid[c]	Chuanxiong
8	55.3	419[M+H]+;177[M+H-CO2-198]+	835[2M-H]-;417[M-H]-;373[M-H-CO2]-;175[M-H-CO2-198]-	418	Salvianolic acid D	Danshen
9	60.6	225[M+H]+;207[M+H-H2O]+;189[M+H-H2O-H2O]+;161[M+H-H2O-HCOOH]+	n.d.	224	Senkyunolide I	Chuanxiong
10	60.9	361[M+H]+;181[M+H-180]+;163[M+H-198]+	359[M-H]-;197[M-H-162]-;179[M-H-180]-;161[M-H-198]-	360	Rosemary acid[c]	Danshen
11	64.4	495[M+H]+;297[M+H-198]+	493[M-H]-;295[M-H-198]-	494	Isosalvianolic acid A	Danshen
12	71.3	719[M+H]+;521[M+H-198]+;323[M+H-198-198]+	717[M-H]-;519[M-H-198]-;321[M-H-198-198]-	718	Salvianolic acid B[c]	Danshen
13	81.9	495[M+H]+;297[M+H-198]+	987[2M-H]-;493[M-H]-;295[M-H-198]-	494	Salvianolic acid A	Danshen
14	95.6	n.d.	491[M-H]-;293[M-H-198]-	492	Isosalvianolic acid C	Danshen

[a]*Peak No. is consistent with the label of* ***Figure 1****;* [b]*n.d. (not detected) means not detected, no or below the detection limit;* [c]*Compound has been confirmed by reference standard.*

could remove one molecule of H_2O, CO, and CH_3OH to form corresponding fragment ions in the positive mode, remove CH_3• in the methoxy group on the benzene ring to form radical ions of *m/z* 178 in the negative mode, and remove CO_2 of carboxyl group on the side chain to form the fragment ion of *m/z* 134 (Hu et al., 2012). Peak 8 was identified as salvianolic acid D, of which the main fragment ions were formed by firstly removing one molecule of CO_2 and then removing one molecule of tanshinol (198 of molecular weight) in the positive and negative modes of mass spectrometry (Chen et al., 2011). Peak 9 was identified as senkyunolide I, of which the dehydrated ion peak (*m/z* 207) was obtained by removing one hydroxyl group from cyclohexane in the positive mode and the corresponding fragment ions were obtained by further removing the second hydroxyl group on the ring or the ester bond in the lactone ring (Hu et al., 2012). Peak 10 was identified as rosmarinic acid, and its structure was formed by the condensation of one molecule of caffeic acid and one molecule of tanshinol. Therefore, it could remove one molecule of caffeoyl group (162 of molecular weight) or caffeic acid (180 of molecular weight), and a molecule of tanshinol (198 of molecular weight) to form each fragment ion in the mass spectrometry (Chen et al., 2011). Peaks 11, 12, 13, and 14 were identified as isosalvianolic acid A, salvianolic acid B, salvianolic acid A, and isosalvianolic acid C, respectively. These compounds were similarly cleaved in the mass spectrometry, with single or multiple molecules of tanshinol (198 of molecular weight) removed to form each of the major fragment ions (Chen et al., 2011).

Content Quantification of Seven Main Active Ingredients in GXNT

We took two samples each of GXNT, Danshen and Chuanxiong herbs in parallel, calculated the amounts of the seven compounds confirmed by reference standards using the corresponding standard curves listed in **Table 2**, and investigated the changes of the seven compounds in each single Chinese herb and the Chinese compound formula. The results are shown in **Table 3** in detail. In each extract, the seven compounds accounted for about 6.5% of the total amount of extract from GXNT. The amount of salvianolic acid B was much higher in the extract of GXNT and Danshen than that in the extract of Chuanxiong. The current quality standard of GXNT uses salvianolic acid B and ferulic acid to control the quality of Danshen and Chuanxiong, respectively. However, our results indicated that ferulic acid only accounts for 0.316% of the Chuanxiong extract, which is not enough to reflect the quality of the whole Chuanxiong extract. Therefore, the quality control indexes for Chuanxiong need to be improved. In terms of raw drug content, the amount of each compound is similar in the medicinal materials compared to that in the compound formula, with some individual compounds having a slightly lower amount in the compound formula.

Screening of Potential Antithrombotic Targets for Active Ingredients in GXNT

Table 4 shows that different active compounds in GXNT could act on the same target, and the same active compound could also act on different targets, reflecting multi-component and multi-target action mode of GXNT. In specific, 83 unique targets were predicted from the 14 identified components using the Swiss Target Prediction analysis platform. The targets were also mapped to 743 targets possibly related to the occurrence and development of thrombus in the CooLGeN database, and to 725 targets associated with the occurrence and development of thrombus in the GeneCards database. Among them, 23 targets were also found in the GeneCards database, and 25 targets were

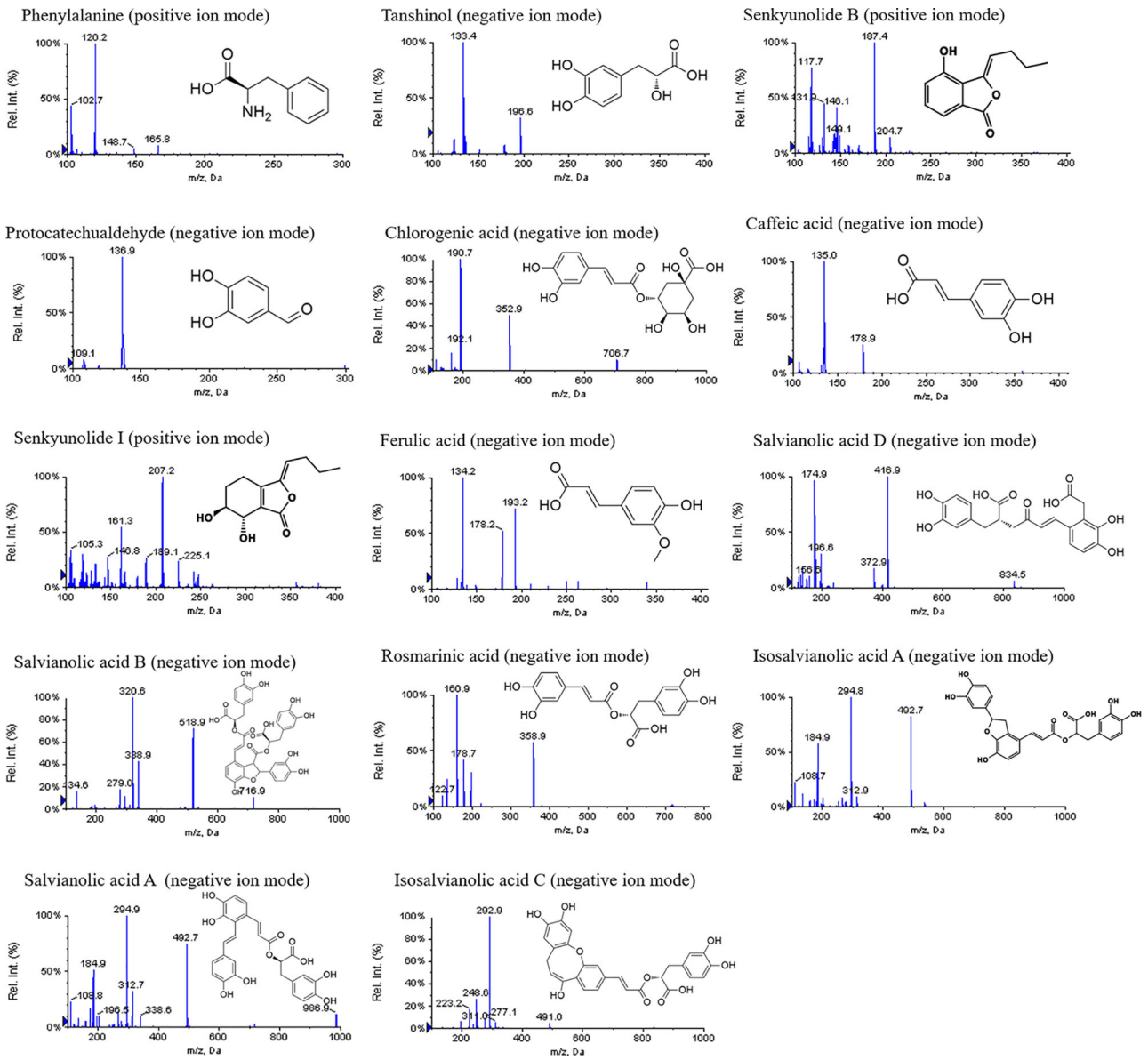

FIGURE 3 | Mass spectrums and chemical structures of main compounds in GXNT.

found in the CooLGeN database. The intersection of these targets resulted in a total of 17 potential antithrombotic targets of GXNT (shown in **Figure 4**), including MAPT, EGFR, KDR, MMP2, MMP9, MMP13, MMP1, MMP10, PTPN1, FYN, SRC, PRKCA, PTGS1, PTGS2, JUN, EDNRA, and ALOX12.

Functional Pathway Notes of Active Component Candidate Targets in GXNT

We performed GO enrichment analysis for the above mentioned 17 candidate targets of the active ingredients from GXNT *via* Metascape biomolecular function annotation system, which includes the analysis of biological process, molecular function and cellular components, and KEGG pathway annotation. And the top 10 terms with $P < 0.05$ are shown in **Table 5**. According to the screening results, the candidate targets for the active components in GXNT were involved in the biological process of response to oxidative stress, response to toxic substance, and response to inorganic substance. In terms of the molecular function, the targets were mainly related to metalloendopeptidase activity, endopeptidase activity, and protein domain specific binding. As for the cellular components, the extracellular matrix and membrane microdomain were the main components related to

TABLE 2 | Standard curves of seven main compounds.

Peak No.	Compound name	RT (min)	Linear relation	R^2	Linear range (μg/mL)
2	Tanshinol sodium	13.7	y = 0.031x - 0.0658	0.9999	40.8~916.0
4	Protocatechualdehyde	21.6	y = 0.2065x - 0.5731	0.9999	23.1~462.4
5	Chlorogenic acid	27.6	y = 0.1021x - 0.2181	0.9999	21.8~436.8
6	Caffeic acid	28.9	y = 0.2006x - 0.4056	0.9999	21.0~419.2
7	Ferulic acid	42.6	y = 0.1855x - 0.4126	0.9999	21.4~428.8
10	Rosmarinic acid[a]	60.7	y = 0.6489x + 5.0937	0.9744	40.2~803.2
12	Salvianolic acid B	71.3	y = 0.0673x - 0.1907	0.9999	198.4~3968

[a]*Rosmarinic acid was quantified by extracting ion peaks by mass spectrometry.*

TABLE 3 | Determination results of seven main compounds.

Peak No.	Compound name	Content in extract (%)			Content of raw drug (%)		
		GXNT	Danshen	Chuanxiong	GXNT	Danshen	Chuanxiong
2	Tanshinol	0.580	1.882	n.d.	0.090	0.125	n.d.
4	Protocatechualdehyde	0.135	0.763	n.d.	0.021	0.051	n.d.
5	Chlorogenic acid	0.084	n.d.	0.111	0.013	n.d.	0.017
6	Caffeic acid	0.097	0.082	0.069	0.015	0.005	0.011
7	Ferulic acid	0.362	n.d.	0.316	0.056	n.d.	0.049
10	Rosmarinic acid	0.551	1.547	n.d.	0.086	0.103	n.d.
12	Salvianolic acid B	4.676	12.337	n.d.	0.728	0.822	n.d.
	Total	6.485	16.611	0.496	1.009	1.107	0.076

n.d. (not detected) means not detected, no or below the detection limit.

TABLE 4 | Potential targets from active ingredient candidates of GXNT.

Active ingredient candidates	Predicted targets
Phenylalanine	CA12, CA1, CA2, ALPL, CA3, ALPI, CA6, CA5A, CA7, CACNA2D1, CA9, CA14, PLAA, CA5B, CA13
Tanshinol	CA12, CA1, CA2, CA3, CA6, CA5A, CA7, CA13, TDP1, CA14, CA5B, MAPT, EGFR, ERBB2, LCK
Senkyunolide B	MBNL1, MBNL2, MBNL3, MAPT, CYP19A1, FLT1, FLT4, KDR, ESR1,ESR2, CDK1, CDK2, CDK4, CDK3, CDK6
Protocatechualdehyde	COMT, CA1, CA2, CA3, CA5A, CA7, CA5B, CA13, TYR, TDP1, MAPT, CA9, KDM4E, KDM4A, KDM4B
Chlorogenic acid	AKR1B10, AKR1B1, AKR1B15, AKR1A1, AKR1E2, MMP2, MMP9, MMP12, MMP13, MMP1, MMP3, MMP10, MMP27,MMP20, TDP1
Caffeic acid	CA12, CA1, CA2, CA3, PTPN2, PTPN1, CA6, CA5A, CA7, CA9, CA13,TDP1, CA14, CA5B, CA4
Ferulic acid	CA12, CA1, CA2, CA3, CA6, CA5A, CA7, CA9, CA13, CA14, CA5B, TDP1, AKR1B10, AKR1B1, AKR1B15
Salvianolic acid D	EGFR, ERBB2, ERBB4, ERBB3, FYN, YES1, FGR, SRC, FRK, ESR1, ESR2, MAPT, AKR1B10, AKR1B1, AKR1B15
Senkyunolide I	PRKCG, PRKCB, PRKCA, PRKCQ, PRKCD, PTGS1, PTGS2, RELA, REL, JUN, JUNB JUND, CRYZ, ADORA1, EDNRA
Rosmarinic acid	AKR1B10, AKR1B1, AKR1B15, TDP1, AKR1A1, AKR1E2, MMP1, MMP2, MMP3, MMP9 MMP12, MMP13, MMP10, MMP27, FYN
Isosalvianolic acid A	MMP1, MMP2, MMP3, MMP9,MMP8, MMP12, MMP13, MMP10, MMP27, AKR1B10, AKR1B1, AKR1B15, AKR1A1, AKR1E2, TDP1
Salvianolic acid B	MMP1, MMP2, MMP3, MMP9, MMP8, MMP12, MMP13, MMP10, MMP27, PTGS1 PTGS2, AKR1B10, AKR1B1, AKR1B15, AKR1A1
Salvianolic acid A	FYN, SRC, YES1, FGR, FRK AKR1B10, AKR1B1, AKR1B15, AKR1A1, AKR1E2, TDP1 MMP1, MMP2, MMP3, MMP9
Isosalvianolic acid C	AKR1B10, AKR1B1, AKR1B15, AKR1A1, AKR1E2, ALOX15, ALOX12, TOP1, TOP1MT EGFR, ERBB2, ERBB4, ERBB3, PTGS1, PTGS2

the targets. In addition, 34 pathways were revealed from the KEGG pathway enrichment analysis, including TNF signaling pathway, IL-17 signaling pathway, focal adhesion, MAPK signaling pathway, and platelet activation. These findings suggest that GXNT may play an antithrombotic role by regulating multi-dimensional signal cascades. In specific, MAPK signaling pathway is known to play an important role in the signal transduction *in vivo* and in maintaining the body's biological metabolic balance (Lien et al., 2017; Manne et al., 2018). Therefore, MAPK signaling pathway was selected in this study to further explore the molecular mechanism of GXNT.

Construction of Component–Target Network

The active component–target network for GXNT on thrombus was constructed using Cytoscape 3.6.1 software. The results showed that a total of 98 nodes and 210 edges were in the identified GXNT component–target network. Network topology

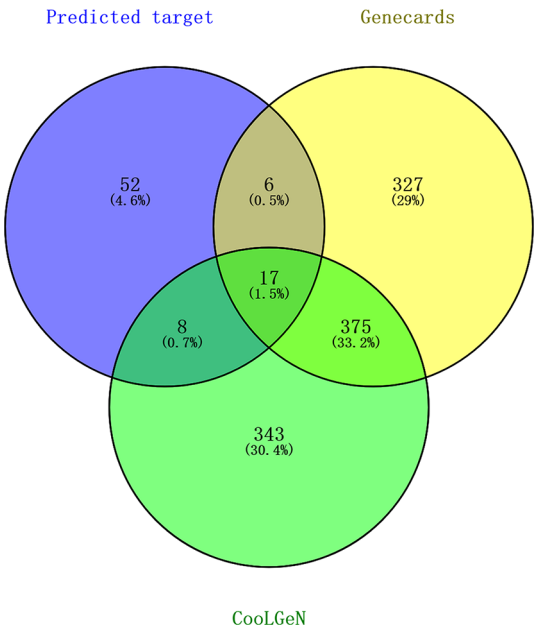

FIGURE 4 | Screening of targets for the identified components of GXNT on thrombus. 83 Predicted targets (in the blue circle) were mapped to 743 thrombus-related targets in CooLGeN (in the green circle), and to 725 thrombus-related targets in the GeneCards database (in the yellow circle), respectively. Among them, 23 targets were found in the GeneCards database, and 25 targets were found in the CooLGeN database. The intersection of these targets resulted in a total of 17 potential antithrombotic targets of GXNT.

analysis showed that the degree and betweenness centrality of Isosalvianolic acid C were the highest (degree=15, betweenness centrality=0.24921196), whereas the degree and betweenness centrality of PTGS1, a target of Isosalvianolic acid C, also ranked among the top (degree=3, betweenness centrality =0.1234151), shown in **Figure 5**.

Construction of Component–Target–Pathway Network

The Cytoscape software was used to construct the identified component–target–pathway network for GXNT on thrombus. As shown in **Figure 6**, the results showed that multiple targets were associated with multiple components, indicating that different components in GXNT had a synergistic effect in the process of exerting efficacy. The action targets of active ingredients in GXNT were distributed in different pathways and were coordinated with each other, suggesting that the action mechanism of GXNT may be related to the currently known effects of GXNT, such as anti-oxidative stress, anti-inflammation, vascular expansion, anti-platelet aggregation, and protection of vascular endothelium. The component–target–pathway network of GXNT revealed through multiple pathways that GXNT has the characteristic of multiple dimensions and functions for treating thrombotic cardiovascular disease.

TABLE 5 | Gene Ontology (GO) and pathway enrichment analysis for active component candidate targets of GXNT.

Category	Term	Number of the targets	P-value
GO Biological process	Response to oxidative stress	9	5.324E-12
	Positive regulation of epithelial cell migration	7	1.274E-11
	Response to inorganic substance	8	1.630E-09
	Circulatory system process	7	4.640E-08
	Regulation of mitochondrial membrane potential	4	1.496E-07
	Positive regulation of blood vessel endothelial cell migration	4	2.702E-07
	Response to toxic substance	6	1.001E-06
	Superoxide anion generation	3	1.559E-06
	Cellular response to amino acid stimulus	3	1.289E-05
GO Molecular Function	Metalloendopeptidase activity	5	7.598E-09
	Ephrin receptor binding	3	8.383E-07
	Metallopeptidase activity	5	1.322E-07
	Endopeptidase activity	5	9.480E-06
	Peptidase activity, acting on L-amino acid peptides	5	4.938E-05
	Peptidase activity	5	5.929E-05
	Serine-type endopeptidase activity	3	0.0001949
	Serine-type peptidase activity	3	0.0002867
	Serine hydrolase activity	3	0.0003050
	Protein domain specific binding	4	0.0012516
GO Cellular Components	Membrane raft	6	5.15E-08
	Membrane microdomain	6	5.24E-08
	Membrane region	6	6.53E-08
	Extracellular matrix	5	2.40E-05
	Cytoplasmic side of membrane	3	0.000232
	Perinuclear region of cytoplasm	4	0.0012385
	Early endosome	3	0.0017933
	Side of membrane	3	0.00704918
	Postsynapse	3	0.0085988
KEGG Pathway	Focal adhesion	6	3.33E-09
	GnRH signaling pathway	5	4.29E-09
	IL-17 signaling pathway	5	4.53E-09
	VEGF signaling pathway	4	7.46E-08
	Adherens junction	4	1.68E-07
	ErbB signaling pathway	4	3.44E-07
	Rap1 signaling pathway	4	1.21E-05
	MAPK signaling pathway	4	2.59E-05
	TNF signaling pathway	3	5.65E-05
	Platelet activation	3	8.32E-05

Effects of GXNT on the Length and Weight of Thrombus

We observed changes of thrombus lengths and weights in each group of rats. As shown in **Figures 7A** and **B**, we observed obvious thrombus and significant weight increases in rats of the model group after induction by $FeCl_3$. When compared to the model group, GXNT with incremental dosages (75, 150, and 300 mg/kg) could significantly reduce the length and weight of thrombus ($P < 0.01$). In particular, 300 mg/kg of GXNT was superior to clopidogrel in suppressing thrombus length. In

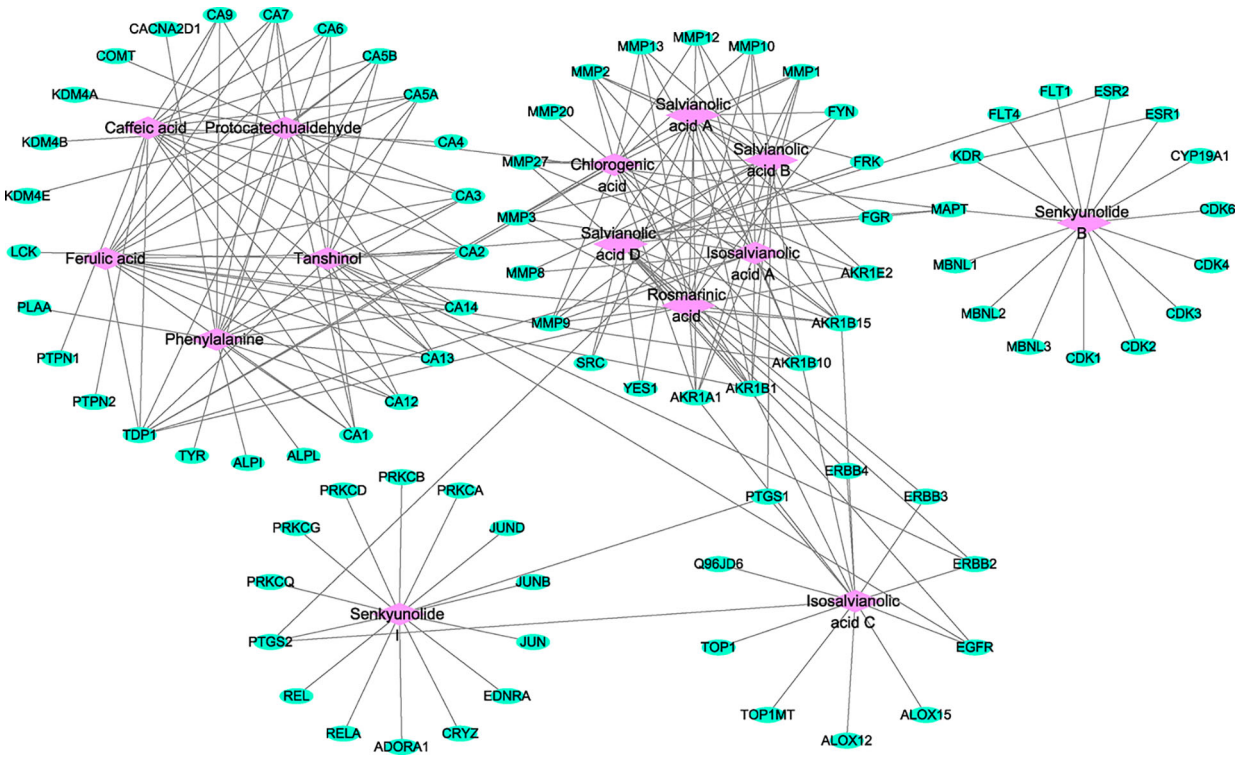

FIGURE 5 | Component–target network for the identified components of GXNT on thrombus. The component–target network was constructed by linking the 14 identified components and their potential targets. The green nodes represent the potential targets and the pink nodes represent the identified components. Edges represent the interactions between the compounds and the targets in the network.

addition, the weight of thrombus decreased significantly as the dosage of GXNT increased ($P < 0.01$).

Effects of GXNT on the Expressions of Fbg, PAI-1, 6-keto-PGF1α, and TXB_2

Fbg is one of the indicators for anticoagulant system activity, and PAI-1, 6-keto-PGF1α, and TXB_2 are the active markers in fibrinolytic system (**Figures 8A–E**). In **Figures 8A, B**, we can see that the Fbg and PAI-1 expression levels in the model group were significantly increased ($P < 0.05$; $P < 0.01$), compared with those in the control group. The expression levels of Fbg and PAI-1 were reduced in all GXNT groups and the positive group (12.5 mg/kg clopidogrel), compared with those in the model group ($P < 0.01$, $P < 0.05$; $P < 0.01$). As shown in **Figure 8C**, compared to the control group, the expression level of 6-keto-PGF1α in the model group was significantly decreased ($P < 0.05$), and there was no significant change in TXB_2 expression ($P > 0.05$). Furthermore, the 150-mg/kg GXNT group markedly increased the level of 6-keto-PGF1α ($P < 0.01$) compared to that in the model group, and no significant change was observed in TXB_2 expression ($P > 0.05$). Meanwhile, the 150- and 300-mg/kg GXNT group significantly decreased the ratio of TXB_2/6-keto-PGF1α compared with that in the model group ($P < 0.01$, $P < 0.01$; **Figure 8E**).

Effects of GXNT on Platelet Aggregation

The effect of GXNT on maximum platelet aggregation rate in rats is shown in **Table 6**. The results showed that GXNT could inhibit maximum platelet aggregation rate induced by ADP. Compared with the control group, maximum platelet aggregation rate significantly increased in the model group ($P < 0.01$). Compared with the model group, GXNT with different dosages could decrease maximum platelet aggregation rate to varying degrees. Among them, 150 and 300 mg/kg of GXNT could markedly reduce maximum platelet aggregation rate in rats ($P < 0.01$).

Effects of GXNT on Proteins Related to MAPK Signaling Pathway in Platelet

We observed expression changes of p-P38, p-ERK1/2 and p-JNK proteins in the MAPK signaling pathways in each group. From **Figures 9A–C**, it could be seen that after platelet was induced by ADP, phosphorylation levels of P38, ERK1/2, and JNK proteins were significantly increased compared with those in the control group ($P < 0.01$; $P < 0.05$). Compared with the model group, 150 mg/kg GXNT significantly decreased the phosphorylation levels of P38 and ERK1/2 ($P < 0.05$), while 300 mg/kg GXNT significantly lowered the phosphorylation levels of P38, ERK1/2, and JNK ($P < 0.01$; $P < 0.05$).

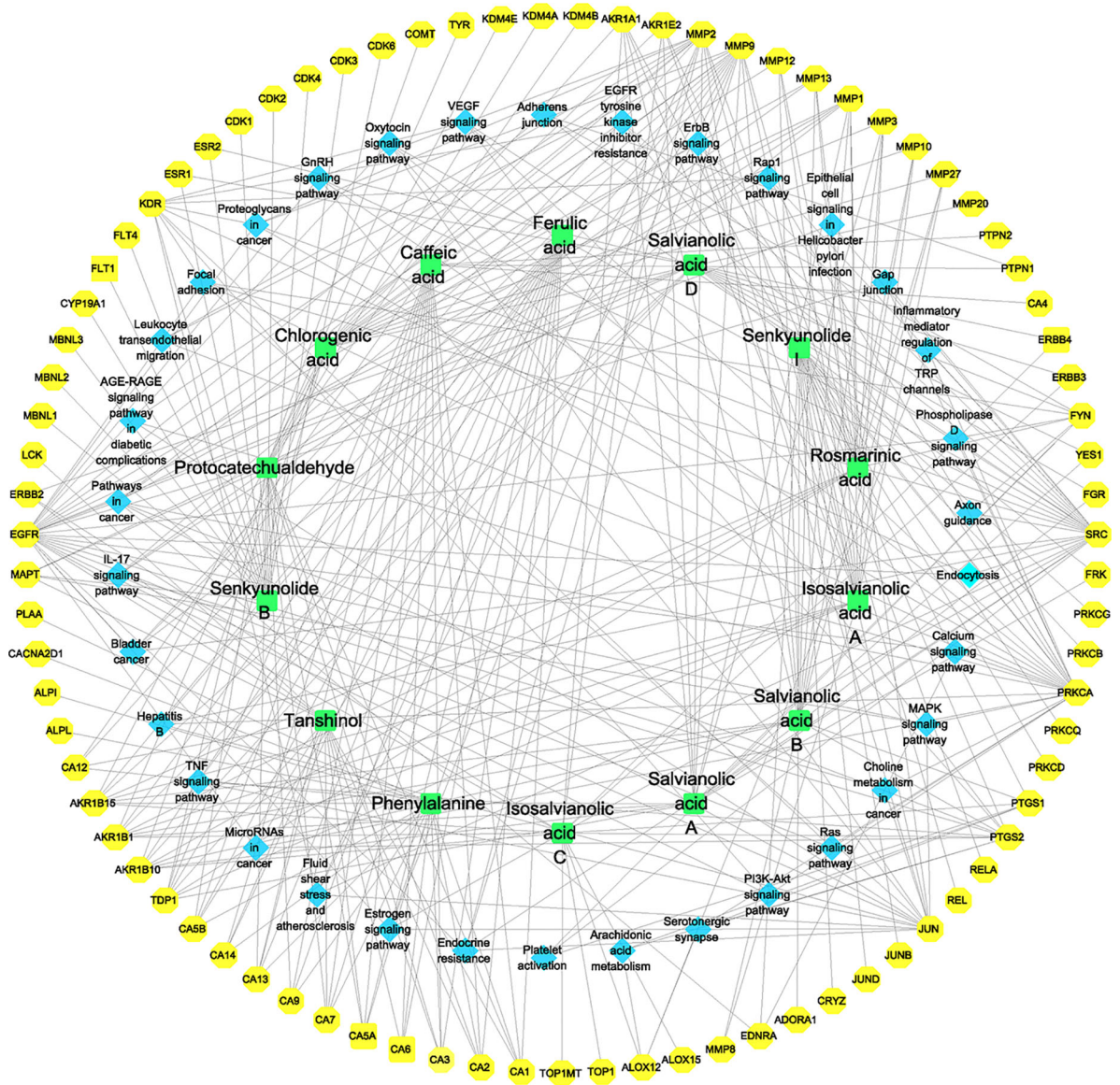

FIGURE 6 | Component–target–pathway network for the identified components of GXNT on thrombus. The green nodes represent the identified components, the blue nodes represent pathways, and the yellow nodes represent targets. Edges represent the interactions between the compounds and the targets in the network.

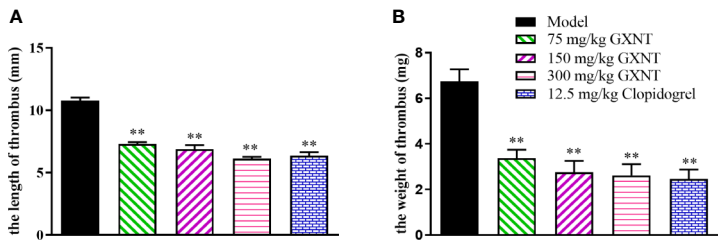

FIGURE 7 | Effects of GXNT on the length and weight of thrombus. **(A)** The length and **(B)** the weight of thrombus were observed after GXNT administration (75, 150, and 300 mg/kg) for 1 h. Data were expressed as the mean ± SEM (± SEM, n=8). $^{**}P < 0.01$ vs. model group.

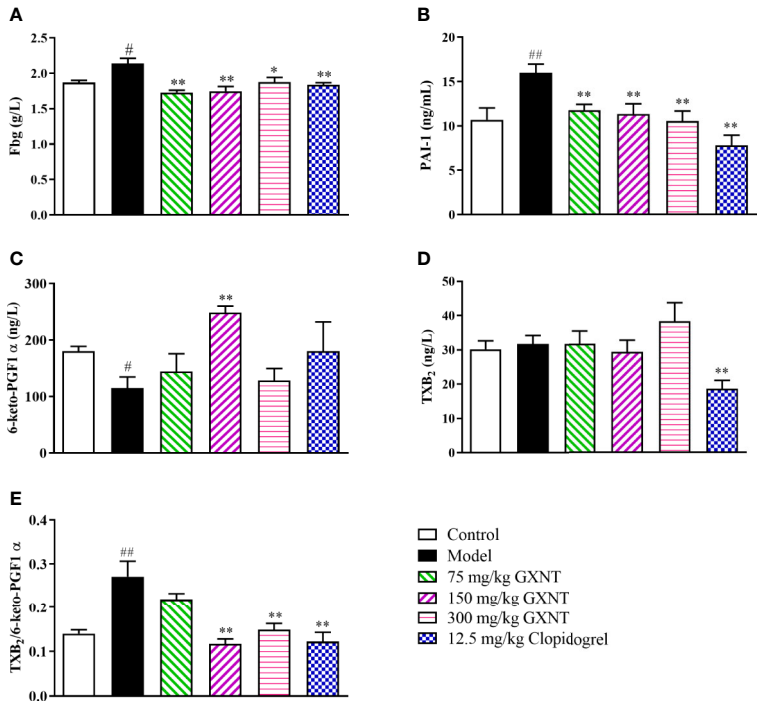

FIGURE 8 | Effects of GXNT on Fbg, PAI-1, 6-keto-PGF1α, TXB2, and TXB2/6-keto-PGF1α. **(A)** Fbg was measured using automatic blood coagulation analyzer. Expression levels of **(B)** PAI-1, **(C)** 6-keto-PGF1α, and **(D)** TXB2 were detected by the enzyme linked immunosorbent assay (ELISA) method. **(E)** The ratio of TXB2/6-keto-PGF1α was then calculated. Data were expressed as the mean ± SEM (± SEM, n=8). $^{\#}P < 0.05$, $^{\#\#}P < 0.01$ vs. normal group; $^{*}P < 0.05$, $^{**}P < 0.01$ vs. model group.

TABLE 6 | Effect of GXNT on maximum platelet aggregation rat.

Groups	Drug and Doses	Maximum platelet aggregation rate (%)
Control	10 mL/kg NS	49.33 ± 1.69
Model	10 mL/kg NS	69.17 ± 1.60$^{\#\#}$
The low-dose group	75 mg/kg GXNT	54.83 ± 6.64
The middle-dose group	150 mg/kg GXNT	53.17 ± 2.39**
The high-dose group	300 mg/kg GXNT	52.00 ± 3.34**
The positive group	12.5 mg/kg Clopidogrel	41.50 ± 3.38**

Data were expressed as the mean ± SEM (± SEM, n=8). $^{\#\#}P < 0.01$ vs. normal group; $^{**}P < 0.01$ vs. model group.

DISCUSSION

GXNT consists of extracts from two Chinese herbal medicines, Danshen and Chuanxiong, with the effect of promoting blood circulation and removing blood stasis. The two herbs are compatible with each other to make the blood and qi of human body run smoothly (Zhang, 2017). GXNT has excellent treatment effects on stable or unstable coronary heart diseases and angina pectoris of qi stagnation and blood stasis type triggered by thrombus in the clinic (Huo et al., 2016; Yang et al., 2017; Li et al., 2018). In this study, the pharmacological active substances of GXNT were analyzed, and the action mechanism of these active ingredients was predicted by the approach of network pharmacology, revealing that multiple pathways (such as MAPKs, VEGF, and TNF) are related to the antithrombotic mechanism. The experiments not only further confirmed the antithrombotic effect of GXNT, but also proved that the MAPKs pathway is an important action target. Thus, it showed that network pharmacology could provide high-value insights and reference information for studying the action mechanism of traditional Chinese medicines with complex components.

Thrombosis is an important pathophysiological process involved in various cardiovascular diseases (Otsuka et al., 2016; Ten et al., 2017), and its formation is a complicated process of multifactor participation and gradual development. Abnormal coagulation of blood occurs in the state of flow, due to activation of platelets and clotting factors (Xu et al., 2009). The conditions of thrombosis include vascular intimal injury, changes in blood state, and increased coagulation. Therefore, inhibiting platelet function and preventing blood coagulation can prevent thrombosis. Currently, antiplatelet and antithrombin drugs are often used clinically for treating thrombus, such as platelet cyclooxygenase inhibitor aspirin, platelet ring nucleotide inhibitor dipyridamole, ADP P2Y12 receptor antagonist clopidogrel, and GPIIb/IIIa receptor inhibitor abicximab. However, most of these drugs only have a single target, therefore often require a combination therapy with the risk of causing gastrointestinal hemorrhage (Rocca and Husted, 2016; Dregan et al., 2018). Hence, developing antithrombotic agents with multiple targets and a low risk of hemorrhage from medicinal

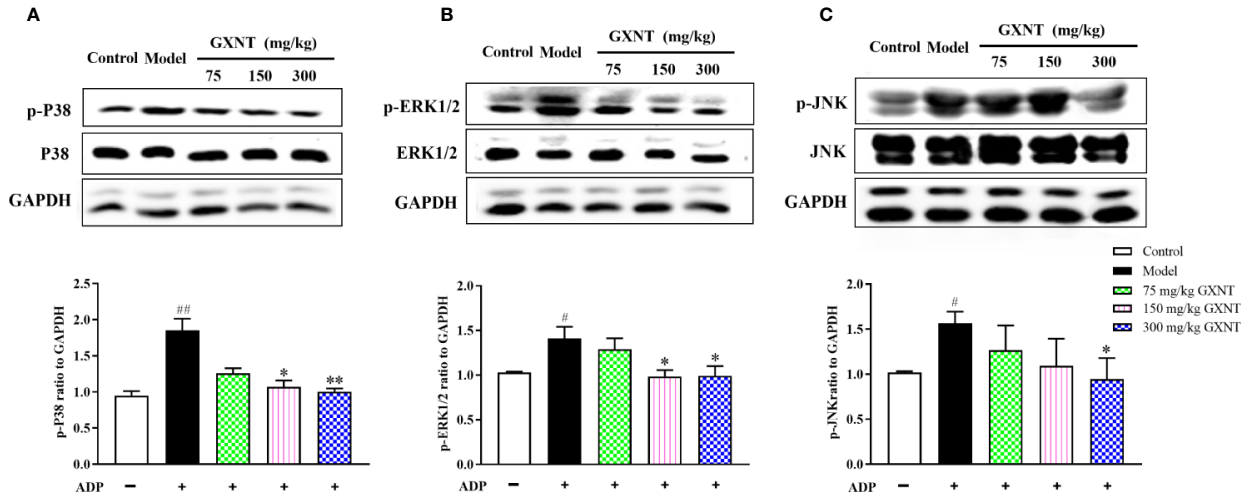

FIGURE 9 | Effects of GXNT on the expressions of p-P38, p-ERK1/2, and p-JNK proteins in platelets. The expressions of **(A)** p-P38, **(B)** p-ERK1/2, and **(C)** p-JNK proteins in platelets were determined by western blotting analysis after GXNT administration (75, 150, and 300 mg/kg). Data were expressed as the mean ± SEM (± SEM, n=3). $^{\#}P < 0.05$, $^{\#\#}P < 0.01$ vs. normal group; $^{*}P < 0.05$, $^{**}P < 0.01$ vs. model group.

herbs is of great significance. Our previous studies have shown that GXNT has anti-platelet aggregation and antithrombotic effects (Chen et al., 2005; Wang et al., 2016), which was again validated using the $FeCl_3$-induced rat thrombus model in this experiment. Common carotid artery thrombus model in rats induced by $FeCl_3$ is widely used in the preparation of arterial models and in the research of antithrombotic drugs (Kurz et al., 1990). The results of this experiment showed that the length and weight of thrombus were increased significantly after the formation of common carotid artery thrombus in rats. The administration of GXNT could significantly reduce the length and weight of thrombus. Furthermore, the antithrombotic effect was dose-dependent, indicating that GXNT is strongly resistant to $FeCl_3$-induced thrombus. Fe^{3+} can damage vascular endothelial cells and cause platelet activation and aggregation, due to a joint action of the coagulation system and the hemolysis system. When endothelial cells are damaged, the internal and external coagulation systems are activated. Thrombin activates platelets and converts Fbg to fibrin, which in turn activates the coagulation response system. Thus, Fbg plays a major role in the blood coagulation process, while PAI plays a major role in regulating plasma fibrinolytic activities. In addition, TXA_2 is a biologically active substance that strongly promotes vasoconstriction and platelet aggregation, whereas PGI_2 can dilate blood vessels and increase platelet cAMP to inhibit platelet aggregation. The dynamic balance between TXA_2 and PGI_2, i.e. ratio of TXA_2/PGI_2, plays an important role in maintaining the function of platelet and vessels and the regulation of thrombosis. Because of the instability of TXA_2 and PGI_2, their stable metabolites (TXB_2 and 6-keto-PGF1α) were used as detection indicators in this study (Xie et al., 2017; Cui et al., 2018). Our results showed that the level of Fbg was increased significantly in the thrombus model rats, whereas GXNT reduced the levels of Fbg and PAI, and regulated the balance of 6-keto-PGF1α and TXB_2. The results demonstrated that GXNT could ameliorate the hypercoagulable state of the body blood, and maintain the balance of the body's coagulation system and anticoagulant system, thereby achieving an antithrombotic effect.

In this study, 14 potential active components were identified using LC-MS technology. In specific, 8 were from Danshen, 4 were from Chuanxiong, and 2 were common components in both. In general, most compounds had a certain response in both positive and negative modes, but the negative mode response was slightly higher than the positive mode response. This is mainly due to the fact that GXNT contains more salvianolic acids from Danshen, which is more prone to give protons in the negative mode to obtain higher ion response. Nevertheless, some of the compounds only responded in the positive mode, mainly due to the fact that the lactones from Chuanxiong could only bind to protons and are difficult to give protons. Among these components, salvianolic acid B, salvianolic acid A, ferulic acid, chlorogenic acid, caffeic acid, rosemary acid, tanshinol, and protocatechualdehyde have already shown antithrombotic effects to some extent in previous studies (Jiang et al., 2005; Moon et al., 2012; Chen et al., 2018b). The modern pharmacological research showed that tanshinol could dilate blood vessels, promote fibrinolysis, reduce blood viscosity, and promote local blood circulation, thereby exerting antithrombotic effects (Dang et al., 2015). Salvianolic acid could inhibit arterial thrombosis by restraining platelet adhesion, aggregation, and downstream Ca^{2+} and cAMP signaling pathways (Hong et al., 2016). In addition, the antithrombotic effect of chlorogenic acid may be closely related to the adenosine A_{2A} receptor/adenylate cyclase/cAMP/PKA signaling pathway (Fuentes et al., 2014). Thus, it can be seen that the multi-level and multi-target effects were determined by multiple active ingredients of GXNT. We will confirm whether these active ingredients have synergistic effects in our future experimental studies.

To understand the antithrombotic mechanism of GXNT, we used network pharmacology for the analysis. It turned out that the 14 components in GXNT were closely related to 83 targets, of which 17 potential antithrombotic targets were obtained through functional enrichment analysis and are involved in pathways including MAPK signaling pathway, TNF signaling pathway, and VEGF signal transduction pathway. Based on this finding, MAPKs signaling pathway, which is known to be strongly linked to thrombotic diseases (Endale et al., 2012; Lien et al., 2017; Manne et al., 2018), was selected to verify the antithrombotic mechanism of GXNT. The MAPKs signaling pathway exists in most cells. Recent studies have shown that the MAPKs signaling pathway is an important platelet activation pathway that can be activated by collagen and thrombin to mediate platelet deformation, adhesion, and aggregation reaction, thereby participating in thrombus formation (Lien et al., 2017; Manne et al., 2018). The signaling pathway includes three subfamilies: extracellular signal regulated protein kinase (ERK), c-Juc amino-terminal kinase (JNK), and p38 protein kinase (p38 MAPK) (Lanna et al., 2017). The study by Yacoub (Yacoub et al., 2006) has shown that the activation of ERK and p38 MAPK plays an important role in the release of TXA_2 mediated by PKC. After being stimulated from collagen and thrombin, the phosphorylation level of PKCδ was increased in platelets, leading to an activation of p38 MAPK and ERK as well as a release of TXA_2. Simultaneously, the p38 MAPK signaling pathway is involved in the synthesis of platelet cells and backbone proteins. Activated p38 MAPK can induce regeneration and reorganization of actin and dynamic changes of platelet cytoskeleton *via* regulating the activity of heat shock protein (HSP27) and the level of downstream vasodilation-stimulated phosphoprotein (VASP), and can therefore cause platelet degeneration and promoting thrombosis (Mazharian et al., 2007). It has been found that JNK1 is involved in platelet aggregation and thrombosis. An *in vitro* study using rats with JNK1 deficiency (Adam et al., 2010) has shown an activation of integrin αIIbβ3 by PKC, a reduction of platelet aggregation, and an occurrence of platelet secretion disorder, indicating that JNK1 may play a key role in platelet biology and thrombosis. Moreover, some active components in GXNT such as caffeic acid (Lu et al., 2015), salvianolic acid B (Li et al., 2010), and ferulic acid (Hong et al., 2016) may be involved in the regulation of MAPKs signaling pathway. In our study, platelet aggregation was promoted by ADP as the inducer, and the phosphorylation levels of ERK, p38, and JNK proteins in MAPKs signal pathway of platelets were determined by Western Blot. The results showed that GXNT inhibited ADP-induced platelet aggregation. In addition, the phosphorylation levels of p38 MAPK, ERK, and JNK in rat platelets were all significantly increased compared to those in the control group, suggesting that ADP may affect platelet function by influencing the phosphorylation levels of p38 MAPK, ERK, and JNK proteins in the MAPKs signaling pathway. After the intervention with GXNT, the phosphorylation levels of p38 MAPK, ERK, and JNK proteins were all decreased, especially the phosphorylation level of p38 MAPK protein. Hence, GXNT had clear anti-platelet aggregation and antithrombotic effects, which may be achieved through reducing the phosphorylation levels of p38 MAPK, ERK, and JNK in MAPKs signaling pathway.

CONCLUSION

In conclusion, 14 active ingredients of GXNT were identified in this study, and the antithrombotic and antiplatelet aggregation effects of GXNT were further confirmed. Through the approach of network pharmacology, 34 signal pathways were predicted to be involved in thrombus (including MAPKs, VEGF, and TNF), and the role of MAPKs signal pathway in thrombotic diseases was verified. We further showed that the antithrombotic mechanism of GXNT may be associated with suppressing the phosphorylation of p38MAPK, ERK, and JNK in the MAPKs signaling pathway. The results from this study provided a reference for future studies on the action mechanism of GXNT for treating thrombotic diseases, as well as demonstrated that network pharmacology approaches can be used to predict the action mechanism of traditional Chinese medicine with complex components.

DATA AVAILABILITY STATEMENT

All datasets generated for this study are included in the article/supplementary material.

ETHICS STATEMENT

The animal study was reviewed and approved by Institutional Animal Care and Use Committee of Zhejiang Chinese Medical University.

AUTHOR CONTRIBUTIONS

M-LC contributed to the design concepts of this whole study. X-HY, Z-WZ, M-LW, and Y-YL carried out the study and collected important background information. M-LW, Y-YL, Q-QY, and Y-SW drafted the manuscript. Q-QY and Q-XM carried out literature search, data acquisition and analysis, and manuscript revision and edition. Q-YS helped perform the analysis with constructive discussions. All authors have read and approved the content of the manuscript.

FUNDING

This research was funded by Key Projects of Zhejiang Provincial Administration of Traditional Chinese medicine (2015ZZ009) and Zhejiang Science and Technology Department Public Welfare (Experimental Animal Platform) Project (2018C37129).

REFERENCES

Adam, F., Kauskot, A., Nurden, P., Sulpice, E., Hoylaerts, M. F., Davis, R. J., et al. (2010). Platelet JNK1 is involved in secretion and thrombus formation. *Blood* 115 (20), 4083–4092. doi: 10.1182/blood-2009-07-233932

Chang, C. C., Chang, Y. C., Hu, W. L., and Hung, Y. C. (2016). Oxidative Stress and Salvia miltiorrhiza in Aging-Associated Cardiovascular Diseases. *Oxid. Med. Cell. Longev.* 2016 (6), 1–11. doi: 10.1155/2016/4797102

Chen, M. L., Shou, Q. Y., Pan, Y. M., Zhang, J. B., Sang, R., Guan, M. W., et al. (2005). Effects of Guanxinning Tablet on anti-platelet aggregation and protection of vascular endothelium in rats with qi stagnation and blood stasis. *Chin. Clin. Pharmacol. Therap.* 10 (5), 586–589. doi: 10.3969/j.issn.1009-2501.2005.05.024

Chen, X. F., Lou, Z. Y., Zhang, H., Tan, G. G., Liu, Z. R., Li, W. H., et al. (2011). Identification of multiple components in Guanxinning injection using hydrophilic interaction liquid chromatography/time-of-flight mass spectrometry and reversed-phase liquid chromatography/time-of-flight mass spectrometry. *Rapid Commun. Mass Spectrom.* 25 (11), 1661–1674. doi: 10.1002/rcm.5003

Chen, L. D., Cao, Y., Zhang, H., Lv, D. Y., Zhao, Y. H., Liu, Y. J., et al. (2018a). Network pharmacology-based strategy for predicting active ingredients and potential targets of Yangxinshi tablet for treating heart failure. *J. Ethnopharmacol.* 219, 359–368. doi: 10.1016/j.jep.2017.12.011

Chen, Z. J., Zhang, C., Gao, F., Fu, Q., Fu, C. M., He, Y., et al. (2018b). A systematic review on the rhizome of Ligusticum chuanxiong Hort. (Chuanxiong). *Food Chem. Toxicol.* 119, 309–325. doi: 10.1016/j.fct.2018.02.050

Cui, L. L., Xing, M. M., Xu, L. T., Wang, J. Y., Zhang, X. F., Ma, C. Y., et al. (2018). Antithrombotic components of Malus halliana Koehne flowers. *Food Chem. Toxicol.* 119, 326–333. doi: 10.1016/j.fct.2018.02.049

Dang, X., Miao, J.J., Chen, A.Q., Li, P., Chen, L., Liang, J. R., et al. (2015). The antithrombotic effect of RSNK in blood-stasis model rats. *J. Ethnopharmacol.* 173, 266–272. doi: 10.1016/j.jep.2015.06.030

Dregan, A., Ravindrarajah, R., Charlton, J., Ashworth, M., and Molokhia, M. (2018). Long-term trends in antithrombotic drug prescriptions among adults aged 80 years and over from primary care: a temporal trends analysis using electronic health records. *Ann. Epidemiol.* 28 (7), 440–446. doi: 10.1016/j.annepidem.2018.03.006

Endale, M., Lee, W. M., Kamruzzaman, S. M., Kim, S. D., Park, J. Y., Park, M. H., et al. (2012). Ginsenoside-Rp1 inhibits platelet activation and thrombus formation via impaired glycoprotein VI signalling pathway, tyrosine phosphorylation and MAPK activation. *Br. J. Pharmacol.* 167 (1), 109–127. doi: 10.1111/j.1476-5381.2012.01967.x

Fuentes, E., Caballero, J., Alarcon, M., Rojas, A., and Palomo, I. (2014). Chlorogenic acid inhibits human platelet activation and thrombus formation. *PloS One* 9 (3), e90699. doi: 10.1371/journal.pone.0090699

Gfeller, D., Grosdidier, A., Wirth, M., Daina, A., Michielin, O., and Zoete, V. (2014). SwissTargetPrediction: a web server for target prediction of bioactive small molecules. *Nucleic Acids Res.* 42, W32–W38. doi: 10.1093/nar/gku293

Gu, W. L. (2010). "Cold coagulation and blood stasis is an important mechanism for the occurrence of blood clots," in The third academic conference of thrombosis of China Association of Chinese Medicine, (Zhengzhou, China: China Association of Chinese Medicine Press), 227–229.

Hong, Q., Ma, Z. C., Huang, H., Wang, Y. G., Tan, H. L., Xiao, C. R., et al. (2016). Antithrombotic activities of ferulic acid via intracellular cyclic nucleotide signaling. *Eur. J. Pharmacol.* 777, 1–8. doi: 10.1016/j.ejphar.2016.01.005

Hopkins, A. L. (2008). Network pharmacology: the next paradigm in drug discovery. *Nat. Chem. Biol.* 4 (11), 682–690. doi: 10.1038/nchembio.118

Hu, Y., Liu, C. M., Hu, Y. M., and Zhang, Y. C. (2012). Determination of chemical composition in extract of ligusticum Chuanxiong by liquid chromatography-electrospray Ionization mass spectrometry. *Lishizhen Med. Mater. Med. Res.* 23 (8), 1868–1869. doi: 10.3969/j.issn.1008-0805.2012.08.009

Huang, T., Ning, Z. W., Hu, D. D., Zhang, M., Zhao, L., Lin, C. Y., et al. (2018). Uncovering the Mechanisms of Chinese Herbal Medicine (MaZiRenWan) for Functional Constipation by Focused Network Pharmacology Approach. *Front. Pharmacol.* 9, 270. doi: 10.3389/fphar.2018.00270

Huo, G. H., Li, J., Niu, Y. Y., and Zhang, Y. Y. (2016). 45 cases of angina pectoris of coronary heart disease with qi deficiency and blood stasis treated by Dunye Guanxinning tablets. *Chin. Med. Res.* 29 (6), 9–11. doi: 10.3969/j.issn.1001-6910.2016.06.05

Jiang, R. W., Lau, K. M., Hon, P. M., Mak, T. C., Woo, K. S., and Fung, K. P. (2005). Chemistry and biological activities of caffeic acid derivatives from Salvia miltiorrhiza. *Curr. Med. Chem.* 12 (2), 237–246. doi: 10.2174/0929867053363397

Kurz, K. D., Main, B. W., and Sandusky, G. E. (1990). Rat model of arterial thrombosis induced by ferric chloride. *Thromb. Res.* 60 (4), 269–280. doi: 10.1016/0049-3848(90)90106-m

Lanna, A., Gomes, D. C., Muller-Durovic, B., Mcdonnell, T., Escors, D., Gilroy, D. W., et al. (2017). A sestrin-dependent Erk-Jnk-p38 MAPK activation complex inhibits immunity during aging. *Nat. Immunol.* 18 (3), 354–363. doi: 10.1038/ni.3665

Li, Q., Han, L. P., Li, Z. H., Zhang, T. J., and Tang, M. K. (2010). Salvianolic acid B alleviate the disruption of blood-brain barrier in rats after cerebral ischemia-reperfusion by inhibiting MAPK pathway. *Acta Pharm. Sin.* 45 (12), 1485–1490. doi: 10.16438/j.0513-4870.2010.12.011

Li, J. G., Ju, J. Q., Chen, Z., Liu, J., Lu, F., Gao, R., et al. (2018). Guanxinning tablet for patients who switch from dual antiplatelet therapy to aspirin alone after percutaneous coronary intervention: study protocol for a cluster randomized controlled trial. *Trials* 19 (1), 93. doi: 10.1186/s13063-017-2373-x

Li, S. (2013). Traditional Chinese medicine network pharmacology: theory, methodology and application. *Chin. J. Nat. Med.* 11 (2), 110–120. doi: 10.1016/S1875-5364(13)60037-0

Lien, L. M., Lin, K. H., Huang, L. T., Tseng, M. F., Chiu, H. C., Chen, R. J., et al. (2017). Licochalcone A Prevents Platelet Activation and Thrombus Formation through the Inhibition of PLCÎ³2-PKC, Akt, and MAPK Pathways. *Int. J. Mol. Sci.* 18 (7), 1500. doi: 10.3390/ijms18071500

Lin, X. J., Chai, J. G., Dai, J. M., Shi, X. P., Shen, Y., and Zhang, W. J. (2017). A method for establishing fingerprint of Guanxinning Tablet and its application. China Patent No CN201510406716.6. China: China National Intellectual Property Administration (CNIPA).

Lu, Y., Li, Q., Liu, Y. Y., Sun, K., Fan, J. Y., Wang, C. S., et al. (2015). Inhibitory effect of caffeic acid on ADP-induced thrombus formation and platelet activation involves mitogen-activated protein kinases. *Sci. Rep.* 5, 13824. doi: 10.1038/srep13824

Manne, B. K., Münzer, P., Badolia, R., Allgaier, B. W., and Rondina, M. T. (2018). PDK1 governs thromboxane generation and thrombosis in platelets by regulating activation of Raf1 in the MAPK pathway. *J. Thromb. Haemost.* 16 (6), 1211–1225. doi: 10.1111/jth.14005

Mazharian, A., Roger, S., Berrou, E., Adam, F., Kauskot, A., Nurden, P., et al. (2007). Protease-activating receptor-4 induces full platelet spreading on a fibrinogen matrix: involvement of ERK2 and p38 and Ca2+ mobilization. *J. Biol. Chem.* 282 (8), 5478–5487. doi: 10.1074/jbc.m609881200

Moon, C. Y., Ku, C. R., Cho, Y. H., and Lee, E. J. (2012). Protocatechuic aldehyde inhibits migration and proliferation of vascular smooth muscle cells and intravascular thrombosis. *Biochem. Bioph. Res. Co.* 423 (1), 116–121. doi: 10.1016/j.bbrc.2012.05.092

Otsuka, F., Yasuda, S., Noguchi, T., and Ishibashi-Ueda, H. (2016). Pathology of coronary atherosclerosis and thrombosis. *Cardiovasc. Diag. Ther.* 6 (4), 396–408. doi: 10.21037/cdt.2016.06.01

Pang, H. Q., Yue, S. J., Tang, Y. P., Chen, Y. Y., Tan, Y. J., Cao, Y. J., et al. (2018). Integrated Metabolomics and Network Pharmacology Approach to Explain Possible Action Mechanisms of Xin-Sheng-Hua Granule for Treating Anemia. *Front. Pharmacol.* 9, 165. doi: 10.3389/fphar.2018.00165

Rocca, B., and Husted, S. (2016). Safety of antithrombotic agents in elderly patients with acute coronary syndromes. *Drugs Aging* 33 (4), 233–248. doi: 10.1007/s40266-016-0359-0

Sadowski, M., Ząbczyk, M., and Undas, A. (2014). Coronary thrombus composition: Links with inflammation, platelet and endothelial markers. *Atherosclerosis* 237 (2), 555–561. doi: 10.1016/j.atherosclerosis.2014.10.020

Shan, C. S., Xu, Q. Q., Shi, Y. H., Wang, Y., He, Z. X., and Zheng, G. Q. (2018). Chuanxiong Formulae for Migraine: A Systematic Review and Meta-Analysis of High-Quality Randomized Controlled Trials. *Front. Pharmacol.* 9, 589. doi: 10.3389/fphar.2018.00589

Ten, C. H., Hackeng, T. M., and García, d. (2017). Coagulation factor and protease pathways in thrombosis and cardiovascular disease. *Thromb. Haemost.* 117 (7), 1265–1271. doi: 10.1160/TH17-02-0079

Wang, M. L., Pan, Y. M., Jin, M., Xu, X. P., Wang, D. J., Ma, Q. X., et al. (2016). Establishment of a zebrafish model of thrombosis and the intervention effect of Guanxinnig tablet. *Acta Lab. Anim. Sci. Sin.* 24 (4), 7. doi: 10.3969/j.issn.1005-4847.2016.04.018

Wang, S. (2018). Compound danshen dropping pill in combination with aspirin for the treatment of coronary heart disease and its effects on blood lipids. *Contemp. Med.* 24 (33), 28–30. doi: 10.3969/j.issn.1009-4393.2018.33.012

Xie, P., Cui, L., Shan, Y., and Kang, W. Y. (2017). Antithrombotic Effect and Mechanism of Radix Paeoniae Rubra. *BioMed. Res. Int.* 2017 (17), 1–9. doi: 10.1155/2017/9475074

Xu, W. T., Zhang, F. F., Luo, Y. B., Ma, L. Y., Kou, X. H., and Huang, K. L. (2009). Antioxidant activity of a water-soluble polysaccharide purified from Pteridium aquilinum. *Carbohydr. Res.* 344 (2), 217–222. doi: 10.1016/j.carres.2008.10.021

Yacoub, D., Theoret, J. L., Abou, S. H., Mourad, W., Allen, B. G., and Merhi, Y. (2006). Essential role of protein kinase C delta in platelet signaling, alpha IIb beta 3 activation, and thromboxane A2 release. *J. Biol. Chem.* 281 (40), 30024–30035. doi: 10.1074/jbc.M604504200

Yang, k., Ma, Y. M., Zhou, X. S., and Liu, W. J. (2017). Clinical study on Guanxinning Tablets combined with esmolol in treatment of angina pectoris. *Drugs Clin.* 32 (10), 1849–1853. doi: 10.7501/j.issn.1674-5515.2017.10.009

Ying, X. H., Liu, M. Y., Liang, Q. L., Jiang, M., Wang, Y. M., Huang, F. K., et al. (2013a). Identification and analysis of absorbed components and their metabolites in rat plasma and tissues after oral administration of 'Ershiwuwei Shanhu' pill extracts by UPLC-DAD/Q-TOF-MS. *J. Ethnopharmacol.* 150 (1), 324–338. doi: 10.1016/j.jep.2013.08.046

Ying, X. H., Ma, J. F., Liang, Q. L., Wang, Y. M., Bai, G., and Luo, G. A. (2013b). Identification and analysis of the constituents in an aqueous extract of tricholoma matsutake by HPLC coupled with diode array detection/electrospray ionization mass spectrometry. *J. Food Sci.* 78 (8), C1173–C1182. doi: 10.1111/1750-3841.12219

Yu, G. H., Zhang, Y. Q., Ren, W. Q., Ling, D., Li, J. F., Geng, Y., et al. (2017). Network pharmacology-based identification of key pharmacological pathways of Yin–Huang–Qing–Fei capsule acting on chronic bronchitis. *Int. J. Chron. Obstruct. Pulmon. Dis.* 12, 85–94. doi: 10.2147/COPD.S121079

Zhang, J. P., Zhang, Y. Y., Zhang, Y., Gao, Y. G., Ma, J. J., Wang, N., et al. (2013). Salvia miltiorrhiza (Danshen) injection ameliorates iron overload-induced cardiac damage in mice. *Planta Med.* 79 (9), 744–752. doi: 10.1055/s-0032-1328588

Zhang, C. Y. (2017). Advanced researches of Danshen-Chuanxiong pair drugs and its prescription of Guanxinning prescriptions in the treatment of cardiovascular and cerebrovascular diseases. *Chin. Tradit. Pat. Med.* 39 (5), 1018–1024. doi: 10.3969/j.issn.1001-1528.2017.05.029

Conflict of Interest: M-LW, X-HY, Z-WZ, were employed by company Chiatai Qingchunbao Pharmaceutical Co., Ltd.

The remaining authors declare that the research was conducted in the absence of any commercial or financial relationships that could be construed as a potential conflict of interest.

Advantages of publishing in Frontiers

OPEN ACCESS
Articles are free to read for greatest visibility and readership

FAST PUBLICATION
Around 90 days from submission to decision

HIGH QUALITY PEER-REVIEW
Rigorous, collaborative, and constructive peer-review

TRANSPARENT PEER-REVIEW
Editors and reviewers acknowledged by name on published articles

Frontiers
Avenue du Tribunal-Fédéral 34
1005 Lausanne | Switzerland

Visit us: www.frontiersin.org
Contact us: frontiersin.org/about/contact

REPRODUCIBILITY OF RESEARCH
Support open data and methods to enhance research reproducibility

DIGITAL PUBLISHING
Articles designed for optimal readership across devices

FOLLOW US
@frontiersin

IMPACT METRICS
Advanced article metrics track visibility across digital media

EXTENSIVE PROMOTION
Marketing and promotion of impactful research

LOOP RESEARCH NETWORK
Our network increases your article's readership